ISSN 0369-5034

NOVA ACTA LEOPOLDINA

Abhandlungen der Deutschen Akademie der Naturforscher Leopoldina
Im Auftrage des Präsidiums herausgegeben von
Benno Parthier, Präsident der Akademie
Neue Folge, Nummer 332, Band 88

Nonlinear Dynamics and the Spatiotemporal Principles of Biology

Leopoldina Symposium

Deutsche Akademie der Naturforscher Leopoldina
in cooperation with
Graduiertenkolleg 340 »Kommunikation in biologischen Systemen« and
Die Junge Akademie

Darmstadt
May 13 to 15, 2002

Organizing Committee:

Friedrich BECK (Darmstadt)

Marc-Thorsten HÜTT (Darmstadt)

Ulrich LÜTTGE (Darmstadt)
Senator of the Academy

Deutsche Akademie der Naturforscher Leopoldina, Halle (Saale) 2003
In Kommission bei Wissenschaftliche Verlagsgesellschaft mbH Stuttgart

NOVA ACTA LEOPOLDINA

Abhandlungen der Deutschen Akademie der Naturforscher Leopoldina

Im Auftrage des Präsidiums herausgegeben von

BENNO PARTHIER

Präsident der Akademie

NEUE FOLGE NUMMER 332 BAND 88

Nonlinear Dynamics and the Spatiotemporal Principles of Biology

Leopoldina Symposium

Deutsche Akademie der Naturforscher Leopoldina
in cooperation with
Graduiertenkolleg 340 "Kommunikation in biologischen Systemen"
and
Die Junge Akademie

Darmstadt
May 13 to 15, 2002

Organizing Committee:

Friedrich BECK (Darmstadt)

Marc-Thorsten HÜTT (Darmstadt)

Ulrich LÜTTGE (Darmstadt)
Senator of the Academy

With 138 Figures and 5 Tables

Deutsche Akademie der Naturforscher Leopoldina, Halle (Saale) 2003
In Kommission bei Wissenschaftliche Verlagsgesellschaft mbH Stuttgart

Redaktion: Dr. Michael KAASCH und Dr. Joachim KAASCH

Die Schriftenreihe Nova Acta Leopoldina erscheint bei der Wissenschaftlichen Verlagsgesellschaft mbH, Stuttgart, Birkenwaldstraße 44, 70191 Stuttgart, Bundesrepublik Deutschland.
Jedes Heft ist einzeln käuflich!

Die Schriftenreihe wird gefördert durch das Bundesministerium für Bildung und Forschung sowie das Kultusministerium des Landes Sachsen-Anhalt.

Bibliografische Information Der Deutschen Bibliothek
Die Deutsche Bibliothek verzeichnet diese Publikation in der Deutschen Nationalbibliografie; detaillierte bibliografische Daten sind im Internet über http://dnb.ddb.de abrufbar.

06019 Halle (Saale), Postschließfach 11 05 43, Tel. (03 45) 4 72 39 34
Hausadresse: 06108 Halle (Saale), Emil-Abderhalden-Straße 37
Herausgeber: Prof. Dr. Dr. h. c. Benno PARTHIER, Präsident der Akademie
Printed in Germany 2003
Gesamtherstellung: druckhaus köthen GmbH
ISBN 3-8047-2077-3
ISSN 0369-5034
Gedruckt auf chlorfrei gebleichtem Papier

Contents

Chaos and Synchronization

Understanding Spatiotemporal Patterns in Biology

Nova Acta Leopoldina NF *88*, Nr. 332, 7–8 (2003)

Welcome Greetings

Benno PARTHIER (Halle/Saale)

President of the Academy

On behalf of the presidium of our academy I have the pleasure to welcome you to this international Leopoldina Symposium here in Darmstadt. It has been scientifically and locally organized by Friedrich BECK, Marc-Thorsten HÜTT, and Ulrich LÜTTGE in cooperation with the Graduiertenkolleg at the Technical University – we enjoy the presence of President WÖRNER of the Technical University – and together with the "Junge Akademie", which is a creation by two parental academies, the Berlin-Brandenburg Academy of Sciences and the Leopoldina Academy, and was founded two years ago in 2000. I think it is a very good opportunity both for the old and for the young academy to organize together scientific events like this one.

Ulrich LÜTTGE has been dreaming of the event of today for several years, as he has told me last night. The result of his dream is a promising program filled up to the rim with lectures and discussions about the topic "Nonlinear Dynamics and the Spatiotemporal Principles of Biology". This is a basic biological topic consisting of theory, modelling and experiments, and therefore meets perfectly the character of the Leopoldina symposia: interdisciplinarity. Our thanks are addressed not only to the colleagues who organized this program, but are likewise directed to the speakers, who came to Darmstadt in order to help demonstrating this symposium as a scientific challenge of the Leopoldina Academy. You probably know that this oldest academy in German speaking countries celebrates its 350th anniversary this year. Celebrations started in Schweinfurt in January and will continue in June in Halle with international academies as our guests.

This gives me a chance to tell you a few sentences about the foundation and history of the Leopoldina Academy. It was founded by four physicians on January 1, 1652, in the Free City of Schweinfurt. They named the society "*Academia Naturae Curiosorum*" because they wanted to know more about what is the cause of sickness. The spiritual rector was Laurentius BAUSCH who was inspired to found this academy by his *peregrinatio academia* in Italy, where he visited the Accademia dei Lincei in Rome and the Accademia Secretorum Naturae in Naples. Italy harboured quite a number of academies at that time; most of them do not exist anymore, but the inspiration came from there and designated the motto of the young academy as "nunquam otiosus". It means "never be idle" and has remained our motto up to date. From the Statutes (*leges*) of the Academy in 1662 I would like to read the first sentence: "The glory of God, the enlightenment of the art of healing and the benefit resulting from this for our fellow men be the goal and the only guide of the Academy of the Natural Scientists." This is also a challenge we have faced until today. A very important point was that the Emperor of the Holy Roman King-

dom of the German Nation, LEOPOLD I., recognized the academy in 1677 as the "Reichsakademie". Ten years later, in 1687, he privileged the imperial academy, which acquired the baroque name *Sacri Romani Imperii Academia Caesareo-Leopoldina Naturae Curiosorum,* but remaining is the abbreviation "Leopoldina". The academy and its presidents, respectively, received a number of remarkable privileges, including the right to award academic degrees, to appoint public notaries and judges, to legalize illegitimate children (as a source for getting money). However, the most important privilege was publishing without censorship. This was important for the development of the academy. For more than 200 years the site of the Academy shifted from one to another of 13 university cities, and since 1878 it has been located in Halle, soon gained property there, and now we have four buildings of our own and have built a new library.

Now I will briefly turn to the more recent time. In the last century we have suffered under two dictatorships in Germany, the "Third Reich" and GDR socialism. The three presidents in office were Emil ABDERHALDEN, Kurt MOTHES and Heinz BETHGE. Each of them was an eager and successful president in saving the Leopoldina from being attacked by both National and State's Socialism, and each of them enhanced the Leopoldina's international reputation. Especially president Kurt MOTHES (1954–1974) saved the academy as both a politically and scientifically independent institution in the Eastern part of Germany. After the reunification in 1990 a new era began also for the academy. Anything the Leopoldina performed in the GDR-period had to happen almost secretly behind the wall, but thereafter the opposite has to be done. Many institutions and persons shed the light of expectations on this academy, and it should response in reflecting the light by activity.

Now a few dates about the present academy. It consists of about 1000 members belonging to 27 disciplinary sections. While during the 300 years of its history the academy comprised only sciences and medical sciences, we decided to extent the disciplines of our sections in the last few years, in order to approach a "real academy" in the eyes of the sister academies and of the society. Thus we have included science theory, technical sciences, empirical social sciences, as well as empirical psychology and cognitive sciences as examples for new sections.

Since 1992 we have been funded through an annual budget of 1.5 Mio Euro jointly provided by the Federal Government and by the Land Sachsen-Anhalt in a ratio of 80 : 20. Our activities comprise quite a number of scientific events, among them are the annual meetings with hundreds of participants every two years. We organize symposia like this one and meetings in a more concentrated form, and we offer, of course, monthly lectures given by our members in the academy. The academy maintains its activity also through 25 staff members in Halle, in order to run the large library, the archives, the administration. We edit two series of journals where our activities are published, and we developed a promotional programme for junior post-doc scientists who are motivated to work in research laboratories all over the world.

Now let us start another of our symposia. I thank the organizers once more for performing this very interesting event here in Darmstadt.

Prof. Dr. Dr. h. c. Benno PARTHIER
Deutsche Akademie der Naturforscher Leopoldina
Emil-Abderhalden-Straße 37
06108 Halle (Saale)
Germany

The Framework

Nova Acta Leopoldina NF *88*, Nr. 332, 11–15 (2003)

From a Static to a Dynamic Description of Living Systems: the Framework (Comment)

Michel THELLIER (Mont-Saint-Aignan)

Historically, the study of life was first approached in an essentially static way. Living species were considered to have been created once for all at the Origin and to have remained unchanged since then; it was only with Charles DARWIN that the notion of evolution was definitively imposed during the 19th century. Up to the discovery of blood circulation by William HARVEY in the first half of the 18th century, the existence of time-dependent processes in animal physiology was practically ignored. Even in recent times, it is striking that molecular biology, however successful it has been, and still is in a number of domains, offers a description of biological systems in which time is almost always absent, or, more precisely, in which the dynamic features of the processes under study are usually ignored. This is really paradoxical! By contrast with simple physical or chemical systems, it is not possible to isolate a living system from exchanges (of heat, energy and/or matter) with its exterior and let it evolve to internal thermodynamic equilibrium. Attempts to do so cause the living system to be rapidly and irrevocably transformed into a dead system: living systems are inseparable from their dynamical behavior.

Endeavoring to unravel the underlying dynamic features of life thus represents an almost entirely new goal for a still restricted number of scientists. There are several reasons why such a dynamic approach is now possible, e. g., the existence of the immense corpus of data previously accumulated by observational and experimental sciences (molecular biology and molecular genetics included), the fact that more and more cooperative multidisciplinary groups or individual researchers with a double (theoretical and biological) culture have taken an interest in the complex modeling of dynamical biological events, and the increasing potential of numerical calculation using computers. At the start of a new century, the international Leopoldina symposium about "Nonlinear dynamics and the spatiotemporal principles of biology" thus may be considered to represent a stage in this newly emerging development to the phenomenon of life. In our present "Framework" session, much attention has been paid to "noisy" systems (BALÁZSI and Moss 2003, HÄNGGI et al. 2003) and to the dynamic behavior of biological networks, especially nerve networks (SINGER 2003, BALÁZSI and MOSS 2003, see also the many original references quoted in these review contributions).

Noise, contrary to the conventional viewing of it as a mere nuisance altering signal purity, is now seen as an indispensable component of fundamental living processes.

Among various other aspects (such as electron transport in DNA, migration of ligands in proteins or protein folding), "cell motors" and "stochastic resonance" have been shown to be of particular relevance to biology.

Material transport within cells and other cases of motion (cytoplasmic streaming, chromosome rearrangement during cell division, plant chloroplast reorientation in light, actin/myosin interactions, cell locomotion, etc.) occur permanently at the subcellular and cellular levels. In most cases, the proteinaceous and other molecular components of the cell motors are well known as well as the exergonic processes energizing them (ALBERTS et al. 1983). How the dynamic functioning of such motors is actually achieved was still to be understood. In the first talk of this session (HÄNGGI et al. 2003) it was shown how movements, such as those of kinesin molecules transporting cargo along the microtubules or those of muscle contraction *via* actin/myosin interaction, could be understood by a generalization of the "temperature-Brownian motor" scheme. In the latter model system, particles immersed in a viscous medium and submitted to alternatively low and high temperature values in an asymmetric saw-tooth potential, tend to progress, in a direction imposed by the potential asymmetry, as a consequence of their random, noisy diffusion at the high temperature while they are trapped in the intervals between the saw teeth at the low temperature. In real cellular systems, energy is provided *via* coupling to exergonic reactions, such as ATP hydrolysis, instead of the mechanism responsible for the temperature changes in the model system; but, although the detail of the functional steps involved is not always clearly understood yet, the random fluctuation of molecules or molecular heads at some stage of the process is an unavoidable requisite for producing the movement.

For its survival, an animal has to be sensitive to signals from its environment, especially those allowing it to detect the presence of a prey or a predator. In some cases, evolution has selected extremely sensitive sensory mechanisms, such as the electric field sensitivity of sharks, rays, catfish and paddlefish, or the crayfish sensitivity to weak mechanical stimuli (BALÁZSI and MOSS 2003). At least in some cases, it seems that the phenomenon of "stochastic resonance" (BALÁZSI and MOSS 2003, HÄNGGI et al. 2003) can enhance the detectability of weak signals. Briefly, a pure signal (e. g. a propagating wave) cannot be detected if it is below the threshold of detection; if the signal is slightly noisy, this will not change the result; with a stronger noise, the threshold may be reached and the signal thus detected (which is especially likely at the level of the signal maxima); with an even more intense noise, the detector will eventually get saturated. In consequence, the curve representing the "signal/noise ratio" as a function of the noise intensity will be negatively curved and exhibiting a maximal value at a medium value of the noise intensity. Such a behavior may be taken as the signature of the manifestation of *stochastic resonance*. A set of experimental data is consistent with *stochastic resonance* actually playing a part in signal detection in various animal systems (BALÁZSI and MOSS 2003), which would mean that "Mother Nature has adapted, during evolution, to use intrinsic ambient noise for the optimization of sensory transduction" (HÄNGGI et al. 2003).

The components involved in a living process at all levels of organization are often arranged in a network. The effect of noise in such network systems was discussed by BALÁZSI and MOSS (2003). By considering model systems made of a network of coupled noisy elements (such as a network of threshold detectors), it has been shown

that noise-enhanced propagation of coherent structures may occur, which has been termed "spatiotemporal stochastic resonance". For instance, Ca^{2+} spiral waves can be nucleated spontaneously, propagate some distance and finally die in the noise in a network of cultured glial cells. The fascinating question whether such "noisy network" effects may have a role in information processing and consciousness in the brain, has begun to be approached *via* various sorts of observations and experiments on human perception and animal behavior.

Apart from these considerations about the possible role of noise, a combination of theoretical reasoning and experimental evidence has begun to shed new light on the way neurones interact with one another to represent objects (SINGER 2003). It was known that permanent hierarchical structures exist in which (*i*) "first-order" neurones respond to the elementary components of an object under observation, (*ii*) several of these first-order neurones are connected to a "second-order" neurone which then responds to the corresponding, specific conjunction of elementary components, (*iii*) several of these second-order neurones may be connected to a "third-order" neurone, and so on. Clearly, such a "smart" system of neurones can be effective in representing items that occur frequently and/or are of particular behavioral importance; however, such a system is poorly adapted to the representation of unexpected or novel objects or of complicated and context-dependent combinations of objects. In these latter cases, it was revealed to be more likely that perception is achieved by the interplay of co-operatively interacting neurones that can participate at different times in different assemblies depending on the task to be carried out (which has the advantage to greatly economize the number of neurones required for accomplishing the different successive tasks). Among various possibilities that can be envisaged for permitting such transient, dynamic associations of subsets of co-operative neurones, synchronization of responses has revealed to be the most likely mechanism assuring that the responses of neurones that constitute an assembly are processed together and not confounded with other, unrelated responses. This is supported by a variety of observations, especially by the finding that the simultaneous recording of discharge from numerous neurones reveals close correlation between the synchronization of cortical neurones and behavioral responses. Another advantage of synchronization is that it can be established and dissolved very rapidly, thus permitting the nervous system to switch from one task to another with short delay.

For a general discussion about synchronization, see also the contribution by PIKOVSKY (2003) in another session of the same symposium, and for an example of the way how cells can become electrically synchronized see for instance data from my own group (LASSALLES et al. 1980, 1981, LETELLIER et al. 2002).

At the sub-cellular level, it has been observed that molecules (especially proteins) involved in a given task (e. g. metabolic pathway or signal transduction) often bind to one another, thus establishing transient functional multimolecular structures (see e. g. MOWBRAY and MOSES 1976, SRERE 1987, HRAZDINA and JENSEN 1992, LETOFFE et al. 1996, MITCHELL 1996, TORSHIN 1999, JORDAN et al. 2000, MORIN-GANET et al. 2000, PETTY and KINDZELSKII 2001, PRESLEY et al. 2002, RAMBOURG et al. 2002). Such transient associations, which are created and maintained by the fact that the system is functioning and which consequently tend to optimize the functioning of this system, have been termed "metabolons" in the case of metabolic pathways (VELOT et al. 1997, NORRIS

et al. 1999), "transducons" in the case of signal transduction (Trewavas and Malh 1997) or, more generally, "hyperstructures" (Norris and Fishov 2001, Amar et al. 2002, Norris et al. 2002); and we have begun to model and study the dynamic behavior of hyperstructures (Le Sceller et al. 2000). The above concept that functional architectures of neuronal connections are not necessarily permanent but may also undergo modifications in a use-dependent way (Singer 2003), thus appears to be a striking equivalent, at the intercellular level, of the original subcellular notion of hyperstructure.

A lot of detailed and stimulating information will be found in the three papers corresponding to the talks given in this first session (Balázsi and Moss 2003, Hänggi et al. 2003, Singer 2003). I would like to end my brief presentation of these contributions by two remarks that seem to my group and me to be of importance for biology. *First*, considering the dynamics of a process is not necessarily restricted to following the time-course of this process; cases exist in living systems in which a dynamic behavior, noise included, is constitutive of the process under consideration. *Second*, beside the traditional "structure → function" couple which was introduced by biochemists to state that they were interested in determining the specific function of each molecular structure which they were discovering, we should now also consider a "function → structure" couple, meaning that living processes exist, at the subcellular and intercellular levels, in which transient operative structures are created and maintained by the very fact that they are accomplishing a function.

References

Alberts, B., Bray, D., Lewis, J., Raff, M., Roberts, K., and Watson, J. D.: Molecular Biology of the Cell. New York: Garland Publishing Inc. 1983

Amar, P., Ballet, P., Bernot, G., Bouligand, Y., Bourgine, P., Delaplece, F., Delosme, J. M., Demarty, M., Fishov, I., Fralick, J., Giavitto, J. L., Gleyse, B., Godin, C., Incitti, R., Kepes, F., Lange, C., Le Sceller, L., Loutellier, C., Michel, O., Moreno, C., Norris, V., Orange, N., Pollard, H., Raine, D., Rambourg, A., Ripoll, C., Rouvière-Yaniv, J., Tracqui, P., Saier, M. H., Jr., Soler, P., Tambourin, P., Thellier, M., Ussery, D., Vannier, J. P., Valleton, J. M., Wiggins, P., and Zemirline, A.: Hyperstructures, genome analysis, and I-cell. Acta Biotheoretica *50*, 357–363 (2002)

Balázsi, G., and Moss, F.: Stochastic resonance: examples from sensory, perceptive and behavioral neuroscience and chemistry. In: Beck, F., Hütt, M.-T., and Lüttge, U. (Eds.): Nonlinear Dynamics and the Spatiotemporal Principles of Biology. Nova Acta Leopoldina NF Bd. *88*, Nr. 332, 57–76 (2003)

Hänggi, P., Schmid, G., and Goychuk, I.: Statistical physics of complexity. In: Beck, F., Hütt, M.-T., and Lüttge, U. (Eds.): Nonlinear Dynamics and the Spatiotemporal Principles of Biology. Nova Acta Leopoldina NF Bd. *88*, Nr. 332, 17–33 (2003)

Hrazdina, G., and Jensen, R. A.: Spatial organization of enzymes in plant metabolic pathways. Annu. Rev. Plant Physiol. Mol. Biol. *43*, 241–267 (1992)

Jordan, J. D., Landau, E. M., and Iyengar, R.: Signaling networks: the origin of cellular multitasking. Cell *103*, 193–200 (2000)

Lassalles, J. P., Hartmann, A., and Thellier, M.: Oscillations of the electrical potential of frog skin under the effect of Li^+: experimental approach. J. Membr. Biol. *56*, 107–119 (1980)

Lassalles, J. P., Hyver, C., and Thellier, M.: Oscillation of the electrical potential of frog skin under the effect of Li^+: theoretical formulation. Biophys. Chem. *14*, 65–80 (1981)

Le Sceller, L., Ripoll, C., Demarty, M., Cabin-Flaman, A., Nystrom, A., Saier, M. H., Jr., and Norris, V.: Modelling bacterial hyperstructures with cellular automata. Interjournal of Complex Systems *366*, http://www.interjournal.org (2000)

Letellier, C., Lassalles, J. P., Norris, V., Ripoll, C., and Thellier, M.: Quasi-periodic behaviour in a model for the lithium-induced oscillations of frog skin. CR Biologies *325*, 917–925 (2002)

Letoffe, S., Delepelaire, P., and Wandersman, C.: Protein secretion in gram-negative bacteria: assembly of the three components of ABC protein mediated exporters is ordered and promoted by substrate binding. EMBO J. *15*, 5804–5811 (1996)

Mitchell, C. G.: Identification of a multienzyme complex of the tricarboxylic acid cycle enzymes containing citrate synthase isoenzymes from *Pseudomonas aeruginosa*. Biochem. J. *313*, 769–774 (1996)

Morin-Ganet, M. N., Rambourg, A., Deitz, S. B., Franzusoff, A., and Képès, F.: Morphogenesis and dynamics of the yeast Golgi apparatus. Traffic *1*, 56–68 (2000)

Mowbray, J., and Moses, V.: The tentative identification in *Escherichia coli* of a multi-enzyme complex with glycolytic activity. Eur. J. Biochem. *66*, 25–36 (1976)

Norris, V., Amar, P., Ballet, P., Bernot, G., Delaplace, F., Demarty, M., Giavitto, J. L., Ripoll, C., Thellier, M., and Zemirline, A.: Hyperstructures. In: Amar, P., Képès, F., Norris, V., and Tracqui, P. (Eds.): Proceedings of the Autrans Seminar on Modelling and Simulation of Biological Processes in the Context of Genomics; pp. 169–191. Bonchamp-lès-Laval (France): Barnéoud 2002

Norris, V., and Fishov, I.: Membrane domains, hyperstructures and cell division. Biochimie *83*, 91–98 (2001)

Norris, V., Gascuel, P., Guespin-Michel, J., Ripoll, C., and Saier, M. H., Jr.: Metabolite-induced metabolons: the activation of transporter-enzyme complexes by substrate binding. Mol. Microbiol. *31*, 1589–1601 (1999)

Petty, H. R., and Kindzelskii, A. L.: Dissipative metabolic patterns respond during neutrophil transmembrane signalling. Proc. Natl. Acad. Sci. USA *98*, 3145–3149 (2001)

Pikovsky, A., and Rosenblum, M.: Synchronization of regular and chaotic oscillators. In: Beck, F., Hütt, M.-T., and Lüttge, U. (Eds.): Nonlinear Dynamics and the Spatiotemporal Principles of Biology. Nova Acta Leopoldina NF Bd. *88*, Nr. 332, 255–268 (2003)

Presley, J. F., Ward, T. H., Pfeifer, A. C., Siggia, E. D., Phair, R. D., and Lippincott-Schwartz, J.: Dissection of COPI and Arf1 dynamics *in vivo* and role in Golgi membrane transport. Nature *417*, 187–193 (2002)

Rambourg, A., Delosme, J. M., Incitti, R., Satiat-Jeunemaître, B., Tracqui, P., and Képès, F.: Modeling the dynamics of secretory compartments. In: Amar, P., Képès, F., Norris, V., and Tracqui, P. (Eds.): Proceedings of the Autrans Seminar on Modelling and Simulation of Biological Processes in the Context of Genomics; pp. 147–168. Bonchamp-lès-Laval (France): Barnéoud 2002

Singer, W.: Oscillations and synchrony: time as coding space in neuronal processing. In: Beck, F., Hütt, M.-T., and Lüttge, U. (Eds.): Nonlinear Dynamics and the Spatiotemporal Principles of Biology. Nova Acta Leopoldina NF Bd. *88*, Nr. 332, 35–56 (2003)

Srere, P. A.: Complexes of sequential metabolic enzymes. Annu. Rev. Biochem. *56*, 21–56 (1987)

Torshin, I.: Activating oligomerization as intermediate level of signal transduction: analysis of protein-protein contacts and active sites in several glycolytic enzymes. Front. Biosci. *4D*, 557–570 (1999)

Trewavas, A. J., and Malh, R.: Signal perception and transduction: the origin of the phenotype. Plant Cell *9*, 1181–1195 (1997)

Velot, C., Mixon, M. B., Teige, M., and Srere, P. A.: Model of a quinary structure between Krebs TCA cycle enzymes: a model for the metabolon. Biochemistry *36*, 14271–14276 (1997)

Prof. Dr. Michel Thellier
Laboratoire "Processus Intégratifs Cellulaires"
Faculté des Sciences de l'Université de Rouen
Mont-Saint-Aignan Cedex
F-76821
France
Phone: +33 (0) 2 35 14 66 82
Fax: +33 (0) 2 35 14 67 55
E-Mail: Michel.Thellier@univ-rouen.fr

Nova Acta Leopoldina NF *88*, Nr. 332, 17–33 (2003)

Statistical Physics of Biocomplexity

Peter HÄNGGI, Gerhard SCHMID, and Igor GOYCHUK (Augsburg)

With 5 Figures

Abstract

Biology and physics share common ancestors. The progress of methods of statistical physics and the developments of new physical tools and various ingenious experimental techniques have triggered dramatic progress for the field of biophysics. Likewise, the two fields fertilized each other repeatedly over the last decades. Most importantly, the complexity of biophysics inspired new developments in physics and chemical physics. In this contribution, we focus on some recent problems that attracted the interest of many statistical physicists. Biological cells contain nanoscale machineries that exhibit a unique combination of high efficiency, high reliability and recognition features and self-assembly properties. Most importantly, these biological machines transport material and perform work in a noisy environment. Here, we will elaborate on the constructive role of noise for the amplification and enhanced detection of weak information-carrying signals (Stochastic Resonance in Biology) and directed transport of vesicles and the like (Brownian Motors in Biology). Quantum statistical physics enters the biological complexity at the interface of electronic transport processes and the interaction with light. In this context, physicists and chemists have become increasingly interested in the electronic properties of the "molecule of life", the DNA. We will comment on the present hot debate whether quantum electronic transport in DNA behaves more like a good molecular wire or whether DNA behaves more like an insulator.

Zusammenfassung

Die beiden Naturwissenschaften Biologie und Physik teilen gemeinsame Interessen: In den letzten Jahrzehnten konnten sich beide Disziplinen immer wieder gegenseitig stimulieren. Der Fortschritt der Biophysik profitiert in hohem Maße von den Methoden der statistischen Physik und von neuen physikalischen Entwicklungen und Technologien. Umgekehrt inspirierte die Vielseitigkeit der Biophysik neue Richtungen in der Physik und der physikalischen Chemie. In diesem Artikel konzentrieren wir uns auf aktuelle Probleme, die insbesondere unter statistischen Physikern auf ein reges Interesse gestoßen sind: Wenige Nanometer große Proteine fungieren in biologischen Zellen als Maschinen und vereinigen dabei eine einzigartige Kombination von hoher Effizienz, hoher Zuverlässigkeit und der Fähigkeit zur Selbstorganisation und Steuerung. Sie transportieren biologisches Material und verrichten physikalische Arbeit in einer thermisch verrauschten Umgebung. Die konstruktive Rolle des Rauschens für die Verstärkung und Detektierung schwacher Signale (Stochastische Resonanz in der Biologie) und für den gerichteten Transport (biologische Brownsche Motoren) werden diskutiert. Die Beschreibung des elektronischen Transports oder der Wechselwirkung mit Licht erfordert sogar quantenphysikalische Ansätze in der Biologie. So interessieren sich Physiker und Chemiker für die elektronischen Eigenschaften des »Moleküls des Lebens«, der DNA. In diesem Zusammenhang soll auf die heiß geführte Debatte eingegangen werden, ob der quantenmechanische elektronische Transport in DNA sich wie in einem guten molekularen Draht oder eher wie in einem Isolator verhält.

1. Introduction

The field of biology underwent dramatic changes in recent years. With the progress and development of new experimental techniques the areas of modern biology and modern physics have fertilized each other repeatedly. One such area involves high-resolution microscopy techniques: Starting from the invention of a first microscope by Zacharias JANSSEN (1588–1630), and the first documentation in form of a book by Robert HOOKE (1635–1703) the first high resolution microscope was built by the Dutchman Antoine VAN LEEWENHOECK (1632–1723). His invention led him to observe bacteria and other micro-organisms. The early 19th century brought further progress with prominent input from Physics. It was the theory of microscopic resolution by Ernst ABBE (1840–1905), in particular his insight into improving resolution *via* a high "numerical aperture" ($n \sin a_1$) by use of a high refraction index material which enabled considerable further progress. The modern age of microscopy arrived with the development of the electron microscopy by Ernst RUSKA (1906–1988) in 1932. This instrument has a resolution of ca. 50 nm, i. e. it became possible to gain insight into the architecture of individual cells and proteins. Finally, the progress culminated with the construction and working of the scanning tunneling microscope (STM), that can provide atomic resolution, by the pioneers Gerd BINNIG and Heinrich ROHRER at IBM during the portentous night of march 16, 1981. The further efforts focused on atomic size imaging techniques for insulating materials. The result has been the construction of the atomic force microscopy (AFM) by BINNIG et al. (1986).

Another root to the progress of molecular biology involves Brownian motion theory as pioneered independently from each other by Marian VON SMOLUCHOWSKI and Albert EINSTEIN. SMOLUCHOWSKI has been working passionately on the theory of Brownian motion since 1900. He, however, delayed the publication of his theoretical findings because he also planned experiments to verify his calculations. After seeing EINSTEIN's (1905) paper in the *Annalen der Physik* he consequently also published his results in 1906 in the same journal.

It is fair to say that Brownian-motion-related phenomena have decisively stimulated many new developments and advances for statistical physics over the last fifty years. As a matter of fact, the field is still very much alive with pioneering contributions covering the physics on the micro-scale and even the nanoscale in situations where novel physics on the quantum level and /or far from thermal equilibrium are ruling the transport behavior.

One of the greatest challenges in the field of molecular biophysics involves the elucidation of the principles by which the nanoscale machineries in biological cells perform their work with such high efficiency, high adaptability to changing environmental conditions and high reliability. Above all, these biological motors must perform all of these functions in the face of inescapable thermal noise that is often much greater than the energy input that we can use to direct their operation. For this reason many physicists are working to understand the elementary mechanisms by which biological motors operate. An important insight is that thermal noise is most likely incorporated as an essential element for controlled motion by biological motors, giving rise to the term *Brownian Motor* (BARTUSSEK and HÄNGGI 1995, HÄNGGI and BARTUSSEK 1996, ASTUMIAN 1997, JÜLICHER et al. 1998, REIMANN and HÄNGGI 2002). For a most comprehensive review,

which in addition provides a wealth of references for this timely research area, we refer the interested reader to the recent *oeuvre* by REIMANN (2002).

From everyday experience, noise is usually thought of as the enemy of order rather than as a constructive influence. In nonlinear systems that possess some sort of threshold, however, random noise can assume a beneficial role in enhancing the detection of weak sensory signals. This phenomenon, termed *Stochastic Resonance* (MOSS 1991, WIESENFELD and MOSS 1995, GAMMAITONI et al. 1998, HÄNGGI 2002) does find useful applications in physical, biological and biomedical contexts. Certain biological systems may even use this effect for optimizing function and behavior (see below).

Statistical quantum physics enters such prominent biological areas as photosynthesis. Clearly, the laws of quantum electron-transfer dynamical processes do in fact determine the mechanism by which sun light is harvested by cells. Most importantly, the structure of proteins and particularly the molecule of life, DNA, which plays a pivotal role as the carrier of genetic information in all living species do obey the laws of quantum mechanics. The structures are by no means fixed but do wobble and shake due to the influence of thermal and non-thermal noise forces. In this context, the question of charge transport in DNA has attracted much enthusiasm within the scientific communities of physics, chemistry and biology. Notably, the potential of DNA with its unique assembly properties, unparalleled recognition features, stability, adaptability and optical qualities together with its electronic properties are far too tempting for not being considered as a prime species for molecular electronics (DEKKER and RATNER 2001).

In the following we elucidate the useful and serviceable role of statistical physics for the description of three salient problems of biocomplexity: These are the phenomena of Brownian motors in biology (Section 2), the phenomenon of Stochastic Resonance (SR, Section 3) and the issue of electronic motion in DNA (Section 4).

2. Brownian Motors in Biology

Parallel to the impressive progress in nanotechnology and the advances in the study and manipulation of small scale biological systems we can witness a tremendous activity in the theoretical understanding of small-scale non-equilibrium transport devices, including a discussion of both the fundamental issues and the limits of the application of the second law of thermodynamics (HÄNGGI and BARTUSSEK 1996, ASTUMIAN 1997, JÜLICHER et al. 1998, REIMANN and HÄNGGI 2002, REIMANN 2002). Brownian motors and Stochastic Resonance have been at the forefront of this new scientific wave; this is mainly due to their intimate connection from the viewpoint of the physics which is at work in these corresponding biological problems.

2.1 Brownian Motor: Proof of Principle

Following the reasoning of REIMANN et al. (1996) a simple example of a Brownian motor is depicted in Figure 1, where micron sized particles move on an asymmetric saw-tooth etched structure, e. g., on a glass slide. Because of the asymmetry of the structure, fluctuations in time between cold and hot temperature cause the particles to move, on average, to

the right. In accordance with the second law of thermodynamics we note, however, that the net transport is zero whenever the temperature is held fixed. The directed motion arises because the cycling in time between cold and hot feeds energy into the system from a hot reservoir and dissipates it to a cold reservoir. In the example, the particles are the "motors" – the elements that undergo directional translation. The fuel is the energy supplied by heating and cooling the device. This simple model in Figure 1 illustrates the three main ingredients necessary for a "Brownian motor" (HÄNGGI and BARTUSSEK 1996, ASTUMIAN 1997, REIMANN and HÄNGGI 2002): (*i*) symmetry breaking, (*ii*) energy input, and (*iii*) thermal noise. Without any one of these the Brownian motor mechanism fails.

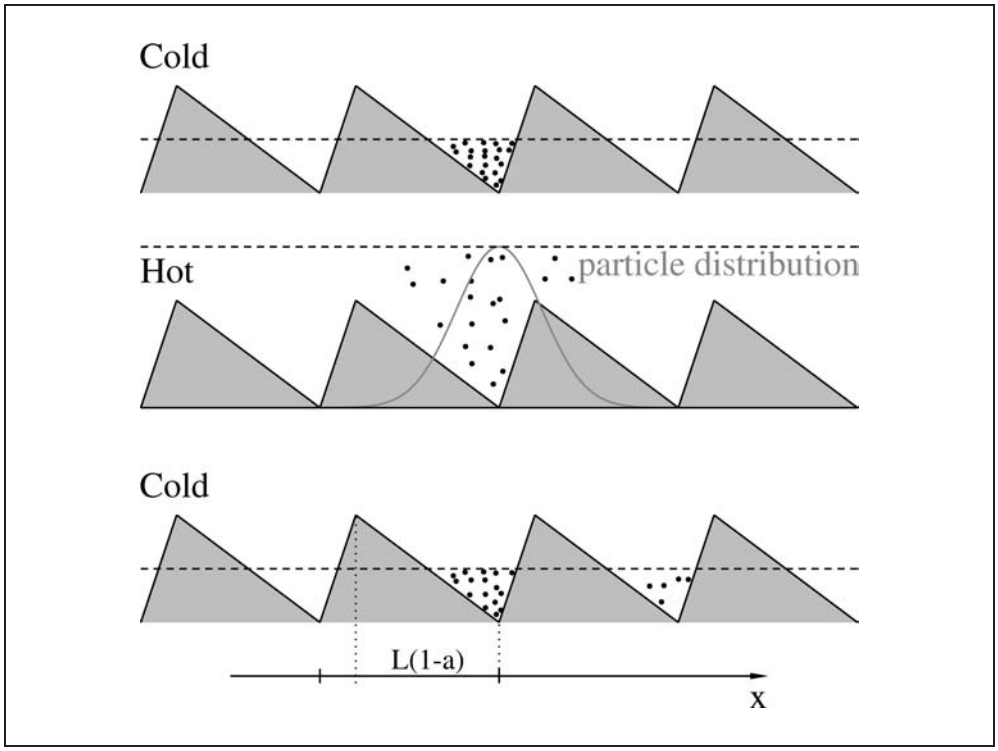

Fig. 1 Following the temperature-Brownian motor scheme by REIMANN et al. (1996) we consider non-interacting particles in a viscous medium moving on an asymmetric saw-tooth potential of period L and height V subject to a temperature that fluctuates in time between "hot" and "cold" ($T \in T_{cold}, T_{hot}$). For simplicity let $V/(k_B T_{hot}) << 1$, and $V/(k_B T_{cold}) >> 1$. The dashed line indicates the level 2 $k_B T$ below which ca. 95 % of the particles are found at any given time. When the temperature is cold, the particles are pinned at a potential minimum. Then, when the temperature is increased, the particles effectively do not "feel" the potential and begin to diffuse. When the temperature is cold again, any particles that have diffused the short distance aL, with $a < ½$, to the right are caught in the well to the right, any particles that have diffused the long distance $(1–a)L$ towards the left are caught in the well to the left, and the rest are pinned again in the original well from which they started. Because the chance for a particle to diffuse the short distance aL during the time when the temperature is hot is much greater than the chance to diffuse the long distance $(1–a)L$, net motion to the right is induced by strong temperature fluctuations. Optimally the system should remain hot long enough for the particles to diffuse the short distance, but not the long distance. The time in the cold state is less critical since pinning the particles is a predominately deterministic process that will be much faster than the diffusive motion.

The scheme in Figure 1 mimics a Brownian motor first proposed by BUG and BERNE (1987) working at Columbia University in New York and AJDARI and PROST (1992) working at the ESPCI in Paris; see also JÜLICHER et al. (1998). The latter researchers in Paris envisioned a situation where turning on and off an asymmetric electric potential would provide a means for separating particles based on diffusion coefficients yielding a so called *flashing* Brownian motor device. Such a scheme has been realized experimentally in several different ways (REIMANN 2002). A most pivotal feature is the rectification property of such Brownian motors. For any *fixed* temperature and an external negative tilt, the particles will move downhill on average. The numerically evaluated load curve, see Figure 2, instead depicts that the opposite is true within an entire interval of negative bias forces when additionally the device is now periodically cycled between two temperatures: Surprisingly indeed, the particles are moving uphill on average, thereby performing work against an external load. In particular, a finite velocity results at zero external load force. Moreover, one needs a finite negative force, the so termed *stall force*, before the average directed motion comes to a standstill.

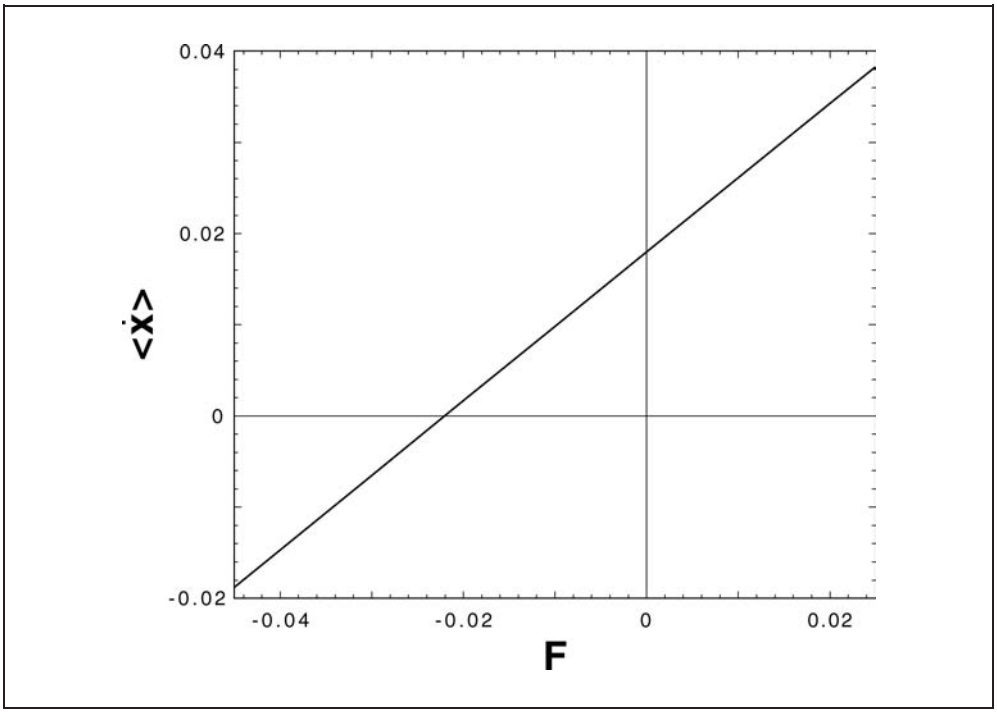

Fig. 2 Numerically determined time- and ensemble-averaged particle current in the long-time limit *versus* an external applied constant force for a temperature-Brownian motor depicted in Figure 1. Notwithstanding a not too large force pulling the particles to the left, the particle move uphill towards the right side. At a finite negative force, the so-called stall force, the average directed motion of the particle becomes reversed. After REIMANN and HÄNGGI (2002).

2.2 From Brownian Motors to Molecular Motors

The principle of such Brownian motor physics is seemingly at work for molecular motors. Nature uses both, linear and rotary molecular motors that transport a variety of biological cargo and propel cells. This rationale of molecular motors in biology is widespread: It is known that such motors drive the replication of DNA, its transcription into messenger RNA as well as, e. g., the injection of DNA into bacteria by bacteriophage (BUSTAMANTE et al. 2000). The latter motor is the strongest presently known molecular motor: It stalls at an amazingly large force of 55 pico-Newton. Yet another astounding rotary motor is the ATPase synthease (the enzyme that uses the H^+-gradients to produce adenosin triphosphate (ATP) – the energy source that powers most molecular motors) which turns at a speed of up to around 4 Hz generating up to 3 ATP molecules per revolution. Notably, we produce and consume every day about half of our body weight in ATP. In all these cases the thermal fluctuations are truly tumultuous and are readily used in pushing stochastically particles over activation barriers. All these motors work in a strong viscous medium (very low Reynolds numbers), i. e., the stochastic motion is strongly overdamped: The situation that cells and bacteria meet is that of a human swimming in very sticky honey. This is also why nature has optimally solved the problem of locomotion under such conditions by use of motors that employ a rotating helical tail, or beating flagella.

In the following we discuss only linear motors, cf. Figure 3, which move tangentially along a periodic structure of cytoskeletal filaments. The motor proteins are divided into

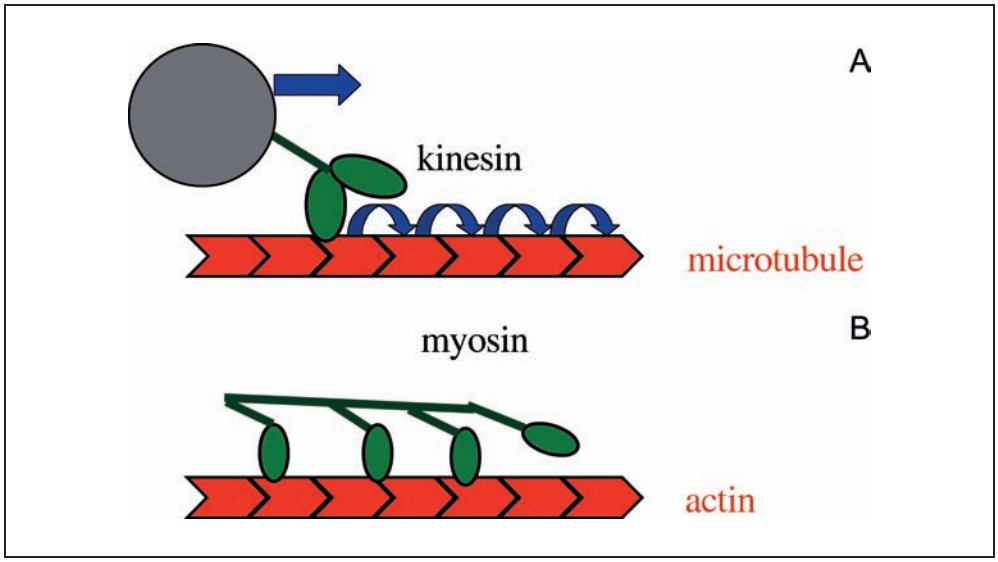

Fig. 3 Sketches of microtubules and actin filaments from the basic scaffolding of cells are depicted. The motor proteins kinesin and myosin are responsible for material transport and muscle motion. (*A*) A kinesin molecule transports cargo along the microtubules by alternate binding and unbinding of the two heads. (*B*) Muscle contractions are caused by aggregated myosin molecules. The motor heads of the myosin filament can bind to the actin filaments. Unbound heads fluctuate freely around their equilibrium positions. By preferentially binding at an angle in a forward direction directed motion occurs.

families by sequence similarities. Myosin-II and myosin-V motors move on actin filaments and operate the contraction of muscles; kinesin and dyenin motors transport cargo along microtubules. These proteins use the chemical energy obtained from the hydrolysis of ATP which is then transformed into mechanical work by the assistance of tempestuous thermal fluctuations. As such the motion becomes a stochastic process, and the key issue in this scenario refers to the problem of the strength of coupling between chemical and mechanical degrees of freedom in this non-equilibrium stochastic process. Important challenges address issues such as (*i*) the role of weak *versus* a tight mechano-chemical coupling, (*ii*) what is the average energy input per cycle, (*iii*) what is the efficiency, and (*iv*) what is the degree of cooperativity among the motors in the process of directed transport.

First ideas of how molecular motors work were put forward by Sir Andrew HUXLEY (1957) in his landmark paper on the contraction of muscles, cf. Figure 3(*B*). It idealizes the myosin-II heads being anchored in the myosin filaments of a sarcomer as harmonic springs with two states. In the bound state the motor heads form a crossbridge between the neighboring myosin and actin filaments; in the unbound state the heads fluctuate freely around their equilibrium positions. Directed motion now occurs when the head binds preferentially at an angle in a forward direction and unbinds after completion of the work. Binding of the head is followed by a backward shift of the actin filament. These spatially asymmetric binding and unbinding rates consequently rectify the thermal fluctuations of the motor head, i. e., this model is an example for a Brownian motor. The myosin-II motors are so termed *nonprocessive* motors with a small duty ratio. The latter refers to the ratio of the average time spent in the bound state and the bound-plus-unbound time interval. Being so, the myosin-II motors must work in groups in order to perform the task. In turn, this feature allows for a fast contraction in response to an external load. A molecular motor that walks over long distances before it detaches and gets lost, possesses consequently a high duty ratio; such motors, like kinesin or myosin-V are termed *processive*. The stochastic nature of the motors is a key ingredient allowing for asymmetric forward *versus* backward rates; indeed, thermal noise is truly essential in overcoming the various activation steps (HÄNGGI et al. 1990). The cooperativity of motor molecules has far reaching consequences: the statistical mechanical treatment of the coupling among the motors can give rise to fascinating phenomena such as phase transitions, normal and anomalous hysteretic behavior, absolute negative mobility and spontaneous oscillatory behaviors, to name but a few (JÜLICHER et al. 1998, REIMANN 2002).

The walking of the processive motor kinesin mimics closely the Brownian motor scenario depicted with Figure 3(*A*). The microtubule is built up periodically with the constituent protein "tubulin". This is a dimer consisting of two quite similar globular proteins, α-tubulin and β-tubulin about 4 nm in diameter and 8 nm long. This asymmetric structure mimics the asymmetric potential profile in Figure 1. Each two-headed kinesin comprises a microtubule binding site as well as an ATP-binding site, termed the ATP-binding pocket, see Figure 3(*A*). Each head can bind and hydrolyze ATP on its own. The chemical reaction cycle consists of the following main four steps. *Step 1*: the motor is interacting with the environment and is attached to the microtubule at a β-tubulin binding site with no ATP bound to the ATP-pocket. *Step 2*: The head binds one ATP out of the environment in its ATP-binding pocket. *Step 3*: The ATP is broken up into adenosine diphosphate (ADP) and inorganic phosphate (the power stroke). In doing so, ca. 20 kT

are gained in energy. *Step 4*: The inorganic phosphate is for a short time (thus implying a high duty ratio) released from the ATP-binding pocket and at the same time the kinesin motor typically detaches and undergoes Brownian motion, cf. the second part in Figure 1. Transition into state 1: ADP is released. The affinity to the binding site increases with the result that after some free diffusion one head will bind preferentially in forward direction again to the microtubule. Typically, a kinesin motor can cover a distance of a few μm with a velocity of ca. 1 μm/s at 10 mM ATP concentration before it looses contact with the microtubule filament. Therefore, a single kinesin molecular motor makes hundreds of unidirectional 8-nanometer steps without detaching from, or freely sliding along the microtubule on which it moves (processive motor). Moreover, it possesses a stall force of ca. 5 pico-Newton. Note also that the two heads coordinate their actions: One head always stays attached and the power stroke energy release of the front head seemingly triggers the rear head to swing forward. How does the forward motion take place? Is it in a hand-over-hand like fashion or more like that of an inchworm (or a caterpillar)? Very recent experiments (Hua et al. 2002) seem to favor an inchworm-like scenario. This would disprove the previously accepted picture that the enzyme's two heads alternately and symmetrically step over each other along the microtubule. Yet, there are still some other schemes thinkable which are still consistent with the present experimental knowledge (Astumian and Derenyi 1999). In any case, the Brownian motor mechanism is at work in all these different mechanisms.

Modern statistical physics clearly is able to provide the necessary tools to describe such non-equilibrium biological transport in terms of Brownian motion theory within coupled flashing potential landscapes (Hänggi and Bartussek 1996, Astumian 1997, Jülicher et al. 1998, Reimann 2002). Clearly, the mere use of a rate description already implies that noise-activated escape events do play an important role in biological transport mechanisms; i. e., a pure deterministic picture can never fully cover the complete story behind microbiological locomotive schemes.

3. Biological Stochastic Resonance

In everyday life, noise is generically viewed as being of harmful influence in detecting and transferring information. In contrast, Stochastic Resonance (SR) (Moss 1991, 1994, Wiesenfeld and Moss 1995, Gammaitoni et al. 1998, Hänggi 2002) refers to a situation where the mere addition of random noise to the dynamics improves a system's sensitivity to discriminate weak information carrying signals. Thus, this phenomenon constitutes yet another example where random perturbations play a beneficial role. Because of its generic nature, this phenomenon boasts universal applications extending from classical and quantum physics to chemistry, engineering, and in recent years, also in biology and biomedicine.

3.1 Introduction to SR

The mechanism of SR works as follows: Consider a particle sitting in one well of a symmetric double well potential – let us say, a marble in an egg carton. A gentle force (per-

iodic or aperiodic) tilts the whole system forth and back. This perturbation may be looked upon as an information carrying signal that is acting on the nonlinear system. Under the influence of this weak force the marble simply rolls around in the bottom of the well. Now, if its movement is detected only when it jumps into the neighboring well, this weak signal will go unnoticed. Adding noise to the system – by rocking randomly the egg carton up and down – will, *a priori,* only mask the weak perturbation further. In fact, however, under some suitable conditions just the opposite is true. The weak signal together with the noise will allow the ball to occasionally exit into the neighboring well. Now the theory of SR (GAMMAITONI et al. 1998) says that these exit events do not occur completely at random, but become correlated with the weak signal. An increasing noise level – correlated with the input signal – enhances the chance for excursions over the barriers. Since these large jump events dominate the response of the system, the small input signal is enlarged. One the other hand, too much noise will deteriorate the coherence of the signal assisted, noise-induced crossings. These barrier-crossing events expose an element of nonlinear system dynamics by which random noise can benefit faint signals by boosting them in a correlated manner over a threshold. The noise-enhanced output response is, therefore, fairly regular with only small fluctuations. From this perspective we find that SR is a cooperative phenomenon in which a weak, coherent input entrains ambient noise.

A typical characteristic of SR consists in its anomalous amplification of input signals by noise. The response itself serves thus as a natural measure of SR. In particular, for a periodic input signal the spectral power amplification (JUNG and HÄNGGI 1989, 1991) evaluates the ratio between the spectral power of the output at the driving frequency and the total power of the input signal. This amplification criterion undergoes a resonance-like behavior: it increases *versus* increasing noise intensity (regime of SR) until it reaches an optimal maximum, and then falls off; hence the term SR, see Figure 4. The spectral power amplification quantifier also yields a criterion of synchronization between the input signal and the noise-activated output dynamics. Note that the effect of SR is *not* a resonance phenomenon for the rate of the weak signal and noise-assisted escape dynamics: The time-averaged rate increases monotonically with both, increasing noise strength and perturbation intensity. Moreover, as a function of increasing driving frequency this time-averaged rate of escape starts out from a plateau-behavior and then decreases monotonically; i. e., no common resonance peak feature is detected for the rate of escape, see JUNG and HÄNGGI (1989) and JUNG (1989). Another common approach to characterize SR is the signal-to-noise ratio (SNR) (MCNAMARA and WIESENFELD 1989). This latter quantity is formed from the ratio obtained from the output spectral power at the driving frequency and the background power spectrum, multiplied by the experimental bin-width, of the driven stochastic dynamics at the driving frequency. Unlike the spectral power amplification, however, this quantifier does, in leading order of the signal strength, not depend on the driving period; consequently, it cannot be related to a synchronization measure. Another indirect measure of SR, which is often used by biologists, is the residence time probability distribution or inter-spike interval histogram. The corresponding measure is composed of a set of separated peaks that vary in width and separation upon increasing the noise intensity. Moreover, the characterization of noise-assisted transduction of realistic, broad-band type biological input-signals typically necessitates the introduction of complexity measures that are based on entropy related con-

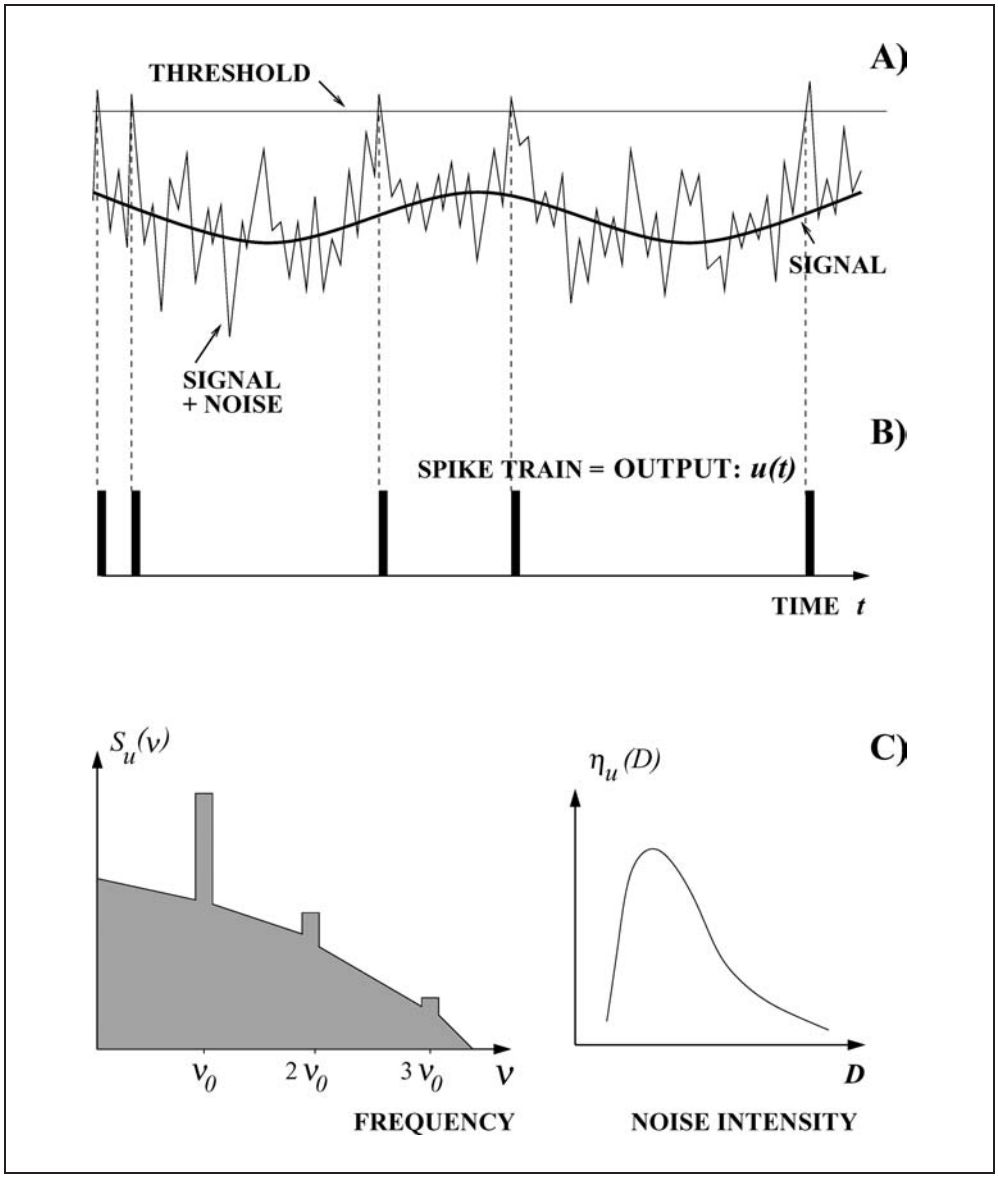

Fig. 4 Threshold stochastic resonance: (*A*) Neuronal-like dynamics detect those events that rise above some threshold value (the thin top line). A weak, periodic subthreshold signal (thick line) can therefore be detected only if its dynamics are assisted by noise (noisy trace). A crossing event occurs most likely when the weak signal assumes its peak value. (*B*) Upward-directed crossing events trigger a firing of spike-train dynamics, u(t). (*C*) The power spectrum $S_u(\nu)$ of the output dynamics is depicted on the left-hand side; superimposed on a typical broadband background the spectrum features sharp peaks at multiples of the driving frequency ν_0. The spectral power amplification, see the right-hand side in part (*C*), exhibits the typical SR signature of a bell-shaped resonance *versus* increasing noise intensity D. The peak value is assumed at an optimal dose of noise for which the periodically modulated threshold crossing rate approximately synchronizes the signal with the firing events.

cepts, like the mutual information, the Kullback entropy, the rate of information gain and diverse cross-correlation measures (GAMMAITONI et al. 1998, ANISHCHENKO et al. 1999, HÄNGGI 2002).

Since its discovery in early 1981, the phenomenon of SR has been demonstrated repeatedly with diverse applications in chemistry, physics and the technical sciences (GAMMAITONI et al. 1998). SR in biology started with benchmark publications in the early nineties wherein the authors discovered SR in sensory neurons that have been subjected to external noise (BULSARA et al. 1991, LONGTIN et al. 1991, CHIALVO and APKARIAN 1993). In a series of experiments the group of Frank MOSS (DOUGLAS et al. 1993, WIESENFELD et al. 1994, PEI et al. 1996) and several other groups as well, convincingly established the effect of SR in a variety of biological systems (HÄNGGI 2002).

Sensory neuronal systems are ideally suited to exhibit SR: they are intrinsically noisy and they do operate as threshold systems, cf. Figure 4. In these neuronal systems a propagating action potential upon reaching the threshold triggers a firing (voltage) spike, which is being followed by a quiescent time interval during which no firing events occur. In this context, a prominent question concerns the role of the internal noise of the sensory systems. Moreover, does the biological system intrinsically use noise-enhanced signal detection, *via* SR, to optimize its operational function? A promising first evidence that SR occurs with internal noise has been shown by PEI et al. (1996) where the internal noise may be varied by altering the light intensity that falls on the photoreceptive areas of crayfishs' hair cells which sense hydrodynamic flows.

3.2 Biological SR on the Subcellular Level: SR in Ion Channels

Ever since the discovery of SR, the Holy Grail of biological SR-related research has been the validation of the premise that mother nature has adapted, during evolution, to use intrinsic ambient noise for the optimization of sensory transduction on its most fundamental level: the ion channels. Presumably, SR has its origin in the stochastic properties of ion channel clusters that are located inside a receptor cell membrane. For an artificial system of ion channels which is composed of a parallel array of the peptide alamethicin, BEZRUKOV and VODYANOY (1995) have found evidence that SR does in fact occur. This result provokes the challenge whether SR in biology is rooted as a collective effect in finite assemblies of natural ion channels or whether SR can occur already within a single ion channel. In recent work, however, it was demonstrated theoretically that SR in a single Shaker potassium channel can indeed occur if the parameters for operation are located within a regime where the channel is predominantly dwelled in the closed state (GOYCHUK and HÄNGGI 2000). This result is not only of interest on its own, but also impacts prominent applications that involve manipulations on the nanoscale, such as the design of a single-molecular biosensor. Where does SR originate from and what is its relevance in biological systems? Membrane patches that are able to exhibit an excitable dynamics must contain ion channels of at least two different kinds – such as potassium and sodium channels. The mean field model of HODGKIN and HUXLEY (1952) for voltage gated ion channels, when subjected to *external* noise, clearly exhibits in its firing dynamics the signature of SR (GAMMAITONI et al. 1998). More challenging, however, is the question of whether this biological system, if

amended by a leakage current due to chloride ions and internal noise that originates from the random fluctuations of stochastic opening and closing of individual channels, is capable to exhibit SR. The intrinsic fluctuations within a given assembly of ion channels scale inversely with its system size. Indeed, the SNR of the spiking dynamics has recently been demonstrated to exhibit SR, which is solely due to internal noise (JUNG and SHUAI 2001, SCHMID et al. 2001). The SNR increases with increasing system size until it assumes a peak value at an optimal area of the assembly of ion channels, cf. Figure 5 *A*. Notice that this SR-behavior mimics SR for the amplification in Figure 4 *C*; but now with the noise intensity being read from right-to-left. Above the optimal area, the SNR decreases with increasing size. Only the addition of external noise will again restore the SR behavior in this regime (see Figure 5 *B*). Put differently, there exists an optimal size for which ambient internal noise is beneficial for the functionality of ion channel patches. For sub-optimal, small sizes of ion channel assemblies, the addition of (external) noise (which simulates even smaller patch-areas) will thus only degrade the transduction behavior. Moreover, there exists an internal noise-induced coherence phenomenon for which the spiking activity assumes for an optimal patch size a "most rhythmic" activity in the absence of any external input-signal that stems solely from spontaneous internal ion channel noise (JUNG and SHUAI 2001, SCHMID et al. 2001). These findings yield support to the conjecture that SR, in fact, is biologically significant. Likewise, the observed SR in biological systems is most likely rooted in a collective property of globally coupled ion channel assemblies.

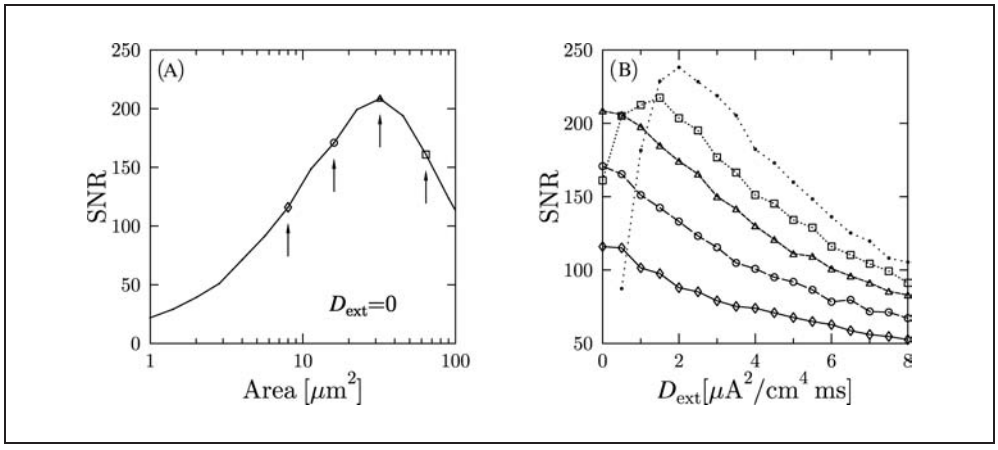

Fig. 5 (*A*) SNR data for a stochastic Hodgkin-Huxley modeling of an assembly of sodium and potassium ion channels and additional leakage channels for an external sinusoidal subthreshold stimulus of amplitude 1.0 μA cm^{-2} and angular driving frequency of 0.3 ms^{-1} (SCHMID et al. 2001). One observes intrinsic SR for a weak stimulus *versus* solely internal noise. The internal noise intensity decreases with increasing area of the membrane patch. (*B*) If additional, external noise D_{ext} is applied for the system sizes marked by the arrows in (*A*), one finds the SNR behavior for the corresponding membrane size *versus* D_{ext}. Notice that adding noise to small assemblies below optimal size only deteriorates the transduction behavior further. In clear contrast, however, for above-optimal sizes the addition of noise yields the conventional SR behavior. For comparison, the situation for infinite size (i. e. the mean field limit) with zero internal noise is depicted by the dotted line through the thin dots.

3.3 Biomedical Benefits from SR

A most appealing feature of SR is the fact that it holds promise for the good of mankind, where numerous physiological functions are marked by threshold behaviors. For example, several disorders of the nervous system are caused by increased sensory thresholds, which lead to a reduced firing rate in the corresponding neurons. Experimental results (COLLINS et al. 1996, RICHARDSON et al. 1998) have offered hope that SR will find its way into applications that are beneficial for mankind in providing some means for the possible cure of, for example, a disordered person's balance, a patient's locomotion and other physiological functions. COLLINS et al. (1996) could establish several experimental SR procedures in order to improve a patient's tactile sensation by employing an optimal dose of mechanical or electrical noise to successfully detect subthreshold stimuli. The human visual perception system (RIANI and SIMONOTTO 1995, SIMONOTTO et al. 1997) and the human blood pressure regulatory system, the so termed "baroreflex system" (HIDAKA et al. 2000) offer yet other examples for biomedical benefits *via* the phenomenon of SR.

4. Electronic Transport in DNA

The molecule of life, DNA, plays a pivotal role in biology for the storage and the propagation of genetic material. Recently, DNA has moved into the limelight as a possible candidate for long range electronic motion. Unlike other proteins such as cytochromes and the photosynthetic reaction centre, DNA is not an ideal electron transfer species. There is also little evidence for the role of DNA-assisted charge migration in biological function and performance. So, why is there so much excitement about DNA being possibly a good conductor? *First*, the DNA with its p-electron system of four bases (guanine [G], cytosine [C], adenine [A], thymine [T]) stacked upon each other resembles certain "molecular metals". *Second*, there are biological implications which pertain to radiation-induced damage, where radical reactions with nucleobases occur. These may be followed by charge migration processes that result in inter-strand and intra-strand chemical reactions which in turn lead to mutations. Most of all, however, DNA with its unique assembly properties, unparalleled recognition features, stability and optical properties make DNA a most potential candidate for the timely area of molecular electronics. It may be used as a toolkit component in building molecular architectures composed of molecular biosensors, molecular switches, molecular-memory elements and molecular rectifiers and the like. Needless to say, that theoretical and experimental DNA assisted charge transport issues have attracted much attention recently (DEKKER and RATNER 2001). According to some recent experiments by physicists with a bundle of DNA of ca. 10 nm in length (FINK and SCHÖNENBERGER 1999), DNA conducts well with ~ 1 mega-Ohm of resistance. Others (KASUMOV et al. 2001) even claim that DNA can conduct charge with virtually no resistance at room temperature; moreover, at extreme low temperatures DNA possibly even exhibits a supercurrent (KASUMOV et al. 2001). In contrast, researchers at Delft University of Technology have shown by a series of reproducible experiments with poly(dG)-poly(dC) DNA of 10–40 nm in length that DNA behaves like a good insulator with a resistance larger than 10^{12} Ohm (PORATH et al. 2000, DEKKER and RATNER 2001).

This result is corroborated in recent experiments of the Princeton group (ZHANG et al. 2002) by two-probe current *versus* voltage measurements with micron based (lambda)-DNA molecular wires bound to two gold electrodes (by incorporating thiol-modified nucleotides into both DNA ends) embedded in a buffer solution. The result is that (lambda)-DNA indeed behaves as an insulator possessing at room temperature a specific resistance $\rho > 10^6$ Ohm/cm. These latter experimental studies are fully consistent with recent electron transfer studies in DNA: Physical chemists have convincingly demonstrated (MEGGERS et al. 1998, GIESE et al. 2001) that long-range electron transfer in DNA occurs either *via* "thermal hopping" when G–C pairing sites are involved, or *via* coherent superexchange (i. e., no energy is exchanged with the molecule and environment) when A–T base pairs must be overcome. In the latter case the reaction rate decreases exponentially with the distance between donor and acceptor.

A satisfactory theoretical treatment of the overall electron (hole)-transport process is still lacking. In particular, this unique combination of incoherent hopping and coherent electron transfer mechanisms calls for a unified treatment that consistently accounts for the effects of coherence and dissipation on the same basis as it had been put forward for the thermally assisted tunneling escape rate (the quantum-Kramers turnover theory) for reactions that occur in condensed phases, see HÄNGGI et al. (1990).

The transport mechanism of DNA when sandwiched between electrodes seems not settled yet. A whole series of mechanisms have been proposed for the problem of bridged hole-transport in DNA: These range from band-like transport, to incoherent hopping, to polaron mechanisms and fluctuation-induced electron transfer. On the bridge itself, however, the dominant mechanisms are, as mentioned above, coherent tunneling and thermal, tunneling assisted hopping events. The confusingly many different claims that range from well-insulating behavior to metal-like and even to the support of superconducting currents may indicate that the parameter range of DNA is indeed extremely huge. The differences might be due to the role of a differing sequencing, the role of solvation on hole motion, differing ambient surroundings such as experiments in liquids, air or vacuum, the structural form of the DNA probe and, in particular, the electrode-DNA molecule interface. As a consequence, the community urgently is in need of careful and reproducible verifications of the different existing experiments and all the seemingly conflicting findings before final conclusions can be drawn.

5. Summary and Outlook

In this article we have discussed the role of modern statistical physics in describing a selection of complex biological phenomena. We elucidated the ubiquitous role of noise for the transduction of biological information, the transport of biological cargo, energy and charge and the function of biological cellular systems. The pursuit of Brownian motor theory, Stochastic Resonance and electron transfer theory into the biological and medical domain is very exciting and promising. Indeed, this change of focus from physical sciences towards life sciences carries a great potential and causes us to rethink and refine some of our usual concepts and issues. The lesson to be learned from all these examples is that noise does provide a useful task for biological activity rather than being a hindrance. It would seem strange when nature would not have taken advantage of the

benefits of the naturally occurring boisterous fluctuations, rather than beating it. There exist many other cases, such as, e. g., the migration of ligands in proteins (ALBERDING et al. 1978, FRAUENFELDER and WOLYNES 1985, FRAUENFELDER and MCMAHON 2001), protein folding and the like, where the methods of modern statistical physics are salient and essential in order to account reliably for the jiggling and wiggling behaviors of biomolecules characterizing biocomplexity. The ultimate goal must be to be able to describe the physical and chemical laws governing the structure, the dynamics and the function of biological materials. At present times, however, we are still far away from being able to provide biology with major predictive power. On the contrary, physics has repeatedly learned fundamental principles and concepts from biological phenomena, and it certainly will continue to do so in the future! In this spirit we (as communicated to us by Hans FRAUENFELDER) may also quote here Stan ULAM:

"Ask not what physics can do for biology, ask what biology can do for physics."

Acknowledgment

The authors do thank present and former members of the theory group in Augsburg for many constructive and critical discussions involving the modeling of biophysical phenomena such as ion channel gating, electron transfer, stochastic resonance, molecular wires, Brownian motors, migration of ligands, etc. One of us (P. H.) owes particular thanks to Professor Hans FRAUENFELDER who introduced him as early as in 1977 into the fascinating field of biological physics. This work has been supported by the *Sonderforschungsbereich der Deutschen Forschungsgemeinschaft*, *SFB* 486 and *Volkswagenstiftung* (grant I/77 217).

References

AJDARI, A., and PROST, J.: Mouvement induit par un potential periodique de basse symmetrie: dielectrophorese pulsee. C. R. Acad. Sci. Ser. II *315*, 1635–1639 (1992)

ALBERDING, N., FRAUENFELDER, H., and HÄNGGI, P.: Stochastic theory of ligand migration in biomolecules. Proc. Natl. Acad. Sci. USA *75*, 26–29 (1978)

ANISHCHENKO, V. S., NEIMAN, A. B., MOSS, F., and SCHIMANSKY-GEIER, L.: Stochastic resonance: noise-enhanced order. Phys.-Usp. *42*, 7–36 (1999)

ASTUMIAN, R. D.: Thermodynamics and kinetics of a brownian motor. Science *276*, 917–922 (1997)

ASTUMIAN, R. D., and DERENYI, I.: A chemical reversable brownian motor: Application to kinesin and Ncd. Biophys. J. *77*, 993–1002 (1999)

BARTUSSEK, R., und HÄNGGI, P.: Brownsche Motoren. Phys. Blätter *51(6)*, 506–507 (1995)

BEZRUKOV, S. M., and VODYANOY, I.: Noise-induced enhancement of signal transduction across voltage-dependent ion channels. Nature *378*, 362–364 (1995)

BINNIG, G., QUATE, C. F., and GERBER, C.: Atomic force microscope. Phys. Rev. Lett. *56*, 930–933 (1986)

BUG, A. L. R., and BERNE, B.: Shaking-induced transition to a non-equilibrium state. Phys. Rev. Lett. *59*, 948 (1987)

BULSARA, A., JACOBS, E. W., ZHOU, T., MOSS, F., and KISS, L.: Stochastic resonance in a single neuron model: Theory and analog simulation. J. Theor. Biol. *152*, 531–555 (1991)

BUSTAMANTE, C., MACOSKO, J. C., and WUITE, G. Z.: Grabbing the cat by the tail: Manipulating molecules one by one. Nature Rev. Mol. Cell Biol. *1*, 130–136 (2000)

CHIALVO, D. R., and APKARIAN, A. V.: Modulated noisy biological dynamics: Three examples. J. Stat. Phys. *70*, 375–391 (1993)

COLLINS, J. J., IMHOFF, T. T., and GRIGG, P.: Noise-enhanced tactile sensation. Nature *383*, 770 (1996)

DEKKER, C., and RATNER, M. A.: Electronic properties of DNA. Physics World *14(8)*, 29–33 (2001)

Douglas, J. K., Wilkens, L., Pantazelou, E., and Moss, F.: Noise enhancement of information transfer in crayfish mechanoreceptors by stochastic resonance. Nature *365*, 337–340 (1993)

Einstein, A.: Über die von der molekularkinetischen Theorie der Wärme geforderte Bewegung von in ruhenden Flüssigkeiten suspendierten Teilchen. Ann. Physik *17*, 549–560 (1905)

Fink, H.-W., and Schönenberger, C.: Electrical conduction through DNA molecules. Nature *398*, 407–410 (1999)

Frauenfelder, H., and McMahon, B. H.: Energy landscapes and fluctuations in proteins. Ann. Physik (Leipzig) *9*, 655–667 (2001)

Frauenfelder, H., and Wolynes, P. G.: Rate theories and puzzles of hemoprotein kinetics. Science *229*, 337–345 (1985)

Gammaitoni, L., Hänggi, P., Jung, P., and Marchesoni, F.: Stochastic resonance. Rev. Mod. Phys. *70*, 223–288 (1998)

Giese, B., Amaudrut, J., Köhler, A.-K., Spormann, M., and Wessely, S.: Direct observation of hole transfer trough DNA by hopping between adenine bases and by tunnelling. Nature *412*, 318–320 (2001)

Goychuk, I., and Hänggi, P.: Stochastic resonance in ion channels characterized by information theory. Phys Rev. E *61*, 4272–4280 (2000)

Hänggi, P.: Stochastic resonance in biology. ChemPhysChem *3*, 285–290 (2002)

Hänggi, P., and Bartussek, R.: Brownian Rectifiers: How to convert Brownian motion into directed transport. Lect. Notes in Physics *476*, 294–308 (1996)

Hänggi, P., Talkner, P., and Borkovec, M.: Reaction-rate theory: fifty years after Kramers. Rev. Mod. Phys. *62*, 251–342 (1990)

Hidaka, I., Nozaki, D., and Yamamoto, Y.: Functional stochastic resonance in the human brain: noise induced sensitization of baroreflex system. Phys. Rev. Lett. *85*, 3740–3743 (2000)

Hodgkin, A. L., and Huxley, A. F.: A quantitative description of the membrane current and its application to conduction and excitation. J. Physiol. (London) *117*, 500–544 (1952)

Hua, W., Chung, J., and Gelles, J.: Distinguishing inchworm and hand-over-hand processive kinesin movement by neck rotation measurements. Science *295*, 844–848 (2002)

Huxley, A. F.: Muscle structure and theories of contraction. Progr. Biophys. *7*, 255–318 (1957)

Jülicher, F., Ajdari, A., and Prost, J.: Modelling molecular motors. Rev. Mod. Phys. *69*, 1269–1281 (1998)

Jung, P.: Thermal activation in bistable systems under external periodic forces. Z. Phys. B *76*, 521–535 (1989)

Jung, P., and Hänggi, P.: Stochastic nonlinear dynamics modulated by external periodic forces. Europhys. Lett. *8*, 505–510 (1989)

Jung, P., and Hänggi, P.: Amplification of small signals via stochastic resonance, Phys. Rev. A *44*, 8032–8042 (1991)

Jung, P., and Shuai, J. W.: Optimal sizes of ion channels clusters. Europhys. Lett. *56*, 29–35 (2001)

Kasumov, A., Kociak, M., Gueron, S., Reulet, B., Volkov, V. T., Klinov, D. V., and Bouchiat, H.: Proximity-induced superconductivity in DNA. Science *291*, 280–282 (2001)

Longtin, A., Bulsara, A., and Moss, F.: Time-interval sequences in bistable systems and the noise-induced transmission of information by sensory neurons. Phys. Rev. Lett. *67*, 656–659 (1991)

McNamara, B., and Wiesenfeld, K.: Theory of stochastic resonance. Phys. Rev. A *39*, 4854–4869 (1989)

Meggers, E., Michel-Beyerle, M. E., and Giese, B.: Sequence dependent long range hole transport in DNA. J. Amer. Chem. Soc. *120*, 12950–12955 (1998)

Moss, F.: Stochastic resonance. Ber. Bunsenges. Phys. Chem. *95*, 303–311 (1991)

Moss, F.: Stochastic resonance: From the ice ages to the monkey's ear. In: Weiss, G. H. (Ed.): Contemporary Problems in Statistical Physics, Chap. 5; pp. 205–253. Philadelphia, PA: SIAM 1994

Pei, X., Wilkens, L., and Moss, F.: Light enhanced hydrodynamic signalling in the candal photoreception interneuron of crayfish. J. Neurophysiol. *76*, 3002–3011 (1996)

Porath, D., Bezryadin, A., de Vries, S., and Dekker, C.: Direct measurement of electrical transport through DNA molecules. Nature *403*, 635–638 (2000)

Reimann, P.: Brownian motors: noisy transport far from thermal equilibrium. Phys. Rep. *361*, 57–265 (2002)

Reimann, P., Bartussek, R., Häussler, R., and Hänggi, P.: Brownian motors driven by temperature oscillations. Phys. Lett. A *215*, 26–31 (1996)

Reimann, P., and Hänggi, P.: Introduction to the physics of Brownian motors. Appl. Phys. A *75*, 169–178 (2002)

Riani, M., and Simonotto, E.: Periodic perturbation of ambiguous figure: A neural-network model and a non-simulated experiment. Il Nuovo Cimento *17* D, 903–913 (1995)
Richardson, K. A., Imhoff, T. T., Grigg, P., and Collins, J. J.: Using electrical noise to enhance the ability of humans to detect subthreshold mechanical cutaneous stimuli. Chaos *8*, 599–603 (1998)
Schmid, G., Goychuk, I., and Hänggi, P.: Stochastic resonance as a collective property of ion channel assemblies. Europhys. Lett. *56*, 22–28 (2001)
Simonotto, E., Riani, M., Seife, C., Roberts, M., Twitty, J., and Moss, F.: Visual perception of stochastic resonance. Phys. Rev. Lett. *78*, 1186–1189 (1997)
Smoluchowski, M. von: Zur kinetischen Theorie der Brownschen Molekularbewegung und der Suspensionen. Ann. Physik *21*, 756–780 (1906)
Wiesenfeld, K., and Moss, F.: Stochastic resonance and the benefits of noise: From ice ages to crayfish and SQUIDs. Nature *373*, 33–36 (1995)
Wiesenfeld, K., Pierson, D., Pantazelou, E., Dames, C., and Moss, F.: Stochastic resonance on a circle. Phys. Rev. Lett. *72*, 2125–2129 (1994)
Zhang, Y., Austin, R. H., Ong, N. P., and Cox, E. C.: On the electrical conductivity of lambda DNA at micron length-scales. Bull. Amer. Phys. Soc., March meeting 2002, *F 29*, 370 (2002)

Prof. Dr. Peter Hänggi
Institut für Physik
Universität Augsburg
Universitätsstraße 1
86135 Augsburg
Germany
Phone: ++49 (0) 82 15 98 32 50
Fax: ++49 (0) 82 15 98 32 32
E-Mail: Peter.Hanggi@physik.uni-augsburg.de

Nova Acta Leopoldina NF *88*, Nr. 332, 35–56 (2003)

Oscillations and Synchrony – Time as Coding Space in Neuronal Processing

Wolf SINGER (Frankfurt am Main)

Member of the Academy

With 6 Figures

Abstract

One of the goals of cognitive neuroscience is to understand how the brain constructs representations of its environment. Knowing the neuronal code of such representations is a prerequisite for any reductionistic explanation of cognitive functions such as perception, memory and learning. At present two hypotheses are pursued: One assumes that perceptual objects are represented by the responses of highly selective, object-specific neurons which are located at the top of hierarchically organized processing streams. The other favors the view that representations are distributed and consist of assemblies of cooperatively interacting neurons. A key feature of assembly coding is that individual neurons can participate at different times in different assemblies which greatly economizes the number of neurons required for the formation of different representations. This, however, requires versatile mechanisms of response selection that permit dynamic association of subsets of distributed neuronal responses for further joint processing. It will be proposed that synchronization of responses could serve as mechanism for the dynamic selection and binding of responses because it raises with great precision and without requiring time consuming temporal integration the saliency of responses containing synchronized epochs. Experiments will be reviewed which have been designed to test predictions derived from the synchronization hypothesis. It will be shown that feature selective neurons in the visual cortex can synchronize their discharges if activated by the outlines of the same visual object and that synchronization probability reflects some of the established Gestalt-criteria for perceptual grouping. Evidence is further provided, that this synchronization is achieved at least in part by cortico-cortical association projections. The functional architecture of these connections can be modified in a use-dependent way. It is proposed that these modifications serve the experience dependent generation of new assemblies such as is required for perceptual learning. Data will be reviewed that reveal close correlations between the synchronization of cortical neurons and behavior. In cats trained to perform a visual discrimination task, zero-phase lag synchronization occurs during preparatory phases and during task performance among cortical areas involved in the task (visual, parietal, frontal) but not while the animal is at rest or consumes the reward. Experiments with stimuli generating rival percepts indicate that synchronization of neuronal discharges in primary visual cortex changes in a context dependent way and correlates with perception. Responses that are perceived exhibit a high degree of synchronicity while responses that are excluded from perception desynchronize. These results suggest that synchronization of distributed neuronal responses serves as a mechanism to select responses and to tag them as related.

Zusammenfassung

Eines der Ziele der kognitiven Neurowissenschaften ist die Beantwortung der Frage, wie das Gehirn Repräsentationen seiner Umwelt strukturiert. Die Kenntnis des neuronalen Codes solcher Repräsentationen ist Voraussetzung für alle reduktionistischen Erklärungsversuche von kognitiven Leistungen wie Wahrnehmen, Erinnern und Lernen. Gegenwärtig werden zwei Hypothesen verfolgt: Eine geht davon aus, daß Objekte der

Wahrnehmung durch die Antworten hochselektiver, objektspezifischer Neurone repräsentiert werden, die sich an der Spitze einer hierarchisch organisierten Verarbeitungspyramide befinden. Die andere Hypothese favorisiert die Annahme, daß Repräsentationen eine distributive Struktur aufweisen und auf Ensembles kooperierender Neurone beruhen. Ein wichtiges Merkmal von Ensemblecodes ist, daß individuelle Neurone zu verschiedenen Zeiten in verschiedene Ensembles eingebunden werden können, wodurch die Zahl der Neurone dramatisch verringert werden kann, die für die Bildung unterschiedlicher Repräsentationen benötigt werden. Zur Realisierung von Ensemblecodes sind jedoch besondere Mechanismen erforderlich, die es gestatten, auf flexible Weise die Antworten weit verteilter Neuronen temporär so zusammenzubinden, daß sie als zusammengehörig erkannt und gemeinsam weiterverarbeitet werden können. Ein Mechanismus, der dies im Prinzip zu leisten vermag, ist die Synchronisation von neuronalen Antworten. Synchronisation erhöht mit hoher zeitlicher Präzision die Wirksamkeit von Antworten bezüglich ihrer Fähigkeit, nachgeschaltete Neuronengruppen zu erregen. Sie stellt somit einen idealen Mechanismus dar, um Antworten auszuwählen und dynamisch zu gruppieren. Im Folgenden werden Experimente diskutiert, die entworfen wurden, um die Voraussagen der Synchronisationshypothese zu überprüfen. Unter anderem wird gezeigt, daß merkmalsselektive Neurone in der Sehrinde ihre Antworten mit hoher zeitlicher Präzision synchronisieren, wenn sie durch die Konturen kohärenter visueller Objekte aktiviert werden, und daß die Synchronisationswahrscheinlichkeit die Gestaltgesetze widerspiegelt, die beim perzeptuellen Gruppieren zum Tragen kommen. Entwicklungsstudien legen nahe, daß diese Synchronisation auf intrakortikalen Assoziationssystemen beruht, deren Ausprägung wesentlich von vorangegangener Erfahrung abhängt. Schließlich werden Daten diskutiert, die enge Korrelationen zwischen dem Auftreten von neuronaler Synchronisation und bestimmten Verhaltensleistungen zeigen. Solche Zusammenhänge bestehen für kognitive Leistungen wie selektive Aufmerksamkeit, Reizantizipation, visuo-motorische Koordination und perzeptuellen Wettstreit. Die diskutierten Daten sind mit der Hypothese kompatibel, daß Synchronisation weit verteilter neuronaler Antworten als Mechanismus genutzt wird, um Antworten auszuwählen und für eine gemeinsame Weiterverarbeitung vorzubereiten. Synchronisation erscheint somit als idealer Mechanismus, um Relationen zwischen verteilten Antworten dynamisch zu definieren.

1. Introduction

Psychophysical and neurophysiological evidence indicates that the brain identifies perceptual objects by decomposing them into components by analyzing the relations among the respective components and representing in a combined code the components and their specific relations. This is an efficient strategy for two reasons. *First*, it permits unambiguous descriptions of a virtually unlimited number of perceptual objects with a limited set of symbols for components and relations. *Second*, it can be scaled and applied also for the description of complex constellations, i. e., for the infinite variety of contextual configurations in which perceptual objects can occur. Linguistic descriptions follow the same principle. By recombining in ever changing configurations a rather limited set of symbols for components, properties and relations, a virtually inexhaustible universe of constellations can be encoded. However, there is an interesting trade-off between the complexity of the symbols and the syntactic rules required for the definition of relations.

In principle, a sentence describing a complex constellation of components can be substituted by a single symbol that captures the full meaning of the sentence. Implementation of such comprehensive symbols may be advantageous for the description of particularly important or frequently occurring constellations. It would make little sense, however, to substitute all possible sentences by specific symbols as this would lead to a combinatorial explosion of the required vocabulary. Conversely, if symbols address only very elementary components only few different symbols are required because the number of elementary components is orders of magnitude smaller than the number of possi-

ble configurations among components: a few dozens of different atoms suffice to generate a universe of molecules and four nucleotides suffice to spell out the alphabet of the genome that instructs the development of organisms. However, if only low-level components are encoded by individual symbols, descriptions of complex objects may become intolerably long and require highly sophisticated syntactic structures in order to cope with the large number of nested relations that need to be specified. Biological systems can be expected to have evolved optimally adapted compromises in this trade-off between the sophistication of descriptors and the complexity of relation defining mechanisms whereby this compromise is likely to differ for different coding tasks. Variables that are likely to be traded against each other are the costs of individual descriptors, the hardware requirements for the generation of complex descriptors, the costs and hardware constraints of relation defining mechanisms and the reliability and speed of the respective coding strategies.

If nervous systems have evolved towards such a compromise between coding strategies one expects to find neurons whose responses signal the presence of elementary components as well as of conjunctions of variable complexity. In addition, one expects the implementation of mechanisms that permit a flexible and context dependent definition of relations among the responses of these neurons.

The numerous investigations of single cell responses performed over the past decades have provided robust support for the existence of neurons in sensory areas of the cerebral cortex that signal the presence of components and some of their conjunctions. The former prevail at early and the latter at late stages of the processing streams. However, until recently, no systematic investigations were devoted to the analysis of mechanisms permitting flexible and context dependent definitions of relations among the responses of these neurons. Reasons were mainly conceptual. *First*, the discovery of neurons responding to highly complex conjunctions of elementary components of perceptual objects suggested that relations are encoded mainly by conjunction specific neurons which acquire their specificity by recombination of input signals. This notion is supported by the evidence that cells responding to elementary components connect in variable constellations onto higher order neurons which then respond to the specific conjunction of components defined by the respective input constellations. This mechanism, if iterated sufficiently often, can in principle cope with the definition of all conceivable relations but, as discussed above, it requires a large number of relation encoding, conjunction specific neurons. Another reason why systematic search for alternative relation coding mechanisms has not been attempted is the explanatory power of models which assume that most of the information conveyed by a neuron is encoded in the amplitude of its response, i. e., in its discharge rate. Accordingly, it was held that all relevant information is retrievable by recording the event related responses of single cells. The numerous and excellent correlations between the response amplitudes of individual cells and particular perceptual and motor functions provided ample support for this notion. For these reasons there was little incentive to record from more than one unit at a time and to investigate the possibility that additional information is contained in the temporal relations among the discharges of simultaneously active neurons.

Systematic search for mechanisms that are complementary to conjunction specific units and permit dynamic definition of relations among distributed responses began after the accidental finding that neurons in the cat visual cortex can engage in oscilla-

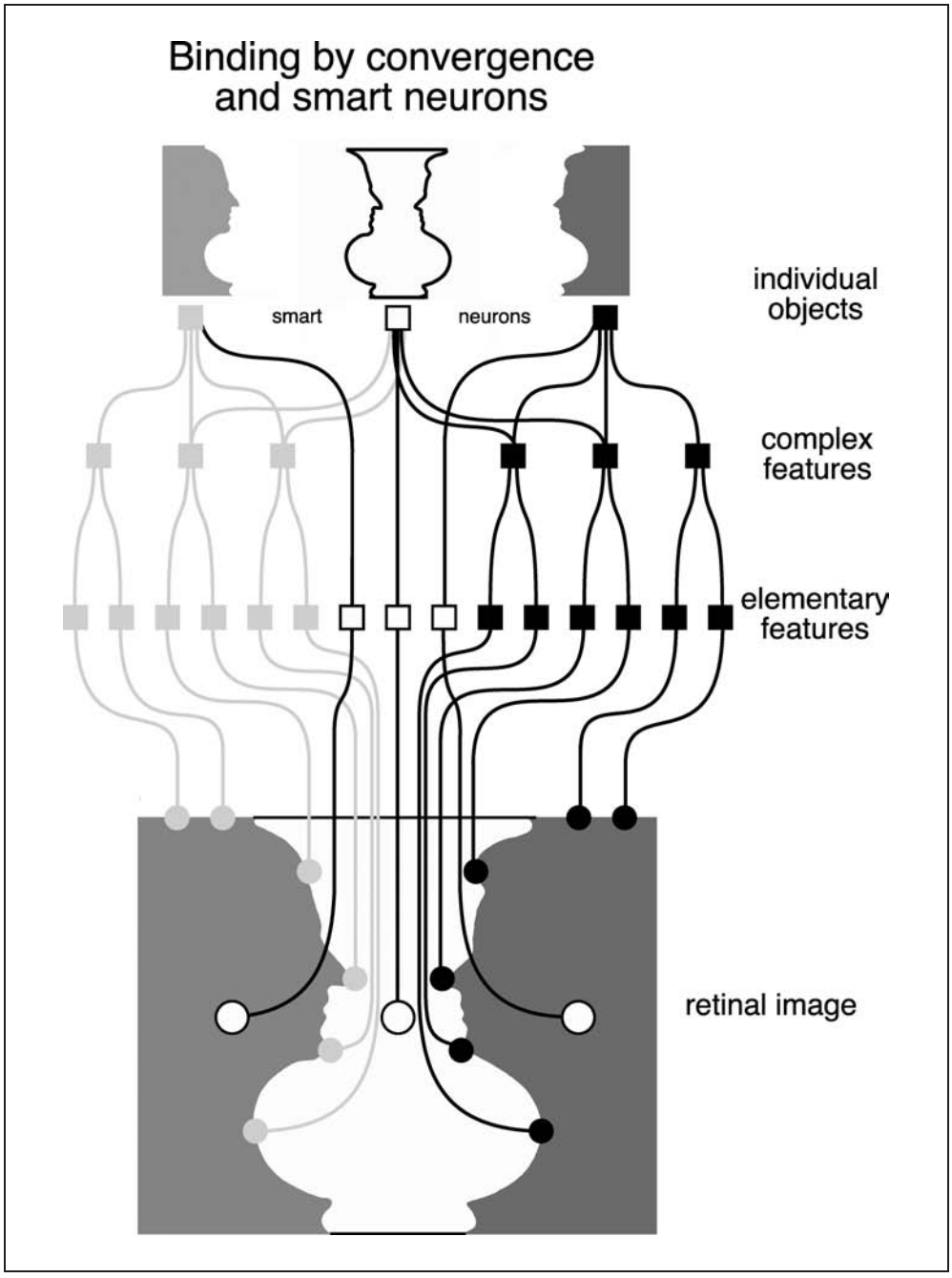

Fig. 1 Schematic wiring diagram of a hierarchically organized feed-forward network that generates conjunction specific neurons which respond selectively to different perceptual objects. Note that the neurons representing the faces and the vase, respectively, receive input from partially the same feature-specific neurons.

tory firing patterns and synchronize their discharges with a precision in the millisecond range (GRAY and SINGER 1987, 1989). This finding suggested the hypothesis that the cerebral cortex can coordinate the temporal fine structure of neuronal discharge sequences and that it exploits this ability in order to define relations among the responses of distributed neurons that are difficult to encode with conjunction neurons. In the following, some of the theoretical considerations are reviewed which led to the hypothesis that temporal synchronization could serve as a strategy to define relations among distributed neurons that is complementary to the encoding of relations by conjunction specific neurons. Subsequently, some of the experiments are discussed that were designed to test predictions derived from the synchronization hypothesis.

2. Smart Neurons and Assemblies

Figure 1 illustrates how relations among features can be encoded by conjunction specific neurons within hierarchically structured feed-forward architectures. Representing relations among components by conjunction units has two undisputed advantages: *First*, it permits rapid processing because it can be realized in feed-forward architectures. *Second*, it is unambiguous because the response of a particular cell always signals the same relation (labeled line coding). However, if not complemented by additional, more dynamic and context sensitive mechanisms for the definition of relations this strategy poses problems. *First*, excessively large numbers of conjunction units are required to cope with the manifold intra- and cross-modal relations between the features of real world objects. *Second*, it is hard to see how the entirely new relations among the features of novel objects can be represented as there cannot be an exhaustive repertoire of *a priori* specified conjunction units for all possible feature constellations. *Third*, unresolved problems arise with the specification of the nested relations that need to be defined to represent composite objects or scenes containing numerous objects. (For a more detailed review of the arguments see GRAY 1999, VON DER MALSBURG 1999, SINGER 1999.)

These shortcomings can be overcome by assembly coding. Here individual cells signal only components of objects and the whole object is represented by the simultaneous responses of the respective component coding cells (see Fig. 2). Individual neurons can then contribute at different times to the representation of different objects by forming ensembles with varying partners. This reduces dramatically the number of required conjunction units. It also solves the problem of representing the novel relations among the features of unfamiliar objects because cells representing elementary features can be grouped dynamically in ever changing constellations and then represent as an assembly the particular combination of features characteristic for the novel object. An essential prerequisite for this coding strategy is a dynamic binding mechanism that can group cells into assemblies and tag their responses such that they are recognizable as related by other centers in the brain. Such dynamic binding of neurons into functionally coherent assemblies requires that neurons interact cooperatively with one another through reciprocal association connections and reentry loops and, therefore, assembly coding cannot be realized in architectures containing only feed-forward connections.

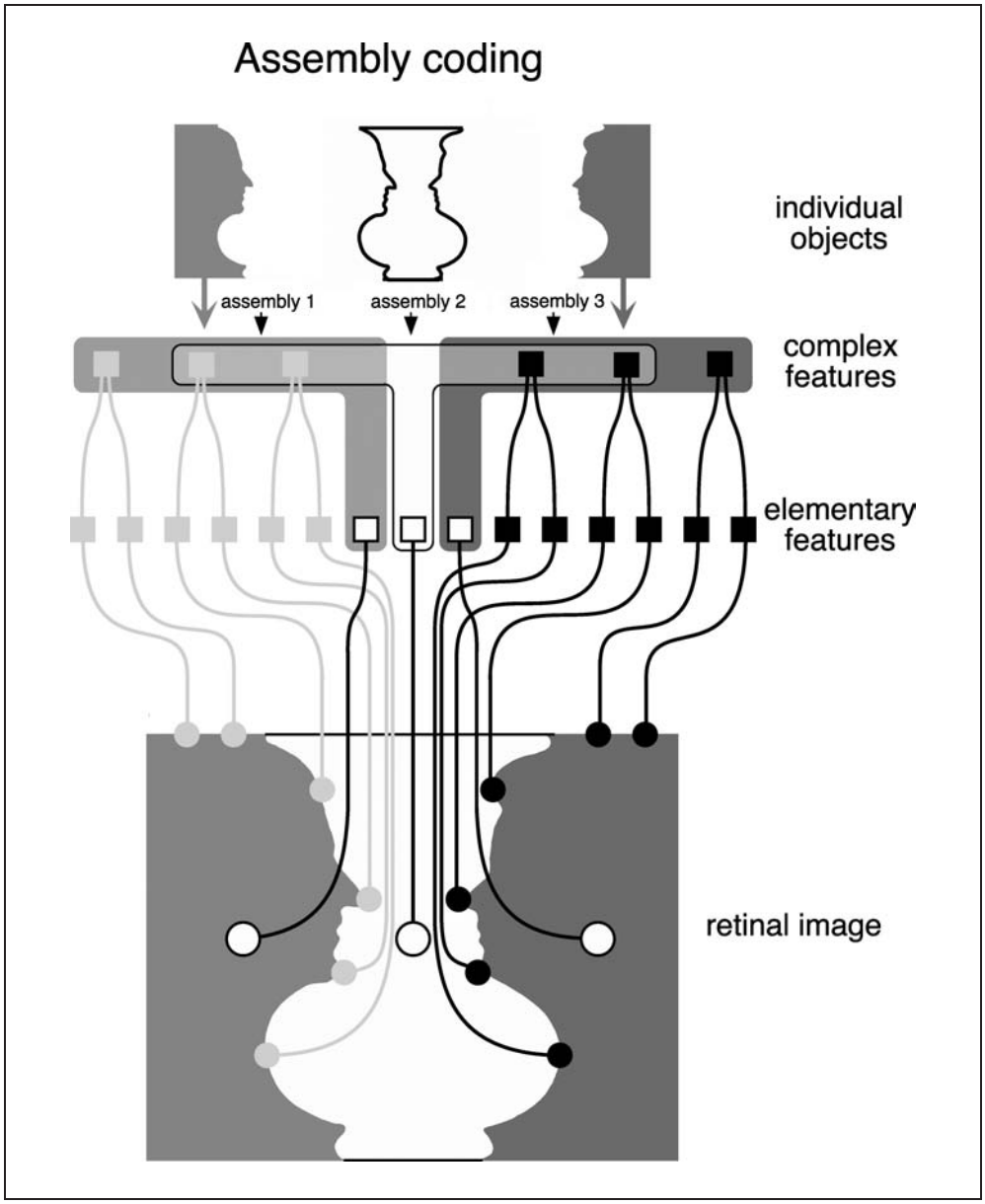

Fig. 2 Schematic wiring diagram of neuronal architectures serving the representation of perceptual objects by assemblies. Note that the assembly representing the vase shares neurons with the assemblies representing the faces. To ensure stability of the respective assemblies, additional reciprocal connections among neurons constituting an assembly are required (shaded regions) that bind responses of neurons belonging to the same assembly.

3. Synchrony as Code for Relations

An unambiguous signature of relatedness is absolutely crucial in assembly coding because, unlike in labeled line codes, the meaning of responses changes with the context in which they are embedded. It needs to be assured that the responses of the neurons that constitute an assembly are processed and evaluated together at subsequent processing stages and are not confounded with other, unrelated responses. In principle, this can be achieved by raising jointly and selectively the saliency of the responses belonging to an assembly and there are three options: *First*, unrelated responses can be inhibited and excluded from further processing. *Second*, the discharge frequency of the selected responses can be enhanced, and *third*, the selected cells can be made to discharge in precise temporal synchrony. All three mechanisms enhance the relative impact of the selected responses and can therefore be used to tag them as related. Problems arise, however, when several assemblies need to be formed at the same time and need to recruit partly the same neurons, – a condition that is likely to occur when a scene contains several objects that have subsets of features in common. This problem has been addressed as the so-called superposition problem and can only be resolved by segregating assemblies in time (see Fig. 3). One option is to jointly raise the discharge frequency of cells belonging to the first assembly for an interval sufficiently long to permit read-out by subsequent stages and to subsequently increase the discharge rate of the cells belonging to the second assembly and so on. Another option to label responses as related is to synchronize the respective discharges. Unlike joint rate increases which exploit temporal summation and enhance the saliency of prolonged response stretches synchronization exploits spatial summation and raises selectively the saliency of coincident discharges. Thus, synchronization can define relations with much higher temporal resolution than rate modulation and in principle permits multiplexing of assemblies on a spike by spike basis as suggested in Figure 3.

Another, potentially important advantage of using synchrony as tag of relatedness is that relations can be specified independently of firing rate. Discharge rates depend on numerous variables such as e. g. the physical energy of stimuli or the match between stimulus and receptive field properties. Response amplitudes are, thus, rather ambiguous indicators of relatedness. As synchrony can be modulated by temporal regrouping of discharges and, thus, can be varied independently of firing rates, synchronicity and rate can be used as orthogonal codes. Signals indicating the presence and the properties of visual features can thus be kept separate from signals indicating how these features are related.

Another advantage is that synchronized input is transmitted with minimal latency jitter (Abeles 1982, Diesmann et al. 1999). Thus, signatures of relatedness can be relayed with great reliability across processing stages, which contributes to reducing the risk of false conjunctions. Finally, synchronization enhances processing speed also by accelerating synaptic transmission *per se* because synchronized excitatory postsynaptic potentials (EPSPs) trigger action potentials with minimal delay.

These features make response synchronization an attractive strategy for the encoding of relations. However, in order to be effective, several additional constraints need to be met. *First*, neuronal networks must be able to modify and to coordinate the temporal patterning of spike trains in a context dependent manner. *Second*, the constellations of

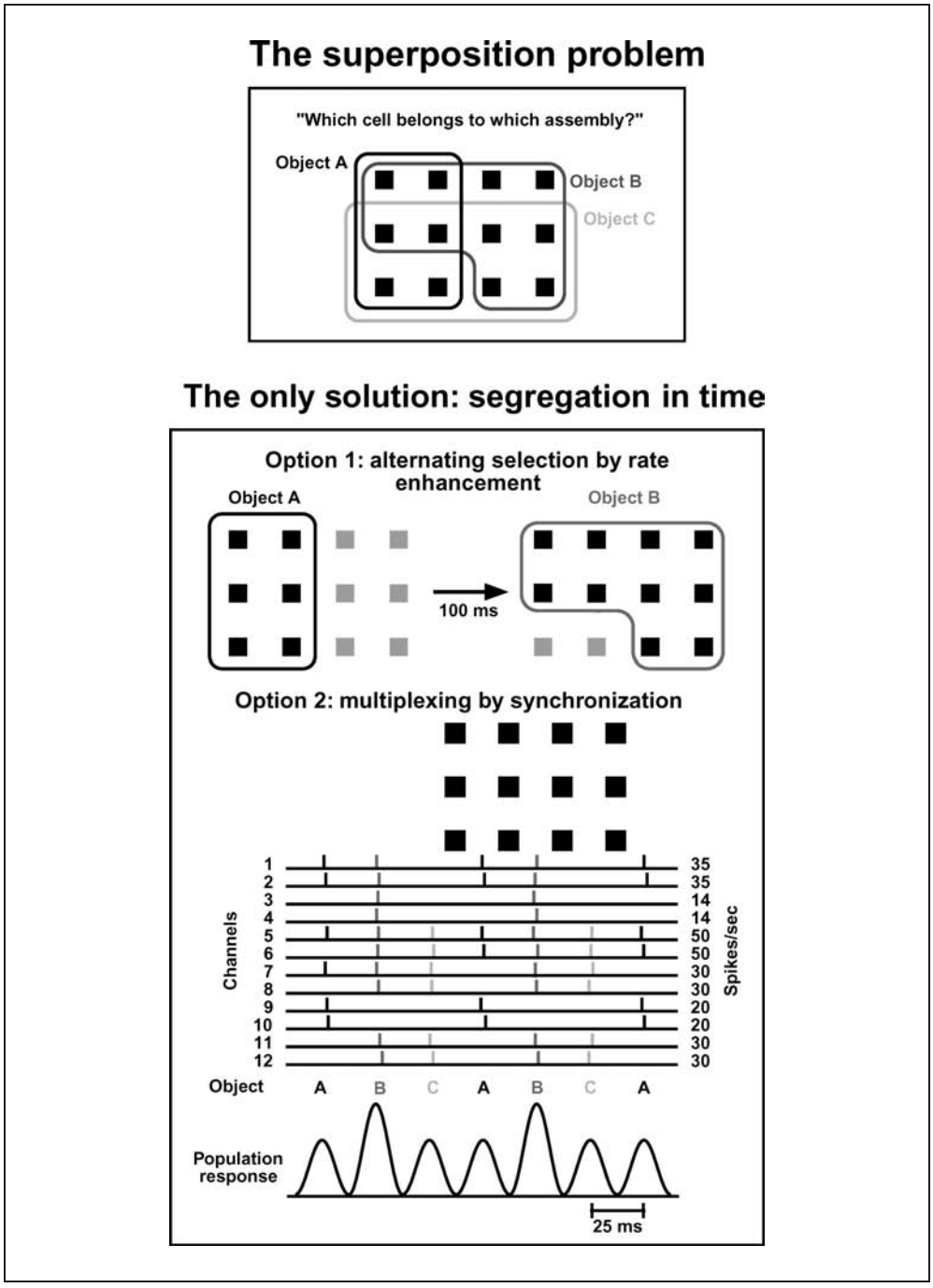
The superposition problem
"Which cell belongs to which assembly?"
Object A
Object B
Object C
The only solution: segregation in time
Option 1: alternating selection by rate enhancement
Object A
Object B
100 ms
Option 2: multiplexing by synchronization
Channels
Spikes/sec
1 35
2 35
3 14
4 14
5 50
6 50
7 30
8 30
9 20
10 20
11 30
12 30
Object
A B C A B C A
Population response
25 ms

synchronously discharging neurons must be changeable within a few tens of milliseconds in order to be compatible with processing speed. *Third*, the temporal signatures of coordinated discharge sequences must be preserved with millisecond precision across processing stages. *Fourth*, neuronal networks must be able to distinguish synchronous from temporally dispersed activity with a precision in the millisecond range, i. e., synchronous input must have a stronger impact on neurons than asynchronous input. *Fifth*, if relations are encoded by synchrony then Hebbian learning, i. e., the use-dependent modifications of synaptic gain, must also depend on the synchronicity of pre- and postsynaptic discharge patterns and not only on the mere covariation of rate changes. Finally, the occurrence and structure of synchronous discharge patterns needs to be related in a meaningful way with perceptual or motor processes that require dynamic grouping of responses.

4. Experimental Evidence

There is growing evidence that neuronal networks are capable of transmitting temporal patterns with high precision and to distinguish between coincident (synchronous) and non-coincident (temporally dispersed) input signals. Psychophysical experiments indicate that the visual system is sensitive to stimulus-onset asynchronies of less than 10 ms (Leonards et al. 1996, Alais et al. 1998, Usher and Donelly 1998, Lee and Blake 1999) supporting the notion that temporally modulated responses can be transmitted over several processing stages with a precision in the millisecond range. Supportive evidence comes from electrophysiological investigations. Cross-correlation analysis between simultaneously recorded responses of retinal ganglion cells, relay neurons in the thalamus and cells of the visual cortex shows that the oscillatory patterning of synchronized retinal responses is reliably transmitted to the cortex (Castelo-Branco et al. 1998). Given the high frequency of the retinal oscillations (up to 100 Hz) this implies high temporal fidelity of synaptic transmission over several stages. The well synchronized cortical responses to flicker stimuli point in the same direction (Rager and Singer 1998). As indicated by the precise temporal modulation of responses in area MT, a high-

◀

Fig. 3 Options for the solution of the superposition problem. Superposition problems arise if perceptual objects are present whose corresponding assemblies share partly the same neurons (upper box). In this case, different assemblies need to be segregated in time to avoid false conjunctions. One option is to raise successively the saliency of responses belonging to the respective assemblies by enhancing the discharge rate of the corresponding responses (lower box, option 1). An alternative solution is to enhance the saliency of responses belonging to a particular assembly by making the discharges of the respective neurons coincident in time (option 2). This permits rapid multiplexing of the different assemblies because coincidence can be evaluated within short time intervals, as it does not require temporal summation. Here it is assumed that the different assemblies alternate at intervals of approximately 25 ms. Note that this temporal structure can be, but does not have to be, obvious in the discharge sequences of individual neurons (channels 1–12) but that the spike density function of the population response shows an oscillatory modulation in the 40 Hz range. Note also that the constellation of neurons contributing spikes to the oscillatory population response changes from cycle to cycle.

er area of the monkey visual cortex, temporal fidelity of synaptic transmission holds also for cortico-cortical connections (BURACAS et al. 1998). Simulation studies indicate that such precision is readily obtained with neurons that operate with conventional time constants. The only prerequisite is that transmission occurs in parallel channels that interact through diverging and converging axon collaterals (DIESMANN et al. 1999). Once neurons at the same processing level have synchronized their discharges, the highly coherent pulse packets are conveyed with minimal dispersion across several synaptic stages as postulated for synfire chains (ABELES 1991).

Evidence is also available that synchronization can be established and dissolved very rapidly. Simulations with spiking neurons revealed that networks of appropriately coupled integrate and fire units can undergo sudden transitions from uncorrelated to synchronized states and *vice versa* (GERSTNER 1996).

The postulate that synchronized activity should have a stronger impact in target structures than temporally dispersed firing is also supported by data. Simultaneous recordings from coupled neuron triplets along thalamo-cortical and intracortical pathways in the visual system have revealed that EPSPs synchronized within intervals below 2 or 3 ms are much more effective than EPSPs dispersed over longer intervals (ALONSO et al. 1996, ALONSO and MARTINEZ 1998, USREY and REID 1999). Multielectrode recordings from several sites of the cat visual cortex and retinotopically corresponding loci in the superior colliculus indicated that the impact which a particular group of cortical neurons has on target cells in the colliculus increases substantially whenever the cortical cells synchronize their discharges with other cortical cell groups projecting to the same site in the tectum (BRECHT et al. 1998). Enhanced saliency of synchronized responses can also be inferred from experiments in amblyopic cats which showed a close correlation between reduced synchrony in primary visual cortex and a loss of responses in higher visual areas (ROELFSEMA et al. 1994, SCHRÖDER et al. 2002). Similar conclusions are suggested by simulation studies (NIEBUR and KOCH 1994, BAIR and KOCH 1996) and *in-vitro* experiments (STEVENS and ZADOR 1998, LARKUM et al. 1999, SCHILLER et al. 2000).

Further evidence that precise temporal relations among neuronal discharges matter in cortical processing comes from investigations of synaptic plasticity. Varying the temporal relations between presynaptic EPSPs and postsynaptic spike responses in simultaneously recorded coupled cortical cells revealed that long-term potentiation (LTP) results when the EPSP precedes the postsynaptic spike within intervals of 10 ms or less while the polarity of the modification reverses to long-term depression (LTD) as soon as the EPSP follows the spike (MARKRAM et al. 1997). Thus, shifts of a few milliseconds in the timing relations between pre- and postsynaptic discharges suffice to invert the polarity of use-dependent synaptic modifications. The mechanism permitting such precise evaluation of the temporal contiguity of pre- and postsynaptic responses is the active dendritic response associated with the back-propagating spike. The following results obtained from visual cortex slices point in the same direction. They suggest that the temporal windows for Hebbian coincidence matching are sharpened further if neurons engage in oscillatory responses.

Pyramidal cells of rat visual cortex slices were made to discharge tonically at 20 or 40 Hz by injecting sinusoidally modulated current through a patch pipette. Simultaneously, EPSPs were evoked at 20 Hz by electrical stimulation of excitatory afferents.

Changing the phase relations between pre- and postsynaptic activity revealed that the stimulated input tended to undergo LTP when the EPSPs were coincident with the spikes while afferents consistently underwent LTD when the EPSPs fell in the troughs of the membrane potential oscillations. Thus, phase shifts of about 12 ms between individual EPSPs and spikes reversed the polarity of the synaptic modifications (WESPATAT et al. in prep.).

In conclusion, there is converging evidence from different experimental approaches that cortical networks can handle temporal patterns with high precision and that precise timing relations among the discharges of distributed neurons are computationally relevant. Thus, the major constraints for the use of synchrony as a relation defining code are met. But does the brain exploit this option?

5. Functional Correlates

Several properties make response synchronization, as it has been observed in the visual cortex, a good candidate mechanism for the definition of relations. *First*, synchronization is sufficiently precise, in particular when it is associated with β- and γ-oscillations, to raise the saliency of the synchronized responses and to be computationally effective. *Second*, joint firing is not simply the result of coherent, stimulus locked variations in discharges rate nor is it a trivial reflection of anatomical connectivity such as shared input. Rather, synchronization is generated by dynamic interactions within the cortical network and its spatiotemporal patterning depends on a large number of variables: among these are the stimulus configuration (GRAY et al. 1989, ENGEL et al. 1991 b), the architecture of the intracortical synchronizing connections (ENGEL et al. 1991 a, LÖWEL and SINGER 1992), the activation state of the cortical network (MUNK et al. 1996, HERCULANO-HOUZEL et al. 1999) and attention dependent effects (ROELFSEMA et al. 1997, STEINMETZ et al. 2000, FRIES et al. 2001 b). These multiple influences endow synchronization with the required context sensitivity. *Third*, synchronization can be established across different cortical areas (ENGEL et al. 1991 c, ROELFSEMA et al. 1997) and even hemispheres (ENGEL et al. 1991 a) which are required for a relational code. *Fourth*, synchrony has been shown to vary independently of rate changes (RIEHLE et al. 1997, HERCULANO-HOUZEL et al. 1999) which is advantageous for the encoding of relations (see above). *Fifth*, synchronization is not an all or none phenomenon. When populations of cells engage in synchronous oscillatory activity, individual cells can skip cycles (BUZSAKI and CHROBAK 1995, BUZSAKI 1996) and cells participating in population oscillations of different frequency can engage in partial correlations (JENSEN and LISMAN 1998). This can be exploited to express graded and nested relations (LUCK and VOGEL 1997). *Sixth*, when cells engage in synchronous oscillatory activity, the probability increases that the same cells synchronize in subsequent trials (HERCULANO-HOUZEL et al. in prep.). This makes it in principle possible to store information about relations by changing synchronization probability.

In the following some of these features of response synchronization will be discussed in more detail whereby emphasis is laid on synchronization phenomena in the visual system and on relations between synchrony and cognitive processes.

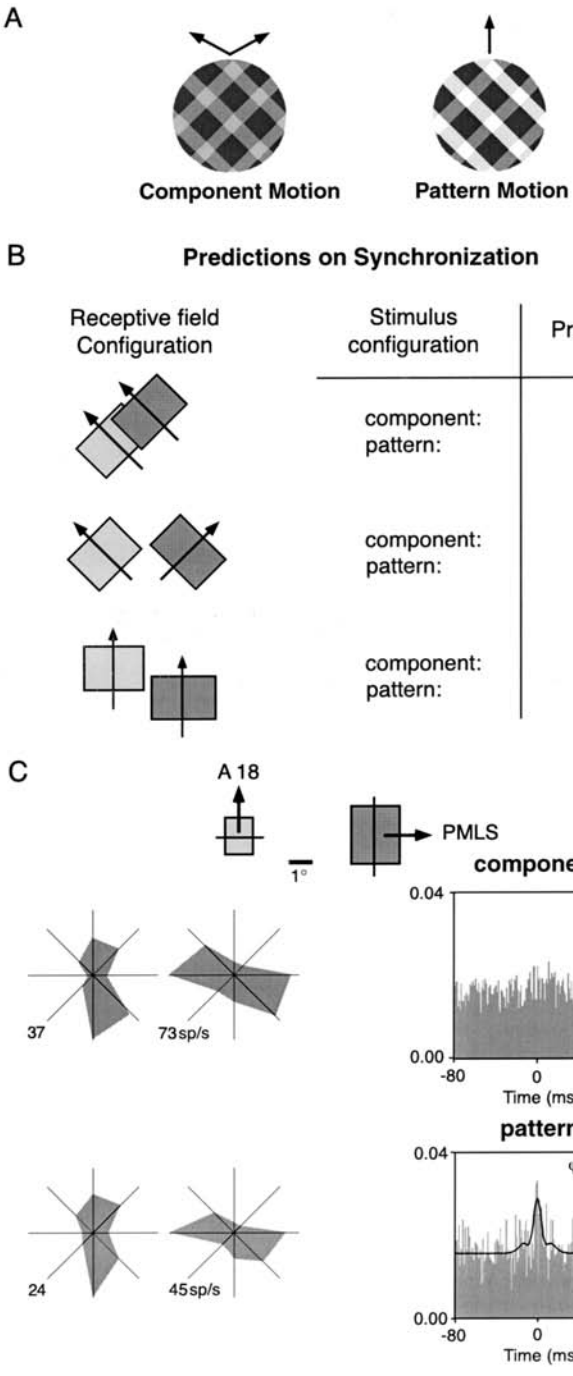
A
Component Motion
Pattern Motion
B
Predictions on Synchronization
Receptive field Configuration
Stimulus configuration
Predictions
component: sync
pattern: sync
component: no sync
pattern: sync
component: no sync
pattern: sync
C
A 18
1°
PMLS
component
0.04
n.s.
0.00
-80
0
80
Time (ms)
Norm coincidences
37
73sp/s
pattern
0.04
φ1.27
0.00
-80
0
80
Time (ms)
Norm coincidences
24
45sp/s

6. Perceptual Grouping

Scene segmentation and perceptual grouping are typical examples of low-level visual functions requiring flexible definition of relations. If internal synchronization of discharges serves to tag responses as related and to assure their joint processing, synchronization probability among neurons in early visual areas should reflect some of the basic Gestalt-criteria according to which the visual system groups related features during scene segmentation. Multielectrode studies designed to test this prediction revealed that neurons distributed across different columns within the same or different visual areas and even across hemispheres tend to synchronize their responses with close to zero phase lag when activated with a single contour but fire independently when stimulated simultaneously with two different contours (Gray et al. 1989, Engel et al. 1991 a, b, c, Freiwald et al. 1995, Kreiter and Singer 1996). Further analysis of the dependence of synchrony on receptive field and stimulus configurations confirmed that the probability and strength of response synchronization reflected elementary Gestalt-criteria for perceptual grouping such as continuity, proximity, similarity in the orientation domain, colinearity, and common fate (for review see Singer 1993, Singer et al. 1997, Gray 1999). These early experiments were performed in anesthetized animals but more recent multielectrode recordings from awake cats and monkeys indicate that these synchronization phenomena are not artifacts of anesthesia but are even more pronounced when the animals are awake and attentive (Kreiter and Singer 1992, Frien et al. 1994, Kreiter and Singer 1996, Fries et al. 1997, Gray and Viana di Prisco 1997, Friedman-Hill et al. 2000, Maldonado et al. 2000). It is noteworthy that none of these systematic changes in synchronization probability have been associated with systematic stimulus dependent changes of the neurons' discharge rate.

A particularly close correlation between neuronal synchrony and perceptual grouping has recently been observed in experiments with plaid stimuli. These stimuli are well suited for the study of dynamic binding mechanisms because minor changes of the stimulus cause a binary switch in perceptual grouping. Two superimposed gratings moving in different directions (plaid stimuli) may be perceived either as two surfaces, one being transparent and sliding on top of the other (component motion), or as a single surface, consisting of crossed bars, that moves in a direction intermediate to the component vectors (pattern motion) (Adelson and Movshon 1982, Stoner et al. 1990). Which percept dominates depends on the luminance of grating intersections because this variable defines the degree of transparency (Albright and Stoner 1995) (Fig. 4 *A*). Here is a

◄

Fig. 4 (*A*) Two superimposed gratings that differ in orientation and drift in different directions are perceived either as two independently moving gratings (component motion) or as a single pattern drifting in the intermediate direction (pattern motion), depending on whether the luminance conditions at the intersections are compatible with transparency. (*B*) Predictions on the synchronization behavior of neurons as a function of their receptive field configuration (*left*) and stimulation conditions (*right*). (*C*) Changes in synchronization behavior of two neurons recorded simultaneously from areas 18 and PMLS that were activated with a plaid stimulus under component (*upper graph*) and pattern motion conditions (*lower graph*). The two neurons preferred gratings with orthogonal orientation (see receptive field configuration, top, and tuning curves obtained with component and pattern, respectively) and synchronized their responses only when activated with the pattern stimulus (compare cross-correlograms on the right). (Adapted from Castelo-Branco et al. 2000.)

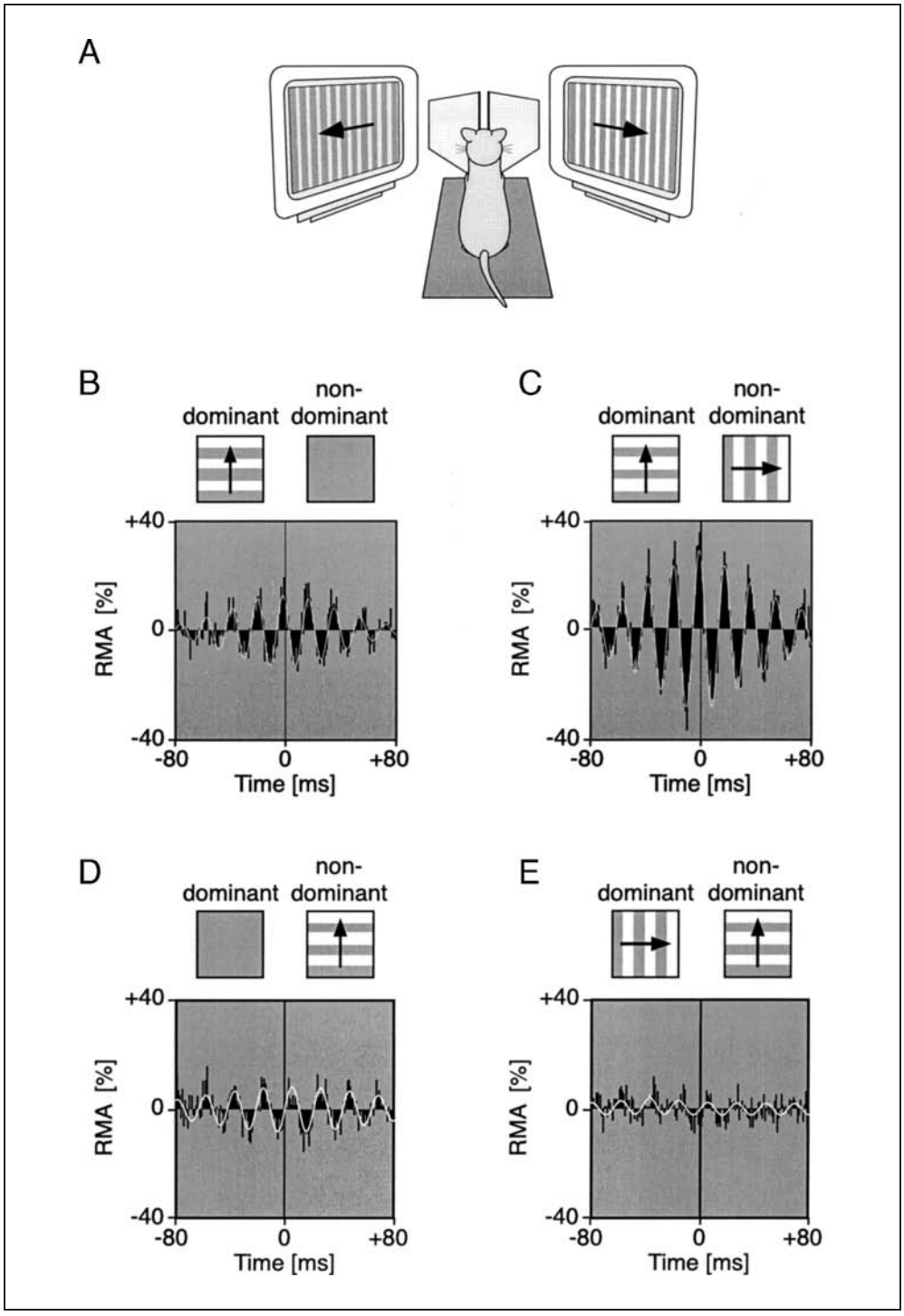
A
B
non-
dominant
dominant
+40
0
-40
RMA [%]
-80
0
+80
Time [ms]
C
non-
dominant
dominant
+40
0
-40
RMA [%]
-80
0
+80
Time [ms]
D
non-
dominant
dominant
+40
0
-40
RMA [%]
-80
0
+80
Time [ms]
E
non-
dominant
dominant
+40
0
-40
RMA [%]
-80
0
+80
Time [ms]

case where the percept changes when the assignment of relations among stimulus components changes. If these relations are defined by selective synchronization, a set of testable predictions can be formulated (see Fig. 4 *B*): One of them is that groups of neurons that are tuned to respond to different gratings should synchronize their responses if they mediate the percept of coherent pattern motion because in this case they must signal that all contours belong to the same surface and are related. By contrast, the same groups of cells should not synchronize if they mediate the percept of component motion because in this case their responses are associated with two different surfaces and must be treated as unrelated.

Cross-correlation analysis of responses from cell pairs recorded from various visual areas of lightly anesthetized cats confirmed this prediction as well as a number of others. Cells synchronized their activity if they responded to contours that are perceived as belonging to the same surface (CASTELO-BRANCO et al. 2000) (Fig. 4 *C*). This is strong support for the hypothesis that synchronization could serve to encode in a context dependent way relations among simultaneous neuronal responses.

7. Perceptual Selection

If synchronization serves to raise the saliency of responses, one should expect that it is used as a mechanism for response selection that is complementary to response selection by rate increases.

An involvement of response synchronization in stimulus selection has been documented in experiments on binocular rivalry (FRIES et al. 1997, 2002). When different stimuli that cannot be fused into a single percept are presented simultaneously to the two eyes perception always alternates between the two eyes. This can be exploited to investigate how neuronal responses to constant stimuli change if they pass from being selected and perceived to being suppressed and excluded from perception and *vice versa* (Fig. 5). The outcome of these experiments was surprising because the responses in early visual areas (areas 17 and 18 in cat) were not enhanced in amplitude when they supported perception and were not attenuated when they were excluded from supporting perception. A close and highly significant correlation existed, however, between changes in the strength of response synchronization and the outcome of rivalry. Cells mediating responses of the eye that won in interocular competition increased the synchronicity of their responses

◄

Fig. 5 Neuronal synchronization under conditions of binocular rivalry. (*A*) Using two mirrors, different patterns were presented to the two eyes of strabismic cats. Panels (*B*–*E*) show normalized cross-correlograms for two pairs of recording sites activated by the eye that won (*B*, *C*) and lost (*D*, *E*) in interocular competition, respectively. Insets above the correlograms indicate stimulation conditions. Under monocular stimulation (*B*), cells driven by the winning eye show a significant correlation which is enhanced after introduction of the rivalrous stimulus to the other eye (*C*). The reverse is the case for cells driven by the losing eye (compare conditions *D* and *E*). The white continuous line superimposed on the correlograms represents a damped *cosine* function fitted to the data. RMA, relative modulation amplitude of the center peak in the correlogram, computed as the ratio of peak amplitude over offset of correlogram modulation. This measure reflects the strength of synchrony. (Modified from FRIES et al. 1997.)

upon presentation of the rival stimulus to the other, losing eye while the reverse was true for cells driven by the eye that became suppressed. This agrees with rivalry experiments in awake, behaving monkeys which showed no systematic relation between the strength of visual responses and perception in early visual areas but a clear correlation between perceptual suppression and loss of neuronal responses in higher visual areas (LOGOTHETIS and SCHALL 1989, LEOPOLD and LOGOTHETIS 1996, SHEINBERG and LOGOTHETIS 1997). This is what one expects if the saliency of the responses from the two eyes is adjusted at early processing stages by modulating synchronization rather than discharge rates.

8. Dependency on Central States and Attention

A characteristic feature of response synchronization is its marked state dependency. It is particularly prominent when the cortex is in an activated state, i. e., when the EEG is desynchronized and exhibits high power in the β- and γ-frequency range (Fig. 6) (MUNK et al. 1996, HERCULANO-HOUZEL et al. 1999). Especially synchronization over long distances, that requires oscillatory patterning of responses, breaks down completely when the EEG gets "synchronized" and exhibits high power in the low frequency range (< 10 Hz). This close correlation between the occurrence of response synchronization on

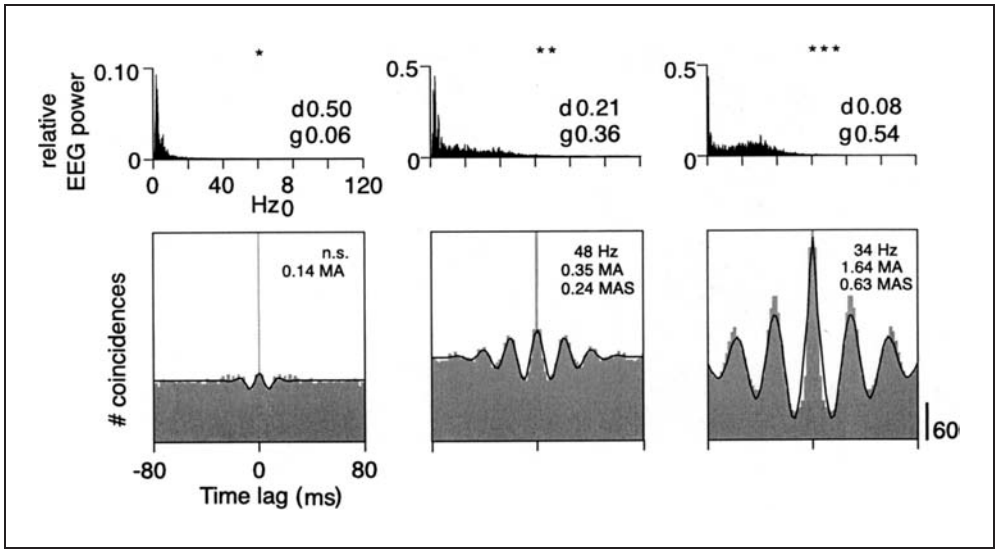

Fig. 6 State dependence of response synchronization. *Upper row*: Power distribution in the EEG recorded during three episodes from an anesthetized cat. *Lower row*: Averaged cross-correlograms of multi unit responses evoked by a drifting grating and recorded from two different sites in A17 during corresponding episodes. Note that the synchronization of the responses and the oscillatory modulation in the γ-frequency range increase with increasing γ-activity in the EEG. Inserts in the power spectra give the relative power in the δ- and γ-frequency range. Inserts in the cross-correlograms give the oscillation frequency (Hz), the relative modulation amplitude of the center peak (MA) and of the first side peak (MAS). (From HERCULANO-HOUZEL et al. 1999.)

the one hand and EEG states characteristic for the aroused and performing brain on the other hand may be taken as support for a functional role of precise synchrony in cortical processing.

The magnitude and precision of synchronization in the β- and γ-frequency range varies also in the fully aroused brain and is then correlated with fluctuations of attention. Such modulation of synchrony has been observed in cats trained to perform a visually triggered motor response. The visual, association, somatosensory and motor areas involved in the execution of the task synchronized their oscillatory activity in the β-frequency range as soon as the animals focused their attention on the relevant stimulus. However, once the reward was available and the animals engaged in consumatory behavior, these coherent patterns collapsed and gave way to low frequency oscillatory activity that did not exhibit any consistent relations with regard to phase and areal topology (ROELFSEMA et al. 1997). These results suggest that an attention related process had imposed a coherent temporal patterning on the activity of cortical areas required for the execution of the task. Such anticipatory enhancement of coherence could facilitate rapid synchronization of responses both within as well as across areas once the stimulus appears, thereby accelerating selection and grouping of responses.

Anticipatory synchronization patterns would be particularly effective if they exhibited some topological specificity and reflected the architecture of intracortical connections. In that case they could serve as a read-out mechanism that translates the grouping criteria defined by intracortical association connections into dynamic patterns of coherent activity against which incoming signals can be matched. Recent evidence supports such a scenario. Measurements of fluctuations in response latency revealed that self-generated oscillatory activity in the γ-frequency range exhibits a specific patterning that reflects intracortical connectivity. Response latencies of neurons in striate cortex fluctuate considerably for identical, repeatedly presented stimuli but these fluctuations are not random. They are correlated across cortical columns sharing certain functional properties (FRIES et al. 2001 a), and these correlations are due to synchronous oscillatory activity that causes coherent shifts in response latency. The effect is that responses of cells located in coherently oscillating columns become synchronized right from the beginning due to latency adjustment. Physiological data suggest that these synchronous oscillations are mediated by cortico-cortical connections (ENGEL et al. 1991 a, LÖWEL and SINGER 1992, KÖNIG et al. 1993) and anatomical evidence indicates that the cortico-cortical association connections link preferentially columns coding for related features that tend to be grouped perceptually (TS'O and GILBERT 1988, GILBERT and WIESEL 1989, MALACH et al. 1993, SCHMIDT et al. 1997). Thus, spontaneously occurring oscillatory activity could serve to continuously translate the functional architecture of the association connections into coordinated fluctuations of neuronal excitability which, in turn, would lead to fast, context dependent synchronization of neuronal responses. These ongoing oscillatory patterns are in addition modified by top-down influences from higher cortical areas and by immediately preceding changes of sensory input. Both effects would be equivalent to the functions commonly attributed to attentional mechanisms, the selection and binding of expected events, either as a consequence of bottom up priming or of intentional top down selection. The observed fluctuations could thus be equivalent with the system's updated expectancy that is determined by the fixed, locally installed grouping rules, by top-down influences and preceding sensory input. Seen in

this context, ongoing activity assumes the function of a predictor against which incoming activity is matched (GROSSBERG 1999). One of the effects of matching these predictions with incoming signals is a rapid temporal regrouping of output activity.

Direct evidence for an attention dependent anticipatory modulation of synchronous γ-oscillations has recently been obtained in area V4 of the monkey visual cortex (FRIES et al. 2001 b). While the monkey expected a visual stimulus that needed to be discriminated, neuronal synchronization increased in the γ-frequency range. This increase was specific for the site where the relevant stimulus was expected to appear and was not associated with a modulation of discharge rate. When the stimulus appeared, responses exhibited better coherence when the stimulus was attended than when attention was directed to another, distracting stimulus. Similar, attention dependent enhancement of synchrony has been observed among neurons in the somatosensory cortex of monkeys engaged in a tactile discrimination task (STEINMETZ et al. 2000).

These results suggest that cognitive processes consist not simply of the extraction and recombination of features but of an active matching operation. Afferent sensory activity is matched against self-generated activity that exhibits an oscillatory time structure and spatially distinct patterns of synchronization (for a detailed review of relations between attention and synchronous oscillations see ENGEL et al. 2001).

9. Conclusion

Taken together, the data and arguments exposed in this chapter support the notion that neuronal networks are capable of evaluating with a precision in the millisecond range the temporal relations among the discharges of neuronal populations and that precise timing relations are computationally relevant both in the context of signal processing and synaptic plasticity. Evidence suggests further that cortical networks exploit this ability not only to transmit with high temporal fidelity the temporal features of stimuli across processing stages but also to impose temporal signatures on neuronal activity that can be used in a variety of ways. Frequently observed signatures are an oscillatory patterning and precise synchronization of discharges. Evidence available so far suggests that the oscillatory patterning serves to synchronize responses at variable time scales and that synchronization enhances with high temporal resolution the saliency of the synchronized discharges. This, in turn, appears to be used for a variety of different functions that have in common to require selection of responses for further joint processing. Changes in synchrony correlate both with preattentive switches in stimulus selection – as indicated by the rivalry experiments – as well as with attention dependent stimulus selection. Furthermore, synchronization appears to be used to label responses as related in the context of both signal processing and use dependent synaptic modifications. This latter function has the characteristics of a binding mechanism that permits rapid and context dependent definition of relations in ever changing constellations. It is, therefore, ideally suited to serve as a selection mechanism in assembly coding that associates distributed responses with one another and assures their joint processing. Assembly coding, in turn, appears necessary in order to cope with the representation of the astronomical number of possible relations that can exist among the features of real world objects and among the objects constituting visual scenes. Thus, both theoretical considerations and

experimental evidence converge in the conclusion that the cerebral cortex applies with all likelihood two complementary strategies in order to encode relations: *First*, an explicit representation of relations by the responses of conjunction specific neurons, and *second*, an implicit representation of relations by dynamically associated assemblies that are characterized by the transient synchronization of discharges of the participating neurons. The first strategy seems to be applied for the representation of a limited set of conjunctions and is with all likelihood reserved for items that occur very frequently and/or are of particular behavioral importance. The second strategy seems to be reserved for the representation of novel conjunctions and all those relations that do not warrant explicit representation, either because these would require too many neurons or because the contents to be represented are too infrequent to justify the implementation of specialized and henceforth committed neurons. Space did not allow me to review the growing literature on correlations between cognitive processes and synchronous β- and γ-oscillations in human subjects and in non-mammalian animal species. Nor was it possible to discuss the numerous *in-vitro* studies that have contributed essentially to our understanding of the mechanisms responsible for the oscillatory patterning and the synchronization of cortical responses. These aspects are dealt with in the recent reviews by TALLON-BAUDRY and BERTRAND (1999) and by WHITTINGTON et al. (2000).

References

ABELES, M.: Role of the cortical neuron: integrator or coincidence detector? Israel J. Med. Sci. *18*, 83–92 (1982)

ABELES, M.: Corticonics. Neural Circuits of Cerebral Cortex. Cambridge: Cambridge University Press 1991

ADELSON, E. H., and MOVSHON, J. A.: Phenomenal coherence of moving visual patterns. Nature *300*, 523–525 (1982)

ALAIS, D., BLAKE, R., and LEE, S.-H.: Visual features that vary together over time group together over space. Nature Neurosci. *1*, 160–164 (1998)

ALBRIGHT, T. D., and STONER, G. R.: Visual motion perception. Proc. Natl. Acad. Sci. USA *92*, 2433–2440 (1995)

ALONSO, J.-M., and MARTINEZ, L. M.: Functional connectivity between simple cells and complex cells in cat striate cortex. Nature Neurosci. *1*, 395–403 (1998)

ALONSO, J.-M., USREY, W. M., and REID, R. C.: Precisely correlated firing in cells of the lateral geniculate nucleus. Nature *383*, 815–819 (1996)

BAIR, W., and KOCH, C.: Temporal precision of spike trains in extrastriate cortex of the behaving macaque monkey. Neural Comput. *8*, 1185–1202 (1996)

BRECHT, M., SINGER, W., and ENGEL, A. K.: Correlation analysis of corticotectal interactions in the cat visual system. J. Neurophysiol. *79*, 2394–2407 (1998)

BURACAS, G., ZADOR, A., DEWEESE, M., and ALBRIGHT, T.: Efficient discrimination of temporal patterns by motion-sensitive neurons in primate visual cortex. Neuron *20*, 959–969 (1998)

BUZSAKI, G.: The hippocampo-neocortical dialogue. Cereb. Cortex *6*, 81–92 (1996)

BUZSAKI, G., and CHROBAK, J. J.: Temporal structure in spatially organized neuronal ensembles: a role for interneuronal networks. Curr. Opin. Neurobiol. *5*, 504–510 (1995)

CASTELO-BRANCO, M., GOEBEL, R., NEUENSCHWANDER, S., and SINGER, W.: Neural synchrony correlates with surface segregation rules. Nature *405*, 685–689 (2000)

CASTELO-BRANCO, M., NEUENSCHWANDER, S., and SINGER, W.: Synchronization of visual responses between the cortex, lateral geniculate nucleus, and retina in the anesthetized cat. J. Neurosci. *18*, 6395–6410 (1998)

DIESMANN, M., GEWALTIG, M.-O., and AERTSEN, A.: Stable propagation of synchronous spiking in cortical neural networks. Nature *402*, 529–533 (1999)

ENGEL, A. K., FRIES, P., and SINGER, W.: Dynamic predictions: oscillations and synchrony in top-down processing. Nature Rev. Neurosci. *2*, 704–716 (2001)

ENGEL, A. K., KÖNIG, P., KREITER, A. K., and SINGER, W.: Interhemispheric synchronization of oscillatory neuronal responses in cat visual cortex. Science *252*, 1177–1179 (1991 a)

ENGEL, A. K., KÖNIG, P., and SINGER, W.: Direct physiological evidence for scene segmentation by temporal coding. Proc. Natl. Acad. Sci. USA *88*, 9136–9140 (1991 b)

ENGEL, A. K., KREITER, A. K., KÖNIG, P., and SINGER, W.: Synchronization of oscillatory neuronal responses between striate and extrastriate visual cortical areas of the cat. Proc. Natl. Acad. Sci. USA *88*, 6048–6052 (1991 c)

FREIWALD, W. A., KREITER, A. K., and SINGER, W.: Stimulus dependent intercolumnar synchronization of single unit responses in cat area 17. Neuroreport *6*, 2348–2352 (1995)

FRIEDMAN-HILL, S., MALDONADO, P. E., and GRAY, C. M.: Dynamics of striate cortical activity in the alert macaque: I. Incidence and stimulus-dependence of gamma-band neuronal oscillations. Cereb. Cortex *10*, 1105–1116 (2000)

FRIEN, A., ECKHORN, R., BAUER, R., WOELBERN, T., and KEHR, H.: Stimulus-specific fast oscillations at zero phase between visual areas V1 and V2 of awake monkey. Neuroreport *5*, 2273–2277 (1994)

FRIES, P., NEUENSCHWANDER, S., ENGEL, A. K., GOEBEL, R., and SINGER, W.: Rapid feature selective neuronal synchronization through correlated latency shifting. Nature Neurosci. *4(2)*, 194–200 (2001 a)

FRIES, P., REYNOLDS, J. H., RORIE, A. E., and DESIMONE, R.: Modulation of oscillatory neuronal synchronization by selective visual attention. Science *291*, 1560–1563 (2001 b)

FRIES, P., ROELFSEMA, P. R., ENGEL, A. K., KÖNIG, P., and SINGER, W.: Synchronization of oscillatory responses in visual cortex correlates with perception in interocular rivalry. Proc. Natl. Acad. Sci. USA *94*, 12699–12704 (1997)

FRIES, P., SCHRÖDER, J.-H., SINGER, W., and ENGEL, A. K.: Oscillatory neuronal synchronization in primary visual cortex as a correlate of perceptual stimulus selection. J. Neurosci. *22*, 3739–3754 (2002)

GERSTNER, W.: Rapid phase locking in systems of pulse-coupled oscillators with delays. Phys. Rev. Letters *76*, 1755–1758 (1996)

GILBERT, C. D., and WIESEL, T. N.: Columnar specificity of intrinsic horizontal and cortico-cortical connections in cat visual cortex. J. Neurosci. *9*, 2432–2442 (1989)

GRAY, C. M.: The temporal correlation hypothesis of visual feature integration: still alive and well. Neuron *24*, 31–47 (1999)

GRAY, C. M., KÖNIG, P., ENGEL, A. K., and SINGER, W.: Oscillatory responses in cat visual cortex exhibit inter-columnar synchronization which reflects global stimulus properties. Nature *338*, 334–337 (1989)

GRAY, C. M., and SINGER, W.: Stimulus-dependent neuronal oscillations in the cat visual cortex: a cortical functional unit. Soc. Neurosci. Abstr. *13*, 404.3 (1987)

GRAY, C. M., and SINGER, W.: Stimulus-specific neuronal oscillations in orientation columns of cat visual cortex. Proc. Natl. Acad. Sci. USA *86*, 1698–1702 (1989)

GRAY, C. M., and VIANA DI PRISCO, G.: Stimulus-dependent neuronal oscillations and local synchronization in striate cortex of the alert cat. J. Neurosci. *17*, 3239–3253 (1997)

GROSSBERG, S.: The link between brain learning, attention, and consciousness. Conscious. Cogn. *8*, 1–44 (1999)

HERCULANO-HOUZEL, S., MUNK, M. H. J., NEUENSCHWANDER, S., and SINGER, W.: Precisely synchronized oscillatory firing patterns require electroencephalographic activation. J. Neurosci. *19*, 3992–4010 (1999)

HERCULANO-HOUZEL, S., SINGER, W., and MUNK, M. H. J.: Use-dependent long-term modification of neuronal synchronization. (2003, in prep.)

JENSEN, O., and LISMAN, J. E.: An oscillatory short-term memory buffer model can account for data on the Sternberg task. J. Neurosci. *18*, 10688–10699 (1998)

KÖNIG, P., ENGEL, A. K., LÖWEL, S., and SINGER, W.: Squint affects synchronization of oscillatory responses in cat visual cortex. Eur. J. Neurosci. *5*, 501–508 (1993)

KREITER, A. K., and SINGER, W.: Oscillatory neuronal responses in the visual cortex of the awake macaque monkey. Eur. J. Neurosci. *4*, 369–375 (1992)

KREITER, A. K., and SINGER, W.: Stimulus-dependent synchronization of neuronal responses in the visual cortex of the awake macaque moneky. J. Neurosci. *16*, 2381–2396 (1996)

LARKUM, M. E., ZHU, J. J., and SAKMANN, B.: A new cellular mechanism for coupling inputs arriving at different cortical layers. Nature *398*, 338–341 (1999)

LEE, S.-H., and BLAKE, R.: Visual form created solely from temporal structure. Science *284*, 1165–1168 (1999)

Leonards, U., Singer, W., and Fahle, M.: The influence of temporal phase differences on texture segmentation. Vision Res. *36*, 2689–2697 (1996)

Leopold, D. A., and Logothetis, N. K.: Activity changes in early visual cortex reflect monkeys' percepts during binocular rivalry. Nature *379*, 549–553 (1996)

Logothetis, N. K., and Schall, J. D.: Neuronal correlates of subjective visual perception. Science *245*, 761–763 (1989)

Löwel, S., and Singer, W.: Selection of intrinsic horizontal connections in the visual cortex by correlated neuronal activity. Science *255*, 209–212 (1992)

Luck, S. J., and Vogel, E. K.: The capacity of visual working memory for features and conjunctions. Nature *390*, 279–281 (1997)

Malach, R., Amir, Y., Harel, M., and Grinvald, A.: Relationship between intrinsic connections and functional architecture revealed by optical imaging and in vivo targeted biocytin injections in primate striate cortex. Proc. Natl. Acad. Sci. USA *90*, 10469–10473 (1993)

Maldonado, P. E., Friedman-Hill, S. R., and Gray, C. M.: Dynamics of striate cortical activity in the alert macaque: II. Fast time scale synchronization. Cereb. Cortex *10*, 1117–1131 (2000)

Malsburg, C. von der: The what and why of binding: the modeler's perspective. Neuron *24*, 95–104 (1999)

Markram, H., Lübke, J., Frotscher, M., and Sakmann, B.: Regulation of synaptic efficacy by coincidence of postsynaptic APs and EPSPs. Science *275*, 213–215 (1997)

Munk, M. H. J., Roelfsema, P. R., König, P., Engel, A. K., and Singer, W.: Role of reticular activation in the modulation of intracortical synchronization. Science *272*, 271–274 (1996)

Niebur, E., and Koch, C.: A model for the neuronal implementation of selective visual attention based on temporal correlation among neurons. J. Comput. Neurosci. *1*, 141–158 (1994)

Rager, G., and Singer, W.: The response of cat visual cortex to flicker stimuli of variable frequency. Eur. J. Neurosci. *10*, 1856–1877 (1998)

Riehle, A., Grün, S., Diesmann, M., and Aertsen, A.: Spike synchronization and rate modulation differentially involved in motor cortical function. Science *278*, 1950–1953 (1997)

Roelfsema, P. R., Engel, A. K., König, P., and Singer, W.: Visuomotor integration is associated with zero time-lag synchronization among cortical areas. Nature *385*, 157–161 (1997)

Roelfsema, P. R., König, P., Engel, A. K., Sireteanu, R., and Singer, W.: Reduced synchronization in the visual cortex of cats with strabismic amblyopia. Eur. J. Neurosci. *6*, 1645–1655 (1994)

Schiller, J., Major, G., Koester, H. J., and Schiller, Y.: NMDA spikes in basal dendrites of cortical pyramidal neurons. Nature *404*, 285–289 (2000)

Schmidt, K. E., Goebel, R., Löwel, S., and Singer, W.: The perceptual grouping criterion of colinearity is reflected by anisotropies of connections in the primary visual cortex. Eur. J. Neurosci. *9*, 1083–1089 (1997)

Schröder, J.-H., Fries, P., Roelfsema, P. R., Singer, W., and Engel, A. K.: Ocular dominance in extrastriate cortex of strabismic amblyopic cats. Vision Res. *42*, 29–39 (2002)

Sheinberg, D. L., and Logothetis, N. K.: The role of temporal cortical areas in perceptual organization. Proc. Natl. Acad. Sci. USA *94*, 3408–3413 (1997)

Singer, W.: Synchronization of cortical activity and its putative role in information processing and learning. Annu. Rev. Physiol. *55*, 349–374 (1993)

Singer, W.: Neuronal synchrony: a versatile code for the definition of relations? Neuron *24*, 49–65 (1999)

Singer, W., Engel, A. K., Kreiter, A. K., Munk, M. H. J., Neuenschwander, S., and Roelfsema, P. R.: Neuronal assemblies: necessity, signature and detectability. Trends Cogn. Sci. *1*, 252–261 (1997)

Steinmetz, P. N., Roy, A., Fitzgerald, P. J., Hsiao, S. S., Johnson, K. O., and Niebur, E.: Attention modulates synchronized neuronal firing in primate somatosensory cortex. Nature *404*, 187–190 (2000)

Stevens, C. F., and Zador, A. M.: Input synchrony and the irregular firing of cortical neurons. Nature Neurosci. *1*, 210–217 (1998)

Stoner, G. R., Albright, T. D., and Ramachandran, V. S.: Transparency and coherence in human motion perception. Nature *344*, 153–155 (1990)

Tallon-Baudry, C., and Bertrand, O.: Oscillatory gamma activity in humans and its role in object representation. Trends Cogn. Sci. *3(4)*, 151–162 (1999)

Ts'o, D. Y., and Gilbert, C. D.: The organization of chromatic and spatial interactions in the primate striate cortex. J. Neurosci. *8*, 1712–1727 (1988)

Usher, M., and Donnelly, N.: Visual synchrony affects binding and segmentation in perception. Nature *394*, 179–182 (1998)

Usrey, W. M., and Reid, R. C.: Synchronous activity in the visual system. Annu. Rev. Physiol. *61*, 435–456 (1999)

Wespatat, V., Tennigkeit, F., and Singer, W.: Phase sensitivity of Hebbian modifications in oscillating cells of rat visual cortex. (2003, in prep.)

Whittington, M. A., Traub, R. D., Kopell, N., Ermentrout, B., and Buhl, E. H.: Inhibition-based rhythms: experimental and mathematical observations on network dynamics. Int. J. Psychophysiol. *38*, 315–336 (2000)

Prof. Dr. Wolf Singer
Max Planck Institute for Brain Research
Deutschordenstraße 46
60528 Frankfurt am Main
Germany
Phone: ++49 (0) 69 96 76 92 18
Fax: ++49 (0) 69 96 76 93 27
E-Mail: singer@mpih-frankfurt.mpg.de

Nova Acta Leopoldina NF *88*, Nr. 332, 57–76 (2003)

Stochastic Resonance: Examples from Sensory, Perceptive and Behavioral Neuroscience and Chemistry

Gabor Balázsi and Frank Moss (St. Louis)

With 8 Figures

Abstract

The idea of stochastic resonance is introduced with examples involving single elements, from single protein molecules to postsynaptic sensory neurons. But perception and behavior surely arise from processes distributed over both space and time, leading us to consider *spatio-temporal* stochastic resonance. The seminal, demonstrative experiment of this phenomenon was created in a chemical system, but preceding this were simulations of strikingly simple construction – networks of stochastic threshold elements. All these showed the phenomenon of noise enhanced propagation of spatiotemporal coherent structures. Though there is a large gap between these elemental demonstrations and operative processes within the brain, we nevertheless finally mention stochastic resonance experiments in human and animal perception and behavior.

Zusammenfassung

Das Konzept der Stochastischen Resonanz wird allgemein an aus einzelnen Elementen bestehenden Beispielen erläutert, wie einzelne Proteinmoleküle oder postsynaptische Sinnesneuronen. Die Tatsache, daß Wahrnehmung und Verhalten innerhalb von Prozessen entstehen, die sowohl räumlich als auch zeitlich ausgedehnt sind, macht die Betrachtung von raum-zeitlicher Stochastischer Resonanz notwendig. Das bahnbrechende Experiment, das dieses Phänomen anschaulich zeigt, wurde innerhalb eines chemischen Systems realisiert. Diesem Experiment sind allerdings bemerkenswert einfache Simulationen vorausgegangen – aus Elementen mit stochastischen Schwellenwerten bestehende Netzwerk – die alle das Phänomen zeigen, daß Rauschen die Übertragung von raum-zeitlich kohärenten Strukturen verstärken kann. Obwohl es ein weiter Weg von derartigen elementaren Darstellungen zu realen Hirnprozessen ist, werden wir am Schluß auf Experimente zur Stochastischen Resonanz in Verhalten und Wahrnehmung bei Menschen und Tieren eingehen.

1. Introduction

Stochastic Resonance (SR) is the somewhat counterintuitive process by which the addition of a random process, or "noise", in a class of nonlinear systems, can actually enhance the detection efficiency or the information content of the detected signal. An optimal noise enhances the signal optimally while too much or too little noise degrades the information content. A convenient measure of the quality of the signal is the signal-to-noise ratio (SNR), a measure that has been traditionally used in SR research. But other measures have sometimes adopted, for example, the transinformation, Fisher information, discrim-

inability, input-output coherence, etc. All of these can be optimized with the introduction of the proper noise intensity either externally or inside a system that shows SR.

For many years, and beginning with its inception as a possible explanation of the periodic recurrences of the Earth's Ice Ages (Benzi et al. 1981, 1982, Nicolis 1982), SR was thought to exist only in bi- or multi-stable dynamical systems (Jung and Hänggi 1989). The most frequently studied system was the infinitely damped motion of a particle moving in a "standard quartic" bistable potential, $U(x) = -x^2/2 + x^4/4$, subject to noise, $\zeta(t)$, and a weak periodic forcing, ε:

$$\dot{x} = x - x^3 + \sqrt{2D}\,\xi(t) + \varepsilon\,\sin(\omega t + \varphi). \qquad [1]$$

The first realization of this type of bistable, noisy dynamics in a physical system, apart from a demonstration in an electronic circuit, was provided by McNamara et al. (1988) using a bistable ring laser. The first dynamical theory of SR soon followed (McNamara and Wiesenfeld 1989). Refinements of the theory followed as reviewed by Jung (1993) as well as a variety of demonstrations in physical systems as reviewed by Moss (1994).

Early on, it was, however, obscure that the barrier crossings of the particle moving in $U(x)$ could encode information about the weak periodic signal. But it was soon shown that the probability density of residence times (how long the particle remained in one potential well) as well as the SNR of the train of barrier crossing marker events could encode a surprising amount of information about the weak periodic signal (Longtin et al. 1991). These observations also gave rise to the first theoretical applications of SR in sensory biology (Longtin et al. 1991, Moss et al. 1994) and the first demonstration of SR in a biological system (Douglass et al. 1993) as discussed in Section 2 below.

The advent of SR in sensory biology stimulated a profusion of research. Summaries can be found in several reviews (Moss 1994, Moss et al. 1994, Wiesenfeld and Moss 1995, Gammaitoni et al. 1998, Anishchenko et al. 1999). SR has also invaded medical science (Chiou-Tan et al. 1996, Collins et al. 1996, Cordo et al. 1996, Morse and Evans 1996, Suki et al. 1998, Chuang et al. 1999, Hidaka et al. 2000) and more recently, plant biology (Busch et al. 2001, Hütt et al. 2002).

But the demonstration of SR in single neurons begs the question of whether, or even if, an animal or human can be consciously aware of the noise enhanced information in its peripheral nervous system. This question leads SR research in two distinct directions. *First*, "awareness" must, perforce, arise from some sort of multi unit processing. We are thus led to investigate SR in networks of coupled systems. Coupling can be either global, or "all-to-all", or it can be some local form, for example nearest neighbor. In the latter case, one observes the noise enhanced propagation of coherent structures, or spatiotemporal stochastic resonance (STSR), as discussed in Section 3 below. *Second*, the only way to actually answer the awareness question is with human psychophysics and animal behavior experiments. These are discussed in Sections 4 and 5. We finally conclude in Section 6 with some brief speculations on future developments.

1.1 Outline of the Threshold Theory of SR

Only three ingredients are necessary for threshold, or nondynamical, SR: a threshold, a subthreshold signal and noise. Nature is replete with examples of systems composed of

these ingredients, so it is not surprising that SR has invaded many scientific and technical fields. Figure 1 *A* shows an example threshold, $\Delta_0 = V_t$, of unit magnitude with a subthreshold sinusoidal signal of peak amplitude, A, plus time series for three intensities of added Gaussian, band limited noise of standard deviation, σ, and cutoff frequency f_n. The time series of the positive going threshold crossings are shown by trains of marker pulses

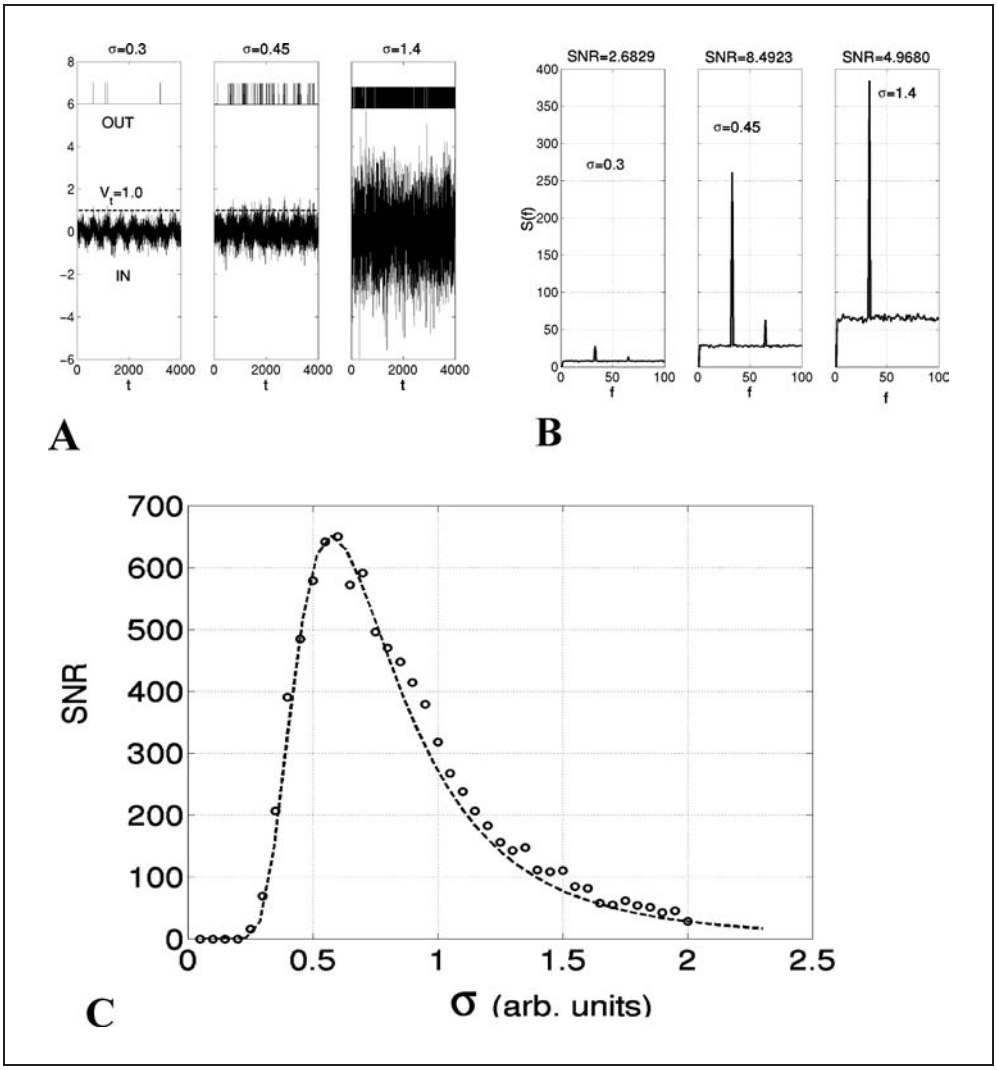

Fig. 1 (*A*) Three time series of a subthreshold sinusoidal signal, the threshold and added Gaussian noise of standard deviation, σ; left-to-right, small to large noise. The threshold is $\Delta_0 = V_t = 1.0$ units and the sine wave signal has peak amplitude $\varepsilon = 0.20$ units. Positive going threshold crossings are marked by the stereotypical spikes above. (*B*) Power spectra of the threshold crossings of the three time series in (*A*). Note the SNRs shown above with maximum SNR value for intermediate noise. (*C*) The SNR *versus* σ, the standard deviation of the noise, showing the optimal value at $\sigma = 0.60$. The dashed line is the theory and the open circles are the numerical simulation.

in the upper parts of the panels. The power spectra of these marker pulse trains are shown in (*B*) with the SNRs (computed as the ratio of power in the signal peak to that in the noise in a 1 Hz bandwidth centered on the signal frequency) shown above. Figure 1 *C* is the *signature* of SR. It shows a maximum in the SNR that occurs for an optimal value of noise intensity, σ_{opt}. The open circles are the results of the numerical simulation and the dashed curve is the theory briefly described below. The noise acts as a signal sampling function. At low noise the signal is under sampled leading to a poor SNR. At high noise the SNR is degraded due to randomization. These effects are clearly seen in Figure 1 *A* and *B*.

Given the three ingredients, the SNR is not difficult to calculate approximately (Moss et al. 1994, Gingl et al. 1995, Freund et al. 2002). Only two approximations are necessary, requiring the signal to be small, $A < \Delta_0$, and the noise cut-off frequency to be large compared to the signal frequency, $f_n >> f_s$ (to insure a large enough signal sampling rate). In practice these approximations are usually well satisfied. The threshold theory (see especially Freund et al. 2002) results in a simple formula for the SNR,

$$SNR = \left[\frac{2f_n \Delta_0^2 A^2}{\sqrt{3}\,\sigma^4}\right] \exp\left(-\frac{\Delta_0^2}{2\sigma^2}\right). \qquad [2]$$

The combination of the inverse σ^4 in the prefactor and inverse σ^2 in the exponent result in a function with a maximum SNR at an optimal noise intensity.

It should be noted that all of the foregoing theory applies to "hard" thresholds, that is a single threshold value characterized by a step function in the input-output relation. Thresholds can, however, be "soft" where a single spike response is determined by a probability function rather that a completely deterministic threshold crossing. In this case, the probability that a spike is fired as a function of the value of some stimulus is often a monotonically increasing, nonlinear function but not a step. Bezrukov and Vodyanoy (1997) have developed an interesting theory that applies to SR without a hard threshold.

1.2 Information Measures

The SNR is not the only information measure that can be used in threshold SR theory or for the analysis of experimental data. It has, however, the advantage that it does not require a clean copy of the input signal as, for example, coherence or transinformation measures do. The transinformation was used in experiments on the cricket cercal system (see Section 2 below) and in a recent theory of SR in single membrane ion channels (Goychuk and Hänggi 2000) stimulated by experiments on ion channels (Petracchi et al. 1994, Bezrukov and Vodyanoy 1997). The behaving animal, of course, does not have a clean copy of the input signal. The following measures also do not require knowledge of the input signal.

The lower bound of the Fisher information, J_{LB}, (Fisher 1949) is particularly useful in sensory biology since it can be obtained from measures of the neural spike train alone. In threshold theory, it is related to the SNR:

$$J_{LB} = \frac{T f_n \Delta_0^2}{\sqrt{3}\,\sigma^4} \exp\left(-\frac{\Delta_0^2}{2\sigma^2}\right) = \frac{T}{2A^2} SNR, \qquad [3]$$

where T is a time window across which the spike train is measured and the interspike time intervals (threshold crossings) are assumed to be Poisson distributed (FREUND et al. 2002).

Finally, we mention the discriminability, d', a measure used frequently to analyze statistical data from human psychophysics experiments. It essentially measures the normalized distance between the means of two distributions, one measured with stimulus or signal present, and one without (see WARD 1999, FREUND et al. 2002). STEMMLER (1996) has shown that in threshold theory, $d' \approx A\sqrt{J_{LB}}$, all of these measures show maxima at optimal values of the noise intensity and can thus be useful in interpreting experimental data in SR experiments.

2. Experimental Stochastic Resonance in Single Elements

SR was first demonstrated in a biological experiment using the hydrodynamically sensitive mechanoreceptor system of the crayfish (DOUGLASS et al. 1993). Studies of this animal have a long history in biology. The crayfish was the animal chosen by Thomas Henry HUXLEY to create and introduce the modern study of physiology, then called zoology (HUXLEY 1880). The crayfish is a successful animal, having spread over the globe from the arctic to the tropics in myriad species. It surely owes this success in large part to a remarkable sensory and motor system for escaping predators. The system is based in part on mechanoreceptors, or hydrodynamically sensitive hairs, spread over the tail fan (WIESE et al. 1976). Each hair moves with the water and can sense the approach of a swimming fish, the crayfish's main predator, *via* its induced water motions. These motions are approximately periodic (4 to 10 Hz) but exist for a short period of time and the system shows optimal response in this frequency range. The hairs are innervated by afferent sensory neurons that converge on the terminal, or 6^{th}, ganglion (located below the 5^{th} ganglion) as shown in Figure 2. Processing takes place in the ganglion which outputs a pair of motor neurons that operate the crayfish's escape reflex, a rapid contraction of abdominal muscles causing the tail to fan the water resulting in a fast backward motion.

These afferents carry action potentials, or spikes, stimulated by water motions to the ganglion. Embedded in the ganglion and postsynaptic to the sensory afferents are a pair of bilaterly symmetric caudal photoreceptor (CPR) neurons (WILKENS 1988). The transduction of a weak hydrodynamic signal is mediated by the light intensity falling on the CPRs.

2.1 Demonstration of SR in Crayfish Mechanoreceptor and Cricket Cercal Systems

In our experiment, the tailfan was excised and mounted in an apparatus such that periodic water motions of 10 to 150 μm in amplitude and 5 to 15 Hz frequency could be applied. Receptors that were relatively free of internal noise were selected. Recordings were made on the sensory root as shown in Figure 2*B*. The amplitude of the periodic stimulus was reduced until just barely visible in the power spectrum of the recording. Noise in the form of random hydrodynamic motions could be added to the periodic stimulus. The SNRs within the sensory afferent neurons were determined from recordings of

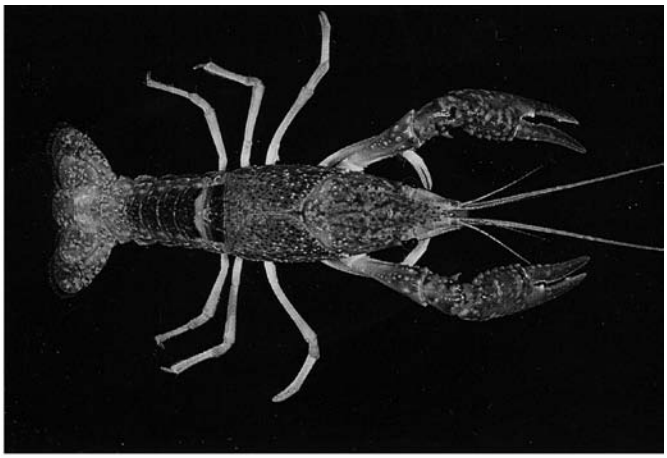

A

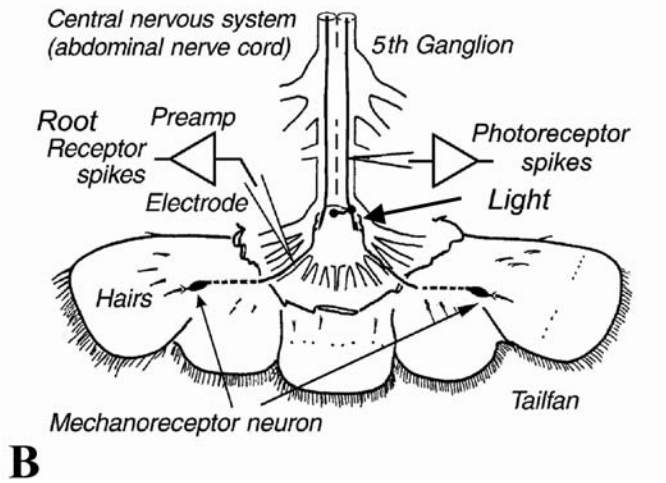

B

Fig. 2 (*A*) The common red swamp crayfish *Procambarus clarkii* reproduced from the *Missouri Conservationist* with permission from the Missouri Department of Conservation. Our interest focuses on the tailfan at left and the 6th or caudal ganglion that lies just beneath the carapace near the last segmentation to the left. The tailfan is covered with approximately 250 hydrodynamically sensitive hairs about 10 by 100 microns in size. Each is connected to a pair of sensory afferents that converge on the interneurons of the 6th ganglion. (*B*) A diagram of the tailfan, hairs, afferents, ganglion and the two embedded caudal photoreceptor neurons. Amplifiers and extracellular recording electrodes are shown positioned on a root sensory afferent (*left*) and on the output of a photoreceptor. The spread tailfans of the crayfish used in these experiments, *Procambarus clarkii*, are typically 3 to 5 cm laterally at the widest.

the spike train as discussed in Section 1. SNRs were measured for various added noise intensities. The results of the crayfish experiment are shown in Figure 3 by the open triangles. The diamonds are the results of an analog simulation of a FitzHugh-Nagumo (FN) model neuron (Moss et al. 1993). The FN model is not a non-dynamical system, but it does have a threshold. Instead it is called excitable. When the threshold is crossed, the system undergoes a Hopf bifurcation and executes one or more cycles. These represent the action potentials, or spikes, of the actual neuron. The fundamental threshold dynamics of a generic excitable system were studied in WIESENFELD et al. (1994). We shall meet the FN model again in Section 3.3 below.

The SR experiment was repeated with a different animal, a cricket, which is a member of the same phylum (Arthropoda) but adapted for living on land and immersed in air instead of water (LEVIN and MILLER 1996). The cricket has a mechanosensory system quite similar in architecture to the crayfish, except its system is optimized to detect periodic air motions in the range 100–140 Hz. These are the signatures of the cricket's main predators, flying wasps and birds, whose approaches induce motions in a set of hairs spread over two appendages posterior to the body of the cricket. Like the crayfish's,

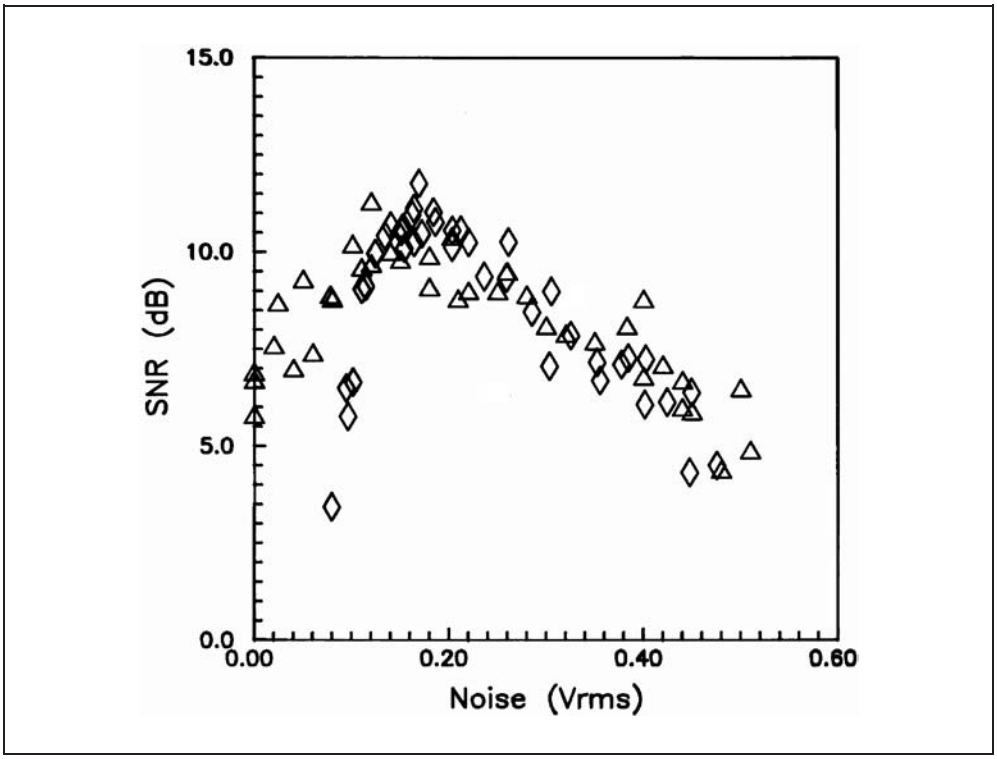

Fig. 3 The SNR in decibels *versus* noise intensity (measured in V-rms as an input to the hydrodynamic motion transducer). The triangles shown the crayfish data and the diamonds shown the results of a noisy Fitz-Hugh-Nagumo simulation. The optimal noise voltage is approximately 0.18 V-rms.

these hairs are innervated by sensory afferents that converge on a ganglion. An escape reflex can also be triggered in the cricket by some combination of air movements. There are no photoreceptors in the cricket ganglion, however.

LEVIN and MILLER's experiment beautifully demonstrated SR in the cricket mechanosensory system (the cercal system). Moreover, they were the first to use a modern information measure, the Shannon transinformation, computed between the responses of the sensory afferents and the air motions to which the tail appendages were subject.

2.2 Postsynaptic SR in the Caudal Photoreceptor and Frog Auditory Neurons

As Figure 2*B* shows the sensory afferents that innervate the hairs converge on and are synaptically connected to a set of some 250 interneurons in the 6th ganglion. Embedded within the ganglion is a pair of bilaterally symmetric caudal photoreceptor neurons (CPRs). The CPRs send, and possibly receive, signals from the 6th ganglion to the higher nervous system. In addition, the 6th ganglion outputs two motor neurons that excite abdominal contractions under certain conditions. The stereotypical contractions lead to the animal swimming backwards at a high speed, a reflexive motion used for escape from approaching predators. In several experiments in this laboratory, it was demonstrated that the light intensity falling on the CPR mediates the transduction efficiency by which the CPRs send mechanosensory signals to the higher nervous system (PEI et al. 1996). Essentially the same experiments described in Section 2.1 above were repeated, except that recordings were made from the CPR outputs in dark and for various levels of light intensity falling on the CPR. The recording site is shown on the right in Figure 2*B*. It was observed that for weak hydrodynamic signals the SNR at the CPR outputs could be enhanced by factors approaching 10 by light in the visible range of wavelengths and for intensities approximating dim room light. These results have since been replicated in additional experiments (BAHAR et al. 2002, BAHAR and MOSS 2003).

They bring us to the question of function. Why does the presence of light enhance the hydrodynamic mechanical signal leaving the ganglion? We can only speculate. The crayfish is primarily a nocturnal animal preferring to stay inside its burrow during daylight hours. It nevertheless does sometimes leave the burrow to forage in the daylight. At such times it is subject to predation by visually hunting fish. So its prospects for survival will be improved if its mechanosensory system is at high sensitivity relative to noise. Thus the "early warning system" is switched on when the crayfish is out in the light. And equally important for survival, the system should be shut down when the animal is safely inside its burrow in the dark. Why? Recall the noise. The sensory afferents in the root send remarkably noisy signals to the ganglion. We look at the ganglion as a statistical calculator. Some combination of signal, noise and light results in the escape reflex being fired with some probability. To enhance survivability, that probability should be very small when the animal is safely within its burrow.

Even though in this Section, we have considered postsynaptic signal processing, the recordings were obtained from single units. This will remain true for the next section on the human median nerve, though the noise is internal and mediates the response of a multi unit organ. We are working our way toward network applications wherein the noise originates within each element, as will be described in Section 3.

2.3 SR in the Human Nerves

The median nerve of the human body carries both sensory and motor neurons down the arms to activate and innervate tactile senses in the hands and fingers. Using standard electromyography (EMG), an SR experiment was performed by transcutaneous electrical stimulation of this nerve at the upper forearm while recording action potentials transmitted along the nerve with surface electrodes on the thumb and second digit of the right hand. There is a threshold for the transmission and detection of the action potentials. Moreover, the system is noisy because of the random firings of the neurons, especially the motor neurons. The noise intensity of the latter could be controlled by subject applied tension in the muscle of the thumb. Thus this was the first biological SR experiment wherein internal noise was generated and controlled (CHIOU-TAN et al. 1996).

In the experiment, a stimulating pulse was applied, received and recorded. With the thumb muscle relaxed, the amplitude of the stimulus was reduced until it vanished beneath the threshold as observed with the detecting EMG machine. The internal noise, the random background motor neuron firing rate, was then adjusted to one of three levels corresponding to three forces exerted by the subject with the thumb pressing against a force gage. The noise intensity (root mean square value) and its density (histogram of amplitudes) were measured with a second EMG machine. Thus the three ingredients necessary for SR were realized. The experiment was successful in that noise enhanced SNRs of the transmitted sensory nerve action potentials were observed at the thumb and digit electrodes. No enhancement was observed for pulses transmitted through the motor neurons. Moreover, the characteristic decrease in SNR at high noise intensities was not observed, possibly because subjects were unable to generate large enough noise intensities through thumb muscle tension. Follow-up studies showed that tension in a remote muscle could also enhance transmission of impulses by the sensory neurons of the median nerve (CHIOU-TAN et al. 1997) even when the locations of the muscles (upper limbs) and the stimulus and recording electrodes (distal leg to lateral ankle through the sural nerve) were interrupted by complete paraplegia (TRAN et al. 2000). These experiments point to the possibility that SR may developed as a useful tool in medical science (GLANZ 1997).

3. Spatiotemporal Stochastic Resonance

Certainly some of the previously cited experiments are evidence of SR in distributed systems. These systems can be represented by networks of noisy elements coupled according to some scheme (JUNG et al. 1992). Perhaps the simplest realization is a network of threshold detectors. The detectors were coupled with exponentially decreasing strength with distance away from an exciting element. Each element was provided with its own independent noise source, but all noise sources had the same intensity. The noise intensity (of the network) was a control parameter. Each element fired a pulse when its threshold was crossed with the pulse being transmitted to neighbors according to the aforementioned exponential rule. After firing the threshold element was refractory for a period of time. Noise enhanced propagation of coherent structures in this simple system

was observed, with an optimal noise corresponding to a maximum in some measure of coherence in the network (JUNG and MAYER-KRESS 1995 a, b). These results represented the first demonstrations of spatiotemporal stochastic resonance (STSR).

3.1 Experimental Realization of STSR in the Belozov-Zhabotinsky Chemical Reaction

An elegant experimental demonstration of STSR has been provided by SHOWALTER and his colleagues using the Belousov-Zhabotinsky (BZ) chemical reaction (KÁDÁR et al. 1998). Noise enhancement and optimization can take many forms in STSR. In this experiment the distance of propagation of a subthreshold signal in a noisy excitable medium was observed.

The classical BZ reaction was modified to include a light sensitive reactant. In essence the threshold for propagation of an excitation could be controlled by light intensity. The reaction was confined to an approximately two-dimensional gel. The medium was divided into a superexcitable region where a propagating wave front was generated. The wave front then entered a subexcitable region where it quickly died out, that is, it was able to propagate only a short distance as shown in Figure 4 *A*. The subexcitable region was then exposed to spatiotemporal noise. This noise was accomplished by dividing the medium up into many small cells, each of which was exposed to light with temporally random intensity (see Fig. 4 *E*). The light intensity in each cell was statistically independent of the intensities in all other cells, but the mean intensity – the control parameter – was the same for all cells. Increasing the noise from zero first enhances the propagation distance for the coherent waves, then causes a loss of coherence as the waves break up at higher noise (see Fig. 4 *B–D*).

3.2 Noise Enhanced Propagation of Spatiotemporal Waves in a FitzHugh-Nagumo Network

This system can be modeled in a number of ways. KÁDÁR et al. (1998) used a BZ model called the Oregonator (FIELD and NOYES 1974) modified to include the photosensitive reactant. JUNG and MAYER-KRESS also demonstrated noise enhanced propagation distance in their network of simple threshold elements. But we are leading to discuss STSR in biological systems. A more biologically relevant model is a network of FitzHugh-Nagumo model neurons (BALÁZSI 2001) defined by

$$\varepsilon \frac{dv}{dt} = v(0.5 - v)\,(v - 1) - w + D\nabla^2 v \qquad [4]$$

$$\frac{dw}{dt} = v - w - b, \qquad [5]$$

where v is the fast and w the slow variable respectively. The difference in time scales is determined by ε and is typically a factor of 500. The slow, or recovery, Equation [5] insures that the system is refractory for a time the order of ε. The system must be refractory in order for coherent structures to propagate. The excitability parameter is b, which has a critical value, $b_{crit} = 0.26$. For $b > b_{crit}$ coherent structures can propagate for inde-

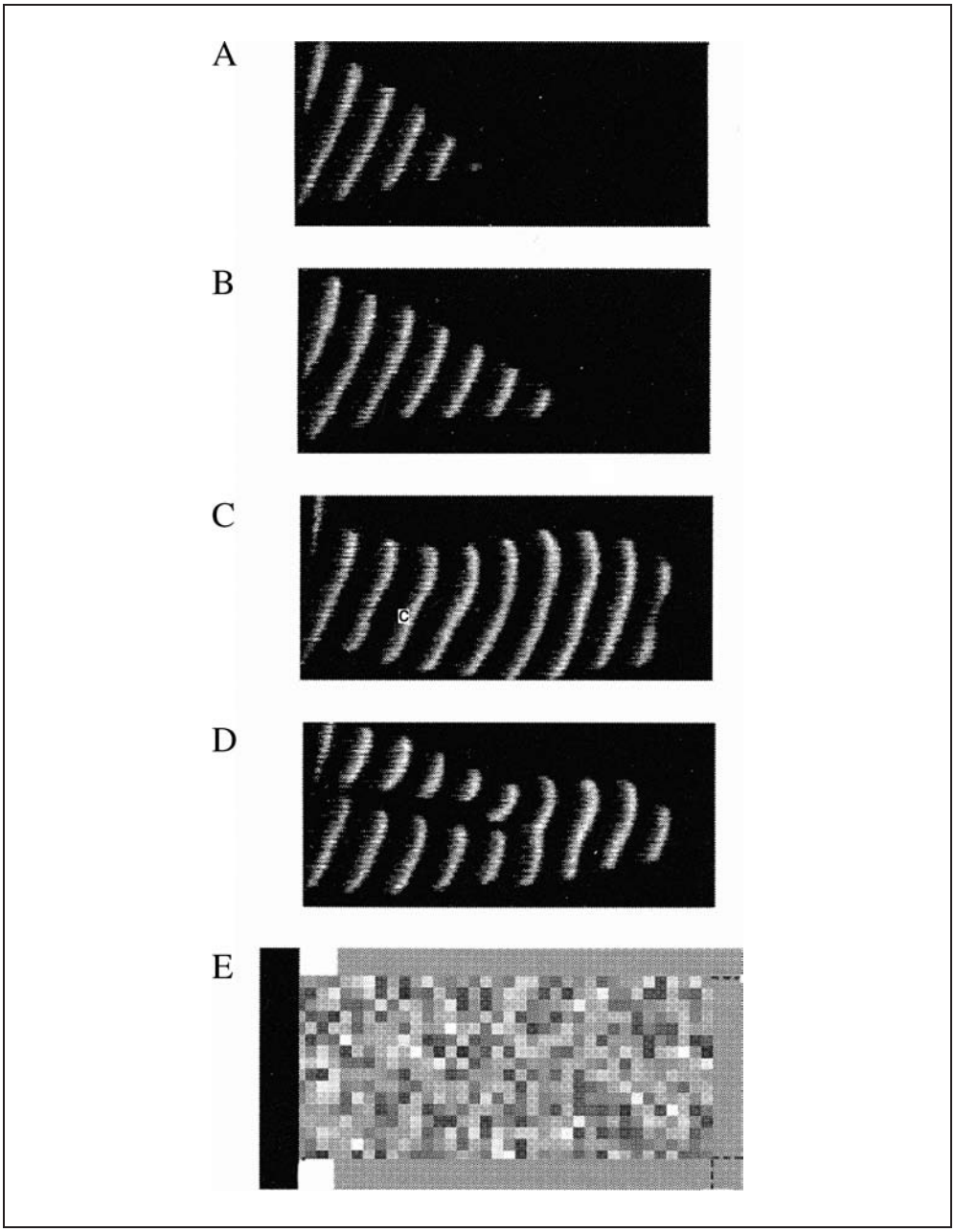

Fig. 4 Spatiotemporal stochastic resonance (STSR) in the Belousov-Zhabotinsky reaction. Mean spatiotemporal noise intensity increases from top to bottom: (*A*) zero, (*B*) 0.3, (*C*) 0.6, and (*D*) 1.0 in normalized units; (*E*) shows a snap-shot picture of the grid of cells with various light intensities. The uniformly grey area on the left identifies the excitable region. Waves are generated in the excitable region and propagate into the sub excitable region on the right. Optimal noise intensity maximizes the coherence and propagation length as shown in *C*. Reproduced with permission from KÁDÁR et al. (1998).

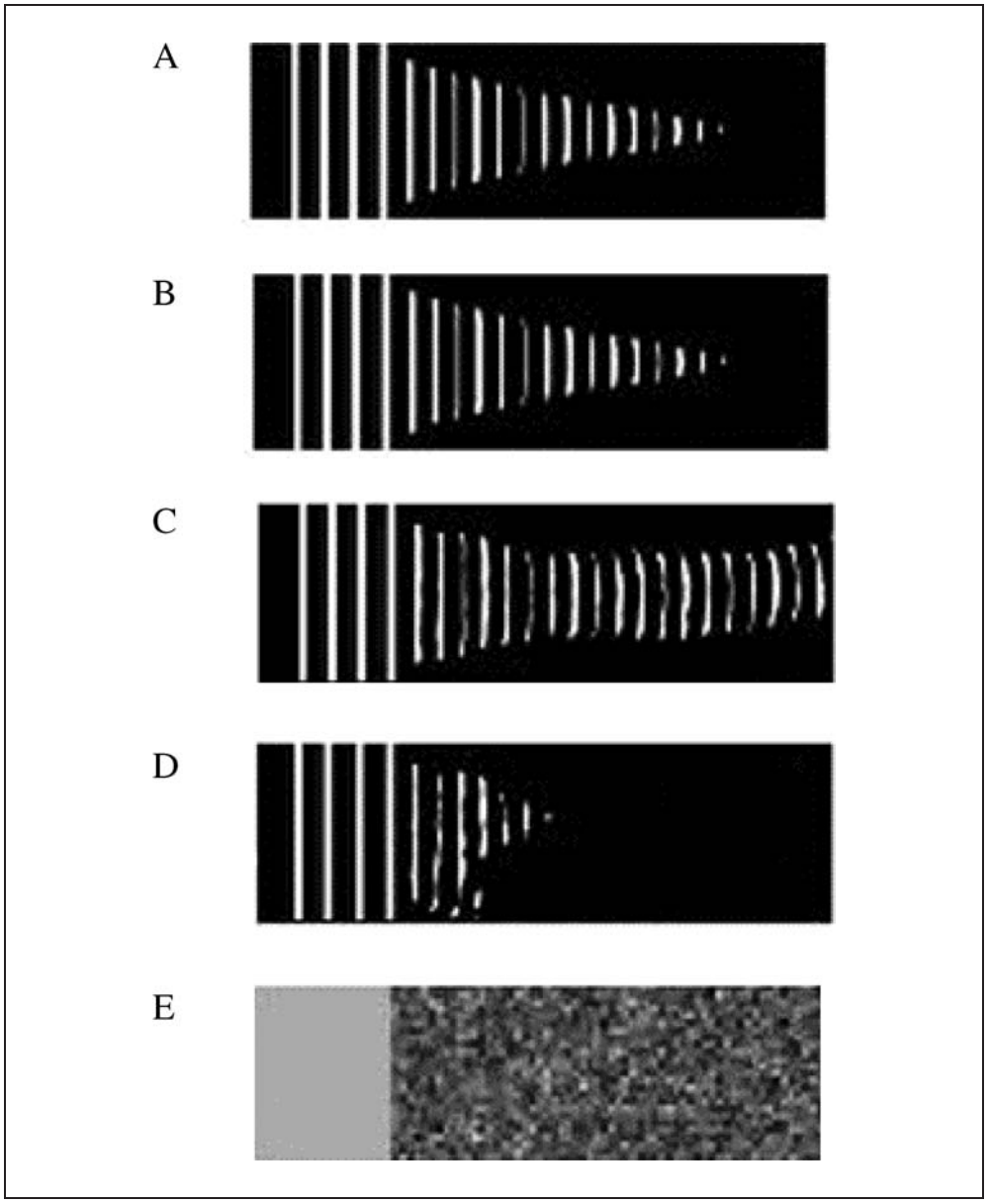

Fig. 5 Spatiotemporal Stochastic Resonance in a network of noisy FitzHugh-Nagumo model neurons. Noise increases top-to-bottom, *A–D*. The sub excitable region ($b = 0.197$) containing the grid of cells with noises is shown in *E* on the right (speckled area), and the excitable region (uniform grey area, $b = 0.245$) is on the left. The panel *E* is in registry with the panels above. Note that in *B–D* waves generated in the excitable region on the left propagate unattenuated into the sub-excitable region on the right. (*A*) No added noise; waves propagate into the sub-excitable region for a distance then die. (*B*) Small noise; waves propagate further. (*C*) Large noise, waves propagate indefinitely (continue to infinity). (*D*) Very large noise, waves again die out after propagating a short distance.

finite lengths in the medium, whereas for $b < b_{crit}$, they die after propagating a finite length. Thus this system also is characterized by a threshold; in this case it is a threshold for propagation of coherent structures. A two dimensional realization of Equations [4] and [5], computed with spatiotemporal noise on a grid similar to that of Figure 4 *E* generates propagating waves and demonstrates STSR in a manner similar to the two-dimensional, light sensitive BZ reaction (BALÁZSI 2001, BALÁZSI et al. 2001) (see Fig. 5).

BALÁZSI has made a detailed study of the noise mediated length of propagation of coherent structures in the FN system. The results are shown in Figure 6 *A*. Moreover, he found that the propagation velocity is also maximized at the optimal noise intensity, as shown in Figure 6 *B*. The latter is an interesting finding, since cognitive processes (in the brain, for example) leading to conscious states must depend not only on the length over which information can propagate, but also the speed of propagation.

When FN system is operated under similar conditions, but starting with somewhat different initial conditions (a straight line initial excitation with truncated ends), the excitable FN medium is capable of generating spiral waves (not shown here). The spirals are nucleated at the truncated ends. Such waves are important in biological applications as we mention in the following section.

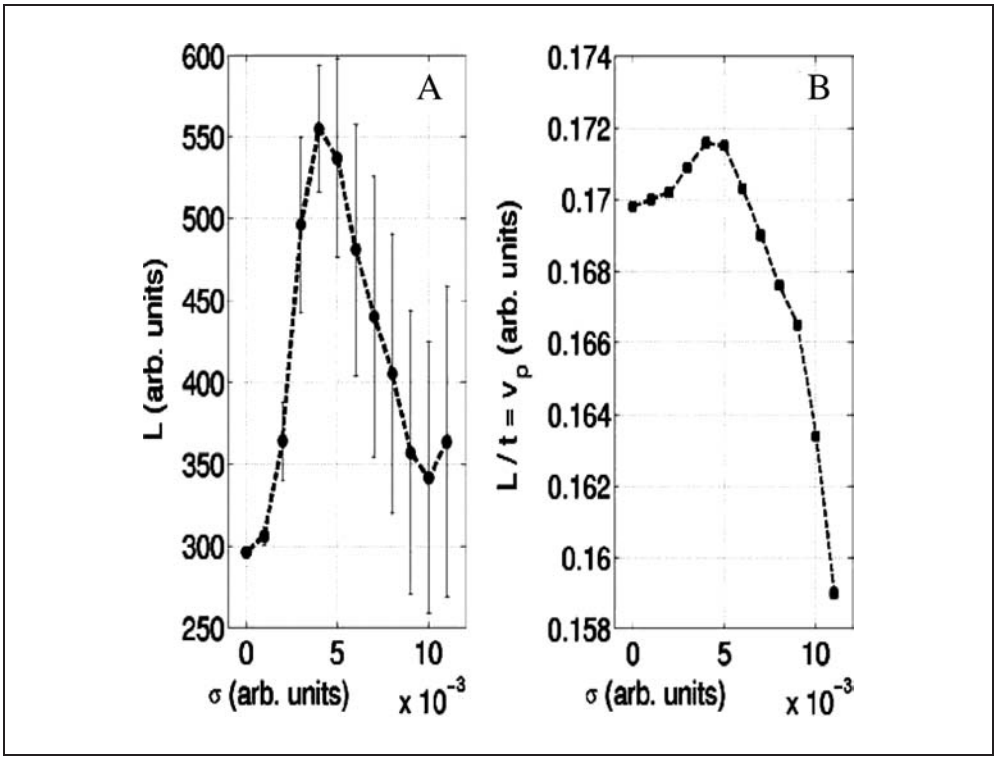

Fig. 6 Noise optimized propagation length and velocity in the FN system. (*A*) Length *versus* noise intensity (the standard deviation, σ, of the Gaussian noise placed in each cell). Error bars are standard deviations based on 40 trials. (*B*) Velocity *versus* noise intensity. For both panels, the excitability parameter was $b = 0.20$ in the sub excitable, noise mediated region.

3.3 Noise Mediated Ca^{++} Waves in Glial Cell Networks

It has been demonstrated that noisy spiral waves can be nucleated spontaneously, propagate a finite distance, then lose coherence and die in the noise in a network of cultured human glial cells (JUNG et al. 1998 b, SHUAI and JUNG 2003, this volume). The noise (and probably also the coupling strength) is determined by the kainate concentration in the perfusion wherein the network has been grown. There is an optimal noise (optimal kainate concentration) that maximizes the coherence, lifetime and propagation distance of the waves. Thus this system demonstrates STSR. An example is shown in Figure 7 where a coherent wave of the doubly ionized calcium ion (Ca^{2+}) is first nucleated spontaneously, lives and grows in size and coherence, then finally loses coherence and dies in the noise. Glial cells – in the human brain they are specifically called astrocytes – are the structure upon which the neurons in the brain live. They are thought to maintain the correct chemical environment for proper functioning of the neural network. However, more recently it has been shown that waves of Ca^{2+} can propagate in networks of glia alone, raising the possibility that they can mediate long distance information flow across the network of neurons.

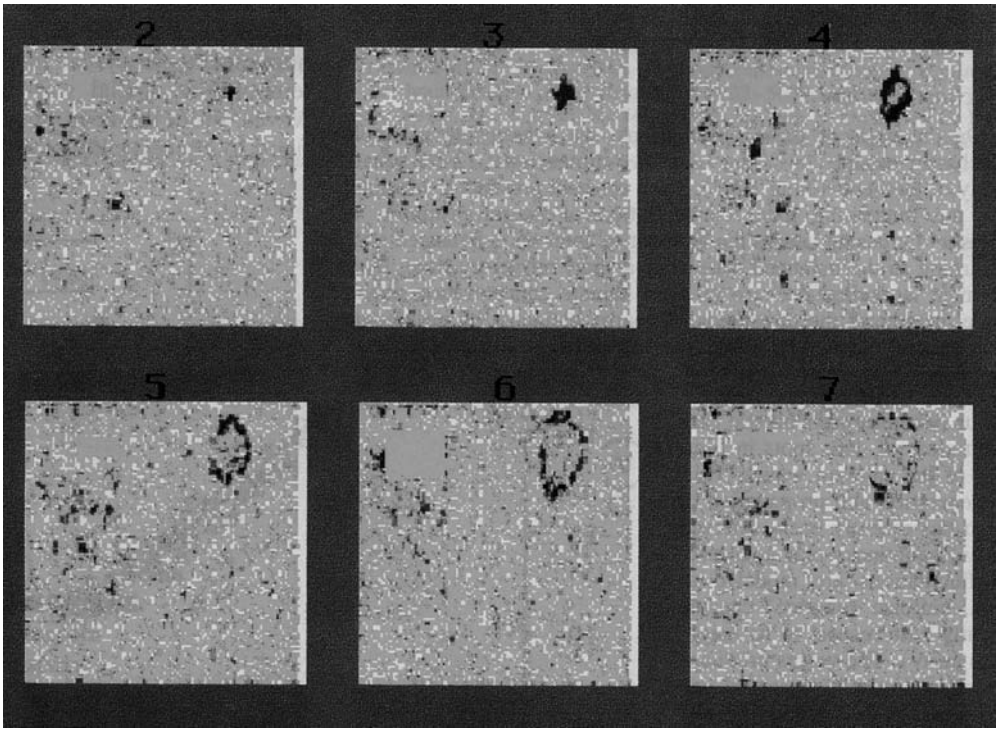

Fig. 7 A propagating spiral wave in a noise mediated network of cultured human glial cells. Snapshot pictures (1 s intervals) of a Ca^{2+} spiral wave nucleated spontaneously by the noise in the upper left panel. Time advances from upper left to lower right. The wave propagates (grows in size and coherence) only to finally die in the noise. The lower right panel shows the dying wave with much degraded coherence. The darker shading indicates a higher concentration of Ca^{2+} ions. The concentration within the perfusion was kainate 50 mM.

Further it has been recently shown that healthy cells cultured from healthy specimens (rat brain) show a kind of disorder that lacks characteristic time and length scales (JUNG et al. 1998 a). The disorder is manifest as a power law distribution of a spatiotemporal coherence measure applied to spontaneously generated structures similar to the one shown in Figure 7. This behavior can be contrasted with that of cultures of cells taken from human epileptic patients during surgery. These often show anomalous oscillations with noisy but definable (in the mean) characteristic time and length scales. Thus in these cultures, the measure of disorder breaks down, a process that has been identified as a signature of epilepsy (BALÁZSI 2001, BALÁZSI et al. 2003).

The results of the BZ chemical experiments and the experiments with cultured cells, together with various simulations, have been reviewed recently (JUNG et al. 1998 a). Such experiments and simulations with noisy networks inevitably lead to questions of information processing, perception and consciousness in the human and animal brain. We briefly touch upon these topics in the next section.

4. Human Perception and Animal Behavior

Of course, the observation of SR in single elements in the peripheral nervous system raises an immediate question: Is the animal *aware* of the enhanced information in its sensory system? In humans, this question can be answered with psychophysics experiments, and there have been a number of them. In animals, the question can only be answered with behavioral experiments. In this section we very briefly review the current literature on these studies.

4.1 Noise Enhanced Perception: Visual, Auditory and Tactile

An experiment on human perception of SR was reported a few years ago wherein subjects observed noisy images on a computer screen (SIMONOTTO et al. 1997). The images, on a 256 grey scale were suppressed below a threshold level. With added noise in each pixel the threshold was crossed with some probability, and that pixel was painted black when its threshold was crossed. The noise in each pixel was dynamical (time dependent) and uncorrelated with that of all other pixels. The information flow in this system has been analyzed (FREUND 2001). The optimum noise intensity (about half the threshold value) resulted in the best perceptive performance by the subjects. Though all subjects showed approximately the same optimal noise intensity, surprisingly, their sensitivity to fine detail in the image was quite different from one subject to the next. This variability was reproducible with the same subject showing the same sensitivity ($\pm 20\,\%$) for the same test repeated even after one year. Later fMRI experiments using a similar visual protocol showed that active brain volume in the visual cortex was the maximum at the optimal noise intensity (SIMONOTTO et al. 1999).

A recent set of carefully performed psychophysics experiments have revealed SR in the human visual and auditory systems (WARD et al. 2001). In contrast to the aforementioned experiments where the threshold was already built into the image, these experiments made use of well known inherent visual and auditory thresholds. The former used

the perceptive threshold of a 3 Hz beat note obtained by two slightly detuned 1 KHz tones. The latter employed the visual contrast threshold. The SR effect is small but statistically significant in human hearing and vision. A previous experiment using the absolute hearing threshold found an approximately 3 dB effect (ZENG et al. 2000).

Another set of psychophysics experiments involved the human tactile sense (COLLINS et al. 1996 a, 1997). In this experiment an indenter applied a momentary mechanical pressure to the skin of an index finger. The indenter could also be actuated with either mechanical or electrical noise. Thus SR could be studied with signal and noise introduced *via* different modalities. Similar experiments were previously performed on a rat cutaneous mechanoreceptor (COLLINS et al. 1996 b).

4.2 Behavioral SR: Environmental Noise at the Edge of Perception

We finally turn our attention to animal behavior. Does the animal know that there exists noise enhanced information in its peripheral nervous system? The question can only be answered with a behavioral experiment. To study this question, a unique fish with a passive electrosense was chosen. The paddlefish, *Polyodon spathula*, is a primitive creature that detects tracks and catches its prey by means of an array of electroreceptors spread over a unique anterior appendage called the rostrum (see Fig. 8). Throughout its entire life the fish feeds exclusively on plankton (1 to 2 mm) which it detects by means of the weak electric field emitted by their feeding and swimming motions (WILKENS et al. 1997).

Can the detectability of the weak electric field signatures of the plankton be enhanced by electrical noise added to the environment? In particular in the presence of noise can the fish detect and capture plankton that is further away from its rostrum than it could in

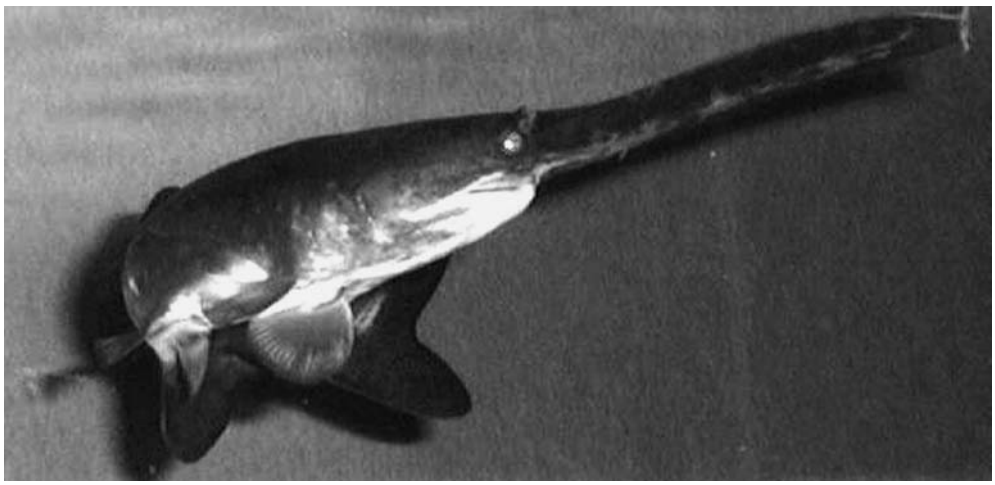

Fig. 8 A juvenile paddlefish *Polyodon spathula.* The fish is about 14 cm long and is less than one year old. The rostrum on the anterior is an electro sensitive detector of planktonic prey.

the absence of noise? The answer to these questions is affirmative. Though the noise induced behavioral effects are small, they are, nevertheless, measurable with quantifiable statistical accuracy (RUSSELL et al. 1999). Juvenile paddlefish were placed in a swim mill and the water stream flowing past them was seeded with *Daphnia* zooplankton. The capture probability distributions were measured in the presence of electric field noise of various strengths and, as controls, in the absence of noise. The capture distributions were observed to widen slightly at the optimal noise intensity. For large noise the feeding rate decreased. The Fisher information at the rostrum due to the plankton signal has been calculated and found to follow the measured capture distribution (GREENWOOD et al. 2000). In the wild it may be that the electrical noise is produced by a swarm of zooplankton. An SR theory based on the threshold model and including modern information measures using the swarm model has recently been published (FREUND et al. 2002, see also FREUND 2003, this volume).

5. Prospects

Does SR endow animals with an evolutionary advantage? This must be one of the most significant research questions that can be addressed, and it presents researchers with a substantial challenge. One can muse and speculate that the evolution of most sensory systems is indeed driven by naturally occurring stimuli (either predator or prey) at the threshold of perception. Otherwise, what has driven some animals to evolve truly remarkable sensory sensitivities? These include the electric field sensitivities, 0.5 to 1 μV/cm for our paddlefish (RUSSELL et al. 1999) and other freshwater passively electrosensitive fish, 1–10 nV/cm for sharks and rays (KALMIJN 2000), 10's of nm water displacements detectable by crayfish (DOUGLASS et al. 1993), 10's of nm vibrational amplitudes detectable by some frogs, etc. (BARTH and SCHMID 2001). For that matter, what was the evolutionary driver for the paddlefish's long anterior rostrum shown in Figure 8 if not the continual competition to detect evermore distant plankton (by sensing ever weaker signals)? If we grant this, and admit that noise is ubiquitous in the natural environment, then the ingredients required for SR were present probably since life began on this planet. Indeed, it has been suggested that SR may have played a role in prebiotic evolution as well (CARERI 2000).

But the only experiment that connects SR directly to evolution was designed and carried out by JARAMILLO and WIESENFELD (1998). They studied bundles of cilia in the inner ear of leopard frogs. They simultaneously measured the neural response while manipulating the mechanical motion of the bundle. They performed an SR experiment by moving the cilia with a near sub-threshold periodic signal to which was added varying amounts of mechanical noise. They found that the optimal noise quantified by its root-mean-square displacement corresponded (±20%) to the *natural* Brownian motion of the cilia bundle. It would seem virtually impossible that this correspondence could have arisen simply by chance. What it almost certainly means is that the frog auditory system evolved to make use of SR at the threshold of detectability.

We can be certain that in the future other bright scientists will devise ways of testing hypotheses based on evolution and SR.

References

Anishchenko, V., Moss, F., Neiman, A., and Schimansky-Geier, L.: Stochastic resonance: noise induced order. Uspekhi Fizicheskih Nauk *169*, 7–38 (1999); Sov. Phys. Usp. *42*(1), 7–36 (1999)

Bahar, S., and Moss, F.: Stochastic phase synchronization and sensory encoding: the crayfish mechanoreceptor/photoreceptor system. Chaos *13*, 138–144 (2003)

Bahar, S., Neiman, A., Wilkens, L. A., and Moss, F.: Phase synchronization and stochastic resonance effects in the crayfish caudal photoreceptor. Phys. Rev. E Rapid *65*, 05090 (2002)

Balázsi, G.: Spatio-Temporal Dynamics of Noisy Excitable Systems: Application to Cultured Human Glial Cell Networks. Ph. D. Diss. Univ. of Missouri 2001

Balázsi, G., Cornell-Bell, A., and Moss, F.: Increased phase synchronization of spontaneous calcium oscillations in epileptic human versus normal rat astrocyte cultures. Chaos *13*, 515–522 (2003)

Balázsi, G., Kish, L. B., and Moss, F.: Spatiotemporal stochastic resonance and its consequences in neural model systems. Chaos *11*, 563–569 (2001)

Barth, F., and Schmid, A. (Eds.): The Ecology of Sensing. Heidelberg, Berlin: Springer 2001

Benzi, R., Parisi, G., Sutera, S., and Vulpiani, A.: Stochastic resonance in climatic change. Tellus *34*, 10–16 (1982)

Benzi, R., Sutera, A., and Vulpiani, A.: The mechanism of stochastic resonance. J. Phys. A *14*, L453–L457 (1981)

Bezrukov, S. M., and Vodyanoy, I.: Noise-induced enhancement of signal transduction across voltage-dependent ion channels. Nature *378*, 362–364 (1995)

Bezrukov, S. M., and Vodyanoy, I.: Stochastic resonance in non-dynamical systems without response thresholds. Nature *385*, 319–321 (1997)

Busch, H., Hütt, M.-T., and Kaiser, F.: Effect of colored noise on networks of nonlinear oscillators. Phys. Rev. E *64*, 021105 (2001)

Careri, G.: Prebiotic selection induced by periodic starlight. In: Chela-Flores, J., et al. (Eds.): The First Steps of Life in the Universe, ICTP. Trieste, Italy: September 2000: Amsterdam: Kluwer (2003, in press)

Chiou-Tan, F. Y., Magee, K., Robinson, L., Nelson, M., Tuel, S., Krouskop, T., and Moss, F.: Enhancement of subthreshold sensory nerve action potentials during muscle tension mediated noise. Int. J. Bifurc. and Chaos *6*, 1389–1396 (1996)

Chiou-Tan, F., Magee, K., Robinson, L. R., Nelson, M. R., Tuel, S. S., Krouskop, A., and Moss, F.: Augmented sensory nerve action potentials during distant muscle contraction. Amer. J. Phys. Med. Rehabil. *76*, 14–18 (1997)

Chuang, T.-Y., Robinson, L. R., Nelson, M. R., Moss, F., and Chiou-Tan, F.: Effect of isometric contraction on threshold somatosensory evoked potentials. Amer. J. Phys. Med. Rehabil. *78*, 2–6 (1999)

Collins, J. J., Imhoff, T. T., and Grigg, P.: Noise-enhanced tactile sensation. Nature *383*, 770–771 (1996 a)

Collins, J. J., Imhoff, T. T., and Grigg, P.: Noise-enhanced information transmission in rat SA1 cutaneous mechanoreceptors via aperiodic stochastic resonance. J. Neurophysiol. *76*, 642–645 (1996 b)

Collins, J. J., Imhoff, T. T., and Grigg, P.: Noise-mediated enhancements and decrements in human tactile sensation. Phys. Rev. E *56*, 923–926 (1997)

Cordo, P., Inglis, T., Verschueren, S., Collins, J., Merfeld, D., Rosenblum, S., Buckley, S., and Moss, F.: Noise in human muscle spindles. Nature *383*, 769–770 (1996)

Douglass, J. K., Wilkens, L., Pantazelou, E., and Moss, F.: Noise enhancement of information transfer in crayfish mechanoreceptors by stochastic resonance. Nature *365*, 337–340 (1993)

Field, R. J., and Noyes, R. M.: Oscillations in chemical systems IV. Limit cycle behavior in a model of a real chemical reaction. J. Chem. Phys. *60*, 1877–1884 (1974)

Fisher, R. A.: The Design of Experiments. 5th ed. Edinburgh: Oliver & Boyd 1949

Freund, J. A.: Stochastic resonance with images and spatially correlated stochastic patterns. In: Freund, J. A., and Poeschel, T. (Eds.): Stochastic Processes in Physics, Chemistry and Biology, Lecture Notes in Physics; pp. 160–171. Berlin: Springer 2001

Freund, J. A.: Behavioral stochastic resonance: modelling and theory. In: Beck, F., Hütt, M.-T., and Lüttge, U. (Eds.): Nonlinear Dynamics and the Spatiotemporal Principles of Biology. Nova Acta Leopoldina NF Bd. *88*, Nr. 332, 105–127 (2003)

Freund, J., Schimansky-Geier, L., Beisner, B., Neiman, A., Russell, D., Yakusheva, T., and Moss, F.:

Behavioral stochastic resonance: How the noise from a *Daphnia* swarm enhances individual prey capture by juvenile paddlefish. J. Theor. Biol. *214*, 71–83 (2002)

GAMMAITONI, L., HÄNGGI, P., JUNG, P., and MARCHESONI, F.: Stochastic resonance. Rev. Mod. Phys. *70*, 223–288 (1998)

GINGL, Z., KISS, L. B., and MOSS, F.: Non-dynamical stochastic resonance: theory and experiments with white and arbitrarily coloured noise. Europhys. Lett. *29*, 191–196 (1995)

GLANZ, J.: Sharpening the senses with neural 'noise'. Science *277*, 1759 (1997)

GOYCHUK, I., and HÄNGGI, P.: Stochastic resonance in ion channels characterized by information theory. Phys. Rev. E *61*, 4272–4284 (2000)

GREENWOOD, P. E., WARD, L. M., RUSSELL, D. F., NEIMAN, A., and MOSS, F.: Stochastic resonance enhances the electrosensory information available to paddlefish for prey capture. Phys. Rev. Lett. *84*, 4773–4776 (2000)

HIDAKA, I., NOZAKI, D., and YAMAMOTO, Y.: Functional stochastic resonance in the human brain: Noise induced sensitization of baroreflex system. Phys. Rev. Lett. *85*, 3740–3743 (2000)

HÜTT, M.-T., NEFF, R., BUSCH, H., and KAISER, F.: Method for detecting the signature of noise-induced structures in spatiotemporal data sets. Phys. Rev. E *66*, 026117 (2002)

HUXLEY, T. H.: The Crayfish. An Introduction to the Study of Zoology. New York: Appleton 1880

JARAMILLO, F., and WIESENFELD, K.: Mechanoelectrical transduction assisted by Brownian motion: a role for noise in the auditory system. Nature Neurosci. *1*, 384–388 (1998)

JUNG, P.: Periodically driven stochastic systems. Phys. Rep. *234*, 175–295 (1993)

JUNG, P., BEHN, U., PANTAZELOU, E., and MOSS, F.: Collective response in globally coupled bistable systems. Phys. Rev. A Rapid Comm. *46*, R1709–R1713 (1992)

JUNG, P., CORNELL-BELL, A., MADDEN, K., and MOSS, F.: Noise induced spiral waves in astrocyte syncytia show evidence of self organized criticality. J. Neurophysiol. *79*, 1098–1101 (1998 b)

JUNG, P., CORNELL-BELL, A., MOSS, F., KADAR, S., WANG, J., and SHOWALTER, K.: Noise sustained waves in subexcitable media: from chemical waves to brain waves. Chaos *8*, 567–575 (1998 a)

JUNG, P., and HÄNGGI, P.: Stochastic nonlinear dynamics modulated by external periodic forces. Europhys. Lett. *8*, 505–509 (1989)

JUNG, P., and MAYER-KRESS, G.: Spatio-temporal stochastic resonance in excitable media. Phys. Rev. Lett. *62*, 2682–2686 (1995 a)

JUNG, P., and MAYER-KRESS, G.: Noise controlled spiral growth in excitable media. Chaos *5*, 458–462 (1995 b)

KÁDÁR, S., WANG, J., and SHOWALTER, K.: Noise-supported traveling waves in sub-excitable media. Nature *391*, 770–772 (1998)

KALMIJN, A. J.: Detection and processing of electromagnetic and near-field acoustic signals in elasmobranch fishes. Phil. Trans. R. Soc. Lond. B *355*, 1135–1141 (2000)

LEVIN, J. E., and MILLER, J. P.: Broadband neural encoding in the cricket cercal sensory system enhanced by stochastic resonance. Nature *380*, 165–168 (1996)

LONGTIN, A., BULSARA, A., and MOSS, F.: Time-interval sequences in bistable systems and the noise-induced transmission of information by sensory neurons. Phys. Rev. Lett. *67*, 656–659 (1991)

MCNAMARA, B., and WIESENFELD, K.: Theory of stochastic resonance. Phys. Rev. A *39*, 4854–4866 (1989)

MCNAMARA, B., WIESENFELD, K., and ROY, R.: Observation of stochastic resonance in a ring laser. Phys. Rev. Lett. *60*, 2626–2630 (1988)

MORSE, R., and EVANS, E.: Enhancement of vowel coding for cochlear implants by addition of noise. Nature Med. *2*, 928–932 (1996)

MOSS, F.: Stochastic resonance: from the ice ages to the monkey's ear. In: WEISS, G. H. (Ed.): Contemporary Problems in Statistical Physics; pp. 205–253. Philadelphia: SIAM 1994

MOSS, F., DOUGLASS, J. K., WILKENS, L., PIERSON, D., and PANTAZELOU, E.: Stochastic resonance in an electronic FitzHugh-Nagumo Model. Ann. New York Acad. Sci. *706*, 26–41 (1993)

MOSS, F., PIERSON, D., and O'GORMAN, D.: Stochastic resonance: Tutorial and update. Int. J. Bifurc. and Chaos *6*, 1383–1397 (1994)

NICOLIS, C.: Stochastic aspects of climatic transitions – response to periodic forcing. Tellus *34*, 1–9 (1982)

PEI, X., WILKENS, L., and MOSS, F.: Light enhances hydrodynamic signaling in the multimodal caudal photoreceptor interneurons of the crayfish. J. Neurophysiol. *76*, 3002–3011 (1996)

PETRACCHI, D., PELLEGRINI, M., PELLEGRINO, M., BARBI, M., and MOSS, F.: Periodic forcing of a K^+ channel at various temperatures. Biophys. J. *66*, 1844–1852 (1994)

Russell, D., Wilkens, L., and Moss, F.: Use of behavioral stochastic resonance by paddlefish for feeding. Nature *402*, 219–223 (1999)

Shuai, J.-W., and Jung, P.: Statistical properties of Ca^{2+} puffs. In: Beck, F., Hütt, M.-T., and Lüttge, U. (Eds.): Nonlinear Dynamics and the Spatiotemporal Principles of Biology. Nova Acta Leopoldina NF Bd. *88*, Nr. 332, 151–167 (2003)

Simonotto, E., Riani, M., Seife, C., Roberts, M., Twitty, J., and Moss, F.: Visual perception of stochastic resonance. Phys. Rev. Lett. *78*, 1186–1189 (1997)

Simonotto, E., Spano, F., Riani, M., Ferrari, A., Levrero, F., Pillot, A., Renzetti, P., Parodi, R., Sardanelli, F., Vitali, P., Twitty, J., Chiou-Tan, F., and Moss, F.: fMRI studies of visual cortical activity during noise stimulation. Neurocomp. *26–27*, 511–516 (1999)

Stemmler, M.: A single spike suffices: the simple form of stochastic resonance in model neurons. Network: Comput. Neural Systems *7*, 687–716 (1996)

Suki, B., Alencar, A., Sujeer, M. K., Lutchen, K. R., Collins, J. J., Andrade, J. S., Ingenito, E. P., Zapperi, S., and Stanley, H. E.: Life-support system benefits from noise. Nature *393*, 127–128 (1998)

Tran, T. M. P., Moss, F., Robinson, L. R., and Chiou-Tan, F. Y.: Increased threshold sural amplitude after upper limb isometric contraction in complete paraplegics. Amer. J. Phys. Med. Rehabil. *79*, 542–546 (2000)

Ward, L. M.: The psychophysics of stochastic resonance. In: Killeen, P., and Tempe, A. Z. (Ed.): Fechner Day 99. International Society for Psychophysics; pp. 389–394. 1999

Ward, L. M., Desai, S., Rootman, D., Tata, M., and Moss, F.: Noise Can Help As Well As Hinder Seeing and Hearing. American Physical Society. Virtual Press Room selected paper http://www.aps.org/meet/MAR01/baps/vpr/layn23–002.html (March 2001)

Wiese, K., Calabrese, R. L., and Kennedy, D.: Integration of directional mechanosensory input by crayfish interneurons. J. Neurophysiol. *39*, 834–843 (1976)

Wiesenfeld, K., and Moss, F.: Stochastic resonance and the benefits of noise: from the ice ages to crayfish and SQUIDs. Nature *373*, 33–36 (1995)

Wiesenfeld, K., Pierson, D., Pantazelou, E., Dames, C., and Moss, F.: Stochastic resonance on a circle. Phys. Rev. Lett. *72*, 2125–2129 (1994)

Wilkens, L. A.: The crayfish caudal photoreceptor: Advances and questions after the first half century. Comp. Biochem. Physiol. *91*, 61–68 (1988)

Wilkens, L. A., Russell, D. F., Pei, X., and Gurgens, C.: The paddlefish rostrum functions as an electrosensory antenna in plankton feeding. Proc. R. Soc. Lond. B *264*, 1723–1729 (1997)

Zeng, F.-G., Fu, Q.-J., and Morse, R.: Human hearing enhanced by noise. Brain Res. *869*, 251–255 (2000)

Prof. Dr. Frank Moss
Dr. Gabor Balázsi
Center for Neurodynamics
University of Missouri at St. Louis
8001 Natural Bridge Road
St. Louis, MO 63121
USA
Phone: ++1 31 45 16 61 50
Fax: ++1 31 45 16 61 52
E-Mail: mossf@umsl.edu

Nonlinear Dynamics and Biology

Nova Acta Leopoldina NF *88*, Nr. 332, 79–86 (2003)

Nonlinear Dynamics and Biology (Comment)

STEFAN C. MÜLLER (Magdeburg)

With 1 Figure

Dynamics has become an interdisciplinary subject today. Initially it was a branch of physics: following LEIBNIZ' and NEWTON'S invention of differential equations and the solution of the two-body problem, many subsequent generations of mathematicians and physicists tried to use extended analytical methods to tackle more complicated tasks such as the three-body problem, which, as we know now, is non-integrable. A major breakthrough was achieved by POINCARÉ who developed a more qualitative way that was very powerful to treat systems for which the temporal evolution is governed by nonlinear rules. In this way nonlinear oscillators could be better understood and their successful application to technologies such as radio and lasers marked an important progress towards the field of nonlinear dynamics as it presents itself today. In fact, it was the availability of powerful computers from the 1950s on that made the experimentation with nonlinear equations possible. Through the pioneering discovery of chaotic motion on strange attractors by LORENZ, as well as from RUELLE and TAKENS theoretical work on the onset of turbulence in hydrodynamics we are now quite familiar with the complex behavior of nonlinear systems, e. g. the occurrence of oscillations, bistability, and deterministic chaos as introduced, for instance, by STROGATZ (1995) and thoroughly reviewed by CROSS and HOHENBERG (1993).

Biology is certainly one of the disciplines that deals with systems of a particularly high degree of complexity, starting with the life of a single cell and culminating in the fascinating structure and function of our brain. Nowadays the ideas and methods of nonlinear dynamics find rapidly increasing applications in biological systems of any hierarchic level of organization and many reviews on that topic are available (HESS 1997, GOLDBETER 1998). Since one of the prerequisites of living nature is their openness to exchange energy and matter with their environment, the concepts of open systems, e. g. nonequilibrium thermodynamics, apply to the elucidation of the mechanisms that are responsible for their complex behavior in time and space. At this point chemistry comes into play, because many of the phenomena of temporal and spatial self-organization are also observed in chemical reactive media evolving far from equilibrium. Periodic and aperiodic oscillations, stationary patterns and traveling waves are quite commonly found in chemical experiments (see SCHNEIDER and MÜNSTER 1996, KAPRAL and SHOWALTER 1995). These serve, therefore, frequently as laboratory models in that their properties may reflect the behavior of "real" systems in the living world. In particular, appli-

cations to biomedical problems, e. g. the treatment of heart diseases or the understanding of the cortex, emphasize the relevance of this field (WINFREE 1987).

Thus, the topic of this section "Nonlinear Dynamics and Biology" encompasses many modern disciplines, all interconnected by the common goal to find answers to important questions such as: can we understand many-component, complex, dynamic phenomena in spatially extended nonlinear systems as they apply to physics, chemistry, biology, medicine, ...? What are well characterized examples where temporal or spatio-temporal pattern formation accomplishes biological function, including the highly diversified structure of the human brain? Might patterns lead to novel medical therapies? What is the role of intrinsic noise on the emergence of organized behavior as compared to the deterministic evolution of the systems?

The majority of the contributions to this Section report on research of complex behavior in time, i. e. the spatial degrees of freedom are not explicitly considered.

To start with, research results on one of the topics of the previous Section are considered, showing the high attention devoted currently to stochastic aspects of biological dynamics. J. A. FREUND gives an account on the modeling and the theory of stochastic resonance, treated before on the experimental level by F. MOSS. FREUND provides an analytical approach to the influence of noise on subthreshold signal detection and applies the idea of beneficial fluctuations to the paddlefish and to Daphnia swarms in their natural environment. The work of J. W. SHUAI and P. JUNG also emphasizes the importance of stochasticity, in this case for the fascinating phenomenon of sparks or puffs of calcium ions in the cell that form transient and fluctuating spatial structures. They introduce a simplified method to describe the statistical properties of these puffs efficiently thus contributing to the work on calcium signaling, which is one of the most fascinating activities in actual biophysical research on cellular events. Calcium dynamics with all its crucial relevance for intracellular signal transduction and communication is also the topic in the contribution by M. WACKE et al. These authors investigate calcium dynamics in Chara algae. They develop a model for the complex behavior of calcium mobilization in this plant cell under electrical stimulation and show good agreement with the corresponding experimental investigations of action potentials.

What happens to the dynamics when several or only a single enzyme become responsible for governing the temporal evolution of a system? This question is treated in the contribution by M. HAUSER: He finds simple and complex rhythmic behavior and describes in this context a recent approach to investigate the dynamical properties of complex biological systems in studying so-called biomimetic systems. These consist of synthetic components, which are specially designed to reproduce the characteristic structural and reactive features of their natural counterparts. By focusing on the key features, biomimetic systems achieve a considerably lower degree of complexity that often allows the investigation of topics that in the natural systems are difficult to approach. Following the relative simplicity of a biomimetic system, the contribution by W. EBELING and F. SCHWEITZER takes us to the other end of high complexity. They discuss in their article on "Self-Organization, Active Brownian Dynamics, and Biological Applications" fundamental aspects of biological networks, a topic which belongs to the frontiers of modern statistical physics. Beyond the consideration of more general aspects of complexity they include chapters on the collective dynamics in swarms, biological aggregation and formation of insect trails and show that the coherent motion underlying these

phenomena can be suitably treated by their approach of active Brownian particles. Swarming is also of high relevance in the article by A. ORDEMANN et al. The authors show and analyze the amazing, self-organized vortex motions of the zooplankton Daphnia under well controlled laboratory conditions. Based on the impressive experimental material a model of random walkers is applied to reproduce the observations by simulations.

Having mentioned earlier the treatment of networks and the dynamics developing on them, we now get into the most complex network of all: the brain. Two important questions related to brain dynamics are addressed. S. GRÜN and coauthors deal with the coordinated firing activity of groups of neurons. They introduce a method to analyze experimental data that provides evidence for different time scales involved in cortical processing, and focus on the possible role of unitary events that they have discovered to occur in short time windows. Finally, the last contribution of this Section by P. A. TASS reports on the desynchronization of clusters of coupled oscillators on the basis of stochastic methods. We see again, how important noise and stochastic effects are in this field. The model calculations are aimed to provide insight into the efficiency of different types of pulses with respect to their interference with the collective dynamics of the system. This study could help to develop better therapies by deep brain stimulation for neurological patients.

This last and several other research results presented in this Section raise the interesting question, how the investigated dynamics develops, if the spatial extent of the system is explicitly taken into account, opening a wide area of additional questions to be addressed in future work.

It may be the appropriate place here to add some more aspects on the rich topic of spatial and spatiotemporal self-organization, as it occurs in many biological systems. Among the large number of possible interactions that can lead to pattern formation there is one "prototype" coupling mechanisms which has attracted specific attention by theorists and in experiments. We allude to the coupling of an autocatalytic (bio)chemical reaction with a transport process such as molecular diffusion, convection, chemotaxis, or others. It is the reaction-diffusion coupling, which has been most thoroughly treated so far. In this case, the patterning process is a consequence of the competition between an activator and an inhibitor substance, and the type of pattern that evolves depends sensitively on the diffusivities of these competing species. One observes stationary structures, some of which are referred to as Turing structures (TURING 1952, see also MEINHARDT 1982) and dynamically moving patterns (waves and fronts, see references below).

As mentioned earlier, one often finds suitable model systems in the chemical laboratory that exhibit behavior analogous to that found in biology: in the case of wave or front propagation one often refers to the famous Belousov-Zhabotinsky reaction, which is the bromination of malonic acid in the presence of a catalyst (ZAIKIN and ZHABOTINSKY 1970). This reaction may be prepared in an oscillating regime and then changes its color periodically between red (reduced) and blue (oxidized state). Or it is prepared as an excitable system, resting in the reduced state until a high enough stimulus leads to the propagation of a blue oxidation pulse through the reduced medium (KAPRAL and SHOWALTER 1995, MÜLLER et al. 1985). Due to a refractory period following the excitation, there evolve wave trains in the layer which can have circular or spiral shaped geometry and are characterized by a specific wavelength (Fig. 1 *A*).

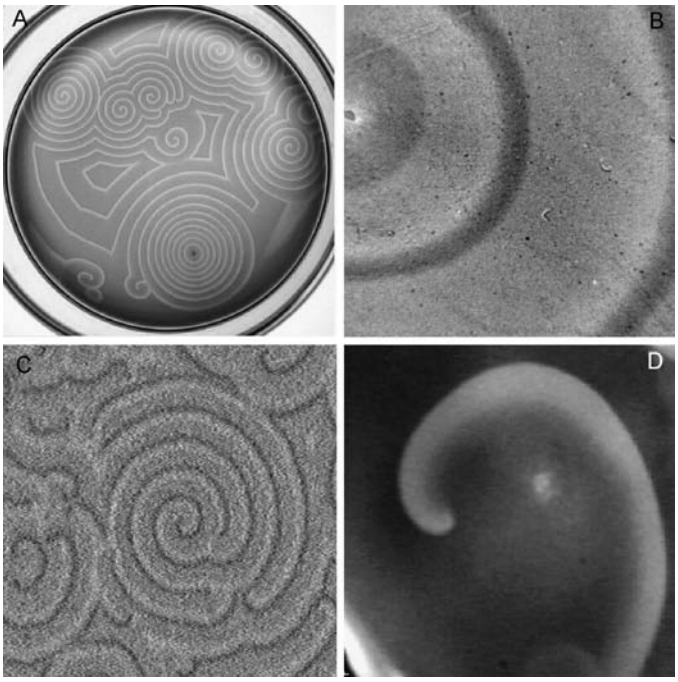

Fig. 1 Four examples of wave propagation in excitable media: (*A*) Spiral wave in the Belousov-Zhabotinsky reaction, (*B*) NADH and proton waves during oscillatory glycolysis, (*C*) wave pattern during the aggregation of amoebae cells of the slime mold *Dictyostelium discoideum*, (*D*) wave of spreading depression in chicken retina.

During the last decade an increasing number of experimental results have demonstrated that traveling waves of concentration changes occur in a variety of different cell types. Some examples are calcium waves in frog oocytes (Lechleiter et al. 1991), heart cells (Wier et al. 1987), liver cells (Lin et al. 1994) and others (for review see Jaffe 1991), NADH- and proton waves in neutrophils (Petty et al. 2000) and yeast extract (Mair and Müller 1996), cAMP-waves in cell layers of slime mould (Tomchik and Devreotes 1981) and spreading depression waves in the cortex (Basarsky et al. 1998).

Intracellular waves: Propagating waves of ionic composition are observed in a multitude of different cell types. Their generation takes place either spontaneously or when the cells are treated with external stimuli of signal transduction pathways. In many cases the initial trigger for generating the waves is the local release of IP_3 from the plasma membrane into the cytosol where it binds to IP_3-receptors of IP_3-sensitive calcium stores (Berridge and Irvine 1989). The subsequent propagation of the wave is mediated by calcium diffusion to adjacent calcium stores. This calcium-induced-calcium release (CICR) mechanism represents a reaction-diffusion coupling and therefore calcium waves exhibit the basic characteristics of excitation waves. For example, mu-

tual annihilation is frequently observed (WUSSLING et al. 1997). An additional feature typical for biological systems is that the high degree of connectivity of metabolic networks and morphological substructures offers several possibilities for increased complexity of these patterns.

Another example of intracellular waves are NADH- and proton waves of the energy metabolism, i. e. glycolysis. Here, an autocatalytic reaction is catalyzed by the enzyme phosphofructokinase (PFK) *via* positive feed-back regulation by its product ADP (GHOSH and CHANCE 1964, HESS et al. 1969). Allosteric regulation and cooperativity of the PFK subunits are the kinetic basis that drives the enzyme into an oscillatory state (GOLDBETER and LEFEVER 1972). Under these circumstances the spontaneous formation of traveling NADH-waves has been observed (MAIR and MÜLLER 1996). They form circular or spiral shaped patterns (Fig. 1 *B*) and show mutual annihilation, thus resembling the patterns and propagation dynamics of calcium waves or chemical reaction-diffusion waves (see Fig. 1 *A*). Corresponding model simulations have confirmed this view (GOLDBETER and LEFEVER 1972). Note, that the generation of calcium waves consumes ATP, whereas glycolysis produces it.

Intercellular waves: Propagation of reaction-diffusion waves from cell to cell are believed to play a crucial role for communication between cells. This kind of waves is generated from some pacemaker cells that excrete ions or metabolites *via* an autocatalytic process. Transmission of the waves through a cell population or tissue is then mediated *via* reaction-diffusion coupling, whereby the excreted substances act concomitantly as the signaling molecules. There are numerous examples of intercellular waves, e. g. electrical waves in the heart muscle (DAVIDENKO et al. 1992), calcium waves in tissue (for review see SANDERSON 1996), aggregation patterns in slime mould (GERISCH 1971) or spreading depression waves in the brain (GORELOVA and BURES 1983).

Let us look closer at two examples: The life cycle of *Dictyostelium discoideum* is characterized by morphogenetic changes that switch the organism between unicellular and multicellular states. The switch between these two states is induced by aggregation of unicellular, motile amoeboid cells into slugs which later develop into fruiting bodies. Directed movement of the cells towards aggregation centers occurs *via* chemotaxis. For this, some pacemaker cells release the chemoattractant cAMP in an autocatalytic process (MARTIEL and GOLDBETER 1987). The external cAMP diffuses to neighboring cells, where it induces a new autocatalytic release of cAMP, leading to a reaction-diffusion wave of the chemoattractant. The shape of the waves can be either circular or spiral shaped (Fig. 1 *C*). Spontaneous break up of circular waves into rotating spirals is more often observed at higher cell densities. Annihilating waves mark the boundary of aggregation territories which result from the multitude of aggregation centers. It should be noted, that propagating waves occur also in the multicellular slug, where a transition between 3-dimensional scroll waves to 2-dimensional planar waves marks the boundary between prestalk and prespore cells, respectively (STEINBOCK et al. 1993).

Spreading depression (SD) is a phenomenon characterized by a sudden break down of neuronal activity in the brain. First observed by LEAO in 1944, it has been the subject of numerous studies. SD spreads over brain tissue in a wave-like manner. It has been observed in the hypothalamus, cortex and retina. Once initiated, the SD waves propagate within the different cell layers of brain tissue from cell to cell, probably mediated *via* extracellular ion changes. At present, there is no conclusive model that can explain

the phenomenon of SD. Despite the lack of information about the basic mechanisms, it is likely that SD waves represent excitation waves, because they show all their characteristics as, for example, unidirectional movement, mutual annihilation, formation of rotating spirals (Fig. 1 *D*), or their dispersion relation (Brand et al. 1997). There are several experimental and theoretical contributions that point to an impact of SD waves for the migraine aura (Lauritzen 1994, Dahlem et al. 2000).

In summary, the contributions to this Section and the discussions of the presented material provide an excellent look into the wide realm of nonlinear dynamic behavior, spatiotemporal self-organization and the either beneficial or destructive effects of noise, emphasizing the important role of this interdisciplinary research field for physics, chemistry, biology and biomedicine.

References

Basarsky, T. A., Duffy, S. N., Andrew, R. D., and MacVicar, B. A.: J. Neurosci. *18*, 7189–7199 (1998)

Berridge, M. J., and Irvine, R. F.: Nature *341*, 197–205 (1989)

Brand, S., Dahlem, M. A., Fernandes de Lima, V. M., Müller, S. C., and Hanke, W.: Int. J. Bifurcat. Chaos *7*, 1359–1365 (1997)

Cross, M. C., and Hohenberg, P.: Rev. Mod. Phys. *65*, 851–1112 (1993)

Dahlem, M. A., Engelmann, R., Löwel, S., and Müller, S. C.: Eur. J. Neurobiol. *12*, 767–770 (2000)

Davidenko, J. M., Pertsov, A. M., Salomonsz, R., Baxter, W., and Jalife, J.: Nature *355*, 349–351 (1992)

Gerisch, G.: Naturwissenschaften *58*, 430–438 (1971)

Ghosh, A., and Chance, B.: Biochem. Biophys. Res. Commun. *16*, 174–181 (1964)

Goldbeter, A. (Ed.): Oscillations, bistability and waves in biochemical and cellular systems. Biophys. Chem. (Special Issue) *72* (1998)

Goldbeter, A., and Lefever, R.: Biophys. J. *12*, 1302–1315 (1972)

Gorelova, N. A., and Bures, J.: J. Neurobiol. *14*, 353–363 (1983)

Hess, B. Q.: Rev. Biophys. *30*, 121–176 (1997)

Hess, B., Boiteux, A., and Krüger, J.: Adv. Enzyme Regul. *7*, 149–167 (1969)

Jaffe, L. F.: Proc. Natl. Acad. Sci. USA *88*, 9883–9887 (1991)

Kapral, R., and Showalter, K. (Eds.): Chemical Waves and Patterns. Dordrecht: Kluwer 1995

Lauritzen, M.: Brain *117*, 199–210 (1994)

Leao, A. J.: Neurophysiol. *7*, 359–390 (1944)

Lechleiter, J., Girard, S., Peralta, E., and Clapham, D.: Science *252*, 123–126 (1991)

Lin, C., Hajnoczky, G., and Thomas, A. P.: Cell Calcium *16*, 247–258 (1994)

Mair, T., and Müller, S. C.: J. Biol. Chem. *271*, 627–630 (1996)

Martiel, J.-L., and Goldbeter, A.: Biophys. J. *52*, 807–828 (1987)

Meinhardt, H.: Models of Biological Pattern Formation. London: Academic Press 1982

Müller, S. C., Plesser, T., and Hess, B.: Science *230*, 661–663 (1985)

Petty, H. R., Worth, R. G., and Kindzelskii, A. L.: Phys. Rev. Lett. *84*, 2754–2757 (2000)

Sanderson, M. J.: News Physiol. Sci. *11*, 262–269 (1996)

Schneider, F. W., und Münster, A. F.: Nichtlineare Dynamik in der Chemie. Heidelberg: Spektrum-Verlag 1996

Steinbock, O., Siegert, F., Müller, S. C., and Weijer, C. J.: Proc. Natl. Acad. Sci. USA *90*, 7332–7335 (1993)

Strogatz, S. H.: Nonlinear Dynamics and Chaos – With applications to Physics, Biology, Chemistry, and Engineering. Reading: Addison-Wesley 1995

Tomchik, K. J., and Devreotes, P. N.: Science *212*, 443–446 (1981)

Turing, A. M.: Phil. Trans. R. Soc. *237*, 37–72 (1952)

Wier, W. G., Cannell, M. B., Berlin, J. R., Marban, E., and Lederer, W. J.: Science *235*, 325–328 (1987)

WINFREE, A. T.: When Time Breaks Down. Princeton: Princeton University Press 1987
WUSSLING, M. H. P., SCHEUFLER, K., SCHMERLING, S., and DRYGALLA, V.: Biophys. J. *73*, 1232–1242 (1997)
ZAIKIN, A. N., and ZHABOTINSKY, A. M.: Nature *225*, 535–537 (1970)

Prof. Dr. Stefan C. MÜLLER
Abteilung Biophysik
Institut für Experimentelle Physik,
Otto-von-Guericke-Universität Magdeburg
39106 Magdeburg
Germany
Phone: ++49 (0) 39 16 71 83 38
Fax: ++49 (0) 39 16 71 11 81
E-Mail: stefan.mueller@physik.uni-magdeburg.de

Nova Acta Leopoldina NF *88*, Nr. 332, 87–103 (2003)

Motions of Daphnia in a Light Field: Random Walks with a Zooplankton

Anke Ordemann, Frank Moss, and Gabor Balázsi (St. Louis)

With 6 Figures

Abstract

To learn more about the self-organized vortex-like motions observed in the field in groups of animals which are swarming as a predator confusing mechanism, such as schools of fish and flocks of birds, we investigate swarms of the common zooplankton *Daphnia*, which infrequently have been observed to perform similar vortex-like motions. Reproducibly inducing swarming *Daphnia* to carry out the vortex motion in our lab reveals that the water between the *Daphnia* also circles in the same direction as the animals. To characterize their behavior in a more defined setup, we study the motion of single *Daphnia*, as well as swarms, with respect to a vertical light shaft, which acts as the optical marker for swarm formation. We observe the development of a circular motion in both directions around this light shaft for swarming *Daphnia* and, surprisingly, also for individual *Daphnia*. Based on experimental data we developed a simple stochastic model of random walkers with short-range correlation and attraction to light to successfully simulate the observed behavior of *Daphnia* in light fields.

Zusammenfassung

Um die Bildung von wirbelförmigen Bewegungen genauer zu verstehen, die selbstorganisierte Tiergruppen wie Fischschulen und Vogelscharen als Verwirrungsmechanismus gegen ihre Jäger einsetzen, untersuchen wir unter Laborbedingungen das Verhalten von Schwärmen des Zooplanktons *Daphnia*, bei welchen auch derartige Wirbelbewegungen beobachtet wurden. Durch reproduzierbares Hervorrufen eines *Daphnia*-Wirbels im Labor konnten wir feststellen, daß sich das Wasser innerhalb eines Wirbels in die gleiche Richtung dreht wie die *Daphnia*. Um das Verhalten von *Daphnia* unter konstanteren Bedingungen untersuchen zu können, haben wir die Bewegung eines Tieres wie auch eines Schwarms im Verhältnis zu einer die Schwarmmarkierung bildenden Lichtsäule untersucht. Es ist zu beobachten, daß sowohl *Daphnia*-Schwärme als erstaunlicherweise auch individuelle *Daphnia* kreisförmige Bewegungen in beide Richtungen um die Lichtsäule ausführen. Basierend auf den experimentellen Daten haben wir ein einfaches *Random-Walk*-Modell mit kurzreichweitiger Korrelation entwickelt, das das beobachtete kreisende Verhalten von *Daphnia* in einem Lichtfeld erfolgreich beschreibt.

1. Introduction

Self-propelled animals living and moving in a three-dimensional environment and being at high risk to be spotted and eaten by visually hunting predators are commonly known to form swarms as a predator confusing mechanism (Humphries and Driver 1967, Ha-

MILTON 1971, PULLIAM 1973, see also PARRISH and EDELSTEIN-KESHET 1999, OKUBO and LEVIN 2002). Examples of such animals are species of planktivore fish, e. g. sardine, mackerel and anchovetta (PARTRIDGE 1982, HALL et al. 1986), as well as some birds (CARACO et al. 1980) and zooplankton (JAKOBSEN et al. 1994, KVAM and KLEIVEN 1995). Since the prey usually cannot flee the predator due to its lower speed, it evolutionarily evolved to form dense groups of animals with a sharp boundary. The confusing effect was shown to increase by increased number of animals in the swarm (NEILL and CULLEN 1974), increased density (MILINSKI 1979), and increased uniformity (OGHUCHI 1978) of the swarm. Animals outside an existing swarm are at the highest risk to become prey (BREWER and COUGHLIN 1996). These prey swarms are self-organized systems (see e. g. PARRISH and EDELSTEIN-KESHET 1999, CAMAZINE et al. 2001, OKUBO and LEVIN 2002), there is no leader or global recipe for the individual animals to react to and the pattern on the global level is an emergent property of the interactions on the local level.

Anecdotal evidence exists about swarming fish and birds performing a fascinating coordinated vortex-like motion in the field. These patterns are not well investigated, mostly due to the size of the animals, and therefore the physical, biological, and chemical reasons for vortex-swarming are not well understood. A feasible behavioral explanation for vortex-swarming to occur might be that circling is the least energy consuming possibility for a group of animals to stay close together as a localized swarm without frequently bumping into each other, although the individual members of the swarm have to constantly move to maintain height in their three-dimensional environment. The aim of the present work is to gain more insight into the physical and behavioral aspects of vortex-swarming in prey animals.

The paper is organized as follows: In the remaining part of Section 1 existing theoretical models of self-propelled particles simulating circular motion in biological systems as well as experimental observations of such motions are briefly reviewed. In Section 2 we first give an introduction into general zooplankton behavior and then explain our experimental setup and the results for tracking the motion of *Daphnia* in a light field as well as in the dark. In Section 3 we present a random walk model with short-range correlation and attraction to light which successfully simulates the observed horizontal circling behavior of *Daphnia* in a light field. Finally, Section 4 summarizes our main observations and concluding remarks.

1.1 Models of Self-propelled Agents Performing a Circular Motion

Lately, models of self-propelled agents simulating the physical aspects of self-organized swarming systems have been found of great interest to theoretical physicists. Based on the models of *Self-propelled Interacting Particles* (VICSEK et al. 1995) and *Active Brownian Particles* (SCHIMANSKY-GEIER et al. 1995) several variants of these models have been developed which lead to a circular behavior of the agents (CZIRÓK et al. 1996, SCHWEITZER et al. 1998, RAPPEL et al. 1999, EBELING and SCHWEITZER 2001, SCHWEITZER et al. 2001, LEVINE et al. 2001, see also VICSEK 2001). Apart from these recent models, several closely related older swarming models exist outside the physics literature (OKUBO and ANDERSON 1984, REYNOLDS 1987, HUTH and WISSEL 1992). It

is instructive to shortly review the ingredients of the two main recent models that successfully lead to circular motion of the agents.

In the discrete two-dimensional many-particle model of LEVINE et al. (2001) each particle, characterized by mass m_i, position $\vec{x}_i$, and velocity $\vec{v}_i$, experiences a self-propelling force $\vec{f}_i$, a friction force with coefficient β as well as an long range attractive and a short range repulsive force between the particles given by an exponentially decaying interaction potential U:

$$m_i \partial_t \vec{v}_i = \alpha \vec{f}_i - \beta \vec{v}_i - \vec{\nabla} U \qquad \partial_i \vec{x}_i = \vec{v}_i. \tag{1}$$

The model has been investigated using two different rules for the determination of the self-propelling force $\vec{f}_i$: either (*i*) without any averaging

$$\vec{f}_i = \vec{v}_i \tag{2}$$

or (*ii*) aligning it with the average velocity direction of the neighboring particles within interaction length l_c,

$$\vec{f}_i = \sum_{j \neq i} \vec{v}_i \exp\left(-\left|\vec{x}_i - \vec{x}_j\right| / l_c\right). \tag{3}$$

For certain parameter settings LEVINE et al. (2001) find stable states with circular motion of the agents, independent of the explicit form of the interaction potential and for various initial conditions such as randomly distributed agents having velocities of constant magnitude but random direction. Depending on the implementation of the self-propelled force the agents either (*i*) circle both clockwise and counterclockwise randomly or (*ii*) circle all in the same direction after a certain transition time, which breaks rotational symmetry and leads to a vortex state. The circular motions are observed to be stable under reasonable noise and the agent density always drops off sharply at the boundary of the agent swarm similar to the boundaries of biological swarms.

In the two-dimensional single-particle model of Active Brownian Particles with an internal energy depot (SCHWEITZER et al. 1998) the agent, characterized by mass m, position $\vec{x}_i$, and velocity $\vec{v}_i$, experiences a self-propelling force which is connected to an energy storage depot $e(t)$, a friction force with friction coefficient γ_0, an external force given by a parabolic potential $U(\vec{v})$, and noise $F(t)$:

$$m \partial_t \vec{v} = d_2 e(t) \vec{v} - \gamma_0 \vec{v} - \vec{\nabla} U(\vec{x}) + F(t), \qquad \partial_t \vec{x} = \vec{v}. \tag{4}$$

The internal energy depot equation consists of the terms for the space dependent take-up of energy $q(\vec{x})$, the internal dissipation, i. e. metabolism, and the conversion of internal energy to kinetic energy:

$$\partial_t e(t) = q(\vec{x}) - c e(t) - d_2 v^2 e(t). \tag{5}$$

SCHWEITZER et al. (1998) consider both a uniform energy supply, i. e. $q(\vec{x}) \equiv q_0$, and patchy energy sources. Carrying out an energy depot analysis for $q(\vec{x}) \equiv q_0$ leads to a Hopf bifurcation with a bifurcation parameter $\mu = \dfrac{q_0}{\gamma_0} - \dfrac{c}{d}$. For $\mu \leq 0$ the model shows simple (passive) Brownian motion while for $\mu > 0$, i. e. supercritical supply of energy $q_0 > q_0^{\text{crit}} = \gamma_0 c / d_2$, the agent moves to a stochastic limit cycle where the circling radius depends on the ratio of energy take-up to used energy. Also, based on this model

many-particle models with various interactions between the Active Brownian Particles were investigated (EBELING and SCHWEITZER 2001, SCHWEITZER et al. 2001). It was found that incorporating an attraction to the center of mass leads to clusters of agents circling in both directions and changing their circling direction due to the noise, while coupling the mean angular momentum of the agents breaks the symmetry of the system under certain conditions leading to circling of all agents in the same direction and thus forming a vortex state.

1.2 Experimental Observations of Self-organized Vortices in Biological Systems

Despite the many theoretical models, experimental observations of circling behavior in biological systems under well defined conditions have up to now only been reported for disc-shaped aggregates of the bacteria *Paenibacillus vortex* (CZIRÓK et al. 1996) and aggregated cells of the amoeba *Dictyostelium* (RAPPEL et al. 1999). These systems are on a low evolutionary level and the physical and behavioral aspects of the observed motions are therefore difficult to compare with the ones for a group of fish or birds. However, several accidental observations of different freshwater zooplankton performing a horizontal circular motion under laboratory conditions (YOUNG and GETTY 1987, YOUNG and TAYLOR 1990, BUSKEY et al. 1996) as well as one vortex-swarming incident of the oceanic zooplankton *Anchylomera blossevilli* at a reef region with sandy bottom near Hawaii (LOBEL and RANDALL 1986) have been reported. It is striking that in all these observed circling events special light conditions were recorded which can be roughly summarized as the existence of a vertical shaft of light in the water to which the animals are attracted. For example in the case of the vortex swarms of *Anchylomera blossevilli,* where several rotating patches 2–3 m in diameter formed at the surface at noon, the water was found to be exceptionally clear and calm with many planktivore fish present. Unfortunately, the observation of individual behavior was not possible, so the physical, chemical and biological basis for the vortex-swarm could not be established. But swarms of zooplankton promise to be a biological system which can be investigated in detail under defined laboratory conditions to learn more about the occurrence of vortex-swarming in birds and fish.

2. Experimental Observations of the Zooplankton *Daphnia*

Infrequently also a swarm of the freshwater zooplankton *Daphnia* (Fig. 1 *A*) has been observed to perform a vortex-like motion in our laboratory (see Fig. 1 *B*), but the specific circumstances for this behavior to occur have been found difficult to define. Reproducibly inducing *Daphnia* to vortex-swarm surprisingly reveals that the water between the *Daphnia* circles in the same direction as the *Daphnia* themselves. The turning direction of the vortex appears to be random. Important conditions for a vortex-swarm to form are the presence of predator kairomones – in our experiment water from a goldfish tank – and freshly crushed *Daphnia,* high enough food density – in our case live green algae *Scenedesmus quadricula* – as well as light from above and the sides and a reflective bottom of the aquarium – in our set-up room light and a 40 cm diameter cylindric glass

aquarium. Although the exact light conditions necessary for a vortex-swarm to occur are again not possible to define for this set-up, the above observations are in good agreement with the conditions reported for the vortex-swarm of *Anchylomera blossevilli* as well as

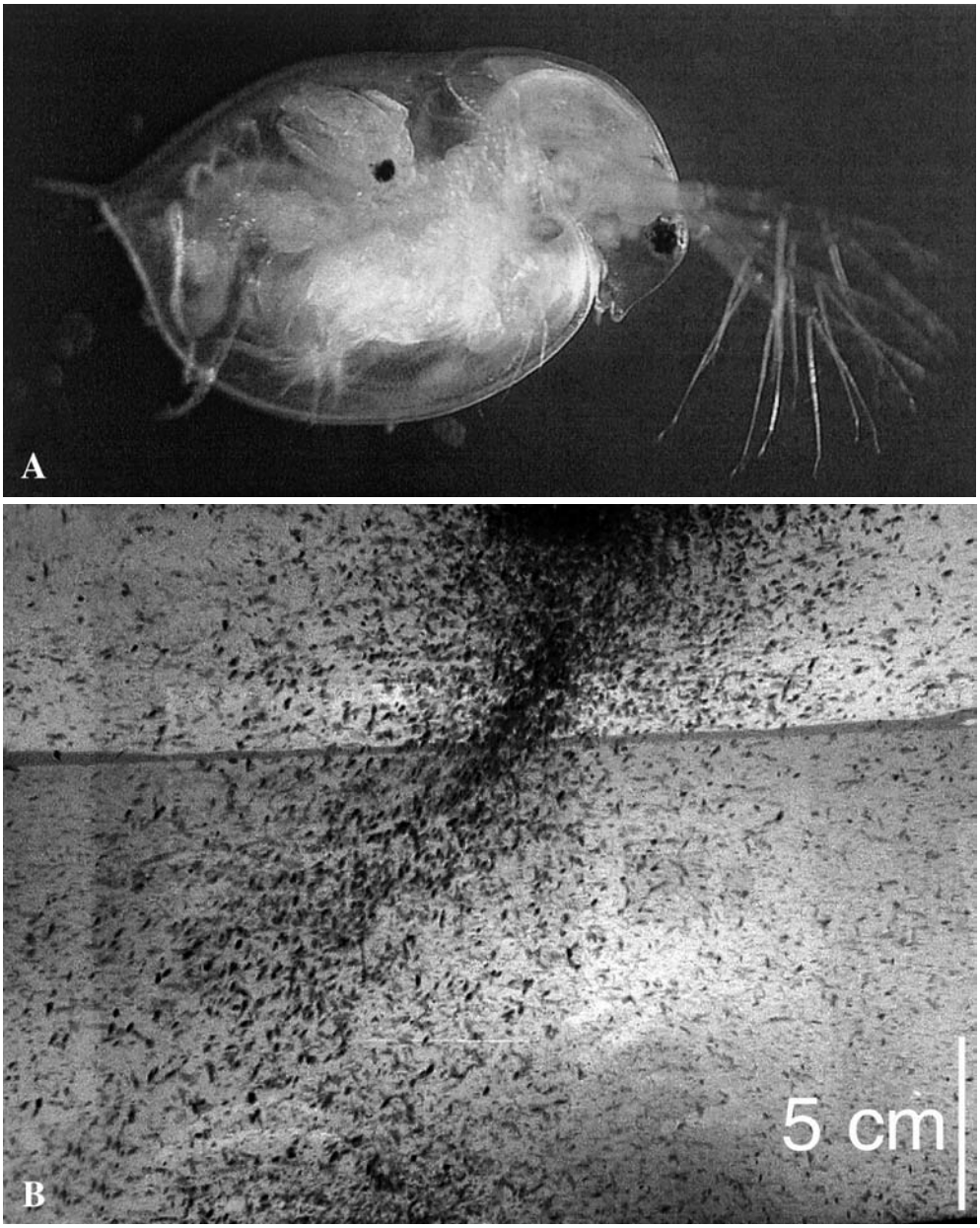

Fig. 1 (*A*) Lateral view of the common zooplankton *Daphnia* (typical body lenght: 0.5–1.5 mm) with a juvenile in the brood pocket, the head with the compound eye and the swimming antennae is visible on the right. Picture by D. RUSSELL with permission. (*B*) Side-view of vortex-swarming *Daphnia* in a rectangular aquarium. Picture by D. RUSSELL with permission.

with earlier experiments. It was reported that the presence of predator kairomones and chemical clues of eaten *Daphnia* enhances the tendency to swarm in *Daphnia* (PIJANOWSKA 1994, KVAM and KLEIVEN 1995, JENSEN et al. 1998), that the major cost of swarming is limited food availability as the food density significantly decreases inside a swarm (BERTRAM 1978, JAKOBSEN and JOHNSEN 1988) and that visual clues are important for swarming behavior in zooplankton (BUSKEY et al. 1996, JENSON et al. 1999).

The above mentioned observation that water inside a vortex-swarm of *Daphnia* forms a vortex itself gives rise to several general questions: (*i*) Is this also the case for swarming fish? Most likely this is not the case (PARTRIDGE and PITCHER 1979), although it is a controversial topic (WEIHS 1973). It clearly is not the case for birds. (*ii*) Do *Daphnia* align with their neighbors as fish (PARTRIDGE and PITCHER 1980) and birds (POTTS 1984) do? In case they do align, what clues do they use for alignment, e. g. phototaxis or mechanoreceptors? It is known that fish (OKUBO 1986) as well as birds (POTTS 1984) align visually. (*iii*) How does a vortex form? To shed more light on these questions it is necessary to perform more defined laboratory experiments with *Daphnia*.

2.1 Known Daphnia Behavior

As *Daphnia* are a well investigated species for various reasons, and are very old from the evolutionary point of view, a possible set-up for a more well defined experiment to investigate vortex-swarming in *Daphnia* should take into account the following observations. *Daphnia* are known to heavily depend on phototaxis to sense their environment, e. g. when searching for food (YOUNG and GETTY 1987) as well as confusing and avoiding their predators by swarm formation (JENSEN et al. 1998) or performing Diel Vertical Migration (ZARET and SUFFERN 1976, RHODE et al. 2001). They are strongly attracted to light in the visual range and repelled from UV light, being more sensitive to relative changes in light intensity than to absolute intensity. Most likely *Daphnia* cannot form an image with their eyes at all, or have very limited visual acuity compared to fish or birds (BUCHANAN and GOLDBERG 1981, OKUBO and LEVIN 2002), but they can determine wavelength, intensity, and direction of the light (SMITH and MACAGNO 1990). No direct visual alignment between *Daphnia* has been detected (OKUBO and LEVIN 2002) besides the observed external alignment perpendicular to the plane of polarization of the light (YOUNG and TAYLOR 1990, SCHWIND 1999, NOVALES and BROWMAN 2000). In addition to phototaxis they also make use of their chemotaxis (LARSON and DODSON 1993) and the sensation of water motion with their mechanoreceptors (HAURY and YAMAZAKI 1995). As it is assumed that no means of direct long range communication between *Daphnia* exists (LARSON and DODSON 1993), they have to be individually attracted to a landmark to aggregate. These landmarks are believed to be the aforementioned shafts of light in the visual range (JENSEN et al. 1999), as it is also the case for the zooplankton copepod (BUSKEY et al. 1996) and mosquitos (GIBSON 1985). The swimming behavior of *Daphnia* is dominated by the fact that they live in a relatively low Reynolds number environment (ZARET 1980), they move with an average "hopping" rate of approximately three moves per second and their overall speed is 4–16 mm/s with a sinking rate of approximately 3 mm/s (DODSON 1996). Therefore their motion can be modeled well by self-propelled discretely maneuvering agents.

2.2 Daphnia in a Light Field

Following the above lines a simpler and more well defined set-up to investigate circular motion of *Daphnia* consists of a rectangular aquarium (50 × 20 cm, water level 25 cm) with a vertical translucent plastic tube mounted in the middle which is illuminated from above by a fiber optic illuminator (see Fig. 2 for details), thus forming a shaft of light in the visual range. Besides this light field with radial symmetry to which the *Daphnia* are attracted, the room is dark. After placing many *Daphnia* in the algae water and leaving them to acclimate and to distribute uniformly for at least 15 min, the fiber optic illuminator is switched on. Being individually attracted to the optical marker a substantial proportion of *Daphnia* can be observed to circle around the shaft in both directions (see Fig. 3 *A*), frequently reversing their circling direction. The radius of their circles is large enough to exclude the possibility that this behavior occurs simply due to the hydrodynamic sensation of an artificial object with their mechanoreceptors, since experiments show that *Daphnia* can sense static objects only in about one body length distance (HAURY and YAMAZAKI 1995), and since a similar circling behavior was observed in recent experiments when using a high intensity flashlight shining vertically into the water instead of the solid light tube (NIHONGI and ORDEMANN 2002). Therefore this artificial vertical solid light shaft induces *Daphnia* to circle around it in both directions in the horizontal plane. No vortex formation, i. e. circling of all *Daphnia* in the same direction, has been observed. This is most likely due to the solid light shaft preventing a fluid dynamic vortex to occur, since for the set-up with the flashlight vortex-swarming can be induced under certain environmental conditions, most importantly by high enough *Daphnia* density (NIHONGI and ORDEMANN 2002).

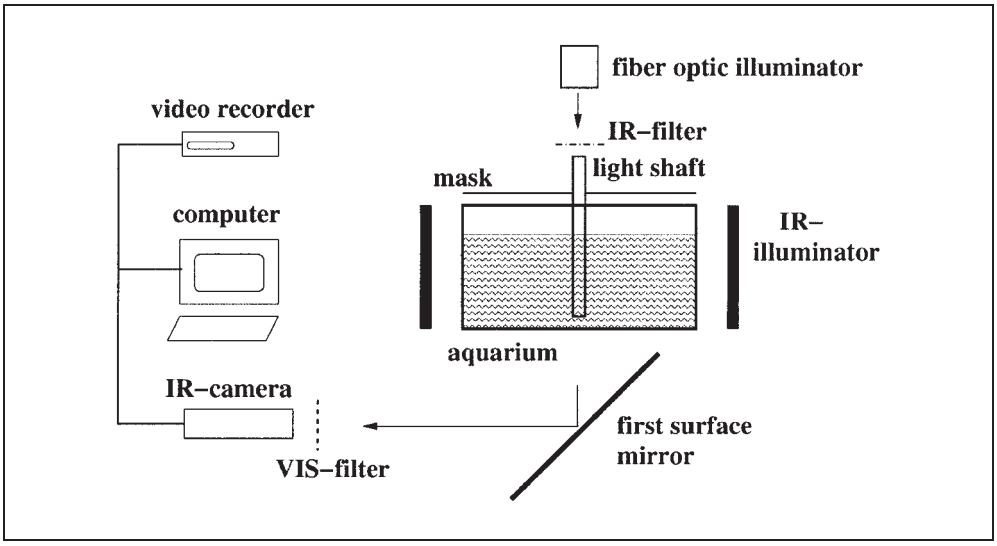

Fig. 2 Design of the experimental setup. For reasons of clarity not shown is the second infrared camera for side-view recording of the aquarium. Near infrared background illumination to which the *Daphnia* are blind (SMITH and MACAGNO 1990) is used for recording purposes, to light up the *Daphnia* independently of the light in the visual range emitted from the light shaft. The light sources, aquarium and cameras are housed in a light-tight room, computer and video recorder are in a separate compartment. Care was taken to reduce any kind of reflection in the aquarium area by using masks of low-pile velvet.

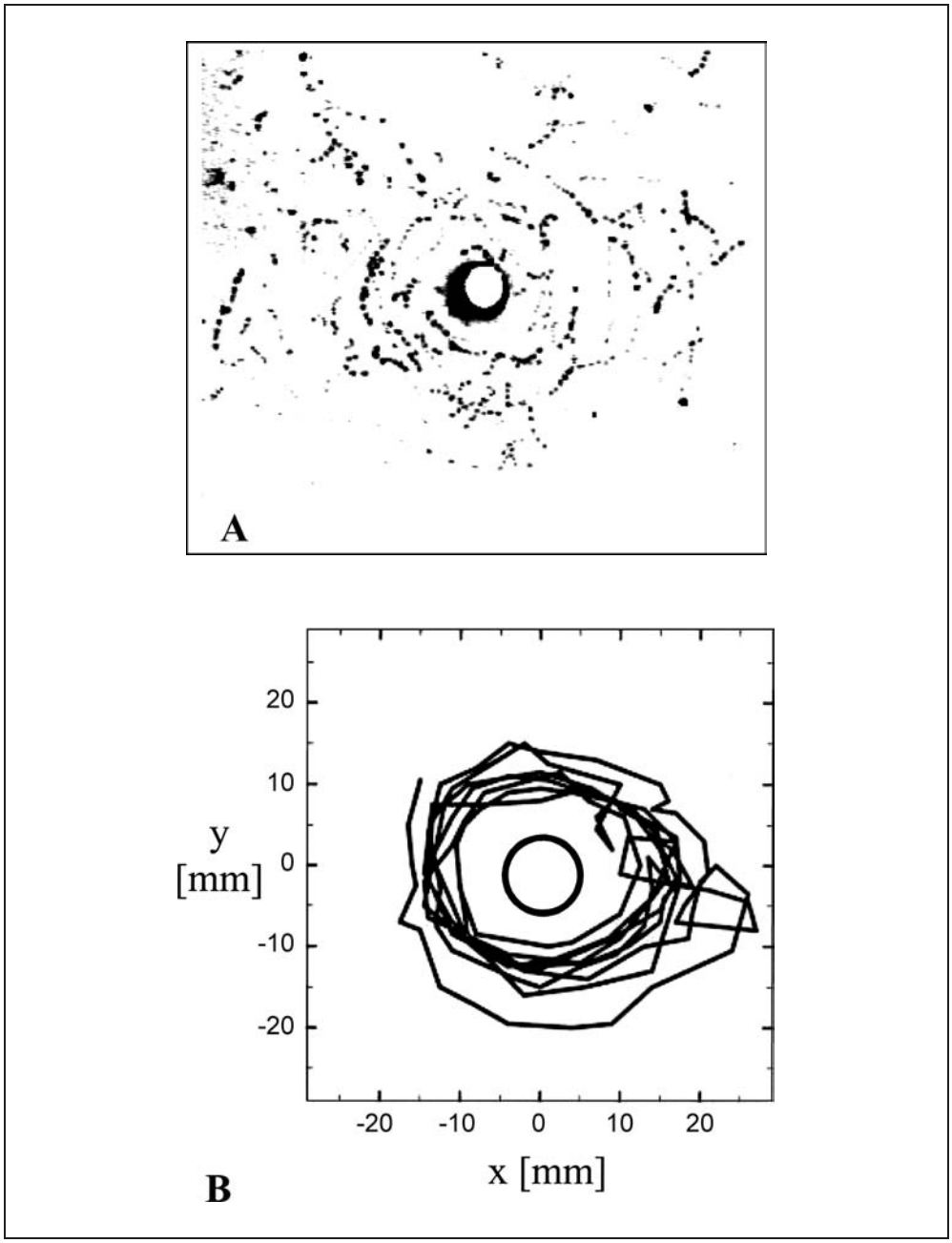

Fig. 3 Observation of *Daphnia* in the aquarium with centred vertical light shaft (radius of light shaft 5 mm, light intensity 10^{-3} W/m^2). (*A*) Bottom view of the aquarium showing five successive positions, taken in intervals of 0.3 s, of many simultaneously moving *Daphnia*. The lighter dots mark the positions earlier in time. Most of the *Daphnia* close to the center can be observed to circle in both directions, in the outer regions several *Daphnia* can be seen to move towards the light. (*B*) Horizontal projection of the track of one Daphnia circling individually around the light shaft (recorded time t_{rec} = 146 s, frame rate 1 picture/s).

To investigate the motion of *Daphnia* in the light field in more detail and to be able to analyze the path of *Daphnia* using the automatic tracking software Chromotrack® Version 4.02 from San Diego Instruments, we placed several single *Daphnia* in the aquarium one after each other. Surprisingly, we found some of them circling around the light shaft. A typical track of an individually circling *Daphnia* is shown in Figure 3 (*B*). Note the nearly constant radius of circling throughout the recording, which might be explained by the observation that *Daphnia* can retrace their own path – or the path of a fellow

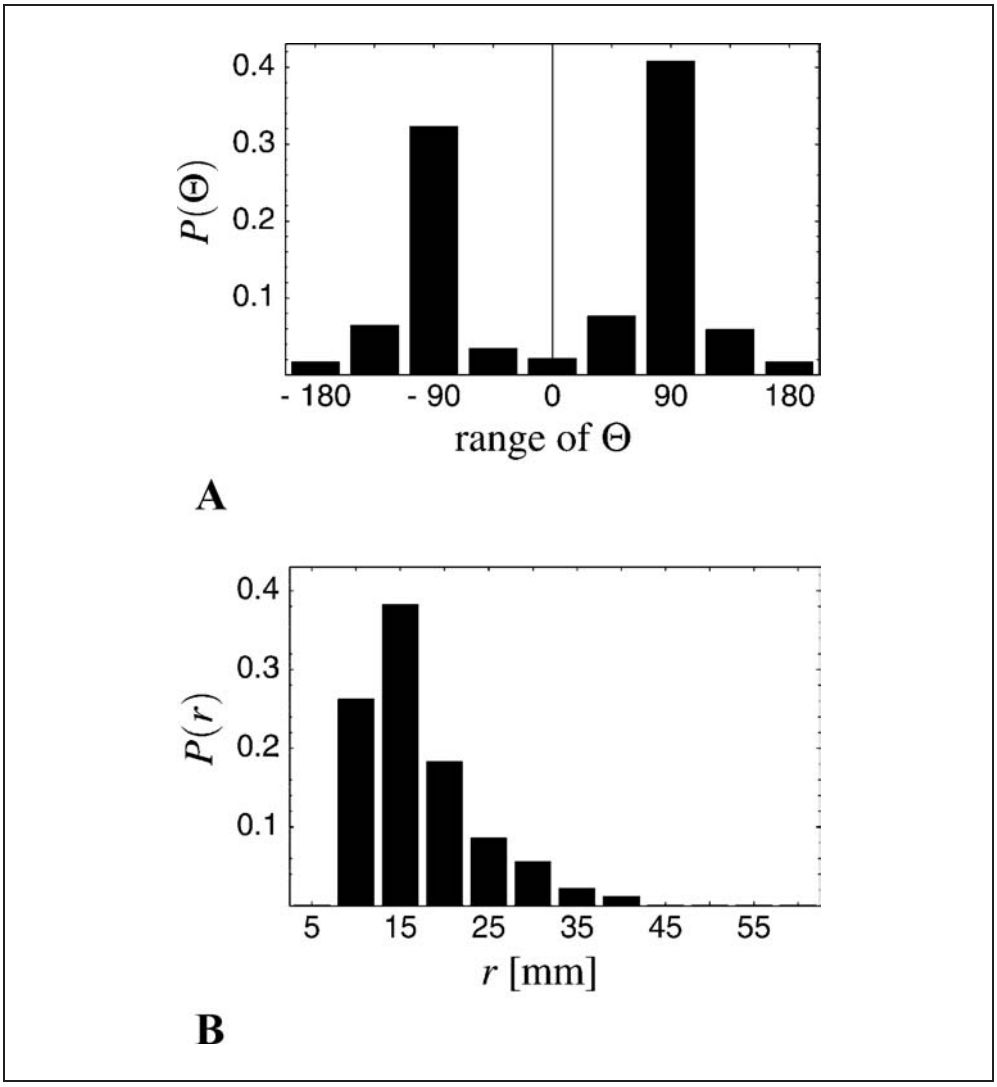

Fig. 4 (*A*) Probability distribution $P(\theta)$ of the angle θ between the heading of the *Daphnia* and the direction to the light shaft for every move, determined from data of 624 moves of the tracks of four different individual *Daphnia* observed circling around the light shaft. (*B*) Probability distribution $P(r)$ of the distance r of the *Daphnia* to the light shaft, determined from the same set of data as in (*A*).

Daphnia – by detecting small density gradients in the water produced by the motion of their feeding legs and antennae (GRIES et al. 1999). The fact that single *Daphnia* also circle indicates that, for *Daphnia,* circling is not a collective motion emerging in a swarm of animals, e. g., due to the alignment of neighboring animals as observed for fish and birds, but an individual reaction to a certain light pattern. This is in agreement with the above mentioned observation that *Daphnia* cannot actively align with their neighbors using their phototaxis (OKUBO and LEVIN 2002). The vortex motion evolving at a natural light marker or a light cone of a flashlight can then be explained as a self-organization phenomenon occurring for high enough *Daphnia* density when due to random fluctuations one circling direction is sufficiently more pronounced and the positive feedback of the water drag forces more and more *Daphnia* to circle in the same direction and thereby breaking the symmetry of the system. The detailed physical aspects of the fluid dynamic vortex to occur need more investigation but most likely are a consequence of the low Reynolds number environment of *Daphnia* (ZARET 1980).

As the dominating part of the motion of single *Daphnia* in the light field takes place in the horizontal plane it is sufficient to restrict the characterization of the observed circling behavior to two dimensions, analyzing only the bottom-view pictures of the aquarium. To quantify the amount of circling we calculated the probability distribution $P(\theta)$ of the angle θ between the heading of the *Daphnia* and the direction to the light shaft for every move for several *Daphnia* observed circling around the light shaft (see Fig. 4 *A*) as well as the probability distribution $P(r)$ of the distance r of these *Daphnia* to the light shaft (see Fig. 4 *B*). For circling to occur it is necessary (but not sufficient) that $P(\theta)$ has maxima at $\pm 90°$ and $P(r)$ shows a maximum relatively close to the light shaft, both of which is visible in Figure 4. Further on we determined the average length of circling in one direction, i. e. either clockwise or counterclockwise, before reversing the direction to be 11.8 moves. This translates to circling more than one full turn on average when combined with the average circling radius (see Fig. 4 *B*) and an approximate average move length of 3 mm.

2.3 Daphnia in the Dark

For comparison with the above described experiment in the light field and with self-propelled agent models it is instructive to observe the behavior of *Daphnia* without them being attracted to light, that is tracking *Daphnia* in the dark. It is assumed that the animals, taking into account their chemotactic and hydrodynamic perception radius, strive to maximize the covered territory to increase their encounter rates (GERRITSON and STRICKLER 1977). A typical track of a *Daphnia* in the dark is shown in Figure 5 *A* in 2-dimensional projection. Measuring the distribution of the turning angle (DTA) between successive moves of such tracks yields a bimodal symmetric distribution with maxima approximately at $\pm 35°$ (see Fig. 5 *B*). Comparing this result with previously reported track analysis is difficult, as usually only the mean of the distribution of the absolute turning angle, which is larger than the maximum of this distribution, is reported in literature. However, for the zooplankton copepod the observed DTA is given by SCHMITT and SEURONT (2001), and is qualitatively and quantitatively very similar to the DTA shown in Figure 5 *B*.

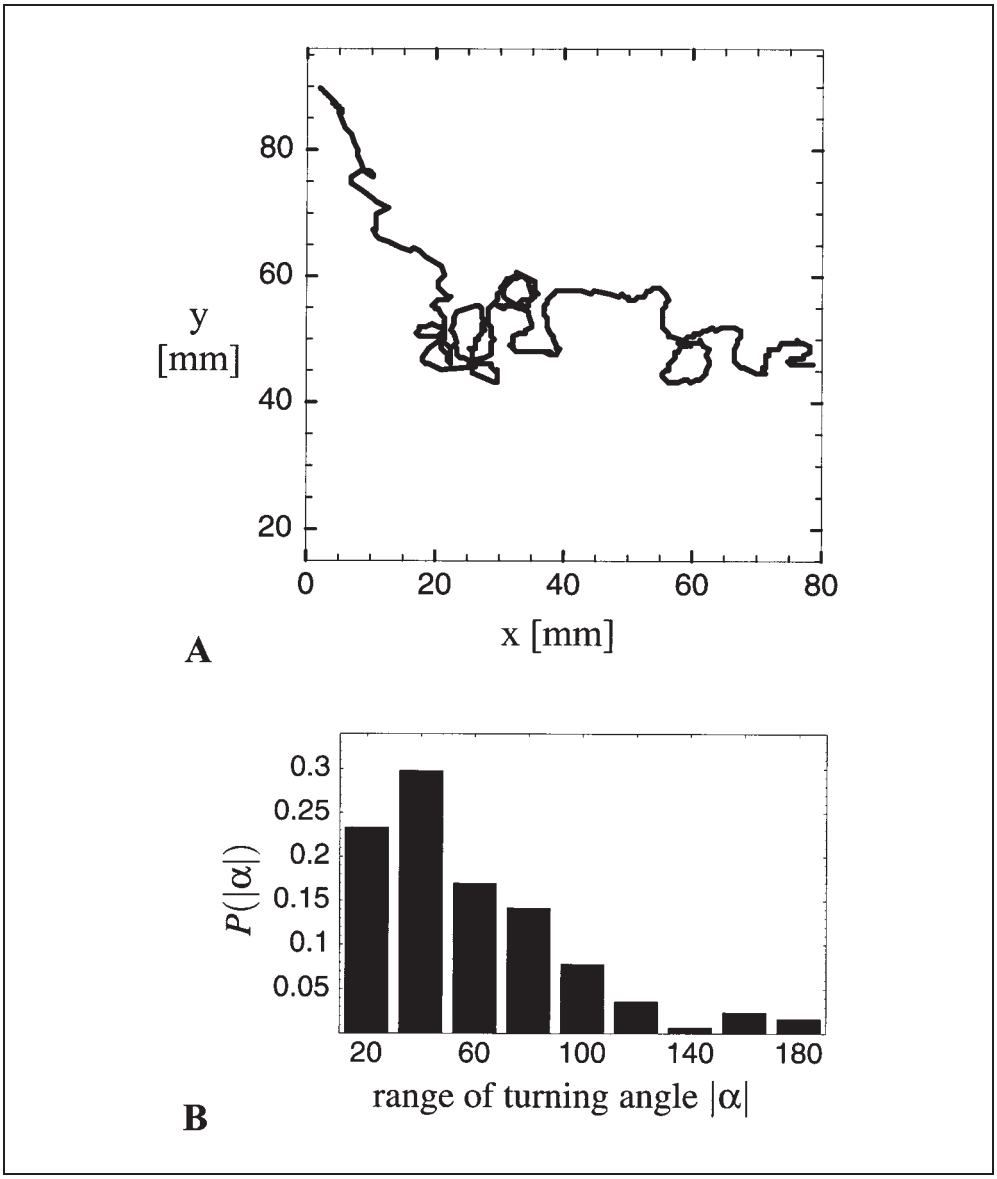

Fig. 5 (*A*) Horizontal projection of a typical track of a *Daphnia* in the dark (200 moves, recorded time $t_{rec} = 60$ s, frame rate 10 pictures/s). (*B*) Probability distribution $P(|\alpha|)$ of the absolute turning angle $|\alpha|$ of *Daphnia* between successive moves, determined from data of 1600 moves of the tracks of eight different *Daphnia* observed in darkness (cumulative recorded time $t_{rec} = 455$ s, frame rate 10 pictures/s). Note that when determining and comparing the cumulative turning angle of all left turns with the one of all right turns as well as the number of left turns and the number of right turns, no preference in the turning behavior of *Daphnia* in darkness can be found. Therefore the probability distribution $P(a)$ of the turning angle a is a symmetric bimodal distribution.

3. Random Walk Model for *Daphnia* Circling in a Light Field

Comparing the experimental results for circling *Daphnia* reported in Section 2 with the theoretical models of self-propelled agents mentioned in Section 1.1 suggests that variants of the model of Self-Propelled Interacting Particles (Vicsek 2001, Levine at al. 2001) are not applicable to these animals, since direct interaction of *Daphnia* was found not to be necessary for circling to occur. The Active Brownian Particle model of Schweitzer et al. (1998) more closely simulates the observed circular motion in single *Daphnia* although the variant of the model that incorporates a patchy energy supply is not fully suitable as the resulting motion is on the wrong time scale for *Daphnia*: *Daphnia* can actively move a considerably longer time without energy take-up than the corresponding agents in the model (Dawidowicz 1999), and *Daphnia* slow down in a food patch (Smith and Macagno 1990) where as the agents speed up significantly when in an energy patch.

A general question arising when comparing the self-propelled agent models which lead to circular motion based on self-organization is which ingredients are necessary for circular motion to occur and which are not necessary? To answer this question and to simulate the observed behavior in single *Daphnia* we developed a self-propelled agent model based on random walks with the aim of being as simple as possible. The final model, being closely related to the model of Schweitzer et al. (1998), consists of two ingredients, a short range temporal correlation to simulate the general movement of the *Daphnia* in darkness and an attraction to light to reproduce the circular motion in the light field.

3.1 Random Walk with Short Range Correlation

Discrete random walk models with interactions and memory or correlation are powerful tools to simulate various biological, chemical and physical processes which are more complex than pure Brownian motion (Hughes 1995). In our case, long range interactions are undesirable as we want to keep the model simple, but it is constructive to incorporate a short range correlation between the moves to take care of the fact that *Daphnia* do not move completely randomly but try to cover as much territory as possible (Gerritson and Strickler 1977). So instead of randomly choosing the direction of the next step from a uniform distribution, as done in the pure random walk model, our walker chooses its direction according to the experimentally determined distribution of turning angle (DTA) between two successive steps of *Daphnia* moving in the dark (see Fig. 5). The memory introduced into our agent by applying the DTA most likely is considerable shorter than the memory of *Daphnia*, but following our aim to keep the model simple the DTA provides us with a reasonable approximation. It takes care of the important fact that due to the shape of their body and their moving devices *Daphnia* are biased to move forward. Since the move length and velocity of *Daphnia* is relatively constant (Dodson 1996), the assumption of moving unit step length in unit time, which is inherently incorporated in the discrete random walk model with constant velocity, is satisfying.

3.2 Random Walk with Short Range Correlation and Attraction to Light

To simulate the behavior of *Daphnia* in a light field with radial symmetry an attraction to the light proportional to the distance of the agent to the light source and proportional to the normalized attraction strength parameter $L/(1–L)$ is incorporated into the random walk model described in *Section 3.1*. For every time step, the walker randomly chooses a direction from the DTA, then a "kick" towards the light is added and the final head-

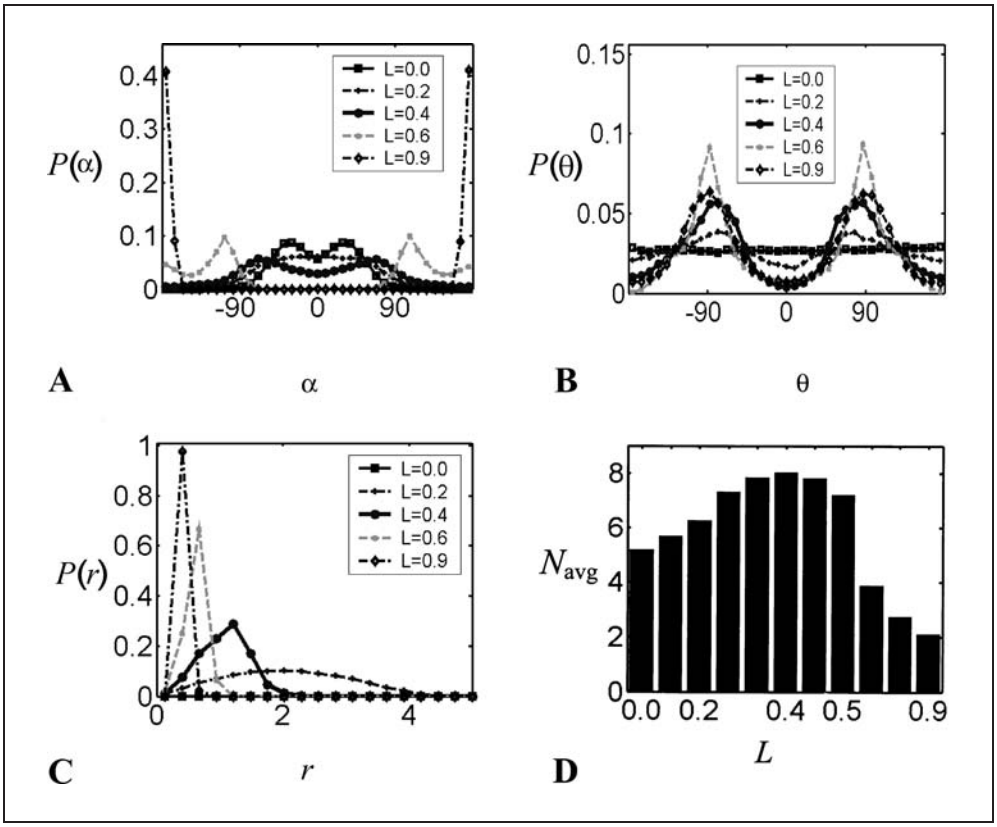

Fig. 6 Characterization of the motion of a random walker with DTA and attraction strength, L, to the light, determined from 50,000 moves for L varying from $L = 0.0$ to $L = 0.9$. (*A*) Probability distribution, $P(\alpha)$, of the turning angle α of the walker between successive moves for $L = 0.0$, 0.2, 0.4, 0.6, 0.9. Note that for the case $L = 0.0$ the DTA inserted in the model is visible. For circling to take place it is necessary that the positions of the maxima are smaller than $\pm 120°$, which is true for $L < 0.7$. (*B*) Probability distribution, $P(\theta)$, of the angle θ between the heading of the walker and the direction to the light shaft for $L = 0.0$, 0.2, 0.4, 0.6, 0.9. Maxima at $\pm 90°$, which occur for $L > 0.3$, are necessary for circling to be present. (*C*) Probability distribution, $P(r)$, of the distance r of the walker to the light shaft for $L = 0.0$, 0.2, 0.4, 0.6, 0.9. (*D*) Average number, N_{avg}, of successive moves circling in one direction before changing the direction for $L = 0.0$, 0.1, 0.2, 0.3, 0.35, 0.4, 0.45, 0.5, 0.6, 0.7, 0.9. Best circling is observed for $L = 0.4$, in accordance with the observations made in (*A*) and (*B*). An average circling duration of $N_{avg} = 8$ moves for $L = 0.4$ combined with an average circling radius of $r = 1.6$ for $L = 0.4$ yields that the walker is almost circling a full orbit on average before changing the direction.

ing is rescaled to unit length to maintain constant velocity of the walker. Simulating the moves of the walker for varying attraction strength $L \in [0, 1)$ and characterizing the movement with the same measures used for the *Daphnia* tracks in *Section 2.2* reveals that the walker circles on average around the light source in both directions for medium attraction strength $L = 0.4$ and frequently changes its circling direction (see Fig. 6). For smaller L the circular motion is less pronounced as the influence of the randomness increases. For larger L the circling breaks down and the walker mainly steps back and forth over the light source as the attraction to light governs the movement, and absolute turning angles $|\alpha| \geq 120°$ dominate. Without including the DTA in the model, no circular motion of the walker develops for any value of the attraction strength, the motion is always dominated by stepping back and forth over the light source.

Comparing the experimentally observed behavior of the *Daphnia* and the above random walk model with aforementioned agent models reveals that the essential ingredients for vortex motion to occur are: (*i*) self-propelled agents with a preference to move forward within a certain velocity range, (*ii*) a point attraction, either directly in form of an external parabolic potential as in the Active Brownian Particle models and the present model or indirectly in form of an effective mean field potential resulting from the particle-particle interaction in a certain parameter range as in the model by Levine et al. (2001), and (*iii*) alignment for symmetry breaking, either directly as in the models of Schweitzer et al. (2001) and Levine et al. (2001) or indirectly *via* the water drag as observed for vortex-swarming *Daphnia*.

4. Discussion and Conclusion

Although for *Daphnia* the interaction that leads to swarming in general and vortex-swarming in particular is not a direct one, as it is the case of birds and fish, and *Daphnia* swarms do not perform complex predator avoidance maneuvers like swarm splitting and combining (Hall 1986), nevertheless, the observation of vortex-swarming *Daphnia* in the lab provides the possibility to learn more about the general physical, chemical and biological aspects of vortex-swarming in prey animals. Further experiments with *Daphnia* have to include systematical investigations of the factors observed to enhance vortex-swarming such as kairomone intensity, *Daphnia* density and food density. In particular the detailed light conditions in the two different tanks as well as the light perception of the *Daphnia* and the physical aspects of the fluid dynamic vortex to occur need more attention.

Apart from this, our simulation indicates that the experimentally observed bimodal symmetric DTA for *Daphnia* and copepods is important for performing a circular motion, and thus might be a general feature detectable for other animals, as well. Why the movement of these animals follows such a distribution and how animals actually choose to turn either left or right is an unsolved question.

Acknowledgements

A. O. gratefully acknowledges financial support by the Alexander von Humboldt Foundation (Feodor Lynen-Fellowship). We thank Beatrix Beisner, Winfried Lampert, David Russell, Rudi Strickler, Allan Tessier, and Lon Wilkens for valuable suggestions concerning zooplankton behavior and experimental set-up as well as Daniel Pflugfelder for the assistance in modeling, supported by the U. S. Office of Naval Research.

References

Bertram, B. C. R.: Living in groups: predators and prey. In: Krebs, J. R., and Davies, N. B. (Eds.): Behavioral Ecology; pp. 64–96. Oxford: Blackwell Scientific Publications 1978

Brewer, M. C., and Coughlin, J. N.: Virtual plankton: A novel approach to the investigation of aquatic predator-prey interactions. In: Lenz, P. H., Hartline, J. E., Purcell, J. E., and Macmillan, D. L. (Eds.): Zooplankton: Sensory Ecology and Physiology. Amsterdam: Gordon and Breach Publishers 1996

Buchanan, C., and Goldberg, B.: The action spectrum of *Daphnia magna* (Crustacea) phototaxis in a simulated natural environment. Photochem. Photobiol. *34,* 711–717 (1981)

Buskey, E. J., Peterson, J. O., and Ambler, J. W.: The role of photoreception in the swarming behavior of the copepod *Dioithona oculata*. In: Lenz, P. H., Hartline, J. E., Purcell, J. E., and Macmillan, D. L. (Eds.): Zooplankton: Sensory Ecology and Physiology. Amsterdam: Gordon and Breach Publishers 1996

Camazine, S., Deneubourg, J.-L., Franks, N. R., Sneyd, J., Theraulaz, G., and Bonabeau, E.: Self-Organization in Biological Systems. Princeton and Oxford: Princeton University Press 2001

Caraco, T. S., Martindale, S., and Pulliam, H. R.: Avian flocking in the presence of a predator. Nature *285*, 400–401 (1980)

Czirók, A., Ben-Jacob, E., Cohen, I., and Vicsek, T.: Formation of complex bacterial patterns via self-generated vortices. Phys. Rev. E *54*, 1791–1801 (1996)

Dawidowicz, P.: Costs of behavioral defense against predation: A model of diel vertical migration in zooplankton. Wiadomosci Ekologiczne *45*, 3–16 (1999)

Dodson, S. I.: Optimal swimming behavior of zooplankton. In: Lenz, P. H., Hartline, J. E., Purcell, J. E., and Macmillan, D. L. (Eds.): Zooplankton: Sensory Ecology and Physiology. Amsterdam: Gordon and Breach Publishers 1996

Ebeling, W., and Schweitzer, F.: Swarm of particle agents with harmonic interactions. Theory Biosci. *120*, 207–224 (2001)

Gerritson, J., and Strickler, J. R.: Encounter probabilities and community structure in zooplankton: a mathematical model. J. Fish. Res. Board Can. *34*, 73–82 (1977)

Gibson, G.: Swarming behaviour of the mosquito *Culex pipens quinquefasciatus*: a quantitative analysis. Physiol. Entom. *10*, 283–296 (1985)

Gries, T., Jöhnk, K., Fields, D., and Strickler, J. R.: Size and structure of 'footprints' produced by *Daphnia*: impact of animal size and density gradients. J. Plankton Res. *21*, 509–523 (1999)

Hall, S. J., Wardle, C. S., and MacLennan, D. N.: Predator evasion in a fish school: test of a model of the fountain effect. Marine Biol. *91*, 143–148 (1986)

Hamilton, W. D.: Geometry for the selfish herd. J. Theor. Biol. *31*, 295–311 (1971)

Haury, L. R., and Yamazaki, H.: The dichotomy of scales in the perception and aggregation behavior of zooplankton. J. Plankton Res. *17*, 191–197 (1995)

Hughes, B. D.: Random Walks and Random Environment. Vol. 1. Random Walks. Oxford: Oxford University Press 1995

Humphries, D. A., and Driver, P. M.: Erratic display as a defense against predators. Science *156*, 1767–1768 (1967)

Huth, A., and Wissel, C.: The simulation of the movement of fish schools. J. Theor. Biol. *156*, 365–385 (1992)

Jakobsen, P. J., Birkeland, K., and Johnsen, G. H.: Swarm location in zooplankton as an anti-predator defense mechanism. Anim. Behav. *47*, 175–178 (1994)

Jakobsen, P. J., and Johnsen, G. H.: The influence of food limitation on swarming behaviour in the waterflea *Bosmina longispina*. Anim. Behav. *36*, 991–995 (1988)

Jensen, K. H., Jakobsen, P. J., and Kleiven, O. T.: Fish kairomone regulation of internal swarm structure in *Daphnia pulex* (Cladocera: Crustacea). Hydrobiologia *368*, 123–127 (1998)

Kvam, O. V., and Kleiven, O. T.: Diel horizontal migration and swarm formation in *Daphnia* in response to *Chaoborus*. Hydrobiologia *307*, 177–184 (1995)

Larson, P., and Dodson, S.: Invited Review: Chemical communication in planktonic animals. Arch. Hydrobiol. *129*, 129–155 (1993)

Levine, H., Rappel, W.-J., and Cohen, I.: Self-organization in systems of self-propelled particles. Phys. Rev. E *63*, 017101–(1–4) (2001)

LOBEL, P. S., and RANDALL, J. E.: Swarming behavior of the hyperiid amphipod *Anchylomera blossevilli*. J. Plankton Res. *8*, 253–262 (1986)
MILINSKI, M.: Can an experienced predator overcome the confusion of swarming prey more easily? Anim. Behav. *27*, 1122–1126 (1979)
NEILL, S. R. S. J., and CULLEN, J. M.: Experiments on whether schooling by their prey affects the hunting behaviour of cephalopods and fish predators. J. Zool. Lond. *172*, 549–469 (1974)
NIHONGI, A., ORDEMANN, A., and STRICKLER, R.: Behavior of zooplankton in a vertical strange attractor under kairomone existence. (In preparation)
NOVALES, F. I., and BROWMAN, H. I.: Wavelength-dependent polarization orientation in *Daphnia*. J. Comp. Physiol. A *186*, 1073–1087 (2000)
OGHUCHI, O.: Experiments on the selection against color oddity of water fleas by the three-spined sticklebacks. Z. Tierpsychol. *47*, 254–267 (1978)
OKUBO, A.: Dynamical aspects of animal grouping: swarms, schools, flocks, and herds. Adv. Biophys. *22*, 1–94 (1986)
OKUBO, A., and ANDERSON, J. J.: Mathematical models for zooplankton swarms: Their formation and maintenance. Eos *65*, 731–733 (1984)
OKUBO, A., and LEVIN, S. A.: Diffusion and Ecological Problems. New York: Springer 2002
PARRISH, J. K., and EDELSTEIN-KESHET, L.: Complexity, pattern, and evolutionary trade-offs in animal aggregation. Science *284*, 99–101 (1999)
PARTRIDGE, B. L.: The structure and function of fish schools. Scientific American *246*, 90–99 (1982)
PARTRIDGE, B. L., and PITCHER, T. J.: Evidence against a hydrodynamic function for fish schools. Nature *279*, 418–419 (1979)
PARTRIDGE, B. L., and PITCHER, T. J.: The 3-D structure of fish schools. Behav. Ecol. Sociobiol. *6*, 277–288 (1980)
PIJANOWSKA, J.: Fish-enhanced patchiness in *Daphnia* distribution. Verh. Int. Ver. Limnol. *25*, 2366–2368 (1994)
POTTS, W. K.: The chorus-line hypothesis of maneuver coordination in avian flocks. Nature *309*, 344–345 (1984)
PULLIAM, H. R.: The advantage of flocking. J. Theor. Biol. *38*, 419–422 (1973)
RAPPEL, W.-J., NICOL, A., SARKISSIAN, A., LEVINE, H., and LOOMIS, W. F.: Self-organized vortex state in two-dimensional *Dictyosetelium* dynamics. Phys. Rev. Lett. *83,* 1247–1250 (1999)
REYNOLDS, C.: Flocks, herds, and schools: a distributed behavioral model. Comp. Graph. *21*, 25–34 (1987)
RHODE, S. C., PAWLOWSKI, M., and TOLLRIAN, R.: The impact of ultraviolet radiation on the vertical distribution of zooplankton of the genus *Daphnia*. Nature *412*, 69–72 (2001)
SCHIMANSKY-GEIER, L., MIETH, M., ROSE, H., and MALCHOW, H.: Structure formation by active Brownian particles. Phys. Lett. A *207*, 140–146 (1995)
SCHMITT, F. G., and SEURONT, L.: Multifractal random walk in copepod behavior. Physics A *301,* 375–396 (2001)
SCHWEITZER, F., EBELING, W., and TILCH, B.: Complex motion of Brownian particles with energy depots. Phys. Rev. Lett. *80*, 5044–5047 (1998)
SCHWEITZER, F., EBELING, W., and TILCH, B.: Statistical mechanics of canonical-dissipative systems and applications to swarm dynamics. Phys. Rev. E *64*, 021110–(1–12) (2001)
SCHWIND, R.: *Daphnia pulex* swims towards the most strongly polarized light – A response that leads to 'shore flight'. J. Exp. Biol. *202*, 3631–3635 (1999)
SMITH, K. C., and MACAGNO, E. R.: UV photoreceptors in the compound eye of *Daphnia magna* (Crustacean, Branchiopoda). A fourth spectral class in single ommatidia. J. Comp. Physiol. A *166*, 597–606 (1990)
VICSEK, T.: Fluctuations and Scaling in Biology. Oxford: Oxford University Press 2001
VICSEK, T., CZIRÓK, A., BEN-JACOB, E., COHEN, I., and SHOCHET, O.: Novel type of phase transition in a system of self-driven particles. Phys. Rev. Lett. *75*, 1226–1229 (1995)
WEIHS, D.: Hydromechanics of fish schooling. Nature *241*, 290–291 (1973)
YOUNG, S., and GETTY, C.: Visually guided feeding behaviour in the filter feeding cladoceran, *Daphnia magna*. Anim. Behav. *35*, 541–548 (1987)
YOUNG, S., and TAYLOR, V. A.: Swimming tracks in two cladoceran species. Anim. Behav. *39*, 10–16 (1990)
ZARET, R. E.: The animal and its viscous environment. In: KERFOOT, W. C. (Ed.): Evolution and Ecology of Zooplankton Communities; pp. 3–9. Hanover: University Press of New England 1980

ZARET, T. M., and SUFFERN, J. S.: Vertical migration in zooplankton as a predator avoidance mechanism. Limnol. Oceanogr. *21*, 804–813 (1976)

Dr. Anke ORDEMANN
Center for Neurodynamics
University of Missouri at St. Louis
8001 Natural Bridge Road
St. Louis, MO 63121
USA
Phone: ++1 31 45 16 61 15
Fax: ++1 31 45 16 61 52
E-Mail: ordemann@neurodyn.umsl.edu

Nova Acta Leopoldina NF *88*, Nr. 332, 105–127 (2003)

Behavioral Stochastic Resonance: Modeling and Theory

Jan A. FREUND (Berlin)

With 14 Figures

Abstract

The phenomenon of behavioral stochastic resonance was discovered by RUSSELL et al. (1999) in a laboratory experiment by observing the feeding behavior of the paddlefish (*Polyodon spathula*) in the presence of well-controlled artificial electrical noise. The additional hypothesis of swarms of *Daphnia* (zooplankton) providing a natural source of electrical noise required further measurements and analyses to evaluate the chances that this effect plays a role in the natural environment of the paddlefish. We briefly sketch analytic approaches to describe the noise-assisted detection mechanism of subthreshold signals using either a bistable or a threshold model. The findings are spatial contour plots of the detectability in the plane spanned by the electroreceptor on the rostrum, the prey (a single outlier *Daphnia*), and the center of the *Daphnia* swarm. The results support the notion of behavioral stochastic resonance in the wild and thus will serve useful in the planning of future behavioral experiments.

Zusammenfassung

Das Phänomen der stochastischen Resonanz in der Verhaltensbiologie wurde von RUSSELL et al. (1999) in einem Laborexperiment entdeckt, in welchem das Freßverhalten des Löffelstörs (*Polyodon spathula*) in der Gegenwart von kontrolliertem elektrischem Rauschen beobachtet wurde. Die zusätzliche Hypothese von Schwärmen von *Daphnien* (Zooplankton) „als natürlicher Rauschquelle" erforderte weiterführende Messungen und Analysen, um die Chancen dafür zu bewerten, daß das Phänomen der stochastischen Resonanz in der Verhaltensbiologie auch unter natürlichen Bedingungen eine Rolle spielt. Wir skizzieren analytische Ansätze zur Beschreibung des rauschunterstützten Detektionsmechanismus von unterschwelligen Signalen, welche auf einem bistabilen oder einem Schwellwertmodell basieren. Die Ergebnisse der Analysen lassen sich durch räumliche Detektionskonturlinien in der Ebene, die von den Elektrorezeptoren auf dem Rostrum, der Beute (einer einzelnen, vom Schwarm isolierten *Daphnia*) und dem Schwarmmittelpunkt aufgespannt wird, darstellen. Insgesamt unterstützen die Analysen die Vorstellung, daß die stochastische Resonanz auch unter natürlichen Bedingungen eine effizientere Jagdstrategie ermöglicht. Die quantitativen Resultate werden bei der Planung zukünftiger Verhaltensexperimente hilfreich sein.

1. Introduction

Historically, the natural sciences of physics and biology have developed side by side with physics primarily aiming at an understanding and description of inanimate phenomena, e. g. celestial mechanics, electromagnetism, or the atomic structure, and with biol-

ogy exclusively investigating objects that are endowed with the "essence of life". Cross-links between physics and biology were established, for instance, when the botanist Robert BROWN in 1882 observed the irregular motion of pollen grains suspended in water. Although he had not discovered the "molecules of life", as he first suspected, his observation still initiated an important research field of physics later termed Brownian motion. Another example proving the cross-fertilization of both natural sciences is the topic of neural networks (HOPFIELD 1982).

It is generally accepted that the fundamental laws of physics, derived from the observation of inanimate objects, should never be in contradiction with the dogmas of biology. Sometimes a paradox could be resolved by careful revision of observations and concepts: the reconciliation of all living systems with the second law of thermodynamics (by a reformulation of the latter for open systems) is one of the most illustrious examples (OSTWALD 1931, SCHRÖDINGER 1948, GLANSDORFF and PRIGOGINE 1971).

Traditional objects of physics are typically understood as a small or large collection of only a few different elementary units. As examples consider a typical solid or a gas that are both built from a huge number of molecules of a few species. Likewise, in granular physics a container filled with sand is successfully modeled as a huge collection of individual grains that are completely characterized by their size and a few constants accounting for their elastic and viscous properties. In contrast, biological objects are complex structures, composed of a myriad of different units each possessing a rich substructure, and being involved in an intricate network of interactions. This statement can be made regardless of a specific scale, be it the DNA, the cellular, tissue, or organ level, be it the behavioral level of individuals or of ecological groups.

From this viewpoint it is intriguing to investigate whether a phenomenon like Stochastic Resonance (SR) could have any functional benefit for the performance of a task relevant in a biological context. If so, evolution provides an explanation how fundamental mechanisms have pervaded the different levels of self-organization of a biological being (EBELING et al. 1990). Nevertheless, and in spite of being used to the success of reductionism: to find an effect from inanimate world, like SR, acting on the highest biological, the behavioral level, is still absolutely remarkable.

This paper is organized as follows: in *Section 2* we briefly review the essential features of SR introducing its two paradigm models: the bistable potential and the threshold system. The phenomenon of phase synchronization in stochastic systems and methods of its description are introduced in *Section 3* and its relation to SR is touched upon. In *Section 4* we introduce the paddlefish, the *Daphnia* and review in brief the behavioral SR experiment performed in St. Louis. *Section 5* is devoted to the measurements and following analysis of the *Daphnia* swarm activity. Eventually, in *Section 6* we outline the steps that lead to the quantitative prediction of behavioral SR in the wild. Discussions and a short summary will close this presentation.

2. A Primer on Stochastic Resonance

In everyday life, noise is considered as being detrimental to the performance of any task, be it a telephone conversation or the perception of a movie on a flickering TV screen. Hence, the assertion that noise or fluctuations can improve some functionality first

comes as a surprise. In fact, the thrust of SR research comes from this counterintuitive central statement. However, the phenomenon immediately becomes intelligible to the layman when mentioning that SR occurs in systems, which in the absence of fluctuations perform no function at all. As an illustration consider the following two paradigm systems in Figures 1 and 2.

In Figure 1 we sketched a double well potential that is modified in time by an external periodic signal. The function is to detect and amplify the subthreshold signal and shall be realized by the overdamped motion of a fictitious particle in this oscillating potential. Subthreshold means here that the external signal amplitude is small enough not to deform the potential in such a way that the barrier separating the two wells is lost. The amplification mechanism requires the fictitious particle – indicated by the little circles in Figure 1 – to make transitions across the barrier. However, in the absence of fluctuations the particle never performs any transition at all but, instead, oscillates in one of the two minima. Only when tuning in noise the particle can jump across the barrier and it does so preferentially when the barrier is lowered by the external signal. Rate theory (HÄNGGI et al. 1990) teaches that high and low barrier situations have transition rates that differ by an exponential (of the barrier asymmetry). For rather high noise intensities it is evident that the particle will practically respond to the large fluctuations alone and no longer feel the comparatively small variations of the potential. Thus, it comes as no surprise that for some intermediate noise intensity the particle can follow the external signal best.

Figure 2 contains three elements: a threshold (dashed horizontal line), a subthreshold periodic signal and fluctuations. As before, the function of this system is to detect and amplify the subthreshold signal. It performs this task by eliciting a spike whenever the

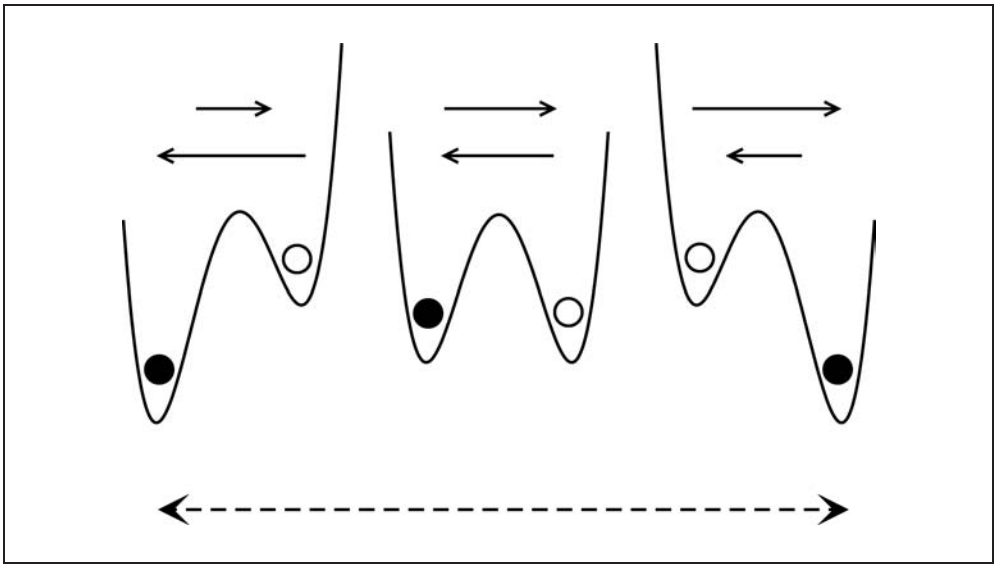

Fig. 1 The double well potential is driven by an oscillating external signal. The amplification mechanism is based on transitions across the barrier separating the two minima.

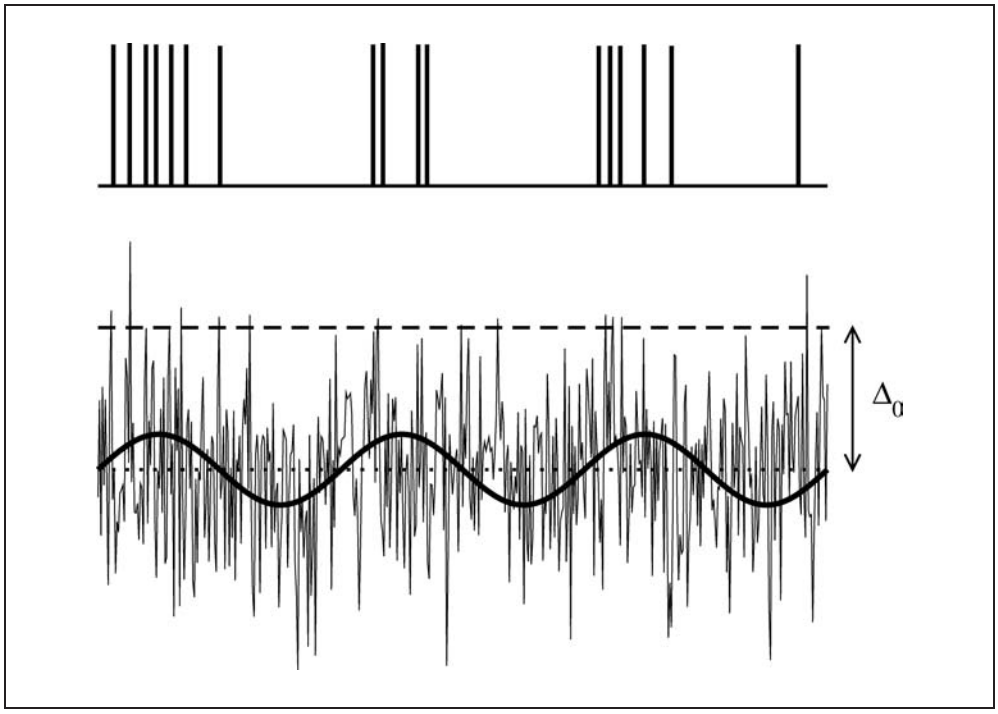

Fig. 2 The threshold system elicits a spike whenever the sum of the subthreshold sinusoidal signal and the instantaneous fluctuation crosses the threshold (dashed horizontal line) from below. The symbol Δ_0 denotes the gap between the signal median and the threshold. Figure adapted from FREUND et al. (2002).

sum of signal and fluctuation crosses the threshold from below. As is evident from the sketch without noise no spike will ever occur and for high noise intensities the small gap between signal and threshold becomes irrelevant for the generation of spikes. Again, for some intermediate noise intensity the correlation between the input signal and the resulting spike pattern will be maximal.

In both systems the effect of SR is rooted in the beneficial role of fluctuations, that cooperate with a subthreshold signal thus enabling and optimizing the functionality of a detector/amplifier. The periodically driven bistable potential was the first model to explain the effect of SR in the context of global climate modeling (glacial periods) (BENZI et al. 1981, NICOLIS 1981). Moreover, it was the basis for a popular adiabatic binary description (MCNAMARA and WIESENFELD 1989) that allows to easily extract analytic expressions for spectral measures of SR (GAMMAITONI et al. 1998), pinpointing the effect quantitatively. The threshold system, on the other hand, played a prominent role after SR was discovered in sensory neurons (LONGTIN et al. 1991, LONGTIN 1993). Since then it was repeatedly used to illustrate what is termed non-dynamical or threshold SR (MOSS et al. 1994).

It has to be noticed that the phenomenon of SR is not restricted to periodic signals but that extensions to aperiodic SR (NEIMAN and SCHIMANSKY-GEIER 1994, COLLINS et al. 1995) exist.

The fluctuations, that occur in the setup of SR, can have a different origin:

– They can be part of the signal. In this case one would adapt the characteristics of the nonlinear system to yield optimal functional performance.
– They can be intrinsic. From the viewpoint of physics internal noise is ubiquitous and related to the temperature of a system. On the one hand, it is widely appreciated that the role of internal noise in information-processing systems is generally negative. An appropriate method to reduce such detrimental effects is to use many elements in parallel (GAILEY et al. 1997). On the other hand, recent theoretical studies on channel noise in excitable membranes have shown that internal fluctuations can be functionally important (SCHMID et al. 2001, JUNG and SHUAI 2001).
– They can be external and additive to the signal. This is the case usually considered. The external character of noise also implies that one can control the intensity of fluctuations.

Of course, a mixed situation is also possible.

It is worth mentioning that an engineer's solution to the detection of subthreshold signals would probably be to lower the detection threshold. In fact, it is easy to show that adapting the threshold of a single unit to the signal median maximizes the transinformation (transmitted mutual information) and outperforms the situation with the original threshold and optimal noise by far. The effect of suprathreshold stochastic resonance (STOCKS 2000) is observed when feeding the signal simultaneously into a summing ensemble of detectors. It is based on the fact that noise effectively generates an ensemble of distributed thresholds that can sample the input signal with a much higher resolution. The optimal distribution of thresholds depends on the signal characteristics; when the latter are not known *a priori* or when the signal is non-stationary Gaussian white noise, indeed, proves to be the best strategy. The original claim of SR in a single element thus retains its validity in situations where the threshold cannot be lowered arbitrarily far, and it can be extended to the suprathreshold case when information is processed by a summing ensemble.

3. Stochastic Resonance and Noise-induced Phase Synchronization

Closely related with SR is the phenomenon of noise-induced phase synchronization (FREUND et al. 2000) or noise-enhanced phase coherence (NEIMAN et al. 1998). To explain the basic mechanism and its connection to SR we have to recall a few facts of synchronization phenomena and their description.

Classically, synchronization describes the adjustment of rhythms of oscillating objects due to their weak interactions (PIKOVSKY et al. 2001). Whereas the bidirectional interaction of two such self-sustained or autonomous oscillators is termed mutual synchronization, the case of unidirectional interaction is interpreted as forced synchronization by an external force and includes the standard setup of SR. In this case the two "rhythms" or, better, the two timescales are given by the external periodic signal and the stochastic flipping dynamics of the bistable system. The description of synchronization is based on a suitably defined phase difference

$$\varphi_{n,m}(t) = n\varphi_{out}(t) - m\varphi_{in}(t) \qquad [1]$$

between the instantaneous phase of the output $\varphi_{out}(t)$ and the instantaneous phase of the input $\varphi_{in}(t)$. The numbers n and m denote the locking mode $m : n$, i. e., after n periods of the input the output has completed m cycles. In the case of a purely deterministic dynamics synchronization in the $m:n$ locking mode reveals itself through the fact that the instantaneous phase difference is bounded for all times, i. e., $|\varphi_{n,m}(t)| < M$. For a stochastic dynamics with unbounded fluctuations, as they occur in standard Gaussian noise, this criterion has to be modified since sufficiently large fluctuations will cause phase slips that interrupt locking episodes. A useful definition is based on the observation that phase synchronization is realized effectively when the average duration of locking episodes $\langle T_{lock}\rangle$ is large in comparison with the period T_0 of the periodic input (Freund et al. 2001 a). The quantity $\langle T_{lock}\rangle$ is determined by both drift and diffusion of the phase difference $\varphi_{n,m}$; this connection is quantified by considering the second moment of the phase difference

$$\langle \varphi_{n,m}^2 \rangle = \langle \omega_{n,m} \rangle^2 \, \langle T_{lock} \rangle^2 + 2D_{n,m} \langle T_{lock} \rangle \qquad [2]$$

where $\langle \omega_{n,m}\rangle$ is the average "frequency", i. e., the generalized difference between the mean switching rate (multiplied with 2π) and the frequency of the external drive, and $D_{n,m}$ is the diffusion coefficient of the related phase difference $\varphi_{n,m}$. Vanishing $\langle \omega_{n,m}\rangle$ means vanishing drift, a situation called $(m:n)$ frequency locking. From Equation [2] it is obvious that frequency locking does not necessarily imply effective phase locking because he latter requires both drift and diffusion to be negligible. To solve for $\langle T_{lock}\rangle$ we have to specify what we understand by a phase slip: since phases are effectively 2π-periodic it is reasonable (at least for $n = m = 1$) to define $\langle \varphi_{n,m}^2 \rangle = \pi^2$ as the condition for a phase slip. From this we arrive at

$$\langle n_{lock} \rangle = \frac{\langle T_{lock} \rangle}{T_0} = \frac{D_{n,m}}{\langle \omega_{n,m} \rangle^2 \, T_0} \left[\sqrt{1 + \left(\frac{\pi \langle \omega_{n,m} \rangle}{D_{n,m}} \right)^2} - 1 \right] >> 1 \qquad [3]$$

which shows that the mean number of locked cycles $\langle n_{lock}\rangle$ can be computed when $\langle \omega_{n,m}\rangle$ and $D_{n,m}$ are known. These two quantities can be either extracted numerically from a time series – in connection with suitable phase definitions[1] – or, for model systems, be derived analytically from a stochastic phase dynamics (Freund et al. 2003). In Figure 3 we plot the analytic result of a calculation that was based on a dichotomous periodic input and a dichotomous output, the latter switching according to a Markovian dynamics formulated *via* a master equation (Freund et al. 2000). As can be seen for intermediate optimal noise intensity $\sigma^2/\Delta U \approx 0.16$ and sufficiently large signal amplitude the mean number of locked cycles can increase significantly.

The fact that noise-induced phase synchronization requires significantly large signals is in contrast to SR which also occurs for weak signals (in the linear response regime) (Gammaitoni et al. 1998). In this context it has to be mentioned that in the neurosciences yet another definition for phase synchronization is common. The criterion is based on the wrapped distribution[2] of the phase difference and states phase coherence

1 For example Hilbert phase, linear interpolating phase or discrete phase (Freund et al. 2001 a, Freund et al. 2003).

2 "wrapped" means that phases outside the interval $(0,2\pi)$ are mapped back using the operation (mod 2π).

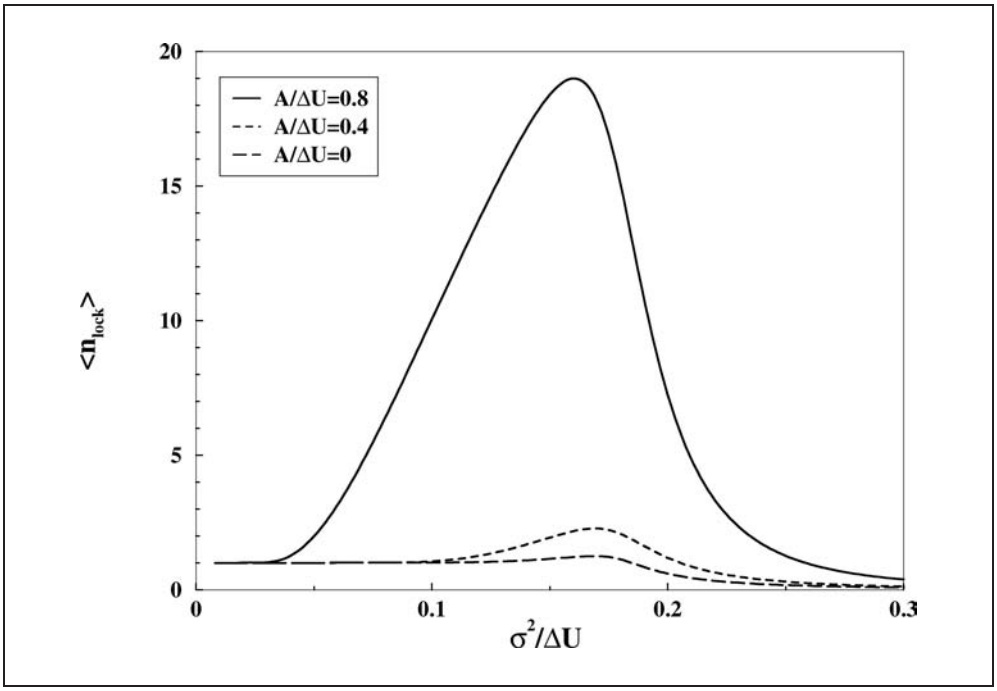

Fig. 3 The average number $\langle n_{lock} \rangle$ of locked cycles as a function of noise intensity $\sigma^2/\Delta U$ (abscissa) and of the relative signal amplitude $A/\Delta U$ (curve parameter). For sufficiently strong signals a pronounced maximum around $\sigma^2/\Delta U = 0.16$ indicates the occurrence of noise-induced phase synchronization.

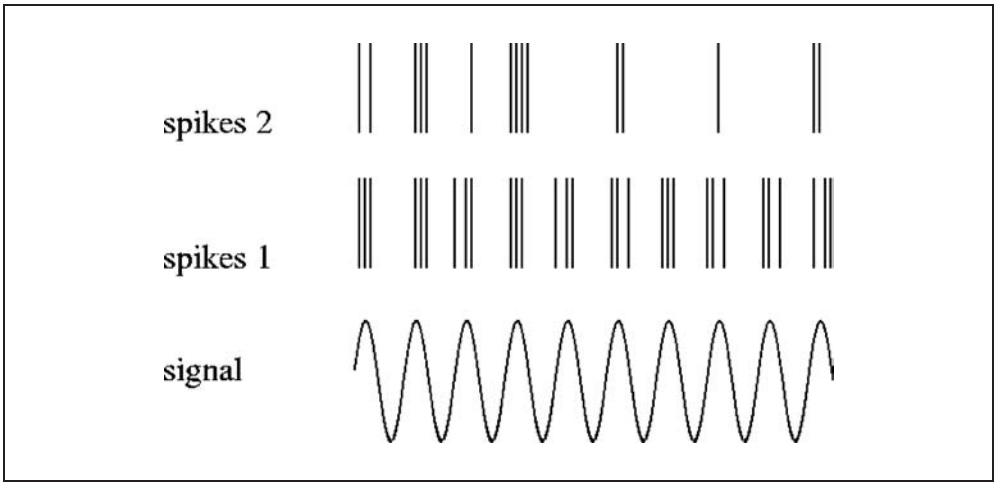

Fig. 4 Two spike patterns in (hypothetic) response to a subthreshold sinusoidal input signal. While both spike patterns yield a sharply peaked wrapped phase distribution ($\varphi_{1,3}$) only the lower row (spikes 1) exhibits an extended locking episode.

in the statistical sense whenever this distribution deviates significantly from the equidistribution. A glance at Figure 4 will immediately convince the reader that both spike patterns yield a sharply peaked wrapped distribution of $\varphi_{3,1}$. However, only one of the spike patterns exhibits an extended locking episode (with each maximum of the sinusoidal input being accompanied by three spikes). Moreover, it is evident that a peaked distribution is even to be expected in the region of suboptimal noise intensity, i. e., outside the SR regime.

4. The Paddlefish, the *Daphnia* and the St. Louis Experiment

In 1999 David RUSSELL and colleagues from St. Louis reported the exciting results of an experiment that established the phenomenon of behavioral SR (RUSSELL et al. 1999). Before actually describing the experiment in brief we have to provide a few important biological facts about the leading actors of the drama: the paddlefish and its favorite food, the *Daphnia* (zooplankton).

Paddlefish, *Polyodon spathula*, are among the largest freshwater fishes found in the river basins of North America and the Yangtze River in China, yet they feed exclusively on planktonic prey. They are found most often near the bottoms of rivers and lakes where

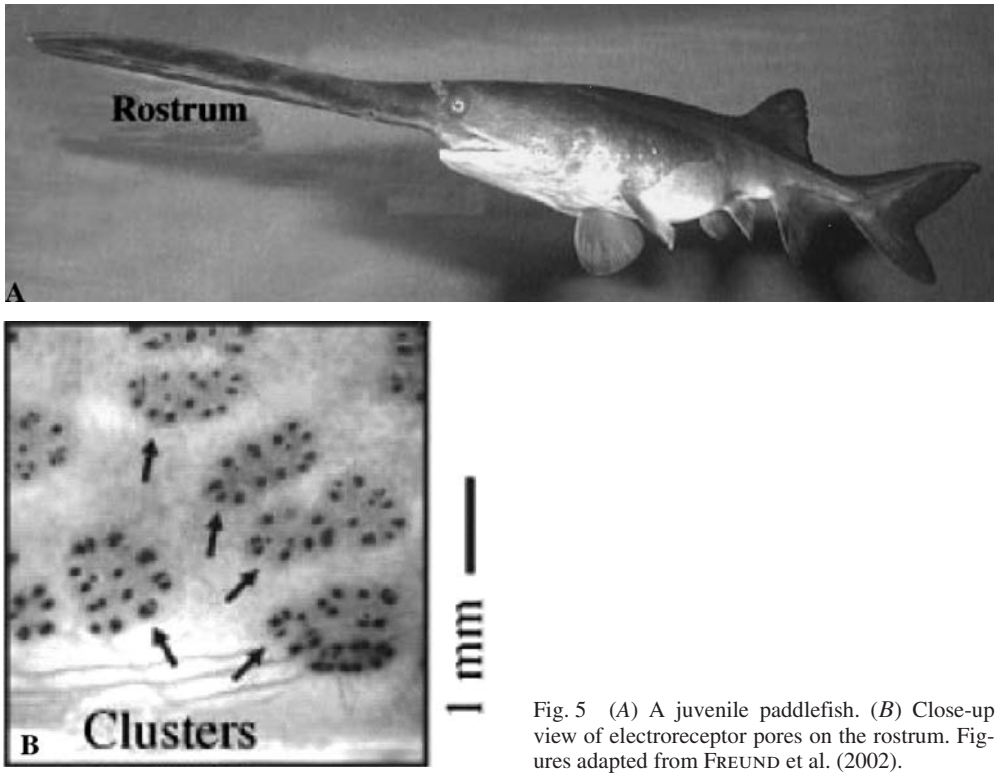

Fig. 5 (*A*) A juvenile paddlefish. (*B*) Close-up view of electroreceptor pores on the rostrum. Figures adapted from FREUND et al. (2002).

turbulence and muddy water obscure normal vision but where plankton is plentiful. In order to adapt to this environment, paddlefish, primeval creatures whose fossil record extends into the Cretaceous (65 million years ago) (GRANDE and BEMIS 1991), have evolved an elaborate array of electroreceptor organs spread over an elongated rostrum anterior to the mouth and head (see Fig. 5 *A*). The organs consist of clusters of ampullae of Lorenzini, which communicate with the water through short (0.1 mm) canals that terminate in pores on the skin surface, as shown in Figure 5 *B*. Prey, for example *Daphnia,* are detected and tracked exclusively by means of an entirely passive electric sensory system provided by the rostral array (WILKENS et al. 1997, NEIMAN et al. 2000, NEIMAN and RUSSELL 2001). This system has evolved to detect the weak electric fields emitted into the surrounding water by the *Daphnia*'s muscular activity associated with its swim-

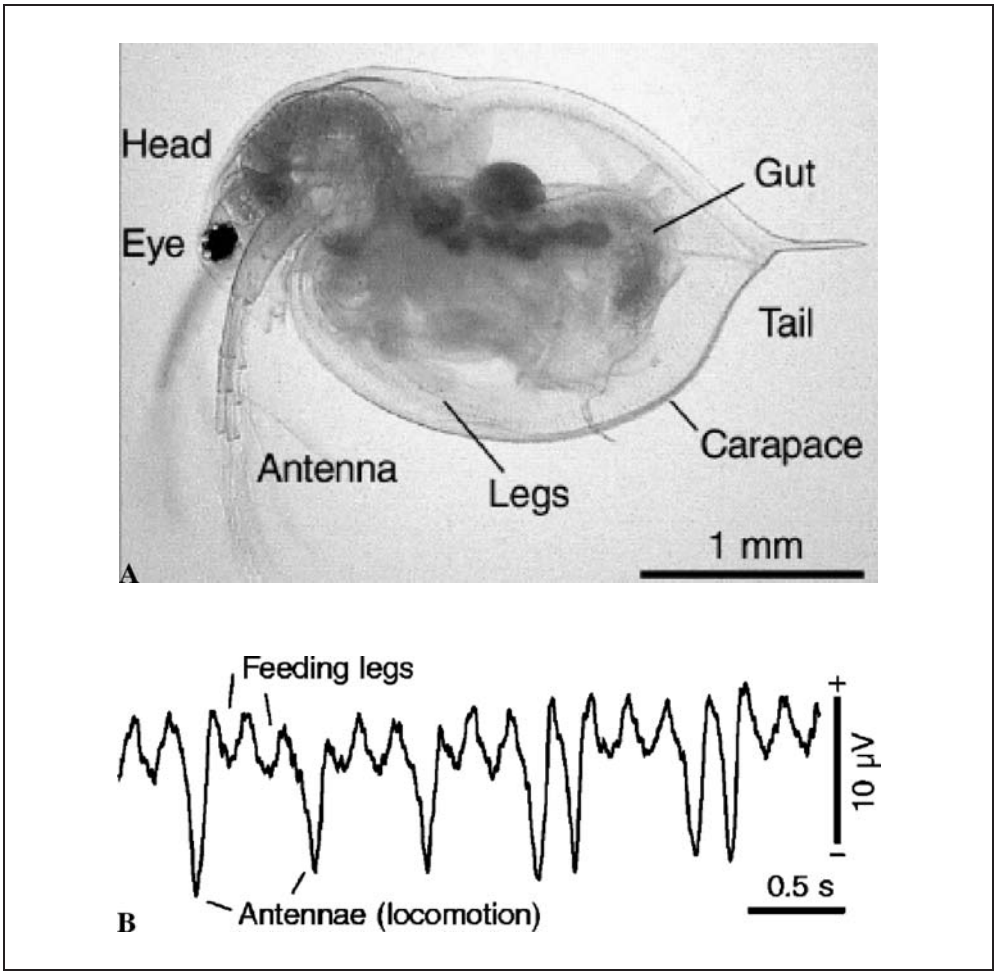

Fig. 6 (*A*) Sketch of a *Daphnia*. (*B*) The electric signal of a tethered *Daphnia* contains two oscillating components related to motion of the feeding legs and the locomotory antennae. Figures adapted from FREUND et al. (2001 b) and FREUND et al. (2002).

ming and feeding motions. Juvenile paddlefish (of less than 1 year old) locate, track and feed on single plankton (WILKENS et al. 1997, NEIMAN et al. 2000), whereas older fish, after having developed gill rakers, filter feed on swarms.

A favorite food of the paddlefish is the *Daphnia*, plankton of 1–2 mm length, commonly found in North American fresh water (see Fig. 6*A*). *Daphnia* emit weak dipole-shaped electric fields with both DC and oscillatory (4–15 Hz) components (see Fig. 6*B*). The intensity of the signal on the surface of the fish's rostrum decreases approximately as the inverse cube of the distance to the *Daphnia* because of the dipole-like shape of the field. Indeed, it has recently been shown, using the $1/r^3$ drop-off characteristic of the dipole field, that the Fisher information at the rostrum from a single *Daphnia* follows the prey capture probability exhibited by the fish (GREENWOOD et al. 2000). *Daphnia* that appear at larger distances from the fish are less likely to be detected and/or captured, because their signals on the rostrum are weaker owing to the $1/r^3$ law. However, external or environmental electrical noise can enhance the detectability of subthreshold signals at the edge of the animal's perception. Consequently, the probability that distant *Daphnia* are captured can be enhanced by the noise in a process called behavioral SR (RUSSELL et al. 1999).

The idea that electric noise, indeed, can enhance the detection of subthreshold signals was actually proven in the St. Louis experiment depicted in Figure 7.

All components of a classical SR experiment are given: a stochastic resonator related to the electroreceptors (or perhaps to some level of perception further downstream in the brain), a subthreshold electrical signal caused by the locomotory or feeding activity of remote *Daphnia*, and spatially homogenous electrical noise provided by a noise generator and a pair of electrodes. The properties, i. e., a typical time course and the spectrum of the artificial noise, are shown in Figure 8.

Projecting the locations of all *Daphnia* at the moment of initial detection onto the *x*–*y* plane (perpendicular to the rostrum axis with the rostrum tip pointing towards the origin,

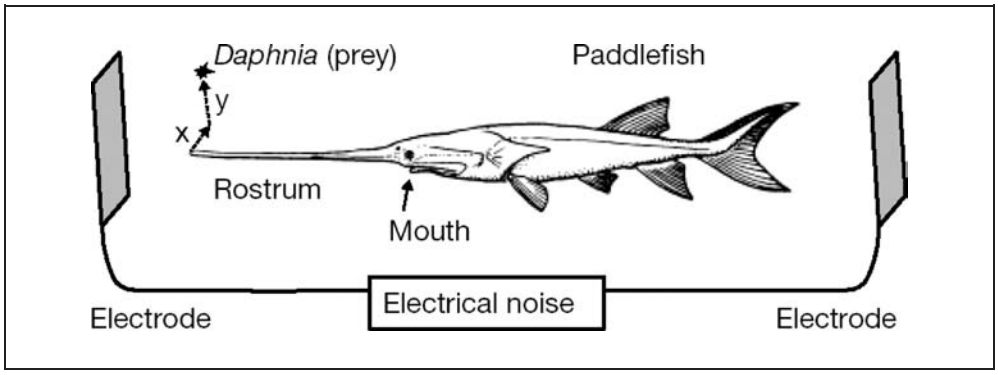

Fig. 7 Sketch of the swim mill that was used in the St. Louis experiment by RUSSELL et al. (1999): water recirculating (from left to right) at the natural swimming velocity of the paddlefish allowed observation of its responses to many passing-by *Daphnia* fed into the stream of water. The prey location at the instant of the first behavioral response (e. g. motion of the pectoral fin) was read from video recordings (side view and bottom view). A pair of electrodes provided spatially homogenous electrical noise. Figure adapted from RUSSELL et al. (1999).

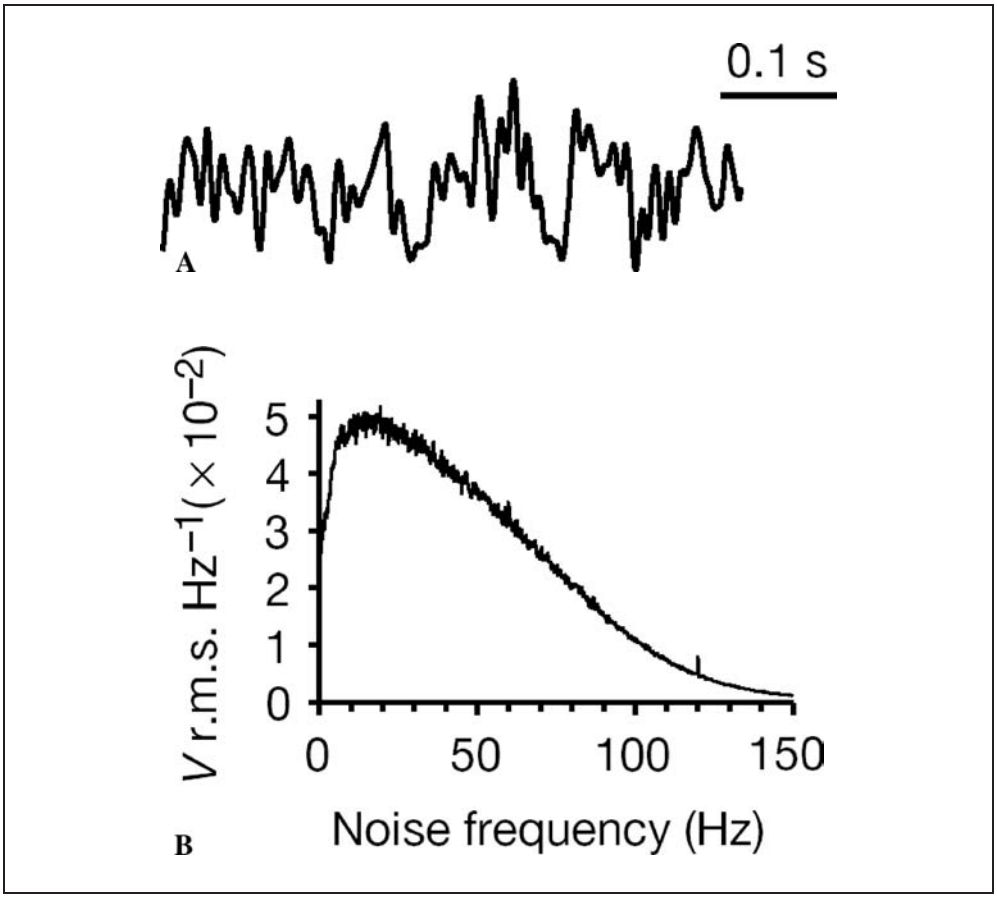

Fig. 8 (*A*) A typical time course of the artificial noise used in the St. Louis experiment; oscillations along the ordinate typically range between 0.05–50 μV cm^{-1} r. m. s. (*B*) The power spectrum of the artificial noise. Figures adapted from RUSSELL et al. (1999).

cf. Fig. 7) yields the scatter plots shown in Figure 9. The widening of the region of detectability in the presence of optimal noise is the key observation of behavioral SR (RUSSELL et al. 1999).

The conclusion of behavioral SR from the laboratory experiment was firmly established by carefully ruling out alternative explanations (RUSSELL et al. 2001). But where in the wild should the paddlefish encounter a natural source of external noise pushing the effect of behavioral SR beyond an academic laboratory experiment towards a realistic behavioral strategy optimized and proven by evolution? The speculative answer was already given by RUSSELL and colleagues (1999): in the natural environment of the paddlefish, i. e., in rivers beneficial fluctuations of the electrical field might be provided by swarms of *Daphnia*. This means the setup of the St. Louis experiment (Fig. 7) has to be replaced by the situation shown in Figure 10.

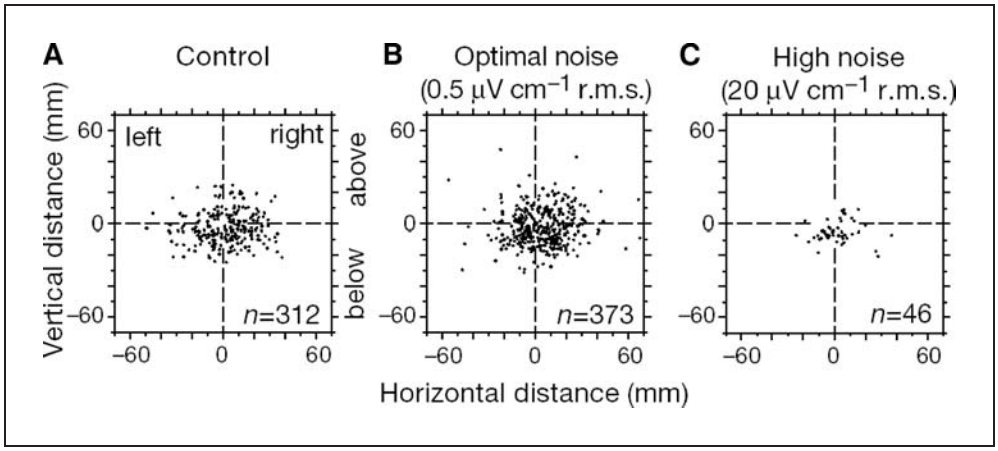

Fig. 9 Scatter plots of *Daphnia* locations at the moment of initial detection shown, (*A*) for the noiseless case (control), (*B*) for optimal noise, and (*C*) for rather high noise, clearly reveal the effect of behavioral SR: outliers that were not detected in the control experiment (*A*) and that evidently emit subthreshold electrical signals can be detected in the presence of optimal noise (*B*). At extremely high noise intensities (*C*) strong fluctuations have the expected detrimental effect. Figures adapted from RUSSELL et al. (1999).

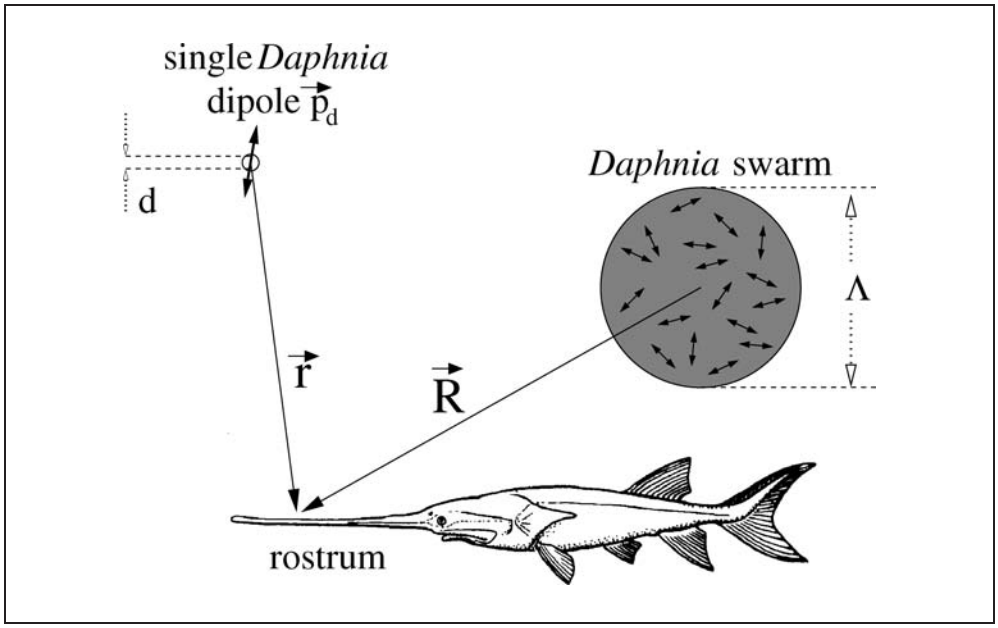

Fig. 10 Sketch of the behavioral SR setup in the wild: the pair of electrodes from the laboratory experiment is replaced by the *Daphnia* swarm. Figure adapted from FREUND et al. (2001 b).

5. *Daphnia* Swarms

The tendency of *Daphnia* to clump in clusters and form swarms of very high density (1000 to 9000 individuals per liter) was reported by many authors (COLEBROOK 1960, BRANDL and FERNANDO 1971, DAVIES 1985, KVAM and KLEIVEN 1995). Several explanations for this swarm formation exist ranging from physical processes in the water column, e. g. Langmuir circulations, to main biological drivers: avoidance of predators, location of food patches and location of mates (FOLT and BURNS 1999).

The avoidance of predators hypothesis is strongly supported by the observation that swarming more often occurs during daylight hours than at night (JAKOBSEN and JOHNSEN 1988, KVAM and KLEIVEN 1995) when visual predators like planktivorous fish and invertebrates would be most threatening. The strongest evidence for swarms induced by predation, however, is from predator kairomone studies (PIJANOWSKA and KOWALCZEWSKI 1997, JENSEN et al. 1998). Kairomones are chemical compounds that act as cues for the prey and are released by fish, invertebrate predators or even crushed bodies of *Daphnia*. When such kairomones are experimentally introduced into the water of *Daphnia* cultures, swarming behavior is induced (PIJANOWSKA and KOWALCZEWSKI 1997). When predators are present, formation of a group benefits the individual, because many identical prey individuals in random motion can distract or confuse predators and decrease their attack rates (MILINSKI 1986). Thus, the dilution effect affords a degree of safety to an individual within a group. The probability of an individual being attacked within a group is lower than for a solitary individual (BERTRAM 1978). Thus, swarming in *Daphnia* is likely a permanent behavioral strategy in systems where predators are abundant (JENSEN et al. 1998).

The signature of the electric fields from *Daphnia* swarms can be measured. In Figure 11 *A*, we show a photograph of a swarm in an aquarium. Figure 11 *B* shows the time course of the noise potential obtained at the location of the measuring electrode depicted in (*A*). The probability density of the amplitude of the potential is plotted in Figure 11 *C*. We note that it is well described by a Gaussian function as indicated by the solid curve. This supports the hypothesis of incoherent activity of *Daphnia* within the swarm. Figure 11 *D* presents the measured power spectrum of the *Daphnia* swarm.

The power spectrum is clearly representative of band-limited noise. Consequently, we shall approximate the swarm signal as Ornstein-Uhlenbeck (OU) doubly filtered noise (UHLENBECK and ORNSTEIN 1930, see also JUNG 1994, DOLAN et al. 1999). This noise, $\xi(t)$ is generated by a double-pole linear filter of white noise according to

$$\frac{\mathrm{d}^2\xi}{\mathrm{d}t^2} + \left(\frac{1}{\tau_1} + \frac{1}{\tau_2}\right)\frac{\mathrm{d}\xi}{\mathrm{d}t} + \frac{1}{\tau_1\tau_2}\xi(t) = \frac{\sqrt{D}}{\tau_1\tau_2}\Gamma(t) \qquad [4]$$

where D is the noise intensity, and $\Gamma(t)$ is white noise with zero mean and a delta autocorrelation function:

$$\langle\Gamma(t)\rangle = 0 \quad \text{and} \quad \langle\Gamma(t)\,\Gamma(t')\rangle = 2\delta(t-t') \qquad [5]$$

The filtered noise, $\xi(t)$, has two correlation times, τ_1 and τ_2 resulting in the stationary autocorrelation function (for $\tau_2 < \tau_1$)

$$C(\tau) = \frac{D}{\tau_1^2 - \tau_2^2}\left[\tau_1 \exp\left(\frac{|\tau|}{\tau_1}\right) - \tau_2 \exp\left(\frac{|\tau|}{\tau_2}\right)\right] \qquad [6]$$

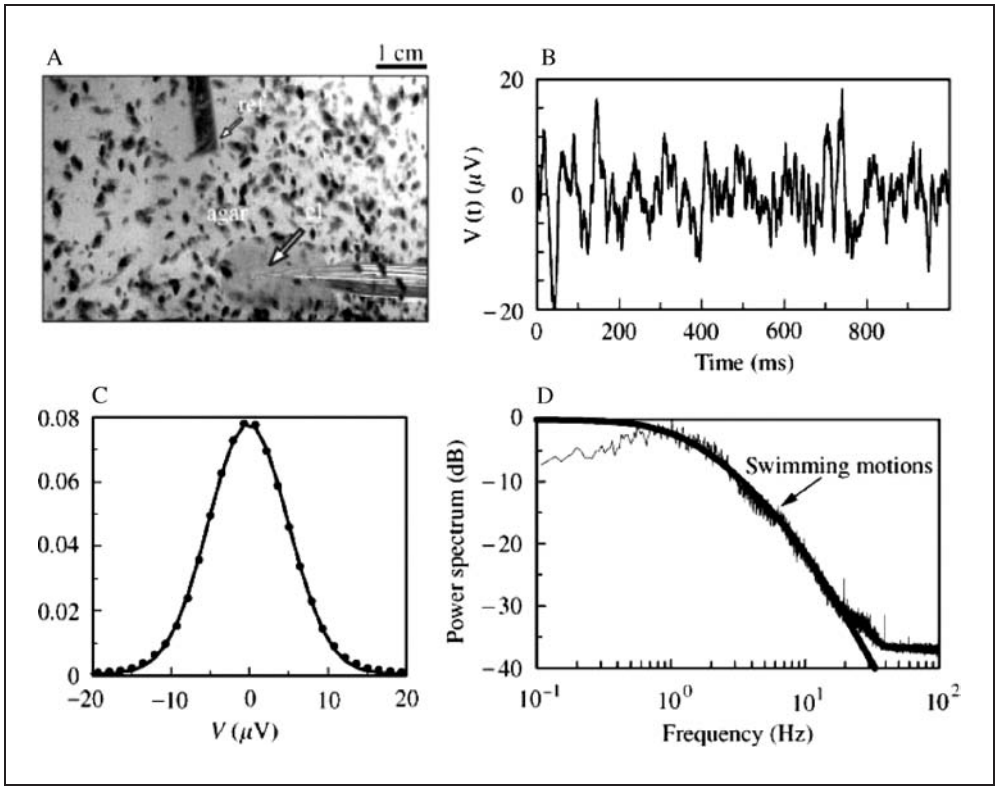

Fig. 11 (*A*) A photograph of a *Daphnia* swarm together with the measuring electrode (*lower arrow*) and the reference electrode (*upper arrow*). The measuring electrode is coated with a bead of agar, an electrically conducting substance, in order to minimize the effects from individual *Daphnia* colliding with the electrode tip. (*B*) Electric potential recorded from the measuring electrode shown in (*A*). (*C*) Measured amplitudes are distributed according to a Gaussian, thus, supporting the hypothesis of incoherent activity of *Daphnia* within the swarm. (*D*) The power spectrum of the measured swarm signal (fluctuating dotted line) together with a fit of Equation [7] (*fat solid line*) demonstrating that we can identify the swarm signal with doubly filtered Ornstein-Uhlenbeck noise. Figures adapted from FREUND et al. (2002).

and the (one-sided) power spectrum is given by

$$S_{\xi\xi}(\omega) = \frac{4D}{(1-\tau_1\tau_2\omega^2)^2+(\tau_1+\tau_2)^2\,\omega^2} \qquad [7]$$

where $\omega = 2\pi f$ is the angular frequency. The two time constants are characteristic of the dynamics of a system that would reproduce the swarm noise. The case $\tau_2 << \tau_1$ corresponds to the overdamped limit of the OU process, and the correlation function reduces to a simple single exponential and the power spectrum reduces to a Lorentzian. However, in the following, we shall need to calculate the mean threshold crossing rate of this noise, and this quantity must be finite. In the strictly overdamped limit, however, this is not the case, so we must retain both correlation times (STRATONOVICH 1963, JUNG 1994).

We note that the experimental power spectrum of the swarm, shown by the dots in Figure. 11 *D*, is very well described by this doubly filtered OU noise (Equation [7] with $\tau_1 = 0.13$ s and $\tau_2 = 0.017$ s) as shown by the solid curve.

Having specified the spectral properties of the swarm noise it remains to quantify its intensity $\sigma^2 = D/(\tau_1 + \tau_2)$ at the location of the receptor (on the rostrum). As is evident from Figure 10 this task involves the relative positions of the swarm and the receptor (paddlefish) and the swarm geometry (shape, diameter Λ, total number N of *Daphnia*, spatial density ρ).

To solve this problem we first note that $d << R$, $r << \lambda$ where d is the size of a *Daphnia* (mm), R (r) are the distances between the detecting site and the swarm center (the outlier *Daphnia*) (1–100 cm), and λ the wavelength of the oscillating signal (far beyond the km scale). Due to this the near-field limit of the electric dipole field applies, yielding

$$E(r,t) \propto \frac{3(n \bullet p_d)\, n - p_d}{r^3} \Rightarrow A = \frac{C_1}{r^3} \qquad [8]$$

$$E(R,t) \propto \int \frac{3[N(x) \bullet P(x,t)]\, N(x) - P(x,t)}{|R-x|^3}\, \rho(x)\, \mathrm{d}^3x \qquad [9]$$

where $\rho(\boldsymbol{x})$ describes the density of *Daphnia* within the swarm. Both expressions [8] and [9] contain the inverse cube of the distance and some dependence on the orientation of the dipole axis with respect to the direction of $\boldsymbol{n} = \boldsymbol{r}/r$ and $\boldsymbol{N}(\boldsymbol{x}) = \boldsymbol{R}(\boldsymbol{x})/R(\boldsymbol{x})$ (cf. Fig. 10 and 12). The signal amplitude A occurring in [8] corresponds to the maximum value of the field component of $\boldsymbol{E}$ at the rostral surface and C_1 denotes a first proportionality

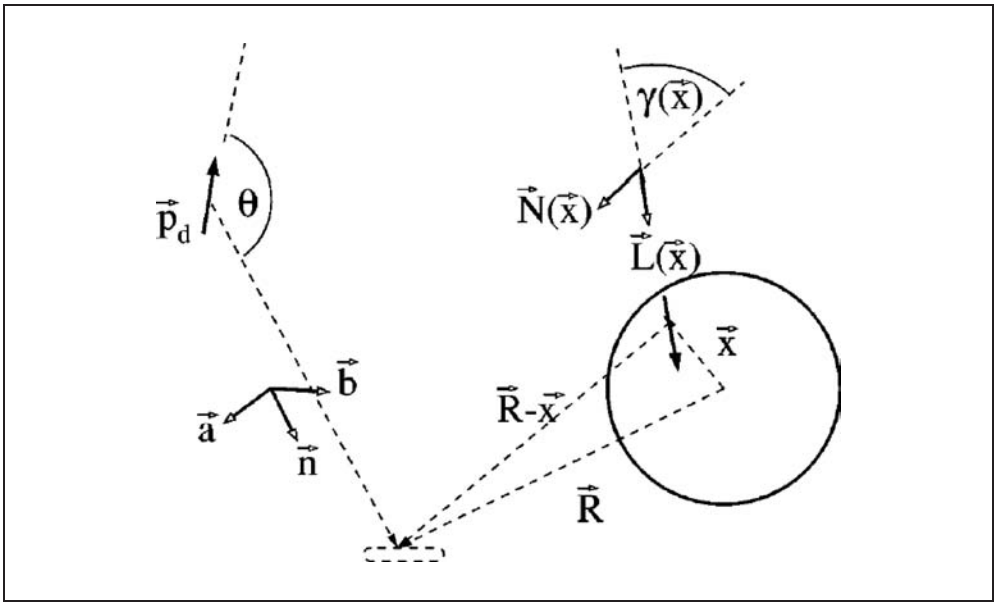

Fig. 12 The geometry of the predator-prey-swarm system. Figure adapted from FREUND et al. (2001 b).

constant. The locally varying net dipolemoment is specified as

$$P(x,t) = p_d L(x)\ e^{\mathrm{i}[\omega(x)t - \Psi(x)]} \qquad [10]$$

with $\boldsymbol{L}(\boldsymbol{x})$, $\omega(\boldsymbol{x})$, and $\psi(\boldsymbol{x})$ denoting the local orientation, frequency and phase of *Daphnia* in a compartment centered around $\boldsymbol{x}$.

Calculation of the swarm spectrum proceeds by writing down an expression for the correlation function of the electric dipole fields of *Daphnia* related to different times t and t' and different positions $\boldsymbol{R}$ and $\boldsymbol{R}'$ within the swarm. The assumption of incoherent *Daphnia* activity – supported by the Gaussian amplitude distribution (cf. Fig. 11 *C*) – is used to perform the average required by the correlation function. Fourier transformation then yields (according to the Wiener-Khinchin theorem) the power spectrum. Comparison with the spectrum of OU noise [7] thus provides an expression for the parameter D controlling the intensity of swarm noise

$$D \propto p_d^2 \int \frac{\rho(\boldsymbol{x})}{|\boldsymbol{R} - \boldsymbol{x}|^6}\ \mathrm{d}^3x \qquad [11]$$

that can be further evaluated when assuming a spherical homogenous density

$$D = \frac{C_2}{R^6} \frac{N}{\left(1 - \dfrac{\Lambda/2}{R}\right)^3 \left(1 + \dfrac{\Lambda/2}{R}\right)^3} \qquad [12]$$

where N is the total number of *Daphnia*, Λ is the diameter of the spherical swarm, and C_2 is a second proportionality constant.

The expressions in [8] and [12] quantify the dependences of the signal amplitude $A = C_1/r^3$ and swarm noise intensity $\sigma^2 = D/(\tau_1 + \tau_2)$ on the geometry of the system. The two proportionality constants C_1 and C_2 were fitted to experimental data (Freund et al. 2001 b).

6. Prediction of Behavioral SR in the Wild

In *Sections 2* and *3* we have outlined the mechanisms underlying SR and noise-induced phase synchronization. Moreover, we have pointed out that, according to our definition $\langle n_{lock} \rangle >> 1$, noise-induced phase synchronization is a stronger demand that also comprises the case of SR. In this section we will indicate how the quantifiers for both subthreshold detection mechanisms depend on the signal amplitude and the noise intensity and, thus, on the geometry of the predator-prey-swarm system. To obtain explicit expressions we have to specify model details for the threshold and the bistable system.

6.1 Behavioural SR Quantified via the Signal-to-noise Ratio

In Section 2 we introduced the threshold system that responds to every crossing of the threshold from below by eliciting a stereotypical pulse, say a rectangle of height Q and width δt. Now we make the additional assumptions that

– the spike generating threshold crossing events can be described as a renewal process, i. e., the events are uncorrelated and
– the adiabatic assumption: $f_0 << \langle \nu \rangle$ and f_n, where f_0 is the frequency of the driving signal (outlier *Daphnia* at 5–7 Hz), $\langle \nu \rangle$ is the mean threshold crossing rate and f_n is an upper cut-off frequency of the swarm noise.

The mean threshold crossing rate $\langle \nu \rangle$, scaled for Gaussian noise with standard deviation σ and a mean distance Δ below the threshold is given by the Rice formula (Rice 1954)

$$\langle \nu \rangle = \frac{\exp\left(-\frac{\Delta^2}{2\sigma^2}\right)}{2\pi} \left[\frac{\int_0^\infty \omega^2 S(\omega)\, \mathrm{d}\omega}{\int_0^\infty S(\omega)\, \mathrm{d}\omega} \right]^{\frac{1}{2}} \qquad [13]$$

where $S(\omega)$ is the one-sided power spectrum of the noise.

The mean amplitude $\langle V \rangle$ of the pulse train is related to this rate by

$$\langle V \rangle = Q\, \delta t \langle \nu \rangle \qquad [14]$$

where Q and δt are the aforementioned pulse height and width, respectively.

The power spectrum of the pulse train due to noise alone is given by Campell's theorem

$$P_n(\omega) = \frac{1}{2} Q^2\, \delta t^2 \langle \nu \rangle. \qquad [15]$$

By virtue of the adiabatic assumption the expressions [13] and [14] for the rate and the mean amplitude, respectively, are valid also for a slowly time varying signal $\Delta(t) = \Delta_0 + A \sin(\omega_0 t)$ with $\omega_0 = 2\pi f_0$ (the angular signal frequency). Sorting terms in the expansion of $\langle V \rangle(t) = \langle V \rangle[\Delta(t)]$ for small signal amplitudes, i. e. $A << \Delta_0$ (linear response regime), allows to extract from the power spectrum of the pulse train $P_s(\omega)$, now in presence of the weak signal, the coefficient of the delta function centered at the signal frequency, i. e., $P_s^\delta(\omega_0)$. In this way we find the signal-to-noise ratio (SNR), defined in the standard way, as

$$\mathrm{SNR} = \frac{P_s^\delta(\omega_0)}{P_n(\omega_0)} = \left[\frac{2 f_n \Delta_0^2 A^2}{\sigma^4 \sqrt{3}} \right] \exp\left(-\frac{\Delta_0^2}{2\sigma^2}\right). \qquad [16]$$

In this expression we have to insert the signal amplitude $A = C_1/r^3$ and the noise intensity $\sigma^2 = D/(\tau_1 + \tau_2)$ (cf. Sec. 5). Remaining parameters can be fitted to experimental data (Freund et al. 2002). We are thus able to compute the SNR [16] for any geometrical configuration of the predator-prey-swarm system.

We illustrate the results in the following way: We place the single *Daphnia* at the origin of a coordinate system and the center of the *Daphnia* swarm is placed along the x-axis at (L, 0, 0). Then, at each point on the sphere $r = \sqrt{x^2 + y^2 + z^2}$, where the rostrum of a paddlefish is located at a distance $R = \sqrt{(x - L)^2 + y^2 + z^2}$ from the center of the swarm (cf. Fig. 10), we can determine the SNR. Assuming the swarm diameter to be $\Delta = 100$ cm together with reported swarm densities in the range of 1000–9000 per liter, we estimate a maximum number for the total *Daphnia* population of N = 5 mil-

lion. With these numbers we finally visualize the SNR as contour plots in Figure 13. The contours are plotted in the X–Y plane containing the single *Daphnia* and the center of the swarm.

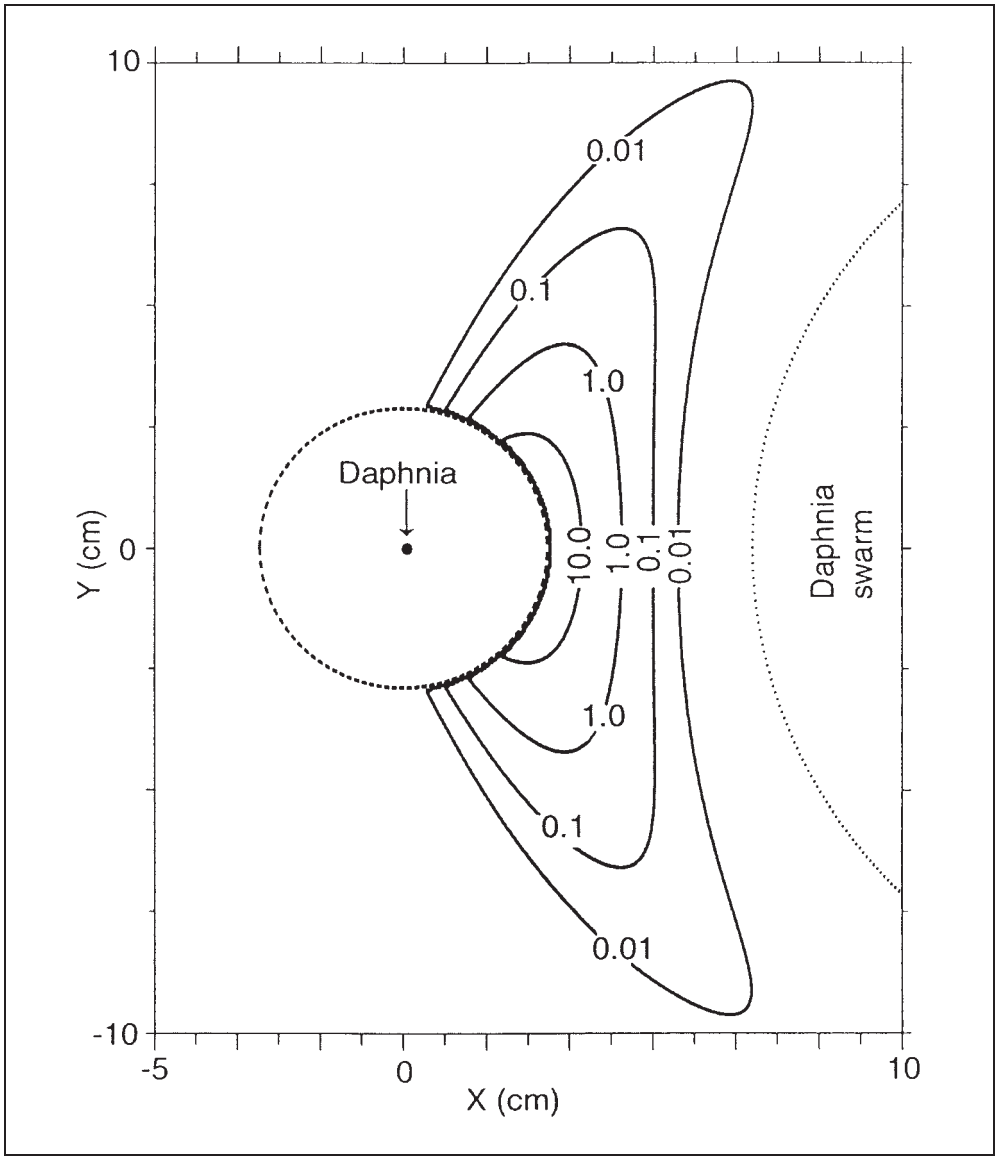

Fig. 13 X–Y contour plot of the SNR according to Equation [16]. In the region outside the dashed circle centered at the origin the signal is subthreshold and can only be detected due to the cooperative role of electric fluctuations provided by *Daphnia* within the swarm to the right. Crossing values above a certain significance level, say SNR = 0.1, should trigger an attack of the cruising juvenile paddlefish. Figure adapted from Freund et al. (2002).

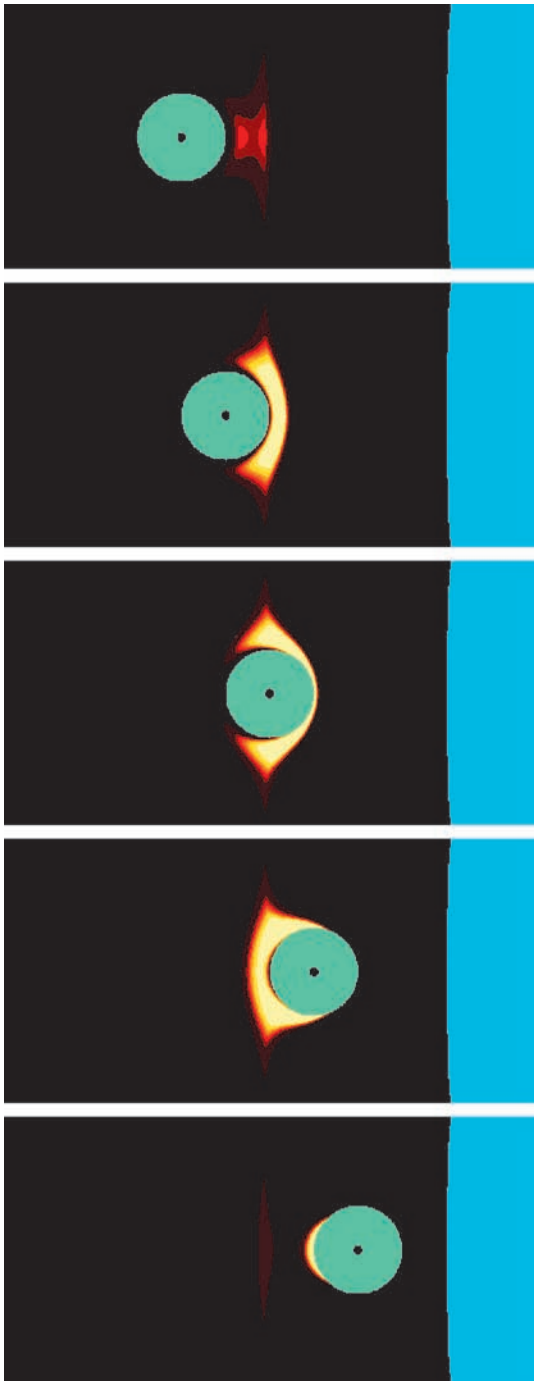

Fig. 14 Behavioral SR quantified *via* the mean number of locked cycles $\langle n_{lock} \rangle$ coded by color: black $\leq \frac{1}{2} <$ dark red to light yellow > 5. The blue region indicates a segment of the swarm and the green circle with the black spot (*Daphnia*) visualizes the region where the signal is above threshold. The outlier *Daphnia* approaching the swarm has to dive through a "firewall" of optimal noise set up by the swarming mates. Figures adapted from FREUND et al. (2001 b).

It should be mentioned that the expression for the SNR [16] is closely related to information theoretical measures, e. g. the Fisher information (Cover and Thomas 1991) or the square discriminability (Stemmler 1996). In fact, for weak signals they are mutually proportional to each other (Freund et al. 2002).

6.2 Behavioural SR Quantified via the Mean Number of Locked Cycles

In *Section 3* we have outlined how the phenomenon of noise-induced phase synchronization occurs when a bistable or threshold system is driven by a subthreshold periodic signal in cooperation with optimal noise. Effective phase locking in stochastic systems means that the average duration of locking episodes $\langle T_{lock} \rangle$ is large compared with the period T_0 of the driving signal, or that the mean number of locked periods $\langle n_{lock} \rangle = \langle T_{lock} \rangle / T_0 >> 1$. In Equation [3] we have expressed how $\langle n_{lock} \rangle$ depends on the drift $\langle \omega_{n,m} \rangle$ and diffusion coefficient $D_{n,m}$ of the phase difference. Now we specify how the latter two quantities vary together with the noise intensity σ^2.

In the following we restrict ourselves to the case of $m : n = 1 : 1$. Analytic expressions for $\langle \omega_{1,1} \rangle$ and $D_{1,1}$ were derived in Freund et al. (2000) based on a dichotomous description for both the input and output signal. At the heart of the analysis were two noise-dependent rates a_1 and a_2 that were adapted (Freund et al. 2001 b) from time-modulated threshold crossing rates specified in (Jung 1994)

$$a_1 = \frac{1}{2\pi\sqrt{\tau_1 \tau_2}} \exp\left(-\frac{1}{2\overline{\sigma^2}}\right) \exp\left(-\frac{\overline{A}\left(1+\overline{A}\right)}{\overline{\sigma^2}}\right) \qquad [17]$$

and

$$a_2 = \frac{1}{2\pi\sqrt{\tau_1 \tau_2}} \exp\left(-\frac{1}{2\overline{\sigma^2}}\right) \exp\left(+\frac{\overline{A}\left(1-\overline{A}\right)}{\overline{\sigma^2}}\right) \qquad [18]$$

where the threshold is denoted by b and $\overline{A} = A/b$ and $\overline{\sigma^2} = \sigma^2/b$ are rescaled signal amplitude and noise intensity, respectively. How A and σ^2 depend on the geometry we have addressed in *Section 5*.

To illustrate the results in Figure 14 we use the same representation scheme as in *Section 6.1*. Now color codes the mean number of locked periods $\langle n_{lock} \rangle$. Noise-induced phase synchronization becomes clearly visible as the red to light yellow regions. The "travelling" outlier *Daphnia* dives through a firewall that is set up by optimal electric fluctuations from the swarm.

7. Discussion and Summary

As can be seen from both Figures 13 and 14, for adequate distances between swarm and outlier *Daphnia* there exists an extra region of noise-induced detectability supporting the hypothesis of behavioral SR in the wild. Even though this extra range does not appear extremely large it might have considerably enhanced the survival chances of juvenile paddlefish that prey on single *Daphnia* – evolutionary systems quite often follow nonlinear laws.

Especially Figure 13 shows that steep gradients exist in the vicinity of the single *Daphnia.* While the steepest gradient is realized by a "head-on" approach from the direction of the center of the swarm, this approach may not be optimal for a juvenile that feels uncomfortable swimming within the swarm. Moreover, the gentler gradients that encircle the swarm on the outside offer substantial detectability at a longer distance. These gradients form a curved path toward the single *Daphnia*, that may indicate an optimal approach trajectory for the cruising juvenile paddlefish, a prediction that appears experimentally testable.

Acknowledgement

Support by the *DFG* (Sfb555) and the *DAAD* (NFS-project no. D/0104610) is greatly acknowledged.

References

Benzi, R., Sutera, A., and Vulpiani, A.: The mechanism of stochastic resonance. J. Phys. A *14*, L453–L457 (1981)

Bertram, B. C. R.: Living in groups: predators and prey. In: Krebs, J. R., and Davies, N. B. (Eds.): Behavioural Ecology; 1st edn., pp. 64–96. Oxford: Blackwell 1978

Brandl, Z., and Fernando, C. H.: Microaggregation of the cladoceran *Ceriodaphnia affinis* Lilljeborg with a possible reason for microaggregations of zooplankton. Can. J. Zool. *49*, 775–778 (1971)

Colebrook, J. M.: Some observations of zooplankton swarms in Windermere. J. Animal Ecol. *29*, 243–252 (1960)

Collins, J. J., Chow, C. C., and Imhoff, T. T.: Aperiodic stochastic resonance in excitable systems. Phys. Rev. E *52*, R3321–R3324 (1995)

Cover, T. M., and Thomas, J. A.: Elements of Information Theory. New York: Wiley-Interscience 1991

Davies, J.: Evidence for a diurnal horizontal migration in *Daphnia hyalina lacustris* Sars. Hydrobiologia *120*, 103–105 (1985)

Dolan, K., Witt, A., Spano, M., Neiman, A., and Moss, F.: Surrogates for finding unstable periodic orbits in noisy data sets. Phys. Rev. E *59*, 5235–5241 (1999)

Ebeling, W., Engel, A., and Feistel, R.: Physik der Evolutionsprozesse. Berlin: Akademie-Verlag 1990

Folt, C. L., and Burns, C. W.: Biological drivers of zooplankton patchiness. Trends Ecol. Evol. *14*, 300–305 (1999)

Freund, J. A., Kienert, J., Schimansky-Geier, L., Beisner, B., Neiman, A., Russell, D. F., Yakusheva, T., and Moss, F.: Behavioral stochastic resonance: how a noisy army betrays its outpost. Phys. Rev. E *63*, 031910 1–11 (2001 b)

Freund, J. A., Neiman, A. B., and Schimansky-Geier, L.: Analytic description of noise-induced phase synchronization. Europhys. Lett. *50*, 8–14 (2000)

Freund, J. A., Neiman, A. B., and Schimansky-Geier, L.: Stochastic resonance and noise-induced phase coherence. Progress in Probability *40*, 309–323 (2001 a)

Freund, J. A., Schimansky-Geier, L., Beisner, B., Neiman, A., Russell, D. F., Yakusheva, T., and Moss, F.: Behavioral stochastic resonance: how the noise from a *Daphnia* swarm enhances individual prey capture by juvenile paddlefish. J. Theor. Biol. *214*, 71–83 (2002)

Freund, J. A., Schimansky-Geier, L., and Hänggi, P.: Frequency and phase synchronization in stochastic systems. Chaos *13*, 225–238 (2003)

Gailey, P. C., Neiman, A., Collins, J. J., and Moss, F.: Stochastic resonance in ensembles of nondynamical elements: the role of internal noise. Phys. Rev. Lett. *79*, 4701–4704 (1997)

Gammaitoni, L., Hänggi, P., Jung, P., and Marchesoni, F.: Stochastic resonance. Rev. Mod. Phys. *70*, 223–288 (1998)

Glansdorff, P., and Prigogine, I.: Thermodynamics of Structure, Stability and Fluctuations. New York: Wiley-Interscience Publishers 1971

Grande, L., and Bemis, W. E.: Osteology and phylogenetic relationships of fossil and recent paddlefishes (Polyodontidae) with comments on the interrelationships of Acipenseriformes. J. Vert. Paleontol. *11* (Memoir 1), 1–121 (1991)

Greenwood, P. E., Ward, L. M., Russell, D. F., Neiman, A., and Moss, F.: Stochastic resonance enhances the electrosensory information available to paddlefish for prey capture. Phys. Rev. Lett. *84*, 4773–4776 (2000)

Hänggi, P., Talkner, P., and Borkovec, M.: Reaction-rate theory: fifty years after Kramers. Rev. Mod. Phys. *62*, 251–341 (1990)

Hopfield, J. J.: Neural networks and physical systems with emergent collective computational properties. Proc. Natl. Acad. Sci. USA *79*, 2554–2558 (1982)

Jakobsen, P. J., and Johnsen, G. H.: The influence of food limitation on swarming behaviour in the waterflea Bosmina longispina. Animal Behav. *36*, 991–995 (1988)

Jensen, K. H., Jakobsen, P. J., and Kleiven, O. T.: Fish kairomone regulation of internal swarm structure in *Daphnia pulex* (Cladocera: Crustacea). Hydrobiologia *368*, 123–127 (1998)

Jung, P.: Threshold devices: fractal noise and neural talk. Phys. Rev. E *50*, 2513–2522 (1994)

Jung, P., and Shuai, J. W.: Optimal sizes of ion channel clusters. Europhys. Lett. *56*, 29–35 (2001)

Kvam, O. V., and Kleiven, O. T.: Diel horizontal migration and swarm formation in *Daphnia* in response to *Chaoborus*. Hydrobiologia *307*, 177–184 (1995)

Longtin, A.: Stochastic resonance in neuron models. J. Stat. Phys. *70*, 309–327 (1993)

Longtin, A., Bulsara, A., and Moss, F.: Time-interval sequences in bistable systems and the noise-induced transmission of information by sensory neurons. Phys. Rev. Lett. *67*, 656–659 (1991)

McNamara, B., and Wiesenfeld, K.: Theory of stochastic resonance. Phys. Rev. A *39*, 4854–4869 (1989)

Milinski, M.: Constraints places by predators on feeding behaviour. In: Pitcher, T. J. (cd.): The Behaviour of Teleost Fishes; pp. 236–252. Baltimore, MD: The Johns Hopkins University Press 1986

Moss, F., Pierson, D., and O'Gorman, D.: Stochastic resonance: tutorial and update. Int. J. Bifurc. Chaos *6*, 1383–1397 (1994)

Neiman, A., and Schimansky-Geier, L.: Stochastic resonance in bistable systems driven by harmonic noise. Phys. Rev. Lett. *72*, 2988–2991 (1994)

Neiman, A., Silchenko, A., Anishchenko, V., and Schimansky-Geier, L.: Stochastic resonance: noise-enhanced phase coherence. Phys. Rev. E *58*, 7118–7125 (1998)

Neiman, A., and Russell, D. F.: Stochastic biperiodic oscillations in the electroreceptors of paddlefish. Phys. Rev. Lett. *86*, 3443–3447 (2001)

Neiman, A. B., Russell, D. F., Pei, X., Wojtenek, W., Twitty, J., Simonotto, E., Wettring, B. A., Wagner, E., Wilkens, L. A., and Moss, F.: Stochastic synchronization of electroreceptors in the paddlefish. Int. J. Bifurc. Chaos *10*, 2499–2517 (2000)

Nicolis, C.: Stochastic aspects of climatic transitions – response to a periodic firing. Sol. Phys. *74*, 473–478 (1981)

Ostwald, W.: Gedanken zur Biosphäre. (1931) Reprint: Ostwalds Klassiker Bd. *257*. Frankfurt: Harri Deutsch 1996

Pijanowska, J., and Kowalczewski, A.: Predators can induce swarming behaviour and locomotory responses in *Daphnia*. Freshwater Biol. *37*, 649–656 (1997)

Pikovsky, A., Rosenblum, M., and Kurths, J.: Synchronization – a Universal Concept in Nonlinear Sciences. Cambridge: Cambridge University Press 2001

Rice, S. O.: Mathematical analysis of random noise. In: Wax, N. (Ed.): Selected Papers on Noise and Stochastic Processes; pp. 189–195. New York: Dover 1954

Russell, D. F., Tucke, A., Wettring, B. A., Neiman, A., Wilkens, L., and Moss, F.: Noise effects on the electrosense-mediated feeding behavior of small paddlefish. Fluct. Noise Lett. *1*, L71–L86 (2001)

Russell, D., Wilkens, L., and Moss, F.: Use of behavioral stochastic resonance by paddlefish for feeding. Nature *402*, 219–223 (1999)

Schmid, G., Goychuk, I., and Hänggi, P.: Stochastic resonance as a collective property of ion channel assemblies. Europhys. Lett. *56*, 22–28 (2001)

Schrödinger, E.: What is Life? Cambridge: Cambridge University Press 1948

Stemmler, M.: A single spike suffices: the simplest form of stochastic resonance in model neurons. Network: Comput. Neural Systems *7*, 687–716 (1996)

Stocks, N. G.: Information transmission in parallel threshold arrays: suprathreshold stochastic resonance. Phys. Rev. E *63*, 041114 1–9. Suprathreshold stochastic resonance in multilevel threshold systems. Phys. Rev. Lett. *84*, 2310–2314 (2000)

Stratonovich, R. L.: Topics in the Theory of Random Noise. Vol. I and II. New York: Gordon and Breach 1963

Uhlenbeck, G. E., and Ornstein, L. S.: On the theory of Brownian motion. Phys. Rev. *36*, 823–841 (1930)

Wilkens, L. A., Russell, D. F., Pei, X., and Gurgens, C.: The paddlefish rostrum functions as an electrosensory antenna in plankton feeding. Proc. R. Soc. Lond. B *264*, 1723–1729 (1997)

Dr. Jan A. Freund
Humboldt-Universität zu Berlin
Institut für Physik
Newtonstraße 15
12489 Berlin
Germany
Phone: ++49 (0) 30 20 93 78 96
Fax: ++49 (0) 30 20 93 76 38
E-Mail: freund@physik.hu-berlin.de

Nova Acta Leopoldina NF *88*, Nr. 332, 129–149 (2003)

Oscillations in Minimal Enzyme Reaction Systems: Origins, Dynamics, and Potential Biological Function

Marcus J. B. HAUSER (Magdeburg)

With 8 Figures and 1 Table

Abstract

Experimental studies on minimal enzyme reaction systems that induce oscillatory (or rhythmic) dynamical behavior are presented. The minimal enzyme systems consist only of a single enzyme (or enzyme model compound) and its substrates. Two reaction systems are discussed in detail: the peroxidase-oxidase reaction and a biomimetic cytochrome P450 model system. The peroxidase-oxidase reaction (i. e. the oxidation of NADH by O_2 catalyzed by peroxidase) displays rich dynamics *in vitro*. Experiments in cell extracts suggest that such oscillations may also occur *in vivo*. Our investigations indicate that one possible function of the oscillations – in addition to provide a means of information transduction – is the protection of the enzyme against inactivation by reactive oxygen species. The second system addressed here is a biomimetic cytochrome P450 model system. It consists of synthetic components which were designed to reproduce the characteristic features of the natural counterpart. Oscillations between different oxidation states of the lipophilic enzyme model compound can be induced. These oscillations require a transport of electrons or substrates into the lipid bilayer of a phospholipid vesicle to be effective. Thus, the experiments indicate that nonlinear dynamics, like oscillatory or rhythmic behavior, are a feature expected to occur in a great variety of single enzyme systems.

Zusammenfassung

Es werden experimentelle Untersuchungen von minimalen Enzymsystemen vorgestellt, die oszillierendes (oder rhythmisches) dynamisches Verhalten hervorrufen. Die minimalen Enzymsysteme bestehen jeweils aus einem einzigen Enzym (oder einer Enzym-Modellverbindung) und dessen Substraten. Zwei derartige Reaktionssysteme werden im Detail vorgestellt: die Peroxidase-Oxidase-Reaktion und ein biomimetisches Cytochrom-P450-Modellsystem. Die Peroxidase-Oxidase-Reaktion (d. h. die durch Peroxidase katalysierte Oxidation von NADH durch O_2) weist unter *In-vitro*-Bedingungen reichhaltige Dynamik auf. Untersuchungen an Zellextrakten deuten darauf hin, daß oszillierendes dynamisches Verhalten auch unter *In-vivo*-Bedingungen auftreten kann. Unsere Arbeiten zeigen ferner, daß Oszillationen – zusätzlich zu ihrer Rolle als Informationsüberträger – eine weitere biologische Funktion zu haben scheinen, nämlich den Schutz von Enzymen gegen irreversible Inaktivierung. Die zweite hier vorgestellte Reaktion ist ein biomimetisches Cytochrom-P450-Modellsystem. Es besteht aus synthetischen Komponenten, die so konzipiert wurden, daß sie die charakteristischen Eigenschaften des natürlichen Vorbilds wiedergeben. In diesem System beobachtet man Oszillationen zwischen den verschiedenen Oxidationsstufen der lipophilen Enzym-Modellverbindung. Damit diese Oszillationen entstehen können, muß ein Transport von Elektronen oder von Substraten in die Lipiddoppelschicht einer Vesikel gewährleistet sein. Die hier vorgestellten experimentellen Befunde zeigen, daß nichtlineares dynamisches Verhalten, wie oszillierende oder rhythmische Dynamik, als eine typische Verhaltensweise von minimalen Enzymssystemen zu erwarten ist.

1. Introduction

The investigation of oscillatory chemical reactions has been in the focus of scientific attention during the last decades (Field and Burger 1985, Epstein and Pojman 1998), due to the interest in studying the dynamics by their own right, and due to the fact that chemical oscillators are considered to be simple model systems for biological rhythms. While chemical oscillators and rhythmic biological systems display the same types of nonlinear dynamical behavior, generally there is a considerable difference in the degree of complexity of the systems under consideration.

Oscillatory chemical reactions involve a relatively small number of chemical species undergoing a set of reactions; the entities giving rise to nonlinear behavior are on the molecular level. By contrast, rhythmic biological systems may frequently be found at the cellular level (e. g. in the concentrations of cytosolic Ca^{2+} in oocytes of *Xenopus laevis*; Camacho and Lechleiter 1993) and the secretion of insulin from pancreatic β-cells (Goodner et al. 1977), at the level of tissues or even organs (e. g. the oscillations in CAM plants; Lüttge 2000, Rascher et al. 2001). The mechanisms that give rise to rhythmic phenomena in biological systems are generally rather complex, involving a large number of species and agents, which may encompass molecules, but also more complex entities, such as receptors, ion channels, or compartmented systems. The high degree of complexity allows for a high specificity and for a precise fine tuning of the physiological processes. However, such high complexity may often make it difficult to obtain fundamental understanding of the underlying mechanisms which give rise to the nonlinear behavior.

Thus, we face the situation where the dynamics of highly complex biological processes that occur at higher hierarchical levels of organization (such as cells, tissues, or organs) are thought to be modeled by comparatively simple chemical oscillators whose constituents are exclusively at the molecular level. Nevertheless, there is ample correspondence in the types of dynamics displayed by both classes of systems. However, the question remains, whether oscillatory or rhythmic behavior may also be generated by biological or biochemical systems at the molecular level of organization. To this purpose, we study the nonlinear dynamics of single enzyme systems. The systems presented in this article consist only of a single enzyme and of its substrates. Therefore, they can be considered as the minimal biochemical systems that generate rhythmic (or oscillatory) behavior. Furthermore, these systems are formed of molecules, thus closing the gap in hierarchical organization levels found in rhythmic biological systems on the one hand, and in simple, "molecular" chemical oscillators on the other hand.

Despite numerous calculations using either the Michaelis-Menten formalism or even more explicit kinetic schemes that show that oscillatory behavior should be a frequently observable feature of single enzyme reaction systems (e. g. Ryde-Petterson 1989, Hübner and Wolna 1994), only a scant number of such systems have unambiguously shown to display rhythmic behavior in experiments. Often, only very few or even a single oscillatory cycle is shown in the publications; in addition, it is frequently impossible to determine whether the time trace really shows an autonomous oscillatory event or if it is due to fluctuations. Among the few unambiguous examples we find oscillations in the cleavage of urea by urease (Temminck Groll 1917), the oxidation of ascorbic acid by catalase (Davison et al. 1986), and the peroxidase-oxidase (PO) reaction (for reviews see

Larter et al. 1993, Scheeline et al. 1997, Hauser and Olsen 1999). Recently, we have added two further model reaction systems to this class, namely a biomimetic cytochrome P450 model system (Schenning et al. 1995) and a pH oscillator based on hemin (Hauser et al. 2001 b, 2002).

In the present article we will focus on two single enzyme systems, namely the peroxidase-oxidase (PO) reaction and a cytochrome P450 model system. First, we will give a brief overview over the dynamical behavior of the peroxidase-oxidase reaction, as observed from experiments where purified enzyme is used. We address the question, whether oscillatory dynamics may occur under *in-vivo* conditions, before we discuss which potential biological functions may be associated with the oscillations in the PO reaction. Next, we will present a completely synthetic model for the cytochrome P450 system which also shows rhythmic behavior. In this biomimetic reaction system transport plays an important role.

2. Materials and Methods

2.1 Experiments with the Peroxidase-Oxidase Reaction

2.1.1 Experiments with Purified Peroxidase

Measurements of the dynamics of the peroxidase-oxidase reaction were performed at 28.0 ± 0.1 °C in a 21.7 mm × 21.7 mm × 42 mm quartz cuvette placed in a Zeiss S10 diode array spectrophotometer. The reactor is equipped with a Clark-type oxygen-sensitive electrode which allows simultaneous detection of the oxygen concentration in the cuvette. Experiments were run in a 10 ml stirred sample, containing 10 ml of a buffer (0.1 M Na-acetate buffer for experiments at $5.1 \leq \text{pH} \leq 5.9$ or a 0.1 M Na-phosphate buffer for $6.1 \leq \text{pH} \leq 6.3$), 1.3–1.6 μM of peroxidase from horseradish (Boehringer Mannheim), 50–100 nM methylene blue (Merck), and a phenolic compound at different concentrations (usually in the range of 25–400 μM). A 0.1 M solution of NADH (Boehringer Mannheim) was infused at a flow rate of 19–40 μl h^{-1} through a capillary tube from a 250 μl Hamilton syringe mounted in a highly accurate syringe pump (Harvard Apparatus, model 22). The gas stream containing a 1.05 % (v/v) O_2/N_2 mixture was purged in the gas volume (10 ml) above the reaction solution. The transfer rate of oxygen v_{O_2} into the liquid is given by

$$v_{O_2} = K\,([O_2]_{eq} - [O_2]) \qquad [1]$$

where $[O_2]_{eq} = 12$ μM is the oxygen concentration in the liquid at equilibrium and K is the oxygen transfer constant. In our experimental set-up $K = (6.0 \pm 0.2) \times 10^{-3}\ s^{-1}$ at a stirring frequency of 17.5 Hz. The spectrophotometric data as well as the recordings of the oxygen electrode were sampled every 2 seconds and stored on a computer for later analysis. The concentrations of NADH and the enzyme species ferric peroxidase (native state), ferroperoxidase, and compound III were measured at 360, 403, 439, and 418 nm, respectively. The concentration of these species was obtained by solving the set equation

$$\mathbf{A} = d \bullet \underline{\varepsilon} \times \boldsymbol{c} \qquad [2]$$

where **A** is a vector containing the absorbancies at the 4 wavelengths mentioned above, *d* is the length of the optical path through the cuvette, **c** the vector of concentrations of NADH and the enzyme species under consideration, and $\underline{\boldsymbol{\varepsilon}}$ is a 4×4 matrix containing the molar absorption coefficients of these four species as determined by HAUSER et al. (2000).

2.1.2 Preparation of Cell Extracts from Horseradish Roots

Extracts of roots from wild growing horseradish plants were prepared using a modified procedure of the one described by ELSTNER and HEUPEL (1976): 30–65 g of horseradish root were sliced and homogenized in ice-cold distilled water (3 ml H_2O per g tissue) using a rod-blender. The homogenate was filtered through cheese-cloth and centrifuged at 1000 *g* for 20 min at 8 °C in a Sorvall RC 5C centrifuge. The pellet was resuspended in 100 ml ice-cold distilled water and recentrifuged. Resuspension and recentrifugation were repeated twice, and the final pellet was resuspended in ice-cold distilled water corresponding to 7 ml of H_2O per 30 g of horseradish root. The extract was used directly without further treatment or stored at –20 °C for later use.

2.1.3 Detection in Experiments with Horseradish Root Extracts

Experiments with horseradish root extracts were performed in the setup mounted in the photometer. The undiluted extract was placed into the cuvette. Methylene blue was added to a final concentration of 200 nM and NADH was supplied from a syringe, similarly to the experiments conducted with purified enzyme. Due to the turbidity of the cell extracts, however, only the oxygen concentration in the extract could be monitored.

2.2 Experimental Conditions for the Biomimetic Cytochrome P450 Model System

Manganese(III) tetrakis(dichlorophenyl)porphyrin **1** was either synthesized according to VAN ESCH et al. (1995) or purchased from Porphyrin Systems. The manganese porphyrin **1** and the amphiphilic Rh complex **2** were incorporated into zwitterionic L-α-diplamitoylphosphatidylcholine (DPPC) by dissolution in ethanol, and subsequent removal of the solvent under N_2. The resulting films were suspended in ethanol and injected into an aqueous 4-ethylmorpholine/sodium formate buffer (pH 7.0), thus forming vesicles.

The dynamic behavior of the biomimetic cytochrome P450 model system was investigated in a cuvette that was placed in the thermostating block of a Hewlett Packard HP 8542 diode array spectrophotometer. This semi-batch reactor was also equipped with an oxygen-sensitive Clark electrode, and its head volume was supplied with a O_2/N_2 gas stream. The experiments were performed at 48 °C under very gentle stirring.

3. Studies on the Peroxidase – Oxidase Reaction

Peroxidases are ubiquitous enzymes which catalyze the oxidation of a large variety of substrates by H_2O_2. However, the enzyme is also able to use molecular oxygen, O_2, as the oxidizing agent, thus acting as an oxidase. When using oxygen as substrate, peroxidase may oxidize electron donors such as reduced nicotinamide adenine dinucleotide (NADH), indole-3-acetic acid, triose reductone, and veratryl alcohol. In the present paper, we shall refer to the peroxidase-catalyzed oxidation of NADH by oxygen as the peroxidase-oxidase (PO) reaction. Although the stoichiometry of the overall reaction is

$$2\,\mathrm{NADH} + 2\,\mathrm{H^+} + \mathrm{O_2} \rightarrow 2\,\mathrm{NAD^+} + 2\,\mathrm{H_2O}, \qquad [3]$$

many elementary steps have been found to be involved in this enzymatic catalysis.

The peroxidase-oxidase reaction has been intensively studied during the last decades. Most frequently, enzyme from horseradish roots is used in experiments, although enzyme from other sources, like soybean, fungi, and milk (Kummer et al. 1996), have also been shown to support rich dynamic behavior. Since about 80 % of the peroxidase found in horseradish root cells is cytosolic (Liu and Lamport 1974), the bulk of experimental studies on the nonlinear dynamic behavior of the PO system has been conducted in spatially uniform systems. The focus of scientific interest has been put on the elucidation of the dynamics of this reaction under *in-vitro* conditions and on its reaction mechanism. These aspects have been recently reviewed (for the dynamics see Hauser and Olsen 1999, for the mechanism Scheeline et al. 1997), we will, therefore, address these issues only briefly.

3.1 Dynamic Behavior

Oscillations in the PO reaction were first observed by Yamazaki and colleagues in 1965, when a N_2/O_2 gas mixture was bubbled through an aqueous solution containing purified peroxidase from horseradish and NADH (Yamazaki et al. 1965). The occurrence of autonomous oscillatory behavior has since been confirmed by many research groups. Meanwhile, the PO system has developed into a prototypical reaction system for the investigation of the various types of oscillatory dynamics (Fig. 1) found in chemical and biochemical reaction systems. Apart from sustained periodic oscillations, the PO system was found to show complex periodic oscillations, i. e. oscillations of higher periodicity. In addition to such periodic oscillations, the PO system also displays chaotic dynamics. In fact, the PO reaction was the first reaction system where chaotic dynamics have been ever observed in chemical or biochemical reaction systems (Olsen and Degn 1977). Later, different routes to chaos have been detected (Geest et al. 1992, Hauser and Olsen 1996), thus providing additional support for the occurrence of deterministic chaos in the PO reaction. Figure 1 shows the so-called period-adding route to chaos. The evidence of chaos has further been substantiated by the application of different tools of time series analysis to the experimental data (Hauck and Schneider 1994). As an example, the time-series analysis of a (homoclinic) chaotic time-series obtained in a period-adding sequence is depicted in Figure 2.

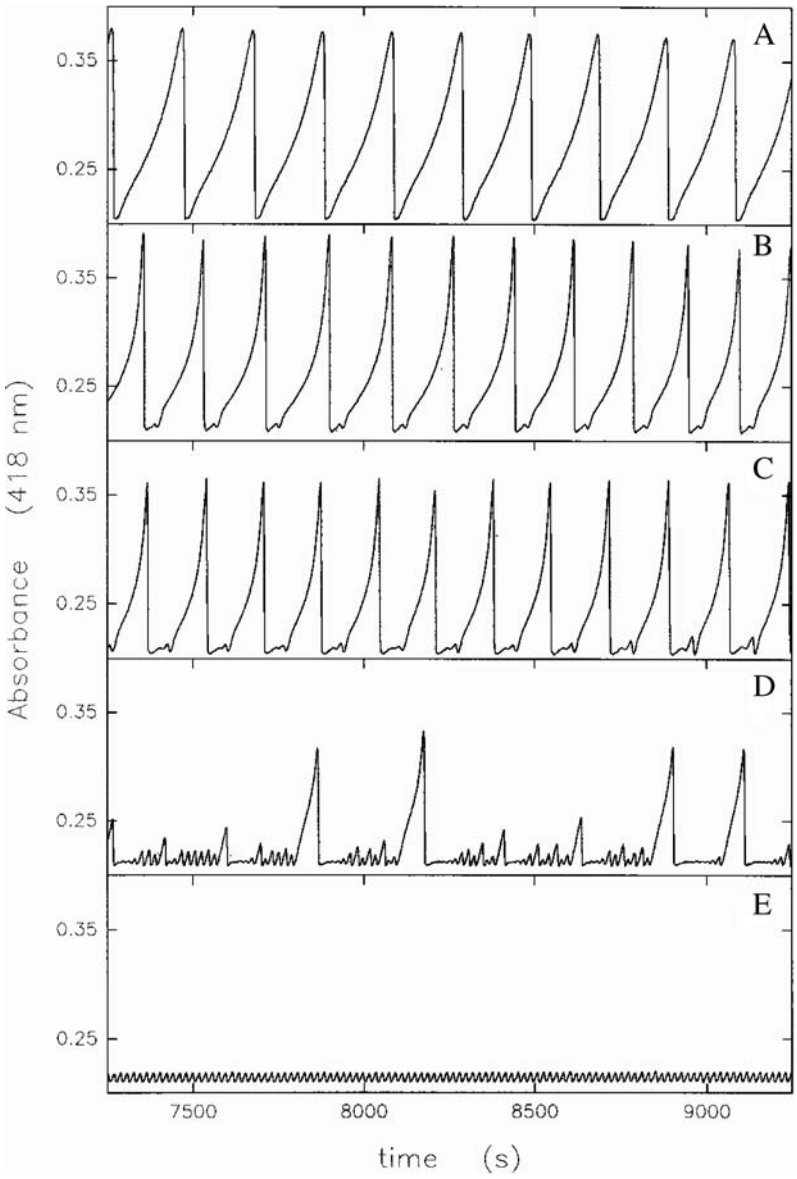

Fig. 1 Examples of different types of oscillatory dynamics observed in the peroxidase-oxidase (PO) reaction. The figure shows a sequence of oscillatory states as response to increasing NADH concentration levels: (*A*) periodic oscillations at $[NADH]_{av}$ = 105 μM; (*B*) mixed mode oscillations composed of one large-amplitude oscillation and one small-amplitude oscillation at $[NADH]_{av}$ = 113 μM; (*C*) mixed mode oscillations composed of one large-amplitude oscillation and two small-amplitude oscillations at $[NADH]_{av}$ = 118 μM; (*D*) chaotic time series at $[NADH]_{av}$ = 125 μM; and (*E*) small-amplitude oscillations at $[NADH]_{av}$ = 128 μM. This sequence is called a period-adding sequence to chaos.

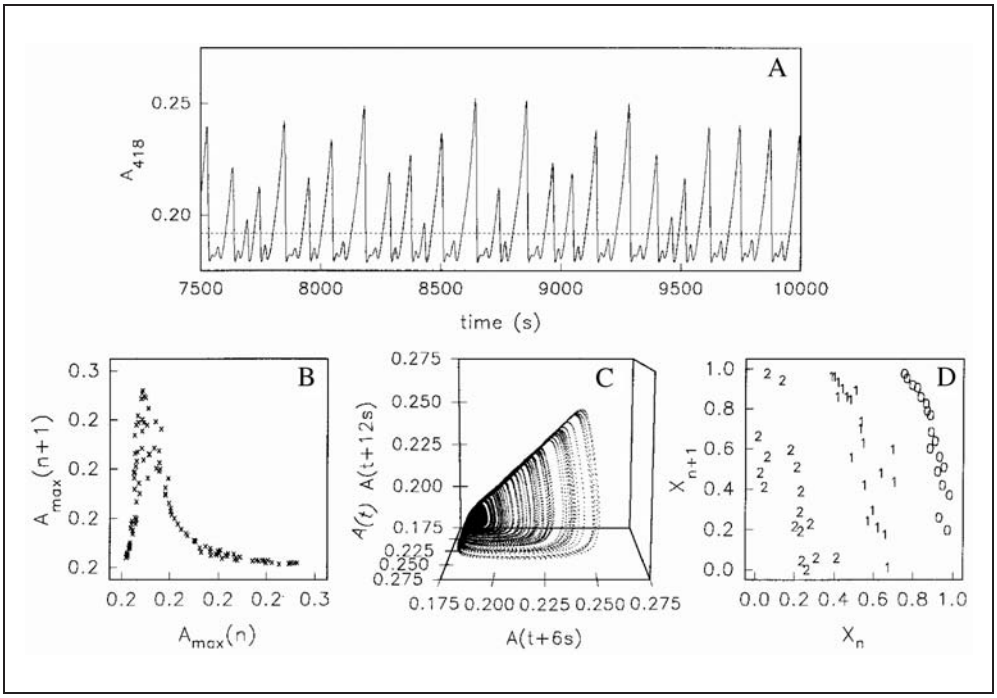

Fig. 2 Example of a time-series analysis of a chaotic time-series observed in a period-adding sequence: (*A*) time-series, monitored as the absorbance of compound III at 418 nm; (*B*) next-amplitude map where the maximum of the amplitude of the $(n + 1)$-th oscillation is plotted against the maximum of the n-th oscillation; (*C*) the attractor reconstructed from the time-series by a time-delay method; and (*D*) the one-dimensional map obtained from a Poincaré section which intersects the inflowing branch of the attractor perpendicular to the direction of flow. The location of the Poincaré section is indicated by the dashed line in the time-series (*A*). The one-dimensional map (*D*) is multi-branched, indicating that the chaotic state is associated with a homoclinic orbit. (For details see HAUSER and OLSEN 1996, HAUSER et al. 1997.)

Another interesting type of behavior encountered in the PO reaction are quasiperiodic oscillations (SAMPLES et al. 1992, HAUCK and SCHNEIDER 1993). In this case, the dynamics are governed by two oscillatory frequencies, the ratio of which is irrational. The resulting time-series consist of a series of sustained oscillations, the amplitude of which presents a regular modulation.

The nonlinearities in the dynamics may also lead to coexistence of dynamical behaviors at a given set of reaction conditions. This phenomenon is called bistability (or multistability, if more than two dynamic states are simultaneously stable). Which of the stable states is actually realized in an experimental system depends on the "history" of the system, i. e., on the way the reaction conditions in the multistable region are approached. Transitions between such simultaneously stable states can be induced. For the PO reaction two parameter regions have been found where bistability occurs. One of them is characterized by the coexistence of two different non-oscillatory, stationary states (DEGN 1968), while the other encompasses the coexistence of a stationary state and an oscillatory state (AGUDA et al. 1990).

3.2 Reaction Mechanism

In their study of the reaction mechanism of the oxidase function of peroxidase enzymes, YAMAZAKI and coworkers ascertained that no less than five different enzyme intermediates were involved in the oxidase cycle (YOKOTA and YAMAZAKI 1965, YAMAZAKI and YOKOTA 1973). The enzyme intermediates represent different oxidation states of the enzyme, where the formal oxidation state of central iron in the heme group may be either + 2 (Per^{2+}, ferrous peroxidase), + 3 (Per^{3+}, ferric peroxidase, i. e. the native enzyme), + 4 (Per^{4+}, compound II), + 5 (Per^{5+}, compound I), or even + 6 (Per^{6+}, compound III). The group of YAMAZAKI worked out the mechanistical fundamentals of the oxidase action of the enzyme (YAMAZAKI and YOKOTA 1973, YOKOTA and YAMAZAKI 1977) which, interestingly, include the elementary reactions forming the typical peroxidase cycle as a subset.

The first detailed reaction models capable of showing periodic oscillations (FED'KINA et al. 1984, AGUDA and LARTER 1991) were based on key steps proposed by YAMAZAKI'S group (YOKOTA and YAMAZAKI 1977). Mechanistic studies have lead to a series of refined detailed mechanistic models, which were recently reviewed by SCHEELINE et al. (1997). Among these refined mechanistic models, the reaction model proposed by BRONNIKOVA et al. (1995) has the virtue of accurately reproducing the dynamical behavior so far observed in the PO reaction and achieving almost quantitative agreement between simulations and experiments. The reactive pathway described by this mechanistic model is shown in Figure 3 and the underlying reactions are compiled in Table 1.

The different detailed reaction mechanisms share common characteristic features. On the one hand, the reaction mechanisms are autocatalytic in NAD• radicals: One NAD• radical reacts with compound III (Per^{6+}) (reaction 8, Tab. 1) to reduce it to the native form of the enzyme (Per^{3+}) (*via* the sequence of reactions 8, 3, and 4, Tab. 1). During this reduction, two NAD• molecules are produced (reactions 3 and 4 of Tab. 1). Thus NAD• radicals catalyze their own production. On the other hand, there are two reactions that limit the increase in NAD• concentration: *first*, oxygen consumes NAD• radicals (reaction 5, Tab. 1), *second*, NAD• radicals form dimers (reaction 9, Tab. 1). These two reactions provide a "feed-back" by limiting the unbound production of NAD•. The interplay of autocatalysis and feed-back leads to nonlinearities in the ordinary differential equations describing the kinetics of the PO reaction. Thus, the origin of the nonlinear behavior of the peroxidase-oxidase system stems form the kinetics of their constituent reactions.

Despite of their relative complexity, the detailed reaction mechanisms usually only consider the reactions of the enzyme species and their substrates (O_2 and NADH). The mechanistic contributions of the two enzymatic cofactors are usually neglected since they are only present in very low concentrations, and they are not necessarily required for the PO reaction to show complex dynamics. However, besides moderating the reactivity of the enzyme, the cofactor methylene blue has been found to protect the enzyme from inactivation (HAUSER et al. 2000). The second cofactor is a phenolic compound (or an aromatic amine), 2,4-dichlorophenol being most frequently used in studies of the oscillatory dynamics. Its effect is to tune the activity of the enzyme.

In parallel to detailed reaction mechanisms which attempt to account for the mechanistic contribution of "all" involved species, a few reduced mechanistic models (i. e. sys-

tems of differential equations) have been developed. These mechanisms were designed to model the dynamic features of the PO reaction system, however, a direct correspondence between the variables of these models and experimentally accessible parameters is not always given. The two typical reduced schemes consist of an autocatalytic step and a chain branching step, the kinetics of which, depending on the model, are either quadratic (DEGN et al. 1979) or cubic (OLSEN 1983). The chain branching acts as feed-back step. Thus, the reduced and the detailed models have the same characteristic features: an autocatalysis and feed-back steps. However, a network analysis showed that the structure of the networks in the reduced models differs from those found to form the cores of the detailed models, which in turn are in better agreement with experimental observations (HUNG and ROSS 1995).

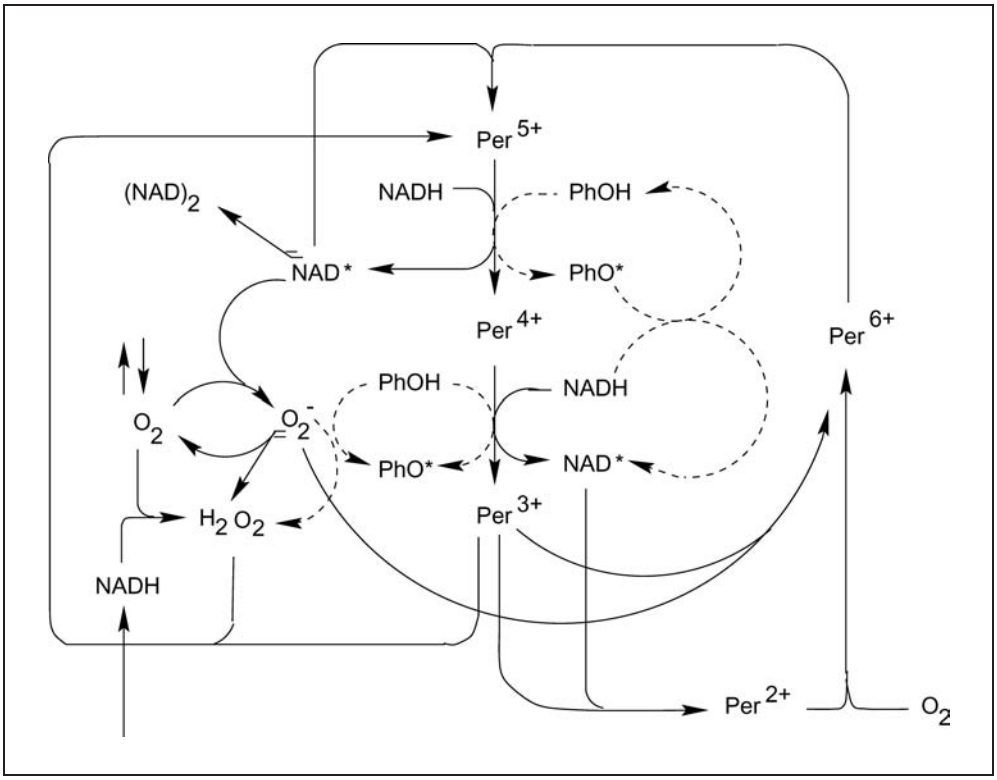

Fig. 3 The model of the PO reaction according to BRONNIKOVA et al. (1995) is shown in solid lines (the reactions are compiled in Tab. 1). The dashed lines indicate the electron mediating loop involving the phenolic cofactor (PhOH), after HAUSER and OLSEN (1998). The reaction involves the following enzyme intermediates: ferrous peroxidase (Per^{2+}), ferric (native) peroxidase (Per^{3+}), compound I (Per^{5+}), compound II (Per^{4+}) and compound III (Per^{6+}), as well as superoxide radicals (O_2^-), hydrogen peroxide, the NAD• radical, and NAD-dimers ($(NAD)_2$). Doubly-barbed arrows indicate that two molecules of a species are consumed during a reaction. The influxes of NADH and O_2 are indicated by single arrows pointing at NADH and a double arrow at O_2.

Tab. 1 Detailed reaction mechanism for the peroxidase-oxidase reaction (according to BRONNIKOVA et al. 1995)

Reaction		Rate constant
[1]	$NADH + O_2 + H^+ \rightarrow NAD^+ + H_2O_2$	$k_1 = 3.0\ M^{-1}\ s^{-1}$
[2]	$H_2O_2 + Per^{3+} \rightarrow Per^{5+}$	$k_2 = 1.8\times10^7\ M^{-1}\ s^{-1}$
[3]	$Per^{5+} + NADH \rightarrow Per^{4+} + NAD\bullet$	$k_3 = 4.0\times10^4\ M^{-1}\ s^{-1}$
[4]	$Per^{3+} + NADH \rightarrow Per^{3+} + NAD\bullet$	$k_4 = 2.6\times10^4\ M^{-1}\ s^{-1}$
[5]	$NAD\bullet + O_2 \rightarrow NAD^+ + O_2^-$	$k_5 = 2.0\times10^7\ M^{-1}\ s^{-1}$
[6]	$O_2^- + Per^{3+} \rightarrow Per^{6+}$	$k_6 = 1.7\times10^7\ M^{-1}\ s^{-1}$
[7]	$2\,O_2^- + 2\,H^+ \rightarrow H_2O_2 + O_2$	$k_7 = 2.0\times10^7\ M^{-1}\ s^{-1}$
[8]	$Per^{6+} + NAD\bullet \rightarrow Per^{5+} + NAD^+$	$k_8 = 1.1\times10^8\ M^{-1}\ s^{-1}$
[9]	$2\,NAD\bullet \rightarrow (NAD)_2$	$k_9 = 5.6\times10^7\ M^{-1}\ s^{-1}$
[10]	$Per^{3+} + NAD\bullet \rightarrow Per^{2+} + NAD^+$	$k_{10} = 1.8\times10^6\ M^{-1}\ s^{-1}$
[11]	$Per^{2+} + O_2 \rightarrow coIII$	$k_{11} = 1.0\times10^5\ M^{-1}\ s^{-1}$
[12]	$(NADH)_0 \rightarrow NADH$	k_{12} = variable
[13]	$O_{2(gas)} \rightarrow O_{2(liquid)}$	$k_2 = 6.0\times10^{-3}\ s^{-1}$
[14]	$O_{2(liquid)} \rightarrow O_{2(gas)}$	$k_2 = 6.0\times10^{-3}\ s^{-1}$

Reaction [12] describes the supply of NADH from its stock solution, $(NADH)_0$. To identify the other reaction species, consult the legend of Figure 3.

3.3 Experiments with Horseradish Root Extracts

The dynamics of the PO reaction was also studied in cell-free extracts from horseradish roots (MØLLER et al. 1998). In such extracts, many enzymes are simultaneously active. In our case, several different oxidases may be competing for NAD(P)H and reactive oxygen species, such as H_2O_2 or O_2^-. Thus, an unambiguous assignment of which enzyme is active is generally not possible. Furthermore, it is not self-evident that the oscillatory dynamics known from *in vitro* experiments should be observable in cell-free extracts.

Figure 4 *A* shows the dynamics in an experiment that starts with a cell extract suspension under anaerobic conditions. At time $t \sim 9150$ s the composition of the gas phase is changed from pure N_2 to an O_2/N_2 mixture containing 1.05 % (v/v) O_2. One observes a rapid but smooth transition from an oxygen-free stationary state to a stationary state containing about 0.8 µM O_2. In an analogous experiment we added small amounts of the cofactors 2,4-dichlorophenol and methylene blue to the cell extract. The rationale for these additions is the following: Natural phenolic compounds present in the cells tend to possess a hydrophobic or partly hydrophobic character, so that a substantial fraction is found in the membranes which we eliminated by preparing cell extract suspensions. Thus, the 2,4-dichlorophenol is added to compensate for any loss of aromatic, more lipophilic cofactors, while methylene blue compensates for the depletion of membrane bound quinoid species, like FMN and FAD or derivates thereof. The dynamic behavior of horseradish cell extracts responds dramatically to the addition of cofactors: When the composition of the gas phase is switched from pure N_2 to 1.05 : 98.95 % (v/v) O_2/N_2, a pronounced activation peak is observed, before the new ("oxygen rich") stationary state of the cell extract suspension is approached *via* strongly damped oscillations (Fig. 4 *B*).

It is remarkable that damped oscillations were only observed in horseradish root extracts prepared from roots harvested in late autumn, and that oscillations were absent in root extracts from plants collected in winter (MØLLER et al. 1998). The seasonal occurrence

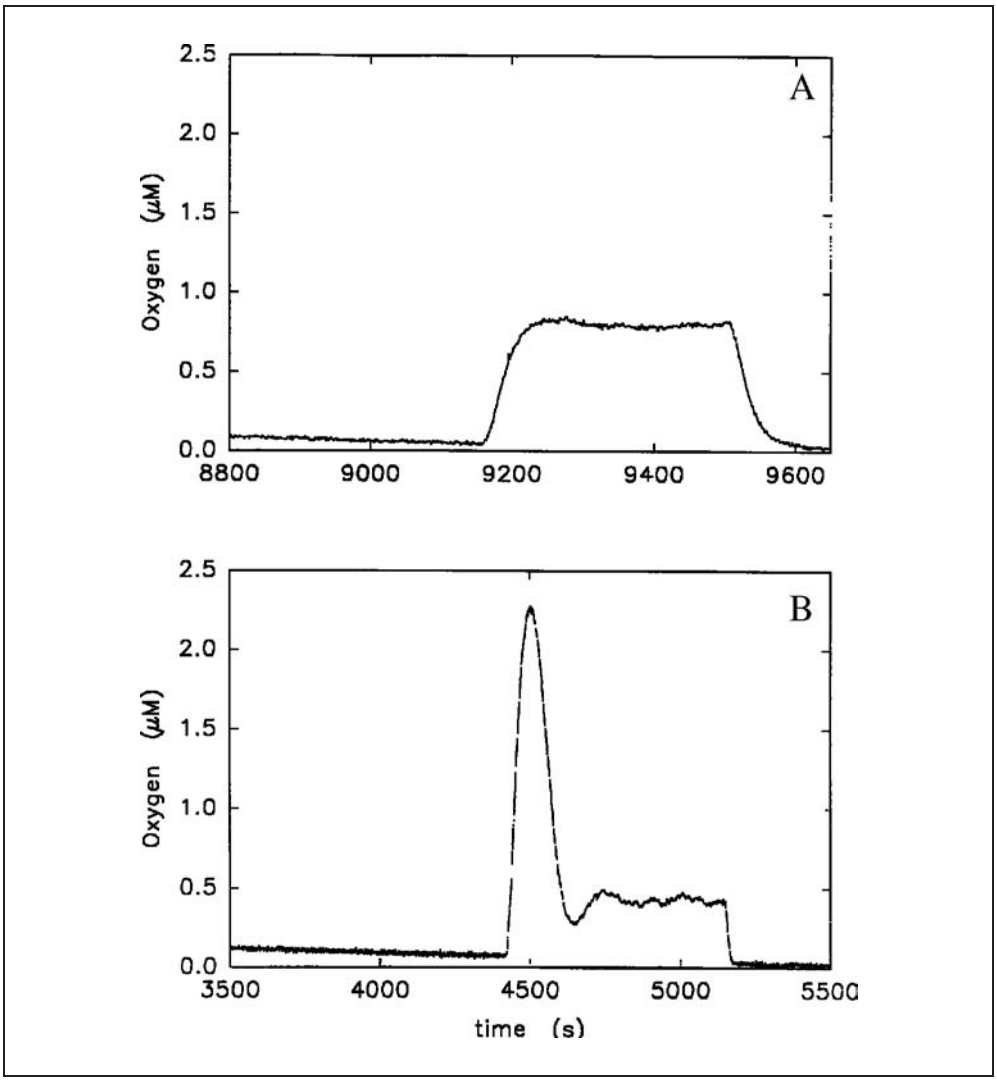

Fig. 4 Dynamic behavior of extracts of horseradish roots: (*A*) Steady state behavior, as seen in the plain extract, i. e., in the absence of any additional phenolic cofactor. (*B*) An activation peak and subsequent relaxation to the new stationary state (*via* strongly damped oscillatory dynamics) are obtained upon addition of 25 μM 2,4-dichlorophenol. Experimental conditions: (*A*) Initially the gas phase above the extract is pure N_2 and 0.1 M NADH is supplied at a rate of 21 μM h^{-1}. At $t \sim 9150$ s the composition of the gas phase is changed to 1.05 : 98.95 (v/v) $O_2 : N_2$. After a further 300 s the oxygen in the gas phase is switched back to 0 %. (*B*) Initial conditions as in (*A*); at $t \sim 4450$ s the oxygen content of the gas phase is changed from 0 % to 1.68 % (v/v). After a further 750 s the gas phase is reset to pure N_2.

of oscillations is most probably due to seasonal variations in the expression of the enzyme in horseradish roots. Since peroxidases are believed to be involved in lignin synthesis by providing the H_2O_2 required for the polymerization of phenolic compounds, like coniferyl alcohol, to form lignin (GROSS et al. 1977, HALLIWELL 1978), the enzyme must be present in higher concentrations in late autumn.

The occurrence of a pronounced activation peak as well as the extremely damped oscillatory approach to the oxygen-rich steady state (Fig. 4 *B*) suggest that a set of experimental conditions may exist, for which sustained oscillations might be obtained. Our results do not provide a definitive proof of the occurrence of PO oscillations, however, they lend support that such behavior is potentially possible in living systems.

3.4 Potential Biological Functions of the Oscillations

The classical biological function ascribed to oscillatory dynamics in biochemical systems is to carry information, like in signal transduction cascades or in oscillations and waves of calcium. We would like to point out an additional possible task of oscillatory dynamics, namely that of protecting the enzyme against inactivation by toxic reaction intermediates.

To this purpose, experimental studies were performed in the parameter region of the PO reaction where periodic oscillations and a stationary state coexist and are simultaneously stable. Which of these dynamic states is approached depends on the "history" of the reaction system. Interestingly, in this bistable regime, the average rates of oxidation of NADH (i. e. the conversion of substrate) have been shown to be the same, independent of the type of dynamics (HAUSER et al. 2001 a). In the experiments, the reaction was run in the absence of the cofactor methylene blue which is known to have a protective role for the enzyme. Spectral deconvolution of the spectrophotometric data of experiments shows that the enzyme is almost exclusively present as ferric peroxidase (Per^{3+}), compound III (Per^{6+}), and ferrous peroxidase (Per^{2+}), while neither compound I (Per^{5+}) nor compound II (Per^{4+}) are present in measurable amounts. Thus, the sum of the concentrations of Per^{2+}, Per^{3+} and Per^{6+} is an excellent approximation to the total enzyme concentration at time *t*.

Experiments performed in the bistable regime show that the rate of enzyme inactivation depends strongly on the type of dynamics, i. e., whether the reaction is in the oscillatory or in the stationary state. Figure 5, which compares the temporal behavior of the sum ($Per^{2+} + Per^{3+} + Per^{6+}$) in the oscillatory and in the non-oscillatory case, illustrates this fact. In both cases the total concentration of enzyme decreases with time due to irreversible side reactions of the enzyme with highly reactive species. However, the rates of enzyme inactivation are very different: While after 12 000 s only about 5 % of the enzyme is inactivated when the reaction proceeds in an oscillatory fashion, roughly 45 % of the enzyme is irreversibly inactivated when the system follows a non-oscillatory pathway (Fig. 5).

The irreversible inactivation of enzymic species is ascribed to reactions of enzyme intermediates with reactive oxygen species. In the PO reaction, the latter may be either superoxide radicals (O_2^-), hydrogen peroxide (H_2O_2), or hydroxyl radicals ($OH\bullet$). To

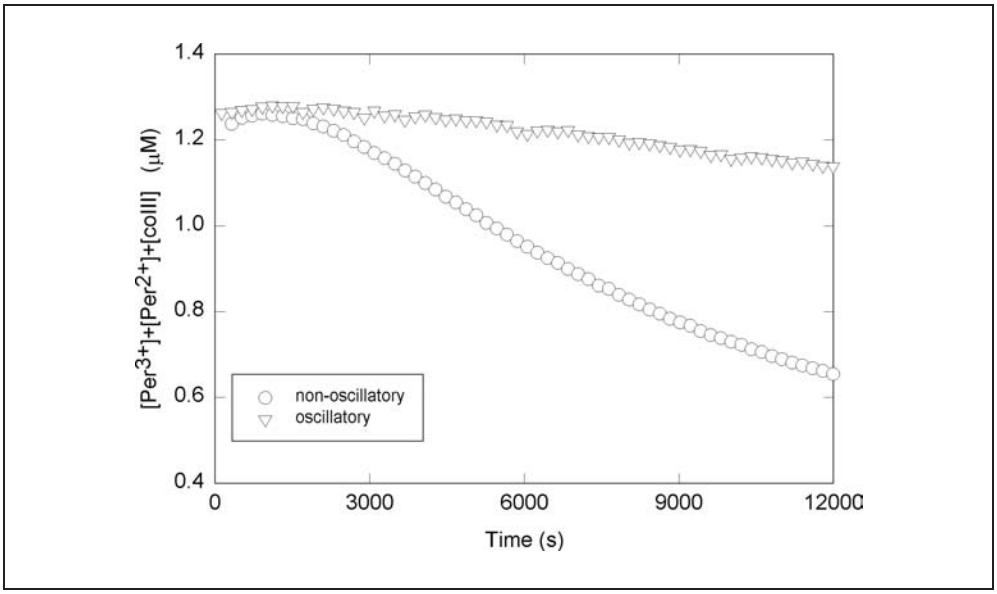

Fig. 5 Total enzyme concentration obtained for oscillatory and non-oscillatory dynamic states in the bistable domain. The sum of the concentrations of ferric peroxidase (Per^{3+}), ferrous peroxidase (Per^{2+}), and compound III (Per^{6+}) of experimental time series are plotted against time. Triangles designate an oscillatory time-series, while circles stand for a non-oscillatory dynamics.

model the effect of enzyme inactivation, we performed numerical simulations using the reaction mechanism shown in Table 1. To account for the inactivation of the enzyme by reactive oxygen species, we introduce the reaction

$$O_2^- + Per^{6+} \rightarrow E' \qquad [4]$$

where E′ stands for the inactivated enzyme. Superoxide radicals need not to be the reactive oxygen species in reality; however, for our simulations the choice of the reactive oxygen species (O_2^-, H_2O_2 or OH•) is not critical. We obtain essentially the same result if we assume that the inactivation is due to reactions of any of the enzyme species with O_2^- or H_2O_2.

Numerical simulations reproduce the experimental observations, i. e., a modest inactivation of the enzyme under oscillatory conditions and a pronounced inactivation when the reaction is run in a non-oscillatory fashion. To understand this difference in the rate of enzyme inactivation on the type of dynamic behavior, we computed the concentrations of O_2^- radicals formed under oscillatory and non-oscillatory conditions (Fig. 6). The simulations reveal that although the maximum O_2^- concentration during oscillations is much higher than the values obtained in the corresponding stationary state, the average concentrations of O_2^- are considerably lower (up to 8 times) during oscillations than during a steady state reaction. Thus, the higher rate of enzyme inactivation observed under stationary dynamics – compared to the oscillations – is linked to the higher concentration level of toxic and reactive oxygen species. These reactive species, which in-

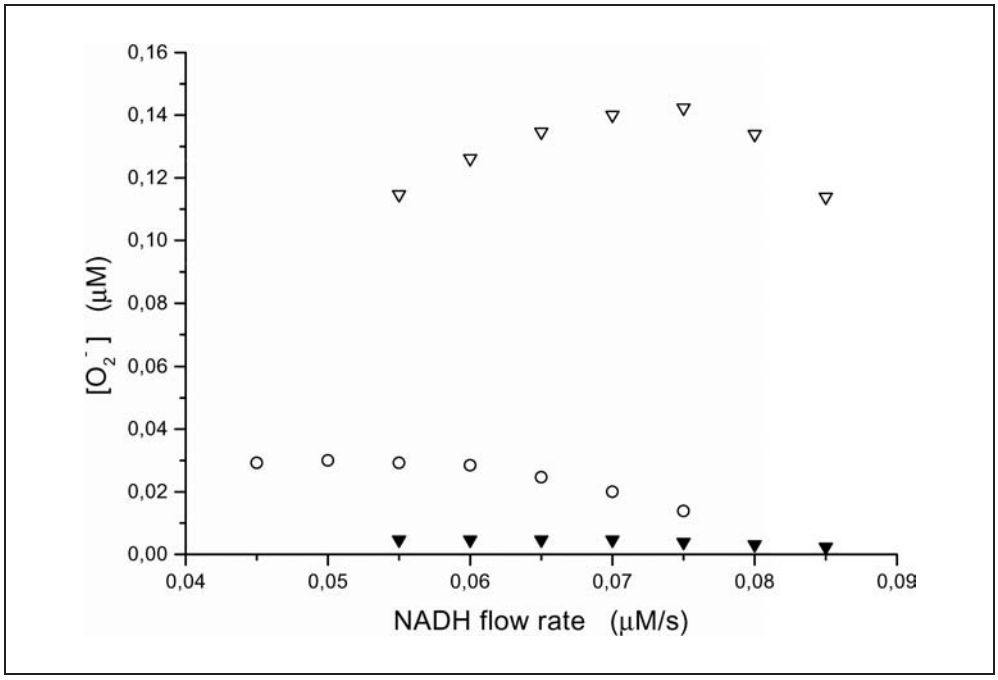

Fig. 6 Concentrations of superoxide radical under steady state and oscillatory conditions obtained from simulations using the reaction model proposed by BRONNIKOVA et al. (1995) (Tab. 1) and the decay reaction $O_2^- + Per^{6+} \rightarrow E'$. The steady state concentration (*circles*), as well as the maximum (*open triangles*) and the average concentration (*solid triangles*) of superoxide are plotted against the rate of NADH inflow.

evitably occur in the PO reaction, lead to irreversible inactivation of the enzyme, thus withdrawing it from the reaction system.

To conclude, the experiments and the numerical simulations strongly suggest that oscillatory dynamics in the PO reaction may be a strategy to protect the enzyme against irreversible inactivation by reactive intermediates. In addition, oscillations also act as information carriers, as can be seen from the high maximum concentrations of O_2^- during oscillations (Fig. 6). During the oscillations, the maxima in O_2^- concentration are very high (they exceed by far the concentrations found in the corresponding stationary state), however their duration is very short. Thus, a compromise between the two important functions of signal transduction and of enzyme protection seems to be achieved when the reaction is performed under oscillatory conditions.

4. Biomimetic Cytochrome P450 Model System

In this section we report on the dynamic behavior of a synthetic, supramolecular reaction system which has specially been designed to reproduce the reactivity, the kinetics, and the most prominent structural features encountered in the natural cytochrome P450 sys-

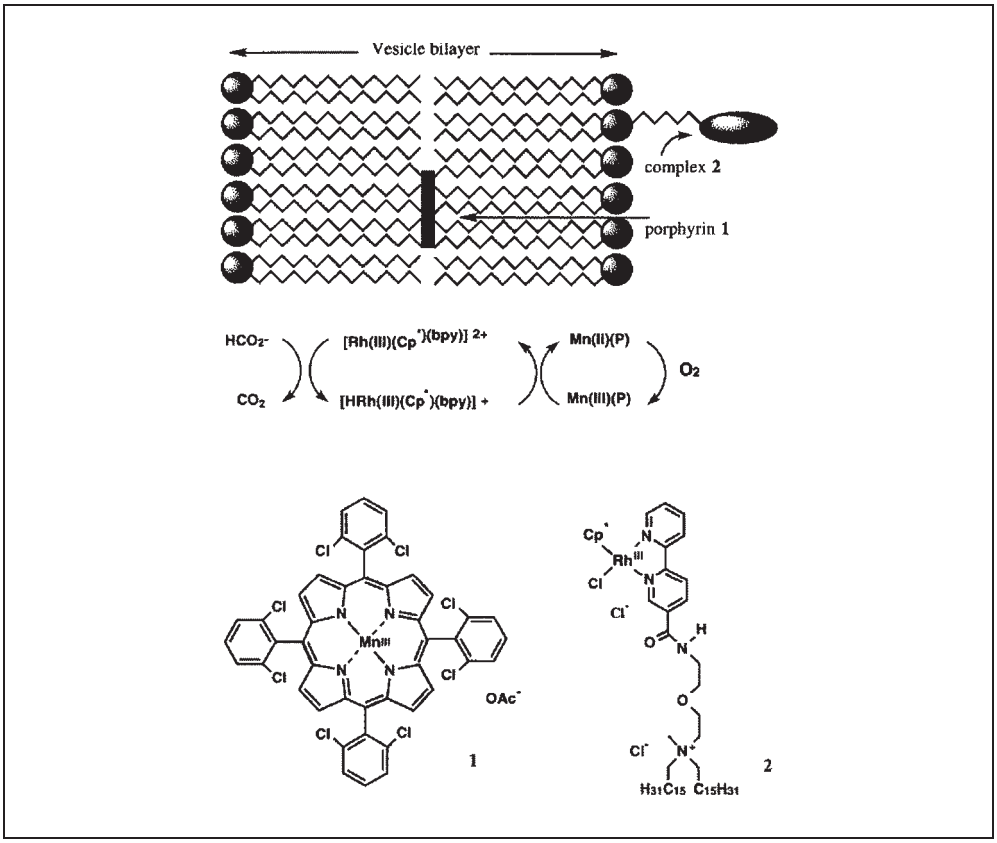

Fig. 7 Schematic representation of the biomimetic cytochrome P450 model system. The vesicles are made of DPPC. The lipid domain of the bilayer hosts the model enzyme compound (the manganese porphyrin **1**). While the model compound for the NADPH-cytochrome P450 reductase (Rh complex **2**) is anchored in the bilayer, its head group is located in the aqueous phase. The sequence of redox cycles forming the reaction cycle of the enzyme model system are shown.

tem (SCHENNING et al. 1994, 1995, VAN ESCH et al. 1995). This biomimetic system consists of a manganese porphyrin (**1**) which is incorporated into the lipid region of a phospholipid bilayer (Fig. 7). The latter is formed of the zwitterionic phospholipid dipalmitoylphosphatidyl choline (DPPC) which hosts an amphiphilic rhodium complex (**2**) in a concentration ratio [DPPC] : [**2**] = 500 : 1. Due to electric repulsion the charged substrates (formate and NADPH) are not capable of penetrating into the hydrophobic domain of the phospholipid bilayer. The aqueous phase contains the substrates sodium formate (or NADPH) and oxygen. In the biomimetic system the porphyrin **1** and the rhodium complex **2** mimic the enzyme cytochrome P450, and the NADPH-cytochrome P450-reductase, respectively.

In the model reaction the substrate formate (or NADPH) transfers electrons to the Rh complex **2**. This reduction induces a change in the charge and the polarity of the head

group of complex **2**, and consequently leads to a conformational change in this molecule. In the reduced form of complex **2**, the Rh moiety is supposed to be neutral and apolar, thus being able to penetrate into the lipid domain of the membrane. There, it transfers the electrons to the manganese porphyrin **1**, which is reduced to its Mn(II) form. By reducing **1**, the Rh complex **2** is re-oxidized and it returns to the aqueous phase. The reduced state of the manganese porphyrin **1** may react with oxygen. A sketch of the reactivity of this enzyme model system is included in Figure 7.

Alkenes present in the lipid domain of the bilayer are epoxidized by the supramolecular reaction system, a reaction that is typical for cytochrome P450. In addition, the turnover numbers for the epoxidations are in the same order of magnitude as those reported for the natural counterpart (SCHENNING et al. 1994). Thus, the supramolecular reaction system can be considered as a good biomimetic model for the natural cytochrome P450 system.

Preliminary studies reveal that the dynamics of the artificial cytochrome P450 model system may show oscillatory kinetics (SCHENNING et al. 1995): at very low concentrations of oxygen, the oxidation state of the membrane-bound model enzyme **1** oscillates periodically between its manganese(II)porphyrin and its manganese(III)porphyrin states. Figure 8 shows the oscillations of the manganese(II)prophyrin-form of the enzyme model compound; the oscillations of the oxidized form are phase shifted by 180°.

It is worth noting that oscillatory dynamics has not yet been directly observed in reactions of the natural cytochrome P450 system. However, when the natural cytochrome P450 system is perturbed by a single light pulse, the reaction products were found to be formed periodically and to accumulate in a step-wise fashion (HÄBERLE et al. 1990, GRULER and MÜLLER-ENOCH 1991). These results are consistent with oscillatory dynamics, and may indicate that oscillations also occur in reactions of natural cytochrome P450.

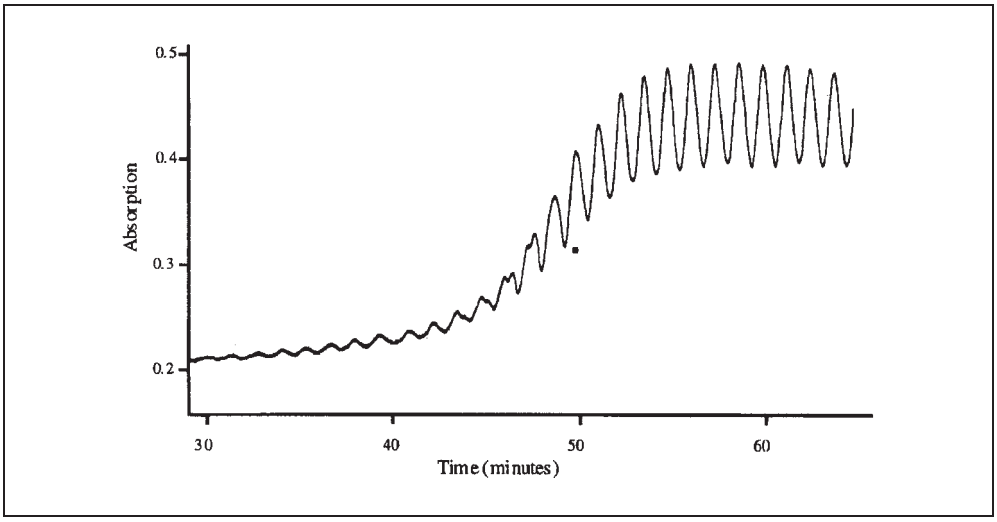

Fig. 8 Temporal oscillations of the oxidation states of the enzyme model compound **1**. The absorbance at 435 nm monitors the concentration of the manganese(II)porphyrin. The oscillations of the manganese(III)porphyrin are complementary to those shown.

However, a confirmation of oscillations in the natural cytochrome P450 system still needs experimental verification.

The involvement of the Rh complex **2** is crucial for the artificial cytochrome P450 system; in its absence no reduction of the manganese(III)porphyrin **1** is observed (VAN ESCH et al. 1995). Complex **2** provides the electron transport from the aqueous phase to the lipid domain of the bilayer. This transport is most likely performed through conformational changes of **2**, however, the exact nature of the mechanism of this electron transport remains to be investigated in detail. Nevertheless, any attempt to model the reaction dynamics must account for the interfacial transport and for the reactions taking place in the different compartments of the biomimetic system. Thus, the source for nonlinearities in the biomimetic cytochrome P450 model system, which lead to the oscillatory dynamics, may stem either from the chemical kinetics of the reaction system, or from the type of the transport, or even from a combination thereof. The identification of the origins of the nonlinearities is an open issue which calls for considerable research efforts. It is quite probable that the reaction–transport equation that eventually describes the dynamics of the biomimetic system may involve a type of transport which so far has not been considered in any study of temporal and spatiotemporal pattern formation (i. e. a type of transport other than diffusion, convection, or ionic migration).

5. Discussion

In the present article, we discussed in detail two single enzyme reaction systems which lead to nonlinear dynamical behavior. Taking into account that the hemin – hydrogen peroxide – sulfite reaction also displays various types of oscillations (HAUSER et al. 2001 b, 2002), and that there are more or less unequivocal reports that other minimal enzymic systems may induce rhythmic dynamics (TEMMINCK GROLL 1917, DAVISON et al. 1986, HÜBNER and WOLNA 1994), it is concluded that oscillatory or rhythmic dynamics are a general behavior of reaction systems consisting only of a single enzyme and their substrates. Thus, systems at the "low" hierarchical level of organization such as that of single enzyme reaction systems, may already exert the function of biological rhythms, pacemakers, or clocks.

The dynamics of single enzyme reactions systems can be very rich. In addition to simple periodic oscillations, periodic oscillations of higher complexity, quasiperiodic, chaotic, and bursting oscillations have been observed in single enzyme (and enzyme-model) systems. While the more complex dynamic regimes are not necessarily realized in every oscillating minimal enzyme system, the "fundamental" rhythmic dynamics, i. e. periodic oscillations of simple periodicity, are found in all of the oscillatory systems. The concrete physiological role of oscillatory behavior differs from enzyme system to enzyme system – and frequently this role is not even known. A physiological role for more complex types of oscillatory dynamics, especially that of quasiperiodic and chaotic dynamics, has not yet been identified. By contrast, periodic and bursting oscillations are known to possess biological significance as pacemakers and as a part of signal transduction cascades (GLASS and MACKEY 1988, GOLDBETER 1996). Typical signal transduction occurs mainly *via* oscillations of second messengers, such

as Ca^{2+}, or H_2O_2 and O_2^-, and the information content is assumed to be encoded in the form and frequency of the oscillations. It is remarkable that one of the detailed single enzyme systems discussed in the present article, the PO reaction, may interact with or even be a part of the signal transduction system involving the secondary messengers H_2O_2 and O_2^-.

Recently, we have presented evidence that oscillations may serve further biological purposes in addition to the classical tasks of generating rhythms and of transporting information. As shown for the PO reaction, oscillatory dynamics may be a tool developed by nature to avoid inactivation of enzymes by toxic reaction intermediates. A similar mechanism may also be effective in the case of Ca^{2+} oscillations, where rhythmic dynamics allow high peaks of Ca^{2+} concentration (and hence signal transduction) by keeping reasonably low average levels of (the otherwise cytotoxic) Ca^{2+}.

The nonlinearities leading to rhythmic dynamics in single enzyme reaction systems may stem from a variety of sources. This is even the case, if one compares single enzyme systems where the enzymes (or enzyme model compounds) carry structurally similar active centers, as in the cases of peroxidase, the cytochrome P450 model compound, and hemin. Here the active centers are always metalloporphyrin moieties. Nevertheless, the sources of nonlinearity are different: In the PO reaction and in the hemin – H_2O_2 – sulfite system, the nonlinearities are found in the kinetic reactions. However, the role of these two enzymes is different in the reaction mechanisms: while the peroxidase (in the PO reaction) is involved in the production of the autocatalytic species (which accounts for the nonlinearities), the task of the hemin (in the hemin – H_2O_2 – sulfite system) is to limit the production of the autocatalytic species. The source of the nonlinearity in the biomimetic cytochrome P450 model system is not known so far, but it is likely that the nonlinearity arises from an interplay between the reaction kinetics and the transport of electrons from the aqueous phase to the lipid domain of the phospholipid bilayer.

To conclude, our studies indicate that minimal enzyme reaction systems, which consist only of a single enzyme and its substrates, may display oscillatory behavior under appropriate reaction conditions. Thus, even reaction systems at the very fundamental molecular level can be the sources for biochemical and biological rhythms. The fact that underlying nonlinearities leading to oscillatory dynamics in such minimal enzyme reactions may arise from a variety of mechanistic sources suggests that rhythmic behavior is a general – and possibly even frequent – feature of single enzyme systems. The biological functions of oscillations are often not yet elucidated, and one might expect that a series of new biological functions (in addition to signal transduction, the action as pacemaker, and the protection against enzyme inactivation) may be carried out by the rhythmic behavior of enzymes. Thus, further research in the area of the dynamics of single enzyme reaction systems is expected to reveal substantial new insights into chronobiological processes.

Acknowledgement

We would like to thank L. F. Olsen (SDU Odense University) for fruitful discussions and a deep and long-standing collaboration on the PO reaction. We are grateful to U. Kummer (*European Media Laboratory*, Heidelberg) and A.-C. Møller (Odense) for discussions and for help in experiments with this reaction system. A. P. H. J. Schenning (University of Eindhoven) and R. J. M. Nolte (University of Enschede) are

acknowledged for collaboration and for introducing the author to the biomimetic system. We gratefully appreciate the intensive collaboration with S. C. Müller (Magdeburg) on the area of nonlinear dynamics of single enzyme model systems, as well as the help with experiments by T. Tosaya (Magdeburg). Financial support provided by the *Deutsche Forschungsgemeinschaft* and *Den naturvidenskabelige Forskninsgråd* (Denmark), and the travel grants from *European Science Foundation programme REACTOR* are acknowledged.

References

Aguda, B. D., Frisch, L.-L. H., and Olsen, L. F.: Experimental evidence for the coexistence of oscillatory and steady states in the peroxidase-oxidase reaction. J. Amer. Chem. Soc. *112*, 6652–6656 (1990)

Aguda, B. D., and Larter, R.: Periodic-chaotic sequences in a detailed mechanism of the peroxidase-oxidase reaction. J. Amer. Chem. Soc. *113*, 7913–7916 (1991)

Bronnikova, T. V., Fed'kina, V. R., Schaffer, W. M., and Olsen, L. F.: Period-doubling bifurcations and chaos in a detailed model of the peroxidase-oxidase reaction. J. Phys. Chem. *99*, 9309–9312 (1995)

Camacho, P., and Lechleiter, J. D.: Increase in frequency of calcium waves in *Xenopus laevis* oocytes that express calcium-ATPase. Science *260*, 226–229 (1993)

Davison, A. J., Kettle, A. J., and Fatur, D. J.: Mechanism of the inhibition of catalase by ascorbate. J. Biol. Chem. *261*, 1193–1200 (1986)

Degn, H.: Bistability caused by substrate inhibition of peroxidase in an open reaction system. Nature *217*, 1047–1050 (1968)

Degn, H., Olsen, L. F., and Perram, J. W.: Bistability, oscillation, and chaos in an enzyme reaction. Ann. New York Acad. Sci. *316*, 623– 637 (1979)

Elstner, E. F., and Heupel, A.: Formation of hydrogen peroxide by isolated cell walls from horseradish (*Armoracia lapathifolia* Gilib.). Planta *130*, 175–180 (1976)

Epstein, I. R., and Pojman, J. A.: An Introduction to Nonlinear Chemical Dynamics. New York: Oxford University Press 1998

Fed'kina, V. R., Attaullakhanov, F. I., and Bronnikova, T. V.: Computer simulations of sustained oscillations in peroxidase-oxidase reaction. Biophys. Chem. *19*, 259–264 (1984)

Field, R. J., and Burger, M. (Eds.): Oscillations and Traveling Waves in Chemical Systems. New York: Wiley 1985

Geest, T., Steinmetz, C. G., Larter, R., and Olsen, L. F.: Period-doubling bifurcations and chaos in an enzyme reaction. J. Phys. Chem. *96*, 5678–5680 (1992)

Glass, L., and Mackey, M. C.: From Clocks to Chaos – The Rhythms of Life. Princeton: Princeton University Press 1988

Goldbeter, A.: Biochemical Oscillations and Cellular Rhythms – The Molecular Bases of Periodic and Chaotic Behaviour. Cambridge: Cambridge University Press 1996

Goodner, C. J., Walike, B. C., Koerker, D. J., Ensinck, J. E., Brown, A. C., Chideckel, E. W., Palmer, J., and Kalnasy, L.: Insulin, glucagon, and glucose exhibit synchronous, sustained oscillations in fasting monkeys. Science *195*, 177–179 (1977)

Gross, G. G., Janse, C., and Elstner, E. F.: Involvement of malate, monophenols, and the superoxide radical in hydrogen peroxide formation by isolated cell walls from horseradish (*Armoracia lapathifolia* Gilib.). Planta *136*, 271–276 (1977)

Gruler, H., and Müller-Enoch, D.: Slaving the cytochrome P-450 dependent monooxygenase system by periodically applied light pulses. Eur. Biophys. J. *19*, 217–219 (1991)

Häberle, W., Gruler, H., Dutkowski, P., and Müller-Enoch, D.: Light-induced activation and synchronization of the cytochrome P-450 dependent monooxygenase. Z. Naturforsch. *45c*, 273–279 (1990)

Halliwell, B.: Lignin synthesis: The generation of hydrogen peroxide and superoxide by horseradish peroxidase and its stimulation by manganese(II) and phenols. Planta *140*, 81–88 (1978)

Hauck, T., and Schneider, F. W.: Mixed-mode and quasiperiodic oscillations in the peroxidase-oxidase reaction. J. Phys. Chem. *97*, 391–397 (1993)

Hauck, T., and Schneider, F. W.: Chaos in a Farey sequence through period doubling in the peroxidase-oxidase reaction. J. Phys. Chem. *98*, 2072–2077 (1994)

Hauser, M. J. B., Fricke, N., Storb, U., and Müller, S. C.: Periodic and bursting pH oscillations in an enzyme model system. Z. Phys. Chem. *216*, 375–390 (2002)

Hauser, M. J. B., Kummer, U., Larsen, A. Z., and Olsen, L. F.: Oscillatory dynamics protect enzymes and possibly cells against toxic substances. Faraday Discuss. *120*, 215–227 (2001 a)

Hauser, M. J. B., Lunding, A., and Olsen, L. F.: On the role of methylene blue in the oscillating peroxidase-oxidase reaction. Phys. Chem. Chem. Phys. *2*, 1685–1692 (2000)

Hauser, M. J. B., and Olsen, L. F.: Mixed-mode oscillations and homoclinic chaos in an enzyme reaction. J. Chem. Soc. Faraday Trans. *92*, 2857–2863 (1996)

Hauser, M. J. B., and Olsen, L. F.: The role of naturally occurring phenols in inducing oscillations in the peroxidase-oxidase reaction. Biochemistry *37*, 2458–2469 (1998)

Hauser, M. J. B., and Olsen, L. F.: Routes to chaos in the peroxidase-oxidase reaction. In: Müller, S. C., Parisi, J., and Zimmermann, W. (Eds.): Transport versus Structure – Their Competitive Roles in Biophysics and Chemistry. Lecture Notes in Physics; pp. 252–272. Heidelberg: Springer 1999

Hauser, M. J. B., Olsen, L. F., Bronnikova, T. V., and Schaffer, W. M.: Routes to chaos in the peroxidase-oxidase reaction. 1. Period-doubling and period-addding. J. Phys. Chem. B *101*, 5075–5083 (1997)

Hauser, M. J. B., Strich, A., Bakos, R., Nagy-Ungvárai, Z., and Müller, S. C.: pH Oscillations in the hemin – hydrogen peroxide – sulfite reaction. Faraday Discuss. *120*, 229–236 (2001 b)

Hübner, G., and Wolna, P.: Nonlinear dynamic processes in open single enzyme systems. Biol. Chem. Hoppe-Seyler *375*, 31–34 (1994)

Hung, Y.-F., and Ross, J.: New experimental methods towards the deduction of the mechanism of the oscillatory perxidase-oxidase reaction. J. Phys. Chem. *99*, 1974–1979 (1995)

Kummer, U., Valeur, K. R., Baier, G., Wegmann, K., and Olsen, L. F.: Oscillations in the peroxidase-oxidase reaction: A comparison of different peroxidases. Biochim. Biophys. Acta *1289*, 397–403 (1996)

Larter, R., Olsen, L. F., Steinmetz, C. G., and Geest, T.: Chaos in biochemical systems: the peroxidase reaction as a case study. In: Field, R. J., and Györgyi, L. (Eds.): Chaos in Chemical and Biological Systems; pp. 175–224. Singapore: World Scientific 1993

Liu, E. H., and Lamport, D. T. A.: An accounting of horseradish peroxidase isoenzymes associated with the cell wall and evidence that peroxidase does not contain hydroxyproline. Plant Physiol. *54*, 870–876 (1974)

Lüttge, U.: The tonoplast functioning as the master switch for circadian regulation of crassulacean acid metabolism. Planta *211*, 761–769 (2000)

Møller, A.-C., Hauser, M. J. B., and Olsen, L. F.: Oscillations in peroxidase-catalyzed reactions and their potential function in vivo. Biophys. Chem. *72*, 63–72 (1998)

Olsen, L. F.: An enzyme reaction with a strange attractor. Phys. Lett. A *94*, 454–457 (1983)

Olsen, L. F., and Degn, H.: Chaos in an enzyme reaction. Nature *267*, 177–178 (1977)

Rascher, U., Hütt, M.-T., Siebke, K., Osmond, B., Beck, F., and Lüttge, U.: Spatiotemporal variation of metabolism in a plant circadian rhythm: The biological clock as an assembly of coupled individual oscillators. Proc. Nat. Acad. Sci. USA *98*, 11801–11805 (2001)

Ryde-Petterson, U.: A theoretical treatment of damped oscillations in the transient state kinetics of single-enzyme reactions. Eur. J. Biochem. *186*, 145–148 (1989)

Samples, M. S., Hung, Y.-F., and Ross, J.: Further experimental studies on the horseradish peroxidase-oxidase reaction. J. Phys. Chem. *96*, 7338–7342 (1992)

Scheeline, A., Olson, D. L., Williksen, E. P., Horras, G. A., Klein, M. L., and Larter, R.: The peroxidase-oxidase oscillator and its constituent chemistries. Chem. Rev. *97*, 793–756 (1997)

Schenning, A. P. H. J., Hubert, D. H. W., van Esch, J. H., Feiters, M. C., und Nolte, R. J. M.: Ein zwei Metalle enthaltendes Modellsystem für Cytochrom P_{450}: Einfluß des Membranmilieus auf die katalytische Oxidation. Angew. Chem. *106*, 2587–2588 (1994)

Schenning, A. P. H. J., Lutje Spelberg, J. H., Driessen, M. C. P. F., Hauser, M. J. B., Feiters, M. C., and Nolte, R. M.: Enzyme mimic displaying oscillatory behavior. Oscillating reduction of manganese(III) porphyrin in a membrane-bound cytochrome P450 system. J. Amer. Chem. Soc. *117*, 12655–12656 (1995)

Temminck Groll, J.: Periodische Erscheinungen bei Fermenten als Folge ihrer kolloiden Beschaffenheit. Kolloid Z. *21*, 138–148 (1917)

van Esch, J. H., Hoffmann, M. A. M., and Nolte, R. J. M.: Reduction of nicotinamides, flavins, and manganese porphyrins by formate, catalyzed by membrane-bound rhodium complexes. J. Org. Chem. *60*, 1599–1610 (1995)

YAMAZAKI, I., YOKOTA, K., and NAKAJIMA, R.: Oscillatory oxidations of reduced pyridine nucleotide by peroxidase. Biochem. Biophys. Res. Commun. *21*, 582–586 (1965)

YAMAZAKI, I., and YOKOTA, K.: Oxidation states of peroxidase. Mol. Cell. Biochem. *2*, 39–52 (1973)

YOKOTA, K., and YAMAZAKI, I.: Reaction of peroxidase with reduced nicotinamide-adenine dinucleotide and reduced nicotineamide-adenine dinucleotide phosphate. Biochim. Biophys. Acta *105*, 301–312 (1965)

YOKOTA, K., and YAMAZAKI, I.: Analysis and computer simulation of aerobic oxidation of reduced nicotinamide adenine dinucleotide by horseradish peroxidase. Biochemistry *16*, 1913–1920 (1977)

Dr. Marcus J. B. HAUSER
Institut für Experimentelle Physik
Abteilung Biophysik,
Otto-von-Guericke-Universität Magdeburg
Universitätsplatz 2
39106 Magdeburg
Germany
Phone: ++49 (0) 3 91 67 18 96
Fax: ++49 (0) 39 16 71 11 81
E-Mail: marcus.hauser@physik.uni-magdeburg.de

Nova Acta Leopoldina NF *88*, Nr. 332, 151–167 (2003)

Statistical Properties of Ca^{2+} Puffs

Jian-Wei SHUAI and Peter JUNG (Athens, USA)

With 10 Figures and 2 Tables

Abstract

Calcium release from clusters of inositol 1,4,5-triphosphate (IP_3) release channels is the basic biophysical mechanism by which Ca^{2+} is released from the endoplasmic reticulum into the cytosol. As small amounts of Ca^{2+} are released they diffuse through the cytosol where they form spatially and temporally limited structures – the Ca^{2+} puffs. We consider Ca^{2+} release through a small cluster of IP_3 release channels and subsequent diffusion through the cytosol using a Markov version of the Li-Rinzel model and a computationally more efficient Langevin approximation. We discuss the effects of Ca^{2+} diffusion on puff amplitude distribution, puff width distribution and inter-puff interval distribution and compare the results of both methods to determine whether the Langevin approximation yields accurate answers.

Zusammenfassung

Calcium-Ionen werden durch kleine Gruppen von Ionenkanälen von intrazellulären Speichern in den intrazellulären Raum transportiert. Dort diffundieren die Calcium-Ionen und werden von Calcium-Pumpen wieder in die Speicher aufgenommen. Als Resultat erhält man räumlich limitierte Calcium-Funken (*sparks* oder *puffs*). Stochastische Effekte sind wegen der kleinen Anzahl von Kanälen pro Gruppe dominierend und werden gewöhnlich durch numerisch aufwendige Markov-Prozesse berücksichtigt. Wir stellen hier eine vereinfachte Methode vor, die auf der Konstruktion von stochastischen Differentialgleichungen für die Zustände der Ionenkanäle beruht. Charakteristische Eigenschaften der Calcium-Funken werden mit Markov-Prozessen und stochastischen Differentialgleichungen simuliert und die Resultate werden verglichen.

1. Introduction

Many important cellular functions are regulated by intra- and intercellular Ca^{2+} signals. They are involved in the insulin production of pancreatic β-cells (CHAY and KEIZER 1983), in the enzyme secretion in liver cells (for a review, see e. g. DUPONT et al. 2000) and the early response to injury of brain tissue (CORNELL-BELL et al. 1990) and corneal epithelia (KLEPEIS et al. 2001).

Key for the Ca^{2+} release is the inositol 1,4,5-triphosphate receptor channel (IP_3R) on the membrane of the endoplasmic reticulum (ER). It is thought (DEYOUNG and KEIZER 1992) that the IP_3 receptor has four subunits where three of them have to be activated for the IP_3R to be open. According to the DeYoung-Keizer model, each subunit has three binding sites, one for IP3 and two for Ca^{2+}. The first Ca^{2+} binding site activates the sub-

unit *via* Ca^{2+} induced Ca^{2+} release (Bezprovanny et al. 1991) while the other Ca^{2+} binding site inactivates the subunit.

Recently, high-resolution recordings have shed new light on the elementary intracellular Ca^{2+} release from internal stores. It has been observed that the IP_3Rs are spatially organized in clusters with only 20–50 release channels and of a size of about 100 nm. The calcium release through such small clusters is subject to random fluctuations due to thermal transitions of individual IP_3Rs. When Ca^{2+} is released from the ER through an IP_3R, it rapidly diffuses within the cluster (in a few μs) and into the intracellular space where it is absorbed by buffers and pumped back into the ER, resulting in a spatially and temporally limited event that has been termed calcium puff or spark (Cheng et al. 1993, Mak and Foskett 1997, Callamaras et al. 1998, Melamed-Book et al. 1999, Gonzalez et al. 2000). Ca^{2+} blips arising from the opening of single release channels have been observed as well (Bootman et al. 1997, Lipp and Niggli 1998, Sun et al. 1998).

In this paper we consider small clusters of Ca^{2+} release channels where the released Ca^{2+} is diffusible in the intracellular space. We study the effects of Ca^{2+} diffusion on the distributions of puff-amplitude (*Section 3*), lifetime (*Section 4*) and interpuff-interval (*Section 5*).

2. Markov Li-Rinzel Model for an Isolated Cluster of IP_3Rs

The first theoretical model for agonist-induced Ca^{2+} oscillations based on the microscopic kinetics of IP_3 and Ca^{2+} gating of the IP_3R was proposed by DeYoung and Keizer (1992). The model assumes that three equivalent and independent subunits are involved in conduction of an IP_3R. Each subunit has one binding site for IP_3 (site 1) and two binding sites for Ca^{2+}; one Ca^{2+} binding site (site 2) for activation, the other (site 3) for inhibition. The subunit is conducting only when site-1 and site-2 are bound and site-3 is unbound. Thus, each subunit may exist in eight states with transitions governed by second-order and first-order rate constants. The scheme in Figure 1 illustrates the processes at a single subunit (DeYoung and Keizer 1992). For the rate constants the same rates as in DeYoung and Keizer (1992) are used (see Tab. 1).

The subunit is activated in the state S_{110} only. The transition rates between the states of an IP_3 channel differ significantly for a large range of intracellular Ca^{2+} concentrations. The binding and unbinding of IP_3 is the fastest process, followed by the binding of Ca^{2+} to the activation binding site (approximately a factor of 10 slower) and by the binding of Ca^{2+} to the inactivation binding site (another factor of 10 slower). Using a type of multiple time-scale expansion, Li and Rinzel (1994) were able to separate the kinetic equations for the IP_3 channel in a fast set, an intermediate set and a slow set of equations. The fast and intermediate sets of equations are solved explicitly, thus eliminating all but the slowest variables. As a result they obtain the following set of differential equations on the slowest time scale with two variables only:

$$\frac{dc}{dt} = -c_1 m_\infty^3 n_\infty^3 h^3 (c - c_{ER}) - c_1 v_2 (c - c_{ER}) - \frac{v_3 c^2}{k_3^2 + c^2}, \quad [1]$$

$$\frac{dh}{dt} = \frac{1}{\tau_h}(h_\infty - h) \quad [2]$$

where c is the intracellular Ca^{2+} concentration and c_{ER} the Ca^{2+} concentration in the ER.

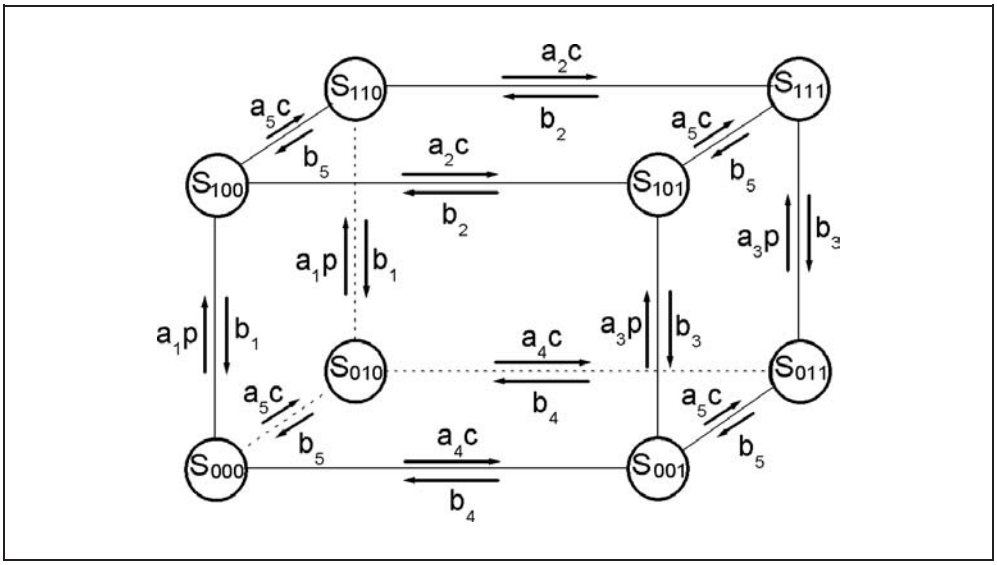

Fig. 1 The binding scheme of a single unit of the IP_3 receptor. S_{nml} denotes the states of the IP_3 receptor where n, m, l can assume the values 0 and 1. The first index indicates the state of the IP_3 binding site, the second the state of the activating Ca^{2+} binding and the third index the state of the inhibiting Ca^{2+} binding site. If an index is 0 the respective binding site is unbound; if it is 1 the respective binding site is bound. The values for the rate constants a_s and b_s are the original values used in DeYoung and Keizer (1992). The concentration of IP_3 is denoted by p and the intracellular concentration of Ca^{2+} is denoted by c.

Tab. 1 Parameter values for the DeYoung-Keizer model of the IP_3 receptor. For the meaning of the rate constants, see Figure 1.

$a_1 = 400/(\mu M\ s)$	$b_1 = 52/s$
$a_2 = 0.2/(\mu M\ s)$	$b_2 = 0.21/s$
$a_3 = 400/(\mu M\ s)$	$b_3 = 377.2/s$
$a_4 = 0.2/(\mu M\ s)$	$b_4 = 0.029/s$
$a_5 = 20/(\mu M\ s)$	$b_5 = 1.64/s$

Tab. 2 Parameter values for Equation [1].

v_1	6/s
v_2	0.11/s
v_3	$0.9/(\mu M\ s)$
k_3	$0.1\ \mu M$

The first term on the right hand side of Equation [1] denotes the channel flux density from the ER into the intracellular space, the second term the leak flux density and the third term the pump flux density from the intracellular space into the ER. Equation [2] for h, defined as the sum of the fractions of the channels in de-inactivated states, has the

form of a two-state gate. The power h^3 in Equation [1] indicates that all three independent subunits have to be de-inactivated in order for the channel to be open. The expressions m_∞^3 and n_∞^3 describe the average fraction of the channels with bound IP_3 and bound activating Ca^{2+}, respectively. The values of the parameters above are

$$n_\infty = \frac{p}{p+d_1}; \quad m_\infty = \frac{c}{c+d_5}; \quad \tau_h = \frac{1}{a_2(Q_2+c)}$$
$$h_\infty = \frac{Q_2}{Q_2+c}; \quad Q_2 = d_2\frac{p+d_1}{p+d_3}; \quad d_i = \frac{b_i}{a_i}. \qquad [3]$$

The dynamic properties of the Li-Rinzel model in comparison with the DeYoung-Keizer model can be summarized in the bifurcation diagram in Figure 2. At concentrations p of IP_3 of less than 0.354 μM and larger than 0.642 μM, the Li-Rinzel model predicts fixed points, i. e., the Ca^{2+} concentration approaches a constant value after an initial transient. A super-critical Hopf bifurcation generates Ca^{2+} oscillations for $0.354\ \mu M < p < 0.642\ \mu M$. The curves in the regime $0.354\ \mu M < p < 0.642\ \mu M$ represent the minima and the maxima of $[Ca^{2+}]$ during the oscillations. The Li-Rinzel model (dashed line) reproduces the bifurcation diagram of the DeYoung-Keizer model (solid line) well. The upper Hopf bifurcation, however, is somewhat shifted. The fixed points for $p > 0.642\ \mu M$ and $p < 0.354\ \mu M$ are reproduced almost exactly.

We consider a cluster of N IP_3Rs, where N can be a small number and thus a stochastic description is necessary. A stochastic version of the Li-Rinzel equations can be obtained by replacing h^3 by the fraction of de-inactivated channels $N_{h\text{-open}}/N$ where N is

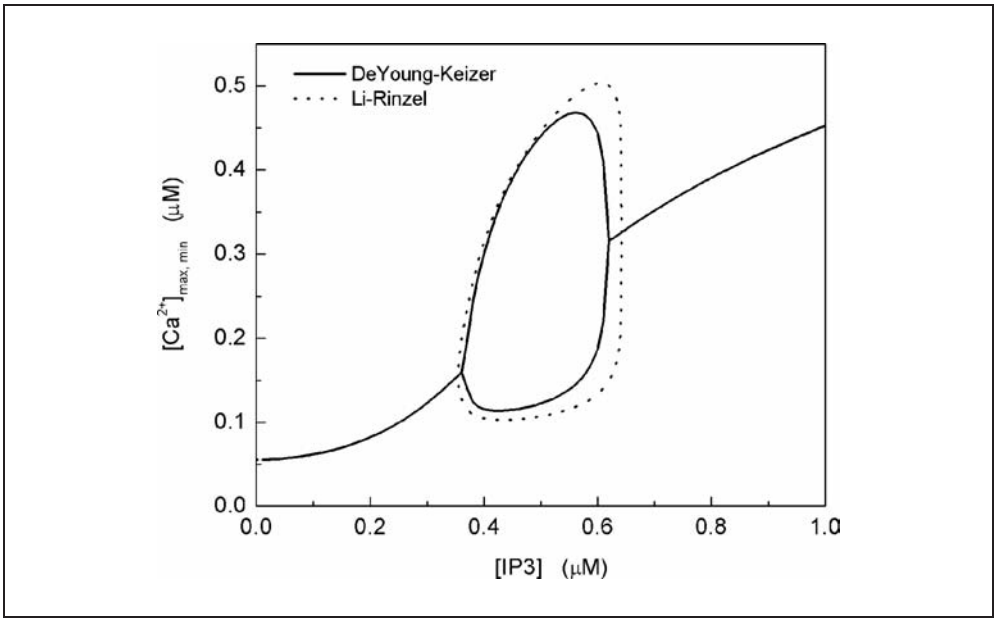

Fig. 2 Bifurcation diagram, i. e. the Ca^{2+} values of the maximum and the minimum as a function of IP_3 concentration p, of the deterministic Li-Rinzel model (dashed line) and the DeYoung-Keizer model (solid line). Oscillations are possible between the two Hopf bifurcations, i. e. $0.354\ \mu M < [IP_3] < 0.642\ \mu M$ in the Li-Rinzel model. For all other values of p, fixed points are observed.

the total number of IP_3Rs, and $N_{h\text{-open}}$ is the number of channels that are de-inactivated (SHUAI and JUNG 2002a), i. e.

$$\frac{dc}{dt} = -c_1 m_\infty^3 n_\infty^3 \frac{N_{h-\text{open}}}{N}(c - c_{ER}) - c_1 v_2 (c - c_{ER}) - \frac{v_3 c^2}{k_3^2 + c^2}. \quad [4]$$

The opening and closing rates $\alpha(p)$ and $\beta(c)$, respectively, of this h-gate can be obtained from Equation [3] as

$$\alpha(p) = a_2 Q_2(p); \quad \beta(c) = a_2 c. \quad [5]$$

The kinetic scheme for the 4 states of the three h-gates of the Li-Rinzel model is given in Figure 3.

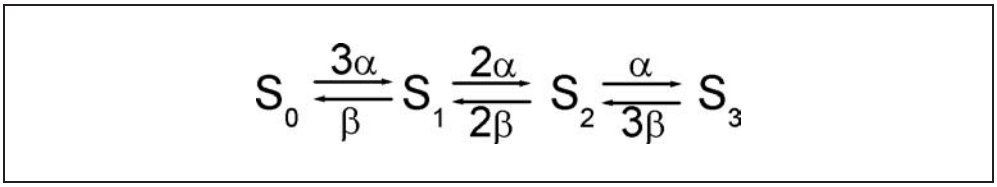

Fig. 3 The kinetic scheme of the h-gates of the Li-Rizel model. The symbol S_n denotes an IP_3R with n h-gates open (not inhibited). The channel is open in the state S_3.

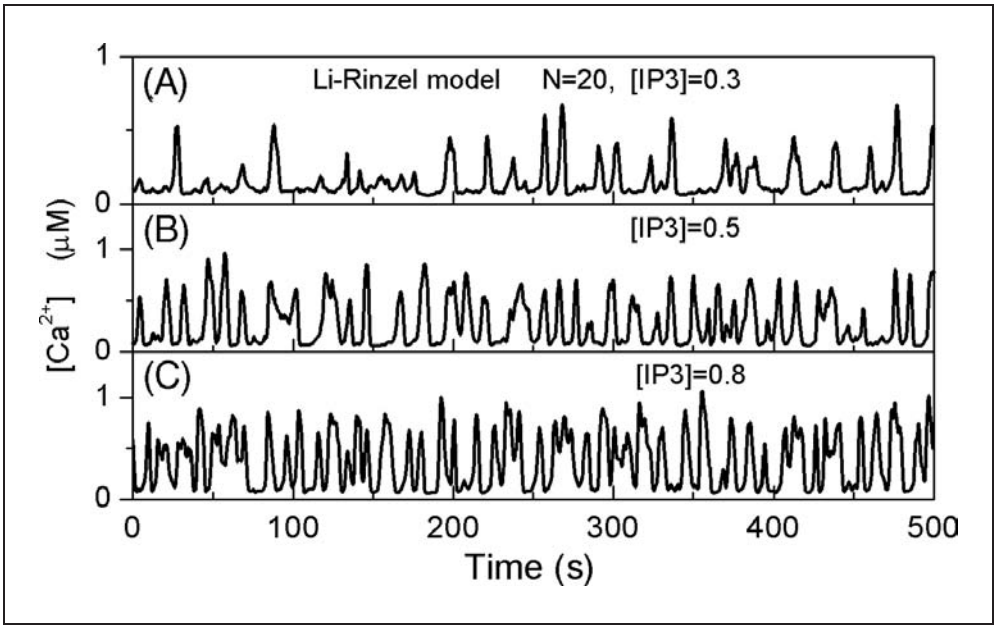

Fig. 4 Calcium traces obtained from the Markov Li-Rinzel model for a cluster of 20 IP_3Rs at three characteristic values of p: (*A*) for $p = 0.3$ μM; (*B*) for $p = 0.5$ μM and (*C*) for $p = 0.8$ μM. The time (horizontal axis) is measured in seconds.

Stochastic simulations of such a scheme can be performed using standard Markov processes (see e. g. SCHNEIDMAN et al. 1998 in different context). As a result one obtains at each time step the number of open h-gates $N_{\text{h-open}}$ which enters into Equation [4] which is subsequently being integrated. Within an isolated cluster of few IP_3Rs the calcium concentration can be assumed uniform across the cluster.

Calcium traces obtained from a cluster of 20 IP3Rs are shown for three different values of IP_3 concentration p in Figure 4. For $p = 0.3$ μM, i. e., below the Hopf bifurcation of the deterministic model ($p = 0.354$ μM), a trace is shown in Figure 4 *A*. While the deterministic equation predicts a fixed point (see Fig. 2), the stochastic dynamics generates release events – the Ca^{2+} puffs. During a puff, a significant fraction of the IP_3Rs open up for a short amount of time to release Ca^{2+} into the intracellular space. The trajectory for $p = 0.5$ μM is shown in Figure 4 *B*. While the deterministic solution (see Fig. 2) predicts periodic calcium oscillations, the stochastic model generates a spike train that looks not very different from the trajectory for subthreshold IP_3 concentration. The situation is similar for $p = 0.8$ μM in Figure 4 *C*.

Detailed studies of the statistical features of calcium puffs generated by isolated clusters have been carried through in previous work (SHUAI and JUNG 2002 a, b, 2003).

3. Ca^{2+} Puffs of a Single Cluster in a Diffusible Medium

The next step towards a more realistic description of Ca^{2+}puffs is to take into account that the released calcium can diffuse into the intracellular space (FALCKE et al. 2000). We study a patch of the ER membrane that we assume to be planar. The cluster of IP_3Rs controls the flux of Ca^{2+} from the ER to the intracellular space. We further assume that the cell is flat so that the concentration of Ca^{2+} is uniform across the cell. The Ca^{2+} concentration thus depends only on the 2D coordinates (x, y) of the flat membrane of the ER. The size of the cluster of IP_3Rs is of the order of 0.1 μm while the diffusion coefficient of Ca^{2+} is of the order of 0.01 $\mu m^2/s$–50 $\mu m^2/s$ resulting in a diffusion length $l \approx \sqrt{D\tau} \approx 0.1\ \mu m - 7\ \mu m$, i. e., at least as large as the size of the cluster of the IP_3R. Combining the Markov Li-Rinzel equation with Ca^{2+} diffusion yields the following stochastic partial differential equation

$$\frac{\partial c}{\partial t} = \left(c_1 v_1 m_\infty^3 n_\infty^3 \frac{N_{h-open}}{N} (c - c_{ER}) - c_1 v_2 (c - c_{ER}) - \frac{v_3 c^2}{k_3^2 + c^2} \right) \Xi(x)\ \Xi(y) + D\nabla^2 c \quad [6]$$

with the form function

$$\Xi(x) = \begin{cases} 1 & \text{for} \quad -L/2 < x < \Lambda/2 \\ 0 & \text{for} \quad |x| > \Lambda/2 \end{cases} \quad [7]$$

With the help of the form function we limit the release of Ca^{2+} from the ER to the intracellular space to a cluster area of L^2. The cluster is located at the origin of the coordinate system and is considered a *point source* of Ca^{2+} regardless of its actual physical size. In order to incorporate the effect of the point source into the numerical solution of Equation [6] (with a finite discretization step x), the form function in Equation [6] must be rescaled with $(L/x)^2$. This procedure is analogous to the point charge concept in electrodynamics where the point charge is represented by a d-function with strength q in the pre-

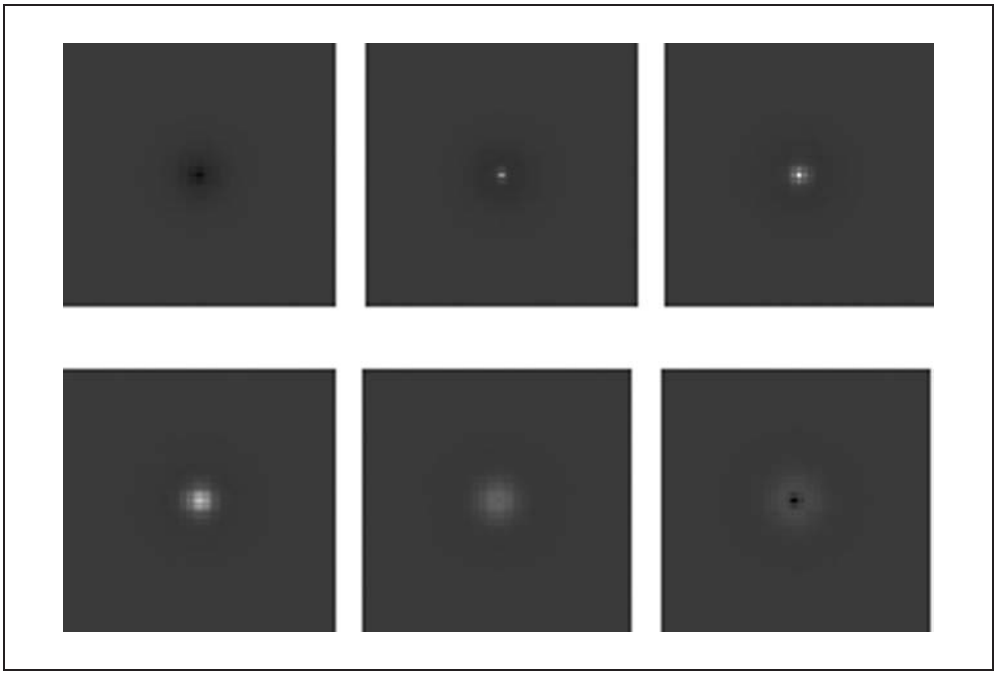

Fig. 5 Snapshots of Ca^{2+} distribution generated by a cluster of IP_3Rs located at the center of the 2D ER membrane. The size of the simulated area is 25 μm^2 while the cluster size is 0.01 μm^2. Lighter gray indicates higher Ca^{2+} concentration. The temporal sequence of the snapshots is from upper left to lower right. The time interval between consecutive snapshots is 2 s.

factor. It saves us to use integration steps that are small in comparison with the size of the release cluster. The Laplacian in Equation [6] is the two dimensional Laplacian in x–y coordinates. The number N represents the total number of IP_3Rs in the cluster and $N_{\text{h-open}}$ denotes the open number of channels at time t. To solve Equations [6] and [7], we used an explicit linear algorithm in combination with a Monte-Carlo Markov simulation of the gating processes of the channels. The cluster of IP_3Rs has been considered Ca^{2+} clamped. In Figure 5, we show a few snapshots of an evolving Ca^{2+} puff. Before we show detailed results of these simulations, we introduce an approximate method for this problem.

4. Langevin Approximation to the Stochastic Li-Rinzel Model

The drawback of the stochastic methods described above is that they become computationally very demanding. In the following we describe an alternative scheme resulting in stochastic differential equations (Langevin equations) that are easy to implement and computationally more efficient. The first approximation is that all three h-subunits can be replaced by a single two-state subunit with the same opening and closing rates $\alpha(p)$ and $\beta(c)$. This assumption can be somewhat motivated but justified only by the success

of the resulting Langevin equations. The motivation is that all subunits are clamped to the same Ca^{2+} concentration and their opening and closing events are thus somewhat correlated. For a fixed Ca^{2+} concentration, the probability of finding N open single-subunit channels in a cluster of N_t channels obeys the birth-death master equation

$$\frac{\partial P(N,t)}{\partial t} = G^{+}(N-1)P(N-1,t) - (G^{+}(N)+G^{-}(N))P(N,t) + G^{-}(N+1)P(N+1,t), \quad [8]$$

where

$$G^{+}(N) = (N_t - N)\,\alpha_h \quad [9]$$
$$G^{-}(N) = N\beta_h\,.$$

The following scaling transformation

$$n = N/N_t$$
$$g+(n) \equiv \frac{G+(N)}{N_t} = (1-n)\,\alpha_h$$
$$g^{-}(n) \equiv \frac{G^{-}(N)}{N_t} = n\beta_h$$
$$\rho(n) \equiv P(N_t n), \quad [10]$$

and the subsequent Taylor expansion in powers of $e = 1/N_t$

$$G^{+}(N-1) = G^{+}(N_t(n-\varepsilon)) = g^{+}(n-\varepsilon) = g^{+}(n) + \sum_{i=1}^{\infty} \frac{1}{i!}\,\varepsilon^{i}\left(-\frac{\partial}{\partial n}\right)^{i} g^{+}(n)$$

$$G^{-}(N+1) = G^{-}(N_t(n+\varepsilon)) = g^{-}(n+\varepsilon) = g^{-}(n) + \sum_{i=1}^{\infty} \frac{1}{i!}\,\varepsilon^{i}\left(\frac{\partial}{\partial n}\right)^{i} g^{-}(n)$$

$$P(N+1) = P(N_t(n+\varepsilon)) = \rho(n+\varepsilon) = \rho(n) + \sum_{i=1}^{\infty} \frac{1}{i!}\,\varepsilon^{i}\left(\frac{\partial}{\partial n}\right)^{i} \rho(n)$$

$$P(N-1) = P(N_t(n-\varepsilon)) = \rho(n-\varepsilon) = \rho(n) + \sum_{i=1}^{\infty} \frac{1}{i!}\,\varepsilon^{i}\left(-\frac{\partial}{\partial n}\right)^{i} \rho(n), \quad [11]$$

yields after inserting Equation [11] into Equation [8] and comparing coefficients of equal powers in ε the Kramers-Moyal expansion

$$\frac{\partial \rho(n,\,t)}{\partial t} = \sum_{i=1}^{\infty} \frac{1}{i!}\,\varepsilon^{i-1}\left(-\frac{\partial}{\partial n}\right)^{i} M_i(n)\,\rho(n,\,t), \quad [12]$$

with the Kramers-Moyal coefficients

$$M_i(n) = g^{+}(n) + (-1)^{i}\,g^{-}(n) = (1-n)\,\alpha_h + (-1)^{i}\,n\beta_h. \quad [13]$$

We truncate the Kramers-Moyal expansion after the second term (the diffusion term) and obtain the Fokker-Planck equation

$$\frac{\partial \rho(n,\ t)}{\partial t} = -\frac{\partial}{\partial n} M_1(n)\ \rho(n,\ t) + \frac{1}{2N_t}\ \frac{\partial^2}{\partial n^2} M_2(n)\ \rho(n,\ t), \qquad [14]$$

with the drift and diffusion coefficients

$$M_1(n) = g^+(n) - g^-(n) = (1-n)\ \alpha_h - n\beta_h$$
$$M_2(n) = g^+(n) + g^-(n) = (1-n)\ \alpha_h + n\beta_h. \qquad [15]$$

Note that this truncation does not guarantee the preservation of the exact stationary probability (HÄNGGI and JUNG 1988). An equivalent Ito-type Langevin equation can be found as

$$\frac{dn}{dt} = \alpha_h(1-n) - \beta_h n + \xi(t)$$
$$\langle \xi(t)\ \xi(t') \rangle = \frac{\alpha_h(1-n) + \beta_h n}{2N_i}\ \delta(t-t')$$
$$\langle \xi(t) \rangle = 0 \qquad [16]$$

with Gaussian white noise $\xi(t)$. FOX and LU (1994) and later SCHMID et al. (2001) have used such a scheme to describe action potentials generated by clusters of neuronal ion channels. The Langevin approximation of the Markov Li-Rinzel model thus reads

$$\frac{dc}{dt} = -c_1 v_1 m_\infty^3 n_\infty^3 h^3 (c - c_{ER}) - c_1 v_2 (c - c_{ER}) - \frac{v_3 c^2}{k_3^2 + c^2}$$
$$\frac{dh}{dt} = \alpha_h(1-h) - \beta_h h + \xi(t)$$
$$\langle \xi(t)\xi(t') \rangle = \frac{\alpha_h(1-h) + \beta_h h}{2N_t}\ \delta(t-t')$$
$$\langle \xi(t) \rangle = 0. \qquad [17]$$

It is almost as simple as the deterministic Li-Rinzel model except for the noise term in the second equation.

Integrating these equations with a first order solver, the stochastic term results in one additional term

$$h(t + \Delta t) = (\alpha_h(1 - h(t)) - \beta_h h(t))\ \Delta t + \sqrt{2K\ \Delta t}\ R_t$$
$$K = \frac{\alpha_h(1-n) + \beta_h n}{2N_t}, \qquad [18]$$

where R_t denotes a Gaussian random number with unit variance. The most significant advantages of the Langevin equations are that they are simple to implement and that their computational demand does not grow with increasing cluster size N_t. In Figure 6, we compare the calcium release and the fraction of de-inactivated channels from an isolated cluster of IP_3Rs obtained with the Markov method and the Langevin method.

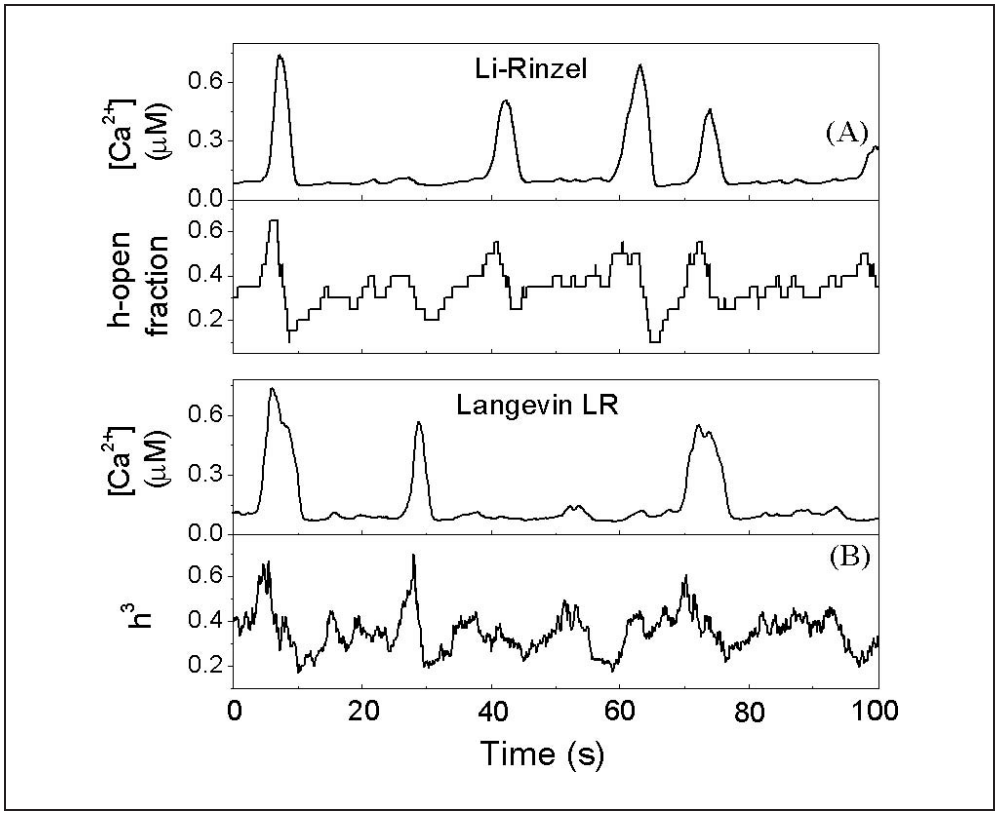

Fig. 6 Simlation results for a cluster of 20 IP_3Rs obtained from the Markov Li-Rinzel model (*A*) and the Langevin model (*B*).

The Langevin approach for the cluster in the diffusible medium results in the following set of nonlinear and stochastic partial differential equations:

$$\frac{\partial c}{\partial t} = \left(c_1 m_\infty^3 n_\infty^3 h^3 (c - c_{ER}) - c_1 v_2 (c - c_{ER}) - \frac{v_3 c^2}{k_3^2 + c^2} \right) \Xi(x)\ \Xi(y) + D\nabla^2 c \qquad [19]$$

$$\frac{\partial h}{\partial t} = \left(-(\alpha_h(p) + \beta_h(c))\ h + \frac{\alpha_h(p)}{\alpha_h(p) + \beta_h(c)} + \xi(t) \right) \Xi(x)\ \Xi(y) \qquad [20]$$

$$\langle \xi(t)\ \xi(t') \rangle = \frac{\alpha_h(1-h) + \beta_h h}{2N_t} \delta(t - t')$$

$$\langle \xi(t) \rangle = 0$$

with the form function in Equation [7]. Note that the single cluster (in the origin of our coordinate system) acts as a point source regardless of the actual physical size of the cluster. The strength of the source in Equation [19] thus must be rescaled by the factor $(L/\Delta x)^2$. The gating variable h is the single gating variable describing the dynamics of the single entire cluster.

5. Results

5.1 Puff Amplitude Distributions

Since the number of open channels is a stochastic variable, the release of Ca^{2+} is also random (see Fig. 6). The amplitudes of calcium puffs have been measured using fluorescent imaging, and although it is hard to gauge the luminocity-Ca^{2+} precisely, histograms of maximum relative luminoscity should be similar to puff amplitude distributions (PRATUSEVICH and BALKE 1996, BOOTMAN et al. 1997, IZU et al. 1998, SMITH et al. 1998, SUN et al. 1998, THOMAS et al. 1998, CHENG et al. 1999, JIANG et al. 1999, CALLAMARAS and PARKER 2000,

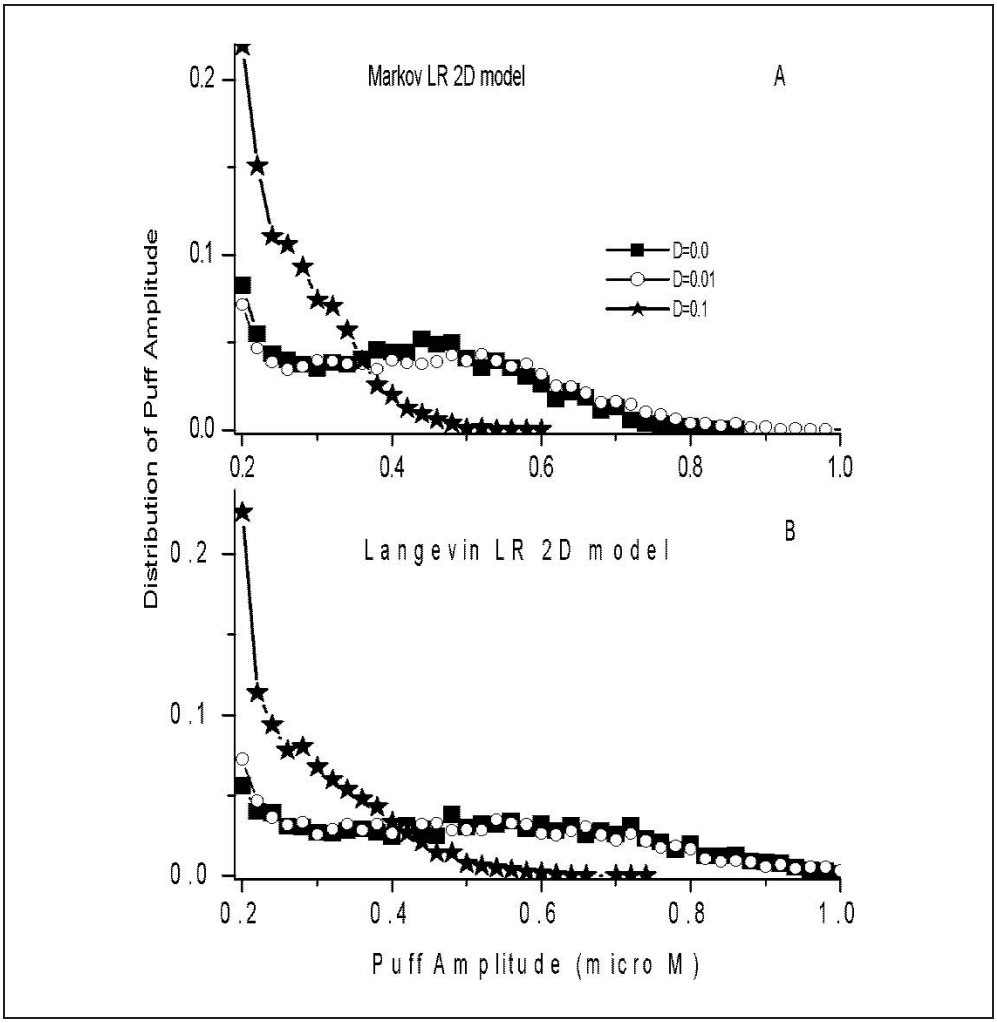

Fig. 7 Ca^{2+} puff amplitude distribution for a cluster of 20 IP_3Rs at $p = 0.3$ μM at various values of the diffusion coefficient. Panel (*A*) is obtained with the Markov Li-Rinzel model (Equations [6] and [7]) while the results in panel (*B*) has been obtained with the Langevin method (Equations [19] and [20]).

Marchant and Parker 2001, Rios et al. 2001). While simulated puff amplitude distributions generated by isolated clusters have been discussed recently (Shuai and Jung 2002 a, 2003), we discuss here the effects of Ca^{2+} diffusion on the puff amplitudes. Calcium diffusion removes Ca^{2+} from the cluster site, smearing out the spatial distribution of Ca^{2+}. The amplitudes are therefore expected to be smaller. In Figure 7 we show puff amplitude distributions for a cluster of 20 IP_3Rs and $p = 0.3$ μM and different values of the Ca^{2+} diffusion constant. The results in panel (*A*) are obtained with the Markov Li-Rinzel model (Equations [6] and [7]), while the results in panel (*B*) are obtained with the Langevin method (Equations [19] and [20]). As expected, diffusion cuts down on the number of large puffs. It actually causes a peaked distribution to become almost simply decaying. The different possible shapes of puff amplitude distributions were subject of a recent controversy. Cheng et al. (1999) suggested that the original calcium puffs should have a monotonically decreasing amplitude distribution. In contrast, Rios et al. (2001) reported on either decaying amplitude distributions or distributions with a central peak. Similarly, we have reported for the isolated clusters (Shuai and Jung 2002 b), various types of puff amplitude distributions are possible based on simulations depending on the size of the cluster, concentration of IP_3 and also the Ca^{2+} diffusion constant. The agreement between the results of the Markov model and the Langevin method is reasonably good.

5.2 Puff width Distributions

Ca^{2+} puffs are temporally limited events. We define the temporal width of a Ca^{2+} puff by the duration the Ca^{2+} concentration remains above half of its peak value during the puff. Puff width distributions have been recorded experimentally (Sun et al. 1998, Thomas et al. 1998, Haak et al. 2001). Ca^{2+} diffusion reduces the Ca^{2+} concentration at the site (see Fig. 7) and thus decreases the closing rates β_h of the h-gates of the stochastic Li-Rinzel model. Thus we expect an increase of the puff width with increasing diffusion coefficients. In Figure 8 (*A*), we show the puff width distributions of a cluster of 20 IP_3Rs at $p = 0.3$ μM at various values of the Ca^{2+} diffusion coefficient. In panel (*B*) we display the results obtained from the computationally faster Langevin method. The Langevin method reproduces the data from the Markov model very well. In general, the distribution broadens with increasing Ca^{2+} diffusion coefficient.

5.3 Inter-puff Interval Distribution

Another quantity that has been used to characterize Ca^{2+} puffs from experiments is the time interval between two consecutive Ca^{2+} puffs (Marchant et al. 1999). These intervals are not constant but distributed according to an interval distribution. In neuroscience such distributions are widely used to characterize neuronal spike patterns. Useful information about recovery times and coherence can be extracted from these distributions. In Figure 9, we show inter-puff interval distributions obtained with the Markov Li-Rinzel model and the Langevin method. While the puff-width distribution becomes broader and the average puff wider with increasing Ca^{2+} diffusion, the opposite is the case for the inter-puff interval distribution. The distribution becomes narrower and shifts to smaller average intervals.

In Figure 10, we show time traces of the Ca^{2+} concentration at the site of the release cluster with a small and a large Ca^{2+} diffusion coefficient. The trace for large Ca^{2+} diffusion coefficients is different in two more aspects. First, the puff frequency is higher, i. e., the time intervals between two spikes is smaller (thus the shift of the average inter-puff interval observed in Figure 9). Second, the Ca^{2+} baseline is a bit higher as in the case with the smaller Ca^{2+} diffusion coefficient. The latter is a consequence of the retreating Ca^{2+} puff after the closing of the cluster (see the dark dot in the center of Figure 5). The larger Ca^{2+} level creates a larger fraction n_∞^3 (see Equations [3] and [6]) and thus explains the larger spiking rate.

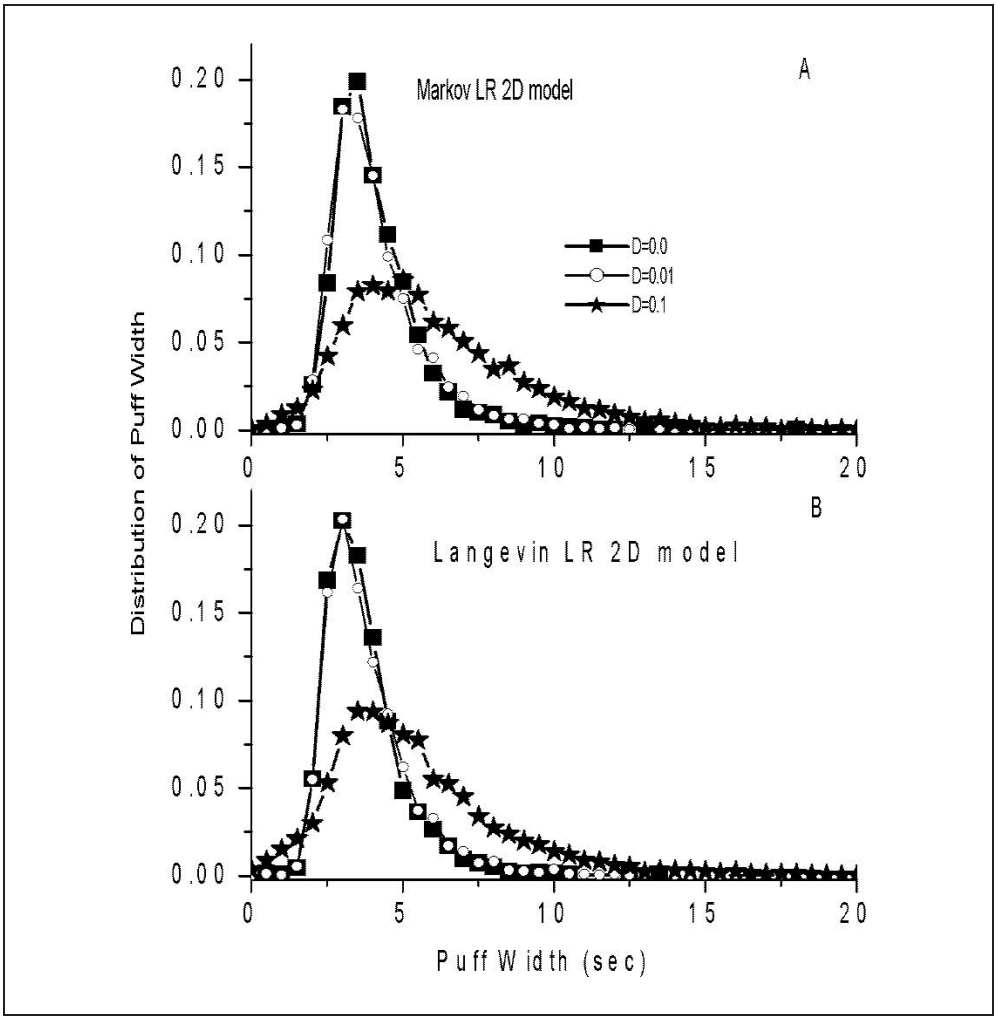

Fig. 8 The distribution of the puff widths is shown for a cluster of 20 IP_3Rs at $p = 0.3$ μM and various values of the Ca^{2+} diffusion constant. Panel (*A*) displays results obtained with the Markov Li-Rinzel model and panel (*B*) results obtained with the Langevin method.

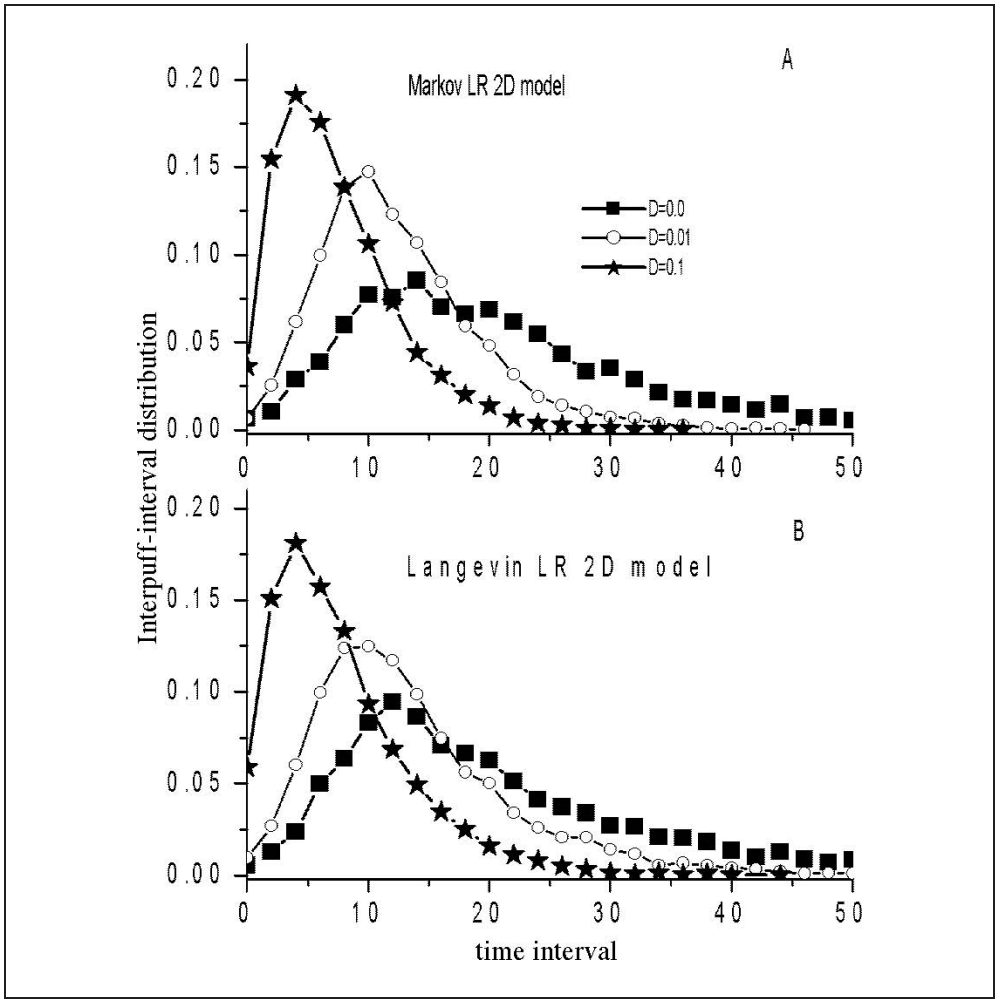

Fig. 9 Inter-puff interval distributions generated by a cluster of 20 IP_3Rs at $p = 0.3$ μM. The results in panel (*A*) are obtained with the Markov Li-Rinzel model while the results in panel (*B*) are obtained with the Langevin method.

6. Conclusions

We have been using a stochastic version of the Li-Rinzel model to describe Ca^{2+} release from the ER into the cytosol through clusters of IP^3Rs with few channels only. Intracellular diffusion of the released Ca^{2+} determines the statistical properties of Ca^{2+} puffs. Diffusion-facilitated puff termination decreases the average Ca^{2+} amplitudes while the puff lifetimes become longer. While the accuracy of the stochastic Li-Rinzel model for isolated clusters of IP_3Rs (without diffusible Ca^{2+}) with respect to the DeYoung-Keizer model has been tested in SHUAI and JUNG (2003), we have tested

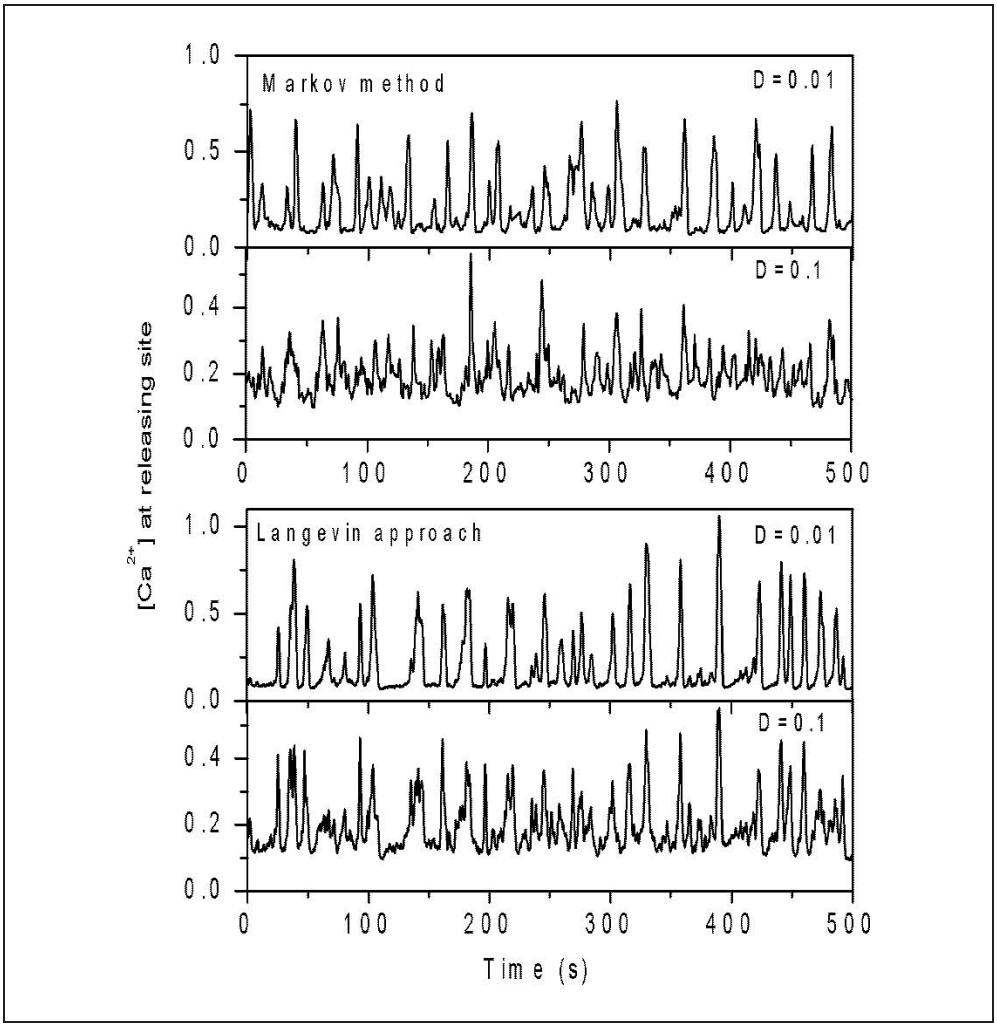

Fig. 10 Traces of Ca^{2+} concentration obtained from the Markov Li-Rinzel model are shown in the upper panel for two values of the Ca^{2+} diffusion coefficient. The lower trace for larger D exhibits a higher puff-frequency. Similar behavior can be obtained with the Langevin method, as shown in the lower panel.

here the accuracy of the Langvin approximation with respect to the Markov Li-Rinzel model in the presence of Ca^{2+} diffusion. Although the Langevin method is much faster and easier to implement than the Markov-Monte-Carlo schemes it delivers results that are in good agreement with the Markov Li-Rinzel model. For larger scale simulations of entire cells or tissues the Monte-Carlo Markov schemes become computationally very demanding and the Langevin approximation offers an alternative that is faster, but still delivers accurate results.

References

Bezprovanny, I., Watras, J., and Ehrlich, B.: Bell-shaped calcium response curves of Ins(1,4,5)P_3- and calcium-gated channels from endoplasmic reticulum of cerebellum. Nature *351*, 751–754 (1991)

Bootman, M., Niggli, E., Berridge, M., and Lipp, P.: Imaging the hierarchical Ca^{2+} signaling system in HeLa cells. J. Physiol. *499*, 307–314 (1997)

Callamaras, N. J., Marchant, S., Sun, X., and Parker, I.: Activation and co-ordination of $InsP_3$ mediated elementary Ca^{2+} events during global Ca^{2+} signals in *Xenopus* oocytes. J. Physiol. *509*, 81–91 (1998)

Callamaras, N., and Parker, I.: Phasic characteristic of elementary Ca^{2+} release sites underlies quantal responses to IP_3. EMBO J. *19*, 3608–3617 (2000)

Chay, T. R., and Keizer, J.: Minimal model for membrane oscillations in the pancreatic beta-cell. Biophys. J. *42*,181–189 (1983)

Cheng, H. W., Lederer, J., and Cannel, M. B.: Calcium sparks elementary events underlying excitation-contraction coupling in heart muscle. Science *262*, 740–744 (1993)

Cheng, H., Song, L., Shirokova, N., Gonzalez, A., Lakatta, E. G., Rios, E., and Stern, M. D.: Amplitude distribution of calcium sparks in confocal images: theory and studies with an automatic detection method. Biophys. J. *76*, 606–617 (1999)

Cornell-Bell, A. H., Finkbeiner, S. M., Cooper, M. S., and Smith, S. J.: Glutamate induces calcium waves in cultured astrocytes: Long-range glial signaling. Science *247*, 470–473 (1990)

DeYoung, G. W., and Keizer, J.: A single-pool inositol 1,4,5-trisphosphate-receptor-based model for agonist-stimulated oscillations in Ca^{2+} concentration. Proc. Natl. Acad. Sci. USA *89*, 9895–9899 (1992)

Dupont, G., Swillens, S., Clair, C., Tordjmann, T., and Combettes, L.: Hierarchical organization of calcium signals in hepatocytes: from experiments to models. Biochim. Biophys. Acta *1498*, 134–152 (2000)

Falcke, M., Tsimring, L., and Levine, H.: Stochastic spreading of intracellular Ca^{2+} release. Phys. Rev. *E62*, 2636–2643 (2000)

Fox, R. F., and Lu, Y.: Emergent collective behavior in large numbers of globally coupled independently stochastic ion channels. Phys. Rev. *E62*, 2636–2643 (1994)

Gonzalez, A., Kirsch, W. G., Shirokova, N., Pizarro, G., Brum, G., Pessah, I. N., Stern, M. D., Cheng, H., and Rios, E.: Involvement of multiple intracellular release channels in calcium sparks of skeletal muscle. Proc. Natl. Acad. Sci. USA *97*, 4380–4385 (2000)

Haak, L. L., Song, L., Molinski, T. F., Pessah, I. N., Cheng, H., and Russell, J. T.: Sparks and puffs in oligodendrocyte progenitors: cross talk between ryanodine receptors and inositol trisphosphate receptors. J. Neurosci. *21*, 3860–3870 (2001)

Hänggi, P., and Jung, P.: Bistability in active circuits: Application of a novel Fokker-Planck approach. IBM J. Res. and Develop. *32*, 119–125 (1988)

Izu, L. G., Wier, W. G., and Balke, C. W.: Theoretical analysis of the Ca^{2+} spark amplitude distribution. Biophys. J. *75*, 1144–1162 (1998)

Jiang, Y., Klein, M. G., and Schneider, M. F.: Numerical simulation of Ca^{2+} sparks in skeletal muscle. Biophys. J. *77*, 2333–2357 (1999)

Klepeis, V. S., Cornell-Bell, A. H., and Trinkaus-Randall, V.: Growth factors but not gap junctions play a role in injury-induced Ca^{2+} waves in epithelial cells. Cell Sci. *114*, 4185–4195 (2001)

Li, Y., and Rinzel, J.: Equations for IP_3 receptor-mediated Ca^{2+} oscillations derived from a detailed kinetic model: a Hodgkin-Huxley like formalism. J. Theor. Biol. *166*, 461–473 (1994)

Lipp, P., and Niggli, E.: Fundamental calcium release events revealed by two-photon excitation photolysis of caged calcium in guinea-pig cardiac myocytes. J. Physiol. *508*, 801–809 (1998)

Mak, D. D., and Foskett, J. K.: Single-channel kinetics inactivation, and spatial distribution of inositol trisphosphate receptors in Xenopus oocyte nucleus. J. Gen. Physiol. *109*, 571–587 (1997)

Marchant, J., Callamaras, N., and Parker, I.: Initiation of IP_3 mediated Ca^{2+} waves in *Xenopus* oocytes. EMBO J. *19*, 5285–5299 (1999)

Marchant, J. S., and Parker, I.: Role of elementary Ca^{2+} puffs in generating repetitive Ca^{2+} oscillations. EMBO J. *20*, 65–76 (2001)

Melamed-Book, N., Kachalsky, S. G., Kaiserman, I., and Rahamimoff, R.: Neuronal calcium sparks and intracellular calcium noise. Proc. Natl. Acad. Sci. USA *26*, 15217–15221 (1999)

Pratusevich, V. R., and Balke, C. W.: Factors shaping the confocal image of the calcium spark in cardiac muscle cells. Biophys. J. *71*, 2942–2957 (1996)

Rios, E. N., Shirokova, W., Kirsch, G., Pizarro, M. D., Stern, H., Cheng, H., and Gonzalez, A.: A preferred amplitude of calcium sparks in skeletal muscle. Biophys. J. *80*, 169–183 (2001)

Schmid, G., Goychuk, I., and Hänggi, P.: Stochastic resonance as a collective property of ion channel assemblies. Europhys. Lett. *56*, 22–30 (2001)

Schneidman, E., Freedman, B., and Segev, I.: Ion channel stochasticity may be critical in determining the reliability and precision of spike timing. Neural Computation *10*, 1679–1703 (1998)

Shuai, J. W., and Jung, P.: Optimal calcium signaling. Phys. Rev. Lett. *88*, 068102 (2002 a)

Shuai, J. W., and Jung, P.: Stochastic properties of Ca^{2+} release of inositol 1,4,5-trisphosphate receptor clusters. Biophys. J. *83*, 87–97 (2002 b)

Shuai, J. W., and Jung, P.: Langevin modeling of intracellular calcium dynamics. In: Deutsch, A., Howard, J., Falcke, M., and Zimmermann, W. (Eds.): Function and Regulation of Cellular Systems: Experiments and Models. New York: Springer 2003 (in press)

Smith, G. D., Keizer, J. E., Stern, M. D., Lederer, W. J., and Cheng, H.: A simple numerical model of calcium spark formation and detection in cardiac myocytes. Biophys. J. *75*, 15–32 (1998)

Sun, X. N., Callamaras, N. J., Marchant, J. S., and Parker, I.: A continuum of $InsP^3$-mediated elementary Ca^{2+} signaling events in Xenopus oocytes. J. Physiol. *509*, 67–80 (1998)

Thomas, D., Lipp, P., Berridge, M. J., and Bootman, M. D.: Hormone-evoked elementary Ca^{2+} signals are not stereotypic, but reflect activation of different size channel clusters and variable recruitment of channels within a cluster. J. Biol. Chem. *273*, 27130–27136 (1998)

Dr. Jian-Wei Shuai
Prof. Dr. Peter Jung
Department of Physics and Astronomy
and Institute for Quantitative Biology
Ohio University
Athens, OH 45701
USA
Phone: ++1 61 45 93 17 20
Fax: ++1 61 45 93 04 33
E-Mail: jung@helios.phy.ohiou.edu

Nova Acta Leopoldina NF *88*, Nr. 332, 169–188 (2003)

Self-Organization, Active Brownian Dynamics, and Biological Applications

Werner EBELING (Berlin) and Frank SCHWEITZER (Berlin, Bonn)

With 9 Figures

Abstract

After summarizing basic features of self-organization such as entropy export, feedbacks and nonlinear dynamics, we discuss several examples in biology. The main part of the paper is devoted to a model of active Brownian motion that allows a stochastic description of the active motion of biological entities based on energy consumption and conversion. This model is applied to the dynamics of swarms with external and interaction potentials. By means of analytical results, we can distinguish between translational, rotational and amoebic modes of swarm motion. We further investigate swarms of active Brownian particles interacting *via* chemical fields and demonstrate the application of this model to phenomena such as biological aggregation and trail formation in insects.

"Every theory, whether in the physical or biological or social sciences, distorts reality in that it oversimplifies. But if it is a good theory, what is omitted is outweighted by the beam of light and understanding thrown over the diverse facts."

Paul A. SAMUELSON

Zusammenfassung

Nach einer Zusammenfassung elementarer Merkmale der Selbstorganisation, wie z. B. Entropie-Export, Feedbacks und nicht lineare Dynamik, werden in diesem Bericht verschiedene Beispiele aus der Biologie erörtert. Der Hauptteil beschäftigt sich mit der aktiven Brownschen Molekularbewegung, welche eine stochastische Beschreibung der Bewegung biologischer Einheiten auf der Basis von Energieverbrauch und -umwandlung ermöglicht. Dieses Model findet bei der Dynamik von Schwärmen mit externalen und Wechselwirkungspotentialen Anwendung. Mit Hilfe analytischer Ergebnisse kann zwischen translationalen, rotationalen und amoebischen Formen der Schwarmbewegung unterschieden werden. Außerdem werden Schwärme aktiver Brownscher Partikel, die über chemische Felder aufeinander wirken, untersucht und die Anwendung des Models bei Phänomenen, wie z. B. biologischer Aggregation und Pfadbildung bei Insekten demonstriert.

„Jede Theorie, ob aus der Physik, der Biologie oder den Sozialwissenschaften, verzerrt die Realität, indem sie vereinfacht. Ist es jedoch eine gute Theorie, wird das, was weggelassen wird, aufgewogen durch den Fokus von Licht und Verständnis, der über die verschiedenen Fakten gelegt wird."

Paul A. SAMUELSON

1. Introduction

About 1845, Hermann VON HELMHOLTZ, the great pioneer in applications of physics to biological systems, developed the concept "*Physics of life*" (MARKL 1995) in compa-

nionship with his fellows Emil DU BOIS-REYMOND, Ernst Wilhelm VON BRÜCKE and Carl LUDWIG. Their statement, that life is not in contradiction to physical laws, was also later elaborated by Ludwig BOLTZMANN and others. But only in the 20th century, the investigations of Erwin SCHRÖDINGER, Max DELBRÜCK, Ludwig VON BERTALANFFY, Ilya PRIGOGINE, Manfred EIGEN, Mikhail VOLKENSTEIN and others led us to some understanding of the necessary conditions for the evolution of living systems (VOLKENSTEIN 1994). Their success was based on a specific theoretical approach to biological problems that also implied some reductionism. "Many biologists do not believe that ... biology can be given a theoretical foundation. Rather they insist in a holistic approach. ... Physicists, on the other hand, have not always appreciated that a theory of biology has to start from biological facts. They often thought that biology is just another field to which they could immediately apply their equations." This quotation from EIGEN'S foreword to VOLKENSTEIN'S (1994) book indicates that the road to a fruitful collaboration between physicists and life scientists the "*Helmholtz road*" – is full of obstacles. Nevertheless, we share the view that at the end of this road we are lead to some useful results, at least to some better understanding of biological facts. This shall also be demonstrated by the examples discussed in the following sections.

We start our considerations with some general remarks on self-organization and nonlinear dynamics in biology. In particular, we summarize some basic physical principles that lead to the emergence of complex structures in biological systems, such as openess, irreversibility, entropy export and feedback processes. It is well known from the thermodynamics of irreversible processes that systems may exhibit a rich variety of complex behavior if there is a supercritical influx of free energy. This energy may be provided in different forms, i. e. matter (chemical components, resources), high temperature radiation, or signals. What kind of complex behavior is observed in a system will of course not only depend on the influx of energy but also on the interaction of the entities that comprise the system. Among the prominent examples that can be observed in biological systems are processes of pattern formation and morphogenesis and different types of collective motion, such as swarming.

The main part of our paper is devoted to the modeling of active motion and coherent motion that in biological systems can be found on different scales, ranging from cells or simple microorganisms up to higher organisms, such as bird or fish. Our investigations are based on a model of active Brownian particles, i. e., particles with an internal energy depot that can be used for active movement. Considering further nonlinear interactions between the particles, such as attractive forces or interactions *via* chemical fields, we are able to derive a rather general framework for the dynamics of swarms.

By means of both, computer simulations and analytical investigations, we demonstrate how the superposition of simple microscopic motions may result in a quite complex dynamics of the macroscopic system. In particular, we derive analytical expressions for the distribution functions that allow distinguishing between different modes of swarming behavior, such as translational, amoebic and rotational modes of collective motion. Eventually, we study the dynamics of swarms coupled to chemical fields and demonstrate the application of this model to phenomena such as biological aggregation and trail formation in insects.

2. Self-Organization and Nonlinear Dynamics in Biology

2.1 General Aspects of Complexity

From our daily life experience we know how fragile and complex biological, ecological and social systems behave. What do we mean by the term "complexity" in a scientific context? According to our view complex systems are comprised of multiple components which interact in a nonlinear manner (cf. Fig. 1), thus the system behavior cannot be inferred from the behavior of the components. More specifically, these systems are characterized by (EBELING et al. 1998):

– structures with many components,
– dynamics with many modes,
– hierarchical level structures,
– couplings of many degrees of freedom,
– long-range spatial-temporal correlations.

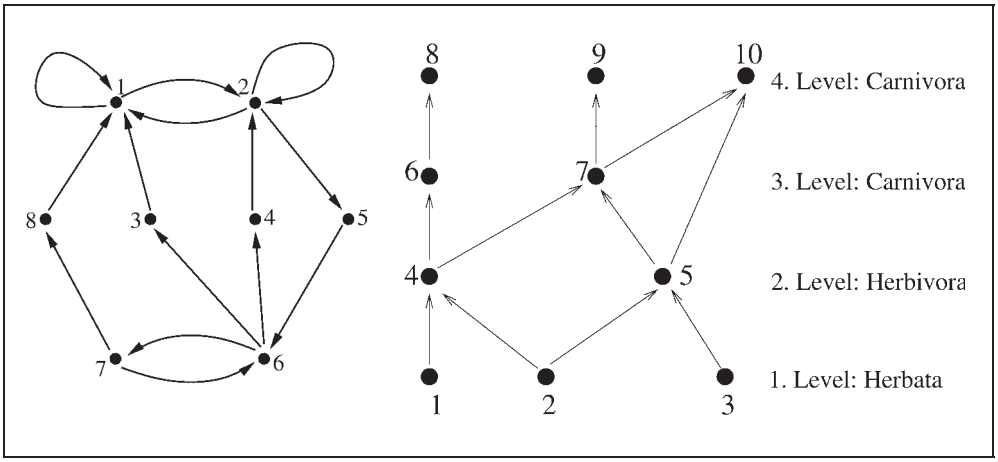

Fig. 1 Two graphical representations of the interaction in complex systems: (*A*) a catalytical network consisting of 8 elements with 14 feedbacks, (*B*) a hierarchical ecological network.

As we have learned from nonlinear dynamics, complexity is not restricted to large hierarchical systems; also relatively simple dynamical models may show complicated behavior. Among the specific features of complex nonlinear processes, we mention:

– complicated trajectories and chaos,
– manifolds of spatial-temporal structures,
– the limited predictability of future behavior (positive Kolmogorov-Sinai entropy).

Further, we note that complexity may arise in dissipative as well as in conservative systems. In general complex systems in nature and society are of dissipative nature, i. e.,

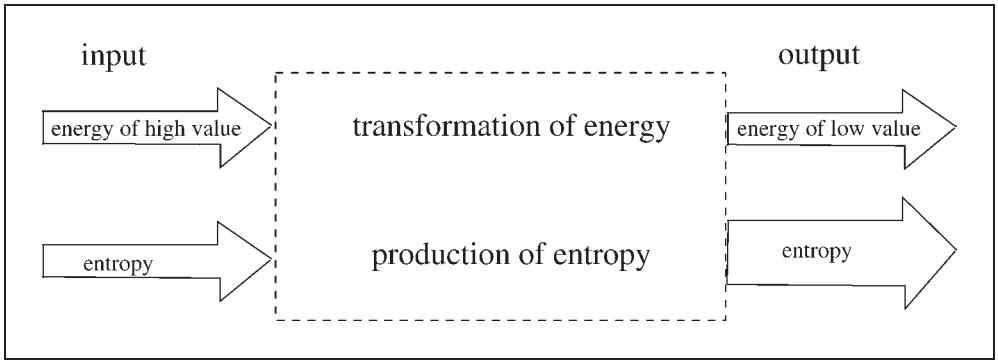

Fig. 2 Transformation of energy and production of entropy in an open system: the export of entropy is a *conditio sine qua non* for self-organization.

they are based on energy "consumption" that allows self-organization processes. This, however, needs some physical requirements, such as:

– thermodynamic openess, i. e., the system exchanges energy, entropy and matter with the environment,
– that on average the system exports entropy, i. e., it imports energy of high value and exports energy of low value (cf. Fig. 2),
– that the system operates far from equilibrium, beyond a critical distance from the equilibrium state (cf. Fig. 3),
– that the causal relations in the system include (positive and negative) feedback and feed-forward processes (cf. Fig. 1), i. e., the dynamics of the system is nonlinear.

For further details we refer to the literature (e. g. Ebeling et al. 1990, Ebeling and Feistel 1994).

2.2 Examples for Physical Models of Biological Systems

It is not intended here to give a complete overview of the vast applications of physical methods and tools to biological systems. Rather, we *pars pro toto* mention here only a few examples, where models based on the theory of self-organization and nonlinear dynamics have contributed to our understanding of biological phenomena (cf. also the other contributions in this volume and references therein):

– *Morphogenesis and biological pattern formation*: After the pioneering work on morphogenesis by Turing, Meinhard, Gierer and others, today a well established theory on biological pattern formation exists that is based on the reaction-diffusion dynamics of several chemical components (morphogens). It has been successfully applied to a range of phenomena, such as patterning of animal coats or sea shells, pattern formation in bacterial colonies or slime molds, biological aggregation – but also to processes of regeneration and wound healing, organ differentiation, etc. (see e. g., the contribution by Technau et al. 2003, this volume).

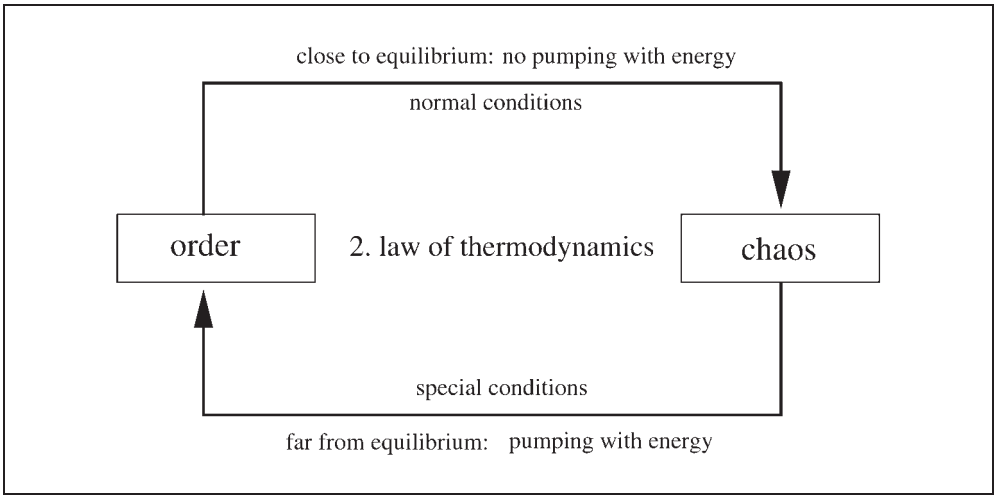

Fig. 3 The 2nd law of thermodynamics allows different processes. Pumping with energy leads the system into states far from equilibrium which may be characterized by the emergence of ordered structures. The relaxation into the thermodynamic equilibrium, on the other hand, is accompanied by the disappearance of ordered structures.

– *Biological rhythms and synchronization phenomena*: Given that the various functional units in biological systems act on different time and length scales, the emergence of synchronized behavior is by no means self-evident. Recent research in this direction has shown for instance how the brain activity is synchronized, or how cardiac cycles are triggered by excitation waves. As another example, the essential role of noise could be revealed in the case of stochastic resonance (see e. g. the contributions by Balázsi and Moss 2003, Braun et al. 2003, Kantz 2003, Mittag 2003, Ordemann et al. 2003, and Singer 2003, this volume).
– *Directed transport and molecular motors*: The ability of living cells to generate motion and forces, e. g. for mobility, contraction of muscles or material transport, could recently be understood within a physical description. For example, biological motor proteins which move along linear filaments can be described by stochastic models coupled to chemical reactions. So-called ratchet models further explain the generation of directed motion on the microscopic level out of an undirected Brownian motion (see e. g., the contribution by Hänggi et al. 2003, this volume).
– *Neural networks and associative memory*: The brain as one of the most complex systems, known in biology, has also attracted the research activities of physicists since the pioneering work of Hodgkin, Huxley, Hebb, Hopfield, and many others. It became clear that information is encoded not only in the response of the individual neural cells but also in the joint activity of a population of neurons. Based on these investigations, new techniques for information storage in associative memories or for pattern recognition, but also for brain stimulation have been developed. Artificial neural networks today also find a wide application in analyzing complex data sets (see e. g., the contributions by Singer 2003, Grün et al. 2003, and Tass 2003, this volume).

Despite a lot of successful investigations, we have to admit that many problems in the (physical) understanding of biological processes are still unsolved. Among the most important are the nature and the origin of biological information processing (EBELING and FEISTEL 1994, VOLKENSTEIN 1994).

In the following, we will restrict the discussion to a particular example, namely *active biological motion*, where we will show in more detail how a physical approach can be derived and on what reductions it is based.

3. Modeling Active Brownian Movement

3.1 Some Historical Remarks

Brownian motion denotes the erratic motion of a small, but larger than molecular, particle in a surrounding medium, e. g. a gas or a liquid. This erratic motion results from the random impacts between the atoms or molecules of the medium and the (Brownian) particle, which cause changes in the direction and the amount of its velocity, $\boldsymbol{v}$.

The motion of the particle is named after the British botanist Robert BROWN (1773–1858), who in 1827 discovered the erratic motion of small pollen grains immersed in a liquid. He was inclined to explain his observation by so-called "active molecules", and it is also reported that he wrote a letter to Charles DARWIN to ask him about his opinion on this subject.

BROWN was not the first who observed such a motion with a microscope. For example, already the Dutch Anton VAN LEEUWENHOEK (1632–1723), who first discovered microorganisms with a simple microscope, knew about the typical erratic motion; however, he considered it a feature of living entities. In 1785, the Dutch physician Jan INGENHOUSZ (1730–1799) also reported the erratic motion of an-organic material dispersed in a liquid, i. e., powdered charcoal floating on alcohol surfaces, but this became not known to the non-Dutch speaking world.

The physical explanation of Brownian motion started about 1900 with the seminal works of Albert EINSTEIN (*On the Theory of Brownian Motion*, 1905) and Marian SMOLUCHOWSKI (*On the Kinetic Theory of Brownian Molecular Motion and Suspensions*, 1906), but it should be noticed that already in 1900 Louis BACHELIER has derived a mathematical theory of this type of stochastic processes while investigating price changes at the stock market.

Brownian motion would be rather considered as *passive motion*, simply because the Brownian particle does not play an active part in this motion. It is an *undirected* motion, driven by thermal noise. Passive motion can also be directed, e. g., if it is driven by convection, currents or by external fields. Active motion, on the other hand relies on the supply of energy, i. e., it occurs under energy consumption and energy conversion and may also involve processes of energy storage. In order to add such a new element to the concept of Brownian motion, we need to investigate possible mechanisms of energy pumping.

The idea of energy supply was first introduced in the context of the theory of sound and music by HELMHOLTZ (*Die Lehre von den Tonempfindungen*, 1870) and RAYLEIGH (*On Maintained Vibrations*, 1883; *The Theory of Sound*, 1877). The Rayleigh model of self-sustained oscillations is based on the assumption of a velocity-dependent coefficient

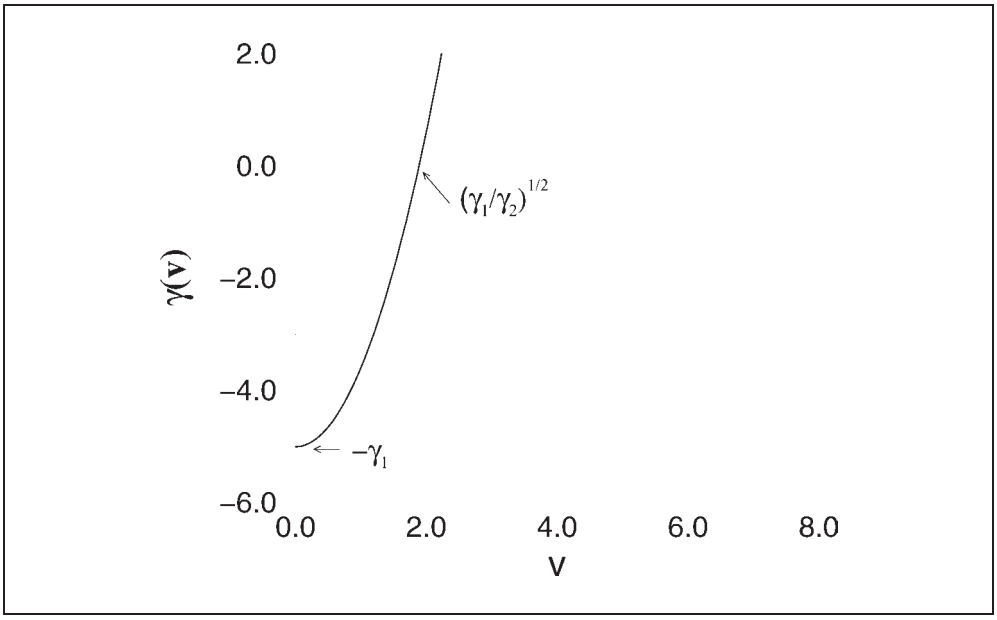

Fig. 4 Rayleigh-type velocity-dependent friction coefficient $\gamma(v) = -\gamma_1 + -\gamma_2 v^2$. For $\gamma(v) < 0$ "pumping" dominates, while for $\gamma(v) > 0$ "dissipation" dominates.

(cf. Fig. 4), that can be negative for a certain range of velocity, i. e., instead of dissipating energy because of friction, energy can be pumped into the system. That means if a violin bow transfers energy to the string *via* friction *negative friction* occurs. Provided a supercritical influx of energy, a self-sustained periodic motion can be obtained, the violin string emits acoustic waves.

In the following we will show how the integration of the ideas about maintained vibrations and Brownian motion leads to a new model of *active movement*. This term will be used now for all kinds of motions in space and time which are driven by sources of free energy.

3.2 Brownian Particles with Energy Supply

In this section, we introduce a simple stochastic model of active movement called "model of active Brownian particles" (Schweitzer et al. 1998, Ebeling et al. 1999). Let us consider $i = 1, \ldots, N$ active Brownian particles with mass m located at the positions $\boldsymbol{r}_i$ and moving with the velocity $\boldsymbol{v}_i$. For the equation of motion we postulate:

$$m\frac{dv_i}{dt} + \frac{\partial U}{dr_i} = \boldsymbol{F}_i + \sqrt{2D}\,\xi_i(t) \qquad [1]$$

The last term denotes the stochastic force acting on the Brownian particle i with a strength D, the random function $\xi_i(t)$ is assumed to be Gaussian white noise. U is the

potential of external and interaction forces and $\boldsymbol{F}_i$ is the dissipative force acting on particle i. It can be specified as:

$$\boldsymbol{F}_i = -m\gamma\boldsymbol{v}_i + de_i\boldsymbol{v}_i. \qquad [2]$$

Here γ is the usual passive friction coefficient with the dimension of a frequency. We assume that the noise intensity D is related to the friction by an Einstein relation $D = m\gamma kT$, where k is the Boltzmann constant and T is the temperature. The second term $(d\boldsymbol{v}_i e_i)$ expresses an acceleration of the particle in the direction of v_i (a forward thrust) which is based on the conversion of energy from a internal energy depot e_i of the particle. More specifically, we assume that the Brownian particle is able to take up energy with the rate q, which can be stored in an internal depot e_i. The internal energy can be converted into kinetic energy with a momentum dependent rate mdv_i^2, which results in the acceleration in the direction of movement. The internal energy dissipates with the rate ce_i, The balance is then expressed by:

$$\frac{de_i}{dt} = q - ce_i - dv_i^2 e_i. \qquad [3]$$

If the internal energy depot relaxes fast compared to the motion of the particle, we find for Equation [2] in adiabatic approximation:

$$\boldsymbol{F}_i = -mv_i g\left(\boldsymbol{v}_i^2\right) = \boldsymbol{v}_i\left(\frac{dq}{c + dv_i^2} - m\gamma\right). \qquad [4]$$

Here $g(v^2)$ denotes a velocity-dependent *friction function*. From now on we will use units corresponding to $m = 1$, i. e. $\boldsymbol{v} = \boldsymbol{p}$. Dependent on the parameter values, the dissipative force $\boldsymbol{F}_i$ may have one zero at $\boldsymbol{v} = 0$, or two more zeros with

$$\boldsymbol{v}_0^2 = \frac{q}{\gamma} - \frac{c}{d}. \qquad [5]$$

A nontrivial velocity $|v_0| > 0$ only exists if $qd > c\gamma$, i. e., if a supercritical supply of energy occurs. In this case, we also speak about "*active particles*". For $0 < |v| < |v_0|$, i. e., in the range of small velocities the dissipative force $\boldsymbol{F}_i$ *is* positive, i. e., the particle is provided with additional free energy. On the other hand, for $0 < |v_0| < |v|$, the dissipative force is negative. Hence, slow particles are accelerated, and fast particles are decelerated.

Assuming $\boldsymbol{v}_0^2 > 0$ we consider now two limiting cases. Introducing the bifurcation parameter $\zeta = (dq/c\gamma) - 1$, we get for small values of the parameter ζ the well-known law of Rayleigh (cf. Fig. 4):

$$\boldsymbol{F} = \gamma\zeta\left(1 - \frac{v^2}{v_0^2}\right)\boldsymbol{v}. \qquad [6]$$

In the opposite case, i. e. for large values of ζ, we get the empirical law found by Schienbein and Gruler (1993) for the dynamics of cells:

$$\boldsymbol{F} = \gamma\left(1 - \frac{v_0}{v}\right)\boldsymbol{v}\,. \qquad [7]$$

This way, our expression for the dissipative force $\boldsymbol{F}_i$, Equation [4] is general enough to cover interesting limiting cases. We mention that in other models of driven motion (Vicsek et al. 1995) the velocity v_0 is postulated without further investigations.

3.3 Velocity Distribution and Mean Squared Displacement of Free Active Motion

We are now interested in how known features of Brownian motion, such as the stationary velocity distribution or the mean squared displacement, change if we consider a supercritical energy take up ($qd > c\gamma$) of the Brownian particles. In order to find the velocity distribution explicitely we have to formulate and to solve the Fokker-Planck equation corresponding to Equation [1]. We restrict our consideration here to the two-dimensional space and $U = 0$, i. e., there are no external or interaction forces. Following standard procedures (KLIMONTOVICH 1995), we find from the Fokker-Planck equation the stationary solution for the velocity distribution (ERDMANN et al. 2000):

$$P^0(\boldsymbol{v}) = C\left(1 + \frac{d}{c}\boldsymbol{v}^2\right)^{\frac{q}{2D}} \exp\left(-\frac{\boldsymbol{v}^2}{2kT}\right). \qquad [8]$$

Compared to the Maxwellian velocity distribution of "simple" Brownian particles, a new prefactor appears in Equation [8] which results from the internal energy depot. For supercritical pumping, $qd > \gamma c$, we find a crater-like velocity distribution, which indicates strong deviations from the Maxwell distribution (cf. Fig. 5).

The distribution represented by Equation [8] is an exact result for non-interacting particles. In the limit of zero noise, $D \to 0$, it obtains the form $d(v^2 - v^2)$. In this small noise limit, a result for the *mean square displacement* is also available (ERDMANN et al. 2000):

$$\left\langle \left(\boldsymbol{r}(t) - \boldsymbol{r}(0)^2\right)\right\rangle = \frac{2v_0^4}{D}t + \frac{v_0^6}{D^2}\left[\exp\left(-\frac{2Dt}{v_0^2}\right) - 1\right]. \qquad [9]$$

From Equation [9], we find the effective spatial diffusion coefficient of active Brownian particles as $D_r^{eff} = v_0^4/D$. This expression leads to rather large values for small D or large v_0. The analytical expressions for the stationary velocity distribution and for the mean square displacement are in good agreement with computer simulations (SCHWEITZER et al. 2001) and with measurements on the active movements of granulocytes (SCHIENBEIN and GRULER 1993). We suggest to compare them also with the observations of the movement of *Daphnia* (see ORDEMANN et al. 2003, this volume).

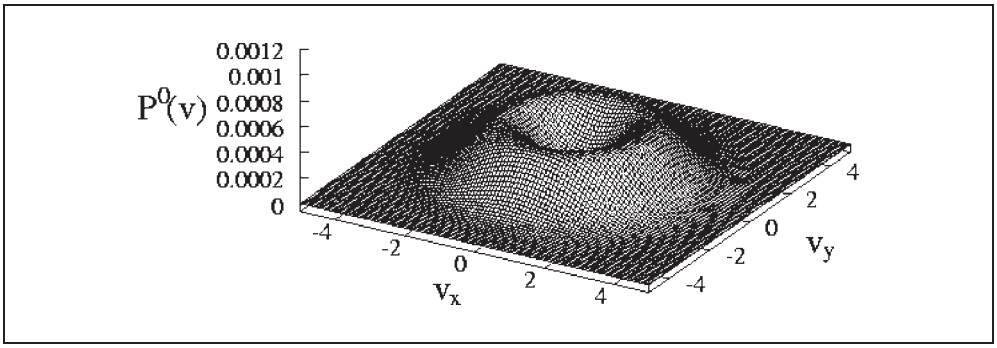

Fig. 5 Stationary velocity distribution $P^0(\boldsymbol{v})$ for active Brownian particles in the case of supercritical energy supply (ERDMANN et al. 2000).

4. Swarm Dynamics with External and Interaction Potentials

4.1 Dynamics in External Potentials

Let us now consider a swarm of active particles in a two-dimensional radially symmetric potential $U(r) = a(x_1^2 + x_1^2)$, that generates an attractive force towards the center, $r = 0$. As the snapshot of the spatial dispersion of the swarm shows Figure 6, we find the occurrence of two branches of the swarm, which after a sufficiently long time move on *two limit cycles*. One of these limit cycles refers to the left-handed, the other one to the right-handed direction of motion in the 2d-space.

The radius of the limit cycles can be calculated with the following considerations: Moving under stationary conditions, the particles have to comply with the additional requirement to balance between centrifugal and attracting forces, which leads to the condition $v^2/r = |U'(r)|$. For the harmonic potential this results in the stationary radius $r_0 = v_0/w_0$ where the frequency of rotations is given by $w_0^2 = a/m$ (ERDMANN et al. 2000).

For the motion on the limit cycle, an exact solution of the equations of motion reads in the deterministic limit:

$$x_1 = r_0 \cos(\omega_0 t + \varphi_0) \qquad v_1 = -r_0\omega_0 \sin(\omega_0 t + \varphi_0)$$
$$x_2 = r_0 \sin(\omega_0 t + \varphi_0) \qquad v_2 = r_0\omega_0 \cos(\omega_0 t + \varphi_0). \qquad [10]$$

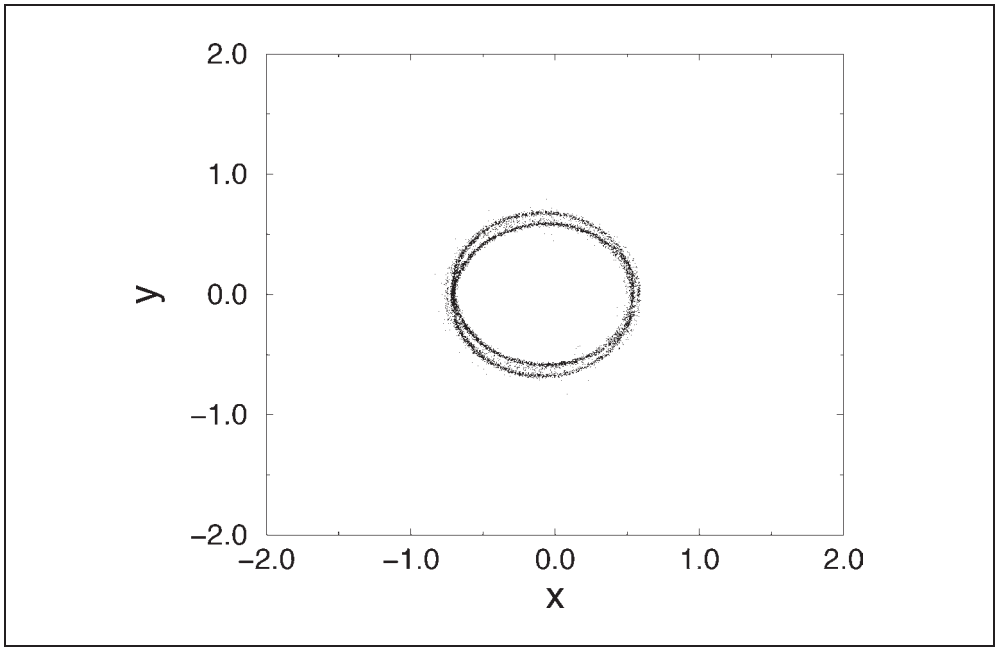

Fig. 6 Spatial snapshot at $t = 99$ of a swarm of 10 000 active particles moving in a parabolic potential (SCHWEITZER et al. 2001).

Another exact solution is obtained by inversion. Any initial state converges to one of these attractor states. In the presence of fluctuations, the particles move in the neighborhood of these two limit cycle orbits, which have circle-like projections and are located on two planes corresponding to the angular momenta $L = \pm v_0^2/w$. In this way, the probability is concentrated on two toroids in the 4-dimensional phase, the stationary distribution may be approximated by:

$$P^0(x_1, x_2, v_1, v_2) = C \left[1 + \frac{d}{2c}\left(v^2 + \omega^2 r^2\right)\right]^{\frac{q}{2D}} \exp\left[-\frac{1}{2k_B T}\left(v^2 + \omega^2 r^2\right)\right] \times \left[1 + \frac{d|L|}{2cr_0^2}\right]^{\frac{q}{2Dr_0^2}} \exp\left[-\frac{L^2}{2k_B T r_0^2}\right]. \quad [11]$$

Here the first factor represents a shell with given energy in the 4-dimensional phase space, while the second factor projects out two planes perpendicular to the two possible directions of the angular momentum, L. In this way two toroids in the 4-dimensional phase space are generated where the occupation density is concentrated.

4.2 Harmonic Swarms

So far we have neglected any coupling within the swarm of active particles. If the swarm is not bound by an external potential as discussed above, the absence of interactions leads to the effect that the swarm eventually disperses in the course of time, whereas a "real" swarm would maintain its coherent motion. A common way to introduce correlations between the moving particles in physical swarm models is the coupling to a mean value. For example Czirok et al. (1996) discuss the coupling of the particles' individual *orientation* (i. e. direction of motion) to the mean orientation of the swarm. Other versions assume the coupling of the particles' velocity to a *local average velocity*, which is calculated over a space interval around the particle (Czirok et al. 1999).

Instead of an external potential $U(\boldsymbol{r})$, let us now assume an *interaction potential*. As the most simple case we may discuss the global coupling of the swarm to the *center of mass*. That means the particle's position $\mathbf{r}_i$ is related to the mean position of the swarm $\boldsymbol{R} = 1/N \Sigma \boldsymbol{r}_i$ *via* a potential $U(\boldsymbol{r}_i, \boldsymbol{R})$. For simplicity, we may assume a parabolic potential, i. e., the Hamiltonian for each particle reads now:

$$H_i = \frac{v_i^2}{2} + \frac{a}{N}\sum_{j \neq i}\left(\boldsymbol{r}_i - \boldsymbol{r}_j\right)^2. \quad [12]$$

With respect to the harmonic interaction potential we call such a swarm a *harmonic* swarm (Ebeling and Schweitzer 2001). The coupling to the center of mass corresponds to the assumption that there is now an attractive force between each two particles i and j which depends linearly on the distance between them. This can be used to control the dispersion of the swarm. A special case of nonlinear (exponential) interactions between particles on a chain has been analyzed in detail by Ebeling et al. (2000).

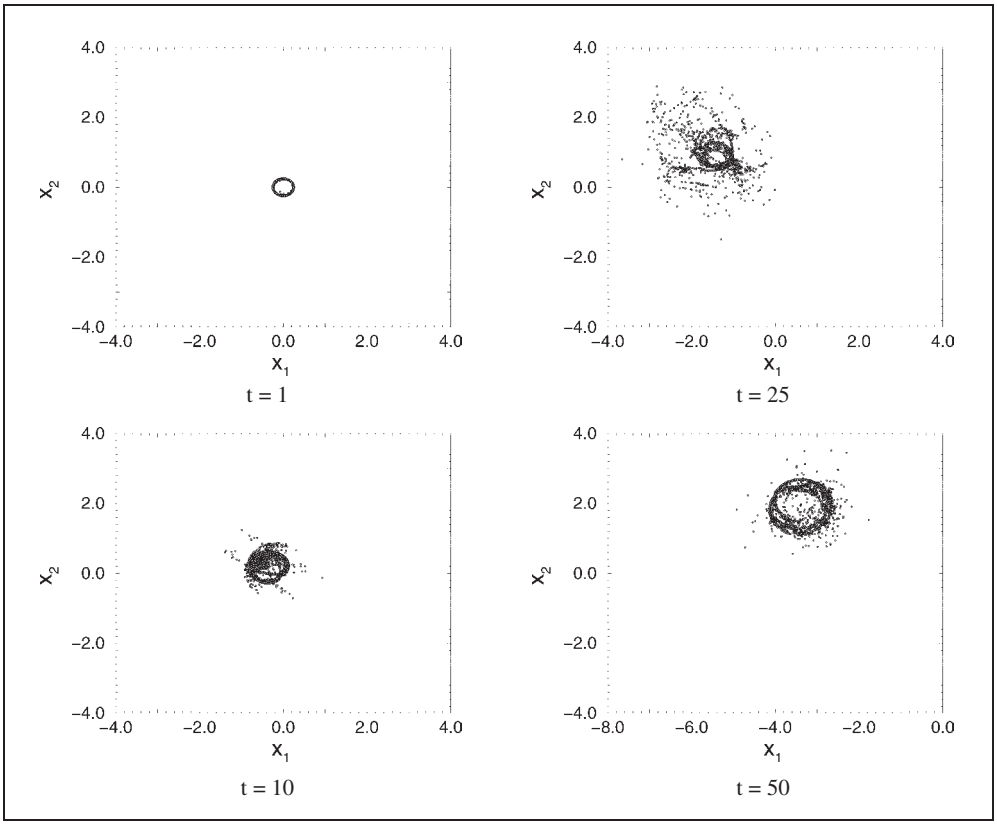

Fig. 7 Snapshots (spatial coordinates) of a harmonic swarm of 2000 active particles. t gives the different times. Initially, the particles were at rest and at the same spatial position. Note that the picture for $t = 50$ has a shifted x_1-axis (EBELING and SCHWEITZER 2001).

Figure 7 presents snapshots of a computer simulation of a harmonic swarm of 2000 active particles.[1] Due to a supercritcal take-up of energy, the particles are able to move actively, the interaction, however, prevents the swarm from simply dispersing in space. Thus, the collective motion of the swarm becomes rather complex, as a compromise between *spatial dispersion* (driven by the energy pumping) and *spatial concentration* (driven by the mutual interaction).

A closer inspection of the swarm dynamics (EBELING and SCHWEITZER 2001, SCHWEITZER et al. 2001) reveals that the system basically possesses two nontrivial dynamic modes. The first mode corresponds to a *flock-like swarm* moving coherently with given direction (translational mode). The second mode corresponds to a *rotating Swarm* while the center of mass is at rest (rotational mode). Which of these modes is the target (attactor) of the collective motion depends both on the initial conditions and on the strength of noise.

1 A movie of these computer simulations – with the same parameters, but a different random seed – can be found at http://ais.gmd. de/~frank/swarm-tb. html.

Let us now characterize the two modes by means of the distribution functions. In the first mode, the particles move parallel to the velocity of the center of mass, *V*. Introducing the relative velocity $d\boldsymbol{v}_i = \boldsymbol{v}_i - \boldsymbol{V}$, we get in first approximation the distribution:

$$P_0(\boldsymbol{r}_i, \boldsymbol{v}_i) = C \left[1 + \frac{d}{c} V^2\right]^{\frac{q}{2D}} \exp\left[-\frac{V^2}{2kT} - \frac{a}{2kT}(\boldsymbol{r}_i - \boldsymbol{R})^2\right] \times \exp\left[-\frac{1}{2\gamma kT}\left(g\left(V^2\right)(\delta v_i)^2 + 2g'\left(V^2\right)(\boldsymbol{V}\cdot\delta v_i)^2\right)\right] \quad [13]$$

Here, $g(V^2)$ denotes the friction function introduced in Equation [4], whereas $g'(V^2)$ is the first derivative of $g(V^2)$. According to Equation [13], the square of the translational velocity V^2 is near to v_0^2 and the deviations fluctuate according to the Boltzmann distribution.

As we have shown by means of computer simulations (Schweitzer et al. 2001), the translational mode breaks down for small initial velocities $\boldsymbol{V}^2 << v_0^2$ (cf. also Fig. 7). In this case the velocities relative to the center of mass are amplified. On the other hand, the translational mode also becomes unstable if the dispersion of the relative velocities approaches the order of v_0^2. In this way, the overall picture is similar to the findings for the one-dimensional case (Mikhailov and Zanette 1999).

In the second stationary mode, where the center of mass is at rest $\boldsymbol{R}$ = const., $\boldsymbol{V} = 0$, the swarm is rotating around the center of mass, and we find in first approximation the distribution, Equation [11] again, with H_i given by Equation [12]:

$$P_0(\boldsymbol{r}_i, \boldsymbol{v}_i) = C \left[1 + \frac{d}{2c} H_i\right]^{\frac{q}{2D}} \exp\left[-\frac{H_i}{2k_BT}\right] \times \left[1 + \frac{d|L_i|}{2cr_0^2}\right]^{\frac{q}{2Dr_0^2}} \exp\left[-\frac{L_i^2}{2k_BTr_0^2}\right]. \quad [14]$$

The two possible branches of the rotating swarm correspond to the positive/negative angular momenta $L = m(x_1v_2 - x_2v_1)$.

There is still a third mode which is realized in the case of very strong noise, $k_BT >> mv_0^2$. In this case the system does not feel the driving force anymore, hence it forms a Boltzmann distributed cluster with a stochastically moving center:

$$P_0(\boldsymbol{r}_i, \boldsymbol{v}_i) = C \exp\left[-\frac{H_i}{k_BT}\right]. \quad [15]$$

In this way, we have – for a rather special model with linear attraction to the center obtained a full stochastic description of three swarming modes. Despite our reductionistic approach, our findings agree also with the qualitative description of Okubo and Levin (2001), who distinguish between three types of collective animal movement:

- *Rectilinear movement*: The animals as a whole tend to perform a rectilinear movement, thus forming a tight (cohesive) group.
- *Doughnut pattern*: When the forward thrust dominates the random force, a group of animals rotates around an empty center, forming the shape of a doughnut.
- *Amoebic movement*: When the random force dominates the forward thrust, the center of mass of animals hardly moves, though the shape of the group fluctuates around a circular pattern.

Hence, we conclude that even in the rather abstract description of physical swarm models, basic features of collective motion and swarm behavior can be recovered and, hopefully, also compared with biological observations of translating/rotating swarms of fish and birds.

5. Swarm Dynamics in the Presence of Chemical Fields

5.1 Models of Biological Aggregation

So far, we have assumed in our model that the linear attraction between any two members of the swarm is of physical nature. The results remain also valid if there is a *chemical* attraction directed to the center of mass of the swarm. This is a reasonable assumption, e. g. for the description of the dynamics of bacterial colonies (Vicsek 2001). Here, the chemotactic attraction might be responsible for the widely observed rotational movements of bacteria as *Bacillus circulans*, *Clostridium tetani*, *Paenibacillus vortex*. If A is the chemotactic coefficient, the attraction of the active particles to the center is now given by a linear chemotactic force $\boldsymbol{F}_{ch} = -A\boldsymbol{r}$. In this case, the two characteristic quantities of our distribution functions derived above read as $w_0^2 = A/m$ and $r_0^2 = v_0^2 m/A$, and the dynamics discussed above remains the same.

A more elaborated investigation has to consider not only the response of the particles to the chemical signal, but also the generation of these chemicals by the particles, i. e. a nonlinear feedback between particles and chemical. In order to describe the chemotactic response of the particles, we modify the Langevin Equation [1], by replacing the potential U with a scalar field $h(\boldsymbol{r}, t)$ that describes the spatiotemporal concentration of the chemical. Assuming that the particles are attracted by higher concentration of the field, we find:

$$m\frac{d\boldsymbol{v}_i}{dt} + \frac{\partial h(\boldsymbol{r},\boldsymbol{t})}{\partial r}|_{r_i} = \boldsymbol{F}_i + \sqrt{2D}\,\xi_i(t). \qquad [16]$$

In a biological context, the chemical field can for example represent pheromones produced, e. g. by ants or other insects in order to communicate with their mates, i. e., it can be envisioned as a communication medium that contains spatial information produced by the insects. The chemotactic response to the field is a basic feature of phenomena such as trail formation in ants (Edelstein-Keshet et al. 1995, Schweitzer et al. 1997), it also plays an important role in the formation of biological patterns in bacteria *Escherichia coli* (Ben-Jacob et al. 1994) or slime molds (Höfer 1999).

For the dynamics of the chemical field $h(\boldsymbol{r}, t)$, we assume the following reaction-diffusion equation:

$$\frac{\partial h(\boldsymbol{r},t)}{\partial t} = \sum_{i=1}^{N} s\delta(\boldsymbol{r} - \boldsymbol{r}_i(t)) - kh(\boldsymbol{r},t) + D_h \Delta_h h(r,t). \qquad [17]$$

It means that changes of the chemical concentration in space and time are governed by three processes: (*i*) production of chemical signals by the particles with a rate s at their current position, $\boldsymbol{r}_i$, (*ii*) decay of the chemical with a rate k, and (*iii*) diffusion (coefficient D_h).

The nonlinear feedback between the particles and the chemical field eventually results in the formation of aggregates, as the snapshots in Figure 8 show. Biological aggregation based on chemotaxis is widely found in biological species, such as insect larvae (DENEUBOURG et al. 1990) or myxobacteria (STEVENS and SCHWEITZER 1997, DEUTSCH 1999) that gather guided by chemical signals originated by the individuals.

5.2 Formation of Trails

A more complex dynamics of the particles can be obtained if instead of the simple chemoattraction described above different chemical fields and a more complex response of the particles to them are considered. So, let us eventually assume that the active particles have another internal degree of freedom θ_i, in addition to their internal energy depot e_i. The individual parameter θ_i may be used to describe different activities and responses to the field, i. e., the active particles then become *agents* with a more complex behavior (SCHWEITZER 2002).

For example, the production rate of the field, s, may now depend on the internal state $\theta_i \in \{-1, +1\}$, i. e., it becomes different for each particle i as follows:

$$s_i(\theta_i, t) = \frac{\theta_i}{2}\left[(1+\theta_i)\, s^0_{+1}\, \exp\left\{-\beta_{+1}\left(t - t^i_{n+}\right)\right\}\right.$$
$$\left. -(1-\theta_i)\, s^0_{-1} \exp\left\{-\beta_{-1}\left(t - t^i_{n-}\right)\right\}\right] \qquad [18]$$

Equation [18] means that the active particle, dependent on its internal state θ_i may produce one of two different chemicals, $\{+1\}$ or $\{-1\}$, with a rate that exponentially decreases in the course of time. Consequently, we now have two different chemical field components that each are assumed to obey the following reaction equation (diffusion is not considered here):

$$\frac{\partial h_\theta(\boldsymbol{r}, t)}{\partial t} = -k h_\theta(\boldsymbol{r}, t) + \sum_{i=1}^{N} s_i(\theta_i, t)\, \delta_{\theta,\theta_i} \delta(\boldsymbol{r} - \boldsymbol{r}_i(t)); \theta \in -1, +1. \qquad [19]$$

The effect of the two field components on each active particle may be described by an *effective field* that also depends on the internal state θ_i of the agent, i. e., the gradient in Equation [16] shall be replaced by the gradient of the effective field (SCHWEITZER and TILCH 2002):

$$\frac{\partial h^e(r,t)}{\partial r} = \frac{\theta_i}{2}\left[(1+\theta_l)\frac{\partial h_{-1}(r,t)}{\partial r} - (1-\theta_l)\frac{\partial h_{+1}(r,t)}{\partial r}\right]. \qquad [20]$$

The nonlinear feedback between the active particles and the chemical field components can be summarized as follows: Particles with an internal state $\theta_i = +1$ contribute to the field by producing component +l, while they are affected by component –1, and particles with an internal state $\theta_i = -1$ contribute to the field by producing component –1 and are affected by component +l.

Eventually, we assume that the particles can change their internal state from $\theta_i = -1$ to +1 and *vice versa*, dependent on environmental conditions or events. To be specific,

we may consider that the active particles are initially concentrated in a "nest" ($\theta_i = +1$) and move out to search for "food", distributed in different spatial locations. Once they found food, their initial state is changed to $\theta_i = -1$, which means that the successful particles begin to produce a different chemical (the "success pheromone"). This gives

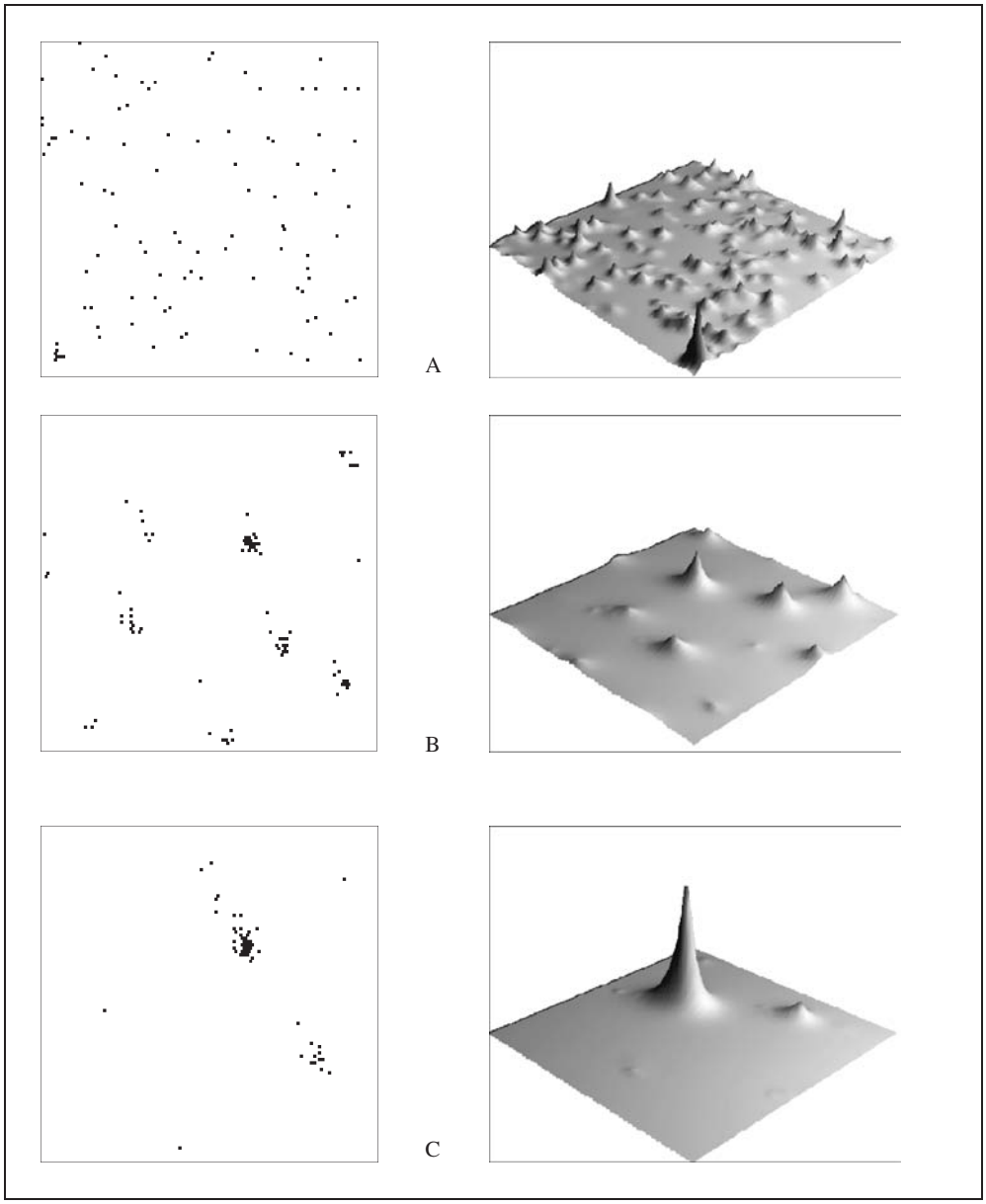

Fig. 8 Snapshots of the positions of the active particles (*left*) and the distribution of the field (*right*) at different times: (*A*) $t = 100$, (*B*) $t = 5000$, (*C*) $t = 50\,000$. (SCHWEITZER and SCHIMANSKY-GEIER 1994)

new information to those particles that are not successful yet to find the food sources, while the successful particle is guided back to the nest by the already existing chemical field component {+1}.

As the result of this nonlinear feedback between the active particles communicating *via* two different chemical field components generated by them, we can observe the formation of directed trails between a nest and different food sources (cf. Fig. 9)

We note that, with respect to biology, there are different parameters which may influence trail following in addition to sensitivity, such as trail fidelity, traffic density, detection distance, endurance of the trail, navigation capabilities etc. (HAEFNER and CRIST

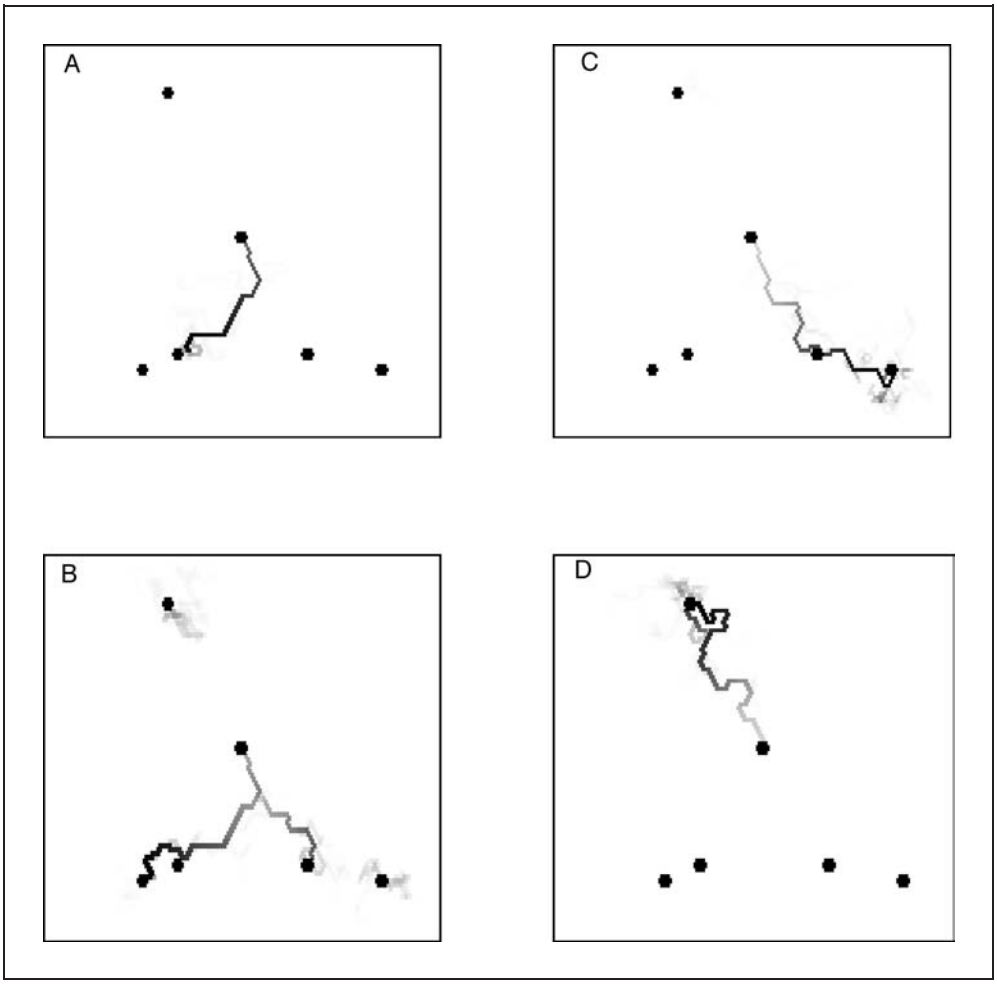

Fig. 9 Formation of trails from a nest (*middle*) to five randomly placed food clusters, which are assumed to be exhausted after a number of visits. The distribution of chemical component (–1) (see text) is shown after (*A*) 2000, (*B*) 4000, (*C*) 8500, and (*D*) 15 000 simulation time steps, respectively (SCHWEITZER et al. 1997).

1994, EDELSTEIN-KESHET et al. 1995). In contrast, our model considers only minimal assumptions for the trail formation. Here, the formation of trail patterns is solely based on simple *local* chemical communication between the particles, with no additional capabilities of orientation or navigation. The spontaneous emergence of a collective trail system by means of the active particles can be described as a self-organizing process. It turns out from the computer simulations that, for different kinds of food sources, the model generates a distinctive trail system to exploit the food sources, and it performs a high flexibility in order to discover and to link new sources.

6. Conclusions

As the examples of the previous sections have shown, the approach of active Brownian particles provides a suitable framework to consider both the *energetic conditions* for active motion and the *interactions* between the particles – two ingredients essential for active and coherent movement in biological systems. The collective motion observed on the "macroscopic" level shows interesting analogies to swarming phenomena found in flocks of bird, schools of fish, but also in cells or insect societies.

With the established collective dynamics, we observe also the *emergence of new system properties* not readily predicted from the basic equations. This process was, in the beginning of this paper, described as *self-organization*, i. e., "the process by which individual subunits achieve, through their cooperative interactions, states characterized by new, emergent properties transcending the properties of their constitutive parts" (BIEBRICHER et al. 1995). Whether or not these emergent properties occur, depends of course, not only on the properties of the system elements and their interactions, but – as we have pointed out in Section 2 – also on suitable external conditions, such as global boundary conditions, the in/outflux of resources (matter, energy, information).

For the prediction of the emergent properties from local interactions fundamental limitations exist which are discussed, e. g. in chaos theory. Moreover, stochastic fluctuations also give unlikely events a certain chance to occur, which in turn affects the real history of the system. This means, the properties of self-organizing systems cannot be determined by a hierarchy of conditions, the system creates its complexity in the course of evolution with respect to its global constraints. Considering, that also the boundary conditions may evolve and new degrees of freedom appear, co-evolutionary processes become important, and the evolution may occur on a qualitatively new level.

Within our physical approach to these phenomena, we are basically interested in the question w*hich extensions* to a known (physical) dynamics might bridge the gap towards a more complex (biological) dynamics. Such a stepping stone strategy is quite promising, as various applications for different biological problems have proven. Of course, many details of real biological phenomena have necessarily to be dropped, in order to focus on particular aspects. Let us quote in this context again from EIGEN'S foreword to the book of VOLKENSTEIN (1994): "The aim of theory is not to *describe* reality in every detail, but rather to *understand* the principles that shape reality."

References

Balázsi, G., and Moss, F.: Stochastic resonance: examples from sensory, perceptive and behavioral neuroscience and chemistry. In: Beck, F., Hütt, M.-T., and Lüttge, U. (Eds.): Nonlinear Dynamics and the Spatiotemporal Principles of Biology. Nova Acta Leopoldina NF Bd. *88*, Nr. 332, 57–76 (2003)

Ben-Jacob, E., Schochet, O., Tenenbaum, A., Cohen, I., Czirok, A., and Vicsek, T.: Generic modelling of cooperative growth patterns in bacterial colonies. Nature *368*, 46–49 (1994)

Biebricher, C. K., Nicolis, G., and Schuster, P.: Self-Organization in the Physico-Chemical and Life Sciences. Vol. *16546* of EU Report (1995)

Braun, H. A., Schäfer, K., Voigt, K., and Huber, M. T.: Temperature encoding in peripheral cold receptors: oscillations, resonances, chaos and noise. In: Beck, F., Hütt, M.-T., and Lüttge, U. (Eds.): Nonlinear Dynamics and the Spatiotemporal Principles of Biology. Nova Acta Leopoldina NF Bd. *88*, Nr. 332, 293–318 (2003)

Czirok, A., Barabasi, A. L., and Vicsek, T.: Collective motion of self-propelled particles: Kinetic phase transition in one dimension. Phys. Rev. Lett. *82/1*, 209–212 (1999)

Czirok, A., Ben-Jacob, E., Cohen, I., and Vicsek, T.: Formation of complex bacterial colonies via self-generated vortices. Phys. Rev. E *54/2*, 1791–1801 (1996)

Deneubourg, J. L., Gregoire, J. C., and Le Fort, E.: Kinetics of larval gregarious behavior in the bark beetle Dendroctonus micans (Coleoptera: Scolytidae). J. Insect Behavior *3/2*, 169–182 (1990)

Deutsch, A.: Principles of morphogenetic motion: swarming and aggregation viewed as self-organization phenomena. J. Biosci. *24/1*, 115–120 (1999)

Ebeling, W., Erdmann, U., Dunkel, J., and Jenssen, M.: Nonlinear dynamics and fluctuations of dissipative Toda chains. J. Stat. Phys. *101*, 443–457 (2000)

Ebeling, W., and Feistel, R.: Chaos und Kosmos – Prinzipien der Evolution. Heidelberg, Berlin, Oxford: Spektrum 1994

Ebeling, W., Feistel, R., and Engel, A.: Physik der Evolutionsprozesse. Berlin: Akademie-Verlag 1990

Ebeling, W., Freund, J., and Schweitzer, F.: Entropie – Information – Komplexität. Stuttgart, Leipzig: Teubner 1998

Ebeling, W., and Schweitzer, F.: Swarms of particle agents with harmonic interactions. Theory BioSci. *120*, 1–18 (2001)

Ebeling, W., Schweitzer, F., and Tilch, B.: Active Brownian motion with energy depots modelling animal mobility. BioSystems *49*, 17–29 (1999)

Edelstein-Keshet, L., Watmough, J., and Ermentrout, G. B.: Trail following in ants: individual properties determine population behaviour. Behav. Ecol. Sociobiol. *361,* 119–133 (1995)

Erdmann, U., Ebeling, W., Schweitzer, F., and Schimansky-Geier, L.: Brownian particles far from equilibrium. Europhys. J. B *15*, 105–113 (2000)

Grün, S., Riehle, A., Aertsen, A., and Diesmann, M.: Temporal scales of cortical interactions. In: Beck, F., Hütt, M.-T., and Lüttge, U. (Eds.): Nonlinear Dynamics and the Spatiotemporal Principles of Biology. Nova Acta Leopoldina NF Bd. *88*, Nr. 332, 189–206 (2003)

Haefner, J. W., and Crist, T. O.: Spatial model of movement and foraging in harvester ants (*Pogonomyrmex*) (I): The Roles of Memory and Communication. J. Theor. Biol. *166*, 299–313 (1994)

Hänggi, P., Schmid, G., and Goychuk, I.: Statistical physics of biocomplexity. In: Beck, F., Hütt, M.-T., and Lüttge, U. (Eds.): Nonlinear Dynamics and the Spatiotemporal Principles of Biology. Nova Acta Leopoldina NF Bd. *88*, Nr. 332, 17–33 (2003)

Höfer, T.: Chemotaxis and aggregation in the cellular slime mould. In: Müller, S. C., Parisi, J., and Zimmermann, W. (Eds.): Transport and Structure. Their Competitive Roles in Biophysics and Chemistry; pp. 137–150. Berlin: Springer 1999

Kantz, H.: Robustness versus sensitivity – can biological systems behave chaotically? In: Beck, F., Hütt, M.-T., and Lüttge, U. (Eds.): Nonlinear Dynamics and the Spatiotemporal Principles of Biology. Nova Acta Leopoldina NF Bd. *88*, Nr. 332, 245–253 (2003)

Klimontovich, Y. L.: Statistical Physics of Open Systems. Dordrecht: Kluwer 1995

Markl, H.: Physik des Lebendigen. A. v. Humboldt-Magazin *65*, 13–24 (1995)

Mikhailov, A. S., and Zanette, D. H.: Noise-induced breakdown of coherent collective motion in swarms. Phys. Rev. E *60*, 4571–4575 (1999)

Mittag, M.: Molecular mechanisms of circadian clocks in microalgae. In: Beck, F., Hütt, M.-T., and Lüttge, U. (Eds.): Nonlinear Dynamics and the Spatiotemporal Principles of Biology. Nova Acta Leopoldina NF Bd. *88*, Nr. 332, 341–351 (2003)

Okubo, M., and Levin, S. A.: Diffusion and Ecological Problems: Modern Perspectives. Berlin: Springer 2001

Ordemann, A., Moss, F., and Balázsi, G.: Motions of daphnia in a light field: random walks with a zooplankton. In: Beck, F., Hütt, M.-T., and Lüttge, U. (Eds.): Nonlinear Dynamics and the Spatiotemporal Principles of Biology. Nova Acta Leopoldina NF Bd. *88*, Nr. 332, 87–103 (2003)

Schienbein, M., and Gruler, H.: Langevin equation, Fokker-Planck equation and cell migration. Bull. Math. Biol. *55*, 585–608 (1993)

Schweitzer, F.: Brownian Agents and Active Particles. Berlin: Springer 2003

Schweitzer, F., Ebeling, W., and Tilch, B.: Complex motion of Brownian particles with energy depots. Phys. Rev. Lett. *80*, 5044–5047 (1998)

Schweitzer, F., Ebeling, W., and Tilch, B.: Statistical mechanics of canonicaldissipative systems and applications to swarm dynamics. Phys. Rev. E *64*, 02110/112 (2001)

Schweitzer, F., Lao, K., and Family, F.: Active random walkers simulate trunk trail formation by ants. BioSystems *41*, 153–166 (1997)

Schweitzer, F., and Schimansky-Geier, L.: Clustering of active walkers in a two-component system. Physica A *206*, 359–379 (1994)

Schweitzer, F., and Tilch, B.: Self-assembling of network in an agent-based model. Phys. Rev. E (2002, in press)

Singer, W.: Oscillations and synchrony – time as coding space in neuronal processing. In: Beck, F., Hütt, M.-T., and Lüttge, U. (Eds.): Nonlinear Dynamics and the Spatiotemporal Principles of Biology. Nova Acta Leopoldina NF Bd. *88*, Nr. 332, 35–56 (2003)

Stevens, A., and Schweitzer, F.: Aggregation induced by diffusing and nondiffusing media. In: Alti, W., Deutsch, A., and Dunn, G. (Eds.): Dynamics of Cell and Tissue Motion; pp. 183–192. Basel: Birkhäuser 1997

Tass, Peter A.: Development of bipolar deep brain stimulation techniques based on stochastic phase resetting. In: Beck, F., Hütt, M.-T., and Lüttge, U. (Eds.): Nonlinear Dynamics and the Spatiotemporal Principles of Biology. Nova Acta Leopoldina NF Bd. *88*, Nr. 332, 207–224 (2003)

Technau, U., Hobmayer, B., Rentzsch, F., and Holstein, T. W.: De-novo formation of the hydra head organizer. In: Beck, F., Hütt, M.-T., and Lüttge, U. (Eds.): Nonlinear Dynamics and the Spatiotemporal Principles of Biology. Nova Acta Leopoldina NF Bd. *88*, Nr. 332, 353–366 (2003)

Vicsek, T.: Fluctuations and Scaling in Biology. Oxford: University Press 2001

Vicsek, T., Czirok, A., Ben-Jacob, E., Cohen, I., and Shochet, O.: Novel type of phase transition in a system of self-driven particles. Phys. Rev. Lett. *75*, 1226–1229 (1995)

Volkenstein, M. V.: Physical Approaches to Biological Evolution. With a foreword by M. Eigen. Berlin: Springer 1994

Prof. Dr. Werner Ebeling
Institute of Physics
Humboldt University
Invalidenstraße 110
10115 Berlin
Germany
Phone: ++49 (0) 30 20 93 76 36
Fax: ++49 (0) 30 20 93 76 38
E-Mail: ebeling@physik.hu-berlin.de

Dr. Frank Schweitzer
Fraunhofer Institute for Autonomous Intelligent Systems
Schloss Birlinghoven
53754 Sankt Augustin
Germany
Phone: ++49 (0) 22 41 14 26 89
Fax: ++49 (0) 22 41 14 23 42
E-Mail: schweitzer@ais.fhg.de

Nova Acta Leopoldina NF *88*, Nr. 332, 189–206 (2003)

Temporal Scales of Cortical Interactions

Sonja GRÜN[1], Alexa RIEHLE[2], Ad AERTSEN[3], and Markus DIESMANN[4]

With 6 Figures

Abstract

Higher brain functions are attributed to the cortex. Over the years it became clear that information is encoded not only in the responses of individual neurons but also in the joint activity of populations of neurons. Based on theoretical studies it has been proposed that the temporally coordinated spiking activity of many neurons is a relevant variable for information processing (VON DER MALSBURG 1981, ABELES 1982 b) and that cortical neurons organize dynamically into coherent functional groups ("cell assemblies", HEBB 1949) that are distinguished by the coordinated activity of the participating neurons. Our research focuses on the development of analysis strategies for the identification of neuronal interactions and assembly activity. We attempt to decipher the spatial and temporal scales of dynamical neuronal interactions, and their relations to the external world (stimuli and/or behavior).

In order to identify neuronal assemblies, simultaneously recorded neuronal spiking activity needs to be analyzed with respect to temporal structure. To that end we developed the "unitary event" analysis method (GRÜN et al. 2002 a, b) that detects the presence of conspicuous spike coincidences and evaluates their statistical significance. The analysis of simultaneously recorded neuronal activity in monkey primary motor and frontal cortex uncovered context-dependent, rapid changes in the patterns of coincident spike activity during performance of a delayed-pointing task (RIEHLE et al. 1997) or a delayed localization task (VAADIA et al. 1989, AERTSEN et al. 1991, VAADIA et al. 1991), respectively. Spike synchronization occurred accompanied by discharge rate modulations and in the absence of spike rate modulations depending on the details of the experimental protocol. The temporal precision of such synchronized events is in the range of a few ms (GRÜN et al. 1999). Data suggest that the composition of significant coincidence patterns changes depending on the computational demands (GRÜN et al. 2002 b), which may be taken as an indication that different assemblies are activated in relation to behavior.

In the unitary event analysis a number of different time scales have to be considered and affect different parameters of the signal. Here we specifically address the different temporal scales and give interpretations in respect to the dynamics of the neuronal processes.

Zusammenfassung

Die Verarbeitung höherer kognitiver Leistungen wird der Großhirnrinde zugeordnet. In den letzten Jahren stellte sich heraus, daß die neuronale Informationsverarbeitung im Kortex nicht nur durch Aktivitäten einzelner Neuronen getragen wird, sondern insbesondere auch durch aufeinander abgestimmte, gemeinsame Akti-

1 Department Neurophysiology, Max Planck Institute for Brain Research, Frankfurt/Main, Germany; present address: Free University Berlin, Institute for Biology, Neurobiology, Berlin, Germany.
2 Equipe Perception and Cognition, INPC-CNRS, Marseille, France.
3 Neurobiology and Biophysics, Albrecht Ludwigs University, Freiburg, Germany.
4 Department Nonlinear Dynamics, Max-Planck-Institut für Strömungsforschung, Göttingen, Germany.

vität von Neuronenverbänden. Auf der Basis theoretischer Untersuchungen wurde die zeitlich abgestimmte Spikeaktivität mehrerer Neuronen als relevante Variable der Informationsverarbeitung vorgeschlagen (VON DER MALSBURG 1981, ABELES 1982 b) und mündet in der Hypothese, daß sich kortikale Neuronen dynamisch in funktionelle Gruppen („cell assemblies", HEBB 1949) formieren, welche sich durch koordinierte Aktivität der teilnehmenden Neuronen auszeichnen. Unsere Forschung konzentriert sich auf die Entwicklung von Analysestrategien, die es erlauben, neuronale Wechselwirkungen und die Aktivität neuronaler Ensembles zu identifizieren. Dabei werden die räumlichen und zeitlichen Skalen dynamischer Wechselwirkungen und deren Bezüge zur äußeren Welt (Reize und/oder Verhalten) untersucht.

Um neuronale Ensembles zu identifizieren, muß gleichzeitig abgeleitete Spikeaktivität in Hinsicht auf ihre zeitliche Struktur untersucht werden. Hierfür haben wir die „Unitary Event"-Analysemethode entwikkelt (GRÜN et al. 2002 a, b), welche auffällige, koinzidente Spikeaktivität detektiert, und auf Signifikanz untersucht. Die Analyse gleichzeitig abgeleiteter neuronaler Aktivität, gemessen im Motorkortex und Frontalkortex von Affen, brachte kontextabhängige, schnelle Änderungen von Koinzidenzmustern während der Ausführung eines „delayed-pointing task" (RIEHLE et al. 1997) bzw. eines „delayed localization task" (VAADIA et al. 1989, AERTSEN et al. 1991, VAADIA et al. 1991) zu Tage. Spikesynchronisation trat sowohl mit als auch ohne gleichzeitiger Ratenmodulationen auf, und variierte je nach experimentellem Protokoll. Die zeitliche Präzision der synchronisierten Ereignisse beträgt nur wenige ms (GRÜN et al. 1999). Die Daten zeigen auch, daß sich die Zusammensetzung der signifikanten Koinzidenzmuster in Abhängigkeit von den Anforderungen ändern kann (GRÜN et al. 2002 b), und deuten darauf hin, daß unterschiedliche neuronale Ensembles in Abhängigkeit vom Verhaltenskontext aktiviert werden.

Im Rahmen der *Unitary-Event*-Analyse werden eine Reihe von Zeitskalen berücksichtigt, die jeweils einen anderen Aspekt des neuronalen Signals betreffen. In dem hier vorliegenden Beitrag liegt der Schwerpunkt auf der Darstellung obengenannter Zeitskalen und deren Interpretation in Hinsicht auf die Dynamik der zugrundeliegenden neuronalen Prozesse.

1. Introduction

Higher brain functions are attributed to the cortex, a highly interconnected network composed of about 10^{10} neurons. Each single neuron receives spike inputs from about 10^4 other neurons and projects its output spikes to about the same number of other neurons (BRAITENBERG and SCHÜZ 1991). Initially, recording techniques were limited to recordings from one channel at a time. Here, the recording was optimized to obtain the spikes from a single neuron only, or the spikes where left unidentified (e. g. in recordings from nerve fibers). Due to this limitation and also guided by early considerations about the integrative properties of the neuron (SHERRINGTON 1906, ECCLES 1957) researchers concentrated on reproducible changes in the spike rate. ADRIAN (1928) observed that the spike rate of neurons is related to changes in the environment and concluded that the intensity of sensation is proportional to sensory spike rates. Single neurons with their specific characteristics became the building blocks of cortical processing (BARLOW 1972, 1992, for reviews see MARTIN 1994, 2000). This approach led to fundamental insights into the neuronal mechanisms of brain function (e. g. LETTVIN 1959, HUBEL 1968) and to important theoretical works on information processing by neuronal networks (MCCULLOCH and PITTS 1943). The influential book by MINSKY and PAPERT (1988) pointed out the limitation of this concept (see also VON DER MALSBURG 1986 b).

The parallel and distributed architecture of the cortex suggested the investigation of the collective properties of neural networks. HEBB (1949) proposed that ensembles of neurons, "cell assemblies", constitute the units of neuronal processing. In this view, functional groups are formed by the coherent activity of the participating neurons. This

hypothesis provided the conceptual framework for successful theoretical work on neural networks (e. g. HOPFIELD 1982, RUMMELHART et al. 1986, AMIT 1989, 1997). These models exhibit multiple attractor states, the attractors being groups of neurons with elevated spike rates. A prominent example from the experimental literature is the demonstration of representation of information by ensembles of neurons (GEORGOPOULOS et al. 1988, 1989).

In parallel, however, conceptual difficulties of the representation of assembly membership by spike rate were pointed out (VON DER MALSBURG 1981, 1986b). The notion was developed that, alternatively, assembly membership could be expressed in the temporal organization of spiking activity (VON DER MALSBURG 1981, ABELES 1982 a, VON DER MALSBURG 1986 a, GERSTEIN et al. 1989, PALM 1990, ABELES 1991, SINGER 1993). Consequently, neuronal processing should be reflected in dynamical changes of spike time correlation. Dynamic modulations of spike correlation at various scales of precision have, in fact, been observed in different cortical areas: visual (ECKHORN et al. 1988, GRAY et al. 1989, for reviews see ENGEL et al. 1992, AERTSEN et al. 1993, SINGER and GRAY 1995, ROELFSEMA et al. 1996, SINGER et al. 1997, SINGER 1999), auditory (AHISSAR et al. 1992, EGGERMONT 1992, DECHARMS et al. 1996, SAKURAI 1996), soma-

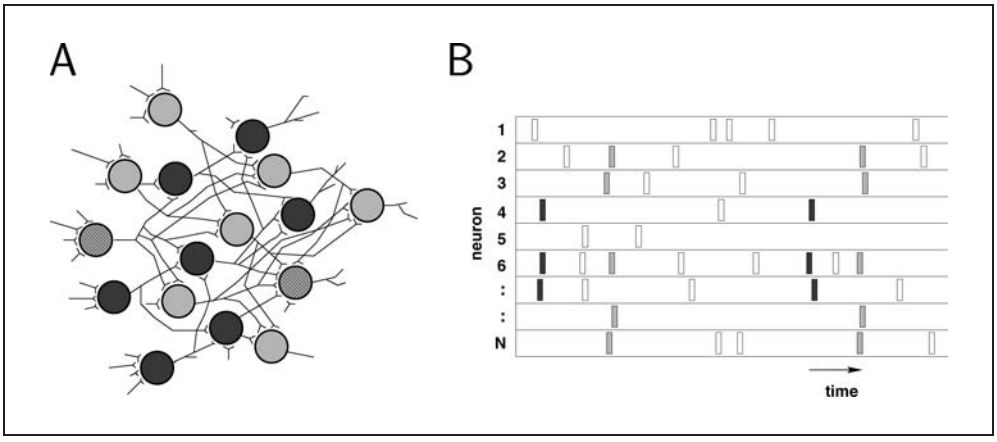

Fig. 1 Cell assemblies. (*A*) Sketch of a piece of the cortical network containing two cell assemblies. The neurons composing the network are indicated by filled circles (black, gray and hatched), the thin lines sketch the connectivity between the neurons. One assembly is composed of the neurons marked in dark gray, the other by the neurons marked in light gray. Hatched disks mark neurons that are members of both assemblies. (*B*) Sketch of the spiking activity of N simultaneously recorded neurons. Part of the recorded neurons are members of the indicated assemblies in (*A*), others are "background" neurons. During the observation interval both assemblies are activated twice, e. g., by a sequence of two different stimuli presented shortly one after the other. Assembly 1 (neurons marked black) is activated first by activity entering the net through the dark gray and hatched neurons on the lower left and is propagating through the subnet composing that assembly. The activation of the assembly is visible by the synchronous activity of recorded member neurons (here numbered as 4, 6, 7). Later the other assembly (neurons marked light gray) is activated by a stimulus entering the network through the gray and hatched neurons on the upper left, expressed by the synchronous spiking activity of recorded member neurons (2,3,6,N-1,N). Interestingly, one neuron (6, corresponding to the hatched neuron on the left) exhibits synchronous activity with neurons of both assemblies. It multiplexes its activity in time while being member of different assemblies. The neuron's assembly membership is expressed by the partner neurons with which it exhibits synchronous activity.

to-sensory (Nicolelis et al. 1995, Laubach et al. 2000, Steinmetz et al. 2000), motor (Murthy and Fetz 1992, Sanes and Donoghue 1993, Riehle et al. 1997, Hatsopoulos et al. 1998), and frontal (Aertsen et al. 1991, Abeles et al. 1993, Vaadia et al. 1995, Prut et al. 1998, Grün et al. 2002 b).

The correlations observed in neuronal data cannot be attributed to the underlying network structure alone (Aertsen et al. 1989, 1991). Parameter changes seem to be able to drive the network into different dynamical regimes or activate different sub-networks. Thus, it was proposed that depending on the behavioral demand neurons organize dynamically into functional groups, which should be reflected in the temporal structure of the spike activity of the neurons involved (sketched in Fig. 1). In order to test this hypothesis and to detect the activity of cell assemblies and their interactions, neuronal activity has to be analyzed for correlation structures. For the analysis of spike coincidence patterns in such simultaneously recorded spike trains we developed the "unitary event" analysis (Grün 1996, Grün et al. 2002 a, b). The method allows to uncover excessive coincident spike events among simultaneously recorded neurons. Such conspicuous coincidences are referred to as "unitary events", and are defined as those joint spike constellations that occur significantly more often than expected by chance. The functional significance of unitary events was tested by investigating their occurrence and composition in relation to sensory stimuli and behavioral events. We were able to define a measure, the joint-surprise, that indicates the presence of an unexpected spike constellation in a time resolved manner. Conspicuous spike patterns can be marked at the point of their occurrence in time. The result is a visualization of the correlation structure of the data as a function of time. The appearance and disappearance of spike patterns can be compared with the stages of the experimental protocol. The time course of pattern occurrence can also be compared to the time course of other time varying features of the data, such as the spike rate. Recordings from awake animals performing a behavioral task enable the experimenter to observe the correlation structure while the neurons are carrying out computational tasks. Various time scales and their interactions are made explicit in the mathematical formulation of unitary event analysis. In this contribution, we use unitary event analysis, which will be introduced in the next section (*Section 2*), as a framework to discuss the multiple time scales that enter our analysis and may be relevant for cortical processing. *Section 3* discusses how temporal coordination is distinguished from changes in spike rate. The following section (*Section 4*) analyzes the time scale of synchronous spiking in cortical data. *Section 5* demonstrates that the time courses of rate modulation are often independent from the modulation of fine temporal coordination.

2. Detection and Statistical Evaluation of Spike Coincidences: Unitary Event Analysis

We developed a method that detects the presence of conspicuous spike coincidences and evaluates their statistical significance (Grün 1996, Grün et al. 2002 a, b). Briefly, the detection algorithm works as follows: The simultaneous observation of spiking events from N neurons can be described mathematically by the joint process, composed of N parallel point processes. By appropriate binning, this can be transformed to an N-fold

binary process, the statistics of which are described by the set of activity vectors reflecting the various (0,1)-constellations that occurred across the recorded neurons (Fig. 2 *A*). Under the null-hypothesis of independently firing neurons, the expected number of occurrences of any activity vector and its probability distribution can be calculated analytically on the basis of the single neuron firing rates. The expected joint-probability of an activity vector is given (assuming statistical independence) by the product of the corresponding firing and non-firing probabilities.

To test the significance of coincident events we developed a new statistical measure: the "joint-p-value" Ψ. For any particular spike activity vector, this joint-p-value meas-

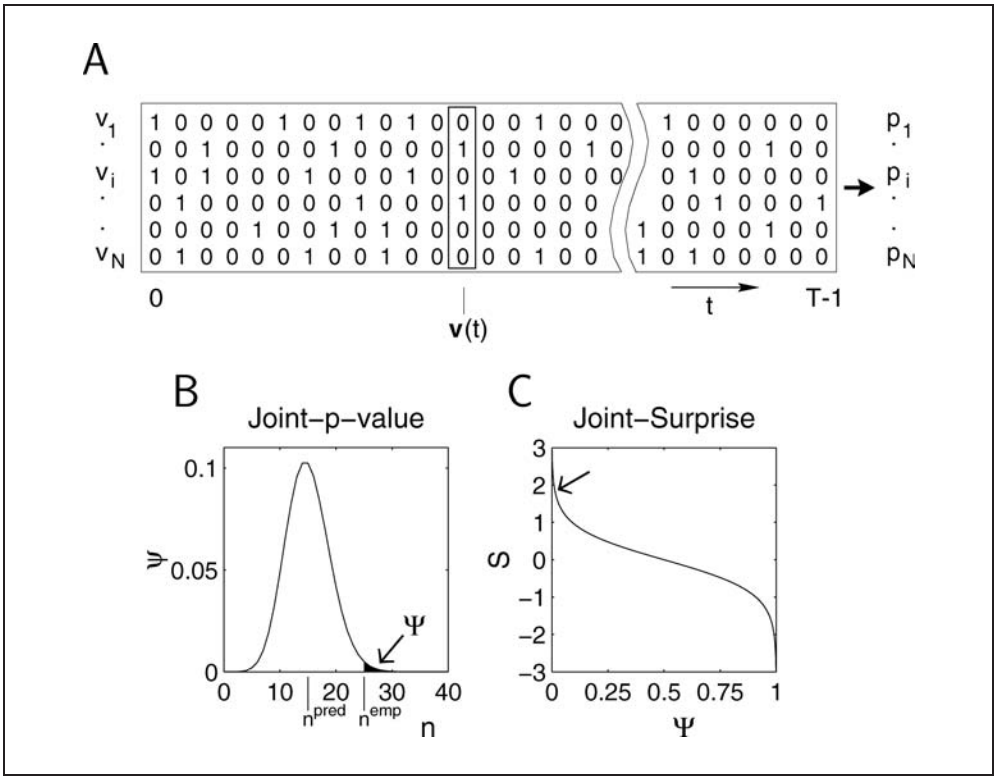

Fig. 2 Unitary Event Analysis. (*A*) Representation of N parallel neuronal spike trains as binary processes. Each horizontal row, consisting of 0's and 1's, represents a realization of a single process v_i observed for T time steps. The 1's mark the occurrences of spike events. The joint activity across the processes at each instant in time can be expressed by a vector **v**(t), as indicated for one example. The empirical firing probability per bin p_i of each single process is evaluated as the marginal probability: the number of spikes in the observation time interval, divided by the number of time steps. (*B*) Distribution of joint-spike events for significance estimation. The black shaded area under the Poisson distribution (with $n^{pred} = 15$) ranging from $n^{emp} = 25$ to ∞, indicates the joint-p-value Ψ as the cumulative probability to get n^{emp} coincidences or an even larger number. For this particular example, the joint-p-value equals 0.0112. C. The joint-surprise S is as a logarithmic scaling function of the joint-p-value. The transformation converts significant joint-p-values to positive numbers, non-significant values to values around 0, and large joint-p-values to negative numbers, indicating significant lack of coincident events. The value of the joint-surprise corresponding to the joint-p-value in the example in (*B*) is S = 1.9459. Figure modified after GRÜN et al. 2002 a.

ures the cumulative probability of observing the actual number of coincidences (or an even larger one) by chance (Fig. 2 *B*):

$$\Psi\left(n^{emp}|n^{pred}\right) = \sum_{n=n^{emp}}^{\infty} \psi\left(n, n^{pred}\right). \quad [1]$$

In order to enhance visual resolution at the relevant low-probability values of Ψ for excessive or lacking coincidences we transform Ψ to a logarithmic scale thereby deriving the joint-surprise measure (Fig. 2 *C*):

$$S = \log \frac{1 - \Psi}{\Psi}, \quad [2]$$

a measure closely related to the surprise measure defined by PALM (1981). Thus, we can calculate for a stationary data set the significance of any joint-activity constellation across the *N* neurons and identify those neurons that exhibit significant (e. g. at a significance level of 5 %: $S(\Psi) = S(\alpha = 0.05)$) synchronous activity presumably indicating signatures of assembly activity (for details see GRÜN et al. 2002 a).

3. Temporal Precision of Coincident Events

The time resolution of data acquisition in extracellular spike recordings is typically 1 ms or better. To define a coincident event implies to know the time scale on which spike events are coincident. Since spikes do not code information by amplitude or shape of the spike we can assume the duration of a spike signal (1–2 ms) as a lower bound. During the last decade there was an intensive debate if neurons could operate on a time scale smaller than a few tens of ms, since neurons were considered to be "noisy" and as units that integrate the spikes over a relatively large time window before emitting a spike. This view is supported by the relatively long time constants of the membrane potential (tens of ms). Note, however, that the degree of this temporal noise has long been questioned (e. g. ABELES 1982 a) and is still under debate (e. g. BRYANT and SEGUNDO 1976, MAINEN and SEJNOWSKI 1995, SHADLEN and NEWSOME 1998, DIESMANN et al. 1999). There is experimental evidence from cross-correlation-, JPST- and, particularly, from spike pattern analysis that the timing accuracy of spiking events which might be relevant for brain function can be as precise as a few ms (ABELES et al. 1993, NOWAK et al. 1995, RIEHLE et al. 1997). Similar suggestions come from modeling studies (DIESMANN et al. 1999).

To detect the relevant time scale of synchronous events in experimental data, we systematically vary the allowed temporal width to detect coincident events and evaluate their significance assuming independence. A straight forward approach to allow synchronous events on a less precise time scale than the time resolution of the data is to section the observation interval into short disjunct time slices ("bins") and consider spikes from different neurons as coincident if they occur within such a time bin. Although coincident spiking events can reliably be detected by using such a discretized process (disjunct binning), the method loses sensitivity for higher temporal jitter of the coincident events (GRÜN et al. 1999). This is mainly due to the nonlinear effect of binning and clipping of the single spike trains, on the one hand, and the application of the same binning grid over multiple spike trains, on the other.

As an alternative approach, we worked out the "multiple shift" method that overcomes the need for binning, and thereby treats the data on their (original) high time resolution (GRÜN et al. 1999). Technically, coincidences are detected by shifting the spike trains against each other over the range of allowed coincidence width and integrating the number of exact coincidences (on the time resolution of the data) over all shifts. In calibration studies we analyzed the sensitivity of the method and the reliability to detect near-coincidences with a given underlying coincidence width. Therefore we simulated data sets in which independent spike trains with a given background rate were "injected" with coincident spikes of a given coincidence width (tolerance) into both trains. For a given data set we varied the analysis coincidence width systematically and evaluated the significance for each coincidence width. It turned out that the significance is maximal, if the analysis bin width corresponds to the underlying jitter (see Fig. 3 *A*).

Thus, we used the method to estimate the underlying "jitter" in experimental data. Neuronal data were taken from a pair of simultaneously recorded neurons (time resolution: h = 1 ms) from the primary motor cortex of a behaving monkey involved in a visuomanual pointing task (see BASTIAN et al. 1998, GRAMMONT and RIEHLE 1999 for experimental details). The results of the analyses of the experimental data using various shift widths (b′) are shown in Figure 3 *B* (solid lines). The joint-surprise function, however, shows a clear peak at b′ = 6 ms. In Figure 3 *B* (*top*) the experimental results are compared to control surrogate data (shown in gray), in which no coincidences were injected. The rates for the simulations were set to correspond to the marginal firing rates of the neuronal data. Simulation results of 30 repetitions (each consisting of 33 trials) are shown as gray bands. The experimental results clearly deviate from the simulation results, indicating that neuronal spike trains do not correspond to the assumption of independence.

As discussed above, according to our model the maximum of S in the experimental data indicates the coincidence width of the underlying data as s = b′, i. e. here 6 ms. Next, surrogate data with injected coincidences were compared to the experimental results. We extracted the coincidence width for the simulation at the maximum of the joint-surprise (here: 6 ms). The firing probabilities of the neurons, measured as the marginal probabilities, were assumed to be a measure for the sum of coincident and background activity. Using the measured marginal probabilites for the two neurons, we obtained estimates for the probability for coincident firing and the "uncorrelated" background firing probabilities. Figure 3 *B* (*bottom*) illustrates the comparison of experimental and simulated data using the derived parameters. The experimentally derived joint-surprise function shows basically the same curve as obtained from the surrogate data. The experimental curve lies within the range of about 1 std of the simulated data (dark gray band), indicating that our model predictions are consistent with the experimental data.

4. Dynamics of Synchronous Spiking Events

In order to account for non-stationarities in the discharge rates of the observed neurons, modulations in spike rates and coincidence rates are determined on the basis of short data segments by sliding a fixed time window (typically 100 ms wide) along the data in

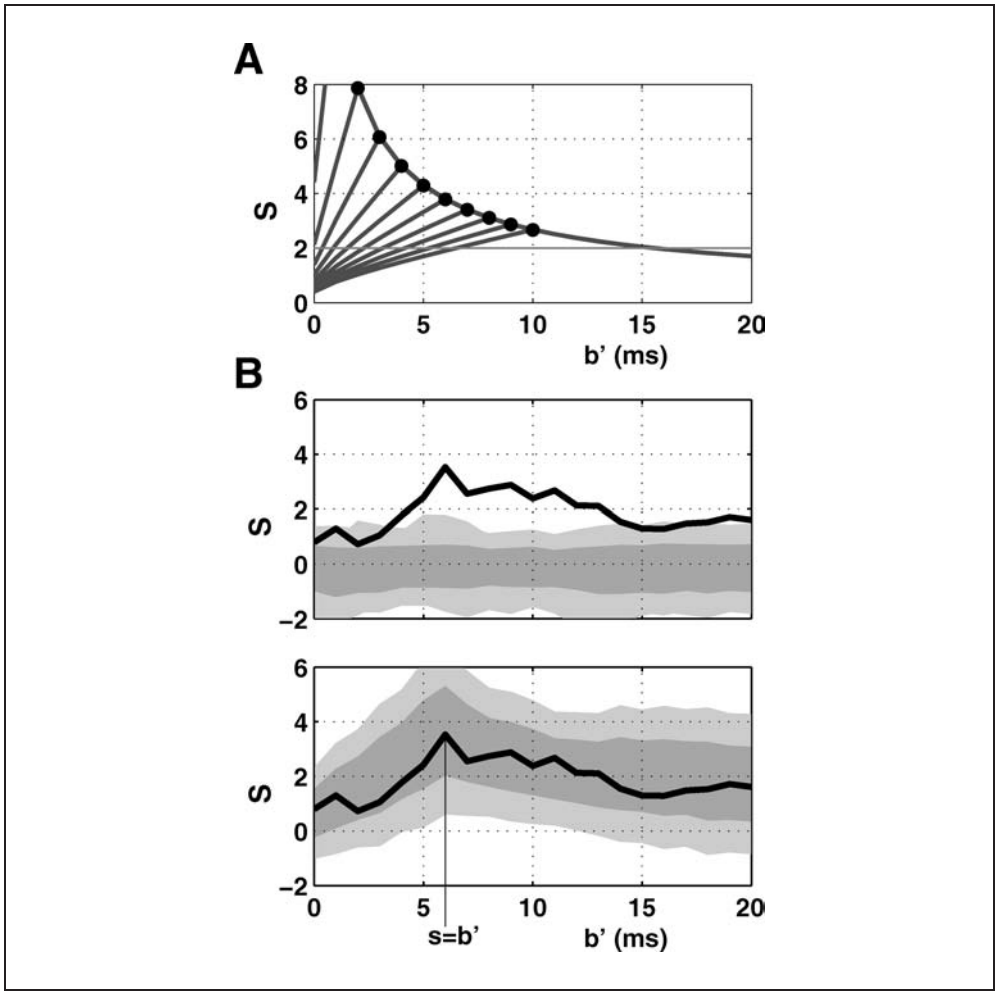

Fig. 3 Temporal precision of coincident activity. (*A*) The detectability of coincident events and their temporal jitter is illustrated for two parallel processes, composed of two independent contributions: background (Poisson processes) and coincident activity with a given homogeneous temporal jitter. For various coincidence widths (from $s = \pm 1 \ldots 10$) the joint-surprise (S) is calculated for increasing analysis widths ($b' = \pm 0 \ldots 20$). For a given temporal jitter s, the joint-surprise as a function of b′ (gray curves) exhibits a maximum at the corresponding analysis jitter ($s = b'$) (marked by filled black circles). For $s = \pm 1$ the maximum of S equals 11.6 at $b' = \pm 1$ (not shown here). The line at $S = 2$ marks the significance level of 1 %, i. e. $S(\alpha = 0.01)$. Data sets were assumed to have the parameters: duration in time as the experimental data shown in (*B*; 33 trials of 800 ms) with a time resolution of $h = 1$ ms; background firing probability for both neurons: $p_r = 0.03$, coincidence firing probability of $p_c = 0.0029$. (*B*) Temporal precision of neuronal spike trains and its comparison with simulated processes. The analysis results expressed by the joint-surprise (S) for increasing shift width b′ of two simultaneously recorded neurons are shown and compared to simulated data. The top graph shows, for control purposes, the simulation experiment performed without injected coincidences, firing probabilities correspond to the measured marginals of the neurons ($p_1 = 0.0321$, $p_2 = 0.0359$). In the bottom graph, coincidences were injected with a coincidence width of $s = \pm 6$ ms, corresponding to the analysis bin width b′ at the maximum of the joint-surprise. The coincidence probability ($p_c = 0.0029$) and the background probabilities of the two neurons ($p_{r1} = 0.0291$ and $p_{r2} = 0.0329$) were

steps of the coincidence bin width. This timing segmentation is applied to each trial, and the data of corresponding segments in all trials are then analyzed as one quasi-stationary data set, using the appropriate rate approximation. Besides the effect that this approach corrects for non-stationary rate variation in time, it also allows us to analyze synchronous activity and its potential modulation as a function of time. Excess coincident activity may occur in a short interval, "triggered" by some external or internal event. When the neuronal processes are observed over repeated trials, the coincident activity appears to some degree locked to certain points in time. We have shown in a modeling study (GRÜN 1996) that loose locking of synchronous activity, e. g. to trial onset, does not contradict precise temporal coordination of the spiking activity related to the assembly activity. Loose locking rather reflects a loose onset of the correspondingly triggered assembly activity. For optimal detection of unitary events using the sliding window procedure, the width of the analysis window has to be adjusted to the temporal spread of the synchronous events. As worked out in detail in GRÜN et al. (2002 b), the shape of the joint-surprise function can indicate the optimal window width, such that the window width can be adjusted accordingly. Further details and calibration of the unitary event analysis technique are described in GRÜN (1996) and GRÜN et al. (2002 b). Recent extensions of the approach are discussed in ROY et al. (2000), PAULUIS and BAKER (2000), GÜTIG et al. (2002). Note that the time window fulfills two different purposes: rate estimation and obtaining a large enough coincidence count for significance testing. In general, both tasks may require windows of different size. Even if the spike rates are known a limited number of trials require a certain window size.

4.1 Temporal Modulation of Synchronous Activity

We tested the hypothesis that such precise synchronization of individual action potentials among groups of neurons in the monkey motor cortex is involved in dynamically organizing the cortical network during the planning and execution of voluntary movements (RIEHLE et al. 1997). We found that simultaneously recorded activities of neurons in monkey primary motor cortex indeed exhibited context-dependent, rapid changes in the patterns of coincident action potentials during performance of a delayed-pointing task. Accurate spike synchronization occurred in relation to external events (visual stimuli, hand movements), commonly accompanied by discharge rate modulations, however without precise time-locking of the spikes to these external events. Accurate spike synchronization also occurred in relation to purely internal events (stimulus expectancy; Fig. 4), where firing rate modulations were distinctly absent. These findings indicate that internally generated synchronization of individual spike discharges may subserve the cortical organization of cognitive motor processes. The clear correlation of spike co-

---

calculated based on the model as assumed in (*A*) (see for details GRÜN et al. 1999). Results from simulations are shown as gray bands. The width of the light gray band represents 95 %, the dark gray band 70 % of 30 repetitions of the simulation experiments. Each simulation had the same duration in time as the experimental data (33 trials of 800 ms) with a time resolution of h = 1 ms. In the upper panel, the light gray band (representing 95 % of the simulation experiments) is well below the threshold for significance of 1 %, i. e. S (0.01) = 2, demonstrating the low probability of the significance measure to generate "false alarms". Figure modified after GRÜN et al. 1999.

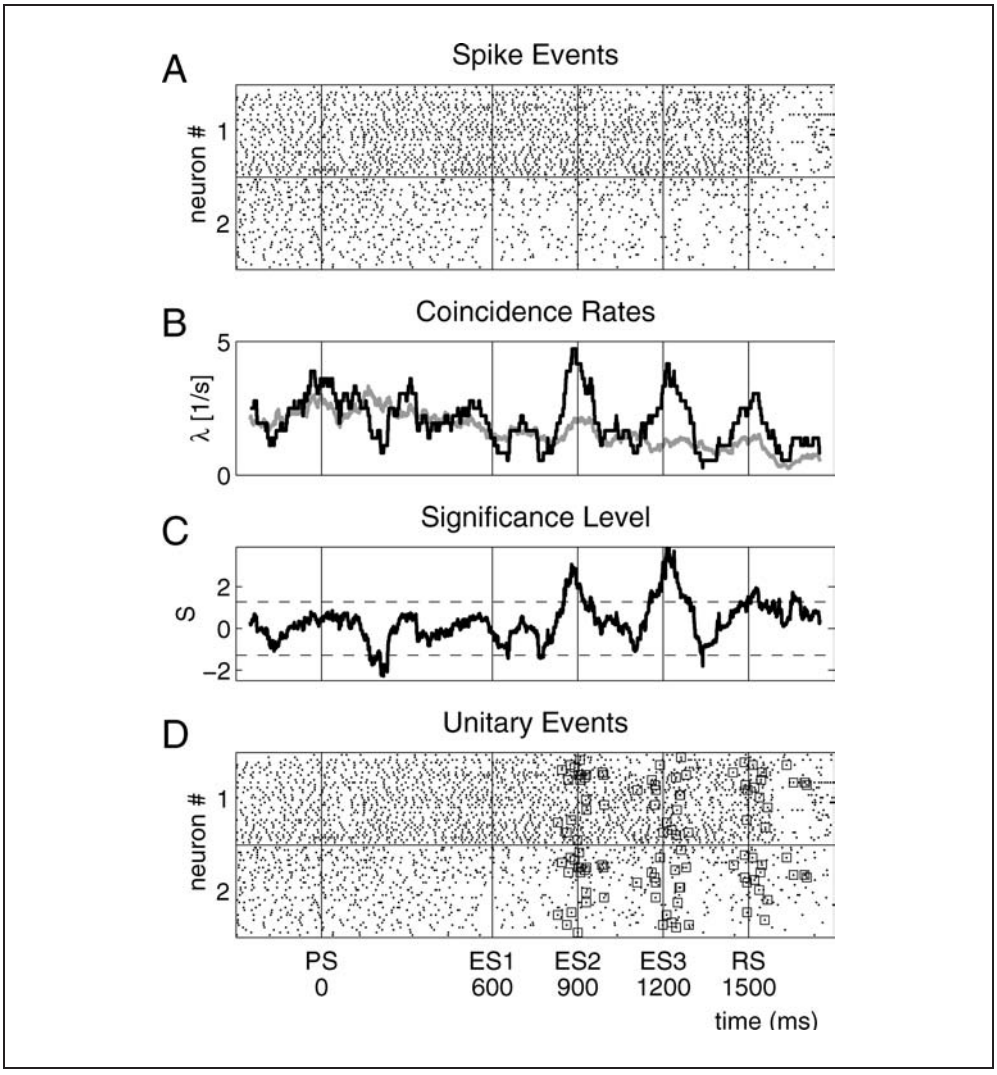

Fig. 4 Temporal modulation of synchronous activity. Unitary event analysis of the spiking activity of two simultaneously recorded single neurons from motor cortex of awake behaving monkey. The monkey was involved in a delayed pointing task, where the duration of the preparation period (after the preparatory signal (PS) up to the reaction signal (RS)) for the movement was selected randomly from 4 possible durations (PP; 600, 900, 1200, 1500 ms) from trial to trial. The 36 trials with longest PP duration (1500 ms) were pooled in this example. Thus the monkey could expect the RS to occur at three successive moments (ES1, ES2, ES3) before it actually occurred at RS. Results of the unitary event analysis in sliding windows of 100 ms over a time interval of 2100 ms, starting at 300 ms before PP and lasting until 300 ms after PS. (*A*) Conventional raster displays of spike discharges of two neurons. Each dot represents an action potential, and each row of action potentials depicts the spiking activity in a single trial. (*B*) Comparison of measured and expected coincidence rates. The measured coincidence rate (black curve) was derived the same way as the firing rates by sliding a box car of 100 ms in steps of 1 ms over the data. Coincident events were detected with an analysis width of $b' = \pm 2$ ms. The expected coincidence rate (gray curve), based on the null-hypothesis of independent firing was calculated as the product of the individual firing rates (see for details GRÜN et al.

incidences with stimuli and behavioral events underlines their functional relevance (FETZ 1997, RIEHLE et al. 1997). Taken together, these findings demonstrate the existence of precise synchronization of individual spike discharges among selected groups of neurons in the motor cortex. This synchronization is associated with distinct phases in the planning and execution of voluntary movements, indicating that it indeed plays a functional role. Moreover, these findings suggest that under behavioral conditions as investigated in this study, the brain uses different strategies in different contextual situations: In order to process a purely cognitive, i. e. an internal and behaviorally relevant event, neurons preferentially synchronize their spike occurrences without changing, at the same time, their firing rates. By contrast, when processing an external, behaviorally relevant event, neurons tend to synchronize their spikes and modulate their firing rates at the same time. Thus, precise synchronization of spike events and modulation of discharge rate may serve different and complementary functions. They act in conjunction at some times, not at others, depending on the behavioral context (RIEHLE et al. 1997).

4.2 Task Dependent Composition of Coincident Spiking Activity

In the second experimental study we discuss, Rhesus monkeys were trained in a "delayed localization" paradigm with two basic tasks (localizing and non-localizing, an example of the latter is shown in Figure 5). In both tasks, the monkey receives a sequence of two stimuli (visual and auditory) out of five possible locations. After a waiting period, a "GO" signal instructed the monkey to move its arm in the direction of the stimulus relevant in the current trial. In the localizing task, the relevant spatial cue was selected by the color of the GO signal. In the non-localizing task, an indicator light between blocks of trials informed the monkey about the reinforced direction for arm movement. Thus, in the latter case, the animal had to ignore the spatial cues given before the GO signal. In the behavioral task analyzed here (non-localizing), neither the spatial cues before the GO signal nor the GO signal itself could be used to determine the correct behavioral response (see VAADIA et al. 1989, AERTSEN et al. 1991, VAADIA et al. 1991 for further details). The activity of several (up to 16) neurons was recorded simultaneously in the frontal cortex by using six microelectrodes during task performance. In each recording session, the microelectrodes were inserted into the cortex with inter-electrode distances of 300–600 μm. Isolation of single units was aided by six spike sorters that could isolate activity of 2–3 single units, based on their spike shape (ABELES and GOLDSTEIN 1977). The spike sorting procedure introduced a deadtime of 600 μs for the spike detection.

Using data from this study, we found that coincident activity in the frontal cortex can be specific to movement direction. We parsed the data of five neurons according to the

---

1999). (*C*) For each time window, the joint-surprise value was computed by comparing the empirical number of coincidences with the expected number (see Fig. 2). (*D*) Whenever the joint-surprise exceeded a fixed threshold (here: $S(\alpha = 0.05)$) this defined an epoch with significantly more coincidences than expected by chance. These precise coincidences were marked as unitary events and are indicated by squares in the raster displays. Reprinted (excerpted) with permission from RIEHLE et al. Science *278*, 1950–1953 (1997). Copyright 1997 American Association for the Advancement of Science.

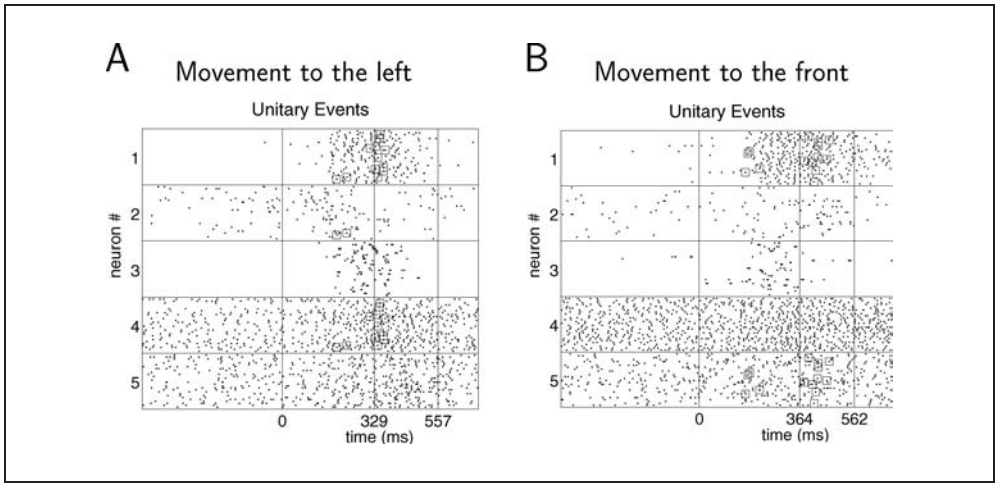

Fig. 5 Task dependence of the composition of coincident spiking activity. The dot displays show the spiking activity of five simultaneously recorded neurons (labeled 1 to 5) from the frontal cortex of a monkey involved in a delayed localization task (28 trials). (*A*) and (*B*) represent two different behavioral conditions: (*A*) movement to the left, (*B*) movement to the front. Unitary event analysis was performed in sliding windows of 60 ms, and with a significance level of $\alpha = 0.01$. Coincident events were detected in disjunct bins with a bin width of 3 ms. Data were taken from segments starting 500 ms before and ending 700 ms after the GO signal (vertical line at 0 ms). Average times of behavioral events (monkey leaves central key, monkey hits the target) are indicated by vertical lines. In (*A*) the monkey leaves the central key at 329 ms and hits the target at 557 ms after the GO signal, in (*B*) leave at 364 ms, and hit target at 562 ms. Unitary events (marked by squares) occur at about the time when the monkey leaves the center key, i. e. at different times in the two conditions. The composition of the correlated spiking activity differs in the two behavioral conditions: related to a movement to the left neuron 1 and 4 are correlated, and related to the movement to the front neuron 1 and 5 are correlated., i. e., neuron 1 seems to switch the partner neuron depending on the behavioral context. Figure modified after Grün et al. (2002 b).

movement direction, and analyzed each of these sub-sets separately. Figure 5 shows the analysis results for two movement directions (*A*: to the left; *B*: to the front); for the three other movement directions there was no significant activity. For each of the two movement directions, there is mainly one cluster of unitary events (besides some sparsely spread individual ones), occurring at the onset of the movement. The clusters of unitary events differ, however, both in their neuronal composition and in their timing. During movement to the left, significant coincidences occur between neurons 1 and 4, for movement to the front they occur between neurons 1 and 5. The timing of the unitary events differs. Both occur shortly after the monkey left the center key (equivalent to reaction time), which differs for the two movement directions (mean reaction time indicated by a line in A: 329 ms after the GO signal, in B: 364 ms after the GO-signal). Thus, unitary events appear to be locked better to the behavioral event than to the external event (GO). The analysis of the same five neurons during the localizing task, where the color of the GO-signal contained the information about the reinforced type of stimulus (data not shown) did not reveal any indications for unitary events related to movement direction. Note, that neuron 1 is participating in significant coincident activity in both movement

directions, however with another coincidence partner in each. This is indicative of a common membership of neuron 1 in two different cell assemblies, one of which is activated depending on the movement direction.

4.3 Changes of Temporal Precision as a Function of Time

In order to study the temporal aspects of neuronal activity during preparatory processes for arm movements, Rhesus monkeys were trained to perform a multi-directional pointing task (RIEHLE et al. 2000). The animal sat in a primate chair in front of a vertical

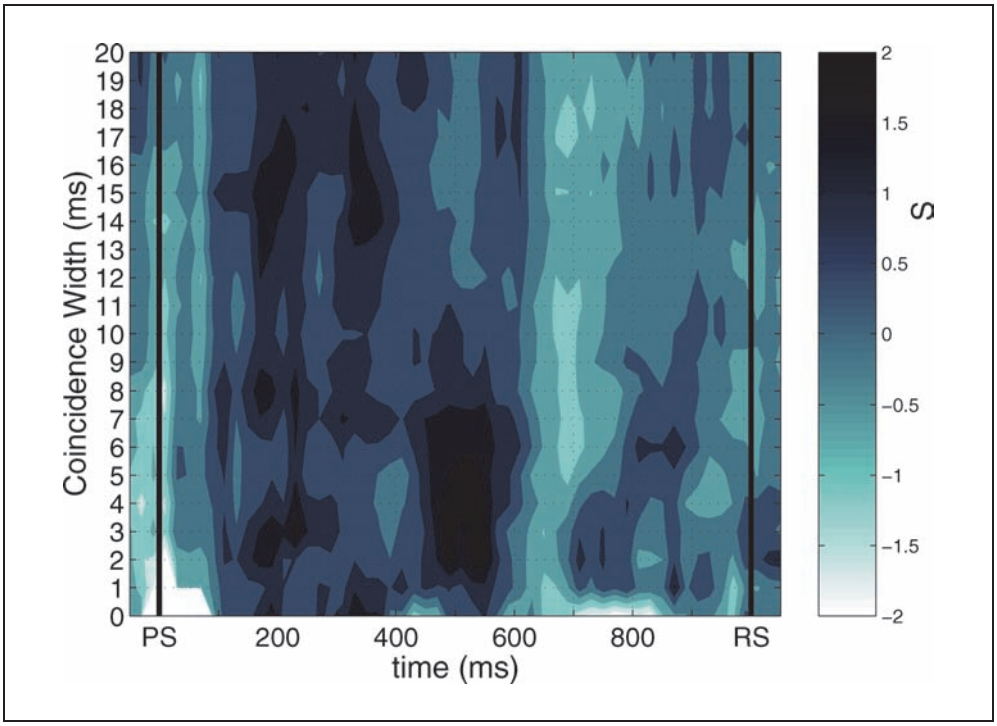

Fig. 6 Temporal precision of coincident spiking events as a function of time. Two simultaneously recorded neurons from a behaving monkey during performance of a delayed multi-directional pointing task. Recording site was primary motor cortex. With the preparatory signal (PS) the monkey was provided with prior information about the target position (1 out of 6; here: movement direction 4) where he had to point at after presentation of the response signal (RS). During the preparatory period (from PS to RS, fixed duration: 1000 ms) the monkey had to sit still, keep the initiating button pressed and the preparatory signal (illuminated in green) was still on. As it turned red it indicated the response signal. The same spike trains were analyzed for varying coincidence widths ranging from $b' = \pm 0 \ldots 20$ ms (vertical). For each coincidence width, the significance level (joint-surprise) was calculated separately. The gray code indicates the joint-surprise values, ranging from –2.19 (white) over 0 (light gray) to 2.42 (black). For symmetry, values were clipped at –2 and 2. The level of statistical significance was $\alpha = 0.05$ for excess coincidences, which corresponds to S = 1.27, correspondingly for lacking coincidences S = –1.27. For calculation of the joint-surprise as a function of time, a sliding window of 100 ms was shifted along the spike trains in steps of 20 ms. Significant coincidences only occurred during the first half of the preparatory period with increasing precision, reaching the strongest synchronicity value at 500 ms with a precision of 2–4 ms (black spot). Figure modified after RIEHLE et al. 2000.

panel on which seven touch sensitive light emitting diodes (LEDs) were mounted, one in the center and six placed equidistantly on a circle around it. In each trial, two signals were presented successively. The first, the preparatory signal (PS), provided prior information about the target which had to be pointed after the occurrence of the second, the response signal. First, the center target was lit and the animal had to press it for initiating the trial. Then, after a fixed delay of 500 ms, the preparatory signal was presented by illuminating one of the targets in green. After another delay (preparatory period), during which the animal still had to continue to press the center target, the color of the peripheral target turned red. This served as a response signal (RS) requesting from the animal to perform the movement to the indicated target. During performance of the task multiple single neurons were recorded and analyzed using the unitary event analysis. For analysis of the time course and modulation of synchronous activity, the joint-surprise values were obtained using the sliding window analysis. In order to observe the temporal precision of synchronous activity, and its potential change during the preparatory period, the allowed temporal precision of synchronous events was varied using the multiple shifts method (Grün et al. 1999).

The analysis of the data revealed two main results. First, synchronous spiking activity in motor cortex during preparation for action is not maintained at a significant level for more than 100–200 ms. Periods of synchrony, however, may occur several times during the trial, with a more or less regular (oscillatory) pattern. Second, for many pairs of neurons, the temporal precision of synchronicity changes over time (comparable to the example shown in Figure 6). If such changes occur, temporal precision typically increases during the preparatory period to be highest towards its end. One possible interpretation is that the increase of temporal precision of synchronous activity facilitates the efficiency of the motor output.

5. Conclusions

We have shown for a number of experimental data sets that several time scales seem to play a role in cortical processing. In order to detect unitary events, we differentiate rate (typically estimated on a time scale of tens to hundreds of ms), and temporal coordination of spiking activity typically on a ms time scale. If synchronous activity occurs more often than expected by chance given the rates, neurons are commonly involved in a fast and active dynamic process.

The temporal precision of significant synchronous activity is in the range of some few ms, an observation that was also found in spatio-temporal spike patterns or in cross-correlation analysis (e. g. Munk et al. 1995, Nowak et al. 1995, Prut et al. 1998). Theoretical work, where the propagation of aperiodic synchronous spiking activity in neural networks is studied, show that the temporal precision of synchronous activity is a function of the rise time of the membrane potential (Diesmann and Aertsen 2001), which is in the range of a few ms (e. g. Fetz et al. 1991). Other models explain the occurrence of synchronous activity in recurrent networks of oscillators. More theoretical studies are required that help to make the link between the connectivity and activity in the neuronal network. Both together define the functional connectivity, i. e. the relationship between neurons in terms of their activity, given the network structure.

The distinction between rate and synchronous activity also depends on the definition of the temporal precision of a synchronous event. If the "coincidence" width is rather in the range of tens or hundreds of ms, one would speak about spike rate correlation or spike count correlation. We found that there can be considerable rate covariation. However, interestingly, rate covariation may occur simultaneously but independent from spike synchronization (GRÜN et al. 2003).

If the expected number of coincidences is estimated on the basis of rate averages across non-stationary rates, the danger of falsely detecting coincident activity as significant is enhanced (GRÜN et al. 2002 b). Therefore, we introduced the sliding window procedure to account for the non-stationarity in firing rates of the neurons. Interestingly, this procedure helped us to uncover another phenomenon, indicating the dynamics of computational processes in time. Unitary events occur mostly only in short time windows, and are typically not constant throughout trial duration. They exhibit "loose locking" of synchronous activity to a trigger event, which does not necessarily correspond to an external behavioral trigger, but presumably rather to "internal" trigger events. Unitary events may be locked to purely internal events, as, e. g., the expectation of a signal (RIEHLE et al. 1997). Thus the timing structure of the modulation of synchronous activity is a reflection of the behavioral design in the experiment. However, also the opposite may be true: data from experiments in which no temporal structure is provided during the preparatory period may also show modulation of synchronous activity (RIEHLE et al. 2000). In the context of the given experiment this could be interpreted as internal "rehearsal".

Both time scales seem to be relevant for cortical processing. Measures derived for the different temporal scales seem to indicate context specific and complementary processes (RIEHLE et al. 1997). In the respective study we have shown, that in motor cortex internal processes seem to be reflected by synchronous activity on a fine temporal scale, whereas stimulus-related unitary events are accompanied by rate changes. However, it is not clear whether this can be generalized to all cortical areas. It is even suspected that the closer to the periphery, the stronger the "locking" to the external changes.

Another prominent activity structure in the cortex are oscillatory features of the signals. Depending on the state of the brain (sleep or awake etc.) there are differing dominant frequencies in mass signals like EEG or LPF. Single units do not obviously exhibit the same oscillatory behavior, and the question arises where does the oscillatory signal come about. There are studies that suggest (KÖRNER et al. 1999, SINGER 1999), that oscillations serve as a timing grid in order to structure the time axis to disentangle different computational processes. Thus, synchronous activity would be limited by the oscillatory period. We are currently studying the interaction of oscillatory activity and synchronous activity.

Acknowledgements

We thank Gordon PIPA and Stefan ROTTER for stimulating discussions. This report summarizes results from a number of ongoing collaborations, and extends an earlier review by part of the authors (AERTSEN et al. 2001). Partial funding was received from the *Deutsche Forschungsgemeinschaft* (*DFG*), the *Human Frontier Science Program* (*HFSP*), the *German-Israel Foundation for Research and Development* (*GIF*), and the *Volkswagen Foundation* (*VW*).

References

Abeles, M.: Local Cortical Circuits: An Electrophysiological Study. Studies of Brain Function. Berlin, Heidelberg, New York: Springer 1982 a

Abeles, M.: Role of cortical neuron: Integrator and coincidence detector? Israel J. Med. Sci. *18*, 83–92 (1982 b)

Abeles, M.: Corticonics: Neural Circuits of the Cerebral Cortex. 1st edn. Cambridge: Cambridge University Press 1991

Abeles, M., Bergman, H., Margalit, E., and Vaadia, E.: Spatiotemporal firing patterns in the frontal cortex of behaving monkeys. J. Neurophysiol. *70*, 1629–1638 (1993)

Abeles, M., and Goldstein, M. H.: Multispike train analysis. Proc. IEEE *65*, 762–773 (1977)

Adrian, E. D.: The Basis of Sensation. London: Christophers 1928

Aertsen, A., and Arndt, M.: Response synchronization in the visual cortex. Curr. Opin. Neurobiol. *3*, 586–594 (1993)

Aertsen, A., Diesmann, M., Gewaltig, M. O., Grün, S., and Rotter, S.: Neural dynamics in cortical networks – precision of joint-spiking events. In: Complexity in Biological Information Processing. Vol. 239 of Novartis Foundation Symposium; pp. 193–204. Chichester: Wiley 2001

Aertsen, A., Gerstein, G., Habib, M., and Palm, G.: Dynamics of neuronal firing correlation: Modulation of 'effective connectivity'. J. Neurophysiol. *61*, 900–917 (1989)

Aertsen, A., Vaadia, E., Abeles, M., Ahissar, E., Bergman, H., Karmon, B., Lavner, Y., Margalit, E., Nelken, I., and Rotter, S.: Neural interactions in the frontal cortex of a behaving monkey: signs of dependence on stimulus context and behavioral state. J. Hirnf. *32*, 735–743 (1991)

Ahissar, M. E. A., Bergman, H., and Vaadia, E.: Encoding of sound-source location and movement: activity of single neurons and interactions between adjacent neurons in the monkey auditory cortex. J. Neurophysiol. *67*, 203–215 (1992)

Amit, D. J.: Modeling Brain Function. Cambridge, New York: Cambridge University Press 1989

Amit, D. J., and Brunel, N.: Model of global spontaneous activity and local structured activity during delay periods in the cerebral cortex. Cereb. Cort. *7*, 237–252 (1997)

Barlow, H.: The biological role of neocortex. In: Aertsen, A., and Braitenberg, V. (Eds.): Information Processing in the Cortex; pp. 53–80. Berlin, Heidelberg, New York: Springer 1992

Barlow, H. B.: Single units and sensation: a neuron doctrine for perceptual psychology? Perception *1*, 371–394 (1972)

Bastian, A., Riehle, A., Erlhagen, W., and Schöner, G.: Prior information preshapes the population representation of movement direction in motor cortex. NeuroReport *9*, 315–319 (1998)

Braitenberg, V., and Schüz, A.: Anatomy of the Cortex: Statistics and Geometry. Berlin: Springer 1991

Bryant, H. L., and Segundo, J. P.: Spike initiation by transmembrane current: a white-noise analysis. Proc. R. Soc. Lond. B *194*, 211–223 (1976)

DeCharms, R. C., and Merzenich, M. M.: Primary cortical representation of sounds by the coordination of action-potential timing. Nature *381*, 610–613 (1996)

Diesmann, M., and Aertsen, A.: Parameter space of synfire activity. Breisach, Germany: Proc 6th Tamagawa Dynamic Brain Forum 2001

Diesmann, M., Gewaltig, M. O., and Aertsen, A.: Stable propagation of synchronous spiking in cortical neural networks. Nature *402*, 529–533 (1999)

Eccles, J. C.: The Physiology of Nerve Cells. Baltimore: Johns Hopkins Press 1957

Eckhorn, R., Bauer, R., Jordan, W., Brosch, M., Kruse, W., Munk, M., and Reitböck, H. J.: Coherent oscillations: A mechanism of feature linking in the visual cortex? Biol. Cybern. *60*, 121–130 (1988)

Eggermont, J. J.: Neural interaction in cat primary auditory cortex. II. Effects of sound stimulation. J. Neurophysiol. *71*, 246–270 (1992)

Engel, A. K., König, P., Schillen, T. B., and Singer, W.: Temporal coding in the visual cortex: new vistas on integration in the nervous system. TINS *15*, 218–226 (1992)

Fetz, E. E: Temporal coding in neural populations. Science *278*, 1901–1902 (1997)

Fetz, E. E., Toyama, K., and Smith, W.: Synaptic interactions between cortical neurons. In: Peters, A. (Ed): Cerebral Cortex. Vol. 9; pp. 1–47. New York: Plenum Publishing Corporation 1991

Georgopoulos, A. P., Kettner, R. E., and Schwartz, A. B.: Primate motor cortex and free arm movements to visual targets in three-dimensional space. II. Coding of the direction of movement by a neuronal population. J. Neurosci. *8*, 2928–2937 (1988)

Georgopoulos, A. P., Lurito, J. T., Petrides, M., Schwartz, A. B., and Massey, J. T.: Mental rotation of the neuronal population vector. Science *243*, 234–236 (1989)

Gerstein, G. L., Bedenbaugh, P., and Aertsen, A.: Neuronal assemblies. IEEE Trans. Biomed. Eng. *36*, 4–14 (1989)

Grammont, F., and Riehle, A.: Precise spike synchronization in monkey motor cortex involved in preparation for movement. Exp. Brain. Res. *128*, 118–122 (1999)

Gray, C. M., and Singer, W.: Stimulus-specific neuronal oscillations in orientation columns of cat visual cortex. Proc. Natl. Acad. Sci. USA *86*, 1698–1702 (1989)

Grün, S.: Unitary Joint-Events in Multiple-Neuron Spiking Activity: Detection, Significance, and Interpretation. Reihe Physik. Band 60. Thun, Frankfurt (Main): Harri Deutsch 1996

Grün, S., Diesmann, M., and Aertsen, A.: Unitary events in multiple single-neuron spiking activity: I. Detection and significance. Neural. Comp. *14*, 43–80 (2002 a)

Grün, S., Diesmann, M., and Aertsen, A.: Unitary Events in multiple single-neuron spiking activity. II. Nonstationary data. Neural. Comp. *14*, 81–119 (2002 b)

Grün, S., Diesmann, M., Grammont, F., Riehle, A., and Aertsen, A.: Detecting unitary events without discretization of time. J. Neurosci. Meth. *94*, 67–79 (1999)

Grün, S., Riehle, A., and Diesmann, M.: Effect of across trial non-stationarity on joint-spike events. Biol. Cybern. *88*(5), 335–351 (2003)

Gütig, R., Aertsen, A., and Rotter, S.: Statistical significance of coincident spikes: Count-based versus rate-based statistics. Neural. Comp. *14*, 121–253 (2002)

Hatsopoulos, N. G., Ojakangas, C. L., Paninski, L., and Donoghue, J. P.: Information about movement direction obtained from synchronous activity of motor cortical areas. Proc. Natl. Acad. Sci. USA *95*, 15706–15711 (1998)

Hebb, D. O.: Organization of Behavior. A Neurophysiological Theory. New York: John Wiley & Sons 1949

Hopfield, J. J.: Neural networks and physical systems with emergent collective computational abilities. Proc. Natl. Acad. Sci. USA *79*, 2554–2558 (1982)

Hubel, D. H., and Wiesel, T. N.: Receptive fields and functional architecture of monkey striate cortex. J. Neurophysiol. *195*, 215–243 (1968)

Körner, E., Gewaltig, M. O., Körner, U., Richter, A., and Rodemann, T.: A model of computation in neocortical architecture. Neural Networks *12* (7–8), 989–1005 (1999)

Laubach, M., Wessberg, J., and Nicolelis, M. A.: Cortical ensemble activity increasingly predicts behaviour outcomes during learning of a motor task. Nature *405*, 567–571 (2000)

Lettvin, J. Y., Maturana, H. R., McCulloch, W. S., and Pitts, W. R.: What the frog's eye tells the frog's brain. Proc. I R E *47*, 1940–1951 (1959)

Mainen, Z. F., and Sejnowski, T. J.: Reliability of spike timing in neocortical neurons. Science *268*, 1503–1506 (1995)

Malsburg, C. von der: The correlation theory of brain function. Internal report 81-2, Max Planck Institute for Biophysical Chemistry, Göttingen, FRG (1981)

Malsburg, C. von der: Am I thinking assemblies? In: Palm, G., and Aertsen, A. (Eds.): Brain Theory; pp. 161–176. Berlin: Springer 1986 a

Malsburg, C. von der: Frank Rosenblatt: Principles of neurodynamics: Perceptrons and the theory of brain mechanisms. In: Palm, G., and Aertsen, A. (Eds.): Brain Theory; pp. 245–248. Berlin: Springer-Verlag 1986 b

Martin, K. A. C.: A brief history of the "feature detector". Cereb. Cort. *4*, 1–7 (1994)

Martin, K. A. C.: The pope and grandmother – a frog's-eye view of theory. Nature Neurosci. *3*, 1169 (2000)

McCulloch, W. S., and Pitts, W.: A logical calculus of the ideas immanent in neural nets. Bull. Math. Biophys. *5*, 115–137 (1943)

Minsky, M. L., and Papert, S.: Perceptrons: An Introduction to Computational Geometry. Expanded edn. Cambridge, Massachusetts: MIT Press 1988

Munk, M. H., Nowak, L. G., Nelson, J. I., and Bullier, J.: Structural basis of cortical synchronization. II. Effects of cortical lesions. J. Neurophysiol. *74*, 2401–2414 (1995)

Murthy, V. N., and Fetz, E. E.: Coherent 25- to 35- Hz oscillations in the sensorimotor cortex of awake behaving monkeys. Proc. Natl. Acad. Sci. USA *89*, 5670–5674 (1992)

Nicolelis, M. A. L., Baccala, L. A., Lin, R. C. S., and Chapin, J. K.: Sensorimotor encoding by synchronous neural assembly activity at multiple levels in the somatosensory system. Science *268*, 1353–1358 (1995)

Nowak, L. G., Munk, M. H., Nelson, J. I., James, A., and Bullier, J.: Structural basis of cortical synchronization. I. Three types of interhemispheric coupling. J. Neurophysiol. *74*, 2379–2400 (1995)

Palm, G.: Evidence, information and surprise. Biol. Cybern. *42*, 57–68 (1981)

Palm, G.: Cell assemblies as a guideline for brain research. Conc. Neurosci. *1*, 133–148 (1990)

Pauluis, Q., and Baker, S. N.: An accurate measure of the instantaneous discharge probability, with application to unitary joint-event analysis. Neural. Comp. *12*, 647–669 (2000)

Prut, Y., Vaadia, E., Bergman, H., Haalman, I., Slovin, H., and Abeles, M.: Spatiotemporal structure of cortical activity: Properties and behavioral relevance. J. Neurophysiol. *79*, 2857–2874 (1998)

Riehle, A., Grammont, F., Diesmann, M., and Grün, S.: Dynamical changes and temporal precision of synchronized spiking activity in monkey motor cortex during movement preparation. J. Physiol. (Paris) *94*, 569–582 (2000)

Riehle, A., Grün, S., Diesmann, M., and Aertsen, A.: Spike synchronization and rate modulation differentially involved in motor cortical function. Science *278*, 1950–1953 (1997)

Roelfsema, P., Engel, A., König, P., and Singer, W.: The role of neuronal synchronization in response selection: A biologically plausible theory of structured representations in the visual cortex. J. Cogn. Neurosci. *8*, 603–625 (1996)

Roy, A., Steinmetz, P. N., and Niebur, E.: Rate limitations of unitary event analysis. Neural. Comp. *12*, 2063–2082 (2000)

Rummelhart, D. E., McClelland, J. L., and *the PDP Research Group*: Parallel Distributed Processing, Explorations in the Microstructure of Cognition: Foundations. Vol. 1. Cambridge, Massachusetts: MIT Press 1986

Sakurai, Y.: Population coding by cell assemblies – what it really is in the brain. Neurosci. Res. *26*, 1–16 (1996)

Sanes, J. N., and Donoghue, J. P.: Oscillations in local field potentials of the primate motor cortex during voluntary movement. Proc. Natl. Acad. Sci. USA *90*, 4470–4474 (1993)

Shadlen, M. N., and Newsome, W. T.: The variable discharge of cortical neurons: Implications for connectivity, computation, and information coding. J. Neurosci. *18*, 3870–3896 (1998)

Sherrington, C. S.: Integrative Action of the Nervous System. New Haven: Yale University Press 1906

Singer, W.: Synchronization of cortical activity and its putative role in information processing and learning. Annu. Rev. Physiol. *55*, 349–374 (1993)

Singer, W.: Striving for coherence. Nature *397*, 391–393 (1999)

Singer, W.: Neural synchrony: a versatile code for the definition of relations. Neuron *24*, 49–65 (1999)

Singer, W., Engel, A. K., Kreiter, A. K., Munk, M. H. J., Neuenschwander, S., and Roelfsema, P. R.: Neuronal assemblies: necessity, signature and detectability. TICS *1*, 252–261 (1997)

Singer, W., and Gray, C.: Visual feature integration and the temporal correlation hypothesis. Annu. Rev. Neurosci. *18*, 555–586 (1995)

Steinmetz, P., Roy, A., Fitzgerald, P., Hsiao, S., Johnson, K., and Niebur, E.: Attention modulates synchronized neuronal firing in primate somatosensory cortex. Nature *404*, 187–190 (2000)

Vaadia, E., Ahissar, E., Bergman, H., and Lavner, Y.: Correlated activity of neurons: A neural code for higher brain functions? In: Krüger, J. (Ed.): Neuronal Cooperativity; pp 249–279. Berlin: Springer 1991

Vaadia, E., Bergman, H., and Abeles, M.: Neuronal activities related to higher brain functions – theoretical and experimental implications. IEEE Trans. Biomed. Eng. *36*, 25–35 (1989)

Vaadia, E., Haalman, I., Abeles, M., Bergman, H., Prut, Y., Slovin, H., and Aertsen, A.: Dynamics of neuronal interactions in monkey cortex in relation to behavioural events. Nature *373*, 515–518 (1995)

Dr. Sonja Grün
Free University Berlin
Institute for Biology
Neurobiology
Königin Luise Str. 28/30
14195 Berlin
Germany
Phone: ++49 (0) 30 83 85 66 35
Fax: ++49 (0) 30 83 85 54 55
E-Mail: gruen@neurobiologie.fu-berlin.de

Nova Acta Leopoldina NF *88*, Nr. 332, 207–224 (2003)

Development of Bipolar Deep Brain Stimulation Techniques Based on Stochastic Phase Resetting

Peter A. Tass (Jülich)

With 5 Figures

Abstract

This paper is devoted to the desynchronizing effects of bipolar stimuli on a synchronized cluster of globally coupled phase oscillators. The bipolar pulses considered here are symmetrical and consist of a positive and a negative monopolar pulse. A bipolar single pulse with the right intensity and duration desynchronizes a synchronized cluster provided the stimulus is administered at a vulnerable initial phase of the cluster's order parameter. A considerably more effective desynchronization is achieved with a bipolar double pulse consisting of two qualitatively different bipolar pulses. The first bipolar pulse is stronger and resets the cluster, so that the second bipolar pulse, which follows after a constant delay, hits the cluster in a vulnerable state and desynchronizes it. A bipolar double pulse desynchronizes the cluster independently of the cluster's dynamical state at the beginning of the stimulation. The dynamics of the order parameter during a bipolar single pulse or a bipolar double pulse is different from the dynamics during a monopolar single pulse or a monopolar double pulse. Nevertheless, concerning their desynchronizing effects the monopolar and the bipolar stimuli are comparable, respectively. This is significant for applications where bipolar stimulation is required. For example, in medicine and physiology charge-balanced stimulation is typically necessary in order to avoid tissue damage. Based on the results presented here, demand-controlled bipolar double pulse stimulation is suggested as a milder and more efficient therapy compared to the standard permanent high-frequency deep brain stimulation in neurological patients.

Zusammenfassung

Im vorliegenden Artikel werden desynchronisierende Effekte bipolarer Stimuli auf synchronisierte Cluster global gekoppelter Phasenoszillatoren untersucht. Die dabei betrachteten bipolaren Pulse sind symmetrisch und bestehen aus einem positiven und einem negativen monopolaren Puls. Ein bipolarer Puls der richtigen Intensität und Dauer desynchronisiert ein synchronisiertes Cluster, vorausgesetzt dieser Reiz wird in einer vulnerablen Phase des Ordnungsparameters appliziert. Eine wesentlich effektivere Desynchronisation läßt sich mit einem bipolaren Doppelpuls erzielen. Letzterer besteht aus zwei qualitativ unterschiedlichen Einzelpulsen: Der erste bipolare Puls ist stärker und führt zu einem Reset, d. h. einem stereotypen Neustart, des Clusters. Der zweite Puls wird mit einer konstanten Zeitverzögerung appliziert und trifft das Cluster verläßlich in einem vulnerablen Zustand. Ein bipolarer Doppelpuls dieser Art entfaltet seine desynchronisierende Wirkung unabhängig von den Anfangsbedingungen, also unabhängig vom dynamischen Zustand des Clusters zu Beginn der Stimulation. Die Dynamik des Ordnungsparameters während eines bipolaren Einzelpulses oder eines bipolaren Doppelpulses ist qualitativ von der Dynamik während eines monopolaren Einzelpulses oder eines monopolaren Doppelpulses verschieden. Dessen ungeachtet sind die bipolaren Reize bezüglich ihrer desynchronisierenden Wirkung jeweils mit ihren monopolaren Pendants vergleichbar. Dies ist für alle die Anwendungen relevant, bei denen bipolare Stimuli benötigt werden. Zum Beispiel in der Medizin und in der Physiologie werden typischerweise Reize verwendet, deren Netto-Ladungseintrag in das

Gewebe gleich Null ist. Aufbauend auf den hier vorgestellten theoretischen Ergebnissen wird eine bedarfsgesteuerte bipolare Doppelpuls-Tiefenhirnstimulation als mildere und effektivere Therapie und somit als Alternative zur standardmäßig verwendeten Hochfrequenz-Tiefenstimulation bei neurologischen Patienten vorgeschlagen.

1. Introduction

Synchronization processes are abundant in physics (Haken 1983, Pikovsky et al. 2001), chemistry (Kuramoto 1984), biology (Winfree 1980, Glass and Mackey 1988, Steriade et al. 1990, Neiman et al. 1999), and medicine (Volkmann et al. 1996, Bergman et al. 1998). Stimulation is a major experimental tool that is used for investigating and manipulating dynamical processes (Winfree 1980, Haken 1983, Kuramoto 1984, Glass and Mackey 1988, Steriade et al. 1990, Volkmann et al. 1996, Bergman et al. 1998, Neiman et al. 1999, Pikovsky et al. 2001). To study desynchronizing effects of pulsatile stimuli, the concept of phase resetting (Winfree 1980, Glass and Mackey 1988) was extended to populations of non-interacting (Tass 1996 a, b) and interacting (Tass 1999, 2000) oscillators subjected to random forces. For this, limit cycle oscillators are approximated by phase oscillators (Kuramoto 1984), and desynchronization is caused by stimuli that exclusively affect the phases of the oscillators.

A single pulse of the right intensity and duration desynchronizes a fully synchronized cluster of oscillators if the pulse hits the cluster in a vulnerable phase range which corresponds to only a small fraction (5 % or even less) of a period of the oscillation (Tass 1999). However, this is tricky to realize under noisy experimental conditions typically encountered in biological systems. What makes single pulse stimulation even less practicable is that the correct stimulation parameters also depend on the extent of the synchronization of a cluster: A weaker pulse has to be used to desynchronize a weakly synchronized cluster, whereas a stronger pulse is necessary for the desynchronization of a cluster that is in its fully synchronized state. Moreover, not only the strength (i. e. intensity and duration) but also the critical phase at which a pulse has to be administered crucially depends on the extent of synchronization of the cluster (Tass 1999, 2001 a).

For this reason, a double-pulse stimulation technique has been developed which makes it possible to effectively desynchronize a cluster of phase oscillators independently of the cluster's dynamic state at the beginning of the stimulation (Tass 2001 a, c). The double pulse consists of two qualitatively different stimuli: The first, stronger pulse resets the cluster, so that after the first pulse the cluster restarts in a stereotyped way. The second, weaker pulse is administered after a fixed delay and hits the cluster in a vulnerable state in order to cause a desynchronization. Instead of the first, strong pulse, alternatively, a high-frequency pulse train (Tass 2001 b) or a low-frequency pulse train (Tass 2002 a) can be used to reset the cluster (for a review see Tass 2002 b).

As yet, in all of these theoretical studies the effects of monopolar pulses were investigated (Tass 1996 a, b, 1999, 2000, 2001 a, b, c, 2002 a, b). In the context of electrical stimulation, a monopolar pulse corresponds to a pulsatile current injection *via* an electrode. In applications to biological systems, however, it is often necessary to use charge-balanced pulses which guarantee that on average the stimulated tissue is not charged, so that tissue damage can be avoided (Steriade et al. 1990, Benabid et al. 1991, Blond et al. 1992). A

charge-balanced stimulation is typically achieved either (*i*) by means of capacitor driven electronic circuits which control the stimulation in a way that after a monopolar pulse the injected charge smoothly flows back, or (*ii*) by means of bipolar pulses, which consist of two opposite monopolar pulses during which on average there is no net current flow (Steriade et al. 1990, Benabid et al. 1991, Blond et al. 1992).

This article is devoted to the desynchronizing effects of bipolar single pulse and bipolar double pulse stimulation on a cluster of globally coupled phase oscillators in the presence of noise. The transient dynamics occurring during administration of the bipolar stimuli are compared with the transients related to the monopolar variants. Finally, it will be discussed how to use the results presented here for the model-based development of demand-controlled deep brain stimulation techniques, which essentially require the use of charge-balanced stimuli. The results presented in this article have been published recently in Tass (2002 c).

2. Model

Along the lines of a first approximation the dynamics of a population of neurons can be modeled by means of a network of phase oscillators (Kuramoto 1984, Ermentrout and Kopell 1991, Grannan et al. 1993, Hansel et al. 1993). This approach was extensively used, in particular, for investigating spontaneous synchronization processes in populations of oscillatory neurons (Kuramoto 1984, Ermentrout and Kopell 1991, Grannan et al. 1993, Hansel et al. 1993). To study stimulus-induced transient dynamics we consider a cluster of coupled phase oscillators subjected to a stimulus S and to random forces, which is governed by the Langevin equation

$$\frac{d\psi_j}{dt} = \Omega + \frac{1}{N}\sum_{k=1}^{N} \Gamma(\psi_j - \psi_k) + F_j(t) \qquad [1]$$

where ψ_j denotes the phase of the *j*th oscillator, i. e. the *j*th model neuron (Tass 1999). For the sake of simplicity all oscillators are assumed to have the same eigenfrequency: ω_j = O. The global coupling is a 2π periodic function. For the time being we consider a simple sine coupling of the form

$$\Gamma(\psi_j - \psi_k) = -K \sin(\psi_j - \psi_k) \qquad [2]$$

where K is a nonnegative coupling constant. This type of coupling is sufficient to explain the basic desynchronization mechanism employed by the bipolar stimulation technique suggested here. The impact of both, cosine couplings like $\cos(\psi_j - \psi_k)$ and coupling terms of second and higher order such as $\sin[2(\psi_j - \psi_k)]$, $\sin[3(\psi_j - \psi_k)]$ has already been analyzed in detail in the context of monopolar stimulation techniques (Tass 1999, 2001 c) and will be discussed below.

The impact of an electrical stimulus on a single neuron depends on the phase of the neuron at which the stimulus is administered (Best 1979, Guttman et al. 1980). Accordingly, the stimulus is modeled by a 2π periodic, explicitly time independent function $S(\psi_j) = S(\psi_j + 2\pi)$. First, we assume that the stimulus is of lowest order and defined by

$$S(\psi_j) = I \cos(\psi_j) \qquad [3]$$

where I is a constant intensity parameter. The effect of more complex stimuli S, e. g., containing higher order terms like $\cos(2\psi_j)$ and $\sin(2\psi_j)$, has already been investigated in monopolar stimulation techniques (Tass 1999, 2001 c) and will be discussed below. Administration of a **monopolar single pulse** is modeled by

$$X(t) = 1 \text{ if stimulus is on at time } t,\ X(t) = 0 \text{ if stimulus is off at time } t \qquad [4]$$

(Fig. 1 *A*).

In contrast, a symmetrical bipolar single pulse consists of a positive monopolar single pulse and a directly following negative monopolar single pulse, which will briefly be denoted as positive and negative pulse below (Fig. 1 *B*). The parameters of the positive and the negative pulse are identical with respect to all parameters except for the sign of X. In particular, positive and negative pulses have identical intensity I and duration. The duration of the positive and the negative pulse will be denoted as $T/2$, so that the duration of the bipolar single pulse is given by T. Accordingly, the administration of a **symmetrical bipolar single pulse** is modeled by

$$\begin{aligned} &X(t) = 1 \text{ if positive pulse is on at time } t, \\ &X(t) = -1 \text{ if negative pulse is on at time } t, \\ &X(t) = 0 \text{ if stimulus is off at time } t. \end{aligned} \qquad [5]$$

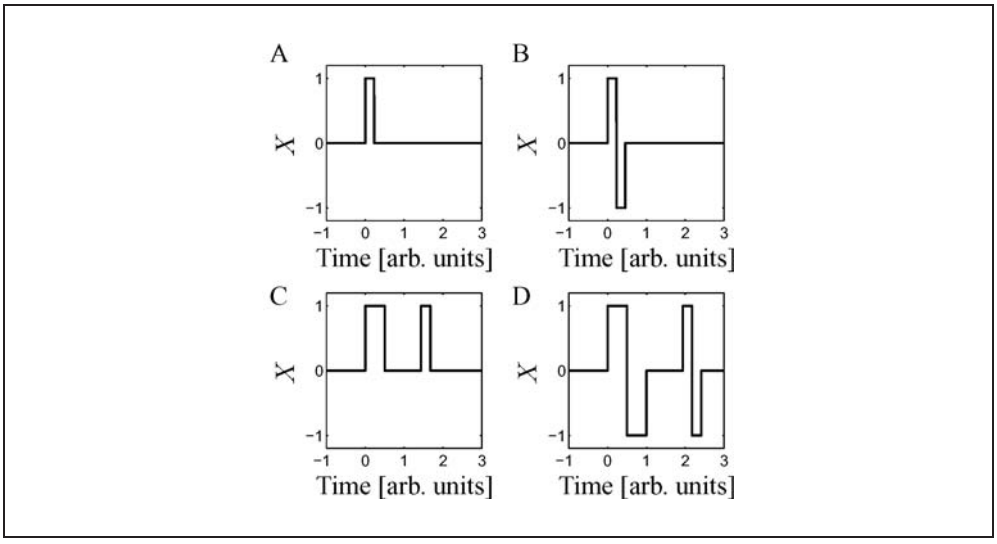

Fig. 1 Time course of X from Equation [4] and Equation [5] during a monopolar single pulse (*A*) (see Equation [4]), during a symmetrical bipolar single pulse (*B*) (see Equation [5]), during a monopolar double pulse (*C*) (see Equation [4]), and during a symmetrical bipolar double pulse (*D*) (see Equation [5]). A symmetrical bipolar single pulse consists of a positive and a directly following negative single pulse (*B*). The positive and the negative pulse are identical with respect to all parameters except for the sign of X. A symmetrical double pulse consists of two symmetrical bipolar single pulses (*D*): The first bipolar single pulse is stronger (i. e. it is longer and has a higher intensity I from Equation [3] and resets the cluster. The second bipolar single pulse follows after a constant delay, is weaker and desynchronizes the cluster by hitting it in a vulnerable state.

In an experimental application a symmetrical bipolar single pulse would guarantee a charge-balanced stimulation. The random forces $F_j(t)$ are modeled by Gaussian white noise which obeys $\langle F_j(t)\rangle = 0$ and $\langle F_j(t)\, F_k(t')\rangle = D\delta_{jk}\delta(t-t')$ with constant noise amplitude D.

To study the dynamics of Equation [1] we first derive the corresponding Fokker-Planck equation which is an evolution equation for the probability density $f(\{\psi_1\}, t)$, where $\{\psi_1\}$ stands for the vector $(\psi_1, \ldots, \psi_N)$. $f(\{\psi_1\}, t)\, d\psi_1 \ldots d\psi_N$ gives the probability of finding the oscillators' phases in the intervals $[\psi_k, \psi_k + d\psi_k]$. In order to simplify the analysis we turn to a more macroscopic level of description by introducing the average number density $n(\psi, t)$ according to

$$n(\psi,t) = \langle n'(\{\psi_l\};\, \psi)\rangle = \int_0^{2\pi} \ldots \int_0^{2\pi} d\psi_1 \ldots d\psi_N n'(\{\psi_l\};\, \psi)\, f(\{\psi_l\}, t) \qquad [6]$$

where the number density is defined by $n'(\{\psi_l\};\, \psi) = \frac{1}{N}\sum_{k=1}^{N}\delta(\psi - \psi_k)$ (Kuramoto 1984). The probability density $f(\{\psi_1\}, t)$ provides us with information concerning the phase of each single oscillator. In contrast, $n(\psi, t)$ tells us how many oscillators of the whole population most probably have phase ψ at time t.

With a little calculation we finally obtain the evolution equation for the average number density

$$\frac{\partial n(\psi,t)}{\partial t} = -\frac{\partial}{\partial \psi}\left\{ n(\psi,t) \int_0^{2\pi} d\psi'\, \Gamma(\psi - \psi')\, n(\psi', t) \right\} - \frac{\partial}{\partial \psi} n(\psi,t)\, X(t)\, S(\psi) - \Omega \frac{\partial}{\partial \psi} n(\psi,t) + \frac{D}{2}\frac{\partial^2 n(\psi,t)}{\partial \psi^2} \qquad [7]$$

which holds for large N (Tass 1999). For the numerical investigation the Fourier transformed model equation [7] was integrated with a 4th order Runge-Kutta algorithm with a time step of 0.0001, where Fourier modes with wave numbers $|k| = 200$ were taken into account. For a detailed analytical and numerical investigation of Equation [7] I refer to Tass (1999).

3. Spontaneously Emerging Synchrony

The time-dependent extent of in-phase synchronization is quantified with

$$Z(t) = R(t)\exp[i\varphi(t)] = \int_0^{2\pi} n(\psi,t)\exp(i\psi)\, d\psi \qquad [8]$$

where $R(t)$ and $\phi(t)$ are the real amplitude and the real phase of Z, respectively (Aizawa 1976, Kuramoto 1984). Because of the normalization condition $\int_0^{2\pi} n(\psi,t)\, d\psi = 1$, the amplitude fulfills $0 = R(t) = 1$ for all times t. Perfect in-phase synchronization corresponds to $R = 1$, whereas an incoherent state, given by $n(\psi, t) = 1/(2\pi)$, is related to $R = 0$. Z(t) corresponds to the center of mass of $n(\psi, t)\, \exp(i\psi)$, the average number density circularly aligned in the Gaussian plane (Fig. 2).

To study the impact of stimulation, first, the cluster's behavior without stimulation (i. e. $X(t) = 0$ in Equation [4] and Equation [5]) has to be clarified. Let us assume that the coupling is given by Equation [2]. Noisy in-phase synchronization emerges out of the incoherent state $n(\psi, t) = 1/(2\pi)$ due to a decrease of the noise amplitude D (KURAMOTO 1984) or, analogously, because of an increase of the coupling strength (TASS 1999). When K exceeds its critical value $K^{crit} = D$, Z from Equation [8] becomes an order parameter (HAKEN 1983) which governs the dynamics of the other, infinitely many stable modes (i. e. frequency components) on the center manifold. In this way a stable limit cycle $Z(t) = Y \exp[i(\Omega + \Omega')\, t\}$ evolves for $K > D$, where Y is a complex constant, and Ω' is a real frequency shift term that depends on model parameters and vanishes if the coupling Γ contains no cosine terms, as in Equations [2] (TASS 1999).

The cluster's collective dynamics will not only be visualized with the order parameter Z, but also by considering the collective firing. A single firing/bursting model neuron fires/bursts whenever its phase vanishes (modulo 2π). Accordingly, the cluster's collective firing is given by the firing density

$$p(t) = n(0, t) \qquad [9]$$

which corresponds to quantities registered in neurophysiological experiments such as multiunit activity (MUA), local field potentials (LFP), and magnetic or electric fields measured with magnetoencephalography (MEG) or electroencephalography (EEG).

4. Single Pulse

4.1 Monopolar Single Pulse

Let us first consider the cluster's dynamics during a single monopolar pulse (TASS 1996 a, TASS 1999). During the monopolar pulse $X(t) = 1$, and S from Equation [3] is constant in time. If the stimulus S is sufficiently strong (i. e., its intensity parameter I is large enough) with respect to the coupling strength, $n(\psi, t)$ tends to a stationary density $n^{stat}(\psi)$ for $t \to \infty$. The latter is the attractor of Equation [7], independently of the initial state $n(\psi, 0)$ at which the stimulation starts (TASS 1999). Correspondingly, the order parameter Z from Equation [8] is attracted by

$$Z^{stat} = \int_0^{2\pi} n^{stat}(\psi) \exp(i\psi)\, d\psi \qquad [10]$$

where t_B and t_E stand for the time of stimulus onset and stimulus end, and $\phi_B = \phi(t_B)$ denotes the initial phase at which the stimulus is administered. In Figure 2 *A* the collective dynamics of the cluster is visualized by plotting the trajectory of Z in the Gaussian plane, where f_B is varied within one cycle $[0, 2\pi]$. A desynchronized state corresponds to $Z = 0$. Thus, to desynchronize the synchronized cluster, the single pulse has to be administered at a critical (vulnerable) initial phase and it has to be turned off as soon as Z reaches the origin of the Gaussian plane (Fig. 2 *B*). The desynchronized state is unstable. Therefore after the desynchronizing stimulation Z spirals back to its stable limit cycle, so that the cluster becomes synchronized again (Fig. 2 *C*).

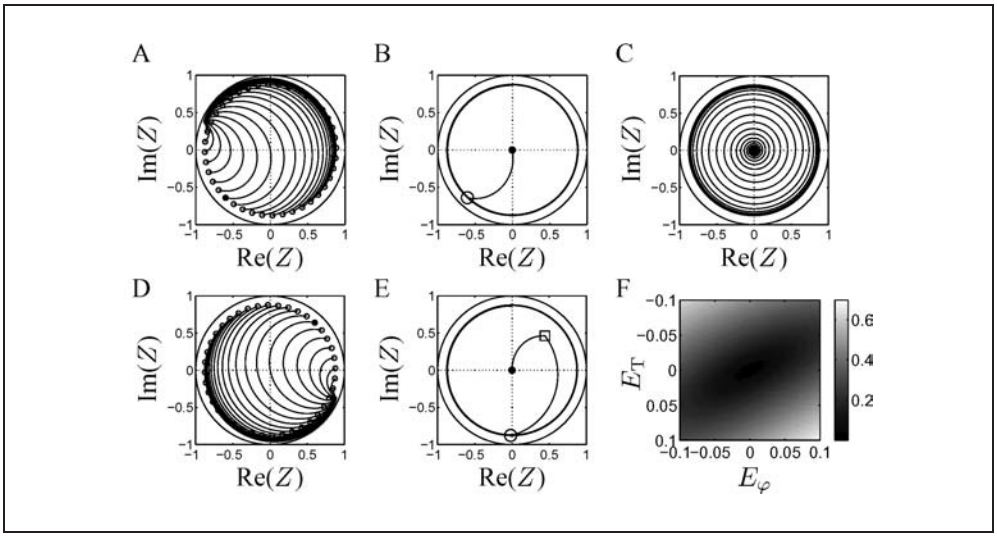

Fig. 2 Trajectory of the order parameter Z from Equation [8] in the Gaussian plane during and after a monopolar single pulse [(*A*)–(*C*)] and during a bipolar single pulse [(*D*), (*E*)]. In (*A*)–(*E* the unit circle indicates the maximal range of |Z| monopolar single pulse: (*A*) Series of identical stimuli with $X(t)\ S(\psi) = I \cos \psi$ (with $I = 7$) administered at different initial phases f_B in the stable synchronized state ('o'). Z approaches its attractor Z_+^{stat} from Equation [10] for $t \to \infty$. Only the stimulus administered at the vulnerable initial phase ('●') moves Z through the origin. Trajectory of Z before and during (*B*) and after (*C*) a desynchronizing monopolar single pulse (parameters as in *A*): (*B*) After running on its stable limit cycle (inner circle) in counterclockwise direction, Z is moved by the pulse into the origin ($Z = 0$). Stimulation starts at 'o' and ends in '●'. (*C*) After the stimulation the cluster spontaneously spirals back to its stable limit cycle. Symmetrical bipolar single pulse: (*D*) Series of identical negative pulses with $X(t)\ S(\psi) = -I \cos \psi$ (with $I = 7$) administered at different initial phases ϕ_B in the stable synchronized state ('o'). For $t \to \infty$ Z approaches its attractor Z_-^{stat}. Only the trajectory starting in '●' runs through the origin. (*E*) Before the bipolar stimulation Z runs on its stable limit cycle (inner circle) in counterclockwise direction. The positive pulse starts in ('o') and moves Z halfway towards the attractor Z_+^{stat} belonging to the positive pulse shown in (*A*), so that at the end of the positive pulse Z is located in '□'. The directly following negative pulse starts in '□' and moves Z towards the attractor Z_-^{stat} of the negative pulse (*D*), so that at the end of the negative pulse Z is located in the origin of the Gaussian plane ('●'). (*F*) The ratio $r = R(t_E)/R(t_B)$ from Equation [13] is calculated for a series of stimulations where the normalized phase and amplitude error E_φ and E_T from Equation [11] and Equation [12] are varied between –0.1 and +0.1. Model parameters: (*A*)–(*F*) $\Gamma(x) = -\sin x$, $D = 0.4$, $\Omega = 2\pi$, $S(\psi) = I \cos \psi$, $I = 7$. Pulse duration $T = 0.31$ of the monopolar single pulse in (*B*), and $T = 0.46$ of the bipolar single pulse in (*E*).

4.2 Symmetrical Bipolar Single Pulse

A symmetrical bipolar single pulse consists of a positive and a directly following negative pulse which are identical with respect to all parameters except for the sign of X (Fig. 1*B*). From Equation [3] and Equation [5] it follows that during the positive pulse $X(t)\ S(\psi_j) = I \cos \psi_j$ holds, so that the Langevin Equation [1] reads $d\psi_j/dt = \Omega + N^{-1} \sum_{l=1}^{N} \Gamma(\psi_j - \psi_l) + I \cos \psi_j + F_j(t)$. In contrast, during the negative pulse $X(t)\ S(\psi_j) = -I \cos \psi_j = I(\cos \psi_j + \pi)$. With this and by applying the transformation $\varphi_j = \psi_j + \pi$ $(j = 1, \ldots, N)$ to Equation [1], $d\varphi_j/dt = \Omega + N^{-1} \sum_{l=1}^{N} \Gamma(\varphi_j - \varphi_l) + I \cos \varphi_j + F_j(t)$, which equals the Langevin equation belonging to the positive pulse.

Hence, except for a shift of all phases by π, the dynamics during a negative pulse is identical to the dynamics during a positive pulse.

This difference is illustrated by comparing Z's trajectories belonging to series of simulations where the same infinitely long positive pulse (Fig. 2 *A*) or the same infinitely long negative pulse (Fig. 2 *D*) is administered at different initial phases, respectively. Rotating the trajectories belonging to the positive pulse by p around the origin of the Gaussian plane yields the trajectories belonging to the negative pulse. Let us denote the attractor from Equation [10] of the infinitely long positive pulse by Z_+^{stat} (Fig. 2 *A*), and the attractor of the infinitely long negative pulse by Z_-^{stat} (Fig. 2 *D*). The two attractors have a phase difference of p, while their amplitudes are identical: $|Z_+^{stat}| = |Z_-^{stat}|$.

To desynchronize the cluster of oscillators with a bipolar single pulse, the stimulus has to be administered at the right initial phase, so that Z runs along a zigzag-like trajectory from the stable limit cycle into the origin of the Gaussian plane (Fig. 2 *E*): Before the bipolar stimulation Z runs on its stable limit cycle in counterclockwise direction. The positive pulse starts in ('o') and moves Z towards the attractor $Z_+^{stat}$of the positive pulse (Fig. 2 *A*). At the end of the positive pulse Z has been shifted halfway to $Z_+^{stat}$and is located in '□'. Due to the directly following negative pulse Z is abruptly shifted towards the attractor Z_-^{stat} of the negative pulse (Fig. 2 *D*), so that Z darts sideways. At the end of the negative pulse, Z is located directly in the origin of the Gaussian plane ('●'). After the bipolar single pulse the cluster resynchronizes (Fig. 2 *C*).

Figure 2 *F* demonstrates that for a given intensity parameter I correct values of the duration T and the initial phase φ_B have to be chosen in order to achieve a strong desynchronization. We denote the values of T and of φ_B which lead to a maximal desynchronization (i. e. $Z = 0$) by T_{crit} and φ_B^{crit}. With this we introduce the normalized phase error

$$E_\varphi = \frac{\varphi - \varphi_B^{crit}}{2\pi} \qquad [11]$$

and the normalized duration error

$$E_T = \frac{T - T_{crit}}{T_{crit}}. \qquad [12]$$

To estimate the extent of desynchronization we define

$$r = \frac{R(t_E)}{R(t_B)}, \qquad [13]$$

i. e. the ratio between the amplitude R of the order parameter at the end of the stimulation and R at the beginning of the stimulation. Figure 2 *F* shows how r depends on E_φ and E_T. Maximal desynchronization ($r = 0$) only occurs for vanishing E_φ and E_T. A strong desynchronization with $r = 0.2$ cannot occur for $|E_\varphi| > 0.05$ and $|E_T| > 0.05$.

5. Double Pulse

5.1 Monopolar Double Pulse

The monopolar double pulse consists of two monopolar single pulses separated by a pause (Fig. 1 *C*) (Tass 2001 a, c). The first pulse resets the cluster, whereas the second pulse causes a desynchronization as explained in Section 4.1. In the stable synchronized

state before the double pulse, Z runs on its limit cycle (Fig. 3 *B*). The first pulse is stronger compared to the second pulse, i. e., the first pulse is longer and/or has a larger intensity parameter I. Therefore during the first pulse Z is quickly attracted by the corresponding attractor Z_+^{stat} (Fig. 3 *A*, *B*). Independently of the initial dynamical state at which the first pulse is administered, at the end of the first pulse Z is sufficiently close to Z_+^{stat} (Fig. 3 *B*). During the pause between the first and the second pulse Z relaxes to its stable limit cycle in a stereotyped way (Fig. 3 *C*). The second pulse is administered at the right initial phase so that Z is moved into the origin of the Gaussian plane, the desynchronized state (Fig. 3 *C*). After the second pulse Z spirals back to its stable limit cycle as shown in Figure 2 *C*.

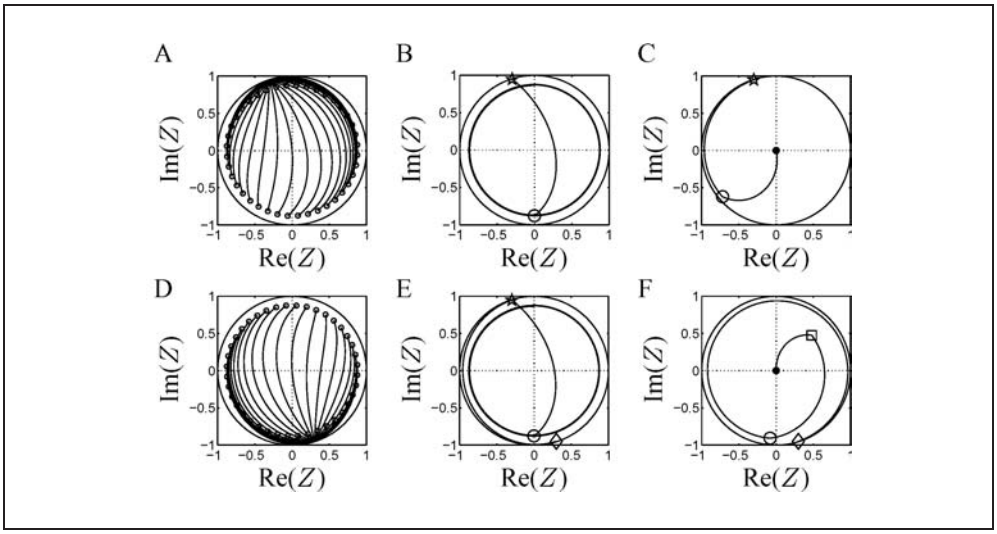

Fig. 3 Trajectories of Z from Equation [8] are plotted in the Gaussian plane (same format as in Fig. 2). **Monopolar single pulse:** (*A*) Series of identical positive pulses with $X(t)\ S(\psi) = I \cos \psi$ (with $I = 21$) administered at different initial phases ϕ_B in the stable synchronized state ('o'). (*D*) Series of identical negative pulses with $X(t)\ S(\psi) = -I \cos \psi$ (with $I = 21$) administered at different initial phases φ_B in the stable synchronized state ('o'). In both cases Z approaches the corresponding attractors Z_+^{stat} (*A*) and Z_-^{stat} (*D*) for $t \to \infty$. Compared to Figure 2 *A*, *D* the intensity I is larger here ($I = 21$ *versus* $I = 7$ in Fig. 2), so that a quick reset is achieved, i. e., Z reaches its attractor rapidly. A **monopolar double pulse** consists of a stronger, resetting monopolar single pulse (parameters as in *A*) and a weaker, desynchronizing monopolar single pulse (parameters as in Fig. 2 *A*). (*B*) Trajectory of Z before and during the first pulse of the double pulse. The first pulse is administered at 'o' and forces Z to the corresponding attractor Z_+^{stat} ('*'). (*C*) After the first pulse Z relaxes from the attractor towards its stable limit cycle. The second pulse of the monopolar double pulse starts at 'o' and moves Z into the origin ('●'). A **bipolar double pulse** consists of a stronger, resetting bipolar single pulse (parameters as in *A* and *D*) and a weaker, desynchronizing bipolar single pulse (parameters as in Fig. 2 *E*). (*E*) Trajectory of Z before and during the first bipolar pulse of the bipolar double pulse. Before the stimulation Z runs on its stable limit cycle (inner circle) in counterclockwise direction. The positive pulse is administered at 'o' and forces Z to its attractor Z_+^{stat} ('*'). The directly following negative pulse then moves Z to the attractor Z_-^{stat} ('◇'). (*F*) At the end of the first bipolar pulse Z is located sufficiently close to Z_-^{stat} ('◇'). During the pause between first and second bipolar pulse Z relaxes back to its stable limit cycle. The desynchronizing bipolar pulse (with parameters as in 2 *E*) moves Z along a zigzag-trajectory: The positive pulse starts in 'o' and moves Z to '□', the directly following negative pulse shifts Z into the origin ('●'). Model parameters: (*A*)–(*F*) $G(x) = -\sin x$, $D = 0.4$, $\Omega = 2\pi$, $S(\psi) = I \cos \psi$. $I = 21$ in (*A*), (*B*), (*D*), and (*E*). $I = 7$ in (C) and (*F*). Pulse duration $T = 0.5$ in (*B*), $T = 0.4$ in (*C*), $T = 1$ in (*E*), and $T = 0.48$ in (*F*).

5.2 Symmetrical Bipolar Double Pulse

The symmetrical bipolar double pulse consists of two bipolar single pulses separated by a pause (Fig. 1 *D*). Similar to the monopolar double pulse, the first bipolar single pulse performs a reset, whereas the second bipolar single pulse desynchronizes the cluster as explained in the former section. The first bipolar single pulse is stronger compared to the second bipolar single pulse, which means that the first bipolar single pulse is longer and/or has a larger intensity parameter *I*. Before stimulus administration Z runs on its stable limit cycle (Fig. 3 *E*). The first bipolar single pulse performs a **double reset**: Independently of Z's initial conditions, the resetting positive pulse shifts Z towards the corresponding attractor Z_+^{stat} (Fig. 3 *A*, *E*), in this way achieving a first reset. The directly following resetting negative pulse then moves Z towards the opposite attractor Z_-^{stat} (Fig. 3 *D*, *E*), so that Z undergoes a second reset. After this zigzag-like reset Z is sufficiently close to Z_-^{stat}, and Z consequently restarts in a stereotyped manner: During the pause between the first and the second bipolar single pulse Z tends to its stable limit cycle (Fig. 3 *F*). The second bipolar single pulse is administered after a constant delay and hits the cluster in a vulnerable state, so that a desynchronization is achieved as explained in Section 4.2. After the stimulation induced desynchronization the cluster resynchronizes: Z spirals back to its stable limit cycle (Fig. 2 *C*).

6. Vulnerability to Stimulation

Figure 4 shows how a bipolar single pulse and a bipolar double pulse affect a cluster in its stable synchronized state, where φ_B, the phase of the order parameter Z at the beginning of the stimulation, is varied within one cycle $[0\ 2\pi]$. We consider R, the amplitude of the order parameter and the firing density $p(t)$. The bipolar single pulse causes a desynchronization only provided it hits Z at or close to a vulnerable phase φ_B^{crit} (Fig. 4 *A*, *B*). In contrast, the bipolar double pulse causes a temporary desynchronization, no matter at which initial phase it is administered (Fig. 4 *C*, *D*).

7. Demand-controlled Desynchronization

The bipolar double pulse explained in Section 5.2 desynchronizes a cluster independently of its initial dynamic state. For this reason a bipolar double pulse can be used to effectively block the cluster's resynchronization. Whenever the cluster tends to resynchronize, the same bipolar double pulse is administered in order to prevent the cluster from resynchronization (Fig. 5). In this way an uncorrelated firing can be maintained. The larger the coupling strength K, the more often a bipolar double pulse has to be administered to cause a desynchronization.

8. Demand-controlled Deep Brain Stimulation

In several neurological diseases such as Parkinson's disease or essential tremor, brain function is severely impaired by pathological synchronization of neuronal firing. Parkin-

sonian resting tremor appears to be caused by a cluster of neurons located in the thalamus and the basal ganglia which fire synchronously at a frequency similar to that of the tremor (LLINÁS and JAHNSEN 1982, PARE et al. 1990, LENZ et al. 1994). For instance, in the anterior nucleus of the ventrolateral thalamus there are the so-called no-response cells which are neither modulated by somatosensory stimuli nor by active or passive

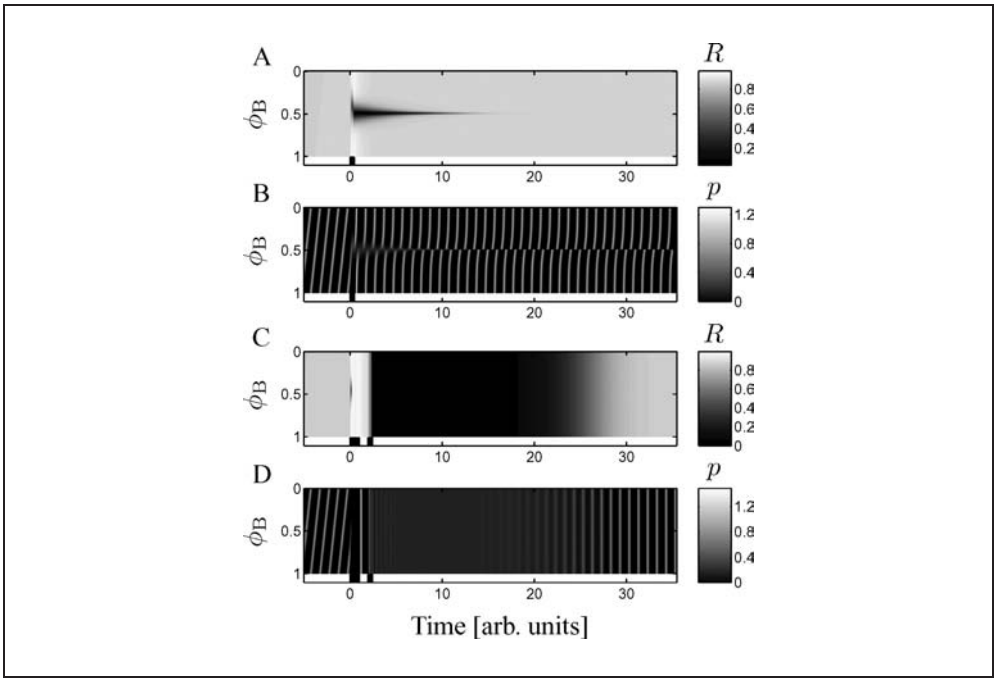

Fig. 4 Time course of the amplitude R of the order parameter from Equation [8] (A, C) and the firing density $p(t) = n(0, t)$ (B, D) before, during and after a bipolar single pulse (A, B) and a bipolar double pulse (C, D), where $\Phi_B = \varphi_B/(2\pi)$ mod1, the normalized phase of the order parameter Z at the beginning of the stimulation, is varied within one cycle. Stimulation starts at $t = 0$. At the bottom of each plot bipolar pulses are indicated by bars. In A, B and C, D same parameters as in Figures 2 E and 3 E, F respectively.

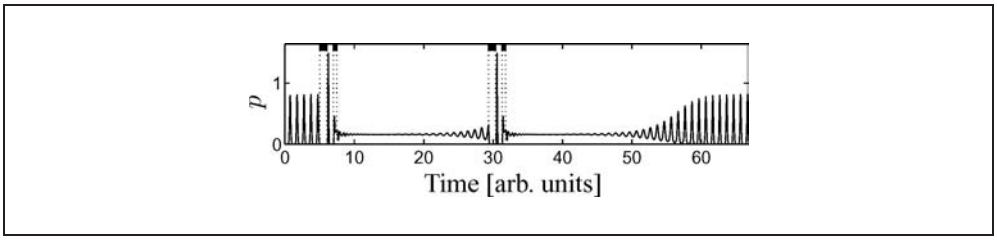

Fig. 5 Time course of the firing density $p(t) = n(0, t)$. Two successively administered bipolar double pulses with identical parameters are administered. The first one desynchronizes the cluster, whereas the second blocks the resynchronization. Model parameters as in Figure 4. Begin and end of bipolar pulses are indicated by dotted vertical lines connected by shaded regions at the top.

movements (Lenz et al. 1994). These cells fire rather periodically in an intrinsic manner, regardless of any feedback signals. In contrast, under physiological conditions the neurons in this cluster fire incoherently (Nini et al. 1995). In patients with Parkinson's disease (PD) this cluster acts like a pacemaker and activates premotor areas (premotor cortex and supplementary motor area) and the motor cortex (Alberts et al. 1969, Lamarre et al. 1971, Nini et al. 1995,Volkmann et al. 1996, Bergman et al. 1998), where the latter synchronize their oscillatory activity (Tass et al. 1998). Similarly, essential tremor also appears to be caused by a central cluster of synchronously firing neurons, which is located in different brain areas compared to PD (Elble and Koller 1990).

In patients with advanced PD or with essential tremor who do not respond to drug therapy any more, depth electrodes are chronically implanted in target areas like the thalamic ventralis intermedius nucleus or the subthalamic nucleus with millimeter precision (Benabid et al. 1991, Blond et al. 1992). Up to now, electrical deep brain stimulation (DBS) is performed by administering a permanent high-frequency (> 100 Hz) periodic pulse train *via* the depth electrodes. DBS at high frequencies suppresses the neuronal activity of the pacemaker-like cluster which, in turn, suppresses the peripheral tremor (Benabid et al. 1991, Blond et al. 1992).

High-frequency DBS has been developed empirically, mainly based on observations during stereotaxic surgery (Benabid et al. 1991, Blond et al. 1992). The mechanism by which DBS at high frequencies suppresses pathological rhythmic activity has not yet been clarified in detail. The permanent high-frequency stimulation basically mimics the effect of tissue lesioning by suppressing neuronal firing (Benabid et al. 1991, Blond et al. 1992, Wielepp et al. 2001). DBS is reversible and has a much lower rate of side effects than lesioning with thermocoagulation (Schuurman et al. 2000). However, permanent high-frequency stimulation is an unphysiological input which may cause an adaptation of the stimulated neuronal networks. This may be one of the reasons why in a number of patients the stimulation amplitude has to be increased in the course of the treatment in order to maintain a therapeutic effect. As a consequence of the increased stimulation strength, neighboring areas may be affected due to current spread, which leads to severe side effects like dysarthria, dysesthesia, and cerebellar ataxia.

For this reason a different therapeutic approach with mild and efficient stimulation techniques based on stochastic phase resetting (Tass 1999) has been suggested: Instead of simply suppressing the neuronal firing in the pacemaker-like cluster, the novel stimulation techniques aim at desynchronizing the pacemaker's pathologically synchronized firing in a demand-controlled way (Tass 2001 a, b, c, 2002 a, b). Accordingly, Equation [1] models the effect of stimulation on the pacemaker-like cluster. In other words, instead of stopping the driving force, I suggest to desynchronize it, so that it is no longer able to entrain other brain areas like premotor areas and the motor cortex.

Up to now in all modelling studies only monopolar pulses have been used (Tass 1996 a, b, 1999, 2000, 2001 a, b, c, 2002 a, b). The results presented here show that at least in a phase oscillator network bipolar pulses are equally suitable for the design of demand-controlled double-pulse stimulation. Based on these results and using a network of phase oscillators as a simple model for a neuronal population (Kuramoto 1984, Ermentrout and Kopell 1991, Grannan et al. 1993, Hansel et al. 1993). I suggest to try to use demand-controlled DBS for the therapy of neurological diseases, like Parkinson's disease or essential tremor. To this end, the depth electrode has to be

used for both stimulation and registration of the feedback signal, i. e. the local field potential (LFP), which in the model corresponds to the firing density p defined by Equation [9]. A desynchronizing bipolar double pulse is administered only and whenever the pacemaker-like cluster becomes synchronized, or put otherwise, whenever its LFP exceeds a critical value (Fig. 5). Note, that the first and the second bipolar single pulse of the bipolar double pulse are delivered to the same site. The goal of this approach is to effectively block the resynchronization and, hence, keep the firing as close to the physiological (i. e. uncorrelated) firing mode as possible. Instead of the LFP registered *via* the depth electrode one could alternatively use an epicortical electrode measuring the neuronal electrical activity in cortical areas (e. g., premotor areas or the motor cortex) which are sufficiently strongly synchronized with the target area stimulated *via* the depth electrode.

9. Discussion

In this study it was shown that a bipolar single pulse with the right intensity and duration desynchronizes a synchronized cluster of phase oscillators provided the stimulus is administered at a vulnerable initial phase φ_B^{crit} of the order parameter. Furthermore, it was shown that a bipolar double pulse consisting of a first, resetting and a second, desynchronizing bipolar pulse desynchronizes the cluster independently of the cluster's dynamical state at the beginning of the stimulation.

The dynamics of the order parameter Z during the bipolar single and double pulse stimulation is different from Z's dynamics during monopolar single and double pulse stimulation (Fig. 2 and 3). Nevertheless, with respect to their desynchronizing effects the monopolar and the bipolar stimuli are comparable. A bipolar single pulse desynchronizes only if it hits the cluster close to the vulnerable phase φ_B^{crit} (Fig. 2 *F* and 4 *A*, *B*). The same holds for a monopolar single pulse (Tass 1999). In contrast, a bipolar double pulse desynchronizes the cluster, regardless of the dynamical state at which it is administered (Fig. 4 *C*, *D*). Thus, a bipolar double pulse can be used to block the resynchronization effectively (Fig. 5). Again, the same is true for a monopolar double pulse.

The fact, that monopolar and bipolar stimuli are exchangeable concerning their desynchronizing effects, is important for all applications where bipolar stimulation is more favorable. For example, in medical and physiological applications charge-balanced stimulation is typically required in order to avoid tissue damage.

The reset attained by means of the first, stronger bipolar pulse of the bipolar double pulse guarantees that a desynchronization is caused independently of the initial dynamical state of the cluster (see Sections 5.2, 6 and 7). The first bipolar pulse shown in Figures 3–5 consists of a positive and a negative monopolar pulse which both are so strong, that they reset the cluster even when applied alone. Consequently, a reset is already achieved after the positive pulse, i. e., the order parameter Z is sufficiently close to the attractor Z_+^{stat} of the positive pulse ('*' in Fig. 3 *E*). In other words, during the first bipolar pulse the cluster undergoes a double reset: The first reset occurs at the end of the positive pulse, the second reset at the end of the negative pulse.

If in an experimental application such a strong reset cannot be performed or should be avoided in order to protect the stimulated system from damage, alternatively a resetting bipolar pulse with reduced strength (i. e. with reduced intensity I and/or duration T)

can be used. In this case both the positive and the negative pulse of the first bipolar single pulse alone perform only an imperfect reset, while the combination of the two is strong enough to reset reliably. Accordingly, after the positive pulse there is still a certain distance between Z and the attractor Z_+^{stat} of the positive pulse, and this distance depends on the initial dynamical sate at the beginning of the stimulation. Nevertheless, after the negative pulse Z is sufficiently close to the corresponding attractor Z_-^{stat} independently of the initial dynamical state. Hence, positive and negative pulse together reset the cluster in a stereotyped manner.

All bipolar single pulses used in this study have a (+, –)-structure, meaning that their first pulse is a positive pulse, whereas their second pulse is negative (Fig. 1). Instead of bipolar single pulses with a (+, –)-structure one can also use bipolar single pulses with a (–, +)-structure, where the first pulse is negative and the second pulse is positive. The exclusive use of stimuli that have a (–, +)-structure corresponds to replacing $X(t) \rightarrow -X(t)$ in Equation [5], which in turn is equivalent to the transformation $\varphi_j \rightarrow \varphi_j + \pi$ (see the reasoning in Section 4.2). Except for this transformation the dynamics of the cluster remains unchanged.

Interesting alternative options, however, ensue from mixing (+, –)- and (–, +)-stimuli. To illustrate this, let us again dwell on the dynamics of the order parameter Z during the bipolar double pulse (Fig. 3 *E*, *F*). After the first, resetting bipolar pulse Z is located in the attractor of the negative pulse Z_+^{stat}. During the pause between the first and the second bipolar pulse Z has to run through nearly one period before the desynchronizing, second bipolar pulse can be administered (Fig. 3 *F*). Such a long pause between the first and the second bipolar pulse may be a disadvantage in experimental applications, since this pause is a period of time where fluctuations or unforeseen external influences can alter the cluster's dynamical state in a way that the desynchronizing impact of the second bipolar pulse gets spoiled. To avoid such a long pause, we can replace the first bipolar pulse with (+, –)-structure by a (–, +)-bipolar pulse. Consequently, at the end of the first bipolar pulse Z is located in Z_+^{stat} ('*' in Fig. 3 *E*). During the pause between the first and the second bipolar pulse Z then runs through less than half a period before the second, desynchronizing (+, –)-bipolar pulse starts (in 'o' in Fig. 3 *E*). In this way the pause between the two bipolar stimuli is reduced by more than a factor of two. Furthermore, since Z then does no longer cross the positive x-axis during the pause, there is no strong burst of firing in between the two bipolar pulses any more (see Fig. 5). Obviously, the cluster's transient reaction during stimulation crucially depends on the pattern of consecutive (+, –)- and/or (–, +)-stimuli.

Characteristic dynamical features of monopolar stimuli are passed on to bipolar stimuli, because bipolar stimuli are combinations of consecutively administered monopolar stimuli. Let us consider the most important aspects.

The right stimulation parameters are reliably determined in an experimental application with calibration procedures that have been developed for the monopolar single pulse stimulation (Tass 1999) and the monopolar double pulse stimulation (Tass 2001 a, c). These procedures work in the same way for the bipolar stimulation techniques presented here: A series of test stimuli is administered. To extract a quantity that corresponds to the phase ϕ of the order parameter Z from Equation [8], the phase of the dominant Fourier mode is extracted out of the experimental data with bandpass filtering and Hilbert transform, and, finally, the correct parameters are obtained with phase resetting curves. The

Hilbert transform $\boldsymbol{S}_H$ of a signal s is generated by a filter which causes a phase shift of $\pi/2$ for all frequencies. Applying such a filter yields the instantaneous phase ψ and amplitude A of s according to $s(t) + \boldsymbol{S}_H(t) = A(t) \exp[i\psi(t)]$ (PANTER 1965).

The bipolar stimulation techniques presented in this article can also be used for desynchronizing cluster states, which are complex synchronized states, where a population of coupled oscillators breaks into distinct clusters, each consisting of phase-locked oscillators (SAKAGUCHI et al. 1987, STROGATZ and MIROLLO 1988, GOLOMB et al. 1992, HAKIM and RAPPEL 1992). Cluster states may even occur in networks of globally coupled oscillators (GOLOMB et al. 1992, HAKIM and RAPPEL 1992). In model Equation [1] noisy clustering may emerge due to coupling terms of higher order like $\Gamma(x) = -K_m \sin(mx)$ (with $K_m > 0$). Increasing K_m above its critical value mD causes an m-cluster state, which consists of m equidistant clusters, where all individual oscillators have the same frequency (TASS 1999). For example, increasing K_2 above its critical value $2D$ gives rise to a two-cluster state, where two clusters are synchronized in anti-phase. Synchronized states of this kind appear to be important in the context of neurological diseases (GOLOMB et al. 1996, TASS et al. 1998). For supercritical coupling $K_m > mD$, the order parameter is given by

$$Z_m(t) = \int_0^{2\pi} n(\psi, t) \exp(im\psi)\, d\psi \qquad [14]$$

(DAIDO 1992, TASS 1999). Note, that Z_1 is equivalent to the order parameter Z defined by Equation [8]. Z_m runs on a limit cycle and has to be desynchronized as illustrated in Figures 2 and 3. For monopolar stimulaton techniques it has already been shown that this is most effectively achieved with a stimulus S containing terms of m-th order, e. g., $S(\psi_j) = I \cos(m\psi_j)$ (TASS 1999, 2001 b, c, 2002 c). These results are also valid for bipolar stimuli, because the latter are made up of monopolar stimuli. Accordingly, also in the case of bipolar single pulse and bipolar double pulse stimulation, stimulation terms of m-th order are favorable for a quick and strong desynchronization.

In this study we considered a stimulus of first order, i. e. a stimulus $S(\psi_j)$ containing only terms with $\sin(\psi_j)$ and/or $\cos(\psi_j)$. Instead of the stimulus $S(\psi_j) = I \cos(\psi_j)$, defined by Equation [3], we can, alternatively, use the general form of a first-order stimulus: $S(\psi_j) = I \cos(\psi_j + \gamma)$ with constant γ. Such a stimulus leads to the same stimulation mechanisms as explained above. This can easily be seen by replacing ψ_j by $\psi_j + \gamma$ and using the same arguing as in Section 4.2.

Applying a stimulus which additionally contains terms of higher order, e. g., $S(\psi_j) = I_1 \cos(\psi_j + \gamma_1) + I_2 \cos(2\psi_j + \gamma_2)$ with constant parameters I_1, I_2, γ_1, γ_2, to the model investigated here, causes a desynchronization in terms of a quenching of the order parameter Z from Equation [8] in the same way as explained in Sections 4.2 and 5.2, provided that the right stimulation parameters are used. The additional stimulation term of second order, $I_2 \cos(2\psi_j + \gamma_2)$, however, gives rise to an excitation of the amplitudes of higher order terms Z_m from Equation [14], in particular, of Z_2 and Z_4, so that $|Z_2|$ and $|Z_4|$ are larger after the stimulation than before. During the transient after the stimulation the vanishing order parameter Z damps the excited modes Z_2 and Z_4, so that Z_2 and Z_4 quickly relax to zero, and the strongest uniform desynchronization occurs with a delay after the end of the desynchronizing stimulation. The order parameter-induced damping of excited modes is due to the slaving principle (HAKEN 1983). This desynchronization

mechanism has been studied in detail in monopolar stimuli (Tass 1999, 2001 c, 2002 b) and holds equally in bipolar stimuli.

In a first approximation a phase oscillator can be used as a simple model for a rhythmically active neurons (Kuramoto 1984, Ermentrout and Kopell 1991, Grannan et al. 1993, Hansel et al. 1993). Accordingly, Equation [1] serves as a simple model for a population of globally interacting neurons subject to stimulation and random forces (Tass 1999). Hence, based on the results presented here I suggest to try to perform demand-controlled electrical deep brain bipolar double pulse stimulation for the therapy of neurological diseases characterized by pathologically synchronized neuronal activity, perturbing brain function. In contrast, standard DBS aims at mimicing the effect of tissue lesioning by simply suppressing neuronal firing (Benabid et al. 1991, Blond et al. 1992, Wielepp et al. 2001). As, for instance, in Parkinson's disease the uncorrelated firing is the physiological mode of functioning in the relevant brain area, the demand controlled block of the resynchronization in that area (Fig. 5) might be the milder and more effective therapy which would aim at reestablishing the physiological function instead of totally suppressing the neuronal firing in that particular target area.

Model-based novel DBS techniques may be more effective and may influence the affected neuronal dynamics in a more subtle way. Correspondingly, statistical physics may contribute to the development of therapies that avoid severe side effects. For this, along the lines of a top-down approach, microscopic models have to be investigated which take into account all relevant neurophysiological features such as the dynamics of single ion channels, the anatomy of synaptic interactions, transmission delays etc. Since microscopic models of this kind are much more complicated than a model of globally coupled phase oscillators, the dynamical mechanisms studied in the more macroscopic models will form a necessary basis and starting point for the study of microscopic models.

Acknowledgements

This study was supported by the *German-Israeli Foundation for Scientific Research and Development* (Grant no. 667/00).

References

Aizawa, Y.: Synergetic approach to the phenomena of mode-locking in nonlinear systems. Prog. Theor. Phys. *56*, 703–716 (1976)

Alberts, W. W., Wright, E. J., and Feinstein, B.: Cortical potentials and parkinsonian tremor. Nature *221*, 670–672 (1969)

Benabid, A. L., Pollak, P., Gervason, C., Hoffmann, D., Gao, D. M., Hommel, M., Perret, J. E., and De Rougemont, J.: Long-term suppression of tremor by chronic stimulation of the ventral intermediate thalamic nucleus. Lancet *337*, 403–406 (1991)

Bergman, H., Raz, A., Feingold, A., Nini, A., Nelken, I., Hansel, D., Ben-Pazi, H., and Reches, A.: Physiology of MPTP tremor. Movement Disorders *13*, Suppl. *3*, 29–34 (1998)

Best, E. N.: Null space in the Hodgkin-Huxley equations: a critical test. Biophys. J. *27*, 87–104 (1979)

Blond, S., Caparros-Lefebvre, D., Parker, F., Assaker, R., Petit, H., Guieu, J.-D., and Christiaens, J.-L.: Control of tremor and involuntary movement disorders by chronic stereotactic stimulation of the ventral intermediate thalamic nucleus. J. Neurosurg. *77*, 62–68 (1992)

Daido, H.: Order function and macroscopic mutual entrainment in uniformly coupled limit-cycle oscillators. Prog. Theor. Phys. *88*, 1213–1218 (1992)

Elble, R. J., and Koller, W. C.: Tremor. Baltimore: Johns Hopkins University Press 1990

Ermentrout, G. B., and Kopell, N.: Multiple pulse interactions and averaging in systems of coupled neural oscillators. J. Math. Biol. *29*, 195–217 (1991)

Glass, L., and Mackey, M. C.: From Clocks to Chaos. The Rhythms of Life. Princeton University Press 1988

Golomb, D., Hansel, D., Shraiman, B., and Sompolinsky, H.: Clustering in globally coupled phase oscillators. Phys. Rev. A *45*, 3516–3530 (1992)

Golomb, D., Wang, X. J., and Rinzel, J.: Propagation of spindle waves in a thalamic slice model. J. Neurophysiol. *75*, 750–769 (1996)

Grannan, E. R., Kleinfeld, D., and Sompolinsky, H.: Stimulus-dependent synchronization of neuronal assemblies. Neural. Comp. *4*, 550–569 (1993)

Guttman, R., Lewis, S., and Rinzel, J.: Control of repetitive firing in squid axon membrane as a model for a neurone oscillator. J. Physiol. (London) *305*, 377–395 (1980)

Haken, H.: Advanced Synergetics. Berlin: Springer (1983)

Hakim, V., and Rappel, W.: Dynamics of the globally coupled complex Ginzburg-Landau equation. Phys. Rev. A *46*, R7347–R7350 (1992)

Hansel, D., Mato, G., and Meunier, C.: Phase dynamics of weakly coupled Hodgkin-Huxley neurons. Europhys. Lett. *23*, 367–372 (1993)

Kuramoto, Y.: Chemical Oscillations, Waves, and Turbulence. Berlin: Springer 1984

Lamarre, Y., DeMontigny, C., Dumont, M., and Weiss, M.: Harmaline-induced rhythmic activity of cerebellar and lower brain stem neurons. Brain. Res. *32*, 246–250 (1971)

Lenz, F. A., Kwan, H. C., Martin, R. L., Tasker, R. R., Dostrovsk, J. O., and Lenz, Y. E.: Single unit analysis of the human ventral thalamic nuclear group. Tremor-related activity in functionally identfied cells. Brain *117*, 531–543 (1994)

Llinás, R., and Jahnsen, H.: Electrophysiology of mammalian thalamic neurons in vitro. Nature *297*, 406–408 (1982)

Neiman, A., Schimansky-Geier, L., Cornell-Bell, A., and Moss, F.: Noise-Enhanced Phase Synchronization in Excitable Media. Phys. Rev. Lett. *83*, 4896–4899 (1999)

Nini, A., Feingold, A., Slovin, H., and Bergman, H.: Neurons in the globus pallidus do not show correlated activity in the normal monkey, but phase-locked oscillations appear in the MPTP model of parkinsonism. J. Neurophysiol. *74*, 1800–1805 (1995)

Panter, P.: Modulation, Noise, and Spectral Analysis. New York: McGraw-Hill 1965

Pare, D., Curro'Dossi, R., and Steriade, M.: Neuronal basis of the parkinsonian resting tremor: a hypothesis and its implications for treatment. Neuroscience *35*, 217–226 (1990)

Pikovsky, A., Rosenblum, M. G., and Kurths, J.: Synchronization: a Universal Concept in Nonlinear Sciences. Cambridge: Cambridge University Press 2001

Sakaguchi, H., Shinomoto, S., and Kuramoto, Y.: Local and global self-entrainments in oscillator lattices. Prog. Theor. Phys. *77*, 1005–1010 (1987)

Schuurman, P. R., Bosch, D. A., Bossuyt, P. M., Bonsel, G. J., van Someren, E. J., de Bie, R. M., Merkus, M. P., and Speelman, J. D.: A comparison of continuous thalamic stimulation and thalamotomy for suppression of severe tremor. New Engl. J. Med. *342*, 461–468 (2000)

Steriade, H., Jones, E. G., and Llinás, R.: Thalamic Oscillations and Signaling. New York: John Wiley & Sons 1990

Strogatz, S. H., and Mirollo, R. E.: Phase-locking and critical phenomena in lattices of coupled nonlinear oscillators with random intrinsic frequencies. Physica D *31*, 143–168 (1988)

Tass, P. A.: Resetting biological oscillators – a stochastic approach. J. Biol. Phys. *22*, 27–64 (1996 a)

Tass, P. A.: Phase resetting associated with changes of burst shape. J. Biol. Phys. *22*, 125–155 (1996 b)

Tass, P. A.: Phase Resetting in Medicine and Biology – Stochastic Modelling and Data Analysis. Berlin: Springer 1999

Tass, P. A.: Stochastic phase resetting: a theory for deep brain stimulation. Prog. Theor. Phys. Suppl. (Kyoto) *139*, 301–313 (2000)

Tass, P. A.: Effective desynchronization by means of double-pulse phase resetting. Europhys. Lett. *53*, 15–21 (2001 a)

Tass, P. A.: Effective desynchronization with a resetting pulse-train followed by a single pulse. Europhys. Lett. *55*, 171–177 (2001 b)

Tass, P. A.: Desynchronizing double-pulse phase resetting and application to deep brain stimulation. Biol. Cybern. *85*, 343–354 (2001 c)

Tass, P. A.: Effective desynchronization with a stimulation technique based on soft phase resetting. Europhys. Lett. *57*, 164–170 (2002 a)

Tass, P. A.: Desynchronization of brain rhythms with soft phase-resetting techniques. Biol. Cybern. *87*, 102–115 (2002 b)

Tass, P. A.: Effective desynchronization with bipolar double pulse stimulation. Phys. Rev. E 66, 0362261–0362269 (2002 c)

Tass, P. A., Rosenblum, M. G., Weule, J., Kurths, J., Pikovsky, A., Volkmann, J., Schnitzler, A., and Freund, H.-J.: Detection of n:m phase locking from noisy data: Application to magnetoencephalography. Phys. Rev. Lett. *81*, 3291–3294 (1998)

Volkmann, J., Joliot, M., Mogilner, A., Ioannides, A. A., Lado, F., Fazzini, E., Ribary, U., and Llinás, R.: Central motor loop oscillations in parkinsonian resting tremor revealed by magnetoencephalography. Neurology *46*, 1359–1370 (1996)

Wielepp, J. P., Burgunder, J. M., Pohle, T., Ritter, E. P., Kinser, J. A., and Krauss, J. K.: Deactivation of thalamocortical activity is responsible for suppression of parkinsonian tremor by thalamic stimulation: a 99mTc-ECD SPECT study. Clin. Neurol. Neurosurg. *103*, 228–231 (2001)

Winfree, A. T.: The Geometry of Biological Time. Berlin: Springer 1980

Prof. Dr. Dr. Peter A. Tass
Institute of Medicine
Research Centre Jülich
52425 Jülich
Germany
Phone: ++49 (0) 24 61 61 20 87
Fax: ++49 (0) 24 61 61 28 20
E-Mail: p.tass@fz-juelich.de

and

Department of Stereotaxic and Functional Neurosurgery
University of Cologne
50924 Cologne
Germany

Nova Acta Leopoldina NF *88*, Nr. 332, 225–238 (2003)

Calcium Dynamics Associated with Electrically Stimulated Action Potential in *Chara*: Experiments and Model Simulations

Michael WACKE, Marc-Thorsten HÜTT, and Gerhard THIEL (Darmstadt)

With 7 Figures and 1 Table

Absract

The electrically stimulated release of Ca^{2+} from internal stores in the green alga *Chara* has the hallmarks of an excitable system. The threshold-like dependence of Ca^{2+} mobilization on electrical stimulation can be simulated by a combined model comprised of (*i*) the voltage dependent synthesis/breakdown of the second messenger inositol 1,4,5-trisphosphate (IP_3) and (*ii*) the concerted action of IP_3 and Ca^{2+} on the gating of the receptor channels, which conduct Ca^{2+} release from internal stores.

The model predicts a complex behavior of Ca^{2+} mobilization under periodic stimulation including higher-order phase locking and irregular responses upon increased stimulation frequency. Similar dependencies on stimulation frequencies were observed experimentally for the activation of action potentials. This demonstrates that the all-or-none type activation of the action potential is in reality only the consequence of the preceding all-or-none type mobilization of Ca^{2+} from internal stores.

Zusammenfassung

Die elektrisch stimulierte Ausschüttung von Ca^{2+} aus internen Speichern in der Grünalge *Chara* hat die Charakteristika eines erregbaren Systems. Die schwellenartige Abhängigkeit der Ca^{2+}-Ausschüttung von der Stärke der elektrischen Stimulation kann durch die Kombination zweier Modelle erfolgreich beschrieben werden. Dieses kombinierte Modell setzt sich zusammen aus: (*a.*) der spannungsabhängigen Synthese/Abbau des sekundären Botenstoffes Inositol 1,4,5-trisphosphat (IP_3) und (*b.*) der konzertierten Wirkung von IP_3 und Calcium auf das Schaltverhalten des Rezeptorkanals, der den Ausfluß von Calcium aus den Ca^{2+}-Speichern leitet.

Das Model sagt ein komplexes Verhalten der Ca^{2+}-Reaktion bei periodischer Stimulation voraus. Dies schließt periodische Verdopplung und zufällige Ca^{2+}-Antworten bei immer schnelleren Stimulationsperioden mit ein. Genau dieses vom Modell vorhergesagte Verhalten findet man in Experimenten bei der Auslösung von Aktionspotentialen in *Chara*. Dies belegt, daß die „Alles-oder-Nichts"-artige Auslösung des Aktionspotentials durch elektrische Pulse in Wirklichkeit lediglich die Konsequenz einer schwellenartigen Empfindlichkeit der Ca^{2+}-Mobilisierung aus internen Speichern gegenüber elektrischen Pulsen widerspiegelt.

1. Introduction

Transient excursions of the concentration of cytoplasmic free Ca^{2+} are important for many stimulus-response-coupling processes in plant cells (REDDY 2001, SANDERS et al 1999). In a variety of higher plants it was found that hormonal or abiotic stimuli generate

very complex Ca^{2+} responses with amplitudes and frequencies characteristic for the nature of the stimulus (SANDERS et al. 1999, REDDY 2001, PLIETH 2001, KNIGHT 2000). The observation of these distinct Ca^{2+} responses to specific stimuli has fostered the view that the information for the generation of stimulus specific responses is encoded by a combination of Ca^{2+} response amplitudes and frequencies (MALHO 1999).

The mechanisms underlying signal/response coupling in plants and even more so the mechanisms responsible for the distinct dynamics of Ca^{2+} responses is still largely unknown. Functional and molecular studies suggest that plants rely on signal transduction cascades very similar to those known from animal cells (SANDERS et al. 1999, REDDY 2001). In this context it has been reported from many different lower and higher plants that Ca^{2+} can be mobilized from internal stores *via* the second messenger IP_3 (REDDY 2001, SANDERS et al. 1999, THIEL et al. 1990). Furthermore stimulus response coupling processes can be blocked by treatments which interfere with the IP_3-signaling pathway (STAXEN et al. 1999, BISKUP et al. 1999). It is therefore perceivable that some of the complex Ca^{2+} responses in plants are generated by the operation of such a signaling cascade.

A promising model system for learning more about the details of signal response coupling in plants is the giant alga *Chara*. This plant belongs to the Characeae, a class of algae considered in evolutionary terms as ancestors of all higher plant cells (KRANZ et al. 1995). So any conserved signaling pathway detected in plants will also be relevant for higher plant cells.

The second benefit of the model system is that the plasma membrane of the Characeae is electrically excitable (UMRATH 1929). Central in this process is a voltage stimulated transient rise in Ca^{2+} which in turn activates the Cl^- channels responsible for the transient membrane depolarization (review in THIEL et al. 2002). Recent experiments have shown that the process of excitation is based on a voltage dependent production of a long lived second messenger (WACKE and THIEL 2001). This second messenger, most likely IP_3 (BISKUP et al. 1999), mobilizes Ca^{2+} from the internal stores and in this way initiates the excitation process. Much of the dynamics of the second messenger and its dependence on voltage stimulation can be extracted from experiments in which Ca^{2+} mobilization in these cells is examined under the influence of graded electrical stimuli. From these studies a kinetic model was proposed, which is able to simulate most of the experimental observations with respect to triggering of excitation with electrical stimuli of variable strength and duration (WACKE and THIEL 2001).

A step forward towards understanding the dynamics of the whole process was obtained by combining the aforementioned model on voltage dependent IP_3 production with a well established model from animal cells. The latter model describes the mobilization of Ca^{2+} from internal stores in relation to the gating of the IP_3 receptor channel, i. e. the channel, which allows Ca^{2+} release from the internal stores into the cytoplasm. A kinetic four state model proposed by TANG and coworkers (1996) is sufficient to explain the bulk of the experimental observations on IP_3-generated Ca^{2+} mobilization in animal cells including complex dynamic processes. The model is based on the assumption that Ca^{2+} binds to the activating site of the channel only after IP_3 has bound the receptor, and that the binding of calcium to the inhibitory site occurs only after Ca^{2+} is bound to the activating site. The present work shows that a combination of the two models is able to simulate a large number of experimental observations with respect to voltage stimulated Ca^{2+} responses and triggering of action potentials in *Chara* cells.

2. Materials and Methods

All recordings were performed with isolated internodal cells of *Chara corallina* Klein *ex* Wild. Culture conditions and handling of cells was described previously (THIEL et al. 1993). For experiments cells were bathed in artificial pond water (APW) containing 0.5 mM KCl, 0.5 mM $CaCl_2$, 1 mM NaCl, 2 mM Hepes/NaOH pH 7.5.

Ratiometric measurements of cytoplasmic Ca^{2+} were done as reported previously (WACKE and THIEL 2001). Membrane voltage was measured with a conventional intracellular microelectrode connected to a voltage recording amplifier (μP, Wye Science, UK). Cells were stimulated with extracellular electrodes placed close to a *Chara* interodal cell. Rectangular stimulation pulses were delivered to the cell by a pulse generator.

3. The Model

In a previous study it was shown that electrical excitation of a *Chara* cell involves a voltage dependent production of a second messenger (THIEL and DITYATEV 1998, WACKE and THIEL 2001). This second messenger in turn promotes the release of Ca^{2+} from internal stores. There is good evidence from experimental work that membrane excitation in *Chara* can be triggered by injection of inositol 1,4,5-trisphosphate (IP_3) (THIEL et al. 1990) and that excitation is blocked by inhibitors of phospholipase C (BISKUP et al. 1999), i. e. the enzyme which catalyses the production of IP_3 from its precursor phosphatidylinositol, 4,5 bisphosphate (PIP_2). This stresses that the second messenger in question involved in the excitation process is IP_3.

Based on previous work (WACKE and THIEL 2001) the voltage stimulated production and subsequent decomposition of IP_3 can be well described by two coupled linear differential equations:

$$\frac{\partial[\mathrm{PIP_2}]_t}{\partial t} = k_1([\mathrm{PIP_2}]_0 - [\mathrm{PIP_2}]_t) - k_2[\mathrm{PIP_2}]_t \qquad [1]$$

$$\frac{\partial[\mathrm{IP_3}]_t}{\partial t} = k_2[\mathrm{PIP_2}]_t - k_3[\mathrm{IP_3}]_t \qquad [2]$$

We further define $k_2 = \dfrac{c_2(i - i_0)}{q}$ for $i\text{-}i_0 > 0$ and $k_2 = 0$ for $i \le i_0$, (WACKE and THIEL 2001). Here i represents the current of a pulse; i_0 is the experimentally fixed minimum current required for an infinite pulse to evoke an effect on $[IP_3]$ and q the minimum charge needed for effective excitation of the cell. c_2 is a dimensionless fitting parameter. The expression $k_2 = C_2[IP_3]/q$ has the dimension $\mathrm{Mol} \cdot C^{-1}$. Hence k_2 is a measure for the voltage dependent production of IP_3, and with the stepwise defined response function

$$f(i) = \begin{cases} \left(1 - \dfrac{i_0}{i}\right) & \text{if} \quad \dfrac{i}{i_0} > 1 \\ 0 & \text{else} \end{cases} \qquad [3]$$

Equation [2], can now be rewritten as

$$\frac{dI}{dt} = k_2 f(i) i - k_3 I. \qquad [4]$$

While this model gives a good quantitative account for the dynamics of the second messenger in the process of membrane excitation it provides no insight into the actual mechanism of the Ca^{2+} release process.

Such a mechanism of IP_3-generated release of Ca^{2+} from internal stores is well understood in animal cells. Several models exist which underline the activity of the IP_3 receptor channel in animal cells as a key step for the explanation of the Ca^{2+} dynamics in animal cells (review Othmer 1997). This channel, which is localized in endomembranes, is the pathway for IP_3-stimulated release of Ca^{2+} from internal stores. A minimal model developed by Tang et al. (1996) successfully describes this IP_3 receptor channel by a four-state model. The four states of the model reflect the fact that the receptor has three distinct binding sites. These sites can either be empty (R), occupied by one IP_3 molecule (RI), by one IP_3 molecule plus one Ca^{2+} ion (RIC_+) and finally by an additional Ca^{2+} ion (RIC_+C_-). The binding order of the ions and molecules to the receptor is not free but proceeds sequentially from R over RI, RIC_+ to RIC_+C_- and back. The channel is only active in the state RIC_+ which accounts for the observation that low concentrations of Ca^{2+} stimulate and high concentrations inhibit an IP_3 generated Ca^{2+} release from internal stores. The state transition scheme for the IP_3 receptor is given by Equation [5]

$$\begin{aligned} &R + I \underset{k_{-4}}{\overset{k_4}{\rightleftharpoons}} RI \\ &RI + C \underset{k_{-45}}{\overset{k_5}{\rightleftharpoons}} RIC_+ \\ &RIC_+ + C \underset{k_{-6}}{\overset{k_6}{\rightleftharpoons}} RIC_+ C_- \end{aligned} \qquad [5]$$

in which the k_i, $i = \pm 4, \pm 5, \pm 6$, are the rate constants of the state transitions.

It is well known for animal cells and plants that excess Ca^{2+} is effectively removed from the cytoplasm back into internal stores by an endogenous Ca^{2+} pump (e. g. Reddy 2001), which can be described by a Hill function:

$$\bar{g}(C) = \frac{\bar{p}_1 C^4}{C^4 + \bar{p}_2^4}. \qquad [6]$$

In this equation $\bar{p}_1$ and $\bar{p}_2$ are the Hill coefficients. For more details see Othmer (1997).

Let x_i, $i = 2, \ldots, 5$ denote the fractions of the receptor channel in states R, RI, RIC_+, RIC_+C_- respectively. We then define $x_1 = C/C_0$ with the volume average calcium concentration C_0. Othmer (1997) defined

$$C_0 = \frac{C + v_r C_s}{(1 + v_r)}, \qquad [7]$$

in which C_s is the Ca^{2+} concentration in the store and v_r the ratio of the endoplasmic reticulum (ER) volume to the volume of the cytoplasm. By defining $\lambda \equiv 1 + v_r$,

$k_5 = \bar{k}_5 C_0$, $k_6 = \bar{k}_6 C_0$, $p_1 = \bar{p}_1 / C_0$ and $p_2 = \bar{p}_2 / C_0$ the model is governed by the following five coupled non linear differential equations:

$$\frac{dx_1}{dt} = \lambda(\gamma_0 + \gamma_1 x_4)\,(1 - x_1) - \frac{p_1\, x_1^4}{p_2^4 + x_1^4},$$

$$\frac{dx_2}{dt} = -k_4 I x_2 + k_{-4} x_3,$$

$$\frac{dx_3}{dt} = -(k_{-4} + k_5 x_1)\, x_3 + k_4 I x_2 + k_{-5} x_4,$$

$$\frac{dx_4}{dt} = k_5 x_1 x_3 + k_{-6} x_5 - (k_{-5} + k_6 x_1)\, x_4,$$

$$\frac{dx_5}{dt} = k_6 x_1 x_4 - k_{-6} x_5. \qquad [8]$$

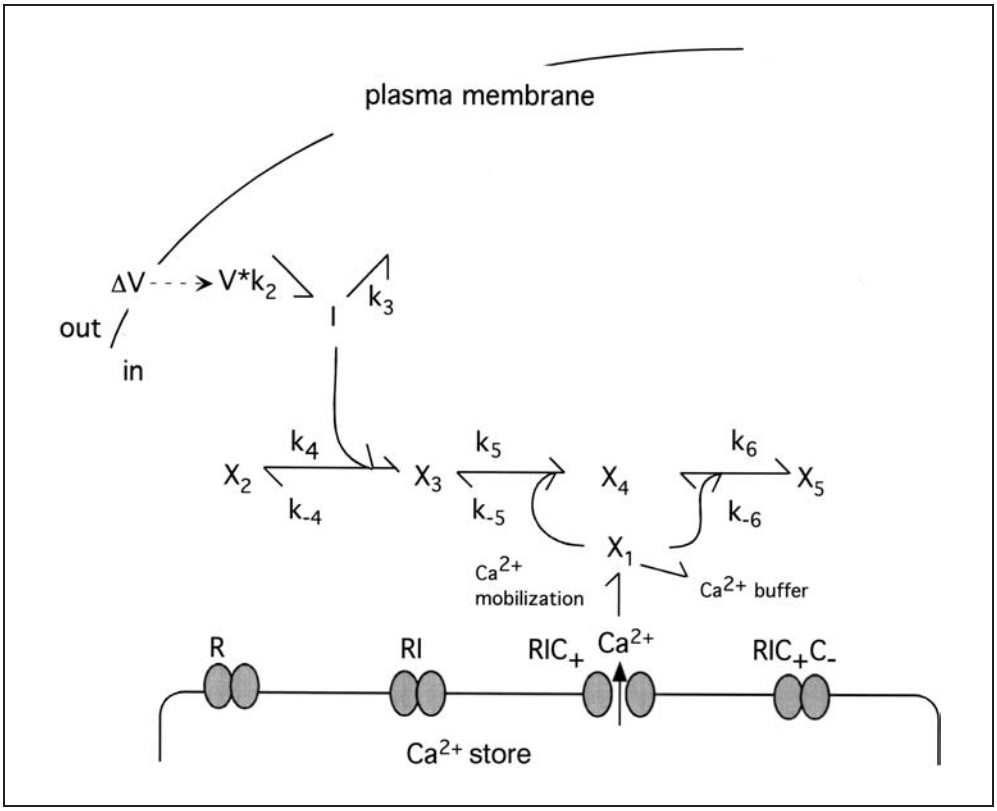

Fig. 1 A schematic of the voltage-stimulated IP_3 (I) production and activation of IP_3/Ca^{2+}-sensitive Ca^{2+} channel on internal store. The receptor channel has three distinct binding sites, which can either be empty (R), occupied in sequential order by one IP_3 molecule (RI), by one IP_3 molecule plus one Ca^{2+} ion (RIC_+) and finally by an additional Ca^{2+} ion (RIC_+C_-). Ca^{2+} release from internal stores only occurs in the state RIC_+.

Here γ_0 represents the leak Ca^{2+} conductance of the Ca^{2+} store membrane in the absence of IP_3 and γ_1 the density of IP_3 sensitive channels, both per unit volume of the ER.

To further understand the dynamics of Ca^{2+} during excitation and the processes underlying this dynamics in *Chara* we combined the model for voltage-stimulated production of IP_3 and the four-state model of the IP_3 receptor channel. In this combined model $[IP_3]_{cyt}$ is no longer – as in the original Othmer model – the input signal. Instead the actual IP_3 concentration resulting from a defined electrical stimulation is now calculated from Equation [4]. In this sense the model gives the full account of the experimental situation with an electrical pulse as input signal and a change in Ca^{2+} as output signal.

For further details of the combined model see WACKE et al. (2003). Numerical integration of the six differential equations (i. e. Equation [8] together with Equation [4]) was obtained by a 6^{th} order Runge-Kutta algorithm, as described in PRESS et al. (1988). A scheme of the model including pools and rate constants is depicted in Figure 1.

4. Determination of the Parameters

In the first approximation we attempted to preserve the dynamics characteristic for the animal system as good as possible. We therefore took – with the exception of k_{-6} – all parameter values in Equation [6] from the original model (OTHMER 1997). The values for k_2 and i_o were taken from WACKE and THIEL (2001).

5. Results and Discussion

The release of Ca^{2+} from internal stores in *Chara* is the consequence of a typical excitable system in which small stimuli are damped while sufficiently large stimuli result in

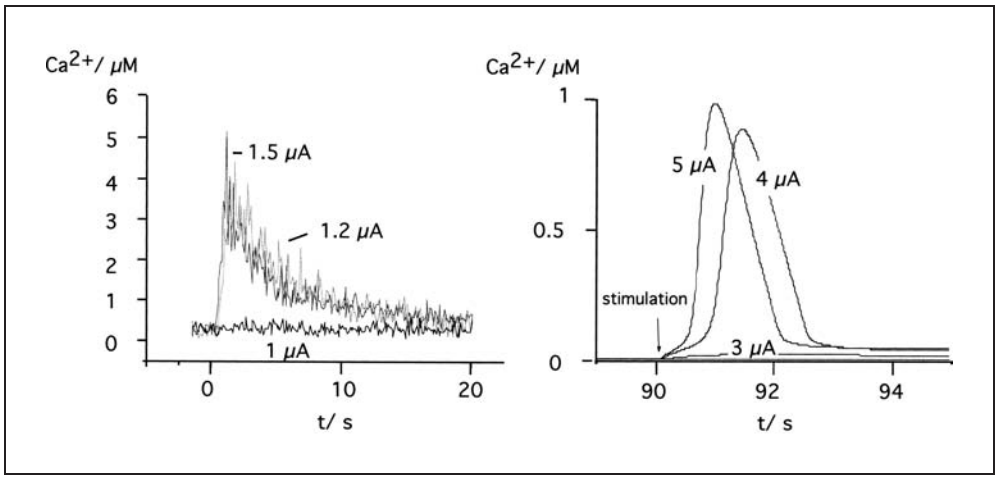

Fig. 2 Effect of pulse strength on experimentally recorded (*left panel*) and simulated (*right panel*) Ca^{2+} transients. In the experiment a *Chara* cell was stimulated with a 100 ms long pulse with amplitudes of 1 μA, 1.2 μA and 1.5 μA. The three simulated Ca^{2+} transients were obtained for 100 long pulses with the strength of 3, 4 and 5 μA. For the values of the parameters see Table 1. In the simulations pulses were started after 90 seconds in which the system was allowed to equilibrate.

Tab. 1 Model parameters used for simulation of the measured time courses.

Parameter	Value	Parameter	Value
ν_r	0.185	k_4	12.0 (μM s)$^{-1}$
γ_0	0.1 s^{-1}	k_5	15.0 (lM s)$^{-1}$
γ_1	20.5 s^{-1}	k_6	1.8 (μM s)$^{-1}$
$\overline{p}_1$	8.5 μM s^{-1}	k_2	21.5 MC^{-1}
$\overline{p}_2$	0.065 μM	k_{-4}	8.0 s^{-1}
C_0	1.56 μM	k_{-5}	1.65 s^{-1}
i_0	2.5 μA	k_{-6}	0.086 s^{-1}
		k_3	0.2 s^{-1}

drastic changes in Ca^{2+}. The left panel in Figure 2 illustrates an experiment in which one *Chara* cell was stimulated by electrical pulses of constant duration and variable strength. A small electrical pulse produced no perceivable effect on Ca^{2+}. Only a small 1.2 fold increase in pulse strength resulted in a marked transient rise in Ca^{2+}. A further increase in pulse strength, however, caused no further increase in the Ca^{2+} response. The Ca^{2+} transient generated by a 1.5 μA pulse was similar in amplitude and kinetics to that evoked by a 1.2 μA pulse. A plot of the peak Ca^{2+} responses from the same cell versus the pulse strength further illustrates this threshold like dependence (Fig. 3).

A similar excitable Ca^{2+} response to electrical stimuli can be simulated with the combined model for voltage stimulated synthesis of IP_3 and a four-state model for the IP_3 receptor. The right panel in Figure 2 illustrates three model simulations with increasing strength of stimulation. Very much like in the experiment the small pulse results in no appreciable Ca^{2+} response. Only a small 1.3 fold increase in pulse strength causes stimu-

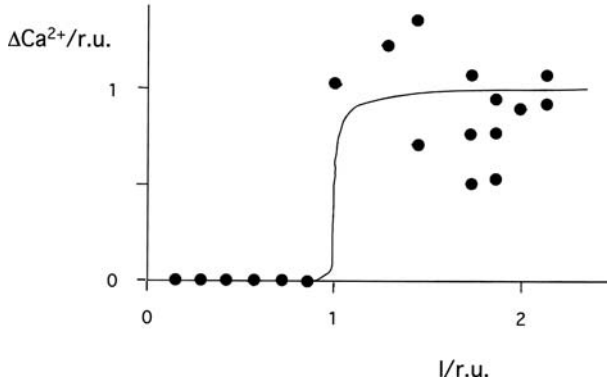

Fig. 3 Measured and simulated all-or-none mechanism. Peak Ca^{2+} response calculated from the model (as in Fig. 2) for pulse strength between 0 and 25 μA (line). Measured peak Ca^{2+} response (closed symbols) evoked in one internodal cell by stimuli with different strength (same as in Fig. 2). Data were normalized to the same ordinate setting of the last pulse which did not evoke an appreciable Ca^{2+} response as 0, and the mean maximal Ca^{2+} response as 1. Hence, I and ΔCa^{2+} are shown in relative units (r. u.).

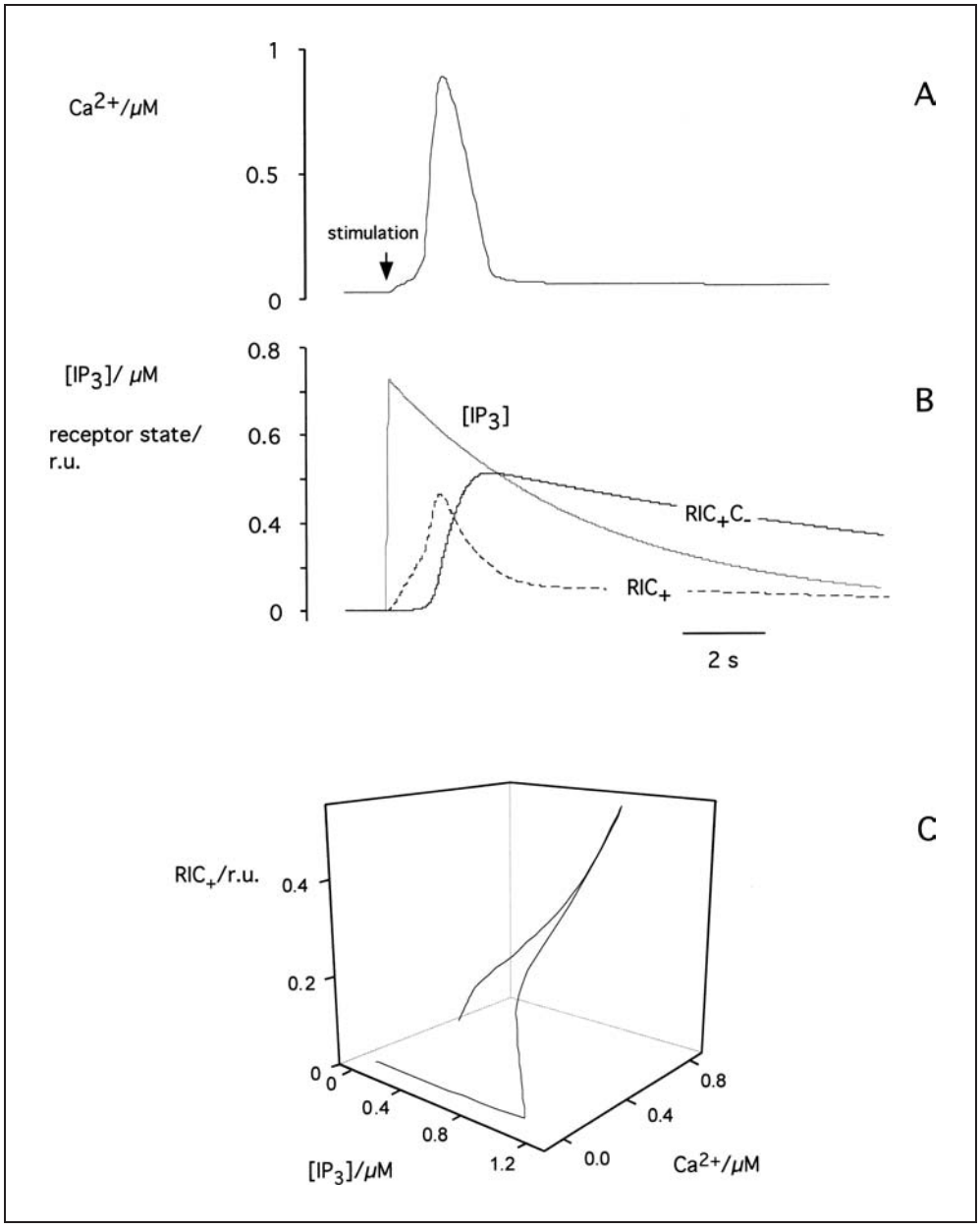

Fig. 4 (*A*) Simulated Ca^{2+} transient in response to a single stimulation (100 ms/5 μA). Data were obtained with the parameters listed in table 1. (*B*) Calculated changes in $[IP_3]$, the active (RIC_+) and the inactivated state (RIC_+C_-) of the receptor channel. (*C*) Dependence of the active state of the receptor channel on Ca^{2+} and $[IP_3]$.

lation of a near maximal response. A plot of the simulated peak Ca^{2+} responses *versus* stimulus strength results in a similar threshold-like dependence of Ca^{2+} release on the strength of stimulation (Fig. 3).

The good agreement between experiment and simulation supports the view that Ca^{2+} is indeed released from internal stores *via* a mechanism which is depending on the voltage-sensitive synthesis of IP_3 and a concerted action of IP_3 and Ca^{2+} for gating of the Ca^{2+} release channel. The model now offers the opportunity to uncover the dynamics of the individual processes. Figure 4 *A* shows a simulated Ca^{2+} response following stimulation with a 100 ms long pulse of 5 μA. Underlying this stimulation is an initial rapid rise in IP_3. This causes a small increase in active receptor channels and hence Ca^{2+} release. The resulting rise in Ca^{2+} amplifies the fraction of receptor channels in the active state, which in turn stimulates further Ca^{2+} release. A further increase in Ca^{2+} together with a decrease in IP_3 favors a transition of the receptor channel into the inactive state RIC_+C_-. As a result the Ca^{2+} release from the stores is accelerated (Fig. 4 *B*). The complex dependence of the active state of the receptor channel on IP_3 and Ca^{2+} during excitation is seen in the 3 *D* plot of Figure 4 *C*.

6. Periodic Stimulation

The model makes clear predictions of the behavior of the system. When a cell is stimulated periodically it is obvious that any second response can only be achieved if the mechanism for IP_3 synthesis is sufficiently recovered from the first stimulation in order to allow a new round of IP_3 synthesis. Previous studies have shown that the recovery of the PIP_2 pool, i. e. of the IP_3 precursor, occurs in the order of about 300 ms (Wacke and Thiel 2001). So a failure of a response to periodic simulations related to limited IP_3 is only relevant in a time frame of some 100 ms.

In addition to IP_3 synthesis also the kinetics of the IP_3 receptor channel is crucial for Ca^{2+} responses under periodic stimulation. Intuitively it is obvious that sufficient receptor channels must have recovered from the inactive state to which they had gone during the first stimulation in order to allow transition into the active state upon a second stimulus. Figure 5 illustrates a simulation of Ca^{2+} responses upon periodic stimulations. The data reveal that at low frequency (0.02 Hz and 0.04 Hz) of stimulation Ca^{2+} is released with a 1 : 1 response. An increase in stimulation frequency (0.11 Hz) results in a period doubling of the Ca^{2+} response. Responses with large amplitudes are periodically followed by responses with very small amplitude. When the stimulation frequency is increased even further (0.20 Hz) the Ca^{2+} responses become irregular. Finally, an ad ditional increase in stimulation frequency (0.23 Hz) results in a complete loss of responsiveness.

The behavior of the system under periodic stimulation can now be better understood in the context of the model. The relevant time window in which the system becomes refractory is at least an order of magnitude larger than that relevant for the regeneration of the PIP_2 pool (Wacke and Thiel 2001). Hence a limitation of IP_3 synthesis can be excluded as an explanation for the failure of the system to respond to each stimulus under high frequency stimulation. The reasons for the refractory behavior are more likely found in the gating kinetics of the IP_3 receptor channel. In this context a critical param-

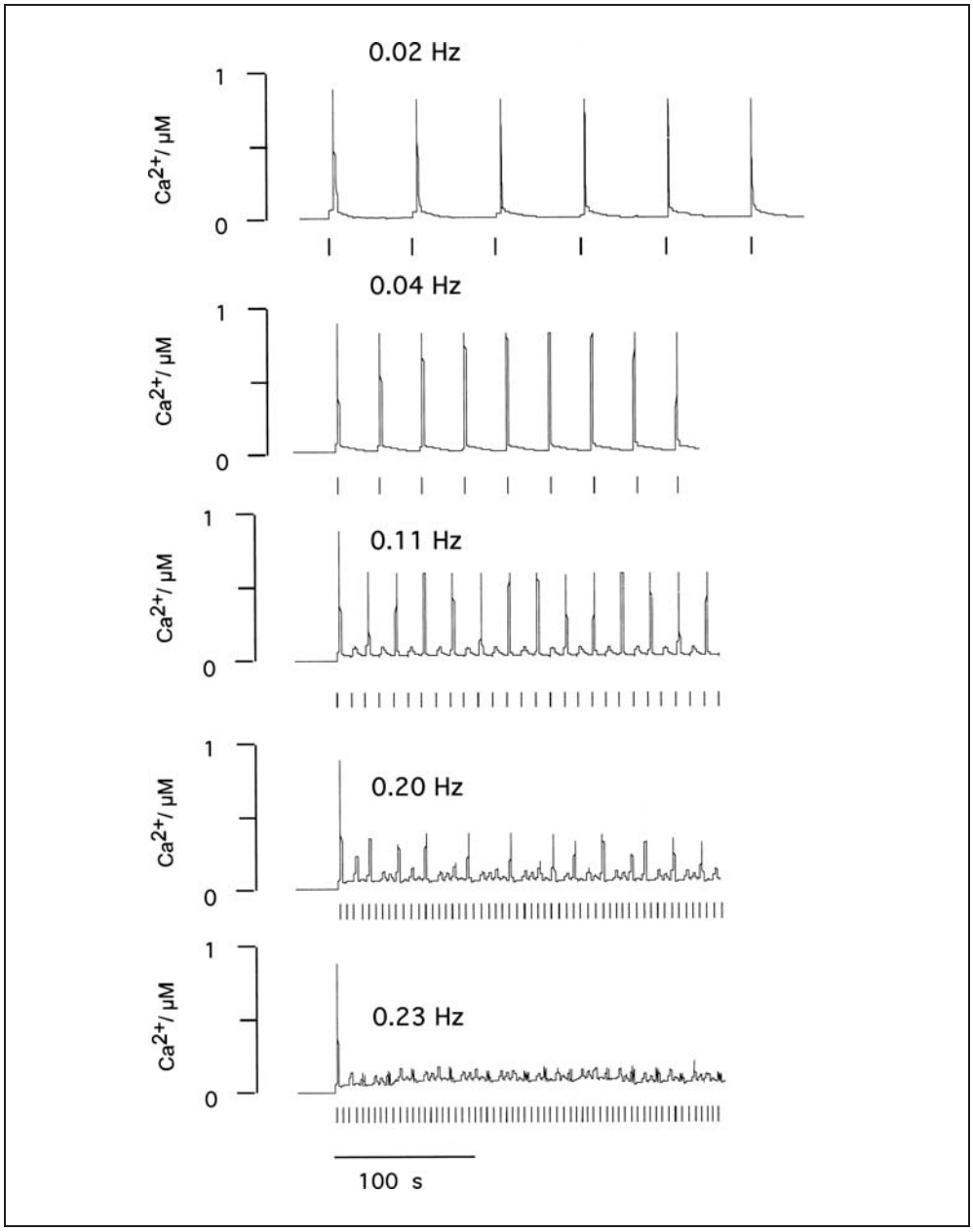

Fig. 5 Simulated Ca^{2+} transients in response to periodic stimulation with increasing frequency. Shown are parts of time courses, which were simulated with the parameters listed in Table 1. The stimulation frequencies are given with corresponding traces. The pulse duration was 100 ms. During the first 330 s of the simulation the system was allowed to equilibrate.

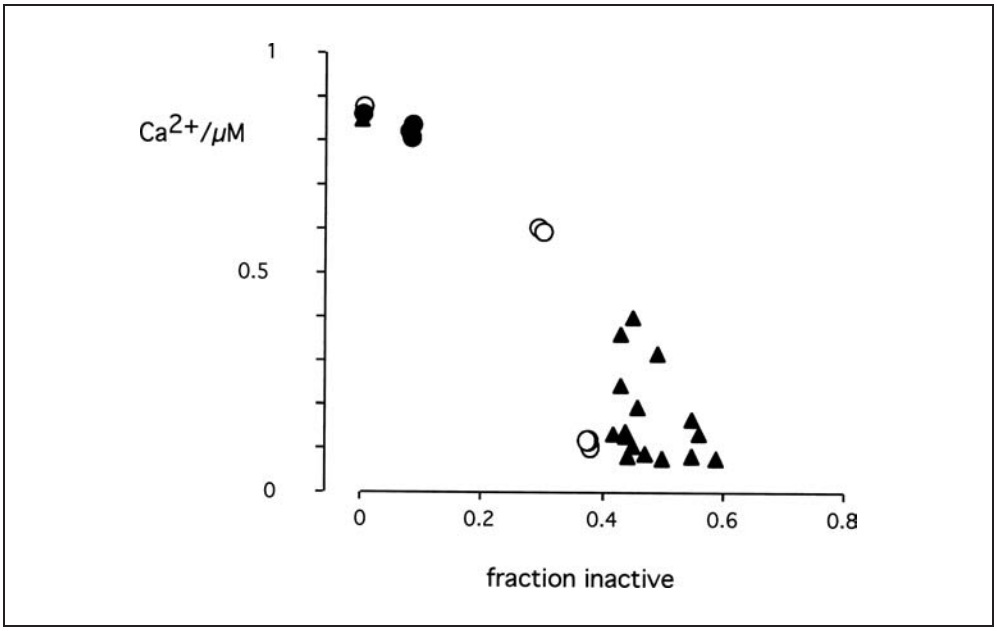

Fig. 6 Peak Ca^{2+} responses from simulations in Figure 5 as a function of the fraction of receptor channels in the inactive state RIC_+C_- at the onset of stimulation. The different symbols represent stimulations with 0.04 Hz (●) 0.11 Hz (○) and 0.20 Hz (▲).

eter for the responsiveness of the system is the recovery of the receptor channel from the inactive state RIC_+C_-. Figure 6 shows a plot of the peak Ca^{2+} response as a function of the fractional occupation of the receptor channel in this state immediately before stimulation. The data show a clear dependence of the Ca^{2+} response amplitude on the inactive state of the receptor channel. Particularly interesting is the finding of a large data scatter under conditions of high frequency stimulation. This result again highlights the fact that the entire system is depending on the interplay of several dynamical variables. The occupancy of the receptor channel is a crucial parameter but not the only one.

Previous experiments have revealed that periodic stimulation of *Chara* cells triggers Ca^{2+} responses similar to those predicted from the simulations (WACKE et al. 2002). This includes the observation of higher order phase locking to the external signal and irregular responses as consequence of progressive stimulation frequency. The irregular response is characterized by an irregular sequence of peak heights provoked by the external periodic signal, which does not fit into a simple phase-locking scheme. To further examine the stimulus response coupling in *Chara* cells under periodic stimulation we measured the response of the membrane voltage to electrical stimulation. The rationale behind this is that the Cl^- channels, which carry the membrane depolarization of the action potential, are thought to be activated as a direct consequence of an elevation of Ca^{2+} (THIEL et at. 2002).

Figure 7 show the representative results from one experiment in which a *Chara* cell was stimulated with a constant pulse (200 ms/5 μA) at different frequencies. The exemplary voltage records shown in Figure 7 reveal that stimulation either caused a clear action

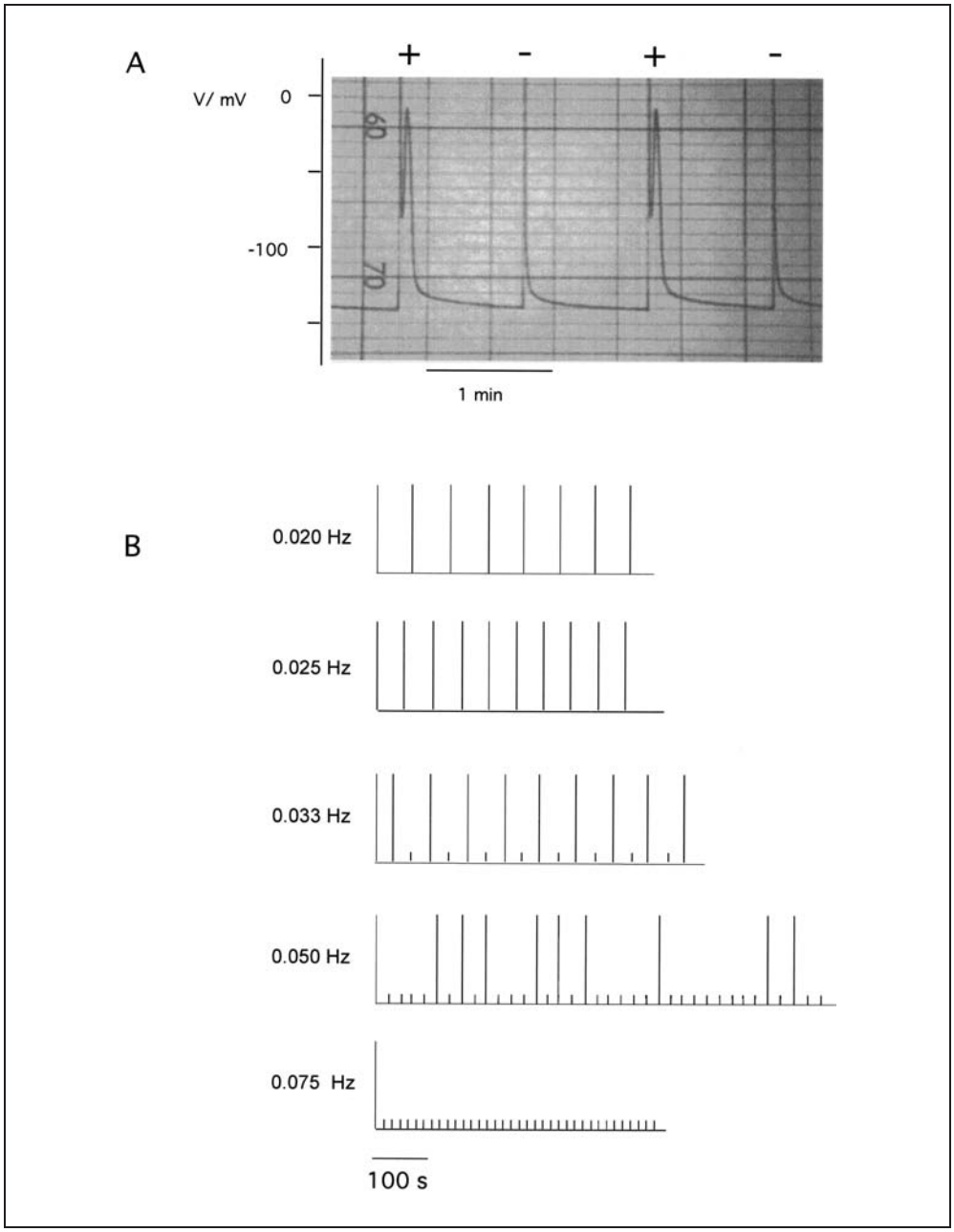

Fig. 7 Triggering of action potentials in a *Chara* cell in response to periodic stimulation (200 ms/5 μA). (*A*) A cell either responded to a stimulation with an action potential (+) or no action potential (–). (*B*) Responses of a cell to periodic stimulation with various frequencies. Stimulations, which evoked an action potential are represented by a long bar; those which failed to elicit an action potential are represented by a short bar. Stimulation frequencies are given on the left of each stimulation cycle. Between each stimulation cycle the cell was allowed to equilibrate for 240 s.

potential or a fast recovering depolarization. For data presentation and analysis the respective responses were identified and presented as long or short dashes for an AP or no AP, respectively. The data in Figure 7 illustrate that low frequency stimulation causes phase-locked APs with a period ratio of 1 : 1. An increase in frequency results in a transition to a 2 : 1 phase locking. After a further increase in stimulation frequency the membrane responses become irregular. Finally the lower panel in Figure 7 shows that an even further increase in stimulation frequency causes after an initial AP a complete silencing of the cell.

The data show that the same dependence on periodic stimulation observed for the Ca^{2+} response is also detectable on the higher level of complexity namely the membrane voltage. This is a clear demonstration of the fact that the activity of the ion channels, which carry the action potential, is the consequence of the changes in cytoplasmic Ca^{2+}. So unlike suggested by others (TAZAWA et al. 1987, KIKUYAMA and TAZAWA 1998, LUNEVSKY et al. 1983), it is indeed the Ca^{2+} release mechanism which makes up the excitable system and not the plasma membrane channels.

7. Conclusions

We have described a model for calcium dynamics in *Chara* in the context of electrical stimulation and generation of action potentials. We could show that model predictions agree with experimental results. The fact that the core of the model is based on a description of the IP_3 receptor channel in animal cells suggests that the stimulus evoked Ca^{2+} dynamics in *Chara* shares many similarities with that in animal cells. This notion is supported by the findings that plant cells have the essential components of the IP_3 signaling cascade including IP_3-sensitive receptor channels (REDDY 2001, SANDERS et al. 1999) and that also *Chara* cells are responsive to elevation of $[IP_3]$ (THIEL et al 1900).

Acknowledgements

We are grateful to the Deutsche Forschungsgemeinschaft for financial support.

References

BISKUP, B., GRADMANN, D., and THIEL, G.: Calcium release from IP_3-sensitve stores initiates action potential in *Chara*. FEBS Lett. *453*, 72–76 (1999)

KRANZ, H. D., MIKS, D., SIEGLER, M. L., CAPESIUS, I., SENSE, C, W., and HUSS, V. A.: The origin of land plants: phylogenetic relationships among charophytes, bryophytes, and vascular plants inferred from complete small-subunit ribosomal RNA gene sequences. J. Mol. Evol. *4*, 74–84 (1995)

KIKUYAMA, M., and TAZAWA, M.: Temporal relationship between action potential and Ca^{2+} transient in characean cells. Plant Cell Physiol. *39*, 1359–1366 (1998)

KNIGHT, H.: Calcium signalling during abiotic stress in plants. Int. Rev. Cytol *195*, 269–324 (2000)

LUNEVSKY, V. Z., ZHERELOVA, O. M., VOSTRIKOV, I. Y., and BERESTOVSKY, G. N.: Excitation of Characeae cell membranes as a result of activation of calcium and chloride channels. J. Membrane Biol. *72*, 43–58 (1983)

Malho, R.: Coding information in plant cells: the multiple roles of Ca^{2+} as a second messenger. Plant Biol. *1*, 487–494 (1999)

Othmer, H. G.: Signal transduction and second messenger Systems. In: Othmer, H. G., Adler, F. R., Lewis, M. A., and Dallon, J. (Eds.): Case Studies in Mathematical Modelling – Ecology, Physiology and Cell Biology. Englewood Cliffs, NJ: Prentice Hall 1997

Press, W., Flannery, B. P., Teukolsky, S. A., and Vettilig W. T.: Numerical Recipes in C: The Art of Scientific Computing. 2nd ed. Cambridge, New York: Cambridge University Press 1992

Reddy, A. S. N.: Calcium: silver bullet in signalling. Plant Science *160*, 381–404 (2001)

Plieth, C.: Plant calcium signalling and monitoring: pros and cons and recent experimental approaches. Protoplasma *218*, 1–23 (2001)

Sanders, D., Brownlee, C., and Harper, J. F.: Communicating with calicum. The Plant Cell. *11*, 691–706 (1999)

Staxen, I. I., Pical, C., Montgomery, L. T., Gray, J. E., Hetherington, A. M., and McAinsh, M. R.: Abscisic acid induces oscillations in guard-cell cytosolic free calcium that involve phosphoinositide-specific phospholipase C. Proc. Natl. Acad. Sci. USA *96*, 1779–1784 (1999)

Tang, Y., Stephenson, J., and Othmer, H. G.: Simplification and analysis of models of calcium dynamics based on $InsP_3$-sensitive calcium channel dynamics. Biophys. J. *70*, 246–263 (1996)

Tazawa, M., Shimmen, T., and Mimura, T.: Membrane control in the Characeae. Annu. Rev. Plant Physiol. *38*, 95–117 (1987)

Thiel, G., and Dityatev, A.: Transient activity of excitatory Cl^- channels in *Chara*: evidence for quantal release of a gating factor. J. Membrane Biol. *163*, 183–191 (1998)

Thiel, G., Homann, U., and Gradmann, D.: Microscopic elements of electrical excitation in Chara: transient activity of Cl^- channels in the plasma membrane. J. Membrane Biol. *134*, 53–66 (1993)

Thiel, G., MacRobbie, E. A. C., and Hanke, D. E.: Raising the intracellular level of inositol 1,4,5-trisphosphate changes plasma membrane ion transport in characean algae. EMBO J. *9*, 1737–1741 (1990)

Thiel, G., Wacke, M., and Foissner, I.: Ca^{2+} Mobilization from internal stores in electrical membrane excitation in *Chara.* Progress in Botany *64*, 217–233 (2002)

Umrath, K.: Über Erregungsleitung bei höheren Pflanzen. Planta *7*, 174–207 (1929)

Wacke, M., and Thiel, G.: Electrically triggered all-or-none Ca^{2+} liberation during action potential in the giant alga *Chara*. J. Gen. Physiol*, 118*, 11–21 (2001)

Wacke, M., Thiel, G., and Hütt, M.-T.: Ca^{2+} dynamics during membrane excitation of green alga *Chara*: model simulations and experimental data. J. Membrane Biol. *191*, 179–192 (2003)

Prof. Dr. Gerhard Thiel
Institute for Botany
University of Technology Darmstadt
Schnittspahnstr. 3
64287 Darmstadt
Germany
Phone: ++49 (0) 61 51 16 60 50
Fax: ++49 (0) 61 51 16 46 30
E-Mail: thiel@bio.tu-darmstadt.de

Chaos and Synchronization

Nova Acta Leopoldina NF *88*, Nr. 332, 241–243 (2003)

Chaos and Synchronization (Comment)

Barbara Drossel (Darmstadt)

With 1 Figure

Session number 3 was entitled "Chaos and Synchronization" and I would like to add "and noise". The five speakers gave interesting talks that stimulated lively discussions. The first talk, by Holger Kantz, discussed how fast chaotic degrees of freedom can act as white noise, opening the fascinating perspective that biological systems might be capable of generating the noise needed for their own functioning. The second talk, by Arkady Pikovsky, showed how chaotic systems can become phase synchronized without loosing their chaotic nature, as manifest for instance in the behavior of the amplitude. Next, Thomas Dittrich focused on quantum aspects of chaotic systems, with the aim of modeling ratchet-like behavior on the small scales relevant for biological processes. Then, Frank Jülicher gave an excellent presentation of the capabilities of hair cells in the inner ear to amplify sound over a wide range of amplitudes and frequencies by acting as connected nonlinear oscillators sitting close to a critical point. Finally, Hans Albert Braun mastered the difficult task of keeping the audience awake after the wine reception by giving us visual and acoustic impressions of the manifold spiking patterns generated by cold receptor neurons, which he could explain using a Hodgkin-Huxley type model.

It was impossible for me to survey these talks in such a way that a single thread or governing theme becomes visible. They are more appropriately compared to the nodes of a highly connected network, with strong links between the talks, and with each talk presenting different facets of the rich interplay between the phenomena chaos, synchronization and noise. Let me briefly discuss each of these links (Fig. 1).

- Kantz–Pikovsky: Both talks mentioned how strange attractors can become deformed. Kantz showed that most attractors have points where a small perturbation creates a new trajectory that does not lead back to the original one, with the consequence that noise deforms these attractors. Pikovsky showed that the phase of a chaotic trajectory can easily be changed by coupling to a periodic driving or another attractor.
- Kantz–Dittrich: There are limits to chaos on small scales. Kantz mentioned limits that are due to the finite amount of information that can be gathered, implying that prediction of the trajectory becomes impossible on sufficiently fine scales. Dittrich pointed out that quantum mechanics imposes a fundamental limit on the density of information in phase space, making quantum systems quasiperiodic.

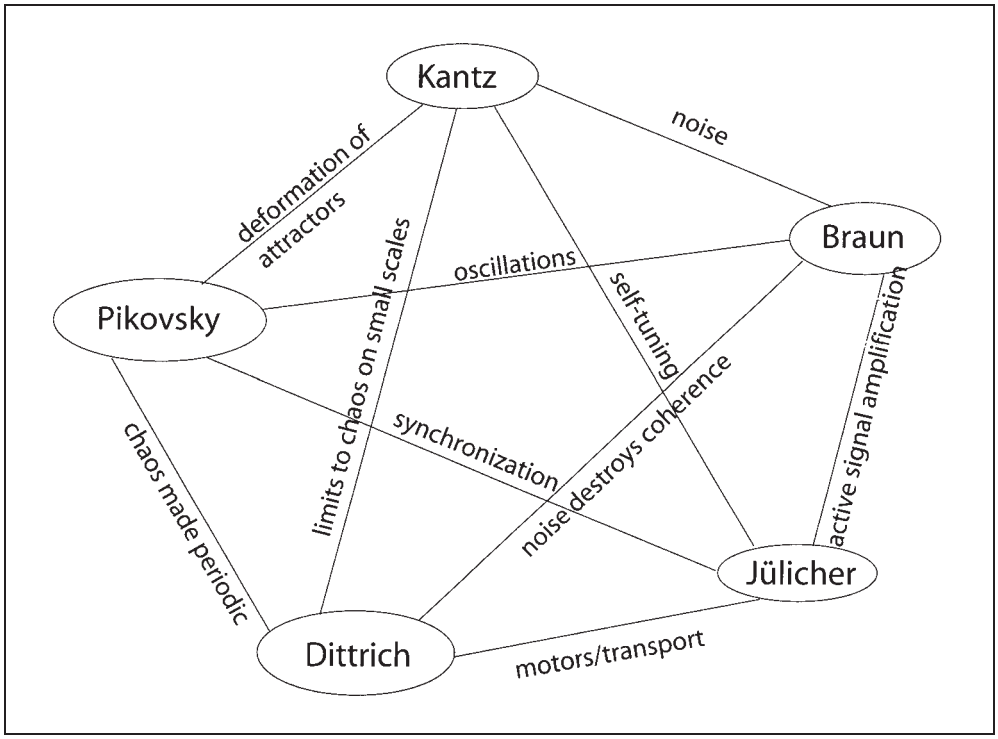

Fig. 1 The network of talks

– KANTZ–JÜLICHER: While KANTZ considered the possibility that biological systems are capable of tuning their own noise, JÜLICHER argued that inner ear hair cells do tune their parameters such that they are close to the critical point where a transition from non oscillating to (spontaneously) oscillating behavior occurs.
– KANTZ–BRAUN: In both talks noise was an important ingredient. KANTZ focused on obtaining noise from fast chaotic degrees of freedom, and BRAUN used noise superimposed to a periodic oscillation in order to generate the observed spike trains.
– PIKOVSKY–DITTRICH: Both talks mentioned chaos becoming periodic, once due to periodic driving, and once due to quantum effects.
– PIKOVSKY–JÜLICHER: Synchronization was the central theme of both talks. PIKOVSKY showed how chaotic attractors can become synchronized with each other, and JÜLICHER showed that the inner ear hair cells move in synchrony.
– PIKOVSKY–BRAUN: One of the main dynamical features in both talks was oscillating behavior, once in the phase of a strange attractor (PIKOVSKY), once in the basic dynamics of a cold receptor neuron (BRAUN).
– DITTRICH–JÜLICHER: Both talks were interested in transport phenomena. While DITTRICH focused on the emergence of transport in quantum systems, JÜLICHER argued that motor proteins drive the oscillations of the inner ear hair cells, although the precise mechanism is not yet understood.

– DITTRICH–BRAUN: Both talks dealt with systems that would have regular behavior in the absence of noise. In quantum systems, coupling to the (noisy) environment causes decoherence and consequently classical behavior, and the cold receptor neurons would fire in a regular sequence in the absence of noise.
– JÜLICHER–BRAUN: Finally, inner ear hair cells and cold receptor neurons both amplify a weak signal, hair cells by using a nonlinear oscillator, and cold receptors by adapting the threshold for firing.

Prof. Dr. Barbara DROSSEL
Institut für Festkörperphysik
Technische Universität Darmstadt
Hochschulstraße 6
64289 Darmstadt
Germany
Phone: ++49 (0) 61 51 16 35 73
Fax: ++49 (0) 61 51 16 36 81
E-Mail: barbara.drossel@physik.tu-darmstadt.de

Nova Acta Leopoldina NF *88*, Nr. 332, 245–253 (2003)

Robustness *versus* Sensitivity – Can Biological Systems Behave Chaotically?

Holger KANTZ (Dresden)

Abstract

We discuss aspects of robustness and of sensitivity of different types in nonlinear dynamics. Chaotic motion is sensitive to changes of initial conditions, to changes of parameters, and to influences of external noises. Due to this lack of robustness the evolutionary advantage of chaotic behavior in biology is unclear. We hence argue that nonlinear dynamics in biology will typically operate in parameter regimes of stable limit cycles.

Zusammenfassung

Für die verschiedenen Typen nichtlinearer Dynamik werden Aspekte von Robustheit und von Empfindlichkeit gegenüber Störungen diskutiert. Chaotische Dynamik reagiert sensibel auf Änderungen der Anfangsbedingungen, Änderungen von Systemparametern und auf eingekoppelte stochastische Störungen, während nichtlineare Grenzzyklusdynamik gegen alle diese Einflüsse robust ist. Aufgrund dieser Empfindlichkeit ist der evolutionäre Vorteil chaotischen Verhaltens in biologischen Systemen unklar. Im Artikel werden verschiedene dynamische Phänomene der Biologie, wie beispielsweise sensorische Einheiten, physiologische Regelkreisläufe und Populationsentwicklungen, auf die Relevanz von Robustheit hin untersucht. Die allgemeine Schlußfolgerung ist, daß in den meisten Fällen eine Robustheit gegen Störungen unerläßlich ist, und somit nichtlineare Systeme in der Biologie evolutionsbedingt in Parameterbereichen operieren sollten, in denen stabile Grenzzyklen existieren.

1. Introduction

Deterministic chaos is a kind of paradox in itself: Despite determinism in the sense that the precise setting of the initial condition leads to a uniquely determined solution for all times into the future, the detailed behavior of exactly this solution is unpredictable, if the initial condition is known only within some measurement error. The reason for this behavior lies in the intrinsic instability of chaotic solutions: Any tiny (more precisely, infinitesimal) change of the initial condition leads with probability one to a very different solution in the long run. This is in strict contrast to regular solutions, where a slight change of the initial condition leads to a modification of the solution by a similar magnitude. Hence, in chaotic systems, similar causes do not have similar actions, but identical causes do have identical actions.

The mathematical theory of dynamical systems, including bifurcation theory and ergodic theory, is well established (GUCKENHEIMER and HOLMES 1983, OTT 1993), so that

the origin of such strange behavior is fully understood. In particular, it is related to linear stretching and nonlinear folding of the phase space by the equations of motion. Nonlinearity hence is required, although not sufficient for chaos. To be more specific, we define a dynamical system by its equations of motion to be of the type

$$\dot{\vec{x}} = \vec{f}(\vec{x}), \qquad [1]$$

where $\vec{x} \in \Gamma \subset \mathbf{R}^d$ and $\vec{f} \in \mathbf{R}^d$ (Γ is called the phase space or state space). If the vector field $\vec{f}$ representing the forces is Lipshitz continuous, i. e., if there exists a finite real number k such that $|\vec{f}(\vec{x}) - \vec{f}(\vec{y})| < k|\vec{x} - \vec{y}|$ for all $\vec{x}$, $\vec{y}$, then the initial value problem $\vec{x}(t = 0) = \vec{x}_0$ has a unique solution $\vec{x}(t)$ for all times t. This property is called determinism.

The theorem of Poincaré-Bendixon states that if the phase space G is two dimensional or less, then the solutions $\vec{x}(t)$ of any initial condition have, if they remain inside a bounded region, no other choice than either becoming periodic or settling down on a fixed point. Hence, in two-dimensional systems of the form of Equation [1], chaos is excluded.

The Poincaré-Bendixon theorem is an important result in order to discuss the notion of nonlinearity in a different way: It is evident that a set of linear equations of motion such as those of the harmonic oscillator,

$$\dot{x} = v, \quad \dot{v} = -\omega^2 x, \qquad [2]$$

can be made nonlinear by a suitable change of coordinates. Still, the solutions (which might be very unfamiliar to us in the transformed coordinates) are the well known harmonic oscillations. So the essential aspect for the possibility of a system to behave chaotically is not the nonlinearity proper, but it is the issue of whether it is decomposable into uncoupled at most two-dimensional subsystems by a suitable change of coordinates. For an arbitrarily high dimensional linear set of equations, this is always possible, whereas nonlinearity generally, but not always, is prohibitive.

Even if such a decoupling of a three- or higher dimensional nonlinear system is not possible, such systems often do not behave chaotically but instead exhibit motion on stable limit cycles or regular motion on tori in phase space. Hence, stable regular motion is as typical of nonlinear dynamical systems as chaos. Unfortunately, due to rather obvious reasons, it makes no sense to quantify how probable either of the two behaviors is for a given set of equations, when we consider to randomly choose its control parameters. As an example of this, let us consider the well known logistic equation

$$x_{n+1} = r x_n \, (1 - x_n) \qquad [3]$$

which is a time discrete dynamical system[1] and can, e. g., be interpreted as a model for the size of a population, x_n, whose reproduction rate goes to zero due to a shortage of food supply when the current population is close to the maximum $x = 1$. In the way this model is written, about 70 % of all possible values of r (which is restricted to the interval [0, 4]) yield periodically oscillating populations. However, by setting $r = \ln q$, the corre-

1 The Poincaré-Bendixon theorem does not apply to discrete time systems, hence this one dimensional noninvertible map can in fact exhibit chaos, depending on the value of r.

sponding percentage when taking $q \in [1, e^4]$ as the control parameter is very different. Hence, since equations of motion always contain some arbitrariness, one cannot specify whether chaos or regular motion is the more typical one, as soon as both have a finite probability to occur.

The literature on mathematical models for biological systems contains many examples of chaotic dynamics. However, as it will be briefly discussed in the following section, empirical evidence for chaos in nature is lacking, but also not to be expected because of the fact that biological systems typically are coupled to a noisy environment. Hence, the analysis of observed data will not yield an answer to whether natural systems can behave chaotically. We therefore want to discuss different issues of robustness of chaotic and of regular motion. We will then compare these results to hypothetical robustness requirements for biological systems in terms of their fitness in order to identify situations or mechanisms, where chaos might be beneficial or destructive for life.

2. Lack of Observations of Chaos from Biological Data

In order to verify the presence of deterministic chaos in an experiment, one has to record a time series of some suitable quantity which can be measured with some precision. Time series analysis (Abarbanel 1996, Kantz and Schreiber 1997) can then tell whether or not the signal represents a chaotic dynamical system. Since typical time series data represent just a single quantity, whereas the dynamics of the system underlying the data lives in some vector valued phase space, embedding techniques are employed to reconstruct a phase space. The clearest signature of determinism then is the confinement of the reconstructed state vectors to a lower dimensional manifold in the embedding space. This is typically studied by numerical dimension estimates of the data set (Grassberger and Procaccia 1983). Low dimensions have been reported for many signals from biological systems such as, e. g. the human heart. However, taking into account current knowledge about the problems in the analysis of intermittent and nonstationary data (as data from field measurements very often are) (Theiler 1986, 1991, Hegger et al. 1997, Schreiber and Kantz 1996), together with other difficulties and the often rather diffuse scaling ranges, almost every of these dimension estimates leaves some doubts whether they are really indications of the existence of low dimensional manifolds.

This does not mean that no finite dimensional manifolds exist, since it is also quite well understood how measurement noise, the high dimensionality of an attractor, or other problems can make it almost impossible to verify for a truly chaotic system the presence of this finite dimensional manifold when working with noisy observations (Schreiber and Kantz 1996). Since systems in nature are never isolated, it is not to be expected to find deterministic chaos, but rather one might see a stochastic process which is unstable also in its deterministic limit. In such a situation, chaos plays an important role for the dynamics, but cannot be detected by dimension estimates due to the lack of determinism.

An alternative to dimension estimates which in most cases would be much more convincing is to construct a deterministic chaotic model of a given system. One then has to verify that the model dynamics is really consistent with the observations and *vice versa*, one should also demonstrate that different model behavior such as regular dynamics perturbed by noise is not consistent with the observed data.

In summary, the author of this article is not aware of any example of data analysis which clearly and unambiguously supports that a biological system behaves chaotically, but there could be many reasons why a system where chaos plays a relevant role cannot be identified as being chaotic on the basis of observations.

3. Robustness *versus* Sensitivity

3.1 Robustness against Initial Conditions

As mentioned before, one striking feature of chaos is its sensitivity with respect to changes in the initial conditions. In a chaotic system, the distance between two different solutions $\vec{x}(t)$ and $\vec{y}(t)$ both subject to exactly the same equations of motion but emerging from slightly different initial conditions $|\vec{x}_0 - \vec{y}_0| = \varepsilon << 1$ grow, on average and with probability one, exponentially in time, i. e., $|\vec{x}(t) - \vec{y}(t)| \cong \varepsilon e^{\lambda t}$, as long as this distance remains much smaller than unity. Such a behavior can also be found in unstable linear systems, but nonlinearity in addition to instability can introduce folding effects such that this exponential divergence can take place despite the fact that in the long run both solutions remain inside a finite domain of the phase space. The latter is a very natural requirement for every physical or biological system, since it guarantees that arbitrary measurement functions yield finite values. Chaoticity expresses itself in a measurement sequence by the irregularity and aperiodicity of the fluctuations observed.

Since an individual solution is a very unstable object, the indecomposable invariant sets are a very useful concept for a description of a system's behavior. In dissipative systems those sets which can be observed in experiments are attractors, i. e., initial conditions from a whole neighborhood of the invariant set (the basin of attraction) yield solutions which enter the set and remain there. Hence, although two slightly different initial conditions create very different trajectories, both fill the same invariant set in an ergodic way if they were both started in its basin of attraction. Quantities which are used to characterize chaotic motion, such as Lyapunov exponents, the Kolmogorov-Sinai entropy, or the attractor dimension are identical for all initial conditions inside the same basin of attraction, when discarding a transient. Hence, ergodic averages along a trajectory are in fact robust against changes of initial conditions, but time dependent properties are not.

As a particular conclusion, we can say that when the initial condition of a chaotic system in biology is set by some stimulus, then the reaction of the system is not well defined, because the slightest change of the stimulus will manifest itself in a macroscopically different reaction after a finite time.

3.2 Robustness against Parameter Changes

We said that ergodic averages along arbitrary trajectories on the same invariant set are identical with probability one. In other words, if we are interested in time averaged quantities only, sensitivity to initial conditions is not a problem, as long as the initial conditions remain inside the basin of attraction. However, also these time averaged quantities

may depend sensitively on some quantities, namely on the system's parameters. Naively one could expect that, e. g., the mean value of $\vec{x}(t)$ inside an invariant set should depend smoothly on the change of system parameters. Unfortunately, this is true only for structurally stable systems, i. e., for systems, where the topological structure of the invariant set does not change abruptly, when a control parameter is modified. More precisely, a system is called structurally stable, if the infinitesimal change of a control parameter can be compensated by a coordinate transform. Structural stability, however, is the exception rather than the rule, when the invariant set supports chaotic dynamics. The formal requirement for structural stability is that the set is hyperbolic, i. e., that expanding and contracting directions are transverse to each other everywhere. This property can be proven to hold for stable and unstable periodic solutions in large ranges of the control parameters, however, for chaotic motion this is known to hold only in a few specific systems.

So what instead happens when changing a system parameter is that bifurcations occur, i. e., periodic orbits change their topology and stability properties. Since infinitely many unstable periodic orbits are densely embedded in chaotic attractors, lack of hyperbolicity means that for any arbitrarily small parameter change some of these orbits undergo a bifurcation. The ergodic averages on the attractor change in a dramatic way, when such a bifurcation yields a stable periodic orbit (Newhouse sinks). In fact, it is well known that inside the parameter ranges of most model systems which create chaotic regimes, arbitrarily many (correspondingly small) windows of parameter values exist, for which the solutions are not chaotic but are complicated periodic orbits (Guckenheimer and Holmes 1983). Hence, when control parameters of a chaotic dynamical system are not precisely fixed, also temporal averages might change their values abruptly, if the system is not structurally stable.

3.3 Robustness against Noises

When external noises are coupled into a system, one is formally leaving the class of dynamical systems (Arnold 1999). Nonetheless, when the noise amplitude is small, it makes sense to compare the behavior of the noisy system to the one of the noise free system. In such a case, the two types of instability discussed in the previous two subsections are relevant. First of all, if we consider an isolated perturbation of a chaotic trajectory at some time t_0, then it is evident from Section 3.1 that the perturbed and the unperturbed solution will diverge exponentially fast after the perturbation. Hence, after some time they will be macroscopically different but they will be on the same invariant set.

If perturbations occur at any time, then we have to study the effect of accumulated perturbations. In such a case it might be more instructive to interpret a perturbation of the current state vector as the perturbation of the parameters of the system, since we have

$$\dot{\vec{x}}(t) = \vec{f}_p(\vec{x}(t) + \eta(t)) = \vec{f}_{\vec{p}}(\vec{x}(t)), \qquad [4]$$

i. e., the vector field for parameters p at the perturbed state $\vec{x}(t) + \eta(t)$ is identical to the vector field for some perturbed parameters $\vec{p}$ at the unperturbed state. Of course, the conversion of noise in the state vector into noise in the parameters changes the distribution of the noise, and requires additional (technical) assumptions about the effect of param-

eter changes on $\vec{f}$. Nonetheless, this interpretation tells us that noise in the state vector can create trajectories which are not close to solutions of the unperturbed system. Exactly this issue is studied in the framework of shadowing: A noisy trajectory is said to be shadowed by a solution of the unperturbed system, if such a solution exists which remains close to the noisy solution for all times. It has been proven (Anosov 1967, Bowen 1975) that such shadowing trajectories exist in systems which are structurally stable. In systems without this stability, noise can drastically modify the ergodic properties, as it has been discussed (e. g. in Jaeger and Kantz 1997, Sommerer et al. 1991).

4. Regular Motion

In the last section we discussed sensitivity and robustness of chaotic motion. The situation is completely different for regular, i. e., non-chaotic solutions of the same system, which may be found by simply changing the control parameters.

When the attracting invariant set is a stable limit cycle or even a fixed point, then typically there is no sensitivity to initial conditions (apart from the case of transient chaos; Kantz and Grassberger 1985). Hence, in the sense of the response to an external stimulus, a system with regular solutions produces reproducible responses also for slightly different stimuli.

Bifurcations occur of course also for stable periodic solutions. However, for a single stable orbit, they are separated by finite intervals of the control parameter. Hence, the ergodic averages over the invariant set are robust against changes of parameters inside a given interval of those, if the corresponding dynamics is regular. In other words, away from the bifurcation points, a periodic orbit is a hyperbolic set and hence changes of the parameters are equivalent to smooth coordinate transforms.

Finally, when noise is coupled into dynamics of limit cycles, shadowing holds: since the invariant set is hyperbolic and hence structurally stable, the perturbed motion close to the limit cycle can be shadowed by an unperturbed solution, which means that the noisy motion looks like measurement noise on an unperturbed solution.

In summary, all the sensitivities which we encounter when the motion is chaotic disappear for limit cycle motion, apart from the vicinity to bifurcation points.

5. Robustness and Fitness

In this section we will attempt to interpret the above observations in terms of fitness in the evolutionary selection process. When asking for the possibility of chaos in biological systems, the hypothesis behind this is that chaos can only exist if it does not reduce the performance of an organism or a population.

5.1 Input-output Systems and Small Signal Amplification

Sensory systems are dynamical input-output systems: A stimulus arrives and causes some reaction of a dynamical system. A prominent limit cycle system is the excitable

Hodgkin-Huxley model for nerve cells. As discussed before, a chaotic system would depend so sensitively on the stimulus that its response would appear to be irreproducible.

Can sensitivity to perturbations be useful? Yes, it can, in the sense of acting as an amplifier. A phenomenon which is known to be relevant in many biological systems and which is discussed thoroughly in several other contributions in this book is stochastic resonance. In this case, the small signal to be amplified is periodic, the system acting on it is nonlinear (often bistable, but never chaotic), and under certain circumstances the nonlinear system starts to synchronize with the very weak periodic perturbation in an optimal way, if it is additionally perturbed by white noise of suitable intensity. In an almost noise free environment, it might be beneficial for a sensory system if it can create its own noise. It has been shown in JUST et al. (2001) that fast chaotic motion coupled to a bistable system can in fact fully replace external noises. The required time scale separation speeds up the chaotic system such that the Kolmogorov-Sinai entropy becomes arbitrarily large, and most details of the chaotic system lose their relevance. However, it is essential that the entropy remains positive, i.e, that the system remains chaotic. The only argument against such an auto-generated stochastic resonance in a living organism is that it should be much easier to use true noises on the cellular level (e. g., coming from ion channels) rather than chaos for the described purpose.

A much more direct amplification mechanism can be used by nonlinear systems close to bifurcations. The dynamics of hair bundles studied by JÜLICHER (2003, this volume) is an excellent example for that. The small signal amplification near bifurcation points has originally been proposed by WIESENFELD (VOHRA and WIESENFELD 1995). Speaking about robustness, it requires a fine tuning of a system parameter in order to be close to the bifurcation point, possibly controlled by a suitable feedback mechanism.

A direct chaotic amplifier, making use of the sensitive dependence on initial conditions, has not been reported and most surely would not work: When two initially very similar states have achieved a macroscopic distance from each other because of the exponential instability, then the relation between the initial conditions and the actual state are described by such a highly nonlinear function that it would be extremely difficult to invert it. Additionally, all noises acting onto the trajectories during this evolution make it impossible to infer the initial states from the final states, because they have been amplified as well.

5.2 Unpredictability as a Benefit?

The striking feature of chaotic time evolution is its unpredictability. So one can think about the existence of situations where unpredictability would be beneficial. One such situation could be population dynamics, similar to how the occurrence of prime number cycles of cicade populations have been interpreted by MARKUS and GOLES (2002): If the population of a prey fluctuates chaotically, the predator cannot rely on its availability and would be forced to prey on another species. Hence, one could study whether populations whose dynamics can be reasonably well described by the logistic equation, Equation [3], correspond to parameters r in the periodic or in the chaotic regime.

5.3 Regulatory Systems

It seems, however, that most regulatory systems, i. e., feedback loops, are operating in periodic regimes. The well known Mackey-Glass delay equations for the production of red blood cells are able to generate chaotic fluctuations. As discussed in MACKEY and GLASS (1977), such chaotic fluctuations have to be considered as a disease. The misbehavior of a system due to wrongly tuned parameters has been called dynamical diseases in BÉLAIR (1995). When looking through the different topics discussed, one observes that chaoticity in this context typically represents a disease whereas regularity represents the healthy state. One exception is the human heart, where regular beating is pathological. However, until now the irregularities of healthy heart dynamics have not been shown in a convincing manner to be deterministically chaotic, but also the pathological chaotic states of, e. g., the Mackey-Glass dynamics have not been verified in experimental data[2].

6. Conclusions

We have discussed aspects of robustness and instability of different types of nonlinear dynamical behavior. Whereas limit cycles are robust with respect to perturbations of any kinds in certain ranges, chaos is not. We discussed some possible scenarios in order to identify beneficial consequences of chaos despite its sensitivity or even through its sensitivity, and there might be situations where chaos could enhance the fitness of an individual or of a species. Although there are several mathematical models of biological phenomena which behave chaotically for suitable adjustments of their parameters, when studying the literature one finds that convincing reports of chaos in real biological systems are almost non-existing. In contrast to that, many examples, some of them being included in this book, show the existence of limit cycle motion. Hence, in this contribution we were clearly unable to present any clear answer, but perhaps the considerations about robustness and sensitivity will allow other researchers for a more specific search for or against chaos in biology.

References

ABARBANEL, H. D. I.: Analysis of Observed Chaotic Data. New York: Springer 1996

ANOSOV, B. V.: Geodesic flows on closed Riemannian manifolds with negative curvature. Proc. Steklov Inst. Math. *90*, 1 (1967)

ARNOLD, L.: Random Dynamical Systems. Heidelberg: Springer 1999

BÉLAIR, J., GLASS, L., AN DER HEIDEN, U., and MILTON, J. (Eds.): Dynamical Disease. AIP Press 1995

BOWEN, R.: Limit sets for axiom A diffeomorphisms. Differential Equations *18*, 333–339 (1975)

GRASSBERGER P., and PROCACCIA, I.: Characterization of strange attractors. Phys. Rev. Lett. *50*, 346 (1983)

GUCKENHEIMER, J., and HOLMES, P.: Nonliner Oscillations, Dynamical Systems, and Bifurcation of Vector Fields. New York: Springer 1983

HEGGER, R., KANTZ, H., and OLBRICH, E.: Dimension estimates for intermittent signals. Phys. Rev. E *5*, 6199–6203 (1997)

2 To be precise, the irregular fluctuations of the number of red blood cells have not been shown to possess a deterministic source.

Jaeger, L., and Kantz, H.: Homoclinic tangencies and non-normal Jacobians – effects of noise in non-hyperbolic systems. Physica D *105*, 79 (1997)

Jülicher, F.: Active amplification in hearing. In: Beck, F., Hütt, M.-T., and Lüttge, U. (Eds.): Nonlinear Dynamics and Spatiotemporal Principles of Biology. Nova Acta Leopoldina NF Bd. *88*, Nr. 332, 269–278 (2003)

Just, W., Kantz, H., Rödenbeck, C., and Helm, M.: Stochastic modelling: Replacing fast degrees of freedom by stochastic processes. J. Phys. A: Math. Gen. *34*, 3199 (2001)

Kantz, H., and Grassberger, P.: Repellers, semi-attractors and long-lived chaotic transients. Physica *17D*, 75–86 (1985)

Kantz, H., and Schreiber, T.: Nonlinear Time Series Analysis. Cambridge, UK : Cambridge University Press 1997

Mackey, M. C., and Glass, L.: Oscillations and chaos in physiological control systems. Science *197*, 287 (1977)

Markus, M., and Goles, E.: Cicadas showing up after a prime number of years. Math. Intelligencer *24*, 30 (2002)

Ott, E.: Chaos in Dynamical Systems. Cambridge University Press 1993

Schreiber, T., and Kantz, H.: Observing and predicting chaotic signals: Is 2 % noise too much? In: Kravtsov, Y, and Kadtke, J. (Eds.): Predictability of Complex Dynamical Systems. Springer Series in Synergetics No. *69*. New York: Springer 1996

Sommerer, J. C., Ott, E., and Grebogi, C.: Scaling law for characteristic times of noise-induced crises. Phys. Rev. A *43*, 1754 (1991)

Theiler, J.: Some comments on the correlation dimension of 1/fá noise. Phys. Lett. A *155*, 480 (1991)

Theiler, J.: Spurious dimension from correlation algorithms applied to limited time series data. Phys. Rev. A *34*, 2427 (1986)

Vohra, S. T., and Wiesenfeld, K.: Experimental test of the normal form for perioid doubling bifurcations. Physica D *86*, 27 (1995)

Prof. Dr. Holger Kantz
Max-Planck-Institut
für Physik komplexer Systeme
Nöthnitzer Straße 38
01187 Dresden
Germany
Phone: ++49 (0) 35 18 71 22 16
Fax: ++49 (0) 35 18 71 19 99
E-Mail: kantz@mpipks-dresden.mpg.de

Nova Acta Leopoldina NF *88*, Nr. 332, 255–268 (2003)

Synchronization: A General Phenomenon in an Oscillatory World

Arkady PIKOVSKY and Michael ROSENBLUM (Potsdam)

With 4 Figures

Abstract

We present a general introduction to synchronization phenomena in nonlinear systems. The notion of self-sustained oscillators is introduced, and effects of phase locking and frequency entrainment are described and illustrated with examples. Different types of synchrony in chaotic systems are also outlined.

Zusammenfassung

In diesem Artikel werden Synchronisationsphänomene in nichtlinearen Systemen diskutiert und zusammengefaßt. Die periodischen selbsterregten Schwingungen lassen sich durch die Phasendynamik charakterisieren. Durch eine Wechselwirkung bzw. äußere Kraft kann die Phase eingefangen werden, was zum Synchronisationszustand führt. Für chaotische Systeme läßt sich die Phase nicht eindeutig definieren, trotzdem ist es möglich, phasensynchronisierte Zustände experimentell zu beobachten. Die vollständige Synchronisation chaotischer Systeme wird auch beschrieben.

1. Introduction

Many natural and human-made nonlinear oscillators exhibit the ability to adjust their rhythms due to weak interaction: two lasers, being coupled, start to generate with a common frequency; cardiac pacemaker cells fire simultaneously; violinists in an orchestra play in unison. Such coordination of rhythms is a manifestation of a fundamental nonlinear phenomenon – s*ynchronization.* Discovered in 17th century by Christiaan HUYGENS, it was observed in physics, chemistry, biology, and even social behavior, as well as found practical applications in engineering and medicine. The notion of synchronization has been recently extended to cover the adjustment of rhythms in chaotic systems, large ensembles of oscillating units, rotating objects, continuous media, etc. In spite of essential progress in theoretical and experimental studies, synchronization remains a challenging problem of nonlinear sciences (for details and further references see PIKOVSKY et al. 2000, 2001, MOSEKILDE et al. 2002).

It is important to emphasize that synchronization is an essentially nonlinear effect. In contrast to many classical physical problems, where consideration of nonlinearity gives a correction to a linear theory, here the account of nonlinearity is crucial: the phenomenon occurs only in the so-called *self-sustained* systems.

2. Self-Sustained Oscillators

Self-sustained oscillators are models of natural oscillating objects, and these models are essentially nonlinear. Mathematically, such an oscillator is described by an autonomous (i. e., without explicit time dependence) nonlinear dynamical system. It differs both from linear oscillators (which, if a damping is present, can oscillate only due to external forcing) and from nonlinear energy conserving systems, whose dynamics essentially depends on initial state.

Dynamics of oscillators is typically described in the phase (state) space. Quite often two state variables suffice to determine unambiguously the state of the system, and we proceed here with this simplest case. As the oscillation is periodic, i. e., it repeats itself after the period T, *x(t)* corresponds to a closed curve in the phase plane, called the *limit cycle.* The reason why we distinguish this curve from all others trajectories in the phase space is thus that it attracts phase trajectories and is therefore called an attractor of the dynamical system. The limit cycle is a simple attractor, in contrast to a *strange (chaotic) attractor.* The latter is a geometrical image of *chaotic* self-sustained oscillations.

Examples of self-sustained oscillatory systems are electronic circuits used for the generation of radio-frequency power, lasers, Belousov-Zhabotinsky and other oscillatory chemical reactions, pacemakers (sino-atrial nodes) of human hearts or artificial pacemakers that are used in cardiac pathologies, and many other natural and artificial systems. An outstanding common feature of such systems is their ability to be synchronized.

This ability of periodic self-sustained oscillators is based on the existence of a special variable, phase ϕ. Mathematically, ϕ can be introduced as the variable parameterizing the motion along the stable limit cycle in the state space of an autonomous continuous-time dynamical system. One can always choose the phase proportional to the fraction of the period, i. e., in a way that it grows uniformly in time,

$$\frac{d\phi}{dt} = \omega_0 \qquad [1]$$

where ω_o is the natural frequency of oscillations. The phase is neutrally stable: its perturbations neither grow nor decay. (In terms of nonlinear dynamics neutral stability means that the phase is a variable that corresponds to the zero Lyapunov exponent of the dynamical system.) Thus, already an infinitely small perturbation (e. g. external periodic forcing or coupling to another system) can cause large deviations of the phase contrary to the amplitude, which is only slightly perturbed due to the transversal stability of the cycle. The main consequence of this fact is that *the phase can be very easily adjusted by an external action, and as a result the oscillator can be synchronized!*

3. Entrainment by External Force

We begin our discussion of synchronization phenomena by considering the simplest case, entrainment of a self-sustained oscillator by external periodic force. Before we describe this effect in mathematical terms, we illustrate it by an example. We will speak about biological clocks that regulate daily and seasonal rhythms of living systems – from bacteria to humans.

3.1 An Example: Circadian Rhythms

In 1729 Jean-Jacques DORTOUS DE MAIRAN, the French astronomer and mathematician, who was later the Secretary of the Académie Royale des Sciences in Paris, reported on his experiments with a haricot bean. He noticed that the leaves of this plant moved up and down in accordance with the change of day into night. Having made this observation, DE MAIRAN put the plant in a dark room and found that the motion of the leaves continued even without variations in the illuminance of the environment. Since that time these and much more complicated experiments have been replicated in different laboratories, and now it is well-known that all biological systems, from rather simple to highly organized ones, have internal biological clocks that provide their "owners" with information on the change between day and night. The origin of these clocks is still a challenging problem. But it is well established that they can adjust their circadian rhythms (from *circa* = about and *dies* = day) to external signals: if the system is completely isolated from the environment and is kept under controlled constant conditions (constant illuminance, temperature, pressure, parameters of electromagnetic fields, etc.), its internal cycle can essentially differ from a 24-hour cycle. Under natural conditions, biological clocks tune their rhythms in accordance with the 24-hour period of the Earth's daily cycle.

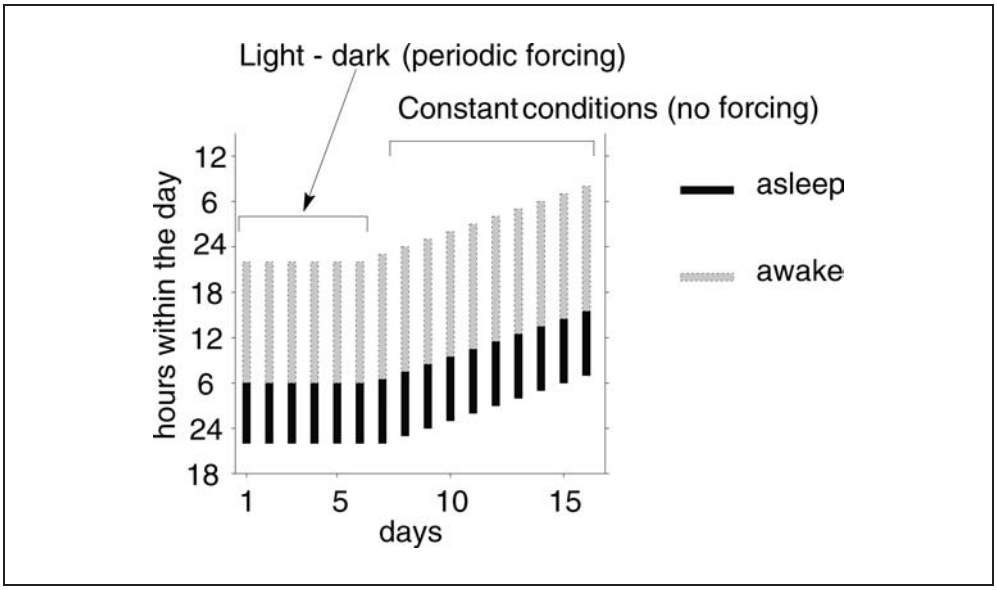

Fig. 1 Schematic diagram of the behavioral sleep-wake rhythm. This cycle (termed circadian rhythm) represents the fundamental adaptation of organisms to an environmental stimulus, the daily cycle of light and dark. Here the circadian rhythm is shown entrained for six days by the environmental light-dark cycle and autonomous for the rest of the experiment when the subject is placed under constant light conditions. The intrinsic period of the circadian oscillator is in this particular case larger than 24 hours. Correspondingly, the phase difference between the sleep-wake cycle and daily cycle increases: the internal "day" begins later and later. Such plots are typically observed in experiments with both, animals and humans (see, e. g., ASCHOFF et al. 1982, CZEISLER et al. 1986, MOORE 1999).

Experiments show that for most people the internal period of biological clocks differs from 24 h, but it is entrained by environmental signals, e. g. illuminance, having the period of the Earth's rotation (Fig. 1); see also the discussion of circadian oscillations of specific biological systems in the contributions by M. MITTAG and U. RASCHER, both in this volume. Obviously, the action here is unidirectional: the revolution of a planet cannot be influenced by mankind (yet); thus, this case constitutes an example of synchronization by an external force. In usual circumstances this force is strong enough to ensure perfect entrainment; in order to desynchronize a biological clock one can either travel to polar regions or go caving. It is interesting that although normally the period of one's activity is exactly locked to that of the Earth's rotation, the phase shift between the internal clock and the external force varies from person to person: some people say that they are "early birds" whereas others call themselves "owls".

Perturbation of the phase shift strongly violates normal activity. Every day many people perform such an experiment by rapidly changing their longitude (e. g. crossing the Atlantic) and experiencing jet lag. It can take up to several days to reestablish a proper phase relation to the force; in the language of nonlinear dynamics one can speak of different lengths of transients leading to the stable synchronous state. As other commonly known examples of synchronization by external force we mention radio-controlled clocks and cardiac pacemakers.

3.2 Phase Dynamics of a Forced Oscillator

For mathematical treatment of synchronization, we recall that the phase of an oscillator is neutrally stable and can be adjusted by a small action, whereas the amplitude is stable. This property allows description of the effect of small forcing/coupling within the framework of the phase approximation. Considering the simplest case of a limit cycle oscillator, driven by a periodic force with frequency ω and amplitude ε, we can write the equation for the perturbed phase dynamics in the form

$$\frac{d\varphi}{dt} = \omega_0 + \varepsilon Q(\varphi, \omega t), \qquad [2]$$

where the coupling function Q depends on the form of the limit cycle and of the forcing. As the states with the phases φ_0 and $\varphi_0 + 2\pi$ are physically equivalent, the function Q is 2π-periodic in its both arguments, and therefore can be represented as a double Fourier series. If the frequency of the external force is close to the natural frequency of the oscillator, $\omega \approx \omega_o$, then the series contains fast oscillating and slow varying terms, the latter can be written as $q(\phi - \omega t)$. Introducing the difference between the phases of the oscillation and of the forcing $\psi = \phi - \omega t$ and performing an averaging over the oscillation period we get rid of the oscillating terms and obtain the following basic equation for the phase dynamics:

$$\frac{d\psi}{dt} = -(\omega - \omega_0) + \varepsilon q(\psi). \qquad [3]$$

Function q is 2π-periodic, and in the simplest case, $q(\cdot) = s\sin(\cdot)$, Equation [3] *is* called the Adler equation. One can easily see that on the plane of the parameters of the external

forcing (ω, ε) there exists a region $\varepsilon q_{\min} < \omega - \omega_0 < \varepsilon q_{\max}$, where Equation [3] has a stable stationary solution. This solution corresponds to the conditions of phase locking (the phase ϕ just follows the phase of the force, he. $\phi = \omega t +$ *c*onstant) and frequency entrainment (the observed frequency of the oscillator $\Omega = \langle \varphi \rangle$ exactly coincides with the forcing frequency ω; brackets $\langle\ \rangle$ denote time averaging).

Generally, synchronization is observed for high-order resonances $n\omega \approx m\omega_0$ as well. In this case the dynamics of the generalized phase difference $\psi = m\varphi - n\omega t$, where *n, m* are integers, is described by an equation similar to Equation [3], namely by $d(\psi)/dt = -(n\omega - m\omega_0) + \varepsilon\tilde{q}(\psi)$. Synchronous regime then means perfect entrainment of the oscillator frequency at the rational multiple of the forcing frequency, $\Omega = \frac{n}{m}\omega$, as well as phase locking $m\varphi = n\omega t +$ constant. The overall picture can be shown on the (ω, ε) plane: there exist a family of triangular-shaped synchronization regions touching the ω-axis at the rationals of the natural frequency $\frac{m}{n}\omega_0$, these regions are usually called Arnold tongues (Fig. 2*A*). This picture is preserved for moderate forcing, although now the shape of the tongues generally differs from being exactly triangular. For a fixed amplitude of the forcing ε and varied driving frequency ω one observes different phase

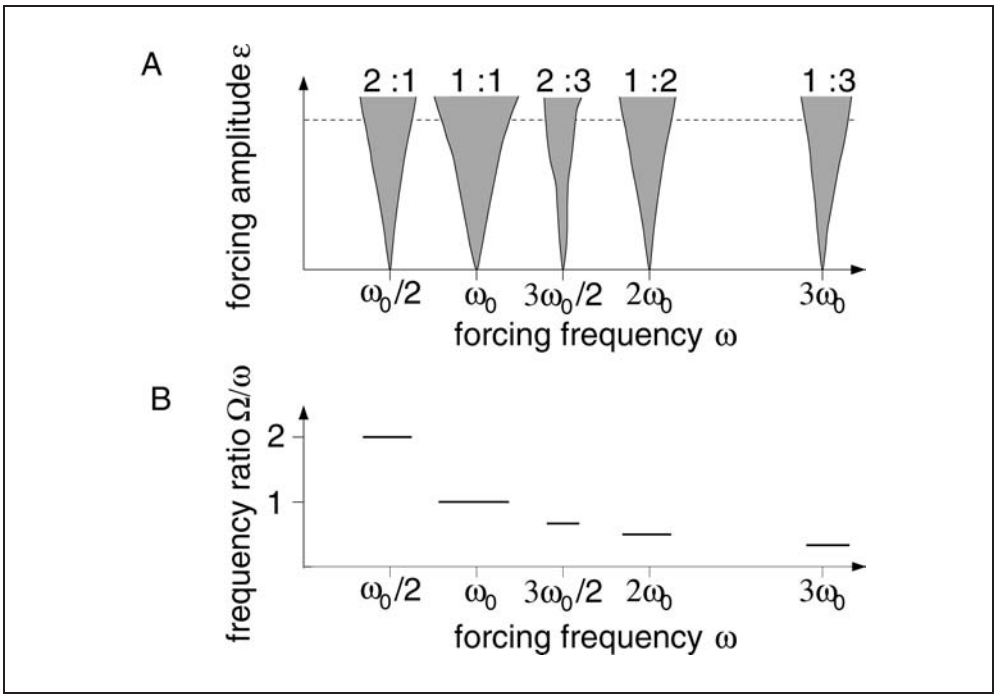

Fig. 2 (*A*) Family of synchronization regions, or Arnold tongues (schematically). The numbers on top of each tongue indicate the order of locking; e. g., 2 : 3 means that the relation $2\omega = 3\Omega$ is fulfilled. (*B*) The Ω/ω *versus* ω plot for a fixed amplitude of the force (shown by the dashed line in (*A*)) has a characteristic shape, known as the *devil's staircase.* (In this scheme the variation of the frequency ratio between the main plateaus of the staircase is not shown.)

locking intervals where the motion is periodic, whereas in between them it is quasiperiodic. The curve Ω *versus* ω thus consists of horizontal plateaus at all possible rational frequency ratios; this fractal curve is called devil's staircase (Fig. 2*B*). A famous example of such a curve is the voltage-current plot for a Josephson junction in an ac electromagnetic field; in this context synchronization plateaus are called Shapiro steps (Shapiro 1963). Note that a junction can be considered as a rotator (rotations are maintained by a dc current); this example demonstrates that synchronization properties of rotators are very close to those of oscillators (Pikovsky et al. 2001).

Finally, we note that the phase difference in the synchronous state is not necessarily constant, but may oscillate around a constant value. Indeed, a solution $m\varphi - n\omega t = \text{constant}$ was obtained from Equation [2] by means of averaging, i. e. by neglecting the fast oscillating terms. If we take this terms into account, then we have to reformulate the condition of phase locking as $|m\phi - n\omega t| < \text{constant}$. Thus, in the synchronous regime the phase difference is bounded, otherwise it grows infinitely.

3.3 Synchronization versus Resonance

At this point we would like to underline the difference to another phenomenon, well-known for oscillatory systems – the resonance. Resonance is a response of a system that is non-active, i. e., demonstrates no oscillations without external driving. In other words, here one cannot speak of an adjustment of intrinsic oscillations to an external force, as this force is the source of the oscillations. In the case of resonance, if the force is switched off, the oscillations disappear, while self-sustained oscillations continue to exist even without forcing.

As a simple example of this difference let us consider *radio-controlled clocks* and *older railway station clocks.* Radio-controlled clocks are self-oscillating, they continue to show time even if there is no radio signal from the high-precision center. The role of the latter is only to adjust – to correct – the oscillations in order to synchronize them with the time standard. The railway station clocks receive signals from a central clock, and if these signals are absent they stop; this is an example of resonance, not of synchronization.

Sometimes, when a system is forced very strongly and operates in a highly nonlinear regime, it is hard to distinguish between synchronization and resonance (especially if one can hardly control the forcing like for circadian rhythms), here the observed features at the resonance may be very close to those at the synchronization (e. g., one can observe the devil's staircase-like dependence on the forcing frequency). Nevertheless, the difference becomes evident if the forcing is reduced or switched off.

4. Two and More Oscillators

4.1 Phase Dynamics of Two Coupled Oscillators

Synchronization of two coupled self-sustained oscillators can be described in a similar way. A weak interaction affects only the phases of two oscillators ϕ_1 and ϕ_2, and Equa-

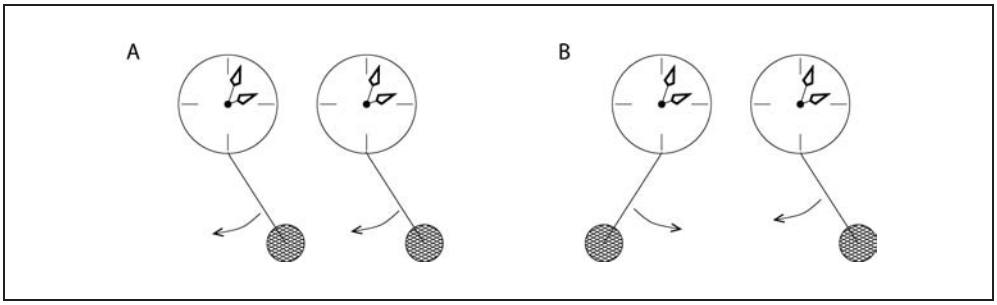

Fig. 3 Two coupled oscillators may be synchronized almost in-phase, i. e., with the phase difference $\phi_2 - \phi_1 \approx 0$ (*A*), or in anti-phase, when $\phi_2 - \phi_1 \approx \pi(B)$, in dependence on how the coupling was introduced. The discoverer of synchronization, Christiaan HUYGENS, observed synchronization in anti-phase. Later experiments, reported in BLEKHMAN (1981) demonstrated that both anti-phase and in-phase synchronous regimes are possible.

tion [1] generalizes to

$$\frac{d\varphi_1}{dt} = \omega_1 + \varepsilon Q_1(\varphi_1, \varphi_2) \qquad \frac{d\varphi_2}{dt} = \omega_2 + \varepsilon Q_2(\varphi_2, \varphi_1). \qquad [4]$$

For the phase difference $\psi = \phi_2 - \phi_1$ one obtains after averaging an equation of the type of Equation [3]. Synchronization now means that two non-identical oscillators start to oscillate with the same frequency (or, more generally, with rationally related frequencies). This common frequency usually lies between ω_1 and ω_2. It is worth mentioning that locking of the phases and frequencies implies no restrictions on the amplitudes, in fact the synchronized oscillators may have very different amplitudes and waveforms (e. g., oscillations may be relaxation [pulse-like] or quasiharmonic).

We conclude the discussion of mutual synchronization of two coupled systems with two remarks. (*i*) Similar to the case of periodic forcing, synchronization of the order $n : m$ is also possible. Examples are synchronization of running and breathing in mammals and locking of breathing and wing beat frequencies in flying birds (see PIKOVSKY et al. 2001 for citations and further examples). (*ii*) Depending on the parameters of coupling two oscillators can be locked almost in-phase or almost in anti-phase (Fig. 3). Moreover, varying the parameters of coupling one can observe transition between different synchronous states. As an example we mention the effect observed by J. A. S. KELSO and later studied by HAKEN, KELSO and co-workers (see HAKEN et al. 1985, HAKEN 1999 for references and details). In their experiments, a subject was instructed to perform an anti-phase oscillatory movement of index fingers and gradually increase the frequency. It turned out that at higher frequency this movement becomes unstable and a rapid transition to the in-phase mode is observed.

4.2 Globally Coupled Oscillators

Now we study synchronization phenomena in large ensembles of oscillators, where each element interacts with all others. This is usually denoted as *global,* or all-to-all coupling.

As a representative example we mention synchronous flashing in a population of fireflies. A very similar phenomenon, self-organization in a large applauding audience, has probably been experienced by every reader of this article, e. g. in a theater. Indeed, if the audience is large enough, then one can often hear a rather fast (several oscillatory periods) transition from noise to a rhythmic, nearly periodic, applause. This happens when the majority of the public applaud in unison, or synchronously.

The each-to-each interaction is also denoted as *mean field* coupling. Indeed, each firefly is influenced by the light field that is created by the whole population. Similarly, each applauding person hears the sound that is produced by all other people in the hall. Thus, we can say that each element is exposed to a force that comes to it from all others by one input from the whole ensemble. Let us denote these outputs of elements by $x_k(t)$, where $k = 1, \ldots, N$ is the index of an oscillator, and N is the number of elements in the ensemble; x can be variation of light intensity or of the acoustic field around some average value, or, generally, any other oscillating quantity. Then the force that drives each oscillator is proportional to $\sum_k x_k(t)$. It is conventional to write this proportionality as $\varepsilon N^1 \sum_k x_k(t)$, so that it includes the normalization by the number of oscillators N. The term $N^{-1}\sum_k x_k(t)$ is just an arithmetic mean of all oscillations, what explains the origin of the term "mean field coupling".

Thus, the oscillators in a globally coupled ensemble are driven by a common force. Clearly, this force can entrain many oscillators if their frequencies are close. The problem is that this force (the mean field) is not predetermined, but arises from interaction within the ensemble. This force determines whether the systems synchronize, but it itself depends on their oscillation – it is a typical example of self-organization (Haken 1993). To explain qualitatively the appearance of this force (or to compute it, as is done in Kuramoto 1984, Pikovsky et al. 2001) one should consider this problem self-consistently.

First, assume for the moment that the mean field is zero. Then all the elements in the population oscillate independently, and their contributions to the mean field nearly cancel each other. Even if the frequencies of these oscillations are identical, but their phases are independent, the average of the outputs of all elements of the ensemble is small if compared with the amplitude of a single oscillator. (According to the law of large numbers, it tends to zero when the number of interacting oscillators tends to infinity; the fluctuations of the mean field are of the order $N^{-1/2}$.) Thus, the asynchronous, zero mean field state obeys the self-consistency condition.

Next, to demonstrate that synchronization in the population is also possible, we suppose that the mean field is non-vanishing. Then, naturally, it entrains at least some part of the population, the outputs of these entrained elements sum up coherently, and the mean field is indeed nonzero, as assumed. Which of these two states – synchronous or asynchronous – is realized, or, in other words, which one is stable, depends on the strength of interaction between each pair and on how different the elements are. The interplay between these two factors, the coupling strength and the distribution of the natural frequencies, also determines how many oscillators are synchronized, and, hence, how strong the mean field is.

We discuss now how the synchronization transition occurs, taking the applause in an audience as an example (experimental study of synchronous clapping is reported in Néda et al. 2000). Initially, each person claps with an individual frequency, and the

sound they all produce is noisy.[1] As long as this sound is weak, and contains no characteristic frequency, it does not essentially affect the ensemble. Each oscillator has its own frequency ω_k, each person applauds and each firefly flashes with its individual rate, but there always exists some value of it that is preferred by the majority. Definitely, some elements behave in a very individualistic manner, but the main part of the population tends to be "like the neighbor". So, the frequencies ω_k are distributed over some range, and this distribution has a maximum around the most probable frequency. Therefore, there are always at least two oscillators that have very close frequencies and, hence, easily synchronize. As a result, the contribution to the mean field at the frequency of these synchronous oscillations increases. This increased component of the driving force naturally entrains other elements that have close frequencies, this leads to the growth of the synchronized cluster and to a further increase of the component of the mean field at a certain frequency. This process develops (quickly for relaxation oscillators, relatively slow for quasilinear ones), and eventually almost all elements join the majority and oscillate in synchrony, and their common output – the mean field – is not noisy any more, but rhythmic. Of course, the synchronization process as described above is not unconscious but depends on the intentions of the audience: in some countries a non-synchronous clapping is preferred, then even a lasting clapping does not synchronize.

The physical mechanism we described is known as the Kuramoto self-synchronization transition (Kuramoto 1975). The scenario of this transition does not depend on the origin of the oscillators (biological, electronic, etc.) or on the origin of interaction. In the above presented examples the coupling occurred *via* an optical or acoustic field. Global coupling of electronic systems can be implemented *via* a common load; in this case the voltage applied to individual systems depends on the sum of the currents of all elements. (As an example we mention an array of Josephson junctions.) Chemical oscillators can be coupled *via* a common medium, where concentration of a reagent depends on the reaction in each oscillator and, on the other hand, influences these reactions. The Kuramoto transition can be treated as a non-equilibrium phase transition, the mean oscillating field serving as an order parameter.

The scenarios of the Kuramoto transition may be also more complicated, e. g., if the distribution of the individual frequencies ω_k has several maxima. Then several synchronous clusters can be formed – they can eventually merge or coexist. Clustering can also happen if, say, the strength of interaction of an element of the population with its nearest (in space) neighbors is larger than with those that are far away.

5. Chaotic Systems

Nowadays it is well-known that self-sustained oscillators, e. g., nonlinear electronic devices, can generate rather complex, *chaotic* signals. Most oscillating natural systems also

1 Naturally, the common (mean) acoustic field is nonzero, because each individual oscillation is always positive; the intensity of the sound cannot be negative, it oscillates between zero and some maximal value. Correspondingly, the sum of these oscillations contains some rather large constant component, and it is the deviation from this constant that we consider as the oscillation of the mean field and that is small. Therefore, the applause is perceived as some noise of almost constant intensity.

exhibit rather complex behavior. Recent studies have revealed that such systems, being coupled, are also capable to undergo synchronization. Certainly, in this case we have to specify this notion more precisely, because it is not obvious, how to characterize the rhythm of a chaotic oscillator. It is helpful that sometimes chaotic waveforms are rather simple, so that a signal is "almost periodic"; we can consider it as consisting of similar cycles with varying amplitude and period (which can be roughly defined as the time interval between the adjacent maxima). Taking a large time interval N_τ we can count the number of cycles within this interval N, compute the *mean frequency* and take it for characterization of the chaotic oscillatory process.

$$\omega_0 = \lim_{\tau\to\infty} 2\pi\frac{N_\tau}{\tau}. \qquad [5]$$

With the help of the mean frequencies we can describe the collective behavior of interacting chaotic systems in the same way as we did it for periodic oscillators. If the coupling is large enough (e. g., in the case of resistively coupled electronic circuits it means that the resistor should be sufficiently small), the mean frequencies of two oscillators become equal, and one can obtain the synchronization region, exactly as in the case of periodic systems. It is important that coincidence of mean frequencies does not imply that the signals coincide as well. It turns out that weak coupling does not affect the chaotic nature of both oscillators; the amplitudes remain irregular and uncorrelated; whereas the frequencies are adjusted in a fashion that allows us to speak of the phase shift between the signals. This regime is denoted as *phase synchronization* of chaotic systems.

Very strong coupling tends to make the states of both oscillators identical. It influences not only the mean frequencies but also the chaotic amplitudes. As a result, the signals coincide (or nearly coincide) and the regime of *complete synchronization* sets in. Known are also the so-called generalized and master slave synchronization (see, e. g. Pikovsky et al. 2001 and references therein); these effects are related to the complete synchronization of chaos.

5.1 Phase Synchronization. An Example: Electrochemical System

Phase synchronization of chaotic systems is mostly close to the classical locking phenomena. It is based on the observation that many chaotic self-sustained oscillators admit determination of the instantaneous phase and the corresponding mean frequency. Below we illustrate this with an electrochemical oscillator, experimentally investigated by Kiss and Hudson (Kiss et al. 2001). An autonomous system demonstrates chaotic dynamics. The strange attractor looks like a smeared limit cycle; this allows one to introduce the phase as a variable that gains 2π with each rotation of the phase space trajectory, and to calculate frequency according to Equation [5].

Having introduced the phase and the frequency for chaotic oscillators we can characterize their synchronization. Now it becomes rather obvious that the effects of phase locking and frequency entrainment, known for periodic self-sustained oscillators, can be observed for chaotic systems as well. The simplest ease is the phase locking by an external periodic signal. When the electrochemical oscillator is driven by a signal with a frequency Ω close to ω_0, the forcing affects the evolution of the phase, and the ob-

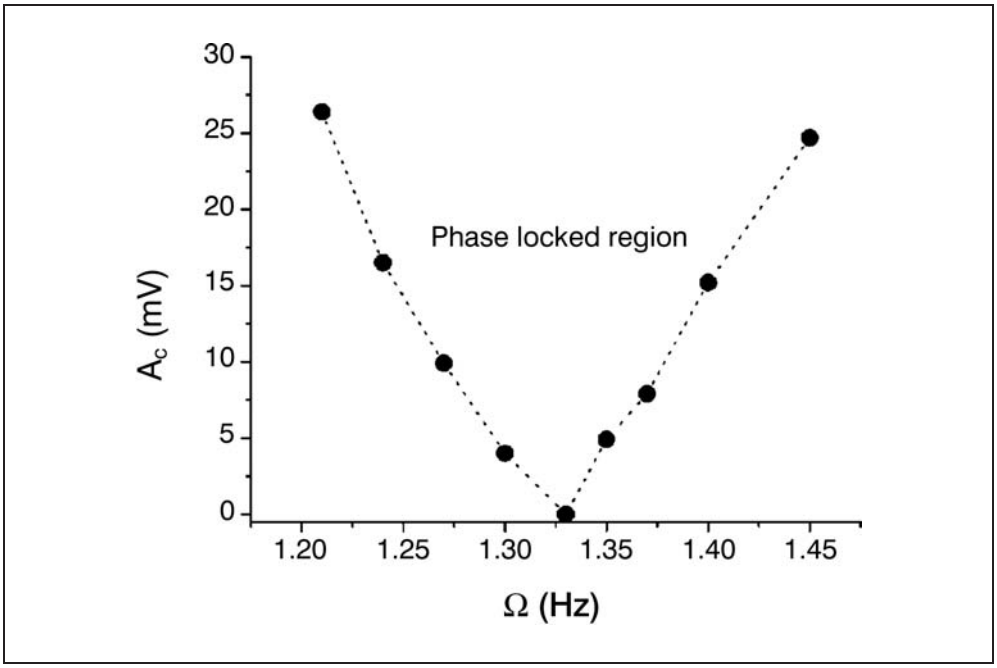

Fig. 4 The synchronization region for the periodically driven chaotic oscillator on the plane "amplitude of the driving – frequency of the driving" (Kiss et al. 2001).

served (mean) frequency ω becomes adjusted to the external one. The results of the experiment for different amplitudes of the forcing allow one to define the synchronization region, where the frequency of the system is completely entrained by the external force, see Figure 4. This region is a complete analog of synchronization regions (Arnold tongues) for periodic oscillators.

It is important to emphasize that the chaos itself is not suppressed by the external force. What happens is not a disappearance of chaos, but an adjustment of the mean oscillation frequency. Chaos may be destroyed by a strong force, but a small forcing affects only the phase, entraining the frequency of its rotation.

Mutual phase synchronization of chaotic oscillators is also quite similar to the classical case. To demonstrate this, one can couple two chaotic electrochemical oscillators. Then the calculation of the observed frequencies Ω_1, Ω_2 characterizes the entrainment. For large enough coupling and for small mismatch of natural frequencies one observes that frequencies becomes equal, $\Omega_1 = \Omega_2$, like in the experiments with periodic oscillators.

5.2 Complete Synchronization

Strong mutual coupling of chaotic oscillators leads to their *Complete Synchronization* when two or more chaotic systems have exactly the same states, and these identical states vary irregularly in time. Contrary to phase synchronization, it can be observed in

any chaotic system, not necessarily autonomous, in particular in periodically driven oscillators or in discrete time systems (maps). In fact, this phenomenon is not close to the classical synchronization of periodic oscillations, as here we do not have adjustment of rhythms. Instead, complete synchronization means suppression of differences in coupled *identical* systems. Therefore, this effect cannot be described as entrainment or locking; it is closer to the onset of symmetry. Maybe another word instead of "synchronization" would better serve for underlining this difference; we will follow the nowadays accepted terminology, using the adjective "complete" to avoid ambiguity.

The main precondition for complete synchronization is that the interacting systems are identical, i. e., they are described by exactly the same equations of motion. This identity implies that if the initial states of these systems are equal, then during the evolution they remain equal at all times. However, in practice this coincidence of states will be realized only if such regime is stable, i. e., if it is restored after a small violation. This imposes a condition on the strength of the coupling between the systems.

To be more concrete in our discussion, let us consider the coupled system of the type

$$\frac{d\vec{x}}{dt} = \vec{F}(\vec{x}) + \varepsilon(\vec{y} - \vec{x}) \qquad \frac{d\vec{y}}{dt} = \vec{F}(\vec{y}) + \varepsilon(\vec{x} - \vec{y}). \qquad [6]$$

Here $\vec{x}$ and $\vec{y}$ are two identical systems, described by the same equations $\vec{F}$, and we will assume that the solutions are chaotic. ε is the coupling parameter, the corresponding terms on the right hand sides describe a so-called diffusive coupling, which tends to equalize the states of two systems (this can be easily seen if one sets $\vec{F} = 0$, then the difference $\vec{y} - \vec{x}$ decreases in time with the rate 2ε).

While the coupling tends to equalize the states of two systems, another mechanism prevents this. This mechanism is the sensitive dependence to initial conditions, inherent for chaos. Suppose that $\varepsilon = 0$, then we have two uncoupled identical systems; they can be regarded as two realizations of one system with different initial conditions. Because chaotic motions sensitively depend on initial conditions (this phenomenon is often called the "Butterfly Effect"), the values $\vec{y}(t)$ and $\vec{x}(t)$ will differ significantly after some time, even if $\vec{y}(0) \approx \vec{x}(0)$.

Summarizing, we see two counter playing tendencies in the diffusive interaction of two identical chaotic systems: intrinsic chaotic instability tends to make the states of the systems different, while coupling tends to equalize them. As a result, there exists a critical value of coupling such that for stronger coupling a completely synchronized state $\vec{y}(t) = \vec{x}(t)$ sets on. At this regime the coupling term in [6] vanishes, and, hence, each of the systems varies chaotically in time as if they were uncoupled. Thus, the complete synchronization is a threshold phenomenon: it occurs only when the coupling exceeds some critical level, proportional to the largest Lyapunov exponent of the individual system. Below the threshold, the states of two chaotic systems are different but close to each other.

6. Conclusions and Outlook

In spite of the long history, theory of synchronization remains a rapidly developing branch of nonlinear science. Among the ongoing directions, not discussed in this arti-

cle, we mention synchronization in spatially-distributed systems and synchronization-like phenomena in stochastic and excitable systems (ANISHCHENKO et al. 2002).

Recent theoretical development was strongly influenced by interdisciplinary studies, especially by widely growing applications to biological and medical problems. It turned out that synchronization is very frequently encountered in live systems (GLASS 2001, PIKOVSKY et al. 2001). In particular, it is believed that the mechanism of the Kuramoto transition plays an important role in dynamics of neural ensembles and is responsible for the emergence of such severe pathologies as epilepsies and Parkinson disease. A popular paradigmatic model, analyzed in this context, is a system of pulse-coupled integrate-and-fire oscillators (see e. g. MIROLLO and STROGATZ 1990). Another direction of research is related to attempts to desynchronize undesirable, pathological collective rhythms and to develop in this way a therapeutic tool (TASS 1999).

Finally we mention that ideas from the synchronization theory are used in analysis of multivariate experimental data. The goal of such an analysis is to detect weak interaction between oscillatory systems, e. g. to reveal a coordination between respiratory and cardiac rhythms in humans (SCHÄFER et al. 1998) or localize the source of pathological brain activity in Parkinson disease (TASS et al. 1998, 2003).

References

ANISHCHENKO, V., NEIMAN, A., ASTAKHOV, V., VADIAVASOVA, T., and SCHIMANSKY-GEIER, L.: Chaotic and Stochastic Processes in Dynamic Systems. Berlin: Springer 2002

ASCHOFF, J., DAAN, S., and GROOS, G. A.: Vertebrate Circadian Systems. Structure and Physiology. Berlin: Springer 1982

BLEKHMAN, I. I.: Synchronization in Science and Technology. Moscow: Nauka 1981 (in Russian); English translation: New York: ASME Press 1988

CZEISLER, C. A., ALLAN, J. S., STROGATZ, S. H., RONDA, J. M, SÄNCHES, R., RÍOS, C. D., FREITAG, W. O., RICHARDSON, G. S., and KRONAUER, R. E.: Bright light resets the human circadian pacemaker independent of the timing of the sleep-wake cycle. Science *233*, 667–671 (1986)

GLASS, L.: Synchronization and rhythmic processes in physiology. Nature *410*, 277–284 (2001)

HAKEN, H.: Advanced Synergetics. Instability Hierarchies of Self-Organizing Systems. Berlin: Springer 1993

HAKEN, H.: Information and Self-Organization. A Macroscopic Approach to Complex Systems. Berlin: Springer 1988; second edition 1999

HAKEN, H., KELSO, J. A. S., and BUNZ, H.: A theoretical model of phase transitions in human hand movements. Biol. Cybern. *51*, 347–356 (1985)

KISS, I. Z., and HUDSON, J. L.: Phase synchronization and suppression of chaos through intermittency in forcing of an electrochemical oscillator. Phys. Rev. E *64*, 046215 (2001)

KURAMOTO, Y.: Self-entrainment of a population of coupled nonlinear oscillators. In: ARAKI, H. (Ed.): International Symposium on Mathematical Problems in Theoretical Physics; p. 420. Lecture Notes Phys. Vol. 39. New York: Springer 1975

KURAMOTO, Y.: Chemical Oscillations, Waves and Turbulence. Berlin: Springer 1984

MIROLLO, R., and STROGATZ, S.: Synchronization of pulse-coupled biological oscillators. SIAM J. Appl. Math. *50*, 1645–1662 (1990)

MOORE, R. Y.: A clock for the ages. Science *284*, 2102–2103 (1999)

MOSEKILDE, E., MAISTRENKO, Y., and POSTNOV, D.: Chaotic Synchronization. Applications to Living Systems. Singapore: World Scientific 2002

NÉDA, Z., RAVASZ, E., BRECHET, Y., VICSEK, T., and BARABÄSI, A.-L.: Tumultuous applause can transform itself into waves of synchronized clapping. Nature *403* (6772), 849–850 (2000)

PIKOVSKY, A. S., ROSENBLUM, M. G., and KURTHS, J.: Phase synchronization in regular and chaotic systems. Int. J. Bifurcation and Chaos *1011*, 2291–2306 (2000)

Pikovsky, A., Rosenblum, M., and Kurths, J.: Synchronization. A Universal Concept in Nonlinear Sciences. Cambridge: Cambridge University Press 2001

Schäfer, C., Rosenblum, M. G., Kurths, J., and Abel, H.-H.: Heartbeat synchronized with ventilation. Nature *392* (6673), 239–240 (1998)

Shapiro, S.: Josephson current in superconducting tunneling. The effect of microwaves and other observations. Phys. Rev. Lett. *11*, 280–282 (1963)

Tass, P. A.: Phase Resetting in Medicine and Biology. Stochastic Modelling and Data Analysis. Berlin: Springer 1999

Tass, P. A., Fieseler, T., Dammers, J., Dolan, K., Morosan, P., Majtanik, M., Boers, F., Muren, A., Zilles, K., and Fink, G. R.: Synchronization tomography. A method for three-dimensional localization of phase synchronized neuronal populations in the human brain using magnetoencephalography. Phys. Rev. Lett *90* (8), 088101 (2003)

Tass, P., Rosenblum, M. G., Weule, J., Kurths, J., Pikovsky, A. S., Volkmann, J., Schnitzler, A., and Freund, H.-J.: Detection of n : m phase locking from noisy data. Application to magnetoencephalography. Phys. Rev. Lett. *81* (15), 3291–3294 (1998)

Prof. Dr. Arkady Pikovsky
Dr. Michael Rosenblum
Department of Physics
University of Potsdam,
Am Neuen Palais 10
14415 Potsdam
Germany
URL:www.stat.physik.uni-potsdam.de/-pikovsky,
www.agnld.uni-potsdam.de/-mros
Phone: ++49 (0) 33 19 77 14 72
Fax: ++49 (0) 33 19 77 17 67
E-Mail: pikovsky@stat.physik.uni-potsdam.de
mros@agnld.uni-potsdam.de

Nova Acta Leopoldina NF *88*, Nr. 332, 269–278 (2003)

Active Amplification in Hearing

Frank JÜLICHER (Dresden)

With 3 Figures

Abstract

In a quiet environment, the ears of many vertebrates emit so-called spontaneous otoacoustic emissions as manifestations of active processes in the inner ear. It has been suggested that the ear employs active dynamical systems self-tuned to the critical point of an oscillating instability. It has recently been discovered that hair bundles, which are the mechanosensitive elements of sensory hair cells in the bull frog's sacculum, have the ability to oscillate spontaneously. In the presence of noise, the bifurcation disappears and is concealed by the noise, however, the principal signatures remain, such as frequency selectivity and nonlinear response. Furthermore, the amount of violation of the fluctuation-dissipation theorem can be quantified.

Zusammenfassung

In einer ruhigen Umgebung senden die Ohren vieler Wirbeltiere sogenannte spontane otoakustische Emissionen als Anzeichen aktiver Prozesse im Innenohr aus. Es wird vermutet, daß das Ohr aktive dynamische Systeme besitzt, die durch einen Selbstregulationsmechanismus an den kritischen Punkten einer oszillierenden Instabilität gebracht werden. Kürzlich ist entdeckt worden, daß Haarbündel, welche die mechanosensitiven Elemente der Sinneshaarzellen im Sacculum des Ochsenfroschs sind, spontan oszillieren können. Bei Vorhandensein von Fluktuationen verschwindet die Bifurkation und wird durch das Rauschen verdeckt. Die Hauptkennzeichen, wie die Frequenzselektivität und die nicht lineare Antwort, bleiben bestehen. Außerdem kann das Ausmaß der Verletzung des Fluktuationsdissipationstheorems quantitativ bestimmt werden.

1. Introduction

The task to detect sounds of the outside world imposes stringent demands on the design of the inner ear, where acoustic stimuli are transduced to electrical signals (HUDSPETH 1989). The cochlea contains highly specialized cells called hair cells, which act as mechanosensors. Each of these cells is responsive to a particular frequency component of the auditory input. Moreover, these sensors need extraordinary sensitivity, since the weakest audible sounds impart an energy, per cycle of oscillation, which is no greater than that of thermal noise (DE VRIES 1949). At the same time, they must operate over a wide range of volumes, responding and adapting to intensities which vary by many orders of magnitude. In order to achieve this goal, non-linear amplification is necessary.

The familiar resonant gain of a passive elastic system is far from sufficient for the required demands, because of the heavy viscous damping at microscopic scales (GOLD 1948). The ear relies on active systems to achieve exquisite sensitivity and sharp frequency selectivity (DALLOS 1992, HUDSPETH 1997, GOLD 1948). The most striking evidence for active behaviors in the ear are so-called otoacoustic emissions which are emitted sounds from the ears of mammals, birds and amphibians (PROBST 1990). It has recently been proposed that the cochlea contains active dynamical systems which are close to the critical point of a Hopf bifurcation (CHOE et al. 1998, CAMALET et al. 2000, EGUILUZ et al. 2000). Proximity to the bifurcation can in general be achieved by a self-tuning mechanism (CAMALET et al. 2000). This concept can explain many of the observed features of the ear, in particular the nonlinearities that are generally observed at resonance conditions (RUGGERO et al. 1997), the interference effects of multiple frequencies (JÜLICHER et al. 2001) as well as the occurrence of spontaneous emissions. While this concept seems to apply essentially to all vertebrate ears, the question of what are the underlying specific mechanisms at the origin of spontaneous oscillations is a subject of active research.

While in mammals, it is widely thought that outer hair cells are the active elements (DALLOS 1992) and thus might contain mechanical oscillators, no spontaneous oscillations have so far been observed. However, in the case of frogs it was discovered that hair bundles of the hair cells themselves could oscillate (MARTIN and HUDSPETH 1999, MARTIN et al. 2000). The observed noisy oscillations exhibit the signature of a system near a Hopf bifurcation: The response to periodic stimuli was nonlinear for sufficiently large amplitudes near the oscillation frequency (MARTIN and HUDSPETH 2001). For small amplitudes, there was a linear response regime which exhibited stable behaviors. Comparing the linear response to the autocorrelation function it was shown that the fluctuation dissipation theorem was violated, indicative for an active system (MARTIN et al. 2001).

The hair bundles of vertebrate hair cells consist of about 50 stereocilia which are stiff, rod-like extensions of the cell with a length of several micron and a diameter of about 300 nm, see Figure 1 (HUDSPETH 1997). The stereocilia merge at the tip and are grouped in a bundle. Fine filaments, so-called tip-links form bridges between neighboring stereocilia (KACHAR et al. 2000). The micromechanical properties of hair bundles in living hair cells can be rich and range from adaptation (slow relaxation involving active elements) (HOWARD and HUDSPETH 1988), twitches (rapid active motion) to spontaneous oscillations (HUDSPETH 1997, MARTIN and HUDSPETH 1999, FETTIPLACE et al. 2001, MARTIN and HUDSPETH 2001).

2. Generic Behaviors near a Hopf Bifurcation

What are the properties that make an oscillatory instability suitable for detection? A dynamical system which is tuned to the proximity of a Hopf bifurcation has very general properties and exhibits a compressive nonlinearity. This compressive nonlinearity permits the system to operate over 6 orders of magnitude in sound pressure. In order to discuss this, first consider the Van der Pol oscillator which is a standard model for nonlinear oscillators (VAN DER POL 1926, STRATONOVICH 1967, NAYFEH and MOOK 1979,

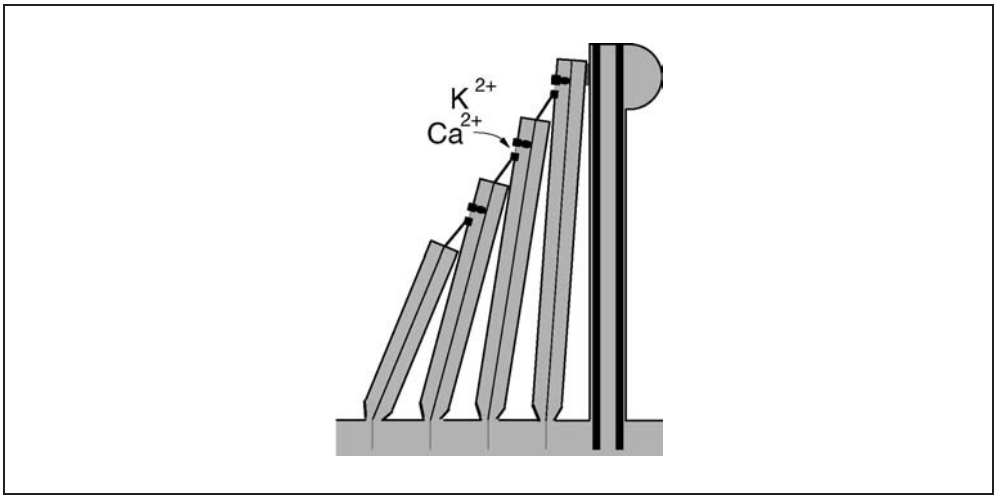

Fig. 1 Schematic representation of the hair bundle, the sensitive element of mechanosensory hair cells. It consists of 10–50 rod-like stereocilia which have a length of 1–10 μm and are connected by fine filaments, called tip-links. The stereocilia contain ion channels which open as a result of mechanical stimulation.

HÄNGGI and RISEBOROUGH 1983). Consider the dynamic equation

$$\gamma\ddot{x} + (\epsilon + \Lambda x^2)\,\dot{x} + kx = f_{\text{ext}}(t); \qquad [1]$$

which represent a damped oscillator with additional nonlinear friction. Here $\times$ is a displacement variable and f_{ext} an external force. γ, k and Λ are positive while ϵ can become negative.

In the absence of external forces, the system is stable for $\epsilon > 0$. It shows damped oscillations or is overdamped, and relaxes to $x = 0$. For $\epsilon = 0$, the system becomes unstable and undergoes a Hopf bifurcation. For $\epsilon < 0$ spontaneous oscillations are generated. In this regime the nonlinearity characterized by Λ is essential to stabilize the system and to determine the oscillation amplitude. In the periodic limit cycle for $f_{\text{ext}} = 0$, we can write

$$x(t) = \sum_n x_n e^{in\omega t} \qquad [2]$$

as a Fourier sum with oscillation frequency ω. Close to the bifurcation point, i. e. for small but negative ϵ, the first Fourier mode x_1 dominates and obeys to lowest order

$$\mathcal{A}x_1 + \mathcal{B}\,|x_1|^2\,x_1 = 0. \qquad [3]$$

Here, higher modes $x_n \sim x_1^n$ are neglected and the complex coefficients are given by $\mathcal{A} = k - \gamma\omega^2 + i\omega\epsilon$ and $\mathcal{B} = 3\Lambda\omega$. Spontaneous oscillations occur with frequency $\omega = \omega_c = (k/\gamma)^{1/2}$. This is the only choice for which Equation [3] has a solution for which the oscillation amplitude

$$|x_1|^2 = -\frac{\mathcal{A}}{\mathcal{B}} = -\frac{\epsilon\gamma}{3\Lambda k} \qquad [4]$$

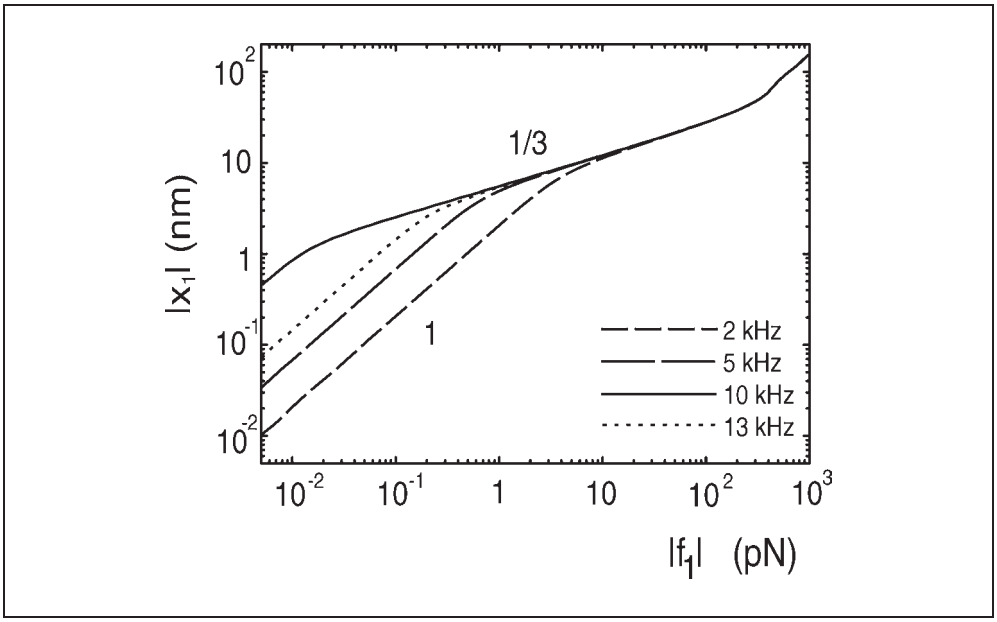

Fig. 2 Fourier amplitude $|x_1|$ of the response of a dynamical system at a Hopf bifurcation to a stimulus force of amplitude $|f_1|$ at different frequencies. The data is obtained by a numerical solution of the model described in the subsequent section, see CAMALET et al. (2000). The power law of the response is indicated.

is real and positive. The bifurcation point $\epsilon = 0$ is characterized by the condition that $A = 0$ vanishes at the critical frequency $\omega = \omega_c$.

Important for sound detection are the mechanical response properties of the oscillator in presence of a periodic stimulus $f_{ext} = f_1 e^{i\omega t} + f_{-1} e^{-i\omega t}$. For simplicity, we assume that only one frequency is present. Equation [3] then becomes

$$f_1 = \mathcal{A} x_1 + \mathcal{B} |x_1|^2 x_1. \qquad [5]$$

While the van der Pol oscillator is a particular choice of a dynamic oscillator, it is important to note that the expressions given in Equations [3] and [5] are generic and describe the mechanical response to any oscillating system in the vicinity of a Hopf bifurcation if it is stimulated at a frequency close to the oscillation frequency. In this case, we replace ϵ by an arbitrary control parameter C, and the linear coefficient $\mathcal{A}(\omega, C)$ is written as a function of C and ω. At the critical point, the control parameter takes a critical value $C = C_c$ and $\mathcal{A}$ vanishes for a critical frequency. We can therefore expand in general:

$$\mathcal{A}(\omega, C) \simeq a(\omega - \omega_c) + \beta(C - C_c). \qquad [6]$$

The van der Pol oscillator is characterized by $C = \epsilon$, $C_c = 0$, $\alpha = 2\gamma\omega_c$ and $\beta = i\omega$.

In order to illustrate the generic mechanical response we focus on the case where $C = C_c$, and the system is exactly at the bifurcation. Two different regimes of the response to an oscillating force can be distinguished, see Figure 2. If the applied

frequency is close to the critical frequency, the linear term can be ignored and

$$|x_1| \simeq |B|^{-1/3}|f_1|^{1/3} \simeq \frac{|f_1|^{1/3}}{(3A\omega_c)^{1/3}} \quad [7]$$

If the frequency mismatch is larger, $|\omega - \omega_c| >> |f_1|^{2/3}\,|B|^{1/3}/|\alpha|$, the cubic term is unimportant and the response becomes linear

$$|x_1| \simeq |A|^{-1}|f_1| = \frac{|f_1|^1}{|\alpha(\omega - \omega_c)|}. \quad [8]$$

The response of the system given by Equation [5] together with the oscillation amplitude [4] characterizes the main properties of an oscillator near the bifurcation point. This approach can be generalized to situations where more than one frequency is present (JÜLICHER et al. 2001).

3. Spontaneous Hair Bundle Oscillations

Spontaneous hair bundle oscillations have been observed experimentally in the sacculus of the frog (FETTIPLACE et al. 2001, MARTIN and HUDSPETH 1999, MARTIN et al. 2000). The observed noisy oscillations can be characterized for small amplitudes by a linear description. We write a dynamic equation for the hair bundle deflection x (MARTIN et al. 2001)

$$\lambda \frac{dx}{dt} = -kx + F_a + f_{\text{ext}} + \eta x + \text{nonlinear terms}; \quad [9]$$

where λ and k are an effective friction and stiffness, respectively, and where we have not specified nonlinearities. Note that we do not include a mass term since at the length scales and frequencies of interest, inertial terms can be ignored. The force F_a is an internally generated force due to active phenomena and active elements such as motor proteins or ion channels, while η is a noise of zero average describing fluctuations both of thermal origin and due to active processes. The system is stimulated by a periodic external force f_{ext}. It can oscillate spontaneously, if the active force F_a itself relaxes and provides a positive feedback to x. We therefore write

$$r^{-1}\frac{dF_a}{dt} = -F_a - \bar{k}x + \eta_a + \text{nonlinear terms}. \quad [10]$$

Here, r is a relaxation rate of the active process and the coupling coefficient $\bar{k}$ has dimensions of a spring constant. Note, that the combined equations for x and F_a represent an active system and cannot be derived from a potential.

In order to simplify our discussion, we focus on the illustrative case where $r = k/\lambda$. Indeed, fitting Equations [9] and [10] to the observed linear response function of a hair bundle leads to the observation $r \simeq k/\lambda$ for this case (MARTIN et al. 2001). Writing $F_a = (k\bar{k})^{1/2}\,y$, where y describes an internal displacement linked to an active process, we can represent the two degrees of freedom by a single complex variable $z = x + iy$. We furthermore add a nonlinearity with complex coefficient $B = (b + ib')$ to stabilize the

system when it starts to oscillate. We thus arrive at the equation

$$\frac{dz}{dt} = -(r + i\omega_0)\, z - B|z^2|\, z + \lambda^{-1} f_{\text{ext}} + \lambda^{-1}\eta, \qquad [11]$$

which is a standard representation of nonlinear oscillators. Here, the frequency of oscillations is given by $\omega_0 = (k\bar{k})^{1/2}/\lambda$. Noise in this system can be described by the complex stochastic force η.

4. Linear Response Function and Hopf Bifurcation

Consider the case where noise is absent, $\eta = 0$. The system undergoes a Hopf bifurcation at $r = 0$ and we identify r with the control parameter C. Writing $z(t) = \Sigma_n z_n e^{-in\omega t}$, we can bring the system into the general form [5]

$$f_1 = \mathcal{A}(\omega, r)\, z_1 + \mathcal{B}|z_1|^2\, z_1. \qquad [12]$$

Here, $B = \lambda B$ and $A = \tilde{\chi}^{-1}$ is related to the Fourier transform of the linear response function χ, defined *via*

$$x(t) = \int_{-\infty}^{t} dt' \chi(t - t')\, f_{\text{ext}}(t'). \qquad [13]$$

In Fourier representation, it is given by

$$\tilde{\chi}(\omega) \simeq \frac{1/2}{i\lambda(\omega_0 - \omega) + k} + \frac{1/2}{-i\lambda(\omega_0 - \omega) + k}. \qquad [14]$$

If the parameter r changes sign and becomes negative, the system undergoes a Hopf bifurcation and has limit-cycle solutions with amplitude

$$|z_1| = \left(\frac{b + b'^2/b}{b^2 + b'^2}\right)^{1/2} |r|^{1/2}, \text{ where } B = b + ib\,! \qquad [15]$$

5. Autocorrelation Function and Fluctuation Dissipation Theorem

In the presence of noise, the system generates noisy oscillations which can be characterized by their autocorrelation function $C(t) = \langle x(t)\, x(0)\rangle$. The noise conceals the Hopf bifurcation and leads together with the nonlinear terms to a renormalization of the parameters. We can still define the linear response function, which is in good approximation of the form given by Equation [14] if the parameters are replaced by their renormalized values. Assuming isotropic, Gaussian noise with auto-correlation $\langle \eta(t)\, \eta(0)\rangle = 2D(t)$, the auto-correlation function in Fourier representation is of the form:

$$\tilde{C}(\omega) \simeq \frac{\tilde{D}(\omega)}{k^2 + \lambda^2(\omega - \omega_0)} + \frac{\tilde{D}(-\omega)}{k^2 + \lambda^2(\omega + \omega_0)^2}. \qquad [16]$$

This is a correlation function characteristic for noisy oscillators with peaks in the spectrum at the oscillation frequency.

From the observation of the spectrum alone, one cannot distinguish between the system being a noisy spontaneous oscillator or a damped passive oscillator, subject to thermal fluctuations. In the former case of a passive system near thermal equilibrium, however, the linear response function is related to the autocorrelation function *via* a fluctuation-dissipation theorem (FTD) (FORSTER 1990): $\tilde{C}(\omega) = 2k_BT\tilde{\chi}(\omega)''/\omega$, where $\chi = \chi' + i\chi''$, i. e. χ'' is the imaginary part of the linear response function. If the system is an active oscillator, this FDT is broken. We characterize the degree to which the system deviates from equilibrium by defining the effective temperature for every frequency

$$\frac{T_{\text{eff}}(\omega)}{T} = \frac{\omega\tilde{C}(\omega)}{2k_BT\tilde{\chi}(\omega)''}. \qquad [17]$$

In our simple model, we expect for $\omega \simeq \omega_0$ this to be of the form

$$\frac{T_{\text{eff}}}{T} \simeq \frac{\tilde{D}(\omega)}{\lambda k_BT}\left(\frac{\omega}{\omega - \omega_c}\right). \qquad [18]$$

The linear response function and the auto-correlation function have been measured for spontaneous hair-bundle oscillations (MARTIN et al. 2001). A fit to the experimental data leads to $k \simeq 1.04 \cdot 10^{-4}$ N/m, $\lambda \simeq 6.5 \cdot 10^{-6}$ Ns/m. The auto-correlation function could be well described by using Gaussian white noise with $\tilde{D}(\omega) = 2D_0$, with $D_0 \simeq 0.14$ pN^{2}s.

6. Self-tuning

While the properties of a Hopf bifurcation can explain the main properties of sound detection by the ear, it raises a number of important questions. In particular, in order to exhibit a nonlinear response for small amplitudes, the system has to be tuned with high precision to its critical point. This requires a fine-tuning of parameters, which raises doubts as to whether a living cell can profit from the special properties at a critical point in a reliable way.

A simple and general mechanism to maintain a dynamical system at a point of operation close to the bifurcation point can be achieved by a feedback regulation of the control parameter (CAMALET et al. 2000, CAMALET 2001). This self-tuning implies that the control parameter is regulated toward the instability as long as the system is not spontaneously oscillating, while it is automatically stabilized as soon as oscillations are detected. This self-tuning works best in the absence of external stimuli, when highest sensitivity is needed, by adapting the control parameter C as a function of the detected amplitude of hair-bundle deflections.

An illustrative example for self-tuning is achieved in a situation where the Ca^{2+} concentration in the hair cell plays the role of the control parameter at the bifurcation (Fig. 3). Since hair-bundle deflections lead to an influx of Ca^{2+} into the hair cell, this provides for a regulation of the control parameter C of the form

$$\frac{dC}{dt} = -\frac{C}{\tau} + JP(x) \qquad [19]$$

where τ is a relaxation time of the control parameter in the absence of hair bundle deflections x. This relaxation drives the system in the oscillatory regime. As soon as deflec-

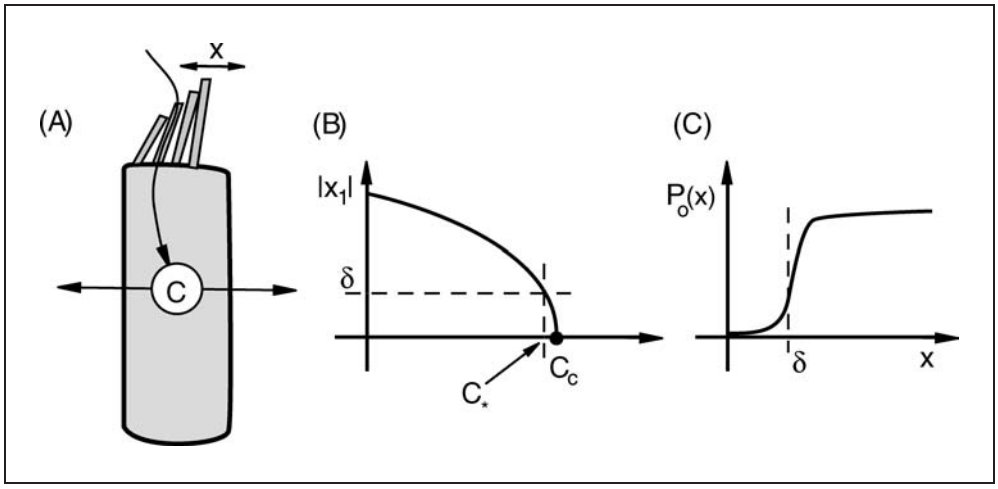

Fig. 3 Simple self-tuning mechanism (schematic). (*A*) Regulation of the control parameter *C* associated with the concentration of ions such as Ca^{2+} which enter the hair cell *via* transduction channels. A permanent outflux drives the system toward the oscillating side of the bifurcation, influx of ions *via* transduction channels provides a stabilizing feedback. (*B*) Fourier amplitude $|x_1|$ of spontaneous oscillations as a function of the control parameter near the bifurcation point C_c. Self-tuning brings the system to an operating point C_*. (*C*) Opening probability $P_o(x)$ of ion channels as a function of the deflection amplitude *x*. A signal is generated for deflections larger than δ.

tions *x* occur, ion channels open with probability

$$P(x) = \frac{1}{1 + e^{-(x-\delta)/\ell}} \qquad [20]$$

and each open channel gives rise to an influx *J* of Ca^{2+}, which drives the system toward the non-oscillating regime. Here we assume $\tau >> \omega^{-1}$, i. e., changes in *C* occur on timescales long compared to the oscillation frequency. The length scale δ, which for hair bundles is of the order of 0.3–1 nm, indicates the smallest deflection amplitudes at which a signal is generated by the hair bundle and the parameter ℓ characterizes the sharpness of the response.

The self-tuning can now be summarized as follows. In the absence of spontaneous oscillations (and if no external sound stimulus is present), the control parameter is decreased within a relaxation time τ. As soon as the critical point C_c is reached, the system starts to oscillate and the decrease of *C* is halted as soon as the typical oscillation amplitude is of the order of magnitude δ (see Fig. 3). Remember that the onset of spontaneous oscillations in the absence of a force given by Equation [4] can be expressed as

$$|x_1| \simeq \Delta \left(\frac{C - C_c}{C_c} \right)^{1/2}, \qquad [21]$$

where Δ is a characteristic saturation amplitude. We can therefore estimate how close to the bifurcation point the system will be tuned *via* this mechanism. Introducing the distance $\Delta C = C_c - C$ from the bifurcation, the self tuning brings the system slightly to the oscillating side of the bifurcation with

$$\Delta C/C_c \sim (\delta/\Delta)^2. \qquad [22]$$

For a typical hair cell we estimate $\delta \sim 1$ nm and $\Delta \sim 100$ nm, thus the system can self-tune with $\Delta C/C_c \simeq 10^{-4}$.

These estimates for the useful amplitude range of hair bundle deflections can also explain the dynamic range of hearing. In the regime of nonlinear response, the hair cell can map changes in force amplitude $|f_1|$ that vary by a factor of $(\Delta/\delta)^3 \simeq 10^6$ onto hair bundle deflections $|x_1|$ which vary over the usable range of Δ/δ. This range of detectable force amplitudes corresponds to a dynamic range of 120 dB.

7. Discussion

The concept of self-tuning to a Hopf bifurcation can explain seemingly disconnected but well-known properties of hearing. In addition to providing an explanation for the high sensitivity at one frequency and a large dynamic range, it can naturally account for what is called adaptation and fatigue. Fatigue implies that the sensitivity to weak stimuli is reduced after a subject is exposed to a loud stimulus which is a natural consequence of self-tuning. In the presence of a stimulus, Equation [19] tunes the system away from the bifurcation point where sensitivity is reduced. The recovery of high sensitivity after a strong stimulus only happens after a relaxation time τ of the self-tuning feedback to its operation point.

This theory of hearing by a generic mechanism could apply to many different animals such as mammals, birds, reptiles and amphibians. These classes of animals, however, have different ears and different types of hair cells and they might thus use different physical systems to realize a Hopf bifurcation and the self-tuning. In the case of mammals, there is some evidence that so-called outer-hair cells are able to generate active motion by contracting the whole cell body (Dallos 1992). Recently, a protein which could play an active role in these contractions has been identified (Zheng et al. 2000). Non-mammalian vertebrates do not possess outer hair-cells. Active oscillators are therefore expected to exist within the hair bundle itself. Spontaneous hair bundle oscillations of amphibian hair-cells have shown that the hair bundle itself could be the active system (Martin and Hudspeth 1999, Martin et al. 2000).

Spontaneous oscillations generated by cells are always noisy and this noise plays an important role for the detection of weak stimuli. The importance of noise has been discussed in the context of stochastic resonance (Gammaitoni et al. 1998, Wiesenfeld and Moss 1995). Near a Hopf bifurcation, there are other aspects of noise which play a role. In the presence of noise, the Hopf bifurcation is concealed, and noisy spontaneous oscillations cannot strictly be distinguished from noise. The difference between noisy spontaneous motion and a periodic stimulus lies mainly in the phase coherence of the stimulus. This phase coherence also appears in the response on top of a noisy oscillation. The detection of phase coherence in the nervous signal generated by the hair cells can thus allow the nervous system to detect weak signals.

Acknowledgement

I thank Sebastien Camalet, Thomas Duke, Pascal Martin, James A. Hudspeth, Björn Nadrowsky, Jacques Prost and Thomas Risler for stimulating collaborations.

References

Camalet, S.: Oscillations critiques de systèmes biologiques. These de doctorat de l'université Paris 6 (2001)

Camalet, S., Duke, T., Jülicher, F., and Prost, J.: Proc. Natl. Acad. Sci. USA *97*, 3183–3188 (2000)

Choe, Y., Magnasco, M., and Hudspeth, A. J.: Proc. Natl. Acad. Sci. USA *95*, 15321–15326 (1998)

Dallos, P.: J. Neurosci. *12*, 4575–4585 (1992)

Eguiluz, V. M., Ospeck, M., Choe Y., Hudspeth, A. J., and Magnasco, M.: Phys. Rev. Lett. *84*, 5232–5235 (2000)

Fettiplace., R., Ricci, A. J., and Hackney, C. M.: Trends Neurosci. *24*, 169–175 (2001)

Forster, D.: Hydrodynamic Fluctuations, Broken Symmetry, and Correlation Functions. Addison-Wesley 1990

Gammaitoni, L., Hänggi, P., Jung, P., and Marchesoni, F.: Rev. Mod. Phys. *70*, 223 (1998)

Gold, T.: Proc. R. Soc. London B *135* (1948)

Hänggi, P., and Riseborough, P.: Amer. J. Phys. *51*, 347–352

Howard, J., and Hudspeth, A. J.: Neuron *1*, 189–199 (1988)

Hudspeth, A. J.: Nature (London) *341*, 397–404 (1989)

Hudspeth, A. J.: Curr. Opin. Neurobiol. *7*, 480–486 (1997)

Jülicher, F., Andor, D., and Duke, T.: Proc. Natl. Acad. Sci. USA *98*, 9080–9085 (2001)

Kachar, B., Parakkal, M., Kurc, M., Zhao, Y., and Gillespie, P. G.: Proc. Natl. Acad. Sci. USA *97*, 13336–13341 (2000)

Martin, P., and Hudspeth, A. J.: Proc. Natl. Acad. Sci. USA *96*, 14306–14311 (1999)

Martin, P., and Hudspeth, A. J.: Proc. Natl. Acad. Sci. USA *98*, 14386–14391 (2001)

Martin, P., Hudspeth, A. J., and Jülicher, F.: Proc. Natl. Acad. Sci. USA *98*, 14386–14391 (2001)

Martin, P., Mehta, A., and Hudspeth, A. J.: Proc. Natl. Acad. Sci. USA *97*, 12026–12031 (2000)

Nayfeh, A. H., and Mook, D. T.: Nonlinear Oscillations, Pure and Applied Mathematics. New York: Wiley 1979

Probst, R.: Adv. Otorhinolaryngol. *44*, 1–91 (1990)

Ruggero, M. A., Rich, N. C., Recio, A., Narayan, S. S., and Robles, L.: J. Acoust. Soc. Amer. *101*, 2151–2163 (1997)

Stratonovich, R. S: Topics in the Theory of Random Noise. Vol. II. New York: Gordon and Breach 1967

Van der Pol, B.: Philos. Mag. *2* (1926)

Vries, H. L. de: Physica *14*, 48–60 (1949)

Wiesenfeld, K., and Moss, F.: Nature *373*, 33 (1995)

Zheng, J., et al.: Nature *405*, 155 (2000)

Prof. Dr. Frank Jülicher
Max-Planck-Institut für Physik komplexer Systeme
Nöthnitzerstraße 38
01187 Dresden
Germany
Phone: ++49 (0) 35 18 71 12 02
Fax: ++49 (0) 35 18 71 12 99
E-Mail: julicher@mpipks-dresden.mpg.de

Nova Acta Leopoldina NF *88*, Nr. 332, 279–291 (2003)

Chaotic Ratchets: Dissipative *versus* Hamiltonian, Classical *versus* Quantum

Walter Acevedo, Thomas Dittrich, and Carlos Pineda
(Santafé de Bogotá)

With 9 Figures

Abstract

For transport on subcellular down to molecular scales, nonlinear dynamics, noise, and eventually quantum effects are the relevant physical concepts. In the framework of *ratchets*, it is studied how these effects conspire to generate directed transport in the absence of any external gradient. We analyze some fundamental physical conditions for directed transport in deterministic chaotic systems, in particular concerning spatial and temporal (a)symmetries. In the presence of dissipation, we point out the relevant structures of the system's attractors and their basins of attraction. For the Hamiltonian case, we present a sum rule implying that transport requires a mixed (chaotic and regular) dynamics. Upon quantizing a Hamiltonian ratchet, new phenomena such as tunneling and localization emerge which profoundly alter the classical scenario.

Zusammenfassung

Die für Transportphänomene auf subzellulären Skalen relevanten physikalischen Konzepte sind nichtlineare Dynamik, thermische Fluktuationen sowie, im molekularen Bereich, Quanteneffekte. Das Modell der *Ratsche* bietet einen geeigneten Rahmen, das Zusammenspiel dieser Effekte beim Zustandekommen gerichteten Transports in Abwesenheit äußerer Gradienten zu studieren. Wir untersuchen die allgemeinen physikalischen Bedingungen für gerichteten Transport bei deterministischen chaotischen Systemen, insbesondere im Hinblick auf räumliche und zeitliche Symmetrien und ihre Brechung. Für den dissipativen Fall weisen wir auf die relevanten Strukturen der dynamischen Attraktoren und ihrer Einzugsbassins hin. Für den Fall hamiltonscher Ratschen impliziert eine Summenregel, daß Transport nur in einem gemischten Phasenraum (chaotisch und regulär) möglich ist. Ihre Quantisierung erlaubt es, den Einfluß von Quanteneffekten wie Tunneln und Lokalisierung auf gerichteten Transport zu analysieren.

1. Introduction

The relevance of nonlinear dynamics for the formation of complex patterns in biological, chemical, geophysical and many other systems is well established and studied since decades by now, as is its role in the recognition of such patterns in perception processes. The formation and change of spatial patterns, in turn, requires transport processes, typically on cellular, subcellular through down to molecular scales. It is a relatively recent insight that nonlinear dynamics plays a fundamental role also here. While pattern formation as such typically can be described as a macroscopic process (with some notable exceptions in chemical patterns), the underlying transport involves microscopic physics. Subcellular

systems are subject to thermal fluctuations. It has been shown that the corresponding Brownian motion is not just a disturbance but rather an active, constructive element in a number of biological functions. A prominent example is stochastic resonance, which forms a crucial ingredient, e. g., in sensual systems (Gammaitoni et al. 1998). In the same spirit, Brownian motion "fuels" transport by Brownian motors, specialized molecules capable of rectifying non-equilibrium noise into directed motion (Reimann 2002). Going further down in scale, quantum effects enter the scene. There is no doubt that they are involved in binding and unbinding, in proton transport and electron exchange. The relevance of quantum effects for more specific biological transport processes remains an open question, since physiological temperature and the strong coupling of functional molecules to the ambient cell plasm and to "parasitic" degrees of freedom within the molecules themselves lead to a rapid decay of quantum coherence. It is clear, however, that quantum mechanics is the only adequate framework once it comes to artificial transport systems, mimicking their biological analogues in nanometer-scale semiconductor devices.

The basic physical concepts involved in subcellular transport therefore are nonlinear dynamics, noise (in space and time), and quantum effects, though close to the classical limit and mitigated by strong decoherence. A fourth crucial ingredient is symmetry, for two reasons: On the one hand, directed transport as such already singles out a certain direction in space, i. e., it breaks reflection symmetry. If the direction of flow is not left to some contingent initial condition but is predetermined, it must reflect an underlying asymmetry in the structure of the motor-rail assembly. On the other hand, rotational molecular motors and the chain molecules serving as rails for their linear cousins are typically characterized by a discrete rotation or translation invariance, respectively. While in classical physics, such discrete symmetries or small deviations from them do not make a big difference, quantum effects are extremely sensitive to them: Suffice to mention coherent tunneling, a phenomenon indicating the presence of a precise discrete symmetry, and Anderson localization, the antagonist of tunneling occurring in disordered systems. The relevance of these interference effects for nonlinear transport is evident (Utermann et al. 1994, Dittrich et al. 2001).

Apart from the problems posed by the specific functioning of each individual molecular motor, the question how directed motion is generated from the interplay of the factors listed above, and under which basic conditions it can come about, represents a formidable problem of physics. It is being studied since a few years in the framework of a class of models designed to reduce the biological diversity to the physically essential: so-called ratchets. In the following paragraphs, we shall retrace the "evolution" of ratchets towards reductionist theoretical constructs, abandoning one by one the aspects of noise and dissipation, and ending up with quantum Hamiltonian ratchets. We shall thereby concentrate on results of our own research, complementing them where necessary to provide a more comprehensive image. A preview of possible directions of the inverse, holistic reconstruction of biological reality that is to follow, will be given in the conclusion.

2. Dissipative Chaotic Ratchets

The thermal fluctuations driving Brownian motors are a standard case of a random process, tractable in the framework of stochastic differential equations (Reimann 2002). It

is tempting, however, to remove this conceptually subtle element from the description, replacing it by deterministic chaos (JUNG et al. 1996). The motivation for this step is to study the response of chaotic systems to completely desymmetrized conditions, and to understand if and how ratchets can function in the absence of random noise.

A model is readily constructed from two elements: A potential periodic in space but asymmetric under space inversion, and a driving periodic in time. The dynamics is then given, for example, by the equation of motion [1]

$$\frac{\mathrm{d}p}{\mathrm{d}t} = \gamma p - V'(x) \sum_{n=-\infty}^{\infty} \delta(t - nT), \qquad \frac{\mathrm{d}x}{\mathrm{d}t} = K'(p) \qquad [1]$$

where

$$V(x) = k(\sin\ x + 2\alpha\ \sin(2x - \beta)) \qquad [2]$$

is a periodic yet asymmetric (for finite α and $\beta \neq n\pi$) potential, and $K(p) = p^2/2m$ is the kinetic energy. The parameter γ gives the rate of dissipation: On the corresponding time scale $t_{\mathrm{diss}} = 1/\gamma$, the system contracts onto an attractor: a point in phase space (point attractor), a limit cycle, or a strange attractor. While an individual trajectory has transients on the scale t_{diss} that need not show any symmetry, the attractors must obey the same symmetry as the potential, that is, periodicity in space and time. This has profound consequences for transport: It requires the mean displacement of point attractors, or any other attractor restricted to a single unit cell, to be "classically quantized", i. e., be given by $v = wX/T$, where X and T are the spatial and temporal periods of the potential, respec-

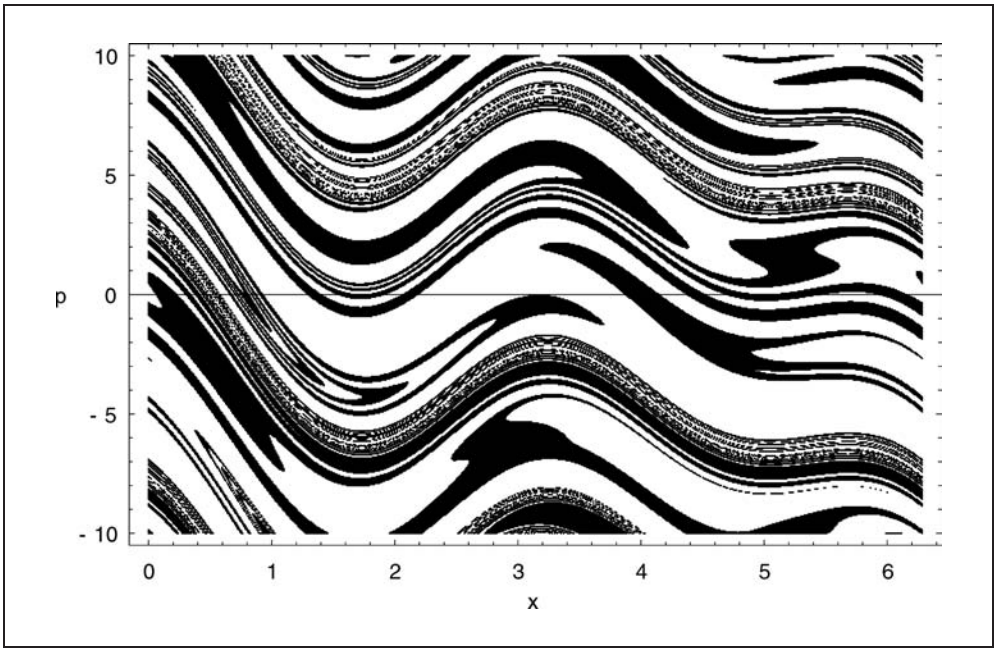

Fig. 1 Basins of attraction of the dissipative chaotic ratchet, Eqations [1], [2], with $\exp(-\gamma) = 0.27$ and $k = 2.5$. The basins of attraction of the two coexisting attractors are filled white and black, respectively.

tively, and $w = n_x/n_t$, with n_x and n_t integer, is a rational winding number. The corresponding projection of the attractor onto the (x, t)-plane is then invariant under shifts by n_x periods in space and n_t periods in time. A finite velocity associated to a given attractor, however, is not yet sufficient for the system to show overall directed transport. For example, the contribution of that attractor might be compensated by the contribution of a counterpart transporting in the opposite direction. In the presence of several attractors, which is the typical case, it is required that their basins of attraction (the region in phase space contracting to a given attractor) be asymmetric, in such a manner that even an initially unbiased velocity distribution converges to a finite mean velocity.

Basins of attraction form a feature of nonlinear dynamical systems not studied as intensely as the attractors themselves, but can be just as rich in their spatial structure. In particular, their boundaries can possess fractal geometry. In this case, not only the motion on the attractor, but also the selection of one attractor among several coexisting ones shows a sensitive dependence on the initial conditions. We have found that in deterministic chaotic ratchets, this is the rule rather than the exception (Fig. 1; ACEVEDO et al. 2002). As a consequence, in phase-space regions where basins of attraction strongly mix, only probabilities for a certain value of transport can be predicted, given by the relative share of phase-space area of the corresponding attraction basin.

In the case of attractors–point, cycle, or strange–not exceeding the boundaries of a single unit cell of the potential, an initially localized ensemble will move with the quantized velocity mentioned above, without any spreading. This situation changes radically

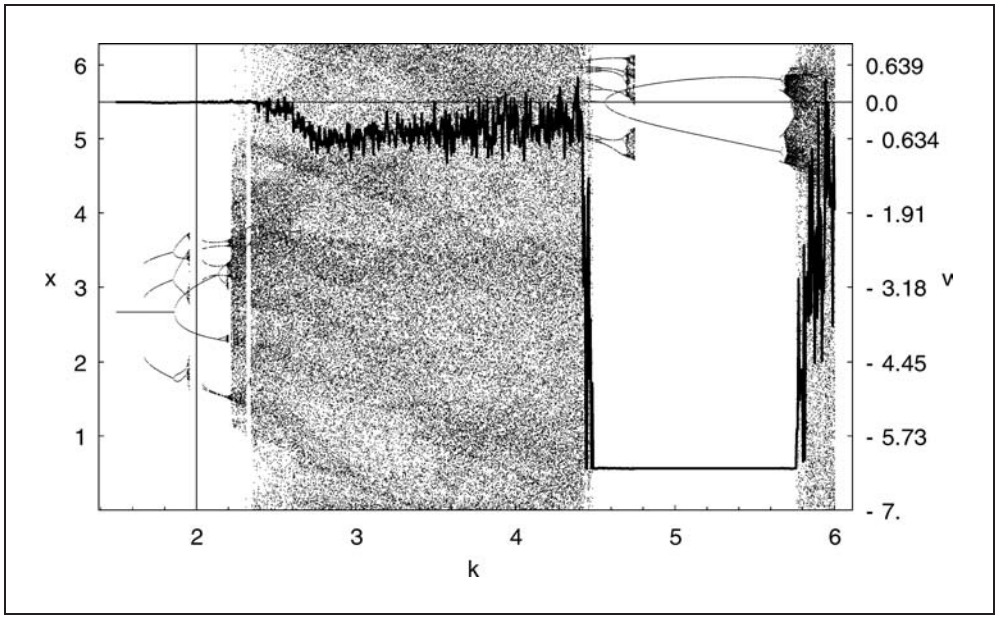

Fig. 2 Bifurcation diagram of the dissipative chaotic ratchet, Eqations [1], [2], at $\exp(-\gamma) = 0.6$, as a function of the parameter k. The fusion of the attractors across the unit-cell boundaries (cf. Fig. 3 below) occurs at $k = 2.4$, giving rise to the onset of transport (black curve). At $k = 4.4$, the strange attractor collapses into a cycle with winding number $w = -1$ (note that here the spatial period is $2p$).

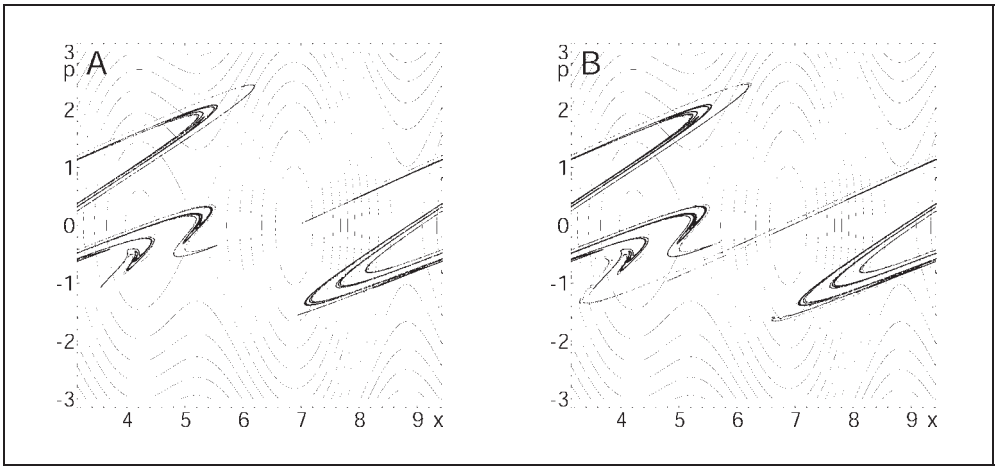

Fig. 3 Crisis of the dissipative chaotic ratchet, Eqations [1], [2], at $\exp(-\gamma) = 0.4$. In (*A*), at $k = 4.1$, the strange attractor is still restricted to a single unit cell, while in (*B*), at $k = 4.2$, two lobes have just merged, connecting the attractor along the entire ratchet. The energy contours of the corresponding system without damping (continuous lines) show that the merger occurs across a separatrix that forms a natural unit-cell boundary.

once, as a function of some parameter like the driving amplitude, a strange attractor merges with its neighbors across the unit-cell boundary (Fig. 2 and 3). The hitherto separate attractors, one per unit cell, thus join to form a single one that extends along the entire ratchet. This topological change, called a crisis, opens the way for trajectories to move freely between unit cells, rendering the motion diffusive instead of ballistic. The full dynamics is then described by a Fokker-Planck equation, comprising free diffusion superposed on a mean drift velocity (JUNG et al. 1996) which no longer needs to be "classically quantized". Similarly abrupt, but less drastic modifications of transport can occur as the consequence of minor conformational changes of strange attractors, upon varying a parameter (MATEOS 2000).

3. Hamiltonian Chaotic Ratchets

3.1 Driven Ratchets

From a fundamental point of view, dissipation is an "emergent phenomenon" that results from restricting consideration to part of a system which in fact is coupled to additional degrees of freedom not directly accounted for in the description. Since these invisible freedoms typically are microscopic ones, dissipation results from assuming a macroscopic point of view, and correspondingly disappears upon going to a complete, microscopic description of the system at hand. Surprisingly enough, the question of directed currents in a Hamiltonian system can arise even on a macroscopic level, for example in models of hydrodynamic flow in the Earth's atmosphere (DEL-CASTILLO-NEGRETE 1998).

So it is legitimate to ask whether the concept of ratchets survives in a Hamiltonian framework where dissipation is excluded. Its role for the functioning of ratchets is twofold: It breaks time-reversal invariance, and it leads to a contraction of phase space. The first effect can be replaced in a Hamiltonian setting by introducing a time-dependent external force that is periodic but not symmetric under time reversal (Flach et al. 2000). For example, one might use the asymmetric function [2], both for the position and the time dependence of the potential,

$$V(x,t) = k_x(\sin x + 2\alpha_x \sin(2x - \beta_x)) + xk_t(\sin t + 2\alpha_t \sin(2t - \beta_t)) . \quad [3]$$

The second modification entailed by a Hamiltonian dynamics – conservation of phase-space volume – turns out to be more severe. Together with the spatiotemporal periodicity of the potential it implies a sum rule: Averaged over a unit cell in phase space, and over a period of the driving in time, transport must vanish identically (Dittrich et al. 2000, Schanz et al. 2001). This has profound consequences since it requires, for example, that in a system with homogeneously chaotic phase space, there can be no transport whatsoever. Likewise, in an integrable system with a phase space completely foliated by tori, transport along tori with positive mean momentum will be exactly cancelled by the contribution of tori with negative mean momentum.

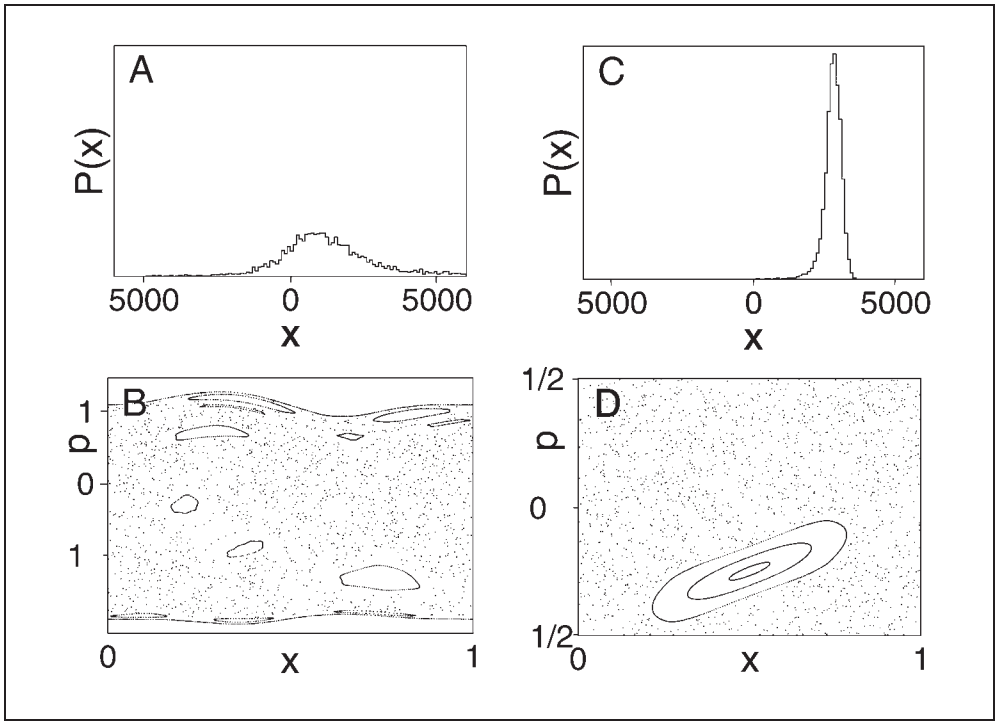

Fig. 4 (*A*) Spatial distribution of the probability density for the continuously driven system, Equation [3], after 20000 periods showing directed transport to the right. (*B*) Poincaré section *p versus x* of a unit cell at integer times. Panels (*C*), (*D*) as (*A*), (*B*), but for a kicked Hamiltonian. The single regular island visible in the lower half of (*D*) has winding number $w = -1$. It gives rise to much more pronounced transport (*C*) than in (*A*).

Is there any loophole left for directed transport? Evidently, it would depend on a persistent inhomogeneity of phase space. This in fact is not the exception but the rule in Hamiltonian systems: For most smooth nonlinear potentials, phase space decomposes into invariant sets, some of them chaotic, some regular, intricately intertwined in a self-similar manner. The coexistence of regular and chaotic regions in a mixed phase space allows to escape the verdict for transport mentioned above. For example, the contribution of a chaotic region can be compensated for by the counterdirected contribution of a regular island. This is easily achieved in a ratchet with smooth potential where close to the minima oscillatory motion prevails, while at intermediate energies, motion is chaotic (Fig. 4). At energies high above the potential's maxima, motion turns regular again.

Moreover, for the same reasons as pointed out in the previous section, the transport velocity of regular islands underlies a classical quantization condition. By the sum rule, this quantization has consequences also for the chaotic contribution to transport. In the chaotic case, however, a diffusive spreading takes place simultaneously. For example, if phase space comprises just a single regular island surrounded by a chaotic sea, the sum rule reads

$$0 = A_{\mathrm{ch}} v_{\mathrm{ch}} + A_{\mathrm{reg}} v_{\mathrm{reg}} \qquad [4]$$

where A_{ch} and A_{reg} are their respective areas. As a consequence, one has $V_{\mathrm{ch}} = -V_{\mathrm{reg}} A_{\mathrm{reg}} / A_{\mathrm{ch}}$ for the chaotic transport velocity.

3.2 Magnetic Billiards

Imposing an asymmetrically time-dependent external force is in fact not the only way to break time-reversal invariance in a Hamiltonian system. Another option is to consider charged particles in a magnetic field. In this case, no driving is needed. On the other hand, to obtain a chaotic dynamics without external time dependence, space now has to be extended to at least two dimensions. One class of models, very popular among nonlinear dynamicists, that combine these features are billiards: areas of free space limited by infinitely high potential walls. The shape of their baselines determines the character of the motion. In the absence of a magnetic field, trajectories are straight lines (geodesics) that undergo specular reflection where they hit a wall. With a constant magnetic field perpendicularly intersecting the plane of the billiard, they turn into arcs of circles with radius $r_{\mathrm{cyc}} = mvc/qB$, the cyclotron radius, where B denotes the field strength, and m, q, v, the mass, charge, and velocity of the particle, respectively. While in the field-free case, convex or concave sections of the boundary have to be introduced to render the dynamics chaotic, the curvature of the trajectories themselves suffices in the presence of the field. It corresponds to an effective concave shape of the boundary if the trajectories are curved towards the walls, and to a convex boundary in the opposite case.

A minimum solution for a magnetic-billiard ratchet therefore is a straight channel with equidistant straight walls attached perpendicularly to one side of the channel (Acevedo et al. 2002). This system is pseudointegrable (Richens and Berry 1981) and integrable in the limits of vanishing field, $r_{\mathrm{cyc}} \to \infty$, and of strong field, $r_{\mathrm{cyc}} \to 0$, respectively, and in the intermediate range shows a similar mixed phase space as discussed above (Fig. 5). Indeed, the breaking of time-reversal invariance by the field, and of the remaining spatial symmetry by the asymmetric configuration of the walls, is sufficient to generate directed transport in the chaotic component of phase space, for all finite values of B (Fig. 6).

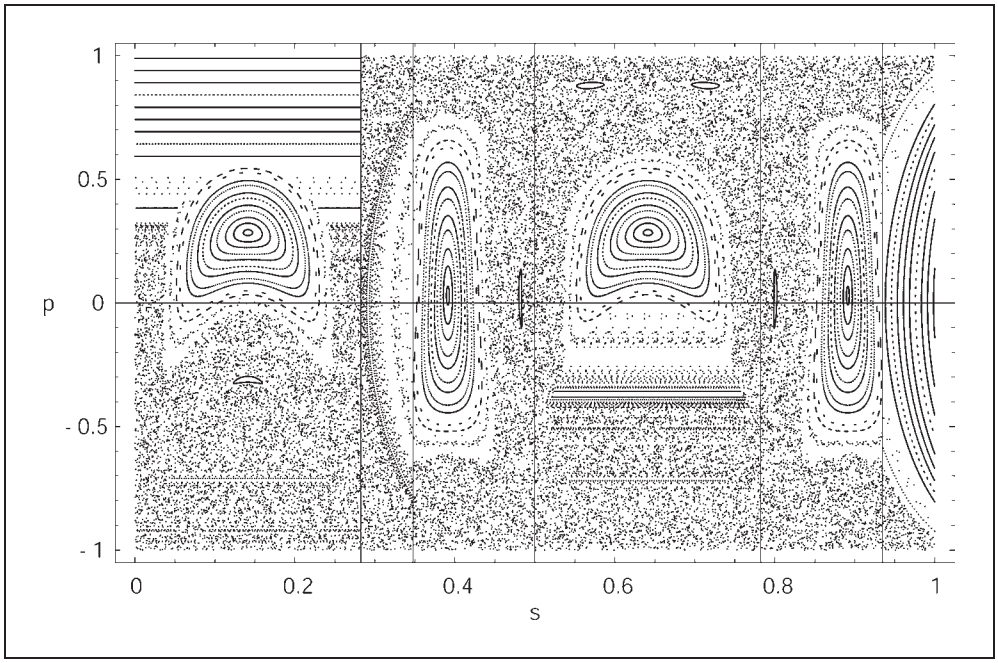

Fig. 5 Phase portraits for various sections of the phase-space unit cell of a magnetic billiard, as shown in the inset in Figure 6 below, for a unit cell of length $l = 1.3$, and $h = 0.7$, $r_{cyc} = 0.7$, in units of the total width of the channel. The coordinate s is measured along the circumference of the rectangular unit cell of the billiard (cf. Fig. 6 below), starting at the lower left corner and continuing counterclockwise. The coordinate p, canonically conjugate to s, is the sine of the angle between the trajectory and the inward normal of the boundary at a reflection. As in Figure 4 *D*, phase space is dominated by a large regular island immersed in the chaotic sea.

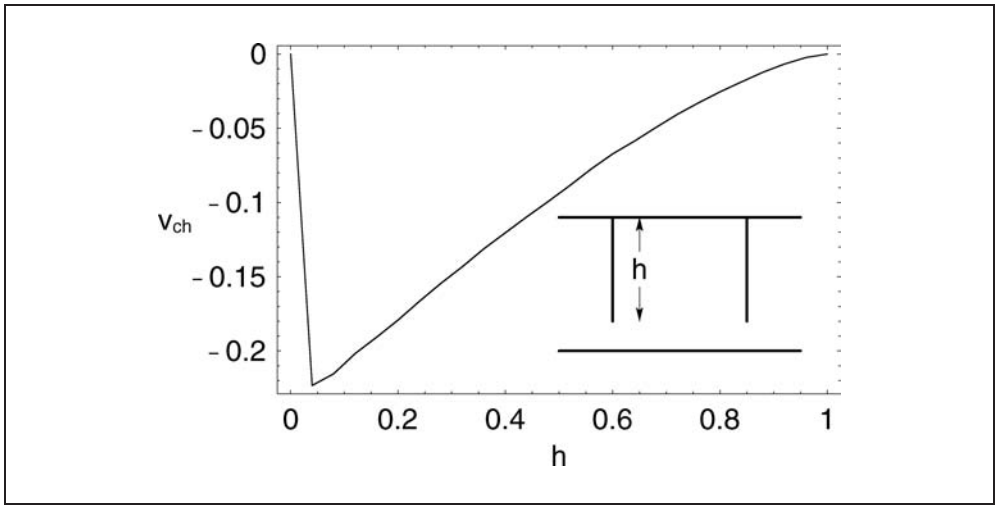

Fig. 6 Transport in the chaotic phase-space component of a magnetic billiard for $r_{cyc} = 2$, with boundary as sketched in the inset, as a function of the relative length h of the transverse walls. Transport vanishes in the limits $h \to 0$, where the billiard looses its asymmetry, and $h \to 1$, of complete closure of the channel.

3.3 Disorder and Noise

Hardly ever in nature are symmetries realized in a perfect manner, except for systems of atomic or smaller scale. The assumption of spatial and temporal periodicity made above therefore may appear artificial, and it is in order to consider the consequences of slight deviations from its exact validity. They can be modeled by superposing the periodic potentials with random functions of appropriate amplitude and autocorrelation properties.

Beginning with static, "frozen" disorder in space, it is immediately clear that a strict distinction between regular islands restricted to a single unit cell of the potential, and tori extending over the entire system, will collapse. In fact we now find regular islands extending over a large but finite number of unit cells, as implied by the large-scale fluctuations of the potential (Fig. 7, ACEVEDO et al. 2002). A trajectory starting in a chaotic region, say, is then more likely to enter the vicinity of a regular island, where it is temporarily trapped and induced to mimic the trajectories within the island. As a consequence, also transport shows much larger fluctuations in the presence of disorder, hence averaging over longer times is required to obtain meaningful results.

The effects of time-dependent noise are more drastic. By random jumps in phase space, trajectories move between the invariant sets of the noise-free system, so that all invariant sets effectively merge into one, on a time scale given by the noise intensity. As transport in the Hamiltonian case depends on the coexistence of disjunct invariant sets, it breaks down on the same time scale (ACEVEDO et al. 2002).

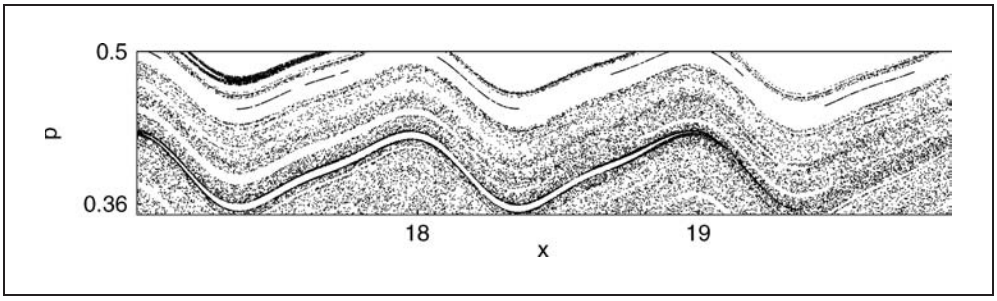

Fig. 7 Phase space of a Hamiltonian ratchet with weak static disorder. A regular island extending over various unit cells of the underlying periodic potential is visible in the lower part of the figure.

4. Quantum Hamiltonian Ratchets

With models of Hamiltonian ratchets at hand, their quantization reduces to a mere technical task (DITTRICH et al. 2000, SCHANZ et al. 2001). Yet some details deserve mentioning: The quantization procedure should respect, and where possible exploit, the spatio-temporal periodicity of ratchet potentials. For both aspects, taylor-made formalisms are readily available, in the form of Bloch theory, for systems with discrete spatial invariance, and Floquet theory, its analogue in the time domain. They entail a number of pertinent consequences for the quantum dynamics: Bloch theory implies that the eigenenergies of the system are organized as bands $E_\alpha(q)$, continuous functions of the quasimomentum q (or Bloch phase ϑ) as an additional independent conserved quantity.

The Floquet formalism, in turn, abandons energy as conserved quantity, replacing it by the Floquet or quasienergy $\varepsilon_\alpha(q)$, actually a phase defined only mod $\hbar\omega$, where $\omega = 2\pi/T$ is the fundamental frequency of the driving.

How is the mechanism of directed transport in classical Hamiltonian ratchets reflected in the structure of quasienergy bands of their quantum counterparts – if indeed it is? The principle of quantum-classical correspondence in fact requires that the quantum dynamics must mimic the classical at least on a finite time scale. To begin with, by the same principle, the partition of phase space into regular and chaotic regions transfers to the quantum realm as a corresponding distinction, as sharp as the Heisenberg uncertainty relation allows, between chaotic and regular eigenstates. A transport velocity is associated to the band α at quasimomentum q by

$$v_\alpha(q) = \frac{\mathrm{d}\varepsilon_\alpha(q)}{\mathrm{d}q}, \qquad [5]$$

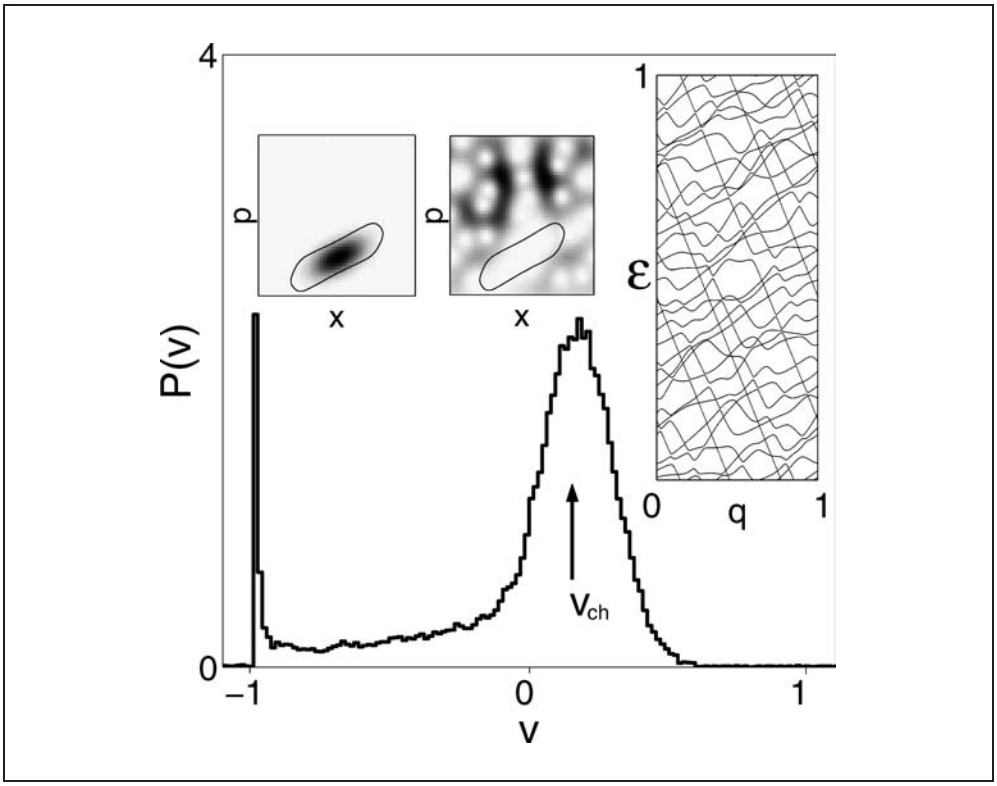

Fig. 8 Typical band structure $e(q)$ and corresponding velocity distribution $P(v)$ for a quantum Hamiltonian ratchet, obtained by quantizing the classical system shown in Figure 4 *C*, *D*. The straight line sections correspond to a classical regular island with winding number $w = -1$ (cf. Fig. 3), reflected in the sharp peak at $v_{reg} = -1$ of the velocity distribution. The remaining wiggly band sections are associated to the chaotic sea in the classical phase space and reflected in the broader peak marked v_{ch}. The small insets show quantum phase-space distributions (Husimi functions) for eigenstates located within the regular island (*left*) and in the chaotic sea (*right*), respectively.

the slope of the band at this point. However, since bands are periodic functions of q, an average of $d\varepsilon_\alpha(q)/dq$ over the entire band vanishes identically. This is the quantum counterpart of the classical sum rule discussed in subsection *3.1* (DITTRICH et al. 2000, SCHANZ et al. 2001).

Also the loophole for directed transport has its quantum analogue: In the typical band structure of a ratchet we distinguish almost straight line sections, with a certain slope, as well as more wiggly curves, with a less well defined yet clearly visible mean slope of opposite sign. It is these band sections that can be associated to classical regular islands and the chaotic sea, respectively. So an initial ensemble localized, say, in a phase-space region corresponding to a regular island of the classical dynamics has weight predominantly on band sections with a slope equal to the classical transport velocity, distributed over various bands (Fig. 8 and 9). In this way the quantum sum rule, which refers to entire bands, is circumvented. Numerical experiments indeed show agreement between quantum and classical transport in every detail of the velocity distribution.

Genuine quantum effects, however, are expected to show up on very long time scales. Spatial periodicity implies that in the long-time average, wave packets will travel along the ratchet by tunneling between unit cells (a phenomenon called Bloch tunneling) with

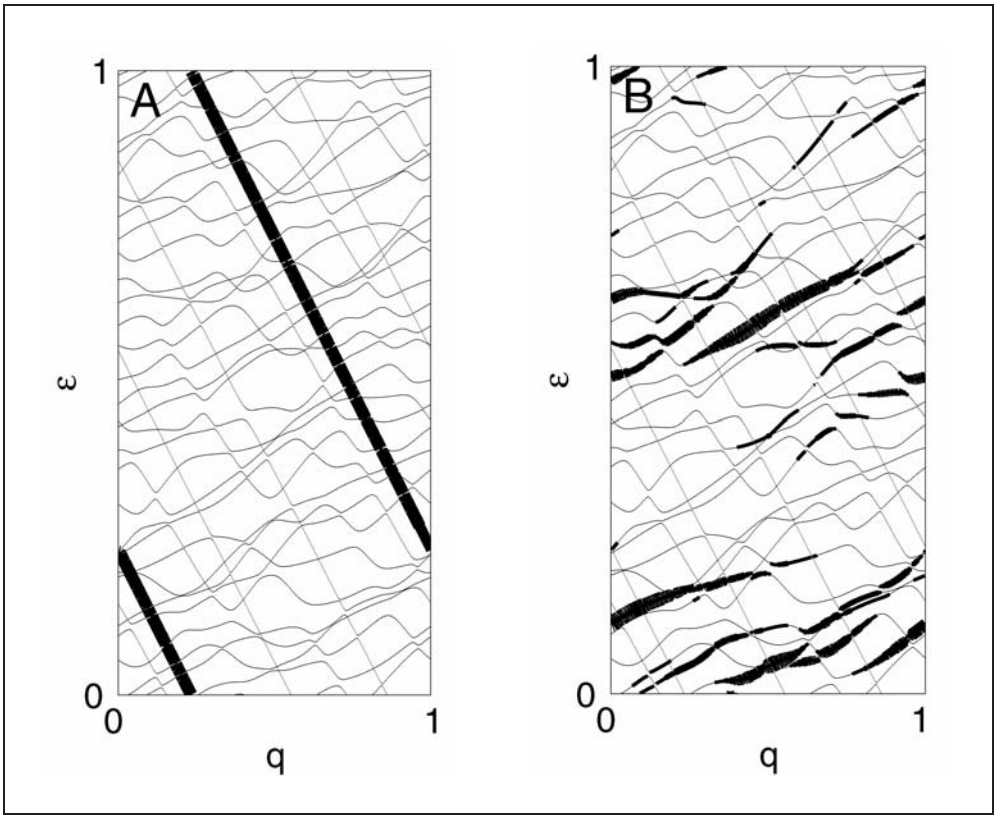

Fig. 9 The same band structure as in the inset in Figure 8, but with the weight distributions for eigenstates localized in the regular island (*A*) and in the chaotic sea (*B*), respectively, indicated by the width of the bands.

a group velocity that is in general different from any classical transport velocity. This quantum interference effect, however, competes with decoherence, which also invariably sets in on sufficiently long time scales.

Breaking periodicity likewise counteracts tunneling: Spatial disorder, however weak, leads to an antagonist effect, Anderson localization (DITTRICH et al. 2001). It is reflected in the quasienergy eigenstates showing an exponential envelope ~ $\exp(-|x|/\lambda)$, characterized by a localization length λ rather than extending over the entire ratchet. In other words, the system changes from conductor to insulator. A wave packet can then move with the corresponding classical transport velocity only until it reaches a distance of the order of λ from where it was launched, whereupon it is stuck.

5. Outlook

The preceding sections have led, in a reductionist spirit, from models directly inspired by molecular motors, to theoretical constructions probing basic features of quantum dynamics. It is time then to return to more complex systems again, step by step adding realistic detail to the models considered. Several directions are of interest:

Dissipation and decoherence are unavoidable phenomena even on the molecular level. They are introduced in a microscopic framework by explicitly including the ambient degrees of freedom that absorb energy from the system of interest. While results on dissipative quantum ratchets with just a few levels already exist (GOYCHUK and HÄNGGI 2001), the technically more demanding problem of quantizing dissipative ratchets in the semiclassical regime where their behavior reflects the classical chaotic motion, has not yet been solved. It would allow to study the full interplay of chaos, quantum effects, and decoherence in directed transport, as pointed out in the introduction.

In order to exclude trivial transport mechanisms, external gradients have intentionally been avoided in the ratchet models presented above. In the living cell, however, molecular motors typically have to work *against* external forces. This changes the physical situation considerably, in particular in Hamiltonian systems where the loss/gain of kinetic energy in moving up/down a potential slope is not counterbalanced by a reservoir. Moreover, in quantizing systems with a mean potential slope, the Bloch theorem, which requires spatial periodicity, no longer applies.

The most striking difference between biophysics-style models of molecular motors and the ratchets considered here is that the latter consist of point particles, void of any internal structure, while the former often represent elaborate molecular machines with complex internal mechanisms. Possibly the most urgent challenge for ratchet research is therefore to gradually add internal degrees of freedom, studying their influence on, and possible constructive role in, directed transport (NAKAGAWA and KANEKO 2002).

Acknowledgements

One of us (TD) thanks the *Max Planck Society* for the hospitality enjoyed during various stays at its Institutes for the Physics of Complex Systems, Dresden, and Flow Research, Göttingen, where part of this work has been performed. We gratefully acknowledge financial support by the *División de Investigación, Sede Bogotá* (DIB, contract 803684), and *Dirección Nacional de Investigación* (DINAIN, contract DI00C1255), of Universidad Nacional de Colombia, and by *Colciencias* (contract 310223).

References

Acevedo, W., Dittrich, T., and Pineda, C.: Matracas clásicas hamiltonianas y disipativas. Rev. Col. Fís. *34*, 380–385 (2002)

del-Castillo-Negrete, D.: Asymmetric transport and non-Gaussian statistics of passive scalars in vortices in shear flow. Phys. Fluids *10*, 576–594 (1998)

Dittrich, T., Ketzmerick, R., Otto, M.-F., and Schanz, H.: Classical and quantum transport in deterministic hamiltonian ratchets. Ann. Phys. (Leipzig) *9*, 755–763 (2000)

Dittrich, T., Mehlig, B., and Schanz, H.: Spectral signatures of chaotic diffusion in systems with and without spatial order. Physica E *9*, 494–497 (2001)

Flach, S., Yevtushenko, O., and Zolotaryuk, Y.: Directed current due to broken time-space symmetry. Phys. Rev. Lett. *84*, 2358–2361 (2000)

Gammaitoni, L., Hänggi, P., Jung, P., and Marchesoni, F.: Stochastic resonance. Rev. Mod. Phys. *70*, 223–287 (1998)

Goychuk, I., and Hänggi, P.: Minimal quantum brownian rectifiers. J. Phys. Chem. B *105*, 6642–6647 (2001)

Jung, P., Kissner, J. G., and Hänggi, P.: Regular and chaotic transport in asymmetric periodic potentials: inertia ratchets. Phys. Rev. Lett. *76*, 3436–3439 (1996)

Mateos, J. L.: Chaotic transport and current reversal in deterministic ratchets. Phys. Rev. Lett. *84*, 258–261 (2000)

Nakagawa, N., and Kaneko, K.: Dynamical mechanism for the conversion of energy at a molecular scale. Phys. Rev. E *67*, 040901–1–4 (2003)

Reimann, P.: Brownian motors: noisy transport far from equilibrium. Phys. Rep. *362*, 57–265 (2002)

Richens, P. J., and Berry, M. V.: Pseudointegrable systems in classical and quantum mechanics. Physica *2D*, 495–512 (1981)

Schanz, H., Otto, M.-F., Ketzmerick, R., and Dittrich, T.*:* Classical and quantum hamiltonian ratchets. Phys. Rev. Lett. *87*, 070601–1–4 (2001)

Utermann, R., Dittrich, T., and Hänggi, P.: Tunneling and the onset of chaos in a driven bistable system. Phys. Rev. E *49*, 273–280 (1994)

Prof. Dr. Thomas Dittrich
Universidad Nacional de Colombia
Departamento de Física
Santafé de Bogotá
Colombia
Phone: +57 13 16 50 00 ext. 1 30 44
Fax: +57 13 16 51 35
E-Mail: dittrich@ciencias.unal.edu.co

Nova Acta Leopoldina NF *88*, Nr. 332, 293–318 (2003)

Temperature Encoding in Peripheral Cold Receptors: Oscillations, Resonances, Chaos, and Noise

Hans Albert Braun[1], Klaus Schäfer[1], Karlheinz Voigt[1], and Martin Tobias Huber[2] (Marburg)

With 6 Figures

Abstract

Peripheral cold receptors belong to the most flexible neuronal impulse pattern generators. Dependent on their physiological stimulus, i. e. temperature, they pass through a fascinating array of impulse sequences of different temporal structures including burst discharges, tonic firing as well as impulse patterns of apparently chaotic origin and others, which can only be understood on the basis of an essential contribution of noise. For a better understanding of the neuronal transduction mechanisms, we compare experimental recordings from cold sensitive nerve fibers with data from deterministic and noisy computer simulations. To focus on the general principles we have used a simplified Hodgkin-Huxley type approach. Impulse sequences, interval-plots (bifurcation diagrams) and return maps demonstrate very close agreement between experimental recordings and noisy simulations. Comparison with deterministic simulations suggests that the major neuromodulatory characteristics can be attributed to varying resonances between two subsystems: the subthreshold oscillations and the spike generating mechanism. However, the results also indicate that the full variety of impulse patterns and smooth transitions can only be obtained with cooperative noise effects which, in specific situations, can become of particular physiological relevance.

Zusammenfassung

Periphere Kälterezeptoren gehören zu den flexibelsten neuronalen Mustergeneratoren. In Abhängigkeit von ihrem physiologisch adäquaten Reiz, der Temperatur, durchlaufen sie eine faszinierende Vielfalt unterschiedlichster Impulsmuster. Dazu gehören tonische Einzelspike-Entladungen und Impulsgruppenentladungen (*Bursts*) genau so wie chaotisch strukturierte Impulssequenzen und wieder andere, die nur unter dem Einfluß von Rauschen zustande kommen können. Für ein besseres Verständnis der zugrundeliegenden neuronalen Prozesse haben wir die experimentellen Befunde im Vergleich mit den Ergebnissen deterministischer und »verrauschter« Computer-Simulationen untersucht. Unser Computer-Modell beruht auf dem sogenannten Hodgkin-Huxley-Ansatz, der aber erheblich vereinfacht wurde, da wir uns für die prinzipiellen Systemeigenschaften interessierten. Impulssequenzen, Intervall-Punktkurven (Bifurkationsdiagramme) und sogenannte »Return-Maps« belegen eine ausgezeichnete Übereinstimmung zwischen den experimentellen Daten und verrauschten Simulationen. Der Vergleich mit deterministischen Simulationen zeigt, daß die neuromodulatorischen Eigenschaften mit verändertem Resonanzverhalten zwischen zwei Teilsystemen, einem unterschwelligen Oszillator und dem Impulsgenerator, zu erklären sind. Die Ergebnisse zeigen aber auch, daß die gesamte Vielfalt der Impulsmuster mit ihren kontinuierlichen Übergängen nur durch die nichtlinearen Wechselwirkungen mit Rauscheffekten zu erhalten ist. Diese kooperativen Effekte zwischen nichtlinearen Systemeigenschaften und Rauschen können unter bestimmten Bedingungen von herausragender physiologischer Bedeutung sein.

1 Institute of Physiology, University Marburg.
2 Department of Psychiatry, University Marburg.

1. Introduction

In experimental recordings of peripheral sensory receptors and central neurons we have seen continuous transitions between different types of oscillatory patterns as a function of physiologically relevant stimuli. Specifically, peripheral cold receptors show a fascinating array of impulse patterns. Depending on the skin temperature, the same neuron can exhibit burst discharges (impulse groups) or tonic activity as well as "irregular" patterns of apparently "chaotic" origin and others which can only be explained with the essential contribution of "noise" (see e. g. BRAUN et al. 1984 a, 1994, 1999). Moreover, in the case of peripheral cold receptors, it is agreed that all these different patterns originate from the neurons' intrinsic dynamical properties. The transduction sites seem to consist of nothing more than free nerve endings of Aδ-fibres which divide into several unmyelinated terminals at the basal epidermal layer of the skin (HENSEL et al. 1974). Any synaptic interactions between these tiny and sparsely distributed nerve endings can be excluded. Hence, it is an almost perfect model to study the neuromodulatory properties of a very flexible endogenous neuronal impulse pattern generator, although there is one major disadvantage: so far, no intracellular recordings of membrane potentials and ion currents have been possible from these tiny nerve endings.

Several groups have tried to obtain further insight into cold transduction with intracellular recordings from the somata of the peripheral nerves assuming that the principle mechanisms of cold transduction might be similar to those at the sensory nerve terminals. Indeed, these groups have detected depolarizing currents in response to cooling as well as on application of menthol (REID and FLONTA 2001, MCKEMY et al. 2002, VIANA et al. 2002). Menthol is a substance of well-known cooling effects and therefore has been used as a marker of cold sensitive neurons. Menthol activates cold receptors and strengthens their temporal patterns (SCHÄFER et al. 1986, 1991) which was attributed to blockade of low-voltage, T-type calcium channels (SWANDULLA et al. 1986, 1987). In the neurons' somata, cold and menthol sensitive membrane receptors have been identified and could also be cloned (MCKEMY et al. 2002, PEIER et al. 2002). In spite of this remarkable success (see also CLAPHAM 2002, MACDERMOTT and Lee 2002), the data from the neurons' somata still leaves open questions and are contradictory in some parts, e. g., with regard to the nature of the cold current (see also MACDERMOTT and Lee 2002). More discrepancies become evident upon comparison of the data from the somata with the neuronal discharges that we and others have recorded from the afferent nerve fibers. The most obvious and important difference is that the neurons' somata only show transient discharges during strong cooling whereas the peripheral receptors are spontaneously active over a broad temperature range and thereby exhibit systematic modifications of impulse patterns which is essential for the encoding of constant temperatures. Hence, the recordings from the neurons' somata might have their particular value in elucidating cold sensitive currents but, so far, cannot contribute to the understanding of neuronal impulse pattern generation and stimulus dependent modulation simply because of the lack of such spontaneous discharges.

Therefore, as a supplement to the experimental recordings we also have made use of computer modeling studies. Our model is based on a simplified Hodgkin-Huxley (HH) type approach (HODGKIN and HUXLEY 1952). It includes two subthreshold currents in

addition to the spike-generating currents (e. g. BRAUN et al. 1998, HUBER et al. 1998, BRAUN et al. 2000) but does not have more dimensions, i. e. differential equations, then the original HH-model. This could be achieved with physiologically justified simplifications as we will describe below (see 3.1). Admittedly, there exist other dimension reduced models – the most prominent being the Fitzhugh-Nagumo model – (FITZHUGH 1965, see also TUCKWELL 1988). However, these are rather abstract mathematical realizations of the neuronal dynamics which sacrificed the clearly specified interrelations between membrane voltage and ion currents of the original Hodgkin-Huxley approach. Such models are preferably used in biophysical studies. For the experimental physiologist, it is of particular importance that the electrophysiological data can be correlated with model parameters of clearly defined physiological meaning. Indeed, our first simulations were done with a detailed model of many dimensions which, for example, had two compartments, one for subthreshold oscillation and one for spike generation (e. g. HUBER et al. 2000 a). Only then, in parallel to these specific simulation studies, we have systematically reduced the dimensions of our model with the goal of not only focusing on the details of cold receptor transduction but also elucidating the general principles of neuronal impulse pattern generation and their stimulus dependent modulation. However, we took care not to loose the link between experimental data and model parameters in the course of dimension reduction and could develop a dimension reduced but physiologically motivated model which, in the meantime, is widely used as a promising approach to attain a better understanding of neuromodulatory properties also under a more general, biophysical point of view (GILMORE 1999, NEIMAN et al. 1999, W. BRAUN et al. 2000, FEUDEL et al. 2000).

In the following we will illustrate the experimental background of our model and then describe our modeling approach and show that all relevant types of impulse pattern can be obtained with systematic, physiologically plausible modulations of the model parameters. We also will emphasize the more general aspects of neuronal impulse pattern generators from the viewpoint of coupled oscillators. We will show that individual patterns reflect distinct resonant behaviors between subthreshold oscillations and spike-generating processes which can lead to comparably regular discharges, e. g. rhythmic bursts or tonic firing, as well as rather complex, e. g. chaotic, patterns.

Last but not least, we will consider the effects of noise, i. e. high dimensional, random dynamics. Biological systems are notoriously noisy which, in neuronal impulse recordings, is manifested in fluctuations of the interspike-intervals. In individual neurons noise might simply arise from the stochastic properties of ion channel gating, whereas neuronal networks also have to consider the stochasticity of synaptic currents (for a more detailed discussion of neuronal noise sources see, for example, LONGTIN and HINZER 1995 or WHITE at al. 2000 and references therein). Irrespective of the origin of noise, it is usually considered detrimental to the encoding process. However, also beneficial effects of noise have been described, e. g. stochastic resonance phenomena (e. g. DOUGLAS et al. 1993, LONGTIN 1993, for review see WIESENFELD and MOSS 1995). In some sensory neurons like shark electroreceptors, noise even seems to be inevitable for stimulus encoding (BRAUN et al. 1994). With the use of computer modeling studies we have the advantage of comparing noisy and deterministic simulations for further elucidation of the noise effects. We will show that the impact of noise can change essentially depending on the dynamical situation.

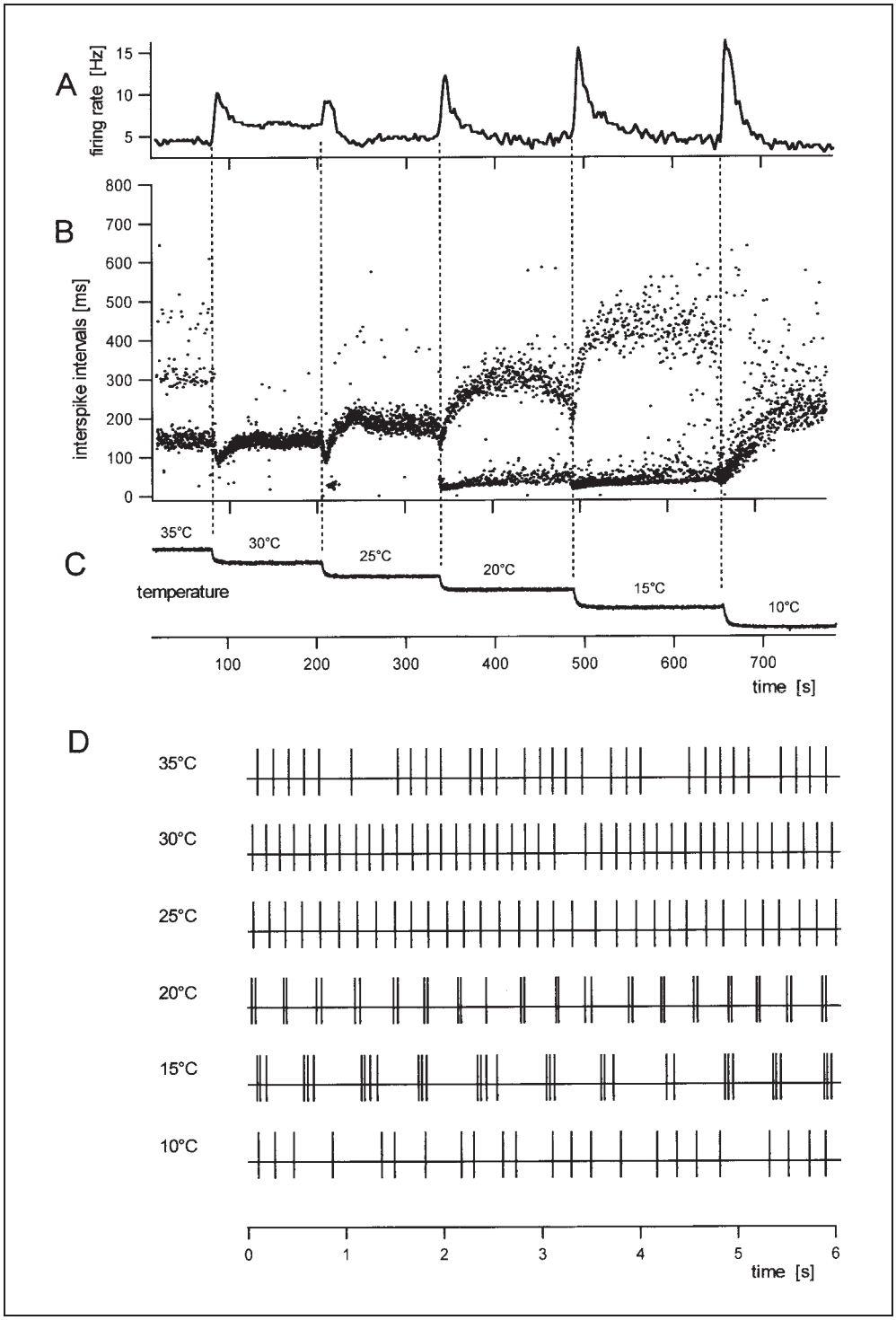
A
firing rate [Hz]
15
10
5
B
interspike intervals [ms]
800
700
600
500
400
300
200
100
0
C
temperature
35°C
30°C
25°C
20°C
15°C
10°C
100
200
300
400
500
600
700
time [s]
D
35°C
30°C
25°C
20°C
15°C
10°C
0
1
2
3
4
5
6
time [s]

2. Experimental Background: the Impulse Patterns of Peripheral Cold Receptors

Stimulus transduction in temperature sensitive skin receptors is based on the modulation of periodically generated impulse patterns. This has been shown for a variety of specific warm and cold receptors of mammals, birds and snakes and also holds true for several temperature sensitive electroreceptors of fish (BRAUN et al. 1980, 1984 b, SCHÄFER et al. 1988, 1989, BRAUN et al. 1990, HEINZ et al. 1990, BRAUN et al. 1994, SCHÄFER et al. 1995). Among all these sensory receptors, peripheral cold receptors are exceptional in so far as they clearly exhibit the greatest variety of impulse patterns (BRAUN et al. 1980, 1984 b). An example of an extracellular impulse recording from a single cold sensitive afferent fiber is shown in Figure 1 (for methods see SCHÄFER et al. 1986). It illustrates how the firing rate (Fig. 1 *A*) and the distribution of interspike-intervals (Fig. 1 *B*) changes as a function of temperature which was successively decreased from 35 to 10 °C in temperature steps of 5 °C each (Fig. 1 *C*). Modifications of the impulse activity are further illustrated in the lower traces with examples of spike sequences (Fig. 1 *D*). Additionally, the serial interdependencies of spike-generation are illustrated in Figure 2 with examples from typical discharge patterns.

2.1 Frequency Responses: The Rate Code

The most prominent feature of the frequency plot (Fig. 1 *A*) is the so-called dynamic frequency overshoot which can be seen at each cooling step (Fig. 1 *C*). This is a transient increase of the firing rate with subsequent adaptation to a new steady state. Fast warming – not shown here – induces the opposite effect, a frequency undershoot, i. e. a transient decrease or complete inhibition of the spike activity. Warm receptors exhibit just the inverse characteristics, a frequency overshoot on warming and undershoot on cooling. For comparison of the frequency-temperature characteristics of warm and cold receptors see for example SCHÄFER et al. (1988).

These dynamic response characteristics provide an unambiguous criterion for distinguishing between cold and warm receptors (see definition in HENSEL et al. 1969). Apart from that, both cold and warm receptors are spontaneously active at constant temperatures over a wide temperature range – here from 35 °C down to 10 °C. However, the static firing rate cannot provide clear information about the actual skin temperature. It generally reaches a maximum around mid-temperatures (mostly 25 °C – 30 °C) and de-

---

Fig. 1 Typical response characteristics of cold receptors illustrated with data from a continuous extracellular recording of action potentials from a peripheral cold receptor in the cat's nose (see SCHÄFER et al. 1986). Firing rate (*A*) and interspike-intervals (*B*) are plotted over a total recording time of about 800 s in parallel with the stimulation temperature (*C*) which was successively decreased from 35 to 10 °C in steps of 5 °C with longer sequences of constant temperatures in between. Recording time is indicated at the abscissae in *C*. Each cooling step (*C*) is accompanied with a sudden change of the interval distribution (*B*) which leads to an immediately increasing firing rate (*A*) as indicated by the vertical dashed lines. The firing rate shows the characteristic frequency overshoot with subsequent adaptation to a new steady state at constant temperatures. The lower traces (*D*) additionally show examples of impulse sequences out of these recordings from static discharges at different constant temperatures which are indicated on the left.

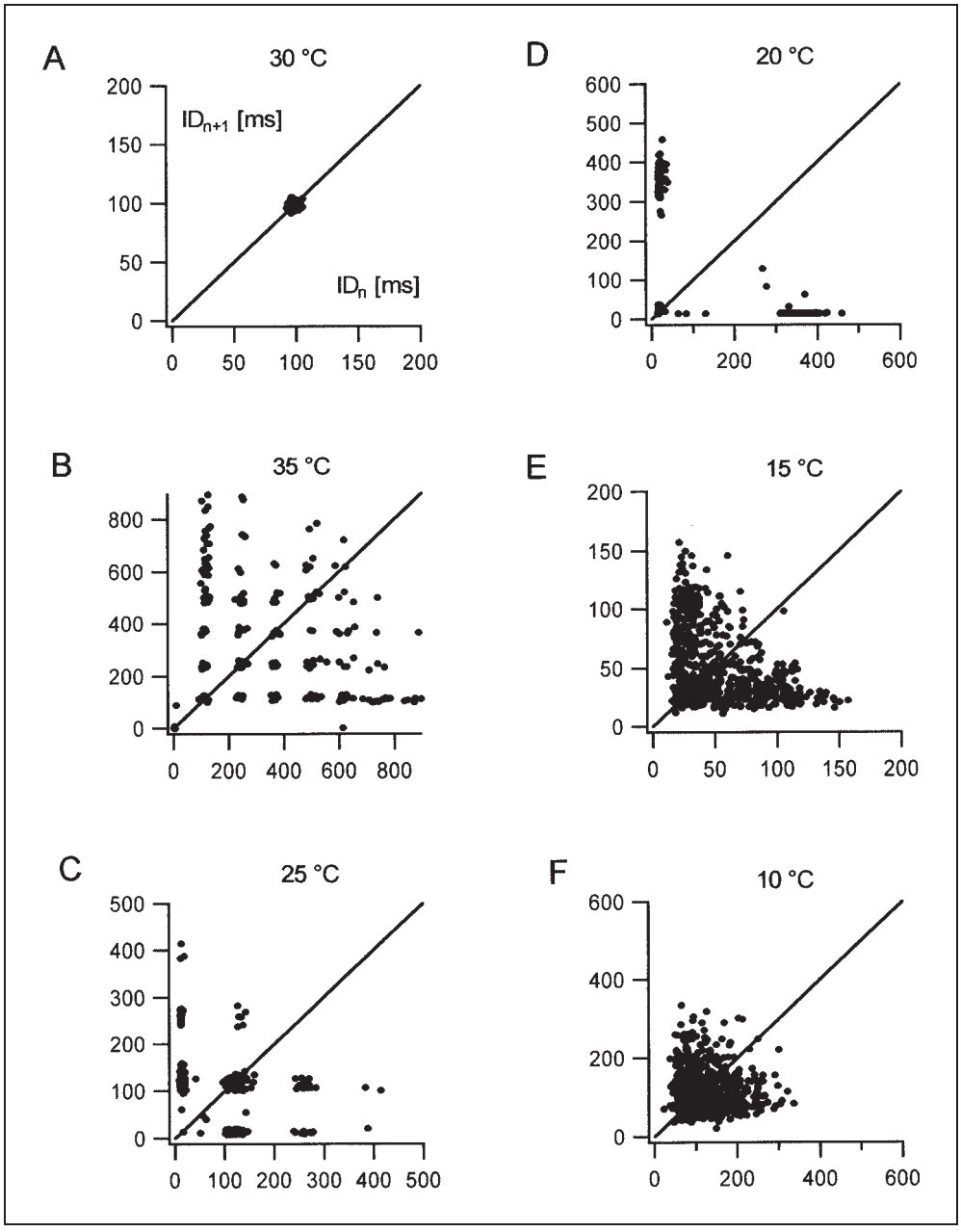

Fig. 2 Return maps of typical impulse patterns of cold receptor discharges illustrate the serial interdependencies of impulse generation. The duration of a given interspike interval at position n (ID_n, ID = interval duration) is plotted as abscissa value. The duration of the following interval ID_{n+1} (position n + 1) is plotted as ordinate value. The 45° line indicates the position of identical values. Recordings are made at different constant temperatures as indicated on the top of each diagram.

creases towards both extremes of the temperature range (see SCHÄFER et al. 1988). In this example, there is a maximum value at 30 °C whereas the frequency values at all other temperatures do not differ very much. Only the static firing rate at 10 °C value is clearly lower. Altogether, cold receptors seem to be far away from being well-designed sensors – at least not for frequency coding of constant temperatures.

2.2 Impulse Patterns: The Temporal Code

While the average firing rate cannot deliver unambiguous information about constant temperatures, the situation changes when we look at the temporal pattern of the discharge. It can be seen already with a superficial look on the spike sequences (Fig. 1 *D*) and even more clearly in the plot of interspike-intervals (Fig. 1 *B*) that the impulse pattern delivers more information than an average firing rate can provide.

In the interval plot (Fig. 1 *B*), we can see distinct bands. At 30 °C and 25 °C most intervals are concentrated in a single, rather narrow band. This corresponds to a comparably regular tonic discharge (see Fig. 1 *D*, 30 °C, 25 °C). Compared to 30 °C the interval band at 25 °C is shifted to higher values indicating a moderate lengthening of the interspike-intervals. The shift of this interval band, including a broadening, continues at 20 °C where, however, an additional band of short intervals occurs. This indicates a qualitative change: the transition from tonic firing to impulse groups, called burst discharges. The additional band of short intervals reflects the high frequency intraburst-discharges. With further temperature decrease to 15 °C a further lengthening of the band of longer intervals is seen and the number of spikes per burst increases (see Fig. 1 *D*, 20 °C and 15 °C). At 10 °C there is again a qualitative change. The band of longer intervals disappears or is melted together with the drastically broadened band of short intervals. The pattern has changed to a comparably irregular tonic discharge (Fig. 1 *D*, 10 °C).

Finally, we have to look at a particular type of a seemingly irregular impulse pattern which, however, is different from that a 10 °C and only can be seen at the highest temperatures of the activity range, i. e. 35 °C or 40 °C (35 °C in Fig. 1 *D*). Figure 1 *B* illustrates that such spike sequences, as here recorded at 35 °C, lead to typical interval distributions. There is a main interval band at approximately the same level as the interval band at 30 °C (around 150 ms). However, at 35 °C, there are additional bands of longer intervals which are located at about integer multiples of the main interval band (around 300 ms and 450 ms).

Altogether, there are systematic modifications of the temporal patterns of the discharge which can provide unambiguous information about constant skin temperatures. Also the frequency overshoots on cooling can be related to characteristic modifications of the impulse patterns: the frequency increase is essentially caused by a transient shortening of the interspike-intervals in the main interval band and by a tendency towards burst discharges with an increasing number of intraburst intervals (for a more detailed analysis see BRAUN et al. 1980). For example, the cooling step from 30 to 25 °C induces a transient, very brief sequence of bursts which disappears during adaptation. Other fibers which we have examined with the same stimulus protocol exhibit burst patterns at 25 °C also in the steady state. Often, the only temperature with regular tonic discharges is 30 °C which is around the "normal" skin temperature, i. e., when no environmental

stimuli are present. Any deviation is clearly indicated by unambiguous modifications of the impulse patterns which allow to distinguish between different temperatures also when the firing rate might be the same.

2.3 Typical Impulse Patterns and their Return Maps (Serial Interdependencis)

For further illustration of characteristic patterns of cold receptor discharges we also have plotted so-called return maps (Fig. 2). The return maps (RM) illustrate the interdependencies between successive interspike-intervals whereby the actual interval is plotted as abscissa value and a following one is plotted as ordinate value. Here we only consider the first-order return maps which means that the actual interval (ID_n) is plotted *versus* the immediately following one (ID_{n+1}).

It is easy to understand that a completely regular tonic discharge, where each interval is of exactly the same length, will give a single point in the return map on the 45 °C line (the line of identity of x- and y-values). In biological systems this can only be obtained with some approximation because of the unavoidable noise.

The RM in Figure 2 *A* is drawn from one of the most regular single-spike discharges that we have recorded. There are only tiny fluctuations around an interval of about 100 ms. This recording was made at 30 °C which, as said before, is the favorite temperature for periodic single-spike discharges. Such extraordinarily regular discharges, however, were only seen during reduction of external Ca^{2+}, or under Ca^{2+}-channel blockade, e. g. with menthol (see SCHÄFER et al. 1986, 1991).

The recording in Figure 2*B* was also obtained under Ca^{2+}-channel blockade – but at the next higher temperature (35 °C) where the dots are heavily scattered across an interval range of 900 ms and more. Nevertheless, the RM shows a clear structure. There are several clusters along the 45 °C line and there are others at approximately the same levels along the abscissa and ordinate. According to Figure 1, 35 °C, this distribution indicates that the spikes are triggered at about integer multiples of a basic discharge period (which is still around 100 ms). The probability for the occurrence of longer intervals is lower than for shorter intervals and additionally decreases with increasing length of the preceding interval which suggests that a purely random, e. g., Poisson-like process contributes to the impulse generation (see also next section for further evidence).

The RM in Figure 2 *C* shows one of the more complex structures which preferably can be seen at 25 °C or 30 °C but in such clarity again could only be recorded under Ca^{2+}-channel blockade. There is still a cluster around the 45 °C line according to regular spike sequences of almost identical intervals (somewhat longer than in *A* and *B*). There are also clusters at higher ordinate and abszissa values around integer multiples according to Figure 1 *B*. But they occur to a clearly less extent (only up to the two-fold, occasionally threefold length of the basic period). Instead, there are additional clusters at shorter abscissa and ordinate values which reflect the occurrence of intraburst intervals. Again, there is a decreasing probability of interval pairs of longer intervals but also the occurrence of successive intraburst intervals is extremely rare.

The return map in Figure 2 *D* is that of a very regular burst discharge. Longer interburst intervals are followed by short intraburst intervals (the right lower cluster) and short intraburst intervals are followed by longer burst pauses (the left upper cluster) but

also can be followed by another intraburst interval (the cluster of short-short intervals). There is no sequence of long-long intervals which means that the cold receptor here generates regular bursts without any single-spike sequence. The extensions of the clusters of long-short and short-long intervals indicate that the fluctuations of the burstpauses are stronger than those of the intraburst intervals.

Figure 2 *E* and 2 *F* illustrate the transitions from regular bursts at mid-temperatures to irregular firing at lower temperatures. In Figure 2 *E* there are still some indications of burst discharges as manifested in preferable occurrences of interval pairs of long-short, short-long and short-short intervals and the lack of long-long intervals. But there are also many interval pairs of intermediate values which means that there is no longer a clear transition from intraburst intervals to burst pauses, as seen in Figure 2 *D*.

Figure 2 *F* finally shows a rather unstructured return map of a type that we only have recorded at the lowest temperatures (10 or 5 °C). It mainly shows broad random fluctuations along the 45 ° line although some indications of serial interdependences can still be seen. There is a slight but clear tendency that longer intervals are preferably followed by shorter ones and *vice versa*.

2.4 Transduction Processes: Oscillations and Noise

As mentioned above, the tiny nerve endings of cold fibers, so far, do not allow intracellular recordings of the membrane potential. However, the occurrence of rhythmic burst discharges immediately implies rhythmic transduction processes of spike generation, i. e. spike-generating oscillations (IGGO and YOUNG 1975). A more detailed analysis of the impulse patterns revealed that also the non-bursting discharges can be related to periodic processes of spike-generation (e. g. BRAUN et al. 1980). Remarkably, it is mainly the irregular pattern at higher temperatures which gives further evidence for spike-triggering oscillations. The fact that the longer intervals are distributed at integer multiples of the shortest intervals suggests an oscillating process which does not trigger groups of impulses but only single-spikes and sometimes even fails to trigger an impulse. Each oscillation cycle without impulse generation lengthens the interspike interval by the oscillation period. Hence, the band of shortest intervals (see Fig. 1 *B*) corresponds to the oscillation period whereas the longer intervals indicate the occurrence of so-called "skippings", i. e. one or more oscillation cycles without spike-generation. The distribution of interval pairs in return maps like those of Figure 2 *B* fits very well to a Poisson distribution which indicates that this pattern, indeed, depends on random, i. e. high-dimensional components rather than on low-dimensional, e. g. "chaotic" dynamics. Hence, it can be concluded that this type of patterns results from cooperative effects between oscillations and noise, whereby the oscillations determine the basic rhythm of the discharge while random components decide whether a spike is triggered or not (see also, for example BRAUN et al. 1980, 1984 b, 1990, 1994).

Regular tonic firing, in principle, can originate from subthreshold oscillations as well as from pacemaker mechanisms. We assume that cold receptors make use of both types of spike-generating processes. Tonic activity in the upper temperature range (at 30 or 25 °C) occurs in an intermediate state between burst discharges and skippings and is often seen in coexistence with these patterns (as in the recording in Figure 2 *C*). Hence,

there can be no doubt that also this type of tonic discharge is generated by subthreshold oscillations which do not produce skippings nor bursts but – more or less regularly – generate one single-spike per oscillation cycle. This assumption is further supported by the equal distributions of the interval pairs in the return map around a periodic fixed point at the 45° line.

The discharges at low temperatures seem to be of different origin. Towards lower temperatures we do not only see a lengthening of the oscillation period, but also found evidence for a reduced amplitude of oscillation as it is indicated, for example, by a lengthening of the intraburst intervals (for details see BRAUN et al. 1980, SCHÄFER et al. 1986). In the extreme, the oscillations seem to be more or less diminished and spike generation essentially seems to reflect some kind of tonic depolarization with stochastic fluctuations. This corresponds to a noisy pacemaker which, of course, does not produce "skippings" but nevertheless will show serial interdependencies (Fig. 2 *F*) simply because it is very unlikely that an extraordinarily long interval again is followed by a another very long interval. Principally, it is the same effect which reduces the probability of long-long intervals at higher temperatures (Fig. 2 *C*) – but without the oscillations.

These findings allowed us to describe the remarkable variety of impulse patterns in peripheral cold receptors on the basis of subthreshold oscillations and noise with comparably simple rules (BRAUN et al. 1980). The assumption is that the noisy subthreshold oscillator is most effective at mid-temperatures where it triggers groups of impulses, i. e. bursts. Increasing temperature increases the oscillation frequency which reduces the number of spikes per oscillation cycle until only single spikes and finally more and more skippings occur. Towards lower temperature, the oscillation period increases, but the more pronounced and qualitative change comes from a simultaneous reduction of the oscillation amplitude which leads to irregular bursts and eventually tonic discharges.

3. The Model: Impulse Generation with Noisy Subthreshold Oscillations

Originally we have used a simple analog computer simulation to illustrate the above described hypothesis of a neuronal pattern generator with noisy subthreshold oscillations (BRAUN et al. 1984 a, b). The analog computer circuit consisted of a leaky integrator which was fed by a sine wave and noise. We could show that continuous transitions between different types of patterns could be obtained with modulation of a single parameter, the sine-wave frequency. Only for the simulations of the bursting-to-tonic transitions at low temperatures we additionally had to reduce the sine-wave amplitude (see Fig. 8 in BRAUN et al. 1984 a).

More recently we – as many others – have taken advantage from the progress in digital computer technologies and developed a Hodgkin-Huxley (HH) type model which additionally allows to evaluate the underlying ionic mechanisms of pattern generation. Our original model (for equations see HUBER et al. 2000 a) had many more dimensions than the present one. It included two electrically coupled compartments: the spike-generating compartment and a transduction compartment for subthreshold oscillations. Accordingly, we had two membrane equations, one with fast sodium and potassium currents for spike-generation and the other one with more slowly activating currents for subthreshold oscillations. Subthreshold oscillations develop from the interplay of a persistent

sodium current with a voltage-dependent calcium current and a calcium-dependent potassium current. They were passively coupled to the spike-generator.

Similar concepts of intrinsically oscillating neurons were first described and modeled for molluscan pacemaker neurons many years ago (e. g. PLANT 1978, 1981), which was at a time when mammalian neurons still were considered as rather passive transduction elements without intrinsic dynamics. During recent years, however, there was growing evidence that also mammalian neurons in the central nervous system (CNS) are far away from being such "platonic nerve cells", but endow a great variety of intrinsic subthreshold mechanisms with a manifold of subthreshold currents (LLINAS 1988). Major experimental evidence came from the analysis of neuronal activity in the thalamus, the entorhinal cortex and amygdala (e. g. LLINAS and YAROM 1986, ALONSO and LLINAS 1989, MCCORMICK and FEESER 1990, LLINAS et al. 1991, KLINK and ALONSO 1993, LAMPL and YAROM 1993, PARE et al. 1995). Also several computer modeling studies have been published which mostly focus on particular properties of the specific neurons (e. g. TOTH and CRUNELLI 1992, WANG 1994, GUTFREUND et al. 1995) but there were also more general approaches (e. g. CHAY et al. 1995, LONGTIN and HINZER 1995). Interestingly, the latter is also referring to peripheral cold receptor discharges because of their "fascinating array of firing patterns" and it is based on the above mentioned model of PLANT.

Our model, in parts, has much in common with the other simulation approaches but also is different in several respects. On the one hand we have considered some particular properties of cold receptor discharges which we have seen in our experiments, e. g. specific Ca effects or serial interdependences of impulse generation (e. g. SCHÄFER et al. 1986). On the other hand we have tried to develop a generalized approach to elucidate the major functional properties of a flexible neuronal pattern generator irrespective of the specific ionic components of individual neurons.

3.1 Modeling Concepts and Model Equations

Here we describe the dimension-reduced version of our cold receptor model. This model has attracted particular attention, not only because it successfully simulates stationary cold receptor discharges, but also as a generalized neuronal pattern generator of enormous flexibility (see, for example, GILMORE 1999, NEIMAN et al. 1999, W. BRAUN et al. 2000, FEUDEL et al. 2000).

This model has only a single compartment (see Fig. 3*A*) and, therefore, only one membrane equation:

$$C_M \, dV/dt = - I_1 - I_d - I_r - I_{sd} - I_{sr} + I_{app} \qquad [1]$$

C_M is the membrane capacitance and V is the membrane voltage. Apart from the leakage current I_1 there are four voltage dependent currents I_d, I_r, I_{sd}, and I_{sr} and a term for external current application I_{app}. For numerical calculations of this and the other differential equations we used the Euler version of integration with time steps dt = 0.1 ms.

According to our generalized approach we do not refer to specific ion currents but to the de- and repolarizing components of the two subsystems, the spike generator and the subthreshold oscillator (see Fig. 3*A*). I_d is the fast depolarizing current and I_r is the fast

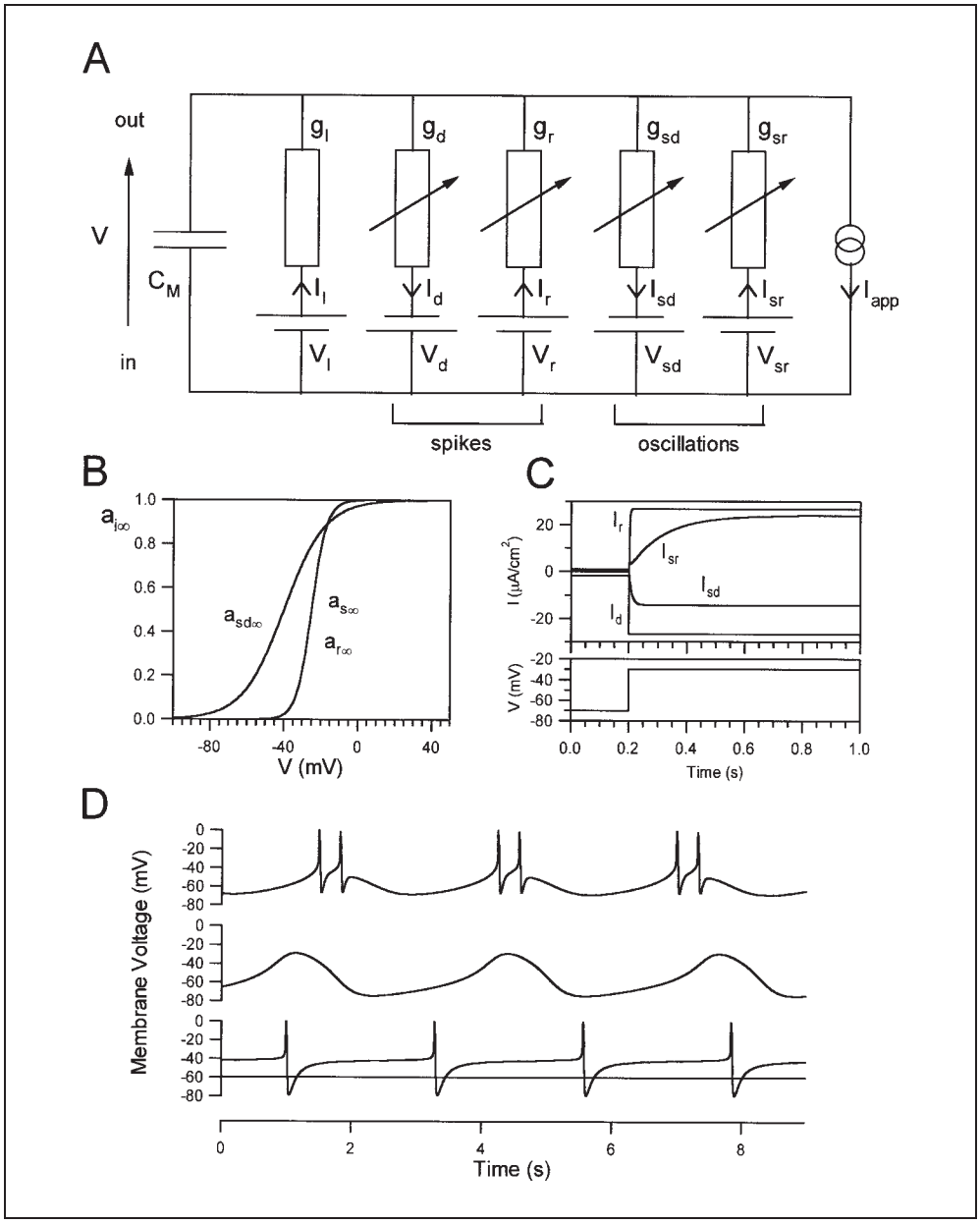

Fig. 3 (*A*) The electrical equivalent circuit of the model with a leak current and two sets of voltage dependent, de- and repolarizing currents for spike generation and for subthreshold oscillations (for details see text). (*B*) The steady-state activation values as functions of the membrane potential. (*C*) The time-dependencies of activation on a depolarizing voltage step. (*D*): Voltage traces at the reference temperature of 25 °C: the response of the complete model (upper trace), of the oscillatory subsystem (mid-trace) and of the spike-generating subsystem (lowest traces). Spikes which are seen in the lowest traces are only generated with external current injection (here $I_{app} = 1.122$). Below this value the spike-generator has a stable potential. The horizontal line indicates the situation at the spike-generator with $I_{app} = 0$.

repolarizing current which reflect the classical Na^+- and K^+-currents for spike generation. The physiological correlates for the other two currents, I_{sd} and I_{sr}, might be different in different neurons. Their major characteristics are that they activate much slower than the spike-currents and at lower membrane potentials (Fig. 3 *B*, *C*). The additional subfix "s" stands for "slow" and "subthreshold" activation.

The leakage current is given by

$$I_1 = g_1(V - V_1) \qquad [2]$$

and the voltage-dependent currents are calculated by:

$$I_i = \rho g_i a_i (V - V_i); \quad \text{for i = d, r, sd, sr.} \qquad [3]$$

V_i are the equilibrium (Nernst) potentials, g_i the maximum conductances and a_i the voltage and time dependent activation parameters. ρ is for temperature-scaling of the ion currents.

The voltage dependencies are given by sigmoidal curves

$$a_{i\infty} = 1/(1 + \exp(-s_i(V - V_{0i}))) \quad \text{for i = d, r, sd} \qquad [4]$$

V_{01} and s_i are half-activation potentials and slopes, respectively, of the steady state activation curves (Fig. 3 *B*).

Time dependent activation of ai is given by

$$da_i/dt = \phi(a_{i\infty} - a_i)/\tau_i; \quad \text{for i = r, sd} \qquad [5]$$

and

$$a_i = a_{i\infty} \quad \text{for i = d} \qquad [6]$$

which means that the fast depolarizing current is modeled with instantaneous activation without time delay:

Activation of the slow repolarizing current is modeled in a different way. It is directly coupled to the slow depolarizing current:

$$da_{sr}/dt = \phi(-\eta I_{sd} - k a_{sr})/\tau_{sr} \qquad [7]$$

with η as coupling constant and k as a relaxation factor.

Compared to the classical HH model (Hodgkin and Huxley 1952), we have included two additional currents but we also have made major simplifications. First of all, we do not go back to the rate constants α and β which describe the state transitions of the ion channels but directly refer to the voltage dependencies of activation which can be approximated quite well with sigmoidal curves ($a_{i\infty}$ in Equ. [4]). Equation [5] accounts for the time delayed activation of a_i with time constants τ_i which here, as another simplification, are voltage independent. Our variables a_i correspond to the activation variables m and n in the HH equations but there is no parameter for the variable h which means we do not consider any inactivation. We also do not use power functions to calculate the ionic conductances. The actual conductance is $g_i \cdot a_i$ (see Equ. [3]) which means that the maximum conductance is multiplied by exactly the same value as it comes from Equation [3] – not with its power of three or four.

Equation [7], which calculates the activation of the slow repolarizing current, seems to be completely different. It is a reduced version of our original model where the slow repolarizing current was modeled as a voltage and Ca-dependent current according to

our experimental recordings from the cold receptor during changed Ca concentrations and Ca-channel blockade which elucidated essential contributions of Ca dynamics to the impulse pattern generation (SCHÄFER et al. 1986, 1991). These are still considered also in this simplified version: The parameter η reflects Ca inflow in dependence on the depolarizing current I_{sd} and leads to Ca accumulation on depolarization. The parameter k serves for Ca relaxation, i. e. active elimination of intracellular Ca with Ca pumps depending on the actual Ca concentration. Indeed, Ca concentration is not explicitly given but it is reflected by the Ca-dependent variable a_{sr}.

The temperature dependencies of the ion currents cannot directly be recorded at the cold receptors. Therefore, we again have used a simplified but physiologically plausible approach (according to the findings from other neurons, see HILLE 1992). We have used the same scaling factors for all voltage dependent currents.

The main temperature effects, relevant for Equations [5] and [7], come from the time constants of activation for which we assume a 3-fold increase over a temperature increase of 10 °C, i. e. a Q_{10} of 3.0:

$$\phi = 3.0^{(T-To)/10}. \quad [8]$$

There is an additional temperature scaling of the maximum conductances which, however, has a Q_{10} of only 1.3 and is only relevant for equation [3]. It has minor effects on the principle model behavior and was mainly done for fine adjustment of the model data with specific cold receptors characteristics:

$$\rho = 1.3^{(T-To)/10}. \quad [9]$$

To account for the effects of random dynamics we have applied Gaussian white noise according to the Box-Mueller algorithm as described in FOX et al. (1988):

$$g_w = (-4d \cdot dt \ln(a))^{1/2} \cos(2\pi b) \quad [10]$$

with a, b random numbers between 0 to 1. Noise intensity is adjusted by the dimensionless control parameter d. The noise value g_w is directly added to the membrane potential:

$$V_{t+dt} = V_t + f(V)\, dt + g_w. \quad [11]$$

The numerical parameter values:

(1.) equilibrium potentials: $V_{sd} = V_d = 50$, $V_{sr} = V_r = -90$, $V_l = -60$ (in mV);
(2.) ionic conductances: $g_l = 0.1$, $g_d = 1.5$, $g_r = 2.0$, $g_{sd} = 0.25$, $g_{sr} = 0.4$ (in mS/cm^2);
(3.) membrane capacitance: $C_M = 1$ (in µF/cm^2)
gives a passive time constant: $\tau_M = C_M/g_l = 10$ (in ms);
(4.) activation time constants: $\tau_r = 2$, $\tau_{sd} = 10$, $\tau_{sr} = 20$ (in ms);
(5.) slope of steady state activation: $s_d = s_r = 0.25$, $s_{sd} = 0.09$;
(6.) half activation potentials: $V_{0d} = V_{0r} = -25$, $V_{0ds} = -40$ (in mV);
(7.) coupling and relaxation constants for I_{sr}: $\eta = 0.012$, $k = 0.17$;
(8.) reference temperature: $T_O = 25$ (in °C).

These parameter values were chosen to obtain a period-two burst discharge at the reference temperature of 25 °C (Fig. 3 *D*, upper trace) according to the situation most often observed in our experimental recordings. Figure 3 *D* also illustrates the voltage responses of the isolated subsystems. With only subthreshold currents (mid-trace in Fig. 3 *D*) the oscillations are a little bit slower compared to the complete system where

spike-generation obviously accelerates the rhythm. This is due to the resettings from each spike which prevent the subthreshold oscillations to fully develop. With only spike-generating currents (lowest traces in Figure 3 *D*) this system would be completely silent with a stable membrane potential of about – 60 mV close to the leakage potential V_1 (horizontal line in the lowest diagram in Fig. 3 *D*). Voltage traces with spike-activity that are also shown in this diagram were obtained with additional constant current injection. It is evident that the dynamics are totally different from that of the complete system with coupled oscillations and spike-generation.

Remarkably, when the system has been adjusted to these specific dynamics, the full variety of experimentally observed impulse patterns almost naturally evolves with simple temperature scaling as implemented in the model equations.

3.2 Impulse Pattern at Different Temperature in Deterministic and Noisy Simulations

In Figure 4 we have once more plotted the most characteristic impulse sequences from experimental recordings for direct comparison with the results from our modeling studies which are shown in the traces below. It can easily be seen that the model almost perfectly mimics all types of cold receptor discharges. But it also becomes evident that one particular type of pattern can only be simulated with addition of noise as we already have expected from previous analysis of our experimental data (see 2.3). This is the pattern which consists of a mixture of spike-generating and subthreshold oscillations (skippings) that typically occurs in the upper temperature range, and can here be seen in both experimental and modeling data (35 °C, left diagrams) but not in the lowest diagram which is from a completely deterministic simulation (d = 0). In this situation only the addition of noise allows the subthreshold oscillations to randomly exceed the threshold for spike-generation.

The second row shows tonic firing patterns which preferably occur in experimental recordings at "normal" skin temperatures around 30 °C and which also can be seen in our simulations with corresponding temperature scaling. Noise does not seem to have major influence on the pattern generation. There is a regular tonic discharge because each oscillation cycle succeeds to trigger a spike – with a single exception: at d = 0.5 one of the oscillation cycles obviously fails. The upper trace indicates that something similar might happen also in experimental recordings: a spike is missing within an otherwise regular tonic discharge. Although these are only singular events, their pure occurrence suggests that noise cannot only induce spiking in otherwise completely subthreshold oscillations (as shown in the left traces) but also can prevent impulse generation in deterministically regularly spiking sequences. As we will see below, such situations can cover very broad ranges of stimulus encoding.

In the next, third row of Figure 4 we are comparing electrophysiological recordings and model simulations of different noise levels in the range of burst discharges. Here, indeed, we cannot see a qualitative effect of noise. More random input simply seems to induce more random fluctuations of spike-generation without any qualitative change of the pattern.

This also seems to be the case at the lowest temperatures where the experimental recordings often exhibit irregular tonic discharges. The deterministic simulations gener-

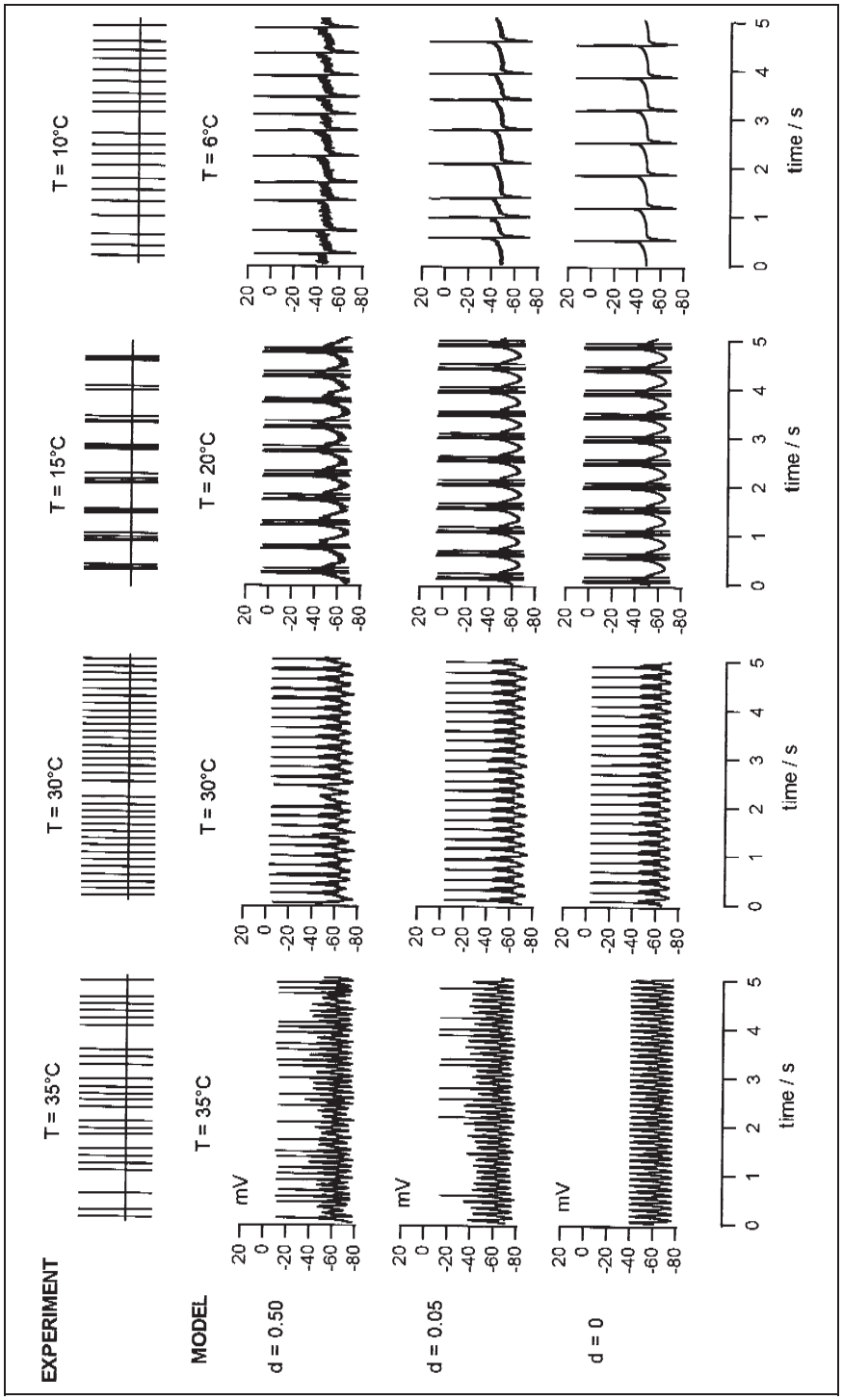

Fig. 4 Typical impulse patterns at different temperatures (T). Comparison of experimentally recorded spike sequences (upper traces) and modelling data from deterministic simulations (d = 0, lowest traces) and with addition of noise (d = 0.05 and d = 0.5).

ate completely regular discharges and it needs addition of noise to produce the more realistically appearing irregular spike sequences. However, a qualitative change of the patterns seems not to be associated with the presence of noise. But this might not be the complete truth as we will see with a more thorough look at the interspike distributions and the return maps.

3.3 Temperature Dependent Bifurcations and Noise Effects

With linear temperature scaling our model shows continuous transitions between a manifold of impulse patterns which is illustrated in Figure 5 with so-called bifurcation diagrams of interspike intervals to illustrate where qualitative changes of the system behavior occur. Figure 5 *A* shows the bifurcation diagram of the deterministic simulation which is plotted again in Figure 5 *B* (in black) together with the data from noisy simulations (in red and blue). Additionally, in Figure 5*C*, the frequency curves are plotted. Moreover, in Figure 6, we have plotted the deterministic and noisy return maps (RM) from different temperatures to further illustrate the most relevant transitions in the bifurcation diagrams.

As described above, it is necessary to add noise to simulate all relevant types of patterns that can be recorded from peripheral cold receptors. This specifically holds true for the mixed pattern of spike-generating and subthreshold oscillations at higher temperatures which cannot be seen without noise. The deterministic simulation (Fig. 5 *A*) shows a very abrupt transition from zero activity to regular firing between 35 and 34 °C and accordingly, a sudden increase in the frequency plot (Fig. 5 *C*, black curve). There is again an abrupt transition when tonic firing changes to burst discharges at about 28 °C in a so-called period-adding bifurcation. More of such bifurcations can be seen towards lower temperatures whenever an additional spike is added to the bursts. The resonant behavior between spikes and subthreshold oscillations thereby changes from 1 : 1 (1 spike per oscillation cycle) to 4 : 1 (bursts of 4 spikes) until the bifurcation scenario becomes completely different at about 15 °C. In deterministic simulations, the transitions from n to n + 1 resonances are rather abrupt. There are only very narrow ranges where auto-resonances between the two subsystems lead to complicated fine structures of the patterns (described in more detail in W. Braun et al. 2000). These fine structures are destroyed already with very low levels of noise. Higher noise levels can even smooth completely the bifurcation structures of the deterministic simulation and induce a variety of mixed patterns, including the above mentioned "skippings".

The bifurcation scenario of the deterministic simulation leads to a sawtooth-like frequency curve (Fig. 5*C*, black curve): the frequency suddenly increases whenever the lengthened oscillations can trigger one impulse more and then gradually decreases due to the temperature dependent lengthening of the oscillations until the next spike is added. Addition of noise also smoothes these multiple maxima. At d = 0.5 (blue curve in Figure 5*C*) there is a broad range of almost constant frequency and, in accordance with the experimental data, a frequency decline towards the extremes of the temperature range.

We will describe these transitions in more detail below but first we will pay attention on another remarkable pattern which occurs when we further decrease the temperature. At around 15 °C the regular bifurcation adding scenario is destroyed (Fig. 5*A*). Instead,

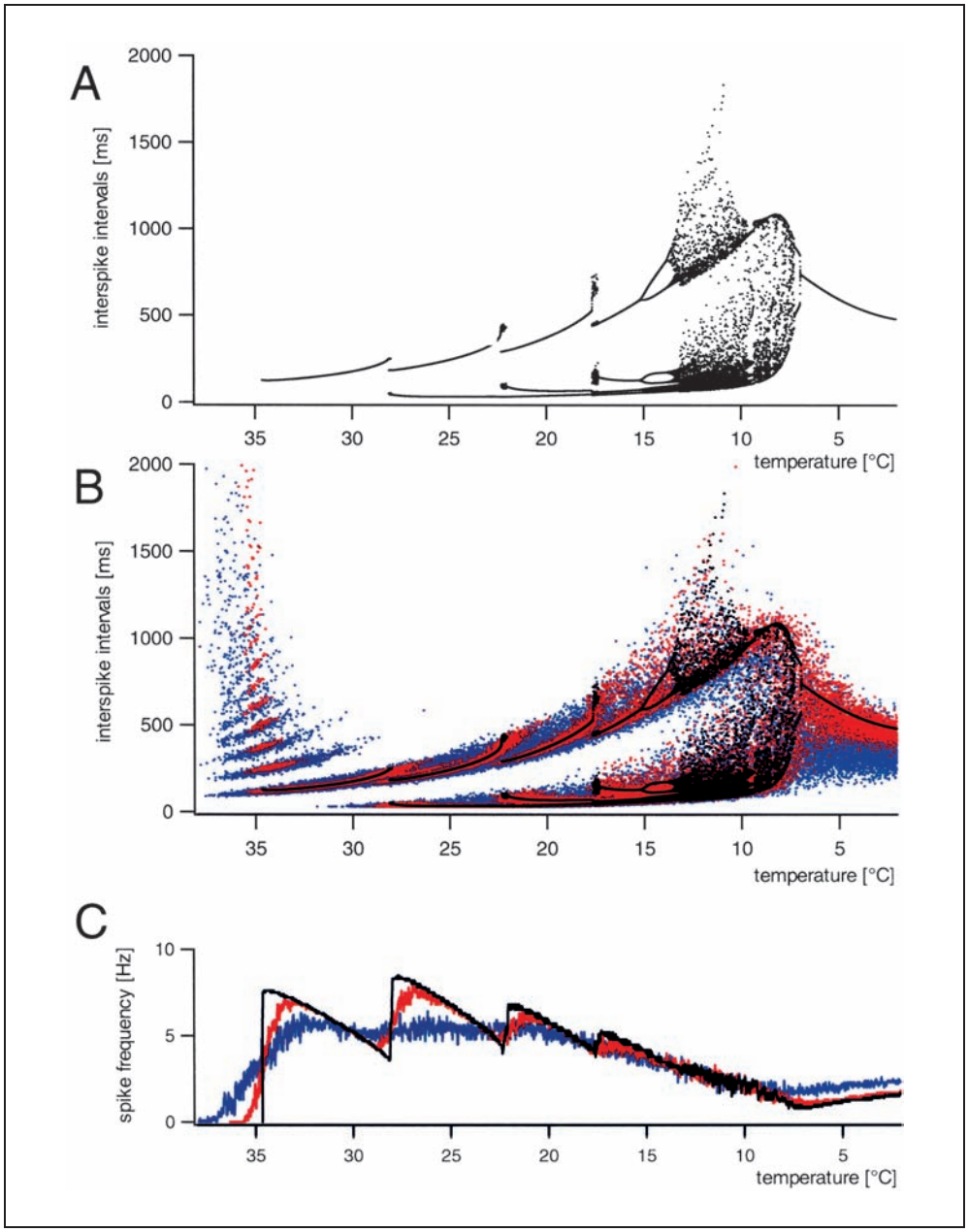

Fig. 5 Plots of successive interspike-intervals (bifurcation diagrams) and spike-frequency plots of deterministic and noisy model simulations with linear temperature scaling from 38 °C down to 2 °C. (*A*) Deterministic bifurcation diagram. (*B*) Deterministic bifurcation diagram (black dots, same as in (*A*)) compared to noisy simulations with two different noise intensities d (red dots: d = 0.05, blue dots: d = 0.5). (*C*) Spike-frequency of the deterministic and noisy simulations (same color code as in (*B*)) plotted as peri-stimulus-time histograms (bin width: 2s). In (*B*) and (*C*), lower noise values (red) are overwriting the higher noise values (blue) and the deterministic values (black) are dominating over the others.

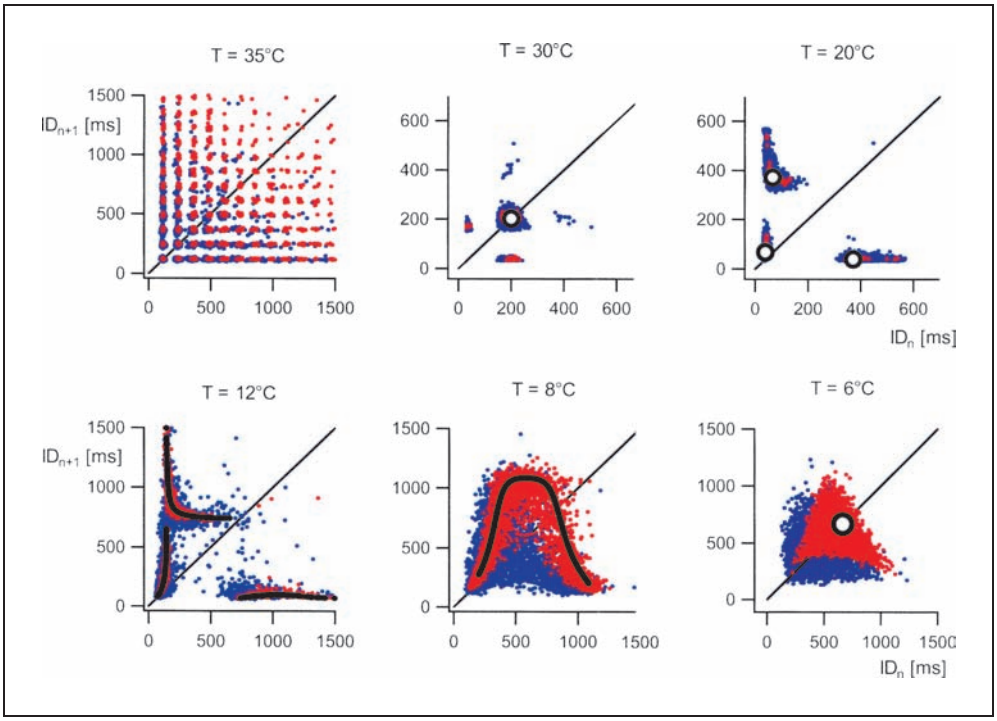

Fig. 6 Return maps of typical impulse patterns of the model from deterministic simulations (black dots) and with addition of noise (red dots: d = 0.05, blue dots: d = 0.5). Each plot consists of 3000 interval pairs from simulations at constant temperatures, as indicated. According to Figure 3, the duration of a given interspike interval at position n is plotted as abscissa value (ID_n) and the duration of the immediately following interval (at position n + 1) is plotted as ordinate value ID_{n+1}. ID stands for interval duration. The deterministic black dots are dominant over the red dots (low noise) which, in turn, are dominant over the blue dots (high noise). Single dots of periodic discharges are enhanced as circles. The 45° line indicates the position of interval pairs of equal duration.

there is a suddenly increasing number of other types of bifurcations which soon leads to completely "chaotic" discharges over a broad temperature range (between about 13 and 7 °C) until again a tonically firing pattern, i. e. a period-one discharge, occurs. Much effort has already been made for a better understanding of these transitions and the underlying system dynamics (e. g. GILMORE et al. 1999, BRAUN et al. 2000, W. BRAUN et al. 2000, FEUDEL et al. 2000, BRAUN et al. 2001) but there are still many aspects which are awaiting further elucidation specifically with regard to the noise effects.

In the following we will have a more thorough look on such transitions between different dynamical states with special emphasis on the effects of noise. We first will describe the transition from skippings to bursts *via* the tonic firing pattern (which is typical for the upper temperature range) and than will focus on the transitions from burst to tonic firing *via* "chaos" (which occurs at lower temperatures).

3.3.1 From Skippings to Tonic Firing and Bursts

The impact of noise becomes most obvious in the upper temperature range with the occurrence of additional interval bands (Fig. 5 *B*, around 35 °C) which only can be seen in the presence of noise (red dots: d = 0.05, blue dots: d = 0.5), while the deterministic simulation (black dots: d = 0) is silent or regularly discharging. This means that noise can induce spiking in previously subthreshold oscillations but also can induce skipping in deterministically tonic discharges. This effect becomes stronger with increasing noise: the bands of longer intervals are spreading over a broader temperature range.

The corresponding return map (Fig. 6, the same color code as in the bifurcation diagrams) is drawn for 35 °C which is a deterministically subthreshold situation closely above the transition to regular firing. There is, of course, no data from the subthreshold oscillations but there is the typical clustering from noisy simulations which shows principally the same characteristics as already described for the experimental data (see Fig. 2 *B*). At first, it might appear surprising that the distribution of the clusters is narrowed with increasing noise (blue dots from high noise simulations are not as widely scattered as red dots from low noise simulations). However, this can easily be understood considering that the probability of spike-generation is increasing with increasing noise which means that the probability for the occurrence of very long intervals, i. e. long sequences of subthreshold oscillations, decreases. This effect is also manifested in the increasing firing rate with increasing noise (Fig. 5 *C*, 35 °C and above). This is the range where stochastic resonance phenomena can occur (see Douglass et al. 1993, Wiesenfeld and Moss 1995) which, however, here we will not discuss.

The situation drastically changes when we reach the deterministically tonic-firing range, e. g. 34 °C, where addition of noise reduces the firing rate which is due to noise-induced skippings (Fig. 5 *B*, *C*). The situation changes again, still in the deterministically tonic-firing range, e. g. around 29 °C, where noise induced bursts increase the firing rate. The probability of noise induced skippings, of course, is higher closer to the range of deterministically subthreshold oscillations whereas noise induced bursts can more often be expected in the neighborhood of the deterministically bursting range. Somewhere in between, both effects should be balanced. This is the point where the deterministic and noisy frequency curves are crossing again. Hence, within a sequence of regular period-adding bifurcations, crossings of the frequency curves, where the noise effects are inversed, must not only be expected at each bifurcation point but also at these "equilibrium" points in between (Fig. 5 *C*). The coexistence of different patterns close to such "equilibrium" points is also illustrated in the return map at 30 °C (Fig. 6). At d = 0.05 clusters of short intraburst-intervals occur and at d = 0.5 also skippings are indicated. This return map has its experimental counterpart in Figure 2 *C* where, of course, we cannot see the deterministic period-one fixed-point which here gives a single dot on the 45° line (in Fig. 6 emphasized as a circle).

The simulated return map from 20 °C in Figure 6 has its experimental counterpart in Figure 2 *D*. These return maps are exclusively built up from burst discharges. The deterministic simulation induces a period-three pattern where the burst-pause is followed by two intraburst-intervals until exactly the same sequence starts again (a 3 : 1 resonance between spikes and oscillations). Noise seems not to disturb this burst pattern very

much. Of course, there are noise induced fluctuations around the deterministic points whereby the interval pairs with burst pauses preferably extend along the x-and y-axis. This effect, is also seen in the experimental data (Fig. 2 *D*) and has already been described there. However, in the model data, there additionally is an elongation of the cluster of intraburst intervals along the ordinate and of short-long intervals towards the 45° line. We will come back to these phenomena below because it might indicate that we are approaching the range of deterministic chaos.

3.3.2 From Bursts to Tonic Firing – via Chaos

The return map which is drawn for 12 °C (Fig. 6) already reflects chaotic dynamics. Even in the deterministic simulation the interval pairs do not form individual dots – according to a certain periodic discharge – but are scattered along distinct lines (see also W. Braun et al. 2000). Remarkably, the particular shape seems already anticipated by the noisy simulations from 20 °C (see above) although this was from a deterministically regular period-3 discharge far away from the chaotic regime. At 12 °C noise does not change the principle structure of the return map.

However, distinct modifications can be seen when we further decrease the temperature and thereby pass through the deterministic chaos, e. g. return maps that show additional elongations at the 45° line and then attain almost rectangular and later parabolic shapes (see also Feudel et al. 2000). The return map that we have drawn from 8 °C (Fig. 6) is somehow at the transition from the more rectangular to the more parabolic shape. The most interesting effects, however, occur with the addition of noise which drastically changes the distribution. At d = 0.05 the dots are still scattered around the deterministic curve but with extraordinarily strong fluctuations. However, at d = 0.5 almost nothing seems to be left from the original parabolic distribution. This return map rather resembles those from experimental recordings with irregular bursts as shown in Figure 2*E*. There is a broad distribution along the 45° line with some extensions to short-short, long-short and short-long interval pairs which is the typical burst pattern. The area where the deterministic curve crosses the 45° line is almost free.

Remarkable noise effects can also be seen in the return map at 6 °C (Fig. 6) which is below the chaotic regime in the deterministically period-one situation. Accordingly, the deterministic simulation gives a single dot (enhanced as circle). But already low noise of d = 0.05 leads to extremely strong fluctuations which are clearly different from a random, even distribution around the deterministic fixed-point. The shape rather reminds to a filled triangle (or parabola?). Further increase of noise to d = 0.5 destroys this particular shape and leads to a rather unstructured distribution, although with some preferences for short-short, short-long and long-short intervals according to very irregular burst discharges. It corresponds to the experimental return map shown in Figure 2*F*, including some details as described there.

4. Summary and Conclusions

We have described the impulse patterns of extracellular recordings of peripheral cold receptors as an example of an enormously flexible neuronal impulse pattern generator. To our knowledge, so far no other neuron is known that passes through such a manifold of patterns as a function of the physiologically relevant input which here is the temperature. Synaptic interactions can be excluded, which implies that these patterns are generated by intrinsic properties of nerve endings.

Supplementary to the electrophysiological experiments, we use computer modeling studies to attain further insights into the underlying neuronal dynamics. Indeed, several models of neuronal oscillations already exist and partly use similar approaches as described here (e. g. WANG 1994, CHAY et al. 1995, LONGTIN and HINZER 1995). However, most of these models consist of a very long set of equations with many different ion currents and with complex activation and inactivation dynamics according to the classical HH-type equations. Instead, our model uses a strongly simplified approach and is systematically reduced to only four dimensions, i. e. differential equations. It nevertheless includes the physiologically relevant ion currents as suggested by the experimental data, and can simulate continuous transitions between a manifold of impulse patterns as recorded from peripheral cold receptors. Similar transitions, although not all together, have been seen in many other neurons. Hence, impulse generation with subthreshold oscillations seems to be a widespread principle of information processing in the peripheral and central nervous system although the specific ionic currents might be different.

This generic property was the reason for examining the model's dynamics from the viewpoint of a generalized neuronal impulse pattern generator, i. e. not to focus on the details of ion currents but on their principle functional interrelations. As a promising approach, suggested by recent analysis of the model's dynamics (see BRAUN et al. 2000, W. BRAUN et al. 2000, FEUDEL et al. 2000), we have examined the resonant behavior between the spike-generator and subthreshold oscillator. Moreover, we have paid particular attention to the effects of noise, because it was clear from previous theoretical and modeling studies (e. g. LONGTIN et al. 1991, LONGTIN and HINZER 1995, WIESENFELD and MOSS 1995, BULSARA and GAMMAITONI 1996) as well as from experimental data (e. g. BRAUN et al. 1980, 1984b, SCHÄFER et al. 1986, 1991, BRAUN et al. 1994, NEIMAN et al. 1999, WHITE et al. 2000) that nonlinear, cooperative noise-effects, can become relevant factors for neuronal encoding. The results that we have described here essentially reflect noise mediated resonance behavior of a minimal model of oscillating and spike-generating mechanisms.

Not only the model equations but also the model's behavior is comparably simple when we look at the two subsystems separately: the spike generator is silent without the input from the oscillator and the subthreshold mechanisms can only produce regular oscillations without the spike-generator. It is the coupling of these two subsystems that leads to more complex activity patterns, and it needs noise to see the full variety of them.

We have illustrated the transitions between the different types of impulse patterns using a simple but physiologically plausible temperature scaling. Qualitatively identical transitions can be expected with other scaling parameters (an example is shown in BRAUN et al. 2000). Temperature scaling has the advantage that we can demonstrate the

efficiency of this approach in direct comparison with our own experimental data from cold receptors, as shown in Figure 1 and Figure 2. In comparison with the model data from Figure 5 and Figure 6 it is evident that this minimal model successfully mimics the experimental data in remarkable detail.

To briefly summarize the major characteristics, it seems easiest to begin in the range of bursting activity which indicates a very strong coupling between subthreshold oscillations and spike-generating mechanisms. Strong depolarization of the subthreshold oscillations can repeatedly activate the spike generating mechanisms. The number of spikes per oscillation cycle simply depends on strength and duration of the slow-wave depolarization. Noise smooths the deterministically abrupt transitions but does not qualitatively change the impulse patterns. The same holds true up to 1 : 1 resonances, i. e. single-spike discharges.

The situation changes when amplitude and/or duration of the subthreshold oscillations are too small for spike generation as it is the case in the upper temperature range. There is an intermediate state where the subthreshold oscillations can still activate the spike-generating processes, but only with the help of stochastic fluctuations. However, noise also can prevent spike generation in the otherwise regularly firing mode. Such "cooperative noise effects" (Bulsara and Gammaitoni 1996, Gammaitoni et al. 1998) were first described – as far as we know – more than 50 years ago (Brink et al. 1946) with chemical excitation of the nerve axons. Many years later, their detection in experimental recordings from cold afferents has led to the first theoretical description of sensory transduction with oscillations and noise (Braun et al. 1980). During recent years, such patterns have been recorded in many other peripheral sensory afferents (Braun et al. 1984, Schäfer et al. 1988, 1989, Braun et al. 1990, Heinz et al. 1990, Braun et al. 1994, Schäfer et al. 1995), and also play a role in information processing in the central nervous system (e. g. Llinas and Yarom 1986, Alonso and Llinas 1989, Klink and Alonso 1993, Lampl and Yarom 1993, Pare et al. 1995). Remarkably, similar effects can become of pathophysiological relevance in systemic functions, for example, when random components interfere with periodic processes in the course of psychiatric disorders (see e. g. Huber et al. 1999, 2000 b, 2002).

The impulse patterns which we have seen in the lower temperature range are far from being completely understood. The deterministic simulations clearly show a broad range of "deterministic chaos" which seems to occur in a transitory state when the oscillatory dynamics change to pacemaker activity (Braun et al. 2000). Dynamical system theory indicates a route through deterministic chaos via homoclinic bifurcations (W. Braun et al. 2000, Feudel et al. 2000). In noisy simulations and particularly in experimental recordings, however, it cannot be immediately seen whether the fluctuations in the impulse sequences are due to noise, i. e. high-dimensional dynamics, or reflects chaotic low-dimensional dynamics. With use of the so-called »recurrence-method« (Pierson and Moss 1995), indeed, we found statistically significant indications of deterministic chaos in experimental recordings (Braun et al. 1999) and noisy simulations (Braun et al. 2001) which occur preferably at low temperatures around the transitions from tonic-to-bursting activity, where chaotic dynamics can be expected. But the model also exhibits remarkable noise effects in the deterministically periodic situations which can be seen best in the return maps (Fig. 6, 20 °C and 6 °C), and which reflect "cooperative" effects between the nonlinear systems dynamics and noise which are not yet fully understood.

With contribution of noise there are obviously very complex dynamics also out of the chaotic regime which reaches far into the range of deterministically regular discharges. The high rate of agreement of the noisy simulations and experimental data indicate that such cooperative noise effects are not only model specific characteristics, but might also be of relevance for neuronal transduction processes in real life, as it has already been experimentally proven for other situations, i. e. noise induced "skippings".

Acknowledgements

The work was supported by the DFG and INTAS grant 01-2061.

References

Alonso, A., and Llinas, R.: Differential electroresponsiveness of stellate- and pyramidal-like cells of medial entorhinal cortex layer II. Nature *342*, 175–177 (1989)

Braun, H. A., Bade, H., and Hensel, H.: Static and dynamic discharge patterns of bursting cold fibers related to hypothetical receptor mechanisms. Pflügers Arch. *386*, 1–9 (1980)

Braun, H. A., Huber, M. T., Anthes, N., Voigt, K., Neiman, A., and Moss, F.: Noise induced impulse pattern modifications at different dynamical period-one situations in a computer-model of temperature encoding. Biosystems *62*, 99–112 (2001)

Braun, H. A., Huber, M. T., Anthes, N., Voigt, K., Neiman, A., Pei, X., and Moss, F.: Interactions between slow and fast conductances in the Huber/Braun model of cold receptor discharges. Neurocomputing *32–33*, 61–66 (2000)

Braun, H. A., Huber, M. T., Dewald, M., Schäfer, K., and Voigt, K.: Computer simulations of neuronal signal transduction: the role of nonlinear dynamics and noise. Intern. J. Bifurcation and Chaos *8*, 881–889 (1998)

Braun, H. A., Schäfer, K., Voigt, K., Peters, R., Bretschneider, F., Pei, X., Wilkens, L., and Moss, F.: Low dimensional dynamics in sensory biology. II: Facial cold receptors of rat. J. Comp. Neurosci. *7*, 17–32 (1999)

Braun, H. A., Schäfer, K., und Wissing, H.: Theorien und Modelle zum Übertragungsverhalten thermosensitiver Rezeptoren. Funkt. Biol. Med. *3*, 26–36 (1984 a)

Braun, H. A., Schäfer, K., Wissing, H., and Hensel, H.: Periodic transduction processes in thermosensitive receptors. In: Hamann, W., and Iggo, A. (Eds.): Sensory Receptor Mechanisms; pp. 147–156. Singapore: World Scientific Publication 1984 b

Braun, H. A., Schäfer, K., and Wissing, H.: Theories and models of temperature-transduction. In: Bligh, J., and Voigt, K. H. (Eds.): Thermoreception and Temperature Regulation; pp. 19–29. Heidelberg: Springer 1990

Braun, H. A., Wissing, H., Schäfer, K., and Hirsch, M. C.: Oscillation and noise determine signal transduction in shark multimodal sensory cells. Nature *367*, 270–273 (1994)

Braun, W., Eckhardt, B., Braun, H. A., and Huber, M. T.: Phase space structure of a thermoreceptor. Phys. Rev. E *62*, 6352–6360 (2000)

Brink, F., Bronk, D. W., and Larrabee, M. G.: Chemical excitation of nerve. Ann. New York Acad. Sci. *47*, 457–485 (1946)

Bulsara, A., and Gammaitoni, L.: Tuning in to noise. Phys. Today March Issue, 39–45 (1996)

Chay, T. R., Fan, Y. S., and Lee, Y. S.: Bursting, spiking, chaos, fractals and universality in biological rhythms. Int. J. Bifurcation and Chaos *5*, 595–635 (1995)

Clapham, D. E.: Hot and cold TRP ion channels. Science *295*, 2228–2229 (2002)

Douglass, J. K., Wilkens, L., Pantazelou, E., and Moss, F.: Noise enhancement of information transfer in crayfish mechanoreceptors by stochastic resonance. Nature *365*, 337–340 (1993)

Feudel, U., Neiman, A., Pei, X., Wojtenek, W., Braun, H. A., Huber, M. T., and Moss, F.: Homoclinic bifurcations in a Hodgkin-Huxley model of thermally sensitive neurons. Chaos *10*, 231–239 (2000)

FITZHUGH, R.: A kinetic model of the conductance changes in nerve membrane. J. Cell. Comp. Physiol. *66*, 111–117 (1965)

FOX, R. F., GATLAND, I. R., ROY, R., and VEMURI, G.: Fast, accurate algorithm for numerical simulation of exponentially correlated colored noise. Phys. Rev. A *38*, 5938–5940 (1988)

GAMMAITONI, L., HANGGI, P., JUNG, P., and MARCHESONI, F.: Stochastic resonance. Rev. Modern Physics *70*, 223–288 (1998)

GILMORE, R., PEI, X., and MOSS, F.: Topological analysis of chaos in neural spike train bursts. Chaos *9*, 812–817 (1999)

GUTFREUND, Y., YAROM, Y., and SEGEV, I.: Subthreshold oscillations and resonant frequencies in guinea-pig cortical neurons: physiology and modelling. J. Physiol. *483.3*, 621–640 (1995)

HEINZ, M., SCHÄFER, K., and BRAUN, H. A.: Analysis of facial cold receptor activity in the rat. Brain Res. *521*, 289–295 (1990)

HENSEL, H., ANDRES, K. H., and DÜRING, M. VON: Structure and function of cold receptors. Pflügers Arch. *352*, 1–10 (1974)

HENSEL, H., IGGO, A., and WITT, I.: A quantitative study of sensitive cutaneous thermoreceptors with C afferent fibres. J. Physiol. *204*, 99–112 (1969)

HILLE, B.: Ionic Channels of Excitable Membranes. Sunderland, Mass.: Sinauer Associates Inc. 1992

HODGKIN, A. L., and HUXLEY, A. F.: A quantitative description of membrane current and its application to conductance and excitation in nerve. J. Physiol. (London) *117*, 500–544 (1952)

HUBER, M. T., BRAUN, H. A., and KRIEG, J. C.: Consequences of deterministic and random dynamics for the course of affective disorders. Biol. Psychiatry *46*, 256–262 (1999)

HUBER, M. T., BRAUN, H. A., and KRIEG, J. C.: Effects of noise on different disease states of recurrent affective disorders. Biol. Psychiatry *47*, 634–642 (2000 b)

HUBER, M. T., BRAUN, H. A., and KRIEG, J. C.: Recurrent affective disorders: nonlinear and stochastic models of disease dynamics. Int. J. of Bifurcation and Chaos (2002 in press)

HUBER, M. T., KRIEG, J. C., DEWALD, M., VOIGT, K., and BRAUN, H. A.: Stochastic encoding in sensory neurons: impulse patterns of mammalian cold receptors. Chaos, Solitons and Fractals *11*, 1896–1904 (2000a)

HUBER, M. T., KRIEG, J. C., DEWALD, M., VOIGT, K., and BRAUN, H. A.: Stimulus sensitivity and neuromodulatory properties of noisy intrinsic neuronal oscillators. Biosystems *48*, 95–104 (1998)

IGGO, A., and YOUNG, D. W.: Cutaneous thermoreceptors and thermal nociceptors. In: KORNHUBER, H. H. (Ed.): The Somatosensory System; pp. 5–25. Stuttgart: Georg Thieme 1975

KLINK, K., and ALONSO, A.: Ionic mechanisms for the subthreshold oscillations and differential electroresponsiveness of medial entorhinal cortex layer II neurons. J. Neurophysiol. *70*, 144–157 (1993)

LAMPL, I., and YAROM, Y.: Subthreshold oscillations of the membrane potential: a functional synchronizing and timing device. J. Neurophysiol. *70*, 2181–2186 (1993)

LLINAS, R. R.: The intrinsic eletrophysiological properties of mammalian neurons: insights into central nervous system function. Science *242*, 1654–1664 (1988)

LLINAS, R. R., GRACE, A. A., and YAROM, Y.: In vitro neurons in mammalian cortical layer 4 exhibit intrinsic oscillatory activity in the 10- to 50-Hz frequency range. Proc. Natl. Acad. Sci. USA *88*, 897–901 (1991)

LLINAS, R. R., and YAROM, Y.: Oscillatory properties of guinea pig inferior olivary neurones and their pharmacological modulation: an in vitro study. J. Physiol. *376*, 163–182 (1986)

LONGTIN, A.: Stochastic resonance in neuron models. J. Stat. Phys. *70*, 309–327 (1993)

LONGTIN, A., BULSARA, A., and MOSS, F.: Time interval sequences in bistable systems and the noise induced transmission of information by sensory neurons. Phys. Rev. Lett. *67*, 656–660 (1991)

LONGTIN, A., and HINZER, K.: Encoding with bursting, subthreshold oscillations and noise in mammalian cold receptors. Neural Comput. *8*, 215–255 (1995)

MACDERMOTT, A. B., and LEE, J. C.: Cold emerging from the fog. Nature Neurosci. *5*, 189 (2002)

MCCORMICK, D. A., and FEESER, H. R.: Functional implications of burst firing and single spike activity in lateral geniculate relay neurons. Neuroscience *39*, 103–113 (1990)

MCKEMY, D. D., NEUHAUSSER, W. M., and JULIUS, D.: Identification of a cold receptor reveals a general role for TRP channels in thermosensation. Nature *416*, 52–58 (2002)

NEIMAN, A., PEI, X., RUSSELL, D., WOJTENEK, W., WILKENS, L., MOSS, F., BRAUN, H., HUBER, M., and VOIGT, K.: Synchronization of the electrosensitive noisy cells in the paddlefish. Phys. Rev. Lett. *82*, 660–663 (1999)

PARE, D., PAPE, H. C., and DONG, J.: Bursting and oscillating neurons of the cat basolateral amygdaloid com-

plex in vivo: electrophysiological properties and morphological features. J. Neurophysiol. *74*, 1179–1191 (1995)

Peier, A. M., Moqrich, A., Hergarden, A. C., Reeve, A. J., Anderson, D. A., Story, G. M., Earley, T. J., Dragoni, I., McIntyre, P., Bevan, S., and Patapoutian, A.: A TRP channel that senses cold stimuli and menthol. Cell *108*, 705–715 (2002)

Pierson, D., and Moss, F.: Detecting periodic unstable points in noisy chaotic and limit cycle attractors with applications to biology. Phys. Rev. Lett. *75*, 2124–2127 (1995)

Plant, R. E.: The effects of Ca on butsting neurions: a modelling study. Biophys. J. *21*, 217–237 (1978)

Plant, R. E.: Bifurcation and resonance in a model for bursting nerve cells. J. Math. Biol. *11*, 15–32 (1981)

Reid, G., and Flonta, M.-L.: Cold currents in thermoreceptive neurons. Nature *413*, 480 (2001)

Schäfer, K., Braun, H. A., and Isenberg, C.: Effect of menthol on cold receptor activity: Analysis of receptor processes. J. Gen. Physiol. *88*, 557–576 (1986)

Schäfer, K., Braun, H. A., and Kürten, L.: Analysis of cold and warm receptor activity in vampire bats and mice. Pflügers Arch. *412*, 188–194 (1988)

Schäfer, K., Braun, H. A., Peters, R. C., and Bretschneider, F.: Periodic firing pattern in afferent discharges from electroreceptor organs of catfish. Pflügers Arch. *429*, 378–385 (1995)

Schäfer, K., Braun, H. A., and Rempe, L.: Discharge pattern analysis suggests existence of a low-threshold calcium channel in cold receptors. Experientia *47*, 47–50 (1991)

Schäfer, K., Necker, R., and Braun, H. A.: Analysis of avian cold receptor function. Brain Res. *501*, 66–72 (1989)

Swandulla, D., Carbone, E., Schäfer, K., and Lux, H. D.: Effect of menthol on two types of calcium currents in cultured sensory neurons of vertebrates. Pflügers Arch. *409*, 52–59 (1987)

Swandulla, D., Schäfer, K., and Lux, H. D.: Calcium channel current inactivation is selectively modulated by menthol. Neurosci. Lett. *68*, 23–28 (1986)

Tuckwell, H. C.: Introduction to Theoretical Neurobiology. Vol. 2 Nonlinear and Stochastic Theories. Cambridge: Cambridge University Press 1988

Viana, F., de la Peña, E., and Belmonte, C.: Specifity of cold thermotransduction is determined by differential ionic channel expression. Nature Neurosci. *5*, 254–260 (2002)

Wang, X.-J.: Multiple dynamical modes of thalamic relay neurons: rhythmic bursting and intermittent phase-locking. Neuroscience *59*, 21–32 (1994)

White, J. A., Rubinstein, J. T., and Kay, A. R.: Channel nosie in neurons. TINS *23*, 131–137 (2000)

Wiesenfeld, K., and Moss, F.: Stochastic resonance and the benefits of noise: from ice ages to crayfish and SQUID. Nature *373*, 33–36 (1995)

Dr. Hans Albert Braun
Institut für Normale und Pathologische Physiologie
Deutschhausstraße 2
35037 Marburg
Germany
Phone: ++49 (0) 6 42 12 86 23 05
Fax: ++49 (0) 6 42 12 86 69 67
E-Mail: braun@mailer.uni-marburg.de

Understanding Spatiotemporal Patterns in Biology

Nova Acta Leopoldina NF *88*, Nr. 332, 321–324 (2003)

Understanding Spatiotemporal Patterns in Biology (Comment)

H. Ulrich GÖRINGER (Darmstadt)

> "Nature uses only the longest threads to weave her patterns, so each small piece of her fabric reveals the organization of the entire tapestry."
>
> Richard FEYNMAN
> The character of physical law.

A biological version of the famous "Bauhaus principle" – *form follows function* – is perhaps that – *form and pattern dictate function* –. This is a concept that biologists are very familiar with since the shape and structures of biological entities such as proteins, nucleic acids, (sub)cellular assemblies, organs, extremities or even behavioral aspects of living communities are shaped to optimally provide a species for survival. However, pattern and complexity are by no means characteristics of living systems only. They are created by physical and chemical principles and are observable in non-living systems as well. The fact that complex biological patterns rely on simple deterministic substructures has become a very "trendy" scientific paradigm. However, the recent increase in our biological knowledge has drawn the attention away from a mere description of the inventory of components towards a description of the interactions of the various players. In this manner, biological complexity is the result of a large number of interactive connections of many components, which form a dynamic network. Unfortunately, networks are intrinsically difficult to understand. This is due to a variety of parameters, among them the high complexity of such networks, the diversity of interactions and of course dynamical aspects of networks because patterns can vary over time and can influence each other. Only these few characteristics demonstrate that the description of complex biological systems must use mathematical models in order to capture the central features of the phenomenon. This in turn calls for an interdisciplinary approach to study biological networks and pattern formation, which was adequately addressed during this symposium.

The session entitled "Understanding spatiotemporal patterns in biology" included five presentations. Three talks were given by biologists, one by a mathematician and one by a physicist. The aim of the organizers was to look at new experimental data in light of fostering a discussion between the three scientific disciplines. As prime examples of today's powerful genomic era two talks focused on spatiotemporal patterns within gene regulatory networks. T. HOLSTEIN from the Darmstadt University of Technology talked about transcriptional gene regulatory interactions required for the self organization and pattern formation in *Hydra*. M. MITTAG (Friedrich Schiller University Jena) presented her work on the molecular mechanisms of circadian clocks in microalgae, which involves posttranscriptional gene regulatory processes. U. RASCHER (Columbia University) showed a remarkable image analysis of spatiotemporal variations in the photosyn-

thetic activity in simple leaves, and M. T. HÜTT (Darmstadt University of Technology) talked on the effect of biological variability on spatiotemporal patterns. Lastly, H. MALCHOW from the University of Osnabrück gave an overview on spatiotemporal pattern formation in population dynamics. Below, I have summarized my personal synopsis of the five talks specifically focusing on two questions: (*i*) Does nature have an unlimited choice of players and patterns, or must it select from just a few? (*ii*) Are the presented data surprising examples or do they just reflect our limited level of knowledge?

Thomas HOLSTEIN talked about the "*De-novo* Formation of the *Hydra* Head Organizer" as an example of a so-called signaling center or organizer tissue. Signaling centers can be defined as an assembly of a small number of embryonic cells that execute positional information for the definition of the main body axis of a developing multicellular organism. The cells secrete growth factors which act as morphogens during cell differentiation. At its core, the phenomenon deals with the problem of symmetry breaking and pattern formation by chemical diffusion as initially proposed by Alan TURING in 1952. TURING described a hypothetical chemical reaction that could generate spontaneous symmetry breaking, leading to stable spatial patterns, in an initially uniform mixture of chemical compounds. Hans MEINHARDT and Alfred GIERER later on showed that short-range activation and long-range inhibition are the chief elements of the Turing patterns.

HOLSTEIN convincingly demonstrated that the *Hydra* head organizer represents a prime example of a reaction-diffusion system and that it relies on the molecular components of the Wnt pathway and the TGF*ß*/Bmp antagonist Chordin. The molecules act during the *de-novo* formation of the head organizer as well as in cell aggregates derived from suspensions of dissociated cells. The highly conserved *HyWnt* and *HyBra1* genes are expressed in these cells; they activate surrounding cells and generate a field of lateral inhibition as expected from an archetypical Gierer/Meinhardt "short-range activation/long-range inhibition" system. HOLSTEIN'S data further verify that the pattern formation system of higher animals also exists in early multicellular animals, which demonstrates an astonishing evolutionary conservation of a self-organizing system. On a genetic level, the data conclude that the expression of only a few regulatory genes in a few cells are sufficient to execute the body plan of a whole organism. Transcription factors play a central role in the function of signaling centers and thus, on a biophysical level the phenomenon relies on the interaction between protein components and DNA molecules.

However, transcriptional control is not everything. Posttranscriptional regulatory phenomena as well as translational control can contribute to spatiotemporal phenomena as well. This was demonstrated by Maria MITTAG, who presented an overview of work from her laboratory on the molecular analysis of circadian clocks in microalgae using the eukaryotic microalgae *Gonyaulax polyedra* (*G. polyedra*) and *Chlamydomonas reinhardtii* (*C. reingardtii*) as model systems. Both organisms are characterized by several "rhythmic" characteristics such as cell aggregation, photosynthesis, cell division and bioluminescence, and as a consequence provide amenable experimental systems to study temporal biological phenomena. Although transcriptional regulation as well as phosphorylation and dephosphorylation events clearly contribute to the circadian phenomenon, both organisms are additionally characterized by very interesting posttranscriptional regulatory circuits. In particular, circadian-controlled RNA-binding proteins, which specifically recognize UG-repeat elements within the 3′-untranslated regions (3′-UTR) of cer-

tain mRNAs. In *G. polyhydra* one such protein is called CCTR for "circadian controlled translational regulator" due to the fact that its binding activity changes over the day-night cycle. The analogous "clock-controlled" protein in *C. reinhardtii* was termed CHLAMY 1 and presumably acts as a translational repressor during the night-phase of the organism. Target mRNAs for CHLAMY 1 have been found to encode proteins involved in metabolic reactions to fixate nitrogen and carbon dioxide, which nicely demonstrates that complete metabolic pathways can be regulated by circadian RNA-binding proteins.

Together, the data demonstrate that the circadian phenomenon, at least in these two organisms, is controlled like any other regulatory process in living systems, on the various levels of gene expression. However, how the identified molecular components contribute to such parameters as the amplitude, the phase and the period of a chronobiological phenomenon, is not clear up to now and represents one of the more challenging questions in the field.

Uwe RASCHER contributed a remarkable set of data. By using non-invasive chlorophyll fluorescence measurements he demonstrated the presence of horizontal variations in the steady state photosynthetic activity within individual leaves of the crassulacean acid metabolism (CAM) plant *Kalanchoë daigremontiana*. The CAM cycle represents a well-studied biochemical carbon acquisition reaction in higher plants, which is characterized, among other features, by a distinct circadian pattern of carbon dioxide exchange.

The chlorophyll fluorescence measurements by RASCHER and colleagues revealed propagating wave fronts in the photosynthetic efficiency with clusters of increasing and decreasing activity as well as areas that are out-of-phase. The data were collected by using significantly improved charged coupled device (CCD) camera technology in combination with sophisticated image acquisition software. The spatial and temporal activity patterns could not be correlated with leave tissue substructures since the leaves consist of assemblies of identical tightly packed cells. Therefore, the circadian rhythm of the CAM reaction cycle seems to be the result of a dynamic pattern of independently initiated variations in the photosynthetic efficiency with every activity center representing a biochemical oscillator that operates independently in space and time. Although the described phenomenon is to some extend "iconoclastic" – simple leaves can no longer be viewed as horizontally homogeneous biochemical reaction units – it resembles other biological pattern formation processes such as the generation of periodic pulses of a chemical attractant during colony formation of the slime mold *Dictiostelium discoideum* or the above described "reaction-diffusion" systems that act as morphogens during early embryogenesis. Lastly, RASCHER'S data provided a very nice example on how technological breakthroughs can lead to new interpretations of what is thought to be a well-understood phenomenon.

Biochemical oscillators such as the one's observed and described in RASCHER'S talk were used by Marc-Thorsten HÜTT as a theoretical model system. This is justified based on the fact that biological self-organization can be mathematically described by treating the various interacting elements of a biological network as coupled nonlinear oscillators. In such a system, "noise" has been shown to be an important determinant for pattern formation, and HÜTT now asked the question how "disorder" or in other words "variability" might impact spatiotemporal phenomena. He was able to demonstrate that variability in a system of hypothetical biochemical reactions can induce spatial waves and

long-range spatiotemporal patterns provided that certain conditions are met. Thus, variability in non-linear systems may provide a dynamic attribute to the network.

Lastly, HÜTT's data nicely demonstrate how numerical simulations can function as a seeding point for theory-driven biological experiments. After all, it was Albert EINSTEIN who said: "Die Theorie bestimmt, was wir beobachten können." ("Theory determines the observable.") Within this context it will be interesting to see whether the "theoreticians" will be able to keep up with analyzing and interpreting the immense amounts of experimentally-derived data from such fields as genomics, proteomics or neurobiological networks. If so, without any doubt, experimental biologists will benefit.

Prof. Dr. H. Ulrich GÖRINGER
Genetics, Darmstadt University of Technology
Schnittspahnstr. 10,
64287 Darmstadt
Germany
Phone: ++49 (0) 61 51 16 28 55
Fax: ++49 (0) 61 51 16 56 40
E-Mail: goringer@hrzpub.tu-darmstadt.de

Nova Acta Leopoldina NF *88*, Nr. 332, 325–340 (2003)

Models of Spatiotemporal Pattern Formation in Plankton Dynamics

Horst MALCHOW (Osnabrück), Sergei V. PETROVSKII (Moscow), and Frank M. HILKER (Osnabrück)

With 2 Figures

Abstract

The dynamics of spatial and spatiotemporal pattern formation in nonlinear biosystems far from equilibrium is of growing interest and many mechanisms of structure generation are not known yet. The main aim of modeling biological population dynamics is to improve the understanding of the functioning of food chains and webs as well as their dependence on internal and external conditions. Hence, mathematical models of biological population dynamics have not only to account for growth and interactions but also for spatiotemporal processes like random or directed and joint or relative motion of species, as well as the variability of the environment. Early attempts began with physico-chemical diffusion, exponential growth and Lotka-Volterra type interactions. These approaches have been continuously refined to more realistic descriptions of the development of natural populations. The aim of this paper is to give an extensive introduction to the subject and the bibliography. The fascinating variety of spatiotemporal patterns in such systems and the governing mechanisms of their generation and further dynamics are described and related to plankton.

Zusammenfassung

Die Dynamik der räumlichen und raumzeitlichen Strukturierung in nichtlinearen Biosystemen fern vom Gleichgewicht ist von wachsendem Interesse, und viele Mechanismen der Strukturbildung sind noch unklar. Das Ziel der mathematischen Modellierung der Dynamik biologischer Populationen ist ein besseres Verständnis der Wirkungsweise von Nahrungsketten und -netzen sowie ihrer Abhängigkeiten von inneren und äußeren Bedingungen. Mathematische Modelle biologischer Populationsdynamik müssen nicht nur Wachstum und Wechselwirkungen beschreiben, sondern auch raumzeitliche Prozesse wie die zufällige oder gerichtete und gemeinsame oder relative Bewegung von Spezies und die Variabilität der Umwelt. Die ersten Versuche begannen mit physiko-chemischer Diffusion und Lotka-Volterra-Wechselwirkungen. Diese Ansätze sind stetig zu realistischeren Beschreibungen der Entwicklung biologischer Populationen verfeinert worden. Die vorliegende Arbeit gibt eine ausführliche Einführung in das Forschungsgebiet und die Bibliographie. Die faszinierende Vielfalt der raumzeitlichen Strukturen in solchen Systemen und die wichtigsten Mechanismen ihrer Erzeugung und weiteren Entwicklung werden anhand der Planktondynamik beschrieben.

1. Introduction to Reaction-Diffusion Models of Population Dynamics

The exploration of pattern formation mechanisms in nonlinear complex systems is one of the central problems of natural, social, and technological sciences. The development of the theory of self-organized temporal, spatial or functional structuring of nonlinear sys-

tems far from equilibrium has been one of the milestones of structure research (HAKEN 1977, NICOLIS and PRIGOGINE 1977). The occurrence of multiple steady states and transitions from one to another after critical fluctuations, the phenomena of excitability, oscillations, waves and, in general, the emergence of macroscopic order from microscopic interactions in various nonlinear nonequilibrium systems in nature and society has required and stimulated many theoretical and, if possible, experimental studies. Mathematical modeling has turned out to be one of the useful methods to improve the understanding of such structure generating mechanisms. The classical method for space-time continuous population-dynamical systems in theoretical ecology and biology is the use of ordinary and partial differential equation models

$$\frac{\partial X_i(\vec{r},t)}{\partial t} = f_i[\underline{X}(\vec{r},t), \Lambda] - \vec{\nabla} \times \left(\vec{v}_i X_i(\vec{r},t) - \sum_{j=1}^{N} D_{ij} \cdot \left[\vec{\nabla} X_j(\vec{r},t) \right] \right); i = 1,2,\ldots,N. \quad [1]$$

The vector $\underline{X}$ contains the N population densities X_i at time t and position $\vec{r}$. $\underline{f}$ is the vector of the growth and interaction functions f_i, i. e., it describes for instance exponential or logistic growth and mutualism, predation or competition. Λ is the set of system parameters. $\vec{v}_i$ is the velocity vector of species i, D_{ij} is the matrix of self- and cross-diffusivities and $\vec{\nabla}$ the Nabla operator. A good introduction to the latter field has been provided by HOLMES et al. (1994). All parameters might be state-dependent, i. e., dependent on time, space and population density due to environmental variability.

In this paper, the mobility of populations is simply modeled as neutral Fickian diffusion with constant diffusion coefficient D_i. Equation [1] then reads

$$\frac{\partial X_i(\vec{r},t)}{\partial t} = f_i[\underline{X}(\vec{r},t), \Lambda] + D_i \Delta X_i(\vec{r},t); i = 1,2,\ldots,N; \quad [2]$$

where $\Delta = \vec{\nabla}^2$ is the Laplace operator.

The simplest form of nonlinear growth of a single population is, maybe, the exponential growth with

$$f = rX \quad [3]$$

where r is the constant positive growth rate. The latter has been assumed by MALTHUS (1798) as a model for the growth of mankind. Coupling a localized population patch to diffusion, one finds an explosive propagating population front with velocity

$$v_F = 2\sqrt{rD} \quad [4]$$

what has been estimated by LUTHER (1906) for chemical reactions. Finally, one obtains a spatially uniform growing population. It was VERHULST (1838) who introduced a carrying capacity K in order to limit the population growth,

$$f = rX\left(1 - \frac{X}{K}\right). \quad [5]$$

Now, any initial population size will converge to K. Considering again the coupling of a localized patch to diffusion, one finds the surprising result that $v_F = 2\sqrt{rD}$ is now the

minimum front speed (FISHER 1937, KOLMOGOROV et al. 1937). FISHER applied this simple model to the spread of an advantageous gene in a population, however, this so-called logistic limitation of growth is often used in population-dynamical models for the lowest trophic levels. The only stable solution for large times is a uniform distribution of the population at its carrying capacity. For populations with a strong Allee effect (ALLEE 1931, ALLEE et al. 1949), i. e., the existence of a minimum viable population size K_-, one finds two stable population densities, extinction ($X = 0$) and survival ($X = K$). The growth function reads

$$f = rX\left(1 - \frac{X}{K}\right)\left(\frac{X}{K_-} - 1\right). \qquad [6]$$

Populations with initial densities less than K_- go extinct whereas larger populations survive at their carrying capacity K. Here, localized initial population patches also show a critical spatial size (SCHLÖGL 1972, NITZAN et al. 1974, EBELING and SCHIMANSKY-GEIER 1980, MALCHOW and SCHIMANSKY-GEIER 1985, LEWIS and KAREIVA 1993, PETROVSKII 1994). Patches greater than the critical size will grow and survive, the others will decay and go extinct. This is sketched in Figure 1.

Bistability and the emergence of a critical spatial size do not necessarily require an Allee effect, also logistically growing preys with a parameterized predator of Holling-type II or III functional response (HOLLING 1959) can exhibit two stable steady states and the related hysteresis loops (cf. LUDWIG et al. 1978, WISSEL 1989). However, finally one finds spatially uniform population distributions. Only one exception is known for single population systems: Bistable systems with Dirichlet boundary conditions can exhibit stable solutions with one spatial minimum or maximum value (JETSCHKE 1979).

The whole variety of temporal, spatial, and spatiotemporal population patterns can be found in models of two and more interacting populations. The pioneers in this field have been LOTKA (1925) and VOLTERRA (1926) with their simple prey-predator model

$$f_1 = a_1X_1 - b_{12}X_2; \qquad f_2 = b_{21}X_1 - a_2X_2, \qquad [7]$$

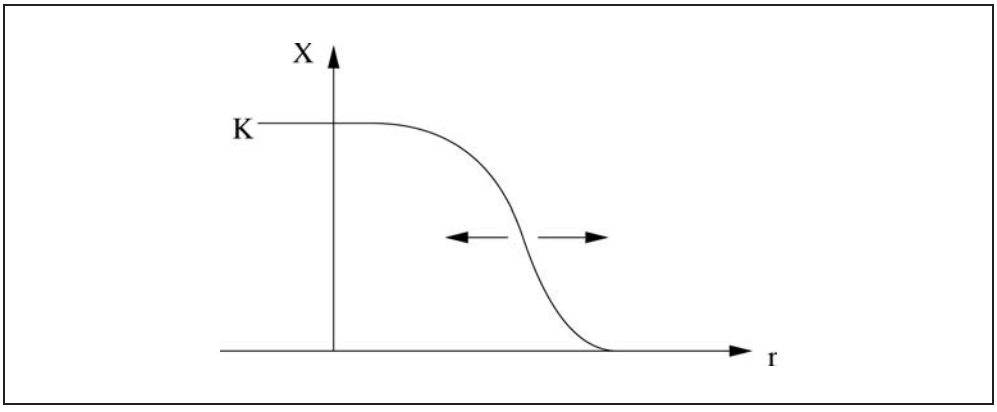

Fig. 1 Sketch of the propagation of a population wave.

with prey X_1 and predator X_2, e. g. snow-shoe hares and silver foxes or, in the case of VOLTERRA, adriatic fishes. All parameters are greater than zero. This model shows the typical prey-predator oscillations, however, they are structurally unstable, i.e., it is not a stable limit cycle. The general Volterra systems

$$f_i = \left(a_i + \sum_{j=1}^{N} b_{ij} X_j \right) X_i; \quad i = 1, 2, \ldots, N; \qquad [8]$$

describe all basic possible interactions with negative, positive or vanishing parameters, though these models are not very realistic and, therefore, not of much use in ecological modeling.

The already mentioned Holling-type response terms (HOLLING 1959) which are also known from Monod or Michaelis-Menten saturation models of enzyme kinetics (MICHAELIS and MENTEN 1913, MONOD and JACOB 1961) make the Volterra models more realistic. Here is an example for a N-component food chain:

$$f_i = e_i \alpha_i \frac{X_{i-1}^{n_{i-1}}}{H_{i-1}^{n_{i-1}} + X_{i-1}^{n_{i-1}}} X_i - \delta_i X_i^{m_i} - \alpha_{i+1} \frac{X_i^{n_i}}{H_i^{n_i} + X_i^{n_i}} X_{i+1}; \quad i = 1, 2, \ldots, N. \qquad [9]$$

The chain needs "boundary conditions", e. g., $X_0 \to \infty$ and X_{N+1} = const. The e_i are the efficiencies of conversion of biomass of species i–1 into species i, α_i is the maximum predation rate of species i, δ_i its mortality rate and H_i the half saturation constant of its functional response. The exponents n_{i-1} and $n_i = 1, 2$ stand for Holling-type *II*, *III* responses, respectively. The $m_i = 1, 2$ describe natural mortality or intraspecific competition. For the later on often mentioned and used Scheffer model of plankton dynamics (SCHEFFER 1991a) one has $N = 2$: X_0 = const (nutrients), X_1 (phytoplankton), X_2 (zooplankton), X_3 = const (planktivorous fish), $n_0 = n_1 = 1$, $n_2 = 2$, $m_1 = 2$, $m_2 = 1$:

$$f_1 = e_1 \alpha_1 \frac{X_0}{H_0 + X_0} X_1 - \delta_1 X_1^2 - \alpha_2 \frac{X_1}{H_1 + X_1} X_2, \qquad [10]$$

$$f_2 = \left(e_2 \alpha_2 \frac{X_1}{H_1 + X_1} - \delta_2 \right) X_2 - \alpha_3 \frac{X_2^2}{H_2^2 + X_2^2} X_3. \qquad [11]$$

Further scenarios of pattern formation in reaction-diffusion systems will be described now, using models of plankton dynamics as an example.

2. Models of Plankton Population Dynamics: Overview and Bibliography

Because of its apparent importance, the dynamics of plankton systems have been under continuous investigation during more than a hundred years. From the very beginning, regular plankton studies have combined field observations, laboratory experiments and mathematical modeling. In the 17th century, the Dutch pioneer microscopist Anton VAN LEEUWENHOEK was probably the first human being to see minute creatures, which he called *animalcules*, in pond water (HALLEGRAEFF 1988). The German Victor HENSEN who organized Germany's first big oceanographic expedition in 1889 (HENSEN 1892, POREP 1970) introduced the term *plankton* (due to the Greek *planktos* = made to wander).

It was in the 19th century that fisheries stimulated the interest in plankton dynamics because strong positive correlations between zooplankton and fish abundance were found. The already mentioned German plankton expedition of 1889 was mainly motivated by fisheries interests. At the same time, fishery science began to develop. In the beginning of the 20th century, first mathematical models were developed in order to understand and to predict fish stock dynamics and its correlations with biological and physical factors and human interventions (cf. CUSHING 1975, GULLAND 1977, STEELE 1977).

Phytoplankton are microscopic plants that drive all marine ecological communities and the life within them. Due to their photosynthetic growth, the world's phytoplankton generate half of the oxygen that mankind needs for maintaining life, and it absorbs half of the carbon dioxide that may be contributing to global warming. It is not only oxygen and carbon dioxide but there are also other substances and gases that are recycled by phytoplankton, e. g. phosphorus, nitrogen and sulphur compounds (BAIN 1968, DUINKER and WEFER 1994, MALIN 1997, RITSCHARD 1992). Hence, the phytoplankton is one of the main factors controlling the further development of the world's climate, and there is a vast literature supporting that (cf. CHARLSON et al. 1987, WILLIAMSON and GRIBBIN 1991).

Zooplankton are the animals in plankton. In marine zooplankton both herbivores and predators occur. Herbivores graze on phytoplankton and are eaten by zooplankton predators. Together, phyto- and zooplankton form the basis for all food chains and webs in the sea. In its turn, the abundance of the plankton species is affected by a number of environmental factors such as water temperature, salinity, sunlight intensity, biogen availability, etc. (RAYMONT 1980, SOMMER 1994). Temporal variability of the species composition is caused by seasonal changes and trophical prey-predator interactions between phyto- and zooplankton.

The contemporary mathematical modeling of phytoplankton productivity has its roots in the work by FLEMING (1939), IVLEV (1945), RILEY (1946), ODUM (1956) and others. A review of the developments has been given by DROOP (1983). Recently, a collection of most frequently used models has been published (BEHRENFELDT and FALKOWSKI 1997).

The control of phytoplankton blooming by zooplankton grazing has been modeled first by FLEMING (1939), using a single ordinary differential equation for the temporal dynamics of phytoplankton biomass. Other approaches have been the construction of data fitted functions (RILEY 1946, 1963) and the application of standard Lotka-Volterra equations to describe the prey-predator relation of phytoplankton and zooplankton (SEGEL and JACKSON 1972, DUBOIS 1975, LEVIN and SEGEL 1976, VINOGRADOV and MENSHUTKIN 1977, MIMURA and MURRAY 1978). More realistic descriptions of zooplankton grazing with functional responses to phytoplankton abundance have been introduced by IVLEV (1945) with a certain modification by MAYZAUD and POULET (1978). Holling-type response terms are just as much in use (cf. STEELE and HENDERSON 1981, 1992 a, b, SCHEFFER 1991 a, b, 1998, MALCHOW 1993, PASCUAL 1993, TRUSCOTT and BRINDLEY 1994 a, b). Observed temporal patterns are the well-known stable prey-predator oscillations as well as the oscillatory or monotonous relaxation to one of the possible multiple steady states. Excitable systems are of special interest because their long-lasting relaxation to the steady state after a supercritical external perturbation like a sudden temperature increase or nutrient inflow is very suitable to model red or brown tides (BELTRAMI 1989, 1996, TRUSCOTT and BRINDLEY 1994 a, b).

Concerning the temporal variability of plankton species abundance, the limits of its predictability are of particular interest. At early stages, the development of mathematical models of marine ecosystems was driven by the idea that the more species were explicitely included into the model the higher would be its predictive ability. As a result, a number of many-species models appeared allowing for a detailed structure of the food web of the community (cf. DeAngelis 1992, Jørgensen 1994, Yodzis 1994). However, the real predictive ability of this class of models is not very high and rarely exceeds a few weeks. Moreover, an increasing number of model agents may sometimes even worsen the properties of the model. This apparent paradox can be explained in terms of dynamical chaos (May 1974). Although the strict evidence of chaotic behavior of natural populations is still absent, there appear stronger and stronger indications in favor of its existence (Scheffer 1991 b, 1998, Costatino et al. 1995, Dennis et al. 1995, Costatino et al. 1997, Godfray and Hassell 1997, Huisman and Weissing 1999). Chaotic population dynamics essentially changes the approach to the system predictability and makes conceptual few-species models of as much use as many-species ones. Moreover, few-species models can sometimes be even more instructive since they take into account only the principal features of the community functioning (cf. Pascual 1993, Petrovskii and Malchow 1999, 2001).

Another interesting problem is the dynamics of externally forced systems. This ideally periodic forcing appears rather naturally due to daily, seasonal or annual cycles of photosynthetically active radiation, temperature, nutrient availability, etc. (Evans and Parslow 1985, Popova et al. 1997, Ryabchenko et al. 1997, Truscott 1995). Natural forcings are of course subject to a certain environmental noise. A number of forced models for parts or the complete food chain from nutrients, phytoplankton and zooplankton to planktivoros fish has been investigated and many different routes to chaotic dynamics have been demonstrated (Kuznetsov et al. 1992, Rinaldi and Muratori 1992, Ascioti et al. 1993, Doveri et al. 1993, Rinaldi et al. 1993, Steffen and Malchow 1996a,b, Scheffer et al. 1997, Steffen et al. 1997).

The abundance of plankton species is not only subject to temporal changes but also depends on space. The distinct spatial heterogeneity of plankton distribution (patchiness) is found in many field observations (Steele 1974, 1978, Fasham 1978, Mackas and Boyd 1979, Greene et al. 1992, Abbott 1993). This phenomenon takes place on all scales, from centimeters to thousands of kilometers. A number of explanations has been suggested, particularly, relating the spatial structure of a plankton system to marine turbulence (Platt 1972) or to the inhomogeneity of the temperature field in the ocean (Denman 1976). A well-studied stripy plankton pattern is due to the trapping of populations of sinking microorganisms in Langmuir circulation cells (Stommel 1948, Leibovich 1993). Other physically determined plankton distributions like steep density gradients due to local temperature differences, nutrient upwelling, turbulent mixing or internal waves have been reported too (Yoder et al. 1994, Franks 1997, Abraham 1998).

On a small spatial scale of some ten's of centimeters and under relative physical uniformity also differences in the "diffusive" mobility of individuals and the ability of locomotion might create finer spatial structures, e. g. due to bioconvection and gyrotaxis (Platt 1961, Winet and Jahn 1972, Pedley and Kessler 1992, Timm and Okubo 1994). Till now not for plankton but for certain bacteria, the mechanism of diffusion-limited aggregation (Witten and Sander 1981) has been proposed and experimentally

proven for the spatial fingering of colonies (MATSUSHITA and FUJIKAWA 1990, BEN-JACOB et al. 1992).

Thus, mathematical models of plankton population dynamics have not only to account for growth and interactions but also for spatial processes like random or directed and joint or relative motion of species as well as the variability of the environment.

The interplay of phytoplankton and zooplankton growth, interactions and transport yields the whole spectrum of spatio-temporal population structures, in particular the phenomenon of plankton patchiness (cf. FASHAM 1978, OKUBO 1980). As mentioned before, the mathematical modeling requires the use of reaction-diffusion and perhaps advection equations.

Since the classic paper by TURING (1952) on the role of nonequilibrium reaction-diffusion patterns in biomorphogenesis, dissipative mechanisms of spontaneous spatial and spatiotemporal pattern formation in a homogeneous environment are of continuous interest in theoretical biology and ecology. TURING showed that the nonlinear interaction of at least two agents with considerably different diffusion coefficients can give rise to spatial structure. SEGEL and JACKSON (1972) were the first to apply TURING's idea to a problem in population dynamics: the dissipative instability in the prey-predator interaction of phytoplankton and herbivorous copepods with higher herbivore motility. LEVIN and SEGEL (1976) suggested this scenario of spatial pattern formation for a possible origin of planktonic patchiness. Local bistability, predator-prey limit-cycle oscillations, plankton front propagation and the generation and drift of planktonic Turing patches were found in a minimal phytoplankton-zooplankton interaction model (MALCHOW 1993, 1994) that was originally formulated by SCHEFFER (1991a), accounting for the effects of nutrients and planktivoros fish on alternative local equilibria of the plankton community.

KIERSTEAD and SLOBODKIN (1953) and SKELLAM (1951) were perhaps the first to think of the critical size problem for plankton patches, presenting their nowadays called KISS model with the coupling of exponential growth and diffusion of a single population. However, as explained in the introduction, these patches are unstable because this coupling leads to an explosive spatial spread of the initial patch of species with surprisingly the same diffusive front speed as the asymptotic speed of a logistically growing population.

Spatial and spatiotemporal patterns like regular and irregular oscillations, propagating fronts, target patterns and spiral waves, pulses as well as stationary spatial patterns were first known from oscillating chemical reactions (cf. FIELD and BURGER 1985), but have never been observed in natural plankton populations. Spirals often appear as solutions of reaction-diffusion models of active media, i.e., also in models of plankton dynamics (MALCHOW 2000 a). In order to blur these artificial structures, environmental gradients (MALCHOW et al. 2000) and/or noise have been added, resulting in a more realistic patchy structure (MALCHOW et al. 2002, 2003). However, physically generated spirals have been seen in the ocean as rotary motions of plankton patches on a kilometer scale (WYATT 1973). Furthermore, they have been found important in parasitoid-host systems (BOERLIJST et al. 1993). For other motile microorganisms, travelling waves like targets or spirals have been found in the cellular slime mold *Dictyostelium discoideum* (GERISCH 1968, 1971, SEGEL and STOECKLY 1972, NEWELL 1983, SEGEL 1977, ALT and HOFFMANN 1990, IVANITSKY et al. 1994, KELLER and SEGEL 1970, SIEGERT and

WEIJER 1991, STEINBOCK et al. 1991, VASIEV et al. 1994, HÖFER et al. 1995). These amoebae are chemotactic species, i. e., they move actively up the gradient of a chemical attractant and aggregate. Chemotaxis is a kind of density-dependent cross-diffusion (KELLER and SEGEL 1971a,b), and it is an interesting open question whether there is preytaxis in plankton or not. However, there is some evidence of chemotaxis in certain phytoplankton species (IKEGAMI et al. 1995). Recently, a zooplankton generated noise based taxis of fish has been reported (FREUND et al. 2002). Bacteria, such as *Escherichia coli* or *Bacillus subtilis*, also show a number of complex colony growth patterns (SHAPIRO and HSU 1989, SHAPIRO and TRUBATCH 1991), different to the already mentioned diffusion-limited aggregation patterns. Their emergence requires as well cooperativity and active motion of the species which has also been modeled as density-dependent diffusion and predation (KAWASAKI et al. 1995 a, b).

An important point is that the spatial dimensions of the plankton community functioning provide also new routes to chaotic dynamics. The emergence of diffusion-induced spatio-temporal chaos has been found along a linear nutrient gradient (PASCUAL 1993). Chaotic oscillations behind propagating diffusive fronts are found in a prey-predator model (SHERRATT et al. 1995, 1997); a similar phenomenon is observed in a mathematically similar model of a chemical reactor (MERKIN et al. 1996, DAVIDSON 1998). Recently it has been shown that the appearance of chaotic spatiotemporal oscillations in a prey-predator system is a somewhat more general phenomenon and must not be attributed to front propagation or to an inhomogeneity of environmental parameters (PETROVSKII and MALCHOW 1999, 2001).

Conditions for the emergence of three-dimensional spatial and spatiotemporal patterns after differential-flow-induced instabilities (EVANS 1977, ROVINSKY and MENZINGER 1992) of spatially uniform populations were derived (MALCHOW 1995, 1996, 1998) and illustrated by patterns in SCHEFFER's model. Instabilities of the spatially uniform distribution can appear if phytoplankton and zooplankton move with different velocities but regardless of which one is faster. This mechanism of generating patchy patterns is more general than the Turing mechanism which depends on strong conditions on the diffusion coefficients; therefore, one can expect a wide range of its applications in population dynamics (KLAUSMEIER 1999, MALCHOW 2000 a, b).

Thus, the dynamics of the plankton communities, particularly processes of pattern formation, have been under intensive investigation during the few last decades. As a result, considerable progress in understanding principal features of plankton systems functioning has been achieved. Still, many mechanisms of the spatiotemporal variability of natural plankton populations are not known yet. Pronounced physical patterns like thermoclines, upwelling, fronts and eddies often set the frame for the biological processes. However, under conditions of relative physical uniformity, the temporal and spatiotemporal variability can be a consequence of the coupled nonlinear biological and chemical dynamics (LEVIN and SEGEL 1976, STEELE and HENDERSON 1992 a, b). SOMMER (1994, 1996) has emphasized the importance of biological dynamics during phytoplankton blooms. DALY and SMITH (1993) concluded: "... that biological processes may be more important at smaller scales where behaviour such as vertical migration and predation may control the plankton production, whereas physical processes may be more important at larger scales in structuring biological communities ..." O'BRIEN and WROBLEWSKI (1973) introduced a dimensionless parameter, containing the characteristic water speed

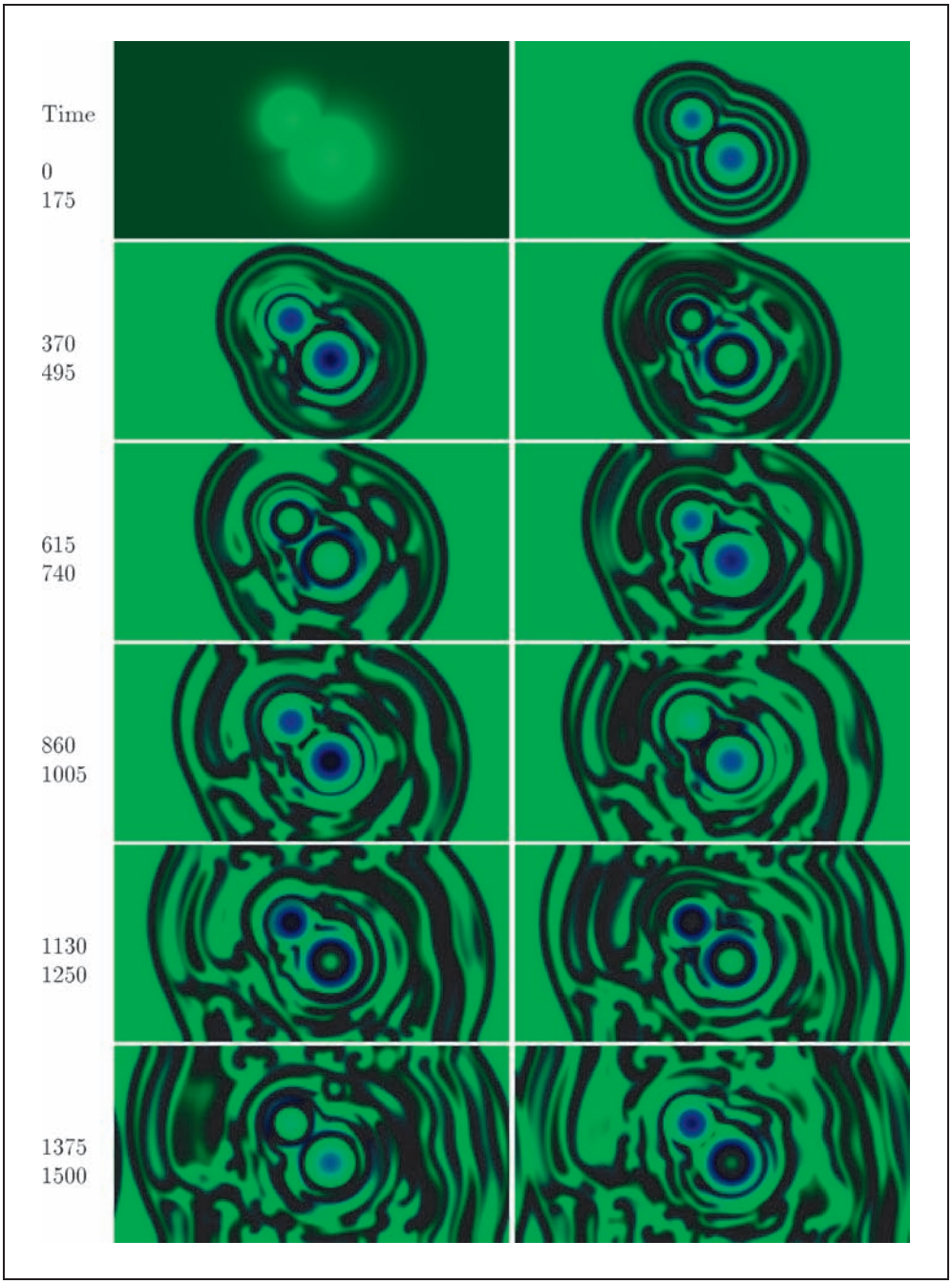

Fig. 2 Phytoplankton patterns in Scheffer's model with two stationary nutrient patches.

and the maximum specific biological growth rate, to distinguish parameter regions of biological and physical dominance (cf. also WROBLEWSKI et al. 1975, WROBLEWSKI and O'BRIEN 1976).

Physical and biological processes may differ significantly not only on spatial but also on temporal scales. Particularly, the effect of external hydrodynamical forcing on the appearance and stability of nonequilibrium spatiotemporal patterns has been studied (MALCHOW and SHIGESADA 1994), making use of the separation of the different time scales of biological and physical processes. A channel under tidal forcing served as a hydrodynamical model system with a relatively high detention time of matter. Examples were provided on different time scales: The simple physical transport and deformation of a spatially nonuniform initial plankton distribution as well as the biologically determined formation of a localized spatial maximum of phytoplankton biomass.

Plankton pattern formation is essentially dependent on the interference of various physical (light, temperature, hydrodynamics) and biological (nutrient supply, predation) factors (cf. PLATT 1972, DENMAN 1976, FASHAM 1978). In nature, it has been observed that the direction of motion of plankton patches does not always coincide with the direction of the water flow (WYATT 1971, 1973), and as the spatial scale becomes larger than approximately 100 meters, phytoplankton behaves successively less like a simple passive quantity distributed by turbulence (NAKATA and ISHIKAWA 1975, POWELL et al. 1975, POWELL and OKUBO 1994). Similarly, the spatial variability of zooplankton abundance differs essentially from the environmental variability on scales less than a few dozens of kilometers (WEBER et al. 1986). This indicates that biological factors play an essential role in the emergence of plankton patchiness (STEELE and HENDERSON 1992 a, b).

For illustration, the formation and spread of a spatiotemporal structure in the Scheffer model is demonstrated in Figure 2. The upper and lower boundaries are reflecting whereas the left and right boundaries are periodic. The existence of two stationary nutrient patches is assumed. The system dynamics is in the parameter interval of prey-predator oscillations. Therefore, the nutrient peaks act as local perturbations and, hence, as sources of concentric populations waves which break up through local interferences and boundary effects. Finally, the whole space is filled with a dynamic patchy structure.

3. Conclusion

This paper was an attempt to give an introduction to and an overview of the mathematical modeling of biologically controlled spatiotemporal pattern formation in nonequilibrium plankton dynamics with a certain focus on prey-predator interactions of diffusive phytoplankton and zooplankton. Such a summary cannot be complete. Only partial differential equation-based models have been introduced, using the Scheffer model (SCHEFFER 1991 a) with diffusion as an example. Though these models already exhibit a wide spectrum of structures, also other modeling tools, such as integro-differential and difference equations, metapopulation models, cellular automata and further rule-based tools or complex adaptive systems or combinations of different methods, show promising results as well and need further attention and development.

References

Abbott, M.: Phytoplankton patchiness: ecological implications and observation methods. In: Levin, S. A., Powell, T. M., and Steele, J. H. (Eds.): Patch Dynamics. Lecture Notes in Biomathematics. Vol. *96*, pp. 37–49. Berlin: Springer 1993

Abraham, E. R.: The generation of plankton patchiness by turbulent stirring. Nature *391*, 577–580 (1998)

Allee, W. C.: Animal Aggregations: A Study in General Sociology. Chicago: University of Chicago Press 1931

Allee, W. C., Emerson, A. E., Park, O., Park, T., and Schmidt, K. P.: Principles of Animal Ecology. Philadelphia: Saunders 1949

Alt, W., and Hoffmann, G. (Eds.): Biological Motion. Lecture Notes in Biomathematics. Vol. *89*. Berlin: Springer 1990

Ascioti, F. A., Beltrami, E., Carroll, T. O., and Wirick, C.: Is there chaos in plankton dynamics? J. Plankt. Res. *15*, 603–617 (1993)

Bain, R. C. Jr.: Predicting DO variations caused by algae. J. Sanitary Engineering Division, Proc. Amer. Soc. Civil Engineers, pp. 867–881 (1968)

Behrenfeldt, M. J., and Falkowski, P. G.: A consumer's guide to phytoplankton primary productivity models. Limnology and Oceanography *42*, 1479–1491 (1997)

Beltrami, E.: A mathematical model of the brown tide. Estuaries *12*, 13–17 (1989)

Beltrami, E.: Unusual algal blooms as excitable systems: The case of "brown-tides". Environm. Modeling & Assessment *1*, 19–24 (1996)

Ben-Jacob, E., Shmueli, H., Shochet, O., and Tenenbaum, A.: Adaptive self-organization during growth of bacterial colonies. Physica *A87*, 378–424 (1992)

Boerlijst, M. C., Lamers, M. E., and Hogeweg, P.: Evolutionary consequences of spiral waves in a host parasitoid system. Proc. R. Soc. London *B 253*, 15–18 (1993)

Charlson, R. J., Lovelock, J. E., Andreae, M. O., and Warren, S. G.: Oceanic phytoplankton, atmospheric sulphur, cloud albedo and climate. Nature *326*, 655–661 (1987)

Costantino, R. F., Cushing, J. M., Dennis, B., and Desharnais, R. A.: Experimentally induced transitions in the dynamic behaviour of insect populations. Nature *375*, 227–230 (1995)

Costantino, R. F., Desharnais, R. A., Cushing, J. M., and Dennis, B.: Chaotic dynamics in an insect population. Science *275*, 389–391 (1997)

Cushing, D. H.: Marine Ecology and Fisheries. Cambridge: Cambridge University Press 1975

Daly, K. L., and Smith, W. O. Jr.: Physical-biological interactions influencing marine plankton production. Annu. Rev. Ecol. Syst. *24*, 555–585 (1993)

Davidson, F. A.: Chaotic wakes and other wave-induced behavior in a system of reaction-diffusion equations. Int. J. Bifurcation and Chaos *8*, 1303–1313 (1998)

DeAngelis, D. L.: Dynamics of Nutrient Cycling and Food Webs. London: Chapman and Hall 1992

Denman, K. L.: Covariability of chlorophyll and temperature in the sea. Deep Sea Res. *23*, 539–550 (1976)

Dennis, B., Desharnais, R. A., Cushing, J. M., and Costantino, R. F.: Nonlinear demographic dynamics: Mathematical models, statistical methods, and biological experiments. Ecol. Monogr. *65*, 261–281 (1995)

Doveri, F., Scheffer, M., Rinaldi, S., Muratori, S., and Kuznetsov, Y. A.: Seasonality and chaos in a plankton-fish model. Theor. Popul. Biol. *43*, 159–183 (1993)

Droop, M. R.: 25 years of algal growth kinetics. Botanica Marina *XXVI*, 99–112 (1983)

Dubois, D.: A model of patchiness for prey-predator plankton populations. Ecol. Model. *1*, 67–80 (1975)

Duinker, J., and Wefer, G.: Das CO_2-Problem und die Rolle des Ozeans. Naturwissenschaften *81*, 237–242 (1994)

Ebeling, W., and Schimansky-Geier, L.: Nonequilibrium phase transitions and nucleation in reacting systems. Proceedings of the 6th International Conference on Thermodynamics; pp. 95–100. Merseburg 1980

Evans, G.: A two-layer shear diffusion model. Deep-Sea Res. *24*, 931–936 (1977)

Evans, G. T., and Parslow, S.: A model of annual plankton cycles. Biol. Oceanogr. *3*, 327–347 (1985)

Fasham, M. J. R.: The statistical and mathematical analysis of plankton patchiness. Oceanogr. and Marine Biol. Annu. Rev. *16*, 43–79 (1978)

Field, R. J., and Burger, M. (Eds.): Oscillations and Traveling Waves in Chemical Systems. New York: Wiley 1985

Fisher, R. A.: The wave of advance of advantageous genes. Ann. Eugenics *7*, 355–369 (1937)
Fleming, R. H.: The control of diatom populations by grazing. J. du Conseil Permanent Int. pour l'Exploration de la Mer *14*, 210–227 (1939)
Franks, P. J. S.: Spatial patterns in dense algal blooms. Limnology and Oceanography *42*, 1297–1305 (1997)
Freund, J., Schimansky-Geier, L., Beisner, B., Neiman, A., Russell, D. F., Yakusheva, T., and Moss, F.: Behavioral stochastic resonance: How the noise from a *Daphnia* swarm enhances individual prey capture by juvenile paddlefish. J. Theor. Biol. *214*, 71–83 (2002)
Gerisch, G.: Cell aggregation and differentiation in *Dictyostelium*. In: Moscona, A. A., and Montroy, A. (Eds.): Current Topics in Developmental Biology. Vol. 3, pp. 157–197. New York: Academic Press 1968
Gerisch, G.: Periodische Signale steuern die Musterbildung in Zellverbänden. Naturwissenschaften *58*, 430–438 (1971)
Godfray, C., and Hassell, M.: Chaotic beetles. Science *275*, 323–326 (1997)
Greene, C. H., Widder, E. A., Youngbluth, M. J., Tamse, A., and Johnson, G. E.: The migration behavior, fine structure, and bioluminescent activity of krill sound-scattering layer. Limnology and Oceanography *37*, 650–658 (1992)
Gulland, J. A. (Ed.): Fish Population Dynamics. London: Wiley 1977
Haken, H.: Synergetics. An Introduction. Springer Series in Synergetics. Vol. 1. Berlin: Springer 1977
Hallegraeff, G. M.: Plankton. A Microscopic World. Leiden: E. J. Brill 1988
Hensen, V. (Ed.): Ergebnisse der in dem Atlantischen Ocean von Mitte Juli bis Anfang November 1889 ausgeführten Plankton-Expedition der Humboldt-Stiftung. Kiel und Leipzig 1892
Höfer, T., Sherratt, J. A., and Maini, P. K.: Cellular pattern formation during *Dictyostelium* aggregation. Physica *D85*, 425–444 (1995)
Holling, C. S.: Some characteristics of simple types of predation and parasitism. Canad. Entomologist *91*, 385–398 (1959)
Holmes, E. E., Lewis, M. A., Banks, J. E., and Veit, R. R.: Partial differential equations in ecology: Spatial interactions and population dynamics. Ecology *75*, 17–29 (1994)
Huisman, J., and Weissing, F. J.: Biodiversity of plankton by species oscillations and chaos. Nature *402*, 407–410 (1999)
Ikegami, S., Imai, I., Kato, J., and Ohtake, H.: Chemotaxis toward inorganic phosphate in the red tide alga *Chattonella antiqua*. J. Plankt. Res. *17*, 1587–1591 (1995)
Ivanitsky, G. R., Medvinsky, A. B., and Tsyganov, M. A.: From the dynamics of population autowaves generated by living cells to neuroinformatics. Physics – Uspekhi *37*, 961–989 (1994)
Ivlev, V. S.: Biologicheskaya produktivnost' vodoemov. Uspekhi Sovremennoi Biologii *XIX*, 98–120 (1945)
Jetschke, G.: General stability analysis of dissipative structures in reaction-diffusion systems with one degree of freedom. Phys. Lett. *A72*, 265–268 (1979)
Jørgensen, S. E.: Fundamentals of Ecological Modelling. Amsterdam: Elsevier 1994
Kawasaki, K., Mochizuki, A., Matsushita, M., and Shigesada, N.: A mathematical model of pattern formation in a bacterial colony (in Japanese). Control and Measurement *34*, 811–816 (1995a)
Kawasaki, K., Mochizuki, A., Matsushita, M., Umeda, T. , and Shigesada, N.: Modeling spatio-temporal patterns generated by *Bacillus subtilis*. J. Theor. Biol. *188*, 177–185 (1995b)
Keller, E. F., and Segel, L. A.: Initiation of slime mold aggregation viewed as an instability. J. Theor. Biol. *26*, 399–415 (1970)
Keller, E. F., and Segel, L. A.: Model for chemotaxis. J. Theor. Biol. *30*, 225–234 (1971a)
Keller, E. F., and Segel, L. A.: Traveling bands of chemotactic bacteria: A theoretical analysis. J. Theor. Biol. *30*, 235–248 (1971b)
Kierstead, H., and Slobodkin, L. B.: The size of water masses containing plankton blooms. J. Marine Res. *XII*, 141–147 (1953)
Klausmeier, C.: Regular and irregular patterns in semiarid vegetation. Science *284*, 1826–1828 (1999)
Kolmogorov, A., Petrovskii, I., and Piskunov, N.: Étude de l'equation de la diffusion avec croissance de la quantité de matière et son application à un problème biologique. Bull. d'Université de Moscou, Serie Internationale, Section *A1*, 1–25 (1937)
Kuznetsov, Yu. A., Muratori, S., and Rinaldi, S.: Bifurcations and chaos in a periodic predator-prey model. Int. J. Bifurcation and Chaos *2*, 117–128 (1992)
Leibovich, S.: Spatial aggregation arising from convective processes. In: Levin, S. A., Powell, T. M., and Steele, J. H. (Eds.): Patch Dynamics. Lecture Notes in Biomathematics. Vol. *96*, pp. 110–124. Berlin: Springer 1993

Levin, S. A., and Segel, L. A.: Hypothesis for origin of planktonic patchiness. Nature *259*, 659 (1976)
Lewis, M. A., and Kareiva, P.: Allee dynamics and the spread of invading organisms. Theor. Popul. Biol. *43*, 141–158 (1993)
Lotka, A. J.: Elements of Physical Biology. Baltimore: Williams and Wilkins 1925
Ludwig, D., Jones, D. D., and Holling, C. S.: Qualitative analysis of insect outbreak systems: the spruce budworm and forest. J. Anim. Ecol. *47*, 315–332 (1978)
Luther, R.: Räumliche Ausbreitung chemischer Reaktionen. Z. Elektrochem. *12*, 596–600 (1906)
Mackas, D. L., and Boyd, C. M.: Spectral analysis of zooplankton spatial heterogeneity. Science *204*, 62–64 (1979)
Malchow, H.: Spatio-temporal pattern formation in nonlinear nonequilibrium plankton dynamics. Proc. R. Soc. London *B 251*, 103–109 (1993)
Malchow, H.: Nonequilibrium structures in plankton dynamics. Ecol. Model. *75/76* 123–134 (1994)
Malchow, H.: Flow- and locomotion-induced pattern formation in nonlinear population dynamics. Ecol. Model. *82*, 257–264 (1995)
Malchow, H.: Nonlinear plankton dynamics and pattern formation in an ecohydrodynamic model system. J. Marine Systems *7*, 193–202 (1996)
Malchow, H.: Flux-induced instabilities in ionic and population-dynamical interaction systems. Z. Phys. Chem. *204*, 35–107 (1998)
Malchow, H.: Non-equilibrium spatio-temporal patterns in models of non-linear plankton dynamics. Freshwater Biol. *45*, 239–251 (2000 a)
Malchow, H.: Motional instabilities in predator-prey systems. J. Theor. Biol. *204*, 639–647 (2000 b)
Malchow, H., Hilker, F. M., and Petrovskii, S. V.: Noise and productivity dependence of spatiotemporal pattern formation in a prey-predator system. Discrete and Continuous Dynamical Systems, Series B (2003, in press)
Malchow, H., Petrovskii, S. V., and Medvinsky, A. B.: Numerical study of plankton-fish dynamics in a spatially structured and noisy environment. Ecol. Model. *149*, 247–255 (2002)
Malchow, H., Radtke, B., Kallache, M., Medvinsky, A. B., Tikhonov, D. A., and Petrovskii, S. V.: Spatio-temporal pattern formation in coupled models of plankton dynamics and fish school motion. Nonlinear Analysis: Real World Applications *1*, 53–67 (2000)
Malchow, H., and Schimansky-Geier, L.: Noise and Diffusion in Bistable Nonequilibrium Systems. Teubner-Texte zur Physik. Vol. *5*. Leipzig: Teubner 1985
Malchow, H., and Shigesada, N.: Nonequilibrium plankton community structures in an ecohydrodynamic model system. Nonlinear Processes in Geophysics *1*, 3–11 (1994)
Malin, G.: Sulphur, climate and the microbial maze. Nature *387*, 857–859 (1997)
Malthus, T.: An Essay on the Principle of Population. London: J. Johnson in St. Paul's Churchyard 1798
Matsushita, M., and Fujikawa, H.: Diffusion-limited growth in bacterial colony formation. Physica *A168*, 498–506 (1990)
May, R.: Biological populations with nonoverlapping generations: stable ponts, stable cycles and chaos. Science *186*, 645–667 (1974)
Mayzaud, P., and Poulet, S. A.: The importance of the time factor in the response of zooplankton to varying concentrations of naturally occurring particulate matter. Limnology and Oceanography *23*, 1144–1154 (1978)
Merkin, J. H., Petrov, V., Scott, S. K., and Showalter, K.: Wave-induced chemical chaos. Phys. Rev. Lett. *76*, 546–549 (1996)
Michaelis, L., and Menten, M.: Die Kinetik der Invertinwirkung. Biochem. Z. *49*, 333–369 (1913)
Mimura, M., and Murray, J. D.: On a diffusive prey-predator model which exhibits patchiness. J. Theor. Biol. *75*, 249–262 (1978)
Monod, J., and Jacob, F.: General conclusions: Teleonomic mechanisms in cellular metabolism, growth and differentiation. Cold Spring Harbor Symposia on Quantitative Biology *26*, 389–401 (1961)
Nakata, K., and Ishikawa, R.: Fluctuation of local phytoplankton abundance in coastal waters. Japanese J. Ecol. *25*, 201–205 (1975)
Newell, P. C.: Attraction and adhesion in the slime mold *Dictyostelium*. In: Smith, J. E. (Ed.): Fungal Differentiation. A Contemporary Synthesis. Mycology Series. Vol. *43*, pp. 43–71. New York: Marcel Dekker 1983
Nicolis, G., and Prigogine, I.: Self-organization in Nonequilibrium Systems. New York: Wiley 1977
Nitzan, A., Ortoleva, P., and Ross, J.: Nucleation in systems with multiple stationary states. Faraday Symposia of The Chem. Soc. *9*, 241–253 (1974)

O'Brien, J. J., and Wroblewski, J. S.: On advection in phytoplankton models. J. Theor. Biol. *38*, 197–202 (1973)

Odum, H. T.: Primary production in flowing waters. Limnology and Oceanography *1*, 102–117 (1956)

Okubo, A.: Diffusion and Ecological Problems: Mathematical Models. Biomathematics. Vol. *10*. Berlin: Springer 1980

Pascual, M.: Diffusion-induced chaos in a spatial predator-prey system. Proc. R. Soc. London *B 251*, 1–7 (1993)

Pedley, T. J., and Kessler, J. O.: Hydrodynamic phenomena in suspensions of swimming microorganisms. Annu. Rev. Fluid Mechanics *24*, 313–358 (1992)

Petrovskii, S. V.: Approximate determination of the magnitude of the critical size in the problem of the evolution of an ecological impact. J. Engineering Physics and Thermophysics *66*, 346–352 (1994)

Petrovskii, S. V., and Malchow, H.: A minimal model of pattern formation in a prey-predator system. Math. and Computer Modelling *29*, 49–63 (1999)

Petrovskii, S. V., and Malchow, H.: Wave of chaos: new mechanism of pattern formation in spatiotemporal population dynamics. Theor. Popul. Biol. *59*, 157–174 (2001)

Platt, J. R.: Bioconvection patterns in cultures of free-swimming organisms. Science *133*, 1766–1767 (1961)

Platt, T.: Local phytoplankton abundance and turbulence. Deep Sea Res. *19*, 183–187 (1972)

Popova, E. E., Fasham, M. J. R., Osipov, A. V., and Ryabchenko, V. A.: Chaotic behaviour of an ocean ecosystem model under seasonal forcing. J. Plankt. Res. *19*, 1495–1515 (1997)

Porep, R.: Der Physiologe und Planktonforscher Victor Hensen (1835–1924). Sein Leben und Werk. In: Herrlinger, R., Kudlien, F., und Dann, G. E. (Eds.): Kieler Beiträge zur Geschichte der Medizin und Pharmazie. Vol. *9*. Neumünster: Karl Wachholtz Verlag 1970

Powell, T. M., and Okuba, A.: Turbulence, diffusion and patchiness in the sea. Proc. R. Soc. London *B 343*, 11–18 (1994)

Powell, T. M., Richerson, P. J., Dillon, T. M., Agee, B. A., Dozier, B. J., Godden, D. A., and Myrup, L. O.: Spatial scales of current speed and phytoplankton biomass fluctuations in Lake Tahoe. Science *189*, 1088–1090 (1975)

Raymont, J. E. G.: Plankton and Productivity in the Oceans. Oxford: Pergamon Press 1980

Riley, G. A.: Factors controlling phytoplankton populations on Georges Bank. J. Marine Res. *6*, 54–73 (1946)

Riley, G. A.: Theory of food-chain relations in the ocean. In: Hill, M. N. (Ed.): The Sea. Vol. *2*, pp. 438–463. New York: Wiley 1963

Rinaldi, S., and Muratori, S.: Conditioned chaos in seasonally perturbed predator-prey models. Ecol. Model. *69*, 79–97 (1993)

Rinaldi, S., Muratori, S., and Kuznetsov, Yu. A.: Multiple attractors, catastrophes and chaos in seasonally perturbed predator-prey communities. Bull. Math. Biol. *55*, 15–35 (1993)

Ritschard, R. L.: Marine algae as a CO_2 sink. Water, Air and Soil Pollution *64*, 289–303 (1992)

Rovinsky, A. B., and Menzinger, M.: Chemical instability induced by a differential flow. Phys. Rev. Lett. *69*, 1193–1196 (1992)

Ryabchenko, V. A., Fasham, M. J. R., Kagan, B. A., and Popova, E. E.: What causes short term oscillations in ecosystem models of the ocean mixed layer? J. Marine Systems *13*, 33–50 (1997)

Scheffer, M.: Fish and nutrients interplay determines algal biomass: a minimal model. OIKOS *62*, 271–282 (1991 a)

Scheffer, M.: Should we expect strange attractors behind plankton dynamics – and if so, should we bother? J. Plankt. Res. *13*, 1291–1305 (1991b)

Scheffer, M.: Ecology of Shallow Lakes. Population and Community Biology Series. Vol. 22. London: Chapman and Hall 1998

Scheffer, M., Rinaldi, S., Kuznetsov, Y. A., and van Nes, E. H.: Seasonal dynamics of *Daphnia* and algae explained as a periodically forced predator-prey system. OIKOS *80*, 519–532 (1997)

Schlögl, F.: Chemical reaction models for nonequilibrium phase transitions. Z. f. Physik *253*, 147–161 (1972)

Segel, L. A.: A theoretical study of receptor mechanisms in bacterial chemotaxis. SIAM J. Appl. Math. *32*, 653–665 (1977)

Segel, L. A., and Jackson, J. L.: Dissipative structure: an explanation and an ecological example. J. Theor. Biol. *37*, 545–559 (1972)

Segel, L. A., and Stoeckly, B.: Instability of a layer of chemotactic cells, attractant and degrading enzyme. J. Theor. Biol. *37*, 561–585 (1972)

Shapiro, J. A., and Hsu, C.: *Escherichia coli* K-12 cell-cell interactions seen by time-lapse video. J. Bacteriol. *171*, 5963–5974 (1989)
Shapiro, J. A., and Trubatch, D.: Sequential events in bacterial colony morphogenesis. Physica *D49*, 214–223 (1991)
Sherratt, J. A., Eagan, B. T., and Lewis, M. A.: Oscillations and chaos behind predator-prey invasion: mathematical artifact or ecological reality? Phil. Trans. R. Soc. London *B 352*, 21–38 (1997)
Sherratt, J. A., Lewis, M. A., and Fowler, A. C.: Ecological chaos in the wake of invasion. Proc. Natl. Acad. Sci. USA *92*, 2524–2528 (1995)
Siegert, F., and Weijer, C. J.: Analysis of optical density wave propagation and cell movement in the cellular slime mold *Dictyostelium discoideum*. Physica *D 49*, 224–232 (1991)
Skellam, J. G.: Random dispersal in theoretical populations. Biometrika *38*, 196–218 (1951)
Sommer, U.: Planktologie. Berlin: Springer 1994
Sommer, U.: Algen, Quallen, Wasserfloh. Die Welt des Planktons. Berlin: Springer 1996
Steele, J. H.: The Structure of Marine Ecosystems. Harvard University Press: Cambridge MA 1974
Steele, J. H. (Ed.): Fisheries Mathematics. London: Academic Press 1977
Steele, J. H. (Ed.): Spatial Pattern in Plankton Communities. NATO Conference Series: IV, Marine Sciences, Vol. *3*. New York: Plenum Press 1978
Steele, J. H., and Henderson, E. W.: A simple plankton model. Amer. Naturalist *117*, 676–691 (1981)
Steele, J. H., and Henderson, E. W.: The role of predation in plankton models. J. Plankt. Res. *14*, 157–172 (1992 a)
Steele, J. H., and Henderson, E.W.: A simple model for plankton patchiness. J. Plankt. Res. *14*, 1397–1403 (1992 b)
Steffen, E., and Malchow, H.: Chaotic behaviour of a model plankton community in a heterogeneous environment. In: Schweitzer, F. (Ed.): Selforganisation of Complex Structures: From Individual to Collective Dynamics; pp. 331–340. London: Gordon and Breach 1996 a
Steffen, E., and Malchow, H.: Multiple equilibria, periodicity, and quasiperiodicity in a model plankton community. Senckenbergiana Maritima *27*, 137–143 (1996 b)
Steffen, E., Malchow, H., and Medvinsky, A. B.: Effects of seasonal perturbations on a model plankton community. Environm. Modeling & Assessment *2*, 43– 48 (1997)
Steinbock, O., Hashimoto, H., and Müller, S. C.: Quantitative analysis of periodic chemotaxis in aggregation patterns of *Dictyostelium discoideum*. Physica *D49*, 233–239 (1991)
Stommel, H.: Trajectories of small bodies sinking slowly through convection cells. J. Marine Res. *8*, 24–29 (1948)
Timm, U., and Okubo, A.: Gyrotaxis: A plume model for self-focusing micro-organisms. Bull. Math. Biol. *56*, 187–206 (1994)
Truscott, J. E.: Environmental forcing of simple plankton models. J. Plankt. Res. *17*, 2207–2232 (1995)
Truscott, J. E., and Brindley, J.: Ocean plankton populations as excitable media. Bull. Math. Biol. *56*, 981–998 (1994 a)
Truscott, J. E., and Brindley, J.: Equilibria, stability and excitability in a general class of plankton population models. Phil. Trans. R. Soc. London *A 347*, 703–718 (1994 b)
Turing, A. M.: On the chemical basis of morphogenesis. Phil. Trans. R. Soc. London *B 237*, 37–72 (1952)
Vasiev, B. N., Hogeweg, P., and Panfilov, A. V.: Simulation of *Dictyostelium discoideum* aggregation via reaction-diffusion model. Phys. Rev. Lett. *73*, 3173–3176 (1994)
Verhulst, P.: Notice sur la loi que la population suit dans son accroissement. Corresp. Math. et Phys. *10*, 113–121 (1838)
Vinogradov, M. E., and Menshutkin, V. V.: The modelling of open-sea ecosystems. In: Goldberg, E. D. (Ed.): The Sea: Ideas and Observations on Progress in the Study of the Seas. Vol. 6, pp. 891–921. Berlin: Wiley 1977
Volterra, V.: Variazioni e fluttuazioni del numero d'individui in specie animali conviventi. Mem. Acad. Lincei *III*, 6, 31–113 (1926)
Weber, L. H., El-Sayed, S. Z., and Hampton, I.: The variance spectra of phytoplankton, krill and water temperature in the Antarctic ocean south of Africa. Deep Sea Res. *33*, 1327–1343 (1986)
Williamson, P., and Gribbin, J.: How plankton change the climate. New Scientist 16 March 1991, pp. 48–52 (1991)
Winet, H., and Jahn, T.: On the origin of bioconvection fluid instabilities in *Tetrahymena* culture systems. Biorheology *9*, 87–104 (1972)
Wissel, C.: Theoretische Ökologie. Berlin: Springer 1989

Witten, T. A., and Sander, L. M.: Diffusion-limited aggregation, a kinetic critical phenomenon. Phys. Rev. Lett. *47*, 1400–1403 (1981)

Wroblewski, J. S., and O'Brien, J. J.: A spatial model of phytoplankton patchiness. Marine Biol. *35*, 161–175 (1976)

Wroblewski, J. S., O'Brien, J. J., and Platt, T.: On the physical and biological scales of phytoplankton patchiness in the ocean. Mémoires Soc. R. des Sciences de Liège *VII*, 43–57 (1975)

Wyatt, T.: Production dynamics of *Oikopleura dioica* in the Southern North Sea, and the role of fish larvae which prey on them. Thalassia Jugoslavica *7*, 435–444 (1971)

Wyatt, T.: The biology of *Oikopleura dioica* and *Fritillaria borealis* in the Southern Bight. Marine Biol. *22*, 137–158 (1973)

Yoder, J. A., Ackleson, S. G., Barber, R. T., Flament, P., and Balch, W. M.: A line in the sea. Nature *371*, 689–692 (1994)

Yodzis, P.: The trophodynamics of whole ecological communities. In: Levin, S. (Ed.): Frontiers in Mathematical Biology. Lecture Notes in Biomathematics. Vol. 100, pp. 443–453. Berlin: Springer 1994

Prof. Dr. Horst Malchow
Institute for Environmental Systems Research
Department of Mathematics and Computer Science
University of Osnabrück
49069 Osnabrück
Germany
Phone: ++49 (0) 54 19 69 24 99
Fax: ++49 (0) 54 19 69 25 99
E-Mail: malchow@uos.de
http://www.usf.uos.de/~malchow

Sergei V. Pertrovskii
Shirshov Institute for Oceanology
Russian Academy of Sciences
Nakhimovsky Prospekt 36
Moscow, 117218
Russia
E-Mail: spetrovs@sio.rssi.ru

Frank M. Hilker
Institute for Environmental Systems Research
Department of Mathematics and Computer Science
University of Osnabrück
49069 Osnabrück
Germany
Phone: ++49 (0) 54 19 69 25 75
Fax: ++49 (0) 54 19 69 25 99
E-Mail: fhilker@uos.de

Nova Acta Leopoldina NF *88*, Nr. 332, 341–351 (2003)

Molecular Mechanisms of Circadian Clocks in Microalgae

Maria MITTAG (Jena)

With 1 Table

Abstract

The occurrence of temporal patterns in biology can either be found during development or within rhythmic processes, whose period can vary from seconds to years. Biological rhythms that have a period of about 24 hours under constant conditions (light, temperature) are called circadian (*circa* = about; *dies* = day). In microalgae, a variety of processes, such as phototaxis, chemotaxis, cell aggregation, cell division or bioluminescence, are controlled by an endogenous circadian clock. The molecular mechanism by which this clock regulates temporal gene expression has been studied primarily in two of the microalgae, namely the dinoflagellate *Gonyaulax polyedra* and the green alga *Chlamydomonas reinhardtii*. Although both algae are phylogenetically widely apart they share a certain type of circadian controlled RNA binding proteins that recognize specifically uridine-guanine-repeat elements of a length of at least seven repeats in row. In both algae this *cis*-acting element can be found in the 3′-untranslated region of certain mRNAs, which encode different proteins. In *G. polyedra*, the mRNA for the luciferin-binding protein, a component of the bioluminescent system, contains such a motif while in *C. reinhardtii* several mRNAs, which encode proteins for nitrogen and CO_2 metabolism, bear this motif.

Zusammenfassung

Temporale Erscheinungen in biologischen Systemen sind sowohl während der Entwicklung eines Organismus als auch bei rhythmischen Prozessen, deren Periode von Sekunden bis hin zu Jahren variieren kann, zu finden. Biologische Rhythmen, welche eine Periode von ca. 24 Stunden unter konstanten Bedingungen (Licht, Temperatur) haben, nennt man circadian (*circa* = ungefähr, about; *dies* = Tag, day). In Mikroalgen werden zahlreiche Prozesse, wie z. B. Phototaxis, Chemotaxis, Zellaggregation oder Biolumineszenz, von einer endogenen circadianen Uhr kontrolliert. Der molekulare Mechanismus, mit dem diese Uhr temporale Genexpression reguliert, wurde hauptsächlich in zwei der untersuchten Mikroalgen, nämlich dem Dinoflagellaten *Gonyaulax polyedra* und der Grünalge *Chlamydomonas reinhardtii*, überprüft. Obwohl beide Algen phylogenetisch sehr weit auseinander liegen, gibt es in beiden ein circadian kontrolliertes RNA-Bindeprotein, das spezifisch Uridin-Guanin-Repetitionen mit einer Mindestlänge von sieben Wiederholungen erkennt. In beiden Algen befindet sich das Bindemotiv in der 3′-nicht-translatierten Region bestimmter mRNAs, die unterschiedliche Proteine kodieren. In *G. polyedra* enthält die mRNA des Luziferin-Bindeproteins, welches eine Komponente des biolumineszenten Systems darstellt, solch ein Motiv, während es in *C. reinhardtii* in mRNAs vorkommt, die für Proteine des Stickstoff- und CO_2-Metabolismus kodieren.

1. Introduction

Spatiotemporal patterns are very widespread in biology. They comprise the formation of structures, which can permanently reorganize themselves. For example, chemotactic

movements of cells and growing tips of neurons always develop new growing areas on surface by removing consequently other parts (MEINHARDT 2001). Thus, the cells are able to move to a certain direction. Spatiotemporal processes represent also the basis for the developmental program of an organism. During the development from an embryonal stage to an adult organism cells become polarized and divide in a programmed manner during a fixed time range. Beside development, temporal programs can also occur in rhythmic patterns during the lifespan of an organism. Hereby, their period can vary from seconds (ultradian), 24 h (circadian), one year (annual) to years (infradian rhythms).

Spatiotemporal organization can be studied in different ways. On one side, one can analyze the molecular basis for such regulation and look for the genes/mRNAs that are switched on or translated during a specific time window or within a given area of a cell or a tissue. Such experiments will usually result in the identification of a network of genes/proteins that interact with each other. In the case of rhythmic processes such proteins have been often shown to be part of a feedback loop with positive and negative elements (summarized in HARMER et al. 2001). On the other side, oscillations, which occur in spatiotemporal pattern formation, can be modeled based on mathematical calculations and their non-linear dynamics can be studied at the level of theoretical physics. Thereby, the already available information about the proteins, which are involved in creating such oscillations, can serve as basis.

This review will first introduce the physiological characteristics of circadian clocks and will then focus on the molecular biology based approach for the investigation of rhythmic patterns within the microalgae. It will describe so far characterized proteins of circadian output processes and their regulation. In future, these proteins can serve as a platform for modeling studies as mentioned above.

The daily change of light and darkness governs the environment on earth and some prokaryotes, and most likely all eukaryotes have adapted a variety of biological processes, which exhibit a period of 24 hours, according to this oscillation. In many cases these processes are regulated by an internal biological clock, called circadian clock. This timekeeper tells the organism at what time of the day it has to transcribe certain genes or start the translation of their mRNAs.

The circadian clock has certain physiological features, which are well conserved from cyanobacteria up to humans (ASCHOFF 1981, KONDO et al. 1993). The most important is the fact that the rhythm continues with a period of about 24 h when the organism is put from a light-dark cycle to constant conditions of light (dim-light or darkness) and temperature. Hence, the name circadian deriving from the latin (circa = about; dies = day) was defined. As desirable for a well functioning clock, circadian rhythms are temperature compensated. In contrast to biochemical reactions, which have an accelerated rate with an increase of temperature of 10 °C (Q_{10}) by a factor of 2, their Q_{10} ranges from 0,8 to 1,3. Another important feature is their ability for entrainment. When an organism is put from a light-dark regime into a reverse cycle (dark-light) it will adapt to this new cycle within a few days. In addition, light pulses can influence the phase of the rhythm, a phenomenon called phase shifting. Depending on the time of the circadian cycle when the light pulse is given the phase can be either advanced or delayed. Even in multicellular organisms, including animals, the generation of circadian rhythms is a property of single cells (WELSH et al. 1995). Thus, unicellular organisms such as microalgae are perfectly suited to study the basics of the circadian clock and its molecular mechanism.

This review will focus on two microalgae that have been extensively used to study circadian rhythms in eukaryotic microalgae, namely the dinoflagellate *Gonyaulax polyedra* and the green alga *Chlamydomonas reinhardtii*.

2. *Gonyaulax polyedra* and its Relevance in Chronobiology

The marine unicellular alga *Gonyaulax polyedra* belongs to the dinoflagellates, which are unique in several respects (Lee et al. 1993). Some of them are able to exhibit bioluminescence naturally (Schmitter et al. 1976). The bioluminescence rhythm of *G. polyedra* was indeed one of the first rhythms, which was well studied by chronobiologists (Hastings and Sweeney 1958). But in this alga, other circadian rhythms such as cell aggregation, photosynthesis and cell division can also be observed (summarized in Roenneberg and Mittag 1996). While bioluminescence reaches its maximum during the night-phase, photosynthesis and cell aggregation peaks during the day-phase, and cell division occurs just at dawn. Due to the fact, that bioluminescence is easily measurable and suited for automatic monitoring (Roenneberg and Hastings 1992), this rhythm has provided the basis for studying the circadian system at the physiological level (Roenneberg 1996). Cultures of *G. polyedra* were exposed to different light qualities or drugs and nutrients were added to them. Consequently, the effect on the period and phase of the bioluminescence rhythm was examined. From these studies, conclusions could be drawn on the light input pathway, which provides information for the central pacemaker, the oscillator. Some of them will be shortly presented here, a more complete overview can be found in Roenneberg (1996) and Mittag (2001). There are at least two light-input pathways in the *G. polyedra* system, one being blue sensitive and another, which is red and blue sensitive (Roenneberg and Hastings 1991). By drug application, it was found, that inhibitors of kinases and phosphatases are strongly affecting the period and phase of the bioluminescence rhythm (Comolli et al. 1994, 1996, Comolli and Hastings 1999). Thus, it seems likely that phosphorylation and dephosphorylation plays a significant role in the circadian system of this alga. Nutrient studies revealed that nitrate acts as a nonphotic *Zeitgeber* signal. It influences all canonical properties of circadian rhythms: amplitude, phase and period (Roenneberg and Rehman 1996). Beside these physiological examinations, circadian bioluminescence was also studied at the cellular, biochemical and molecular biology level.

2.1 Cell Biology and Biochemistry of Circadian Bioluminescence

The bioluminescent system of *G. polyedra* is entirely controlled by the circadian clock. All the components of this system are localized in small organelles named scintillons. They represent extensions in the form of bubbles, which reach from the cytoplasm into the celluar vacuole and are surrounded by the vacuolar membrane (Fogel et al. 1972, Nicolas et al. 1987). They are, however, still connected by a narrow strip with the cytoplasm. Their number fluctuates during the day-night cycle changing from about 40 during the day-phase to ca. 400 during the night-phase. These organelles can be visualized by the fluorescence of the substrate luciferin (Fritz et al. 1991). At pH 7.5, the substrate

is bound to a so called luciferin-binding protein (LBP), which prevents its oxidation. In addition, the enzyme luciferase (LCF) catalyzing the bioluminescence reaction, is inactive at this pH. Due to a drop of pH to 6,5, LBP undergoes some conformational change and releases the substrate (Morse et al. 1989 b, Morse and Mittag 2000). Since the enzyme LCF is activated at this pH, the bioluminescence reaction can take place. Luciferin is oxidized by molecular oxygen, which leads to an electronically excited state. Its decay results in the emission of visible light. It is hypothesized that an action potential across the vacuolar membrane is caused by mechanical stimulation resulting in an influx of protons into the scintillons, which reduces the pH in these organelles.

All three, the substrate luciferin, LBP and LCF are present at high amounts during the night phase and at a low rate during the day-phase (Johnson et al. 1984, Morse et al. 1989 a). Each day, they are synthesized and destroyed again, a process, which is in accordance with the formation and destruction of the scintillons.

2.2 The Molecular Mechanism of Circadian Bioluminescence

In many cases of circadian output regulation, it was found that the amount of mRNA cycles during the light-dark regime. Typical examples are the genes for chlorophyll a/b-binding proteins (*cab*) (Piechulla 1999) or the so-called clock-controlled genes in the fungi *Neurospora crassa* (Bell-Pedersen et al. 1996). In all these cases, circadian gene expression is controlled at the level of transcription. When circadian regulation of LBP and later on LCF were studied, it was surprising that the level of both mRNAs was constantly at a high rate during the entire day-night cycle indicating that both genes are controlled at the level of translation (Morse et al. 1989a, Mittag et al. 1998). Indeed, it appears that translational control is very widespread in this alga (Milos et al. 1990, Marcovic et al. 1996, Fagan et al. 1999).

Since the *lbp* gene was available first, most progress of understanding its circadian control has been made in this case. With pulse-chase experiments, it was shown that synthesis of LBP fluctuates; it is maximally synthesized at the beginning of the night-phase resulting in high level of LBP in the middle of the subjective night (Morse et al. 1989 a). At the end of the night, it is degraded by a still unknown mechanism. Since its mRNA is present throughout the day-night cycle it could be clearly concluded that its circadian regulation occurs at the translational level. It was indeed the first example of such a regulation within the circadian system.

Translational regulation can be mediated by the untranslated regions (UTRs) of an mRNA. In several cases, *cis*-acting elements situated either in the 5′- or 3′-UTR are known to be recognized by *trans*-acting factors, which can play a role as activators or repressors of translation (Decker and Parker 1995, Pain 1996). In addition, so-called upstream open reading frames (uORFs) situated in the 5′-UTR can influence translation (Kozak 1991).

In case of *lbp* mRNA such a uORF was found in its 5′-UTR. Characterization of this uORF by *in-vitro* translation experiments of *lbp* mRNA (wildtype and mutagenized variants) showed that two LBP proteins are made, which differ in their N-terminus (Mittag et al. 1997). LBP-A comprises its entire ORF while LBP-B is initiated from a later start codon in the *lbp* ORF. Mutation of the uORF results in the loss of this differential initia-

tion event so that only LBP-A is expressed. *In-vivo* data including Western blot analysis revealed that these two forms are also present in *Gonyaulax*. Due to their similar molecular masses it remains unclear if both forms are up regulated during the night-phase, although it appears that this might be only the case with LBP-A (MITTAG et al. 1997). Also, the function of LBP-B is not solved up to now.

How is the translational control of LBP-A achieved? By mobility shift assays *trans*-acting factors, which might interact with *lbp* 5′- or 3′-UTR, were searched. While no RNA-binding proteins were found that interact specifically with the *lbp* 5′-UTR, an RNA-binding protein could be identified that recognizes a 22-nt long region within the *lbp* 3′-UTR (MITTAG et al. 1994). This protein was called CCTR (circadian controlled translational regulator) since its binding activity changes over the day-night cycle. It increases at the end of the night and decreases again at its beginning. When *G. polyedra* cells were put under constant conditions of dim light, this rhythm of binding activity continued demonstrating that the CCTR is controlled by the circadian clock (MITTAG et al. 1994, MITTAG 2001). Its binding site comprises seven UG-repeat elements with a UUG at position five. Prediction of RNA secondary structure by computer simulation (ABRAHAMS et al. 1990) showed that the UG-repeat is situated within a potential hairpin-loop structure. Since the binding activity of the CCTR correlates negatively with the synthesis of LBP it was hypothesized that this protein acts as repressor of translation preventing that LBP (at least LBP-A) is translated during the day-phase.

3. *Chlamydomonas reinhardtii*, an Eucaryotic Model Organism

During the past years, the green alga *Chlamydomonas reinhardtii* has emerged as a model organism for studying specific processes such as flagella and basal bodies, photosynthesis, metabolic pathways and circadian rhythms (HARRIS 2001). This alga, also named "green yeast" provides numerous molecular tools that facilitate the examination of the processes mentioned above. Similar to yeast, *C. reinhardtii* can be grown in its haploid form, which allows to screen easily for mutants by their phenotype. Under certain environmental conditions, gametes can be produced, which form a zygote; following meiosis, tetrade analysis can be carried out. The alga can be grown quickly to high amounts, either photoautotrophic or heterotrophic (on acetate), both in liquid as well as on solid culture medium. Its nucleus, chloroplast and mitochondria can be stable transformed and several new technologies such as a green fluorescent-protein (GFP) reporter gene or the use of RNAi have been succesfully applied (FUHRMANN et al. 1999, 2001). In addition, international genome projects are on their way: the entire chloroplast genome has been sequenced, and currently there are more than 180 000 expressed sequenced tags (ESTs) available. Also, sequencing of the nuclear genome of this alga is meanwhile completed (http://www.biology.duke.edu/chlamy_genome/crc.html).

3.1 Circadian Rhythms in C. reinhardtii

Since several of the above mentioned advantages of *C. reinhardtii* are known for a long time, investigators have also used this alga for studying circadian rhythms. One of the

first rhythms, described in this alga was phototaxis, which reaches its maximum during the day-phase (Bruce 1970). The algae swim toward a supplied light source preferentially during the day. The environmental advantage of such a behavior seems obvious: the algae are able to capture more light for photosynthesis. This rhythm was even studied in a spacecraft in outer space, where it was robustly expressed (Mergenhagen and Mergenhagen 1987). Based on circadian phototaxis, several clock mutants having an altered period were also described (Bruce 1972, Bruce and Bruce 1978).

There are, however, also circadian rhythms in *C. reinhardtii* that peak during the night-phase including cell stickiness (Straley and Bruce 1979), chemotaxis (Byrne et al. 1992), and cell division (Goto and Johnson 1995). Another circadian rhythm, namely sensitivity to UV radiation, has its maximum at the day-night switch (Nikaido and Johnson 2000). Cell stickiness reflects the ability of the cells to stick to a glass surface, which is due to alterations on the cell surface (Straley and Bruce 1979). The rhythm of chemotaxis was studied by using the chemo-attractant ammonium as nitrogen source. Of note is the fact, that the cells swim maximally towards this nitrogen source during the middle of the night-phase even though the uptake of ammonium (in form of radiolabeled methylammonium), which is also circadian, does not occur until dawn. This is in accordance with the uptake of nitrite, which also occurs maximally at the beginning of the day and with the activity of nitrite reductase (Pajuelo et al. 1995).

3.2 Transcriptional Control of Gene Expression

The strong focus on photosynthesis in *C. reinhardtii*, which is due to the fact that photosynthetic mutants are fertile and can be grown heterotrophically on acetate, has led several investigators to study the expression of genes encoding photosynthetic or related proteins. In this context, several genes were identified whose mRNA levels change during the day-night cycle indicating transcriptional control of circadian gene expression (summarized in Mittag 2001). In some cases, nuclear run-on experiments were carried out in addition and clearly confirmed this indication.

As in higher plants (Piechulla 1999), the expression of nuclear genes encoding the chlorophyll a/b-binding protein of photosystem II (*cab II*, also named *lhcp II*: light harvesting complex protein), which absorbs and transfers light to the reaction center of PS II, is subject to circadian regulation (Jacobshagen and Johnson 1994, Jacobshagen 1996). Further transcriptionally controlled genes comprise *LI818*, which encodes a protein that has 30 % homology to CAB (Savard et al. 1996) and *cah1* (carbonic anhydrase, Fujiwara et al. 1996). All these genes are nuclear encoded and show circadian rhythms of mRNA abundance with a maximum during the day-phase. However, several (possibly all) chloroplast encoded genes exhibit as well circadian rhythms of transcription, with peaks occurring mostly during early day-phase (Salvador et al. 1993, Hwang et al. 1996). In addition, it was found that the supercoiling status of chloroplast DNA oscillates in an endogenous manner in this alga (Salvador et al. 1998). Thus, a general ON/OFF switch could be present in the *C. reinhardtii* chloroplast and nuclear encoded genes encoding chloroplast proteins might have adapted their temporal expression to this event.

3.3 Posttranscriptional/Translational Control of Gene Expression: Conserved RNA-binding Proteins in G. polyedra and C. reinhardtii

The identification of the RNA-binding protein CCTR in *G. polyedra*, which is involved in the circadian LBP expression at the translational level, raised the question if *trans*-acting factors that are controlling circadian output, could be conserved in evolution, even though their targets might be different. To investigate this possibility, clock-controlled RNA-binding proteins that interact specifically with UG-repeat regions were searched in the green alga *C. reinhardtii*, which is phylogenetically widely apart from the dinoflagellates (MELKONIAN et al. 1995). For this purpose, the *lbp* 3′-UTR containing the *cis*-acting element for the CCTR was used as a probe to screen in mobility-shift assays for proteins from *C. reinhardtii*, which can interact specifically to this repeat. By this way, an RNA-binding protein could be identified that fulfills all criteria to be considered as a CCTR analog: it interacts specifically with the UG-repeat, and its binding activity is controlled by the circadian clock (MITTAG 1996). However, in contrast to the CCTR, its binding activity is phase shifted: it increases at the end of the day-phase and decreases again at the end of the night-phase. If this RNA-binding protein, called CHLAMY 1, acts as a translational repressor, it would repress the translation of mRNAs during most part of the night-phase.

One important question was concerned with the target mRNAs in *C. reinhardtii* that are subject to the control of CHLAMY 1. Since EST-projects in this alga are on its way, several candidates could be identified by computer screening that contain UG-repeat rich elements in their 3′-UTRs. But in all cases the UG-repeat was not fully identical with the *lbp* sequence containing seven UG-repeats in row, with an UUG at position five. By *in-vitro* mutagenesis of UG-elements within the *lbp* 3′-UTR, it was determined how many UGs in row are necessary for the binding of either the CCTR or CHLAMY 1 (MITTAG and WALTENBERGER 1997). These examinations led to the conclusion that strong binding of both proteins requires the presence of all seven repeats. Nevertheless, it was still unclear if the lack of the UUG at position five or UG-repeats with more than seven elements, as it was found in several mRNAs from *C. reinhardtii*, would allow binding

Tab. 1 Binding activity of the circadian RNA-binding protein CHLAMY 1 to different mRNAs containing UG-repeat elements in their 3'-UTR

Gene	Protein	Number of UG-repeats in row	Binding strength of CHLAMY 1 (with molar excess for competing 50 % binding)
gs2	Glutamine synthetase2	7	High (1×)
arg7	Arginino-succinate lyase	7	High (1×)
rbcS1	Small subunit of RUBISCO	7 and 2 UUGs	High (2×)
nii1	Nitrite reductase	9	High (3×)
nrt2;3	Nitrite/nitrate transporter	16	High (8×)
lip-36 G1	CO_2-shuffling protein		Medium (11×)
yptc4	G-protein	7	Low (33×)
lpcr-1	NADPH-protochloro-phyllide oxidoreductase	7	Low (36×)

of CHLAMY 1. These questions were answered by analyzing eight mRNAs that contained UG-repeats from seven up to 16 elements in row in their 3′-UTR by mobility-shift assays as well as UV-crosslinking experiments (Waltenberger et al. 2001). CHLAMY 1 could specifically bind to all examined mRNAs (see Tab. 1). By competition assays, it was checked further if the binding affinity of CHLAMY 1 would increase with the number of UG-elements. This was not the case. Since several experiments indicate that the CCTR and CHLAMY 1 require a single stranded nucleic-acid domain, a loop, for binding (Mittag 2001), it could be hypothesized that the number of UG-elements, which are present within the loop may determine binding strength.

Interestingly, the binding activity of CHLAMY 1 correlated with the function of the proteins, which are encoded by the examined mRNAs (Waltenberger et al. 2001). Some of them are key components of nitrogen metabolism and are involved in the uptake of mainly nitrite (NRT2;3), its reduction to ammonium (NII1), the fixation of ammonium as glutamine (GS2), and in arginine biosynthesis (ARG 7). As mentioned earlier, the uptake of nitrogen components in *C. reinhardtii* takes place at the beginning of the day-phase. Since the activities of enzymes/proteins involved in nitrogen metabolism vary in a temporal way that is opposite in phase to that of CHLAMY 1, it may repress the translation of the cognate mRNAs.

In addition to these examples, CHLAMY 1 has strong affinity to mRNAs, which encode proteins involved in CO_2 metabolism such as LIP36-G1, a protein on the outer chloroplast membrane that shuffles CO_2 into the chloroplast or RBCS1, the small subunit of RUBISCO (Waltenberger et al. 2001).

Thus, CHLAMY 1 seems to coordinate entire metabolic pathways in a circadian way. Up to now, it remains open if this protein is purely a component of the transduction pathway from the central oscillator to the circadian output, or if it is also a part of the pacemaker itself.

4. Conclusive Remarks

In the two microalgae *G. polyedra* and *C. reinhardtii* several metabolic processes are regulated by the circadian clock. Some of them are regulated by a conserved clock-controlled RNA-binding protein (CCTR and CHLAMY 1, respectively). Up to now, it remains open if such circadian output processes are entirely controlled by one central oscillator within these single cell organisms or if oscillations within the metabolic network are more complex structured. In case of *G. polyedra* it was already shown that there are two oscillators within a single cell, one of them triggering the bioluminescence rhythm and the other one being involved in the rhythm of cell aggregation (Roenneberg and Morse 1993). In *C. reinhardtii* this possibility remains an open question. The fact that circadian clocks were also found in cyanobacteria (Kondo et al. 1993) would support a hypothesis that one oscillator was given to the eukaryotic cell by its endosymbiont and may have been retained in the organelle (Mittag 2001). If this would be the case, the regulation of the RNA-binding protein CHLAMY 1, which binds to several mRNAs whose proteins are transferred into the chloroplast after translation, could be very com-

plex. One could imagine that in this case both potential oscillators would contribute to this regulation about feedback regulation.

In general, molecular components of the clock machinery could totally differ between two oscillators or they could be shared among them. Such complex organization programs would consist of many variables and would be hard to analyze in their complexity at the molecular level. In this context, it can be of advantage to generate numerical simulations and create mathematical models, which can help understanding such complex systems. The build up of such modeling opens then the possibility to develop further strategies, which will allow a more precise access to studies at the molecular level. In case of the above described circadian RNA-binding proteins such modeling has not been undertaken up to now, but it presents a challenge for future investigations.

References

Abrahams, J. P., Van den Berg, M., Van Batenburg, E., and Pleij, C.: Prediction of RNA secondary structure, including pseudoknotting, by computer simulation. Nucleic Acids Res. *18*, 3035–3044 (1990)

Aschoff, J.: 4. Biological rhythms. In: Aschoff, J. (Ed.): Handbook of Behavioral Neurobiology. New York, NY: Plenum Press 1981

Bell-Pedersen, D., Shinohara, M. L., Loros, J. J., and Dunlap, J. C.: Circadian clock-controlled genes isolated from *Neurospora crassa* are late night- to early morning specific. Proc. Natl. Acad. Sci. USA *93*, 13096–13101 (1996)

Bruce, V. G.: The biological clock in *Chlamydomonas reinhardtii*. J. Protozool. *17*, 328–334 (1970)

Bruce, V. G.: Mutants of the biological clock in *Chlamydomonas reinhardtii*. Genetics *70*, 537–548 (1972)

Bruce, V. G., and Bruce, N. C.: Diploids of clock mutants of *Chlamydomonas reinhardtii*. Genetics *89*, 225–233 (1978)

Byrne, T. E., Wells, M. R., and Johnson, C. H.: Circadian rhythms of chemotaxis to ammonium and methylammonium uptake in *Chlamydomonas*. Plant Physiol. *98*, 879–886 (1992)

Comolli, J., and Hastings, J. W.: Novel effects on the *Gonyaulax* circadian system produced by the protein kinase inhibitor staurosporine. J. Biol. Rhythms *14*, 11–19 (1999)

Comolli, J., Taylor, W., and Hastings, J. W.: An inhibitor of protein phosphorylation stops the circadian oscillator and blocks light-induced phase-shifting in *Gonyaulax polyedra*. J. Biol. Rhythms *9*, 13–26 (1994)

Comolli, J., Taylor, W., Rehman, J., and Hastings, J. W.: Inhibitors of serine/threonine phosphoprotein phosphatases alter circadian properties in *Gonyaulax polyedra*. Plant Physiol. *111*, 285–291 (1996)

Decker, C. J., and Parker, R.: Diversity of cytoplasmic functions for the 3' untranslated region of eukaryotic transcripts. Curr. Opin. Cell Biol. *7*, 386–392 (1995)

Fagan, T., Morse, D., and Hastings, J. W.: Circadian synthesis of a nuclear-encoded chloroplast glyceraldehyde-3-phosphate dehygrogenase in the dinoflagellate *Gonyaulax polyedra* is translationally controlled. Biochemistry *38*, 7689–7695 (1999)

Fogel, M., Schmitter, R. E., and Hastings, J. W.: On the physical identity of scintillons: bioluminescent particles in *Gonyaulax polyedra*. J. Cell Sci. *11*, 305–317 (1972)

Fritz, L., Morse, D., and Hastings, J. W.: The circadian bioluminescence rhythm of *Gonyaulax* is related to daily variations in the number of light-emitting organelles. J. Cell Sci. *95*, 321–328 (1990)

Fuhrmann, M., Oertelt, W., and Hegemann, P.: A synthetic gene coding for the green fluorescent Protein (GFP) is a versatile reporter in *Chlamydomonas reinhardtii*. Plant J. *19*, 353–361 (1999)

Fuhrmann, M., Stahlberg, A., Govoruniva, E., Rank, S., and Hegemann, P.: The abundant retinal protein of the *C. reinhardtii* eye is not the photoreceptor for photophobic responses and phototaxis. J. Cell Sci. *114*, 3857–3863 (2001)

Fujiwara, S., Ishida, N., and Tsuzuki, M.: Circadian expression of the carbonic anhydrase gene, Cah 1, in *Chlamydomonas reinhardtii*. Plant Mol. Biol. *32*, 745–749 (1996)

Goto, K., and Johnson, C. H.: Is the cell division cycle gated by a circadian clock? The case of *Chlamydomonas reinhardtii*. J. Cell Biol. *129*, 1061–1069 (1995)

Harmer, S. L., Satchidananda, P., and Kay, S. A.: Molecular bases of circadian rhythms. Annu. Rev. Cell Dev. Biol. *17*, 215–253 (2001)

Harris, E. H.: *Chlamydomonas* as model organism. Annu. Rev. Plant Physiol. Plant Mol. Biol. *52*, 363–406 (2001)

Hastings, J. W., and Sweeney, B. M.: A persistent diurnal rhythm of luminescence in *Gonyaulax polyedra*. Biol. Bull. *115*, 440–458 (1958)

Hwang, S., Kawazoe, R., and Herrin, D. L.: Transcription of tufA and other chloroplast-encoded genes is controlled by a circadian clock in *Chlamydomonas*. Proc. Natl. Acad. Sci. USA *93*, 996–1000 (1996)

Jacobshagen, S., and Johnson, C. H.: Circadian rhythms of gene expression in *Chlamydomonas reinhardtii*: circadian cycling of mRNA abundance of cab II, and possibly of beta-tubulin and cytochrome c. Eur. J. Cell Biol. *64*, 142–152 (1994)

Jacobshagen, S., Kindle, K. L., and Johnson, C. H.: Transcription of cab II is regulated by the biological clock in *Chlamydomonas reinhardtii*. Plant Mol. Biol. *31*, 1173–1184 (1996)

Johnson, C. H., Roeber, J., and Hastings, J. W.: Circadian changes in enzyme concentration account for rhythm of enzyme activity. Science *223*, 1428–1430 (1984)

Kondo, T., Strayer, C. A., Kulkarni, R. D., Taylor, W., Ishiura, M., Golden, S. S., and Johnson, C. H.: Circadian rhythms in prokaryotes: Luciferase as a reporter of circadian gene expression in cyanobacteria. Proc. Natl. Acad. Sci. USA *90*, 5672–5676 (1993)

Kozak, M.: An analysis of vertebrate mRNA sequences: intimations of translational control. J. Cell Biol. *115*, 887–903 (1991)

Lee, D. H., Mittag, M., Sczekan, S., Morse, D., and Hastings, J. W.: Molecular cloning and genomic organization of a gene for luciferin-binding protein from the dinoflagellate *Gonyaulax polyedra*. J. Biol. Chem. *268*, 8842–8850 (1993)

Marcovic, P., Roenneberg, T., and Morse, D.: Phased proteinsynthesis at several circadian times does not change protein levels in *Gonyaulax*. J. Biol. Rhythms *11*, 57–67 (1996)

Meinhardt, H.: Auf- und Abbau von Mustern in der Biologie. Biologie in uns. Zeit *1*, 22–29 (2001)

Melkonian, M., Marin, B., and Surek, B.: Phylogeny and evolution of the algae. In: Arai, R., Kato, M., and Doi, Y. (Eds.): Biodiversity and Evolution; pp. 153–176. Tokyo: The National Science Museum Foundation 1995

Mergenhagen, D., and Mergenhagen, E.: The biological clock of *Chlamydomonas reinhardtii* in space. Eur. J. Cell Biol. *43*, 203–207 (1987)

Milos, P., Morse, D., and Hastings, J. W.: Circadian control over synthesis of many *Gonyaulax* proteins is at a translational level. Naturwissenschaften *77*, 87–89 (1990)

Mittag, M.: Conserved circadian elements in phylogenetically diverse algae. Proc. Natl. Acad. Sci. USA *93*, 14401–14404 (1996)

Mittag, M.: Circadian rhythms in microalgae. Internat. Rev. Cytol. *206*, 213–247 (2001)

Mittag, M., Eckerskorn, C., Strupat, K., and Hastings, J. W.: Differential translational initiation of *lbp* mRNA is caused by a 5' upstream open reading frame. FEBS Lett. *411*, 245–250 (1997)

Mittag, M., Lee, D.-H., and Hastings, J.W.: Circadian expression of the luciferin-binding protein correlates with the binding of a protein to the 3′ untranslated region of its mRNA. Proc. Natl. Acad. Sci. USA *91*, 5257–5261 (1994)

Mittag, M., Li, L. M., and Hastings, J. W.: The mRNA level of the circadian regulated *Gonyaulax* luciferase remains constant over the cycle. Chronobiol. Int. *15*, 93–98 (1998)

Mittag, M., and Waltenberger, H.: *In vitro* mutagenesis of binding site elements of the clock-controlled proteins CCTR and Chlamy 1. Biol. Chem. *378*, 1167–1170 (1997)

Morse, D., Milos, P. M., Roux, E., and Hastings, J. W.: Circadian regulation of the synthesis of substrate binding protein in the *Gonyaulax* bioluminescent system involves translational control. Proc. Natl. Acad. Sci. USA *86*, 172–176 (1989 a)

Morse, D., and Mittag, M.: Dinoflagellate luciferin-binding protein. Methods in Enzymol. *305*, 258–276 (2000)

Morse, D., Pappenheimer, A. M., and Hastings, J. W.: Role of the luciferin-binding protein in the circadian bioluminescent reaction of *Gonyaulax polyedra*. J. Biol. Chem. *264*, 11822–11826 (1989 b)

Nicolas, M.-T., Nicolas, G., Johnson, C. H., Bassot, J.-M., and Hastings, J. W.: Characterization of the bioluminescent organelles in *Gonyaulax polyedra* (dinoflagellates) after fast-freeze fixation and antiluciferase immunogold staining. J. Cell Biol. *105*, 723–735 (1987)

Nikaido, S. S., and Johnson, C. H.: Daily and circadian variation in survival from ultraviolet radiation in *Chlamydomonas reinhardtii*. Photochem. Photobiol. *71*, 758–765 (2000)

Pain, V. M.: Initiation of protein synthesis in eukaryotic cells. Eur. J. Biochem. *236*, 747–771 (1996)

Pajuelo, E., Pajuelo, P., Clemente, M. T., and Marquez, J.: Regulation of the expression of ferredoxin-nitrite reductase in synchronous cultures of *Chlamydomonas reinhardtii*. Biochim. Biophys. Acta *1249*, 72–78 (1995)

Piechulla, B.: Circadian expression of the light-harvesting complex protein genes in plants. Chronobiol. Int. *16*, 115–128 (1999)

Roenneberg, T.: The complex circadian system of *Gonyaulax polyedra*. Physiol. Plant. *96*, 733–737 (1996)

Roenneberg, T., and Hastings, J. W.: Are the effects of light on the phase and period of the *Gonyaulax* clock mediated by different pathways? Photochem. Photobiol. *53*, 525–533 (1991)

Roenneberg, T., and Hastings, J. W.: Cell movement and pattern formation in *Gonyaulax polyedra*. In: Rensing, L. (Ed.): Oscillations and Morphogenesis; pp. 399–412. New York: Marcel Dekker 1992

Roenneberg, T., and Mittag, M.: The circadian program of algae. Semin. Cell Devel. Biol. *7*, 753–763 (1996)

Roenneberg, T., and Morse, D.: Two circadian oscillators in one cell. Nature *362*, 362–364 (1993)

Roenneberg, T., and Rehman, J.: Nitrate, a nonphotic signal for thecircadian system. FASEB *86*, 1443–1447 (1996)

Salvador, M. L., Klein, U., and Bogorad, L.: Light-regulated and endogeneous fluctuations of chloroplast transcript levels in *Chlamydomonas*. Regulation by transcription and RNA degradation. Plant J. *3*, 213–219 (1993)

Salvador, M. L., Klein, U., and Bogorad, L.: Endogenous fluctuations of DNA topology in the chloroplast of *Chlamydomonas reinhardtii*. Mol. Cell. Biol. *18*, 7235–7242 (1998)

Savard, F., Richard, C., and Guertin, M.: The *Chlamydomonas reinhardtii* LI818 gene represents a distant relative of the cab I/II genes that is regulated during the cell cycle and in response to illumination. Plant Mol. Biol. *32*, 461–473 (1996)

Schmitter, R. E., Njus, D., Sulzman, F. M., Gooch, V. D., and Hastings, J. W.: Dinoflagellate bioluminescence: a comparative study of *in vitro* components. J. Cell. Physiol. *87*, 123–134 (1976)

Straley, S. C., and Bruce, V. G.: Stickiness to glass: circadian changes in the cell surface of *Chlamydomonas reinhardtii*. Plant Physiol. *63*, 1175–1181 (1979)

Waltenberger, H., Schneid, C., Grosch, J. O., Bareiss, A., and Mittag, M.: Identification of target mRNAs from *C. reinhardtii* for the clock-controlled RNA-binding protein Chlamy 1. Mol. Genet. Genomics *265*, 180–188 (2001)

Welsh, D. K., Logothetis, D. E., Meister, M., and Reppert, S. M.: Individual neurons dissociated from rat suprachiasmatic nucleus express independently phased circadian firing rhythms. Neuron *14*, 697–706 (1995)

Prof. Dr. Maria Mittag
Institut für Allgemeine Botanik
Friedrich-Schiller-Universität-Jena
Am Planetarium 1
07743 Jena
Germany
Phone: ++49 (0) 1 36 41 94 92 01
Fax: ++49 (0) 1 36 41 94 92 02
E-Mail: M.Mittag@uni-jena.de

Nova Acta Leopoldina NF *88*, Nr. 332, 353–366 (2003)

De-novo Formation of the *Hydra* Head Organizer

Ulrich TECHNAU[1], Bert HOBMAYER[1,2], Fabian RENTZSCH[1,3], and Thomas W. HOLSTEIN[1]

With 6 Figures

Abstract

Signaling centers or organizers play a pivotal role in the formation of body axes in multicellular animals. In vertebrates, organizers secrete growth factors, which act as short- and long-range morphogens in axis formation and cell differentiation. We studied the evolutionary origin of organizers and identified the Wnt/Wg[4] and TGF*β*/Bmp signaling pathways in *Hydra*, a member of the primitive animal phylum Cnidaria. Molecules of the Wnt/Wg pathway and the TGF*β*/Bmp antagonist Chordin are expressed in the *Hydra* head organizer. These molecules act during *de-novo* formation of the head organizer in aggregates as well. In suspensions of dissociated single cells, such organizers arise by a community effect and form small clusters of 5–15 cells that express the conserved *HyWnt* and *HyBra1* genes. They act as local sources that instruct and recruit, i. e., activate the surrounding cells and generate a field of lateral inhibition that ranges up to 1000 µm. We propose that the highly conserved patterning systems in higher animals originated from extremely robust and flexible molecular self-organizing systems using Wnt and TGF*β*/Bmp signaling in the earliest multicellular animals.

1 Zoologisches Institut, Technische Universität Darmstadt, Schnittspahnstraße 10, 64287 Darmstadt, Germany.
2 Zoologisches Institut, Universität Innsbruck, Technikerstraße 25, 6020 Innsbruck, Austria.
3 MPI für Immunbiologie, Stübeweg 51, 79108 Freiburg, Germany.

4 Wnt/Wg: Wnts/Wg proteins comprise a family of cysteine-rich glycoproteins. Name comes from fusing the name of the *Drosophila* segment polarity gene *wingless* (*wg*) with the name of the first of its vertebrate homolog genes *integrated-1* (*int-1*), which is activated by the Mouse Mammary Tumour Virus (MMTV). TGF-*β*/Bmp: TGF-*β* super family includes the transforming growth factor beta family (TGF-*β*), the Activin family, the Bone morphogenesis proteins (Bmp), Nodal, and other proteins. In *Drosophila*, the gene *decapentaplegic* (*dpp*) is homologous to the vertebrate *bmp-4* gene. Sog/Chordin: The *Drosophila* protein Short gastrulation (Sog) and the homologous vertebrate protein Chordin are cysteine rich extracellular antagonists of Bmp-4/Dpp proteins. GFP: Green fluorescent protein from *Cyanea* (Cnidaria). Tld: The metalloprotease Tolloid (Tld) cleaves Sog/Chordin to free Dpp/Bmps. Bra: Transcription factor Brachyury (Bra) was named after a mouse mutant exhibiting reduced posterior structures (gr. short tail). Dsh, Frz: Dishevelled (Dsh) and Frizzled (Frz) are members of the canonical Wt/Wg pathway; they are encoded by genes, which were named after mutants of *Drosophila* wing development. GSK3: Glycogen synthase protein kinase (GSK3) is a member of the canonical wnt/wg pathway phosphorylating *β*-Catenin. Tcf/Lef: The transcription factor Tcf (T cell factor) or Lef (Lymphoid enhancer factor) interacts with *β*-Catenin and induces down stream target genes. Smad: The Smad family of transcription factors was named by combining the names of the first identified members of the family, i.e. the *Caenorhabditis* Sma protein and the *Drosophila* Mad (Mothers against decapentaplegic) protein.

Zusammenfassung

Signalzentren spielen eine zentrale Rolle in der Achsenbildung multizellulärer Tiere. Bei Vertebraten werden vom Organisator Wachstumsfaktoren abgegeben, die als kurz- und langreichweitige Morphogene die Achsenbildung und Zelldifferenzierung steuern. Wir studieren den evolutionären Ursprung des Organisators und haben bei *Hydra* den Wnt/Wg- und TGF-*β*/Bmp-Signalweg identifiziert; *Hydra* ist Vertreter des evolutiv ursprünglichen Tierstamms der Cnidaria. Moleküle des Wnt/Wg-Signalweg und der TGF-*β*/Bmp-Antagonist Chordin werden im Kopforganisator von *Hydra* exprimiert. Diese Moleküle sind auch in der *De-novo*-Musterbildung des Kopforganisators aus Aggregaten dissoziierter Zellen aktiv. In solchen Suspensionen dissoziierter Zellen entstehen Kopforganisatoren durch einen *community effect* und bilden kleine Cluster aus 5–15 Zellen, die Wnt- und Brachyury-Gene exprimieren. Diese Cluster agieren als lokale Quellen, die Zellen der Umgebung instruieren und zugleich ein Feld lateraler Inhibition mit einer Reichweite von bis zu 1000 µm erzeugen können. Wir gehen davon aus, daß das hoch konservierte Musterbildungssystem höherer Tiere aus einem extrem robusten und flexiblen molekularen Selbstorganisationssystem entstanden ist, wie es von den frühesten multizellulären, tierischen Organismen erfunden wurde.

1. The *Hydra* Head Organizer

Organizer tissues play a pivotal role during early embryonic development and provide positional cues for the definition of the main body axes. They represent distinct areas of an embryo that can instruct and recruit the surrounding tissue to contribute to the formation of a particular structure. The best-studied example of such an organizer tissue is the dorsal lip of the frog embryo, which can induce a secondary body axis when grafted to the ventral side of the embryo (Spemann and Mangold 1924). The discovery that the same set of genes is active in the organizer of all vertebrates further suggested that basic features of the organizer might be conserved (for review see Harland and Gerhart 1997). However, it was unclear when and how the organizer and its molecular composition did arise during animal evolution (Knoll and Caroll 1999).

Organizers are not restricted to vertebrates. In the freshwater polyp *Hydra,* Ethel Browne (1909) showed in the laboratory of Thomas Morgan that a small piece of tissue from the hypostome, the most apical tip of the animal, is able to induce a secondary body axis, when grafted laterally to another polyp (Fig. 1). The hypostome of a *Hydra* is therefore the equivalent of the Spemann organizer in amphibians (see also Broun and Bode 2002).

Hydra is a member of the diploblastic Cnidarians, which belong to the simplest living metazoans. Cnidarians evolved about 700 million years ago and represent the first animals with defined body axis and a nervous system. The fact that *Hydra's* head tissue exhibits a strong axis inducing capacity suggests that organizers are a basic feature of all metazoans, which evolved very early during metazoan evolution. Since *Hydra's* body plan can also be completely re-established from dissociated and re-aggregated single cells, organizers can be set up *de novo*, i. e. by self-organization in a tissue without inherent asymmetry or external cues.

2. Molecules of the Head Organizer

Several transcription factors, e. g., the fork head homolog *budhead* (Martinez et al. 1997), the homeobox gene *goosecoid* (Broun et al. 2000), and the T-box gene *brachyury* (Technau and Bode 1999), that play a role in the organizer of vertebrates, have

Fig. 1 The *Hydra* organizer experiment of Ethel BROWNE. Hypostomal tissue of an aposymbiontic strain of *Hydra viridissima* was transplanted to the body column of a green *Hydra* (*Hydra viridissima*). The small piece of grafted tissue (*white*) induced the formation tentacles and an intact body axis in the host (*green*). From BROWNE (1909).

been isolated from *Hydra*, and all of them are also expressed in the organizer region in *Hydra* (for review see GALLIOT 2000). This indicated that also the two major signaling systems of the vertebrate organizer that act as diffusible morphogens, i. e. the Wnt and the BMP4/7 pathway (for review see DEROBERTIS and SASAI 1996, DEROBERTIS and BOUWMEESTER 2001), might be present in the *Hydra* head organizer.

The key components of the Wnt-signaling pathway, i. e. the Wnt ligand (*HyWnt*), its cytoplasmic mediators Dishevelled (*HyDsh*), GSK3 (*HyGSK3*), and *β*-Catenin (*Hyβ-Cat*) together with its transcriptional co-activator Tcf (*HyTcf*), were cloned by HOBMAYER et al. (2000). A *Hydra* member of the family of Frizzled receptors was published by MINOBE et al. (2000).

In-situ hybridization revealed that Wnt signaling acts in the head organizer of *Hydra*. *HyWnt* is expressed in a small number of about 50 epithelial cells at the apical tip of the hypostome which might represent the *Hydra* head organizer. *HyTcf* expression is also restricted to the hypostome of the polyp, but the *HyTcf* expression domain is broader than the *HyWnt* spot comprising the entire hypostome, and thereby possibly demarcates the range of action of the HyWnt ligand (HOBMAYER et al. 2000). In the budding zone, where the new body axis of the daughter polyp is initiated (OTTO and CAMPBELL 1977), activation of the HyWnt pathway starts with an up-regulation of *Hyβ-Cat* and *HyTcf*, and

is followed by *HyWnt* expression in a spot of 10–15 cells (Fig. 2). Thus, the members of the Wnt-pathway play a pivotal role in setting up the *Hydra* head organizer during normal development.

The second major signaling system involved in early embryonic axis formation of vertebrates, i. e. the TGF*β*/Bmp-signaling pathway and its antagonist Chordin (Chd*)*, is also present in cnidarians (SAMUEL et al. 2001, LELONG et al. 2001, HOBMAYER et al. 2001). In *Hydra*, a Bmp ligand (REINHARDT and BODE, personal communication), a highly conserved receptor-regulated Smad1 homologue (HOBMAYER et al. 2001), and the Bmp antagonist Chordin (our unpublished results) were found. *In-situ* hybridizations of *HySmad1* and *Chordin* mRNA are consistent with the hypothesis that Bmp signaling is suppressed by Chordin in *Hydra* tissues exhibiting a high morphogenetic activity, which would explain a similar function in higher metazoans (for review see DEROBERTIS and BOUWMEESTER 2001, SHILO 2001).

These data demonstrate that a core Wnt-signaling pathway as well as the TGF*β*/Bmp-signaling pathway and its antagonist Chordin are present in *Hydra*. Wnt and TGF*β* signaling clearly existed in the common ancestor of diploblastic cnidarians and the triploblastic Bilateria and hence most likely were a basic feature of early multicellular animals.

3. A Reaction-Diffusion Model of the *Hydra* Head Organizer

On the theoretical level, pattern formation and positional signaling in *Hydra* (WOLPERT et al. 1972) was explained in terms of a reaction-diffusion model by GIERER and MEINHARDT

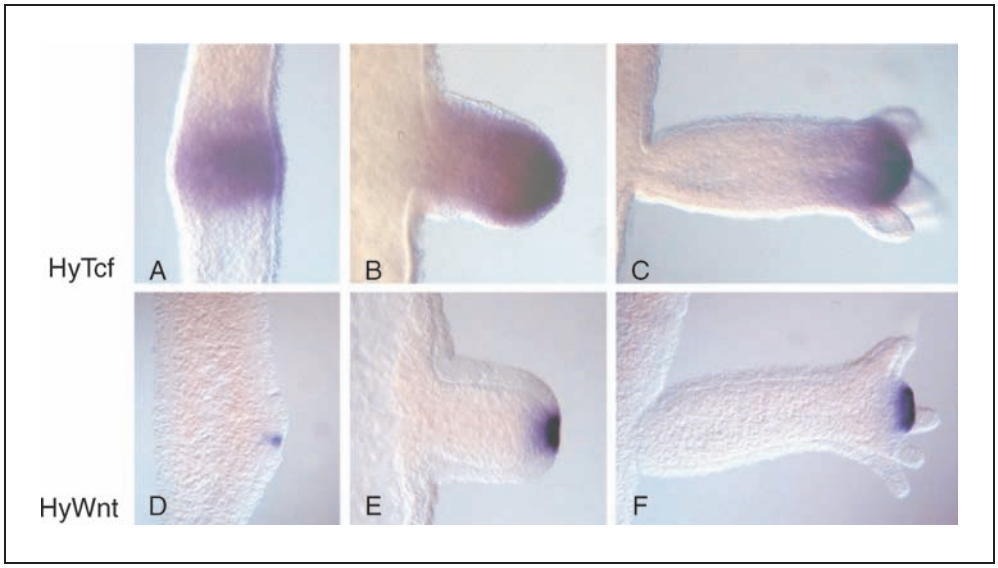

Fig. 2 Expression of *HyTcf* (*A–C*) and *HyWnt* (*D–F*) during bud formation in *Hydra*. Whole mount *in-situ* hybridizations show that the formation of a new bud starts with a broad expression domain of *HyTcf* (*A*); within this domain *HyWnt* is initially expressed in a group of only 15–50 cells (*D*) defining the head organizer region at the tips of an evaginating bud. At later stages the *HyWnt* expression enlarges (*E–F*), while the broad *HyTcf* expression domain becomes restricted to the hypostomal region (*B–C*). (*A–F* from HOBMAYER et al 2000, © Nature Publishing Group, 2000)

(1972). According to this model, a short range activator and a long range inhibitor form a feed-back loop which leads to a local activation of the tissue destined to form a head and a lateral inhibition of further activating centers in the vicinity. It was postulated that both, activator and inhibitor are produced in the head and transmitted to the body column (Gierer and Meinhardt 1972, Meinhardt 1982, Meinhardt 1993, MacWilliams

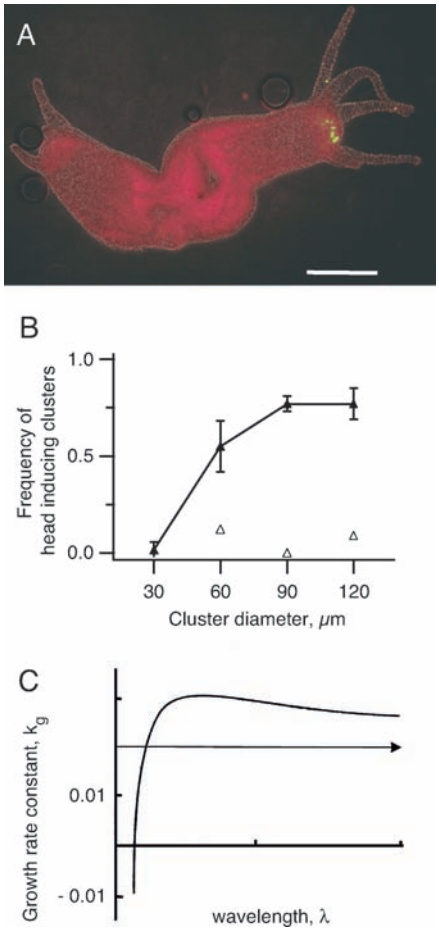

Fig. 3 Head induction by activated cell clusters. (*A*) A two-headed aggregate (96 h) with a head containing a 60 µm cluster of aggregated, green-labeled cells from dissociated 12 h regenerating tip tissue. Bar is 200 µm. (*B*) Efficiency of cell clusters to induce head formation. Head formation frequency of single cells (30 µm) and different cell cluster sizes were scored 80 h after aggregation in carrier tissue derived from the gastric region (*filled symbols*); control clusters were derived from corresponding carrier tissue (*open symbols*). (*C*) A model of Harrison (1993) predicts that in a reaction-diffusion system, which consists of an initial mixture of different wavelengths (λ), one wavelength exists that will be optimally amplified (growth rate k_g). This wavelength is determined by the ratio of activator and inhibitor. (*A–B* from Proc. Nat. Acad. Sci. USA *97*, 12127–12131; © PNAS, 2000)

1982, 1983 a, b). The "head activation gradient" (also termed "source density gradient"; MEINHARDT 1993) maintains axial differentiation and can be measured as a gradient of head formation capacity in transplantation experiments (MACWILLIAMS 1983 b).

The head inhibition gradient prevents head formation in the body column and can also be measured in transplantation experiments (MACWILLIAMS 1983 a). This model can explain organizer formation during reaggregation. After dissociation into a single cell suspension and subsequent reaggregation, all existing gradients of the polyp are destroyed and have to be re-established (GIERER et al. 1972, TECHNAU and HOLSTEIN 1992). Aggregates are therefore an ideal experimental model system to study self-organization. The theoretical model assumes that random fluctuations in the activation level in the aggregate can lead to an amplification of small local peaks resulting in the definition of a new head organizer.

4. The Minimal Size of the *Hydra* Head Organizer

One of the basic questions in the theory of self-organization is, what is the minimal size of such random fluctuations in order to act as an organizer, or in other terms, what is the minimal size of an organizer. To address this question, we modified the classical approach of dissociation and reaggregation by adding clusters of different numbers of fluorescently labeled cells with an elevated level of head activation to an aggregate. The labeled cell clusters were produced from regenerating tips, which have a maximum competence for head induction (MACWILLIAMS, 1983 b). The tips were dissociated into single cells, aggregated in rotary culture, and the resulting cell clusters were fractionated by size (TECHNAU et al. 2000). When small, labeled cell clusters consisting of 10–15 cells (60–120 µm in diameter) were added to the carrier cell suspension, about half of them were found in a developing head (Fig. 3 *A*, *B*). Since the clusters contained only 0.2–4 % of the cells in an aggregate, the high frequency of labeled cell clusters in developing heads was not random indicating that they are involved in head induction. Indeed, the clusters remained confined to the hypostome while the tentacles were formed by host tissue. This shows that a cluster had instructed and recruited surrounding host tissue to the formation of a new head, which is the definition of an organizer *sensu strictu*. Single cells or very small clusters (30 µm in diameter) consisting of one or few epithelial cells have virtually no elevated capacity of induction, while clusters of about 90 µm diameter containing about 50 epithelial cells show maximum inductive capacity (Fig. 3 *B*). Thus, a minimal number of 10–15 cells are necessary and sufficient to act as a head organizer. These data suggest that a "community effect" (GURDON et al. 1993) between these cells is essential to create a stable signaling centre.

5. The Activation Range of the *Hydra* Head Organizer

Besides the minimal organizer size, another crucial parameter in self-organization models is the activation range. Simulations using the reaction-diffusion model of GIERER and MEINHARDT (1972) show that only cluster sizes that are similar to or larger than the activator range will amplify and form stable signaling centers (Fig. 4 *A–B*). Clusters that

are smaller than the activator range will not be amplified since they lose activator too rapidly to the environment by diffusion (Fig. 4 *C*).

We deduced the range of activation from our aggregation experiments (TECHNAU et al. 2000). Based on the experiment shown in Figure 3 *B* one can estimate that the range

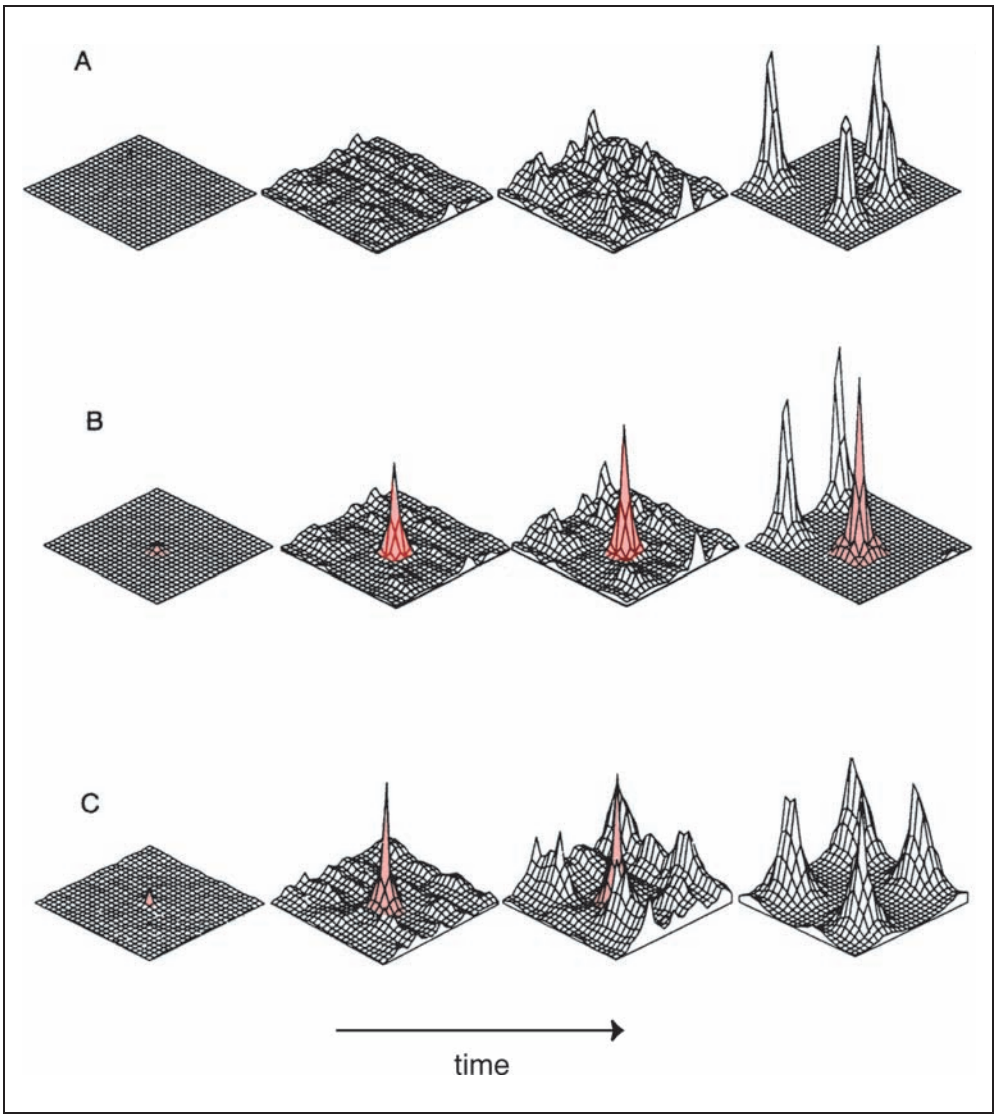

Fig. 4 Computer simulation of head formation in aggregates using the Gierer-Meinhardt model (1972). (*A*) Simulation starts from randomly fluctuating conditions and leads to the formation of four stable head organizers (heads). (*B*) Introduction of a cluster of labeled activated cells (red) with a diameter similar too, or larger than the activator range will amplify and form stable signaling centers. (*C*) Clusters that are smaller than the activator range (red) will be only transiently amplified, since they lose activator too rapidly to the environment by diffusion.

of activation is probably not much larger than the radius of a 90 µm cluster. Larger cluster sizes (120 µm) had no further advantage in inducing heads. This fact can be explained by a prediction made by the model (HARRISON 1993). In a reaction diffusion system, the ratio of activator and inhibitor determines the wavelength (λ) of a chemical diffusion wave. Starting from an initial mixture of different wavelengths (λ), only one wavelength exists that will be optimally amplified (Fig. 3 *C*). This optimal wavelength corresponds to the activator range and determines the optimal cluster size in our aggregation experiments. Since 90 µm clusters exhibited a maximum of activation (Fig. 3 *B*), we conclude that the radius of these clusters corresponds to the activation range of the *Hydra* head organizer. Thus, the activation range measures about 45 µm or 2–3 epithelial cell diameters.

The fact that an activation range of about 45 µm is necessary and sufficient to stable amplify an organizer is consistent with the estimated diffusion range of known morphogens, i. e. Wnt/Wingless in *Drosophila* (GURDON and BOURILLOT 2001). It also indicates that diffusible morphogens like Wnt play an instructive role in the activation process, and we therefore examined the expression pattern of *HyWnt* in early reaggregates. *HyWnt* is first expressed in small spots comprising only a few epithelial cells (Fig. 5) by 24 h. At this time cells have completely sorted out into ectodermal and endodermal layers (GIERER et al. 1972, TECHNAU and HOLSTEIN 1992), indicating that *HyWnt* activation requires an intact epithelial tissue. By 96 h, the *HyWnt* expression domains have enlarged to their final size in future hypostomes (Fig. 5). The size of early *HyWnt* spots is 50–60 µm, which corresponds to the minimal cluster-size that can act as an organizer (see Fig. 3 *B*), while late *HyWnt* domains are similar in size (150–200 µm) to the large clusters, which can induce a head.

6. An Autocatalytic Feedback Control of the Wnt Pathway in the *Hydra* Head Organizer?

An essential element of the reaction-diffusion model is the autocatalytic feed-back loop during the activation process. Preliminary data allow us to propose a feedback control on the HyWnt pathway (see also scheme in Fig. 5). First, HyWnt might activate and stabilize its own expression directly *via* its transcriptional mediators Hy*β*-Cat and HyTcf. During reaggregation, *Hyβ-Cat* and *HyTcf* are expressed uniformly throughout the aggregate and later become restricted to domains where new heads are being formed. Notably, the expression of *HyWnt* always preceded the apparent restriction of domains in the initially symmetrical environment of an aggregate, and all *HyWnt* domains finally form a head (TECHNAU et al. 2000). Of course, subtle differences in the expression level of *HyTcf* and *Hyβ-Cat*, not detectable by the *in-situ* hybridization method, might possibly define the *HyWnt* spots, which in turn enhance up-regulation of *HyTcf* and *Hyβ-Cat* in the surrounding tissue. Alternatively, an ubiquitous, but high level of HyTcf and Hy*β*-Cat might provide a competence to the cells to produce HyWnt. The activation of *HyWnt*, however, might be a stochastic process, which is initiated in single cells, but only maintained if by chance neighboring cells also express *HyWnt*. Both scenarios are consistent with the idea of an autocatalytic feedback loop and that *HyWnt* is a direct target gene of an active Hy*β*-Cat/HyTcf complex. In *Drosophila*, autocatalytic self-activation of Wg

(the *Drosophila* Wnt1 homologue) and a functional Tcf-binding site in the *Wg* promoter have been demonstrated (VAN DE WETERING et al. 1997, LESSING and NUSSE 1998).

We have additional evidence that *HyWnt* might also be positively coupled with another early head gene, *HyBra1*, a *Hydra* homologue of the T-box gene *Brachyury* (TECHNAU and BODE 1999). In aggregates, size and time of appearance of small *HyBra1*-positive spots are equivalent to the *HyWnt* expression dynamics. Interestingly, *HyBra1* also shows synexpression with *HyWnt* during budding and head regeneration as well as in adult polyps, although the *HyBra1*-positive domain in the steady state hypostome is broader than the *HyWnt*-positive domain (TECHNAU and BODE 1999). A putative Tcf-binding site has been recently identified in the *HyBra1* promoter (TECHNAU, unpublished data), which supports the idea that *Brachyury* and *Wnt* are members of a synex-

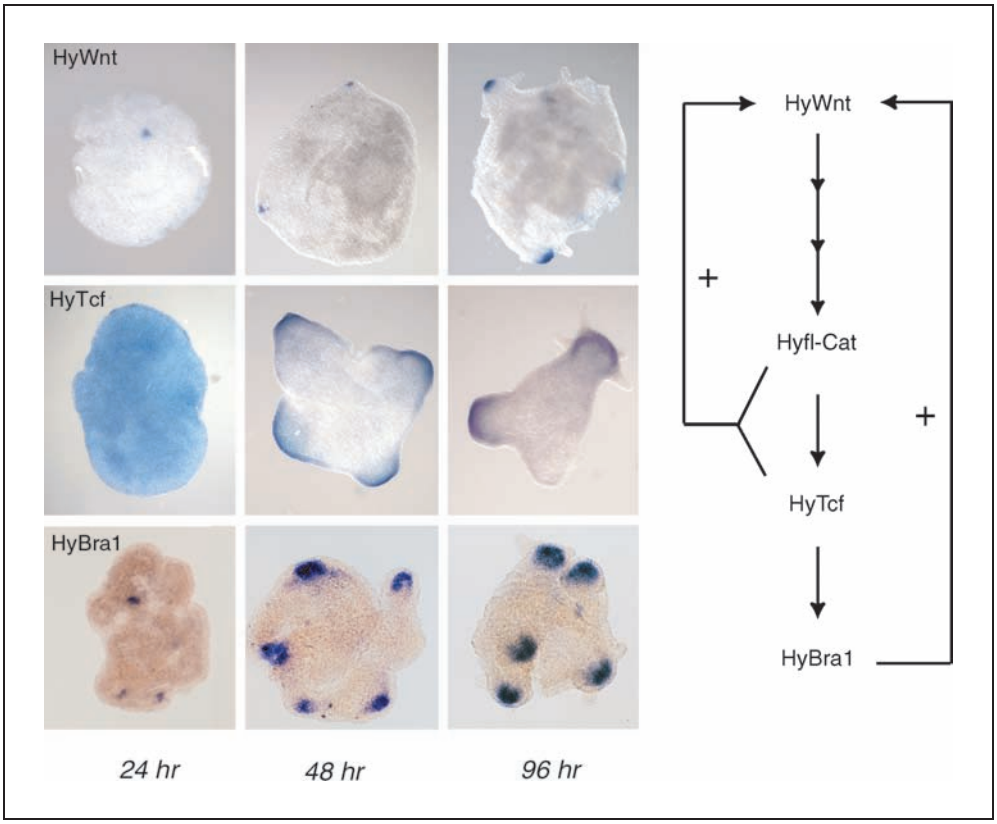

Fig. 5 Expression dynamics of *HyTcf*, *HyWnt*, and *HyBra1* during aggregate development. *In-situ* hybridization reveals patterning events during head organizer formation. *HyWn*t and *HyBra1* appear simultaneously in small spots (24 h), which enlarge during later stages (96 h), and precede formation of morphological head structures by about 2–3 days. All spots eventually develop into heads. (From Proc. Natl. Acad. Sci. USA *97*, 12127–12131, and Nature *407*, 186–189; © Nature Publishing Group, 2000; © PNAS, 2000). The scheme shows the putative positive feedback in *Hydra* Wnt signaling. Preliminary evidence and comparison with higher metazoans support the view that direct, autocatalytic self-activation and indirect feedback between HyWnt and the transcription factor HyBra1 are involved in establishment and maintenance of HyWnt signaling.

pression group in *Hydra*. In mouse embryos and mouse cell lines, *Brachyury* is a direct target gene of Wnt3a signaling (Liu et al. 1999, Galceran et al. 2001), and *Brachyury* itself again activates transcription of *Wnt11* in *Xenopus* (Tada and Smith 2000). Direct experimental proof for such a feedback loop in *Hydra* would be of particular importance.

7. Long-Range Inhibition from the Head Organizer

The second major component in the reaction-diffusion mechanism is the inhibitor which is produced by the activation center and transmitted to the surrounding tissue to prevent the initiation of another activation center (Gierer and Meinhardt 1972). We estimated the range of inhibition in a competition experiment by introducing cell clusters of different size into an aggregate (Technau et al. 2000) where larger cell clusters (120 μm) exerted an inhibitory influence on the smaller clusters (60 μm) (Fig. 6*A–B*). By measuring the distance of small clusters from the nearest head the range of inhibition could be estimated. About 50% of the small clusters were not involved in head formation at a distance of 600 μm, while essentially all of them were in heads at 1000 μm (Fig. 6*C*). This indicates an effective range of inhibition of about 800–900 μm. By comparison, the range of activation as deduced from the size of cell clusters able to induce head formation was about 45 μm, which is easily 20× shorter. These results are in good accord with previous calculations based on the reaction-diffusion model by Gierer and Meinhardt (1972) and on MacWilliams' proportion-regulating version of the model (MacWilliams 1983 a, b) predicting a 15 fold and >20 fold shorter activation range, respectively.

An important prediction of the Gierer and Meinhardt model is that a rise of inhibition is tightly linked to the rise of activation, which should result in an equal spacing of the activation centers in an aggregate, independent of the average head activation level in the aggregate. We found, however, that aggregates from apical tissue (with a high average head activation level) not only formed more heads than aggregates derived from basal tissue (with a low average head activation level), but the spacing of heads formed in apical tissue was also highly irregular. In case that the rise of lateral inhibition would be tightly linked to the rise of activation, the spacing between heads should be always quite regular. Thus, the kinetics of inhibition and activation increase is less tightly linked than previously postulated (Gierer and Meinhardt 1972). This feature allows pattern formation to occur in a broad range of initial conditions (MacWilliams 1991, Technau et al. 2000), and adds a further level of robustness to the system.

The inhibition gradient ensures the size control over a given morphogenetic field. This size control seems to be a general feature in many embryos of higher metazoans that is not well understood. It is also far from clear how inhibition is mediated on the molecular level in *Hydra*. Based on preliminary evidence in higher metazoans, there are two alternative possibilities:

(*i*) Inhibition could be exerted by molecules, which are also involved in growth control, e. g. the insulin pathway (Böhni et al. 1999) or nitric oxide (Kuzin et al. 1996). Mutations in the insulin pathway have been shown to cause a size reduction of the imaginal discs in *Drosophila*, and ectopic NO synthetase (Nos) expression decreases the size of imaginal discs, while inhibition of Nos can increase the leg size in the

dorso-ventral and anterior-posterior axes (KUZIN et al. 1996). NO can rapidly diffuse between the cells, and it could be related to changes in the pattern of rapidly cycling cells during head regeneration and budding (HOLSTEIN et al. 1991).

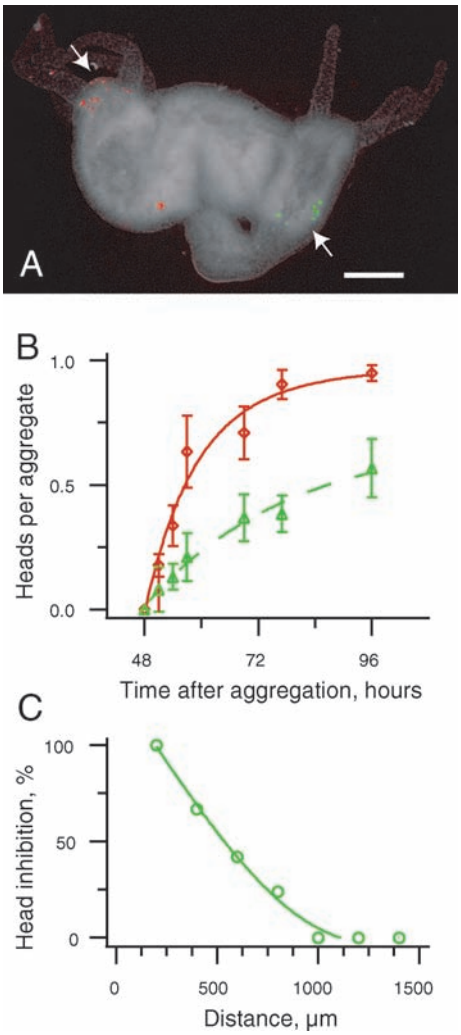

Fig. 6 Effect of head inhibition in aggregates. Aggregates contained competing 120 µm and 60 µm cell clusters in a single aggregate. (*A*) A 120 µm cell cluster (*red*) inhibited the formation of another head from the 60 µm cell cluster (*green*, *arrow*); bar is 200 µm. (*B*) Time course of head induction by the 120 µm cell cluster (*red*) and the 60 µm cell cluster (*green*) when competing in a single aggregate (means ± SEM, $P < 0.001$, n = 42–53). (*C*) Correlation of head formation frequency of 60 µm cell clusters with their distance from the nearest head is shown. The percentage of inhibited cell clusters for a given distance to the next head was calculated (n = 77). (*A–C* from Proc. Natl. Acad. Sci. USA *97*, 12127–12131; © PNAS, 2000)

(*ii*) An alternative explanation for the inhibition gradient could be that its formation is correlated to a more complex interaction of known morphogens with antagonistic factors. The two systems in which size control and morphogen gradients have been extensively studied are the *Drosophila* wing disc and the amphibian blastula animal cap (Lawrence 2001, Day and Lawrence 2000). Here, members of the transforming growth factor beta (TGF-β)/Bmp proteins act as long-range morphogens (100–300 μm), for which concentration dependent effects have been confirmed (Bourillot et al. 2002, Gurdon and Bourillot 2001). Changes in production of Dpp, the *Drosophila* Bmp homolog, can substantially redesign the *Drosophila* wing, indicating a long-range action. Recent studies using GFP-Dpp constructs suggest, however, a more complex mode of gradient formation including endocytotic trafficking and degradation (Entechev et al. 2000). The antagonistic factor to Dpp/BMP2–4 is Sog/Chordin forming an opposing gradient. In *Xenopus* embryos the Chordin gradient can have a range of at least 450 μm when over expressed, although its *in-vivo* range, which is restricted by the metalloprotease Xolloid, appears to be less far (Blitz et al. 2000). In *Drosophila*, it has recently been shown directly that Sog forms a protein gradient in dorsal cells of the embryo (Srinivasan et al. 2002). On the dorsal side, Tolloid (Tld) degradation and a dynamin-dependent retrieval of Sog act as a dorsal sink for active Sog (Srinivasan et al. 2002). This long-range activity of Sog/Chordin and the related degradation by Tolloid/Xolloid could be an important component of the autocatalytic feed back loops involved in the long-range inhibition phenomena and size control of *Hydra*.

8. Conclusion and Outlook

The Wnt and TGF-β pathways, as well as members of the T-box gene family play a crucial role in the patterning of all higher animals. The data reviewed here indicate that *Hydra*, a representative of one of the oldest metazoan phyla, uses these genes in a signaling centre for regulating the establishment of its major body axis. This strongly indicates the antiquity of this patterning system and points towards an origin of signaling centers in the earliest multicellular animals. These genes have also an important function during *de-novo* pattern formation in reaggregates. Aggregates are able to generate complete structures (whole organisms) starting from a broad range of initial conditions. We therefore propose that during early metazoan evolution an extremely robust and flexible self-organization system involving these molecular interactions was selected for, which became conserved during the evolution of higher animals. It is an attractive hypothesis that the signaling molecules identified here, and their putative feedback control, represent a core network of molecular interactions constituting an organizer which might be conserved throughout metazoan evolution.

References

Blitz I. L., Shimmi O., Wunnenberg-Stapleton K., O'Connor M. B., and Cho K. W.: Is chordin a long-range- or short-range-acting factor? Roles for BMP1-related metalloproteases in chordin and BMP4 autofeedback loop regulation. Dev. Biol. *223*, 120–38 (2000)

Bohni, R., Riesgo-Escovar, J., Oldham, S., Brogiolo, W., Stocker, H., Andruss, B. F., Beckingham, K., and Hafen, A.: Autonomous control of cell and organ size by CHICO, a Drosophila homolog of vertebrate IRS 1–4. Cell *97*, 865–875 (1999)

Broun, M., and Bode, H. R.: Characterization of the head organizer in *Hydra*. Development *129*, 875–884 (2002)

Browne, E.: The production of new *Hydra*nths in *Hydra* by the insertion of small grafts. J. Exp. Zool. *8*, 1–23 (1909)

Day S. J., and Lawrence P. A.: Measuring dimensions: the regulation of size and shape. Development *127*, 2977–2987 (2000)

De Robertis, E. M., and Bouwmeester, T.: New twists on embryonic patterning. EMBO Reports *2*, 661–665 (2001)

De Robertis, E. M., and Sasai, Y.: A common plan for dorsoventral patterning in bilateria. Nature *380*, 37–40 (1996)

Entchev, E. V., Schwabedissen, A., and Gonzalez-Gaitan, M.: Gradient formation of the TGFbeta homolog Dpp. Cell *103*, 981–991 (2000)

Galceran, J., Hsu, S.-C., and Grosschedl, R.: Rescue of a Wnt mutation by an activated form of LEF-1: regulation of maintenance but not initiation of Brachyury expression. Proc. Nat. Acad. Sci. USA *98*, 8668–8673 (2001)

Galliot, B.: Conserved and divergent genes in apex and axis development of cnidarians. Curr. Opin. Genetics and Development *10*, 629–637 (2000)

Gierer, A., Berking, S., Bode, H. R., David, C. N., Flick, K., Hansmann, G., Schaller, H., and Trenkner, E.: Regeneration of *Hydra* from reaggregated cells. Nature New Biol. *239*, 98–101 (1972)

Gierer, A., and Meinhardt, H.: A theory of biological pattern formation. Kybernetik *12*, 30–39 (1972)

Gurdon, J. B., and Bourillot, P. Y.: Morphogen gradient interpretation. Nature *413*, 797–803 (2001)

Gurdon, J., Lemaire, P., and Kato, K.: Community effects and related phenomena in development. Cell *75*, 831–834 (1993)

Harland, R., and Gerhart, J.: Formation and function of Spemann's organizer. Annu. Rev. Cell Dev. Biol. *13*, 611–667 (1997)

Harrison, L. G.: Kinetic Theory of Living Pattern. New York: Cambridge University Press 1993

Hobmayer, B., Rentzsch, F., and Holstein, T. W.: Identification and expression of HySmad1, a member of the R-Smad family of TGF-beta signal transducers, in the diploblastic metazoan *Hydra*. Dev. Genes and Evolution *211*, 597–602 (2001)

Hobmayer, B., Rentzsch, F., Kuhn, K., Happel, C. M., Laue, C., Snyder, P., Rothbächer, U., and Holstein, T. W.: Wnt signalling molecules act in axis formation in the diploblastic metazoan *Hydra*. Nature *407*, 186–189 (2000)

Holstein T. W., Hobmayer E., and David C. N.: Pattern of epithelial cell cycling in *Hydra*. Dev. Biol. *148*, 602–611 (1991)

Knoll, A. H., and Carroll, S. B.: Early animal evolution: emerging views from comparative biology and geology. Science *284*, 2129–2137 (1999)

Kuzin, B., Roberts, I., Peunova, N., and Enikolopov, G.: Nitric oxide regulates cell proliferation during *Drosophila* development. Cell *87*, 639–649 (1996)

Lawrence, P. A.: Wingless signalling: more about the Wingless morphogen. Curr. Biol. *11*, R638–639 (2001)

Lelong, C., Mathieu, M., and Favrel, P.: Identification of new bone morphogenetic protein-related members in invertebrates. Biochimie *83*, 423–426 (2001)

Lessing, D., and Nusse, R.: Expression of wingless in the *Drosophila* embryo: a conserved cis-acting element lacking conserved Ci-binding sites is required for patched-mediated repression. Development *125*, 1469–1476 (1998)

Liu, P., Wakamiya, M., Shea, M. J., Albrecht, U., Behringer, R. R., and Bradley, A.: Requirement for Wnt3 in vertebrate axis formation. Nature Genetics *22*, 361–365 (1999)

MacWilliams, H. K.: Numerical simulations of *Hydra* head regeneration using a proportion-regulating version of the Gierer-Meinhardt model. J. Theor. Biol. *99*, 681–703 (1982)

MacWilliams, H. K.: *Hydra* transplantation phenomena and the mechanism of *Hydra* head regeneration. I. Properties of the head inhibition. Dev. Biol. *96*, 217–238 (1983 a)

MacWilliams, H. K.: *Hydra* transplantation phenomena and the mechanism of *Hydra* head regeneration. II. Properties of head activation. Dev. Biol. *96*, 239–257 (1983 b)

MacWilliams, H. K.: Models of pattern formation in *Hydra* and *Dictyostelium*. Semin. Dev. Biol. *2*, 119–128 (1991)

Martinez, D. E., Dirksen, M. L., Bode, P. M., Jamrich, M., Steele, R. E., and Bode, H. R.: Budhead, a fork head/HNF-3 homologue, is expressed during axis formation and head specification in *Hydra*. Dev. Biol. *192*, 523–36 (1997)

Meinhardt, H.: Models of Biological Pattern Formation. London: Academic Press 1982

Meinhardt, H.: A model for pattern formation of hypostome, tentacles, and foot in *Hydra*: how to form structures close to each other, how to form them at a distance. Dev. Biol. *157*, 321–333 (1993)

Minobe, S., Fei, K., Yan, L., Sarras, M. P., and Werle, M. J.: Identification and characterization of the epithelial polarity receptor "Frizzled" in *Hydra vulgaris*. Dev. Genes and Evolution *210*, 258–262 (2000)

Otto, J. J., and Campbell, R. D.: Budding in *Hydra attenuata*: bud stages and fate map. J. Exp. Zool. *200*, 417–428 (1977)

Samuel, G., Miller, D., and Saint, R.: Conservation of a DPP/BMP signalling pathway in the nonbilateral cnidarian *Acropora millepora*. Evolution and Development *3*, 241–250 (2001)

Srinivasan, S., Rashka, K. E., and Bier, E.: Creation of a Sog morphogen gradient in the *Drosophila* embryo. Dev. Cell. *2,* 91–101 (2002)

Shilo, B. Z.: The organizer and beyond. Cell *106*, 17–22 (2001)

Spemann, H., und Mangold, H.: Über die Induktion von Embryonalanlagen durch Implantation artfremder Organisatoren. Arch. mikrosk. Anat. Entwickl. *100*, 599–638 (1924)

Tada, M., and Smith, J. C.: Xwnt11 is a target of *Xenopus* Brachyury: regulation of gastrulation movements via Dishevelled, but not through the canonical Wnt pathway. Development *127*, 2227–2238 (2000)

Technau, U., and Bode, H. R.: HyBra1, a brachyury homologue, acts during head formation in *Hydra*. Development *126*, 999–1010 (1999)

Technau, U., Cramer von Laue, C., Rentzsch, F., Luft, S., Hobmayer, B., Bode, H. R., and Holstein, T. W.: Parameters of self-organisation in *Hydra* aggregates. Proc Nat. Acad. Sci. USA *97*, 12127–12131 (2000)

Technau, U., and Holstein, T. W.: Cell sorting during the regeneration of *Hydra* from reaggregated cells. Dev. Biol. *151*, 117–127 (1992)

van de Wetering, M., Cavallo, R., Dooijes, D., van Beest, M., van Es, J., and Loureiro, J.: Armadillo coactivates transcription driven by the product of the *Drosophila* segment polarity gene dTCF. Cell *88*, 789–799 (1997)

Wolpert, L., Clarke, M. R. B., and Hornbruch, A.: Positional signalling in *Hydra*. Nature New Biol. *239*, 101–105 (1972)

Prof. Dr. Thomas W. Holstein
Technische Universität Darmstadt
Molekulare Zellbiologie
Schnittspahnstraße 10
64287 Darmstadt
Germany
Phone: ++49 (0) 61 51 16 62 48
Fax: ++49 (0) 61 51 16 60 77
E-Mail: holstein@bio.tu-darmstadt.de

Nova Acta Leopoldina NF *88*, Nr. 332, 367–380 (2003)

Imaging and Imagining Spatiotemporal Variations of Photosynthesis on Simple Leaves

Uwe RASCHER (New York)

With 9 Figures

Abstract

Leaves of higher plants are generally considered to act as one physiological unit and photosynthesis is considered to be homogeneously distributed throughout the leaf. Recently this dogma was put into question due to dramatic improvements in CCD camera techniques enabling the development of imaging techniques to quantify photosynthetic efficiency with high resolution using chlorophyll fluorescence. Leaves that were formerly considered homogeneous are now seen as having spatiotemporal variations of photosynthesis. One well investigated example is the crassulacean acid metabolism (CAM) of *Kalanchoë daigremontiana*, which is regarded to be a time-dependent adaptation with a distinct day/night pattern of CO_2 exchange. Its dynamics are expressed as patterns of independently initiated spatial variations in photosynthetic efficiency. Spatiotemporal heterogeneity of photosynthetic efficiency (ϕ_{PSII})[1] governs the subsequent phases of CAM, the different periods of endogenous, circadian rhythm in continuous light and the arrhythmic gas-exchange pattern of CAM. Non-invasive, highly sensitive chlorophyll fluorescence imaging reveals randomly initiated patches of varying ϕ_{PSII} which are propagated within minutes to hours in wave fronts, forming dynamically expanding and contracting clusters and dephased regions of ϕ_{PSII}.

Zusammenfassung

Die Blätter höherer Pflanzen werden im allgemeinen als physiologische Einheiten betrachtet, deren photosynthetische Effizienz gleichmäßig über die Blattfläche verteilt ist. Dieses Dogma wurde erst in den letzten Jahren durch die dramatische Entwicklung moderner CCD-Kamerachips in Frage gestellt. Die hochaufgelöste und nichtdestruktive Messung des Fluoreszenzsignals des Chlorophylls ermöglicht es, die Photosynthese-Effizienz räumlich zu quantifizieren. Hierdurch wurden zahlreiche raum-zeitliche Dynamiken auf Blättern entdeckt, die bisher als homogen betrachtet wurden. Ein gut untersuchtes Beispiel ist der Crassulaceen-Säure-Stoffwechsel (CAM), der eine zeitliche Anpassung der Photosynthese an trockene Standorte darstellt und ein charakteristisches tageszeitliches Muster des CO_2-Gaswechsels zeigt. Blätter der CAM-Pflanze *Kalanchoë daigremontiana* zeigen dynamisch auftretende Muster unterschiedlicher Photosynthese-Effizienz auf einem anatomisch homogenen Blatt. Verschiedene raum-zeitliche Musterbildungsprozesse konnten hierbei während der unterschiedlichen Phasen im Tag- Nachtwechsel, während des endogenen, circadianen Rhythmus und während des arrhythmischen Gaswechsels beobachtet und beschrieben werden. Bildgebende Chlorophyll-Fluoreszenz-Messungen zeigen zufällig auftretende Bereiche ungleichförmiger Photosynthese, die sich zu Wellenfronten formieren können, dynamisch sich ausweitende und zusammenziehende Cluster und eine Phasenentkopplung benachbarter Zellbereiche.

1 ϕPSII: relative quantum efficiency of photosystem II; $\int \phi$PSII: relative quantum efficiency of photosystem II integrated over one leaf; JCO_2: net CO_2 exchange rate [µmol m^{-2} s^{-1}]; PEPCase: phosphoenolpyruvate-carboxylase; Rubisco: ribulose-1,5-bisphosphate-carboxylase-oxygenase.

1. Introduction

1.1 Simple Leaves and Chlorophyll Fluorescence

The understanding of temporal dynamic behavior of biological systems has been in the focus of biomedical research during the last decades. Theories such as non-linear dynamics have revolutionized thinking in physics, biomedical and life sciences research (May 1976, *Editorial* 2000), and nowadays spatiotemporal considerations are advancing our understanding of development, rhythmicity and biological regulation (Rosenblum et al. 1996, Schäfer et al. 1998). Typical examples of spatially extended dynamic systems are the cAMP waves of *Dictyostelium discoideum* (Martiel and Goldbeter 1985), processes of pattern formation during embryogenesis (Grunz 1999, Hudson 2000, Scheres 2000), the fibrillation of the vertebrate heart (Gray et al. 1998), the synchronized activation of brain nerves (Castelo-Branco et al. 2000), or the phase synchronization of spatially extended animal populations (Blasius et al. 1999). However, within plant science those spatiotemporal considerations are rarely found. Plants are not considered to communicate with each other and the single organs are regarded to function as physiological units.

I will focus on green leaves of higher plants in the following communication. Leaves are the organs of photosynthetic activity. Their anatomy has been studied intensively during the last century by various plant anatomists (see e. g. Napp-Zinn 1973). However, most studies investigated the vertical stratification of leaves, and only few studies focused on their horizontal anatomy. Also, plant physiologists seemed to be more interested in the differences in physiology of the different layers of leaves, than in horizontal variations such as base/tip gradients. As a result, photosynthetic efficiency was regarded to be uniformly distributed throughout the leaf.

During the last decade new methods to monitor photosynthesis enabled investigations with high spatial resolution. One of the most powerful methods is based on the monitoring of the fluorescence signal of chlorophyll *a* (Schreiber and Bilger 1993, Schreiber et al. 1995), which allows the quantification of relative quantum efficiency of photosynthesis in a non-destructive manner on healthy, attached leaves (Genty et al. 1989). The fluorescence of chlorophyll *a* of photosystem II is selectively measured just before and during a saturating light pulse (duration: 1 s, intensity: at least 2000 µmol m^{-2} s^{-1}), yielding ground fluorescence (F) and maximum fluorescence (F'_m), respectively. Both values can be used to calculate the quantum efficiency of photosystem II, which will be denoted ϕ_{PSII} in the following: $\phi_{PSII} = (F'_m - F)/F'_m$ (Genty et al. 1989). However, the fluorescence signal is only a fraction of the reflected light. Thus, it is a technical challenge to be able to monitor this signal with fine spatial resolution. Because of the dramatic technical improvements of CCD camera chips during the last decade, quantum efficiency of photosynthesis can now be imaged in space and time using chlorophyll fluorescence techniques.

1.2 Spatial Heterogeneity of Photosynthetic Efficiency

Chlorophyll fluorescence imaging techniques were developed in the late 1980s (Daley et al. 1989), and were applied to monitor the effects of plant pathogens (Balachandran et al.

1994, 1997, LICHTENTHALER et al. 1997), patchy stomatal movements (CARDON et al. 1994, SIEBKE and WEIS 1995 b) and phloem loading and unloading (SIEBKE and WEIS 1995 a). Nowadays, chlorophyll fluorescence imaging is a widely accepted method to monitor the spatial variations of the physiological status of photosynthesis under various conditions (OSMOND et al. 1999, CHAERLE and VAN DER STRAETEN 2001, OSMOND and PARK 2001).

It is not surprising, that the simplified approach to consider one leaf as a physiological unit can no longer be considered sufficient. For example, spatial heterogeneity of photosynthetic activity is shown to occur in optically non-uniform leaves such as variegated *Abutilon striatum* leaves (OSMOND et al. 1998) and in uniform leaves during wilting (OSMOND et al. 1999).

One example in which dynamic, non-anatomy related heterogeneity is visible is that of the endogenous circadian rhythm of crassulacean acid metabolism (CAM), which will be discussed in more detail in the following sections.

1.3 The Endogenous CAM-Rhythm

Crassulacean acid metabolism (CAM) is a specific mechanism of inorganic carbon acquisition during photosynthesis and can be divided into four phases (OSMOND 1978). In phase I nocturnal CO_2 fixation by phosphoenolpyruvate-carboxylase (PEPCase) leads to the formation of malic acid that is removed from the site of its formation in the cytoplasm by active transport to the central cell vacuole. After a transition phase in the early light period (phase II), malic acid is remobilized from the vacuole and decarboxylated. This generates high internal CO_2 concentrations which lead to closure of stomata in the leaf epidermis. The released CO_2 is refixed by ribulose-1,5-bisphosphate-carboxylase-oxygenase (Rubisco) and assimilated *via* the Calvin cycle of photosynthesis (phase III). Finally in the later light period, when malic-acid stores are exhausted, stomata may open, CO_2 may be taken up and assimilated directly *via* Rubisco (phase IV).

In addition to this well known diurnal cycle, the obligatory CAM plant *Kalanchoë daigremontiana* shows an endogenous, circadian rhythm of CO_2 uptake, which may last for several days, under constant external conditions in continuous light (LÜTTGE and BALL 1978, LÜTTGE and BECK 1992) and in continuous darkness and CO_2 free air (WARREN and WILKINS 1961). Stable oscillations in continuous light only persist at intermediate conditions of light intensity and temperature. Above and below thresholds of these parameters rhythmic behavior changes reversibly to non-stochastic arrhythmic behavior (GRAMS et al. 1997). The change between rhythmic and arrhythmic domains may occur in response to very small changes in the control parameters (e. g. within changes of leaf-temperature of less than 1 °C) (LÜTTGE and BECK 1992). From a theoretical point of view the endogenous rhythm can be reproduced by a minimal model that reduces CAM to three metabolic pools, namely internal CO_2 concentration, and cytoplasmic and vacuolar malic acid levels, respectively, connected by several feedback loops that regulate malate influx and efflux of the vacuole (BLASIUS et al. 1997, 1998, 1999, LÜTTGE 2000). Model simulations with spatially arranged individual oscillators (BECK et al. 2001) and observations on the thermal abolition and restoration of the rhythm (RASCHER et al. 1998) led to the hypothesis that spatial decoupling of metabolism dynamics in patches of leaf tissue could underlie the endogenous rhythm.

2. Dynamic Spatial Heterogeneity of Photosynthesis during the Endogenous CAM-Rhythm

2.1 Material and Methods

Plants: Plants of *Kalanchoë daigremontiana* Hamet et Perrier de la Bâthie were raised from adventitious plantlets obtained from leaves of the plant collection of the Botanical Garden, Darmstadt University of Technology. They were grown in soil culture in a glasshouse until they had produced six to seven pairs of fully developed leaves, and were about 0.4 – 0.5 m tall. During winter additional light (HQI-T, 400W, Philips) was provided to extend the daylight period up to 12 h. Prior to the measurements the plants were transferred to a climate-regulated walk-in growth chamber of the phytotron in the University's Botanical Institute, and adapted for at least two days to a controlled 12 h dark and 12 h light period at 21 °C and 28 °C, respectively.

Gas exchange measurements: The measurements of net CO_2 exchange were performed in a climate-regulated chamber of the phytotron, as previously described (Lüttge and Beck 1992, Rascher et al. 1998). Net CO_2 exchange was recorded using the minicuvette system of H. Walz (Effeltrich, Germany). A mature leaf of a plant was enclosed in the gas exchange cuvette while remaining attached to the plant. For a better control of leaf temperature, the thermistor inside the cuvette was carefully attached to the lower side of the leaf. Thus, leaf temperature rather than air temperature was exactly regulated. Gas exchange data were recorded every 5 minutes using a PC and a datalogger program. The relative humidity of the air inside the cuvette was set at $60 \pm 5\,\%$ and was held constant. Irradiance was measured in the range of 400–700 nm using a LICOR quantum sensor. Conditions inside the phytochamber were adapted to conditions inside the gas exchange cuvette. Net CO_2 exchange rate (JCO_2) was calculated according to Farquhar and Sharkey (1982).

Chlorophyll fluorescence imaging: To record the relative quantum yield (ϕ_{PSII}) of photosystem II, a highly sensitive digital-camera system was developed to record fluorescence signal of chlorophyll *a*. The core element is a Peltier cooled digital CCD camera (AP-1, Apogee Instruments Inc., Tucson, USA), which yields intensity images with 14 bit gray resolution on an array of 768×512 pixels. In front of the camera lens a specific cut-off filter (RG655, Fa. Schott, Mainz, Germany) was mounted. The camera was controlled by a PC, images were captured every 20 minutes and transferred to the PC. Light was provided by eight 250W halogen lamps (ENH 120V 250W, Sylvania, Japan), which were mounted in an air-cooled chassis (Dicrolight, Fa. JBSYSTEMS, Germany) and providing a homogeneous illumination over the whole leaf. To selectively measure the fluorescence signal, two filters were mounted in front of the light sources: an infrared cut-off filter (KG-1, Fa. Schott, Mainz, Germany) and a blue-green cut-off filter (No. 9782 4-96 blue-green, Fa Corning Inc., Jamaica, USA). Light intensity was controlled by the personal computer. During the experimental run actinic light intensity was set to different light intensities and held constant. In order to insure a constant light intensity, voltage was stabilized (stabilizer M208L, IREM SpA, Borgone, Italy).

Effective quantum yield of photosynthesis was recorded according to the saturating light pulse method (Genty et al. 1989, Schreiber et al. 1996). A first fluorescence pic-

ture, named 'LOW-picture', was captured during constant light intensity. Subsequently a saturating light pulse (intensity ~ 1500 µmol m^{-2} s^{-1}, duration 1 s) was applied over the whole leaf. At the end of this pulse the second fluorescence picture ('HIGH-picture'), was captured. Relative quantum yield of PSII: ϕ_{PSII} = (HIGH – LOW)/HIGH, was quantified for every pixel of the image, by a computer program (RASCHER 2001).

The values obtained for every pixel were integrated over the leaf in order to obtain the mean value of relative quantum efficiency of a single picture, named $\int \phi_{PSII}$. The maximum $\int \phi_{PSII}$ of a time series was set to 1, all other values of relative quantum efficiency were than scaled to this value. The experimental set-up did not allow to quantify effective quantum yield of PSII numerically, as the system does not operate in a pulsed mode (SCHREIBER et al. 1996). However, within the range of experimental light intensities data obtained by this method were linearly correlated to data measured with the established PAM-measurements (SCHREIBER and BILGER 1993). For a detailed description of the experimental fluorescence set-up see RASCHER (2001).

2.2 Diurnal Day-Night Cycle

The diurnal changes of gas-exchange of *Kalanchoë daigremontiana* show the characteristic CAM pattern with four distinct phases (Fig. 1). Just as the gas-exchange pattern changes with time, $\int \phi_{PSII}$ shows lowest values in the first hour after the onset of light and a distinct drop at the transition from phase III to phase IV (Fig. 1). In addition to these temporal changes, maps of ϕ_{PSII} reveal various patterns of spatial variations

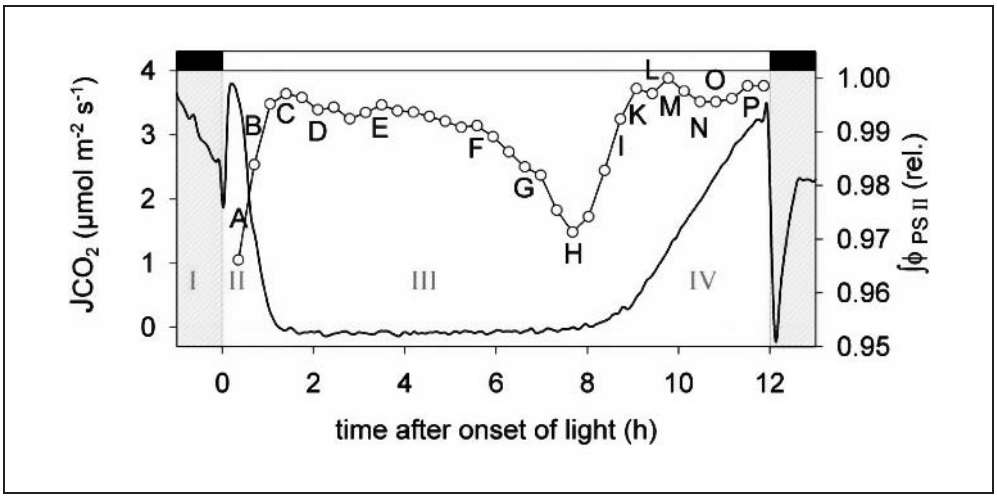

Fig. 1 Light period of the diurnal CAM cycle with net CO_2 exchange rate (JCO_2, ——) and quantum yield of photosynthesis (ϕ_{PSII}, –O–) of an attached leaf of *Kalanchoë daigremontiana* measured simulateneously in a climate-regulated cuvette. $\int \phi_{PSII}$ is obtained by integrating over the leaf area imaged and shown in Fig. 2. Capital letters indicate the time at which maps of Fig. 2 were taken. Experimental conditions were 28 °C and 257 µmol photons m^{-2} s^{-1}; black and white bars indicate dark and light period, respectively. (Data from RASCHER et al. 2001.)

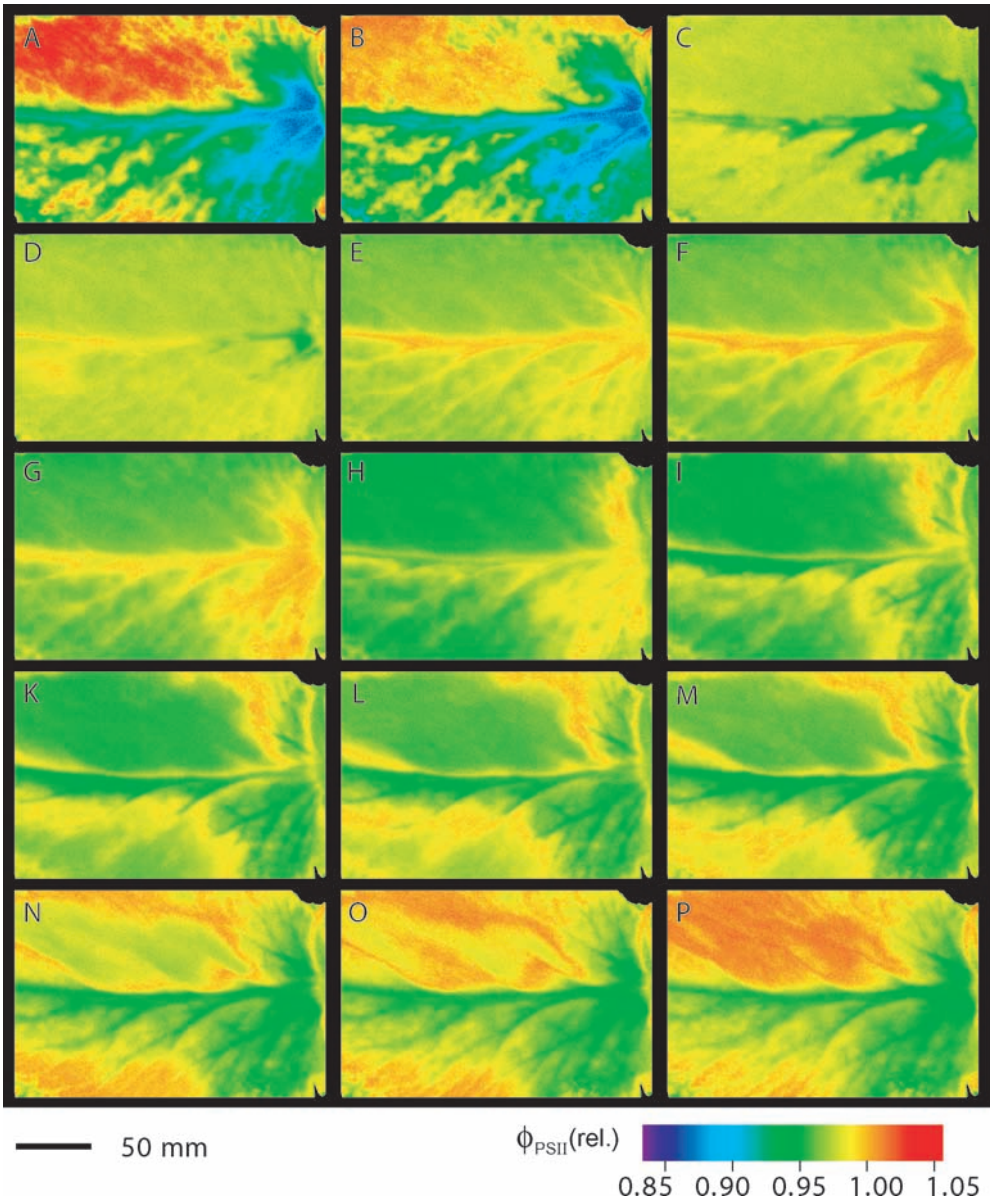

Fig. 2 Spatiotemporal heterogeneity of photosynthetic efficiency (ϕ_{PSII}) in a leaf of *Kalanchoë daigremontiana* during the light period of the diurnal day/night CAM cycle. Maps of ϕ_{PSII} were captured at the times denoted by capital letters in Fig. 1. ϕ_{PSII} was imaged by non-invasive chlorophyll fluorescence measurements at 20-minutes intervals and was normalized to the maximum $\int \phi_{PSII}$ obtained during the experiment, colours code for different efficiency values (see colour code at the lower right). (Data from RASCHER et al. 2001.)

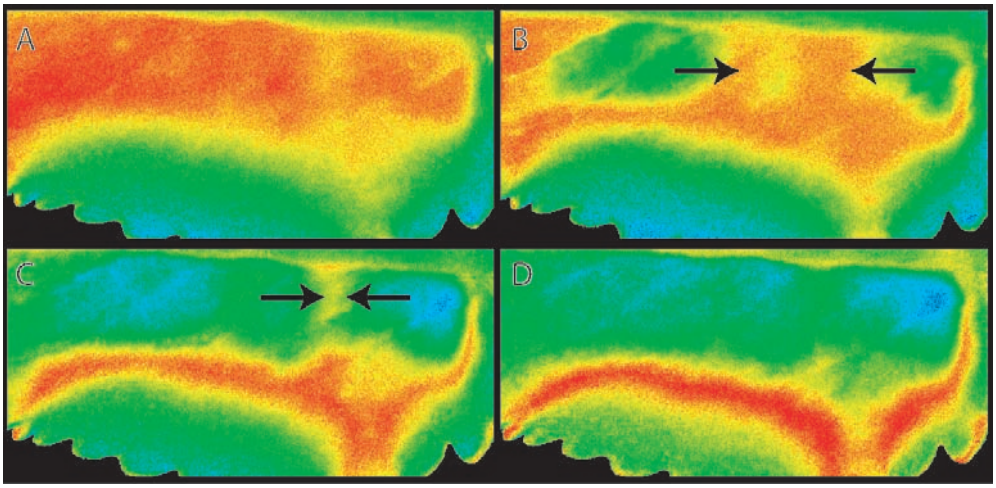

Fig. 3 Maps of photosynthetic efficiency (ϕ_{PSII}), showing two wavefronts, which meet and then disappear rather than reforming. Subsequent pictures were taken in 20-minutes intervals; experimental conditions and colour codes are the same as in Fig. 2. The arrows indicate the direction of the wavefronts.

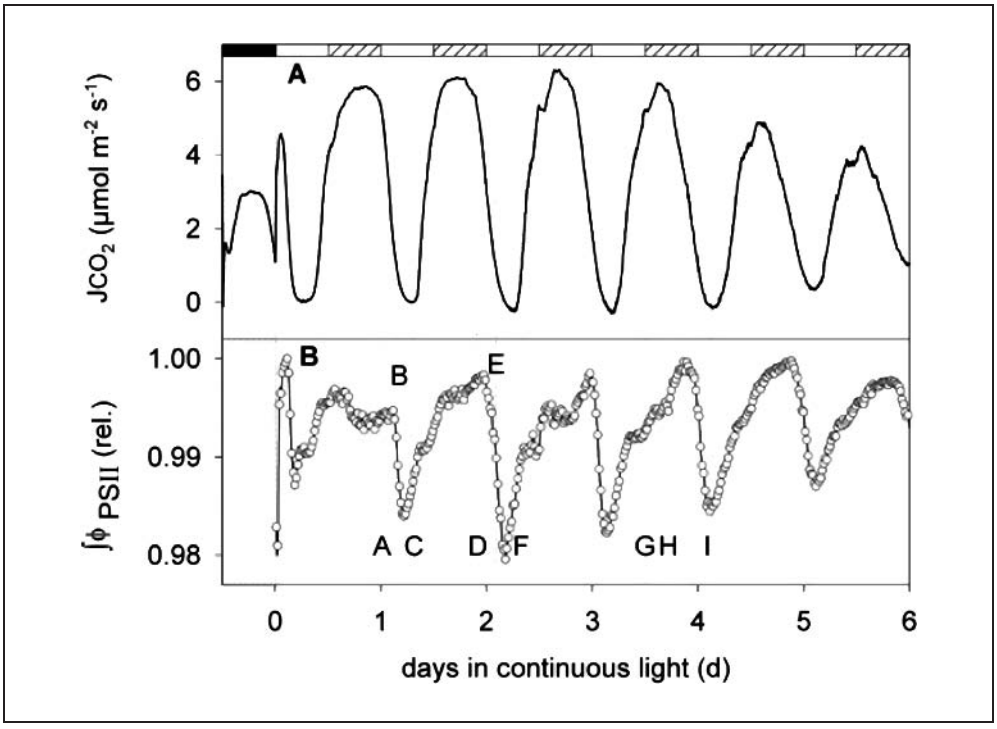

Fig. 4 Endogenous rhythm of net CO_2 exchange rate (JCO_2, *A*) and $\int \phi_{PSII}$ averaged over the entire leaf (*B*) in continuous light. Experimental conditions were the same as in Fig. 1, but leaf temperature was 21 °C and light intensity 194 µmol photons m^{-2} s^{-1}. Hatched bars indicate where a dark period would have occurred in the normal day/night cycle. The capital letters indicate the times, at which maps of ϕ_{PSII} are shown in Fig. 5.

(Fig. 2). Distinct small scale heterogeneity of ϕ_{PSII} is visible during the first hour after the onset of light (Fig. 2 *A*, *B*), ϕ_{PSII} is homogeneously distributed during midday (phase III), when JCO_2 is minimal and leaf-internal CO_2 concentrations are high (Fig. 2 *C–F*). At the transition from phase III to phase IV, wavefronts of high ϕ_{PSII} are initiated at the lower (Fig. 2 *H*) and the upper half (Fig. 2 I) of the leaf. These wavefronts expand with a constant velocity and may run over the entire leaf. Wavefronts which happen to meet each other do not superimpose but rather extinguish each other (Fig. 3).

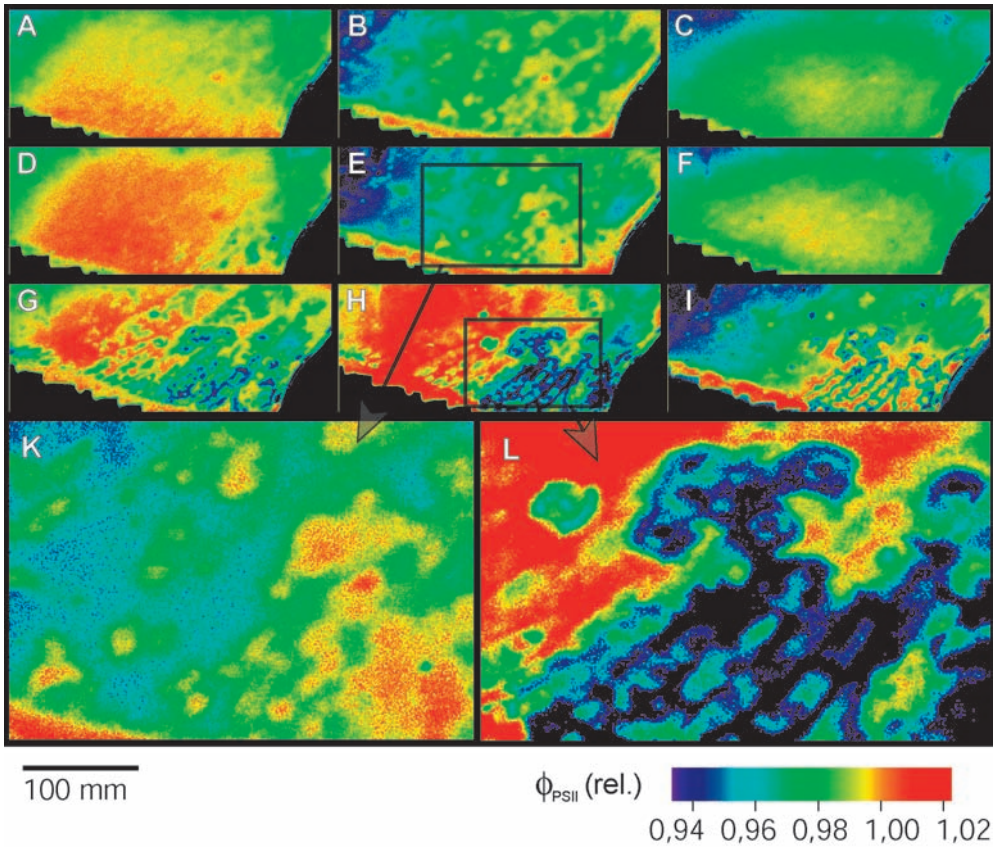

Fig. 5 Spatiotemporal heterogeneity of photosynthetic efficiency (ϕ_{PSII}) in a leaf of *Kalanchoë daigremontiana* during the endogenous, circadian rhythm in continuous light. Two types of heterogeneity can be distinguished as denoted in the text. Type (*i*): panels A – F; type (*ii*); panels G-I. Panels K and L are enlargements of type (*i*) and type (*ii*) patchiness, respectively. Maps were taken at the times denoted by capital letters in Fig. 4. ϕ_{PSII} was imaged by non-invasive chlorophyll fluorescence measurements at 20-minutes intervals and is normalized to the maximum obtained during the experiment, colors code for different efficiency values (see color code at the lower right).

2.3. Endogenous Rhythm

Distinct spatial variations of ϕ_{PSII} are detected by chlorophyll fluorescence imaging during the endogenous CAM rhythm of net CO_2 exchange. Net CO_2 exchange rate (JCO_2) and photosynthetic efficiency (ϕ_{PSII}) both show a closely correlated temporal development (Fig. 4). They are governed by spatial variations of ϕ_{PSII}, which can be divided into two types.

(*i*) The first type only appears at the transition from maximum to minimum JCO_2 or ϕ_{PSII}, respectively (Fig. 5, panels A–F). These patches occur as fine cloud-like structures (Fig. 5, enlargement-panel K) of high ϕ_{PSII}, which emerge out of a homogenous tissue. Closer investigation of the underlying mechanisms revealed that neighbouring patches decouple, and exhibit a phase shift during the transition phase (RASCHER et al. 2001).

(*ii*) The second type of heterogeneity occurs after a few days in continuous light (Fig. 5, panel G–I). Isolated patches cease to oscillate or are phase shifted and occur as areas of low ϕ_{PSII}. They may appear at various spots upon the leaf, widen with time under

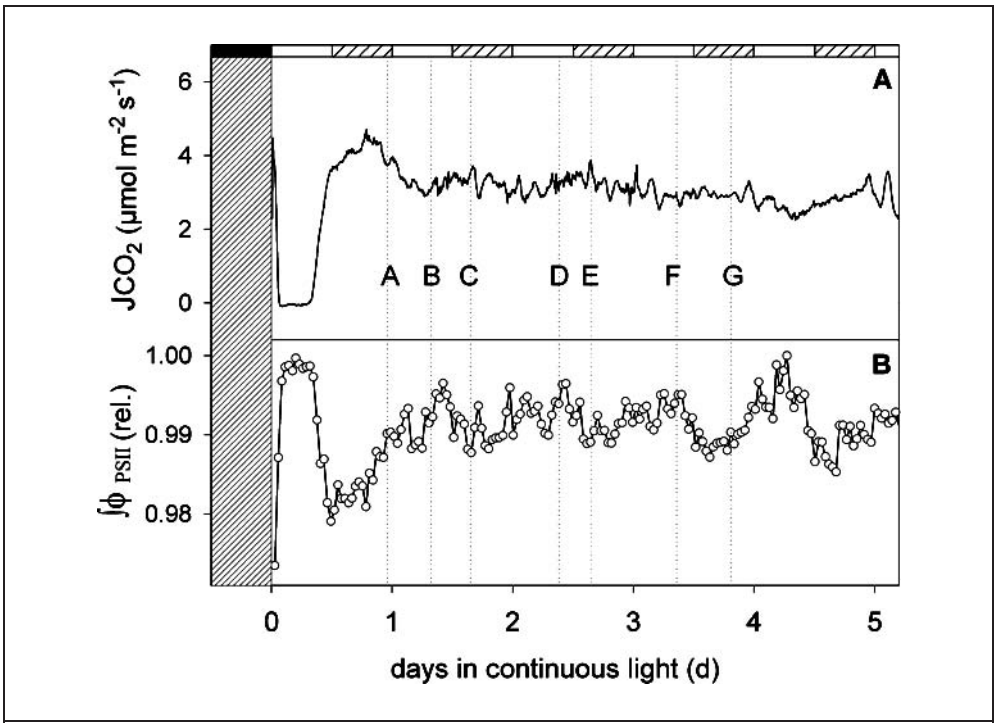

Fig. 6 Arrhythmic net CO_2 exchange rate (JCO_2, *A*) and $\int \phi_{PSII}$ averaged over the entire leaf (*B*) in continuous light at constant higher leaf temperature. Leaf temperature was 28 °C and light intensity 201 µmol photons m^{-2} s^{-1}. Hatched bars indicate where a dark period would occur in normal day-night cycle. The capital letters indicate the times, at which maps of ϕ_{PSII} are shown in Fig. 7.

constant conditions and may exhibit interesting borderlines (Fig. 5, enlargement-panel L). For a more detailed description of these phenomena see RASCHER (2001) and RASCHER et al. (2001).

2.4 Arrhythmic Gas Exchange

Spatial heterogeneity was hypothesized to occur during the arrhythmic gas exchange pattern of CAM in continuous light at higher temperatures. Mathematical model formulations (BECK et al. 2001) and experimental investigations of the abolition and restoration of the endogenous rhythm (RASCHER et al. 1998) suggested a spatial decoupling of individual oscillators. These predictions could not be verified experimentally. However, photosynthesis of leaves of *Kalanchoë daigremontiana* is by no means homogeneously distributed during the arrhythmic regime. ϕ_{PSII} shows spatial differences during the arrhythmic gas exchange at constant high temperatures (28 °C, Figs. 6 and 7), and during a

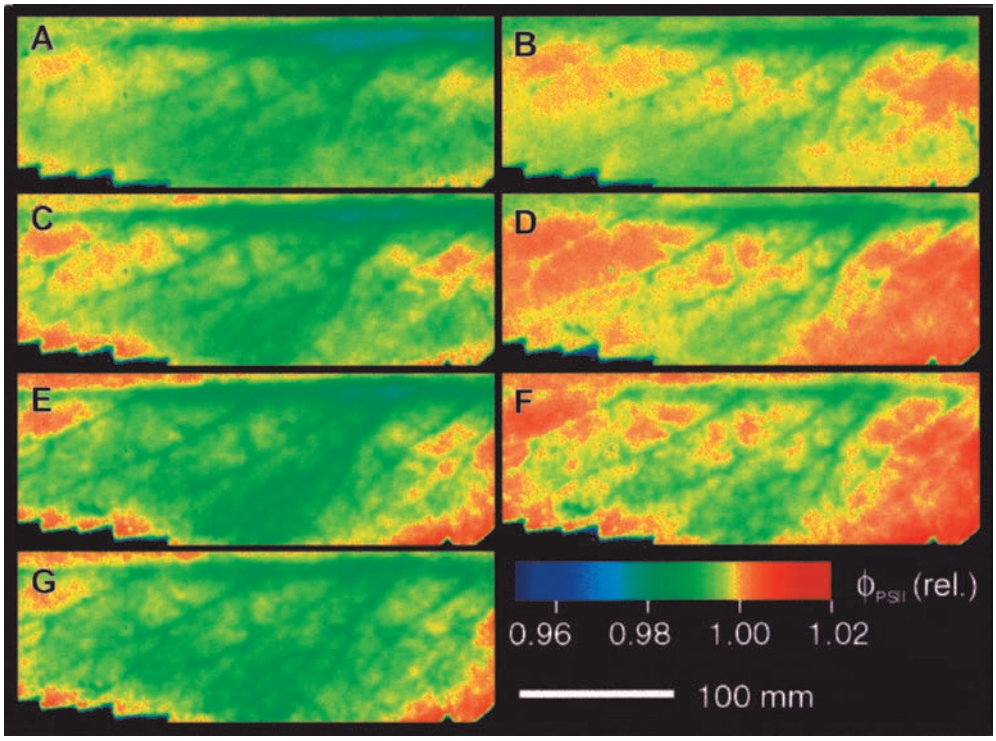

Fig. 7 Spatiotemporal heterogeneity of photosynthetic efficiency (ϕ_{PSII}) in a leaf of *Kalanchoë daigremontiana* during the arrhythmic gas exchange regime at constant temperature (28 °C) in continuous light. Maps were taken at the times denoted by capital letters in Fig. 6. ϕ_{PSII} was imaged by non-invasive chlorophyll fluorescence measurements at 20-minutes intervals and is normalized to the maximum obtained during the experiment, colors code for different efficiency values (see color code at the lower right).

gradual reduction of leaf temperature from the arrhythmic to the rhythmic regime (31 °C to 24 °C, Figs. 8 and 9). The arrhythmic gas exchange, measured over the whole leaf, can be maintained even within a rhythmic temperature regime, if leaf temperature is reduced slowly (RASCHER et al. 1998). It was proposed that during and after a so called "temperature ramp", individual, spatially arranged oscillators may underlie gas-exchange arrhythmicity (BECK et al. 2001).

However, no individual oscillators, which may exhibit circadian oscillations, were found during our measurements. ϕ_{PSII} changed in time and space, but no correlation between the arrhythmic changes of JCO_2 (Figs. 6 and 8, panels A) and ϕ_{PSII} (Figs. 6 and 8, panels B) was found (RASCHER 2001). Spatial variations of ϕ_{PSII} during the arrhythmic regime were small in comparison to the differences during the diurnal day/night cycle or during the endogenous rhythm (see color codes in Figs. 2, 3 and 5 *versus* 7 and 9).

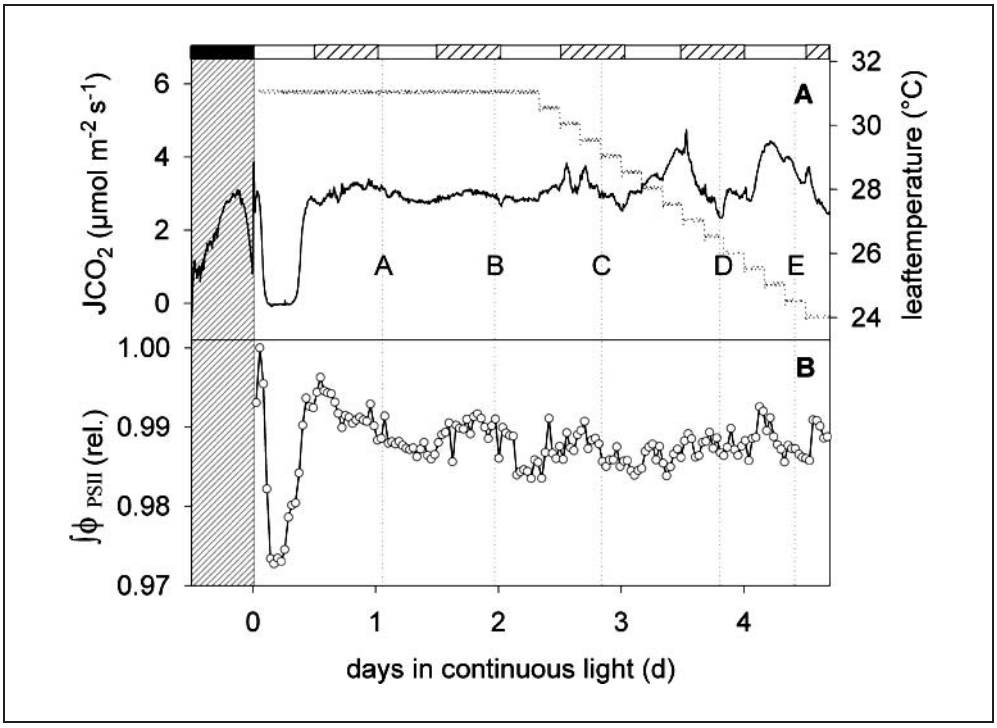

Fig. 8 Arrhythmic net CO_2 exchange rate (JCO_2, *A*) and $\int \phi_{PSII}$ averaged over the entire leaf (*B*) in continuous light before and during a gentle reduction of leaf temperature. Leaf temperature was 31 °C and then was gradually reduced (0.5 °C every 4 h) until 24 °C; light intensity was 201 µmol photons m^{-2} s^{-1}. Hatched bars indicate where a dark period would have occurred in the normal day-night cycle. The capital letters indicate the times, at which maps of ϕ_{PSII} are shown in Fig. 9.

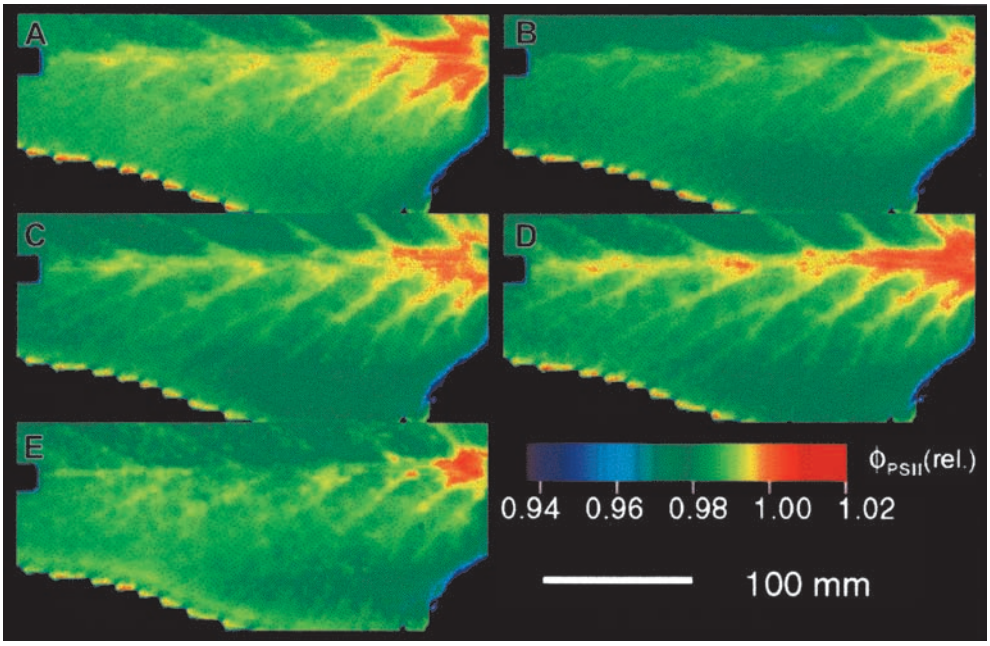

Fig. 9 Spatiotemporal heterogeneity of photosynthetic efficiency (ϕ_{PSII}) in a leaf of *Kalanchoë daigremontiana* before and during a gentle reduction of leaf temperature (31 °C ? 24 °C) in continuous light. Maps were taken at the times denoted by capital letters in Fig. 8. ϕ_{PSII} was imaged by non-invasive chlorophyll fluorescence measurements at 20-minutes intervals and is normalized to the maximum obtained during the experiment, colors code for different efficiency values (see color code at the lower right).

3. Conclusion

"Simple" leaves, which were regarded to have only a vertical stratification may also show various horizontal variations of physiological parameters. In fact, the light response of photosynthesis, which is a highly regulated biophysical process, may be heterogeneously distributed over leaves. Chlorophyll fluorescence imaging has become a powerful tool to reveal such spatial variations. Various external factors, such as herbicides and light intensity have a strong influence on the quantum efficiency and render leaves to become heterogeneous. In addition internal, physiological factors, such as different concentrations of metabolites can cause spatial heterogeneity. One example of dynamic heterogeneity of photosynthetic efficiency is the endogenous, circadian CAM rhythm of *Kalanchoë daigremontiana*, during which various spatial pattern formations were observed under controlled and constant external conditions.

References

Balachandran, S., Hurry, V. M., Kelly, S. E., Osmond, C. B., Robinson, S. A., Rohozinski, J., Seaton, G. G. R., and Sims, D. A.: Concepts of plant biotic stress. Some insights into the stress physiology of virus-infected plants, from the perspective of photosynthesis. Physiologia Plantarum *100*, 203–213 (1997)

Balachandran, S., Osmond, C. B., and Daley, P. F.: Diagnostics of the earliest strain-specific interaction between Tobacco Mosaic Virus and chloroplasts of Tobacco leaves in vivo by means of chlorophyll fluorescence imaging. Plant Physiol. *104*, 1059–1065 (1994)

Beck, F., Blasius, B., Neff, R., Lüttge, U., and Rascher, U.: Stochastic noise interferes coherently with biological clocks and produces specific time structures. Proc. R. Soc. London B *268*, 1307–1313 (2001)

Blasius, B., Beck, F., and Lüttge, U.: A model for photosynthetic oscillations in crassulacean acid metabolism (CAM). J. Theor. Biol. *184*, 345–351 (1997)

Blasius, B., Beck, F., and Lüttge, U.: Oscillatory model of crassulacean acid metabolism: structural analysis and stability boundaries with a discrete hysteresis switch. Plant Cell Environ. *21*, 775–784 (1998)

Blasius, B., Neff, R., Beck, F., and Lüttge, U.: Oscillatory model of crassulacean acid metabolism with a dynamic hysteresis switch. Proc. R. Soc. London B *266*, 93–101 (1999)

Cardon, Z. G., Mott, K. A., and Berry, J. A.: Dynamics of patchy stomatal movements, and their contribution to steady-state and oscillating stomatal conductance calculated using gas-exchange techniques. Plant Cell Environ. *17*, 995–1007 (1994)

Castelo-Branco, M., Goebel, R., Neuenschwander, S., and Singer, W.: Neural synchrony correlates with surface segregation rules. Nature *405*, 685–689 (2000)

Chaerle, L., and Van der Straeten, D.: Seeing is believing: imaging techniques to monitor plant health. Biochim. Biophys. Acta *1519*, 153–166 (2001)

Daley, P. F., Raschke, K., Ball, J. T., and Berry, J. A.: Topography of photosynthetic activity of leaves obtained from video images of chlorophyll fluorescence. Plant Physiol. *90*, 1233–1238 (1989)

Editorial: The changing face of biomedical research. Nature Med. *6*, 113 (2000)

Farquhar, G. D., and Sharkey, T. D.: Stomatal conductance and photosynthesis. Annu. Rev. Plant Physiol. *33*, 317–345 (1982)

Genty, B., Briantais, J. M., and Baker, N. R.: The relationship between the quantum yield of photosynthetic electron transport and quenching of chlorophyll fluorescence. Biochim. Biophys. Acta *990*, 87–92 (1989)

Grams, T. E. E., Borland, A. M., Roberts, A., Griffiths, H., Beck, F., and Lüttge, U.: On the mechanism of reinitiation of endogenous crassulacean acid metabolism rhythm by temperature changes. Plant Physiol. *113*, 1309–1317 (1997)

Gray, R. A., Pertsov, A. M., and Jalife, J.: Spatial and temporal organization during cardiac fibrillation. Nature *392*, 75–78 (1998)

Grunz, H.: Gene expression and pattern formation during early embryonic development in amphibians. J. Bioscience *24*, 515–528 (1999)

Hudson, A.: Development of symmetry in plants. Annu. Rev. Plant Physiol. Plant Mol. Biol. *51*, 349–370 (2000)

Lichtenthaler, H. K., Lang, M., Sowinska, M., Summ, P., Heisel F., and Miehe, J. A.: Uptake of the herbicide diuron as visualised by the fluorescence imaging technique. Bot. Acta *110*, 158–163 (1997)

Lüttge, U.: The tonoplast functioning as master switch for circadian regulation of crassulacean acid metabolism (CAM). Planta *211*, 761–769 (2000)

Lüttge, U., and Ball, E.: Free running oscillations of transpiration and CO_2 exchange in CAM plants without a concomitant rhythm of malate levels. Z. Pflanzenphysiol. *90*, 69–77 (1978)

Lüttge, U., and Beck, F.: Endogenous rhythm and chaos in crassulacean acid metabolism. Planta *188*, 28–38 (1992)

Martiel, J. L., and Goldbeter, A.: Autonomous chaotic behaviour of the slime mould *Dictyostelium discoideum* predicted by a model for cyclic AMP signalling. Nature *313*, 590–592 (1985)

May, R. M.: Simple mathematical models with very complicated dynamics. Nature *261*, 459–467 (1976)

Napp-Zinn, K.: Anatomie des Blattes. II. Blattanatomie der Angiospermen. In: Zimmermann, W., Carlquist, S., Ozenda, P., und Wulff, H. D. (Eds.): Handbuch der Pflanzenanatomie (2. Aufl.). Berlin, Stuttgart: Gebrüder Borntraeger 1973

Osmond, C. B.: Crassulacean acid metabolism: a curiosity in context. Annu. Rev. Plant Physiol. *29*, 379–414 (1978)

Osmond, C. B., Daley, P. F., Badger, M. R., and Lüttge, U.: Chlorophyll fluorescence quenching during photosynthetic induction in leaves of *Abutilon striatum* Dicks. infected with Abutilon mosaic virus, observed with a field-portable imaging system. Bot. Acta *111*, 390–397 (1998)

Osmond, C. B., Kramer, D., and Lüttge, U.: Reversible, water stress-indiced non-uniform chlorophyll fluorescence quenching in wilting leaves of *Potentilla reptans* may not be due to patchy stomatal responses. Plant Biol. *1*, 618–624 (1999)

Osmond, C. B., and Park, Y.-M.: Field-portable imaging systems for measurement of chlorophyll fluorescence quenching. In: Omasa, K., Saji, H., Youssefian, S., and Kondo, N. (Eds.): Air Pollution and Plant Biotechnology – Prospects for Phytomonitoring and Phytoremediation. Tokyo: Springer 2001

Osmond, C. B., Schwartz, O., and Gunning, B.: Photoinhibitory printing on leaves, visualised by chlorophyll fluorescence imaging and confocal microscopy, is due to diminished fluorescence from grana. Aust. J. Plant Physiol. *26*, 717–724 (1999)

Rascher, U.: Der endogene CAM-Rhythmus von *Kalanchoë daigremontiana* als nichtlineares Modellsystem zum Verständnis der raum-zeitlichen Dynamik einer biologischen Uhr. Osnabrück: Der Andere Verlag 2001

Rascher, U., Blasius, B., Beck, F., and Lüttge, U.: Temperature profiles for the expression of endogenous rhythmicity and arrhythmicity of CO_2 exchange in the CAM plant *Kalanchoe daigremontiana* can be shifted by slow temperature changes. Planta *207*, 76–82 (1998)

Rascher, U., Hütt, M.-T., Siebke, K., Osmond, C. B., Beck, F., and Lüttge, U.: Spatio-temporal variations of metabolism in a plant circadian rhythm: the biological clock as an assembly of coupled individual oscillators. Proc. Natl. Acad. Sci. USA *98*, 11801–11805 (2001)

Rosenblum, M. G., Pikovski, A. S., and Kurths, J.: Phase synchronization of chaotic oscillators. Phys. Rev. Lett. *76*, 1804–1807 (1996)

Schäfer, C., Rosenblum, M. G., Kurths, J., and Abel, H.-H.: Synchronization in the human cardiorespiratory system. Nature *392*, 239–240 (1998)

Scheres, B.: Non-linear signalling for pattern formation? Curr. Opin. Plant Biol. *3*, 412–417 (2000)

Schreiber, U., and Bilger, W.: Progress in chlorophyll fluorescence research: major developments during the past years in retrospect. Progr. Botany *54*, 151–172 (1993)

Schreiber, U., Bilger, W., and Neubauer, C.: Chlorophyll fluorescence as a nonintrusive indicator for rapid assessment of in vivo photosynthesis. In: Schulze, E.-D., and Caldwell, M. M. (Eds.): Ecophysiology of Photosynthesis; pp. 49–70. Berlin, Heidelberg, New-York: Springer 1995

Siebke, K., and Weis, E.: Assimilation images of leaves of *Glechoma hederacea*: Analysis of non-synchronous stomata related oscillations. Planta *196*, 155–165 (1995 a)

Siebke, K., and Weis, E.: Images of chlorophyll-a-fluorescence in leaves: topography of photosynthetic oscillations in leaves of *Glechoma hederacea*. Photosynth. Res. *45*, 225–237 (1995 b)

Warren, D. M., and Wilkins, M. B.: An endogenous rhythm in the rate of dark fixation of carbone dioxide in leaves of *Bryophyllum fedtschenkoi*. Nature *191*, 686–688 (1961)

Dr. Uwe Rascher
Columbia University
Biosphere 2 Center
32540 S. Biosphere Road
Oracle, AZ 85623
USA
Phone: +1 52 08 38 50 82
Fax: +1 52 08 38 50 34
E-Mail: urascher@bio2.columbia.edu

Nova Acta Leopoldina NF *88*, Nr. 332, 381–400 (2003)

The Effect of Biological Variability on Spatiotemporal Patterns – Model Simulations for a Network of Biochemical Oscillators

Marc-Thorsten Hütt[1], Hauke Busch[2], and Friedemann Kaiser[2]

With 12 Figures

Abstract

Noise has an important effect on spatiotemporal patterns in biological systems. In contrast to noise, biological variability (or disorder) is a static system property. Nevertheless, it can have dynamical implications, as the magnitude and the statistical properties of the biological variability influence the capabilities of the elements to synchronize or form patterns. We study such influences in a chain of coupled nonlinear oscillators, each of which can be thought of as a simple form of oscillating biochemical reaction. It is seen that under certain conditions an increase in variability can induce spatial waves and complex spatiotemporal patterns. Some properties of the different patterns are discussed and their dependence on the system's parameters is studied. In particular, it is seen that the mutual information quantifying the complexity of the spatiotemporal patterns can depend resonantly on variability. As an outlook, tools for the analysis of such patterns are outlined, which may help to identify similar phenomena in nature.

Zusammenfassung

Rauschen übt einen wichtigen Einfluß auf raumzeitliche Muster biologischer Systeme aus. Im Vergleich zu Rauschen stellt biologische Variabilität (oder Ungeordnetheit) eine statische Systemeigenschaft dar. Dennoch kann Variabilität dynamische Implikationen haben, da ihre Größe und statistischen Eigenschaften die Fähigkeit der Elemente beeinflussen, sich zu synchronisieren und Muster zu bilden. Wir untersuchen solche Einflüsse in einer Kette gekoppelter nichtlinearer Oszillatoren, von denen jeder als eine einfache oszillierende biochemische Reaktion aufgefaßt werden kann. Es zeigt sich, daß Variabilität unter bestimmten Bedingungen räumliche Wellen und komplexe raumzeitliche Strukturen induzieren kann. Eigenschaften dieser Strukturen werden diskutiert und ihre Abhängigkeit von den Systemparametern wird untersucht. Insbesondere zeigt sich, daß die Transinformation als Maß für die Komplexität der raumzeitlichen Muster einen resonanzförmigen Verlauf mit der Variabilität haben kann. Im Ausblick werden Werkzeuge skizziert, mit denen es möglich sein sollte, ähnliche Phänomene in der Natur nachzuweisen.

1. Introduction

A characteristic feature of (self-organized) spatiotemporal patterns in biology is that local (e. g. nearest-neighbor) interactions determine the time development of the individual elements and, in turn, lead to patterns on a large scale (compared to the size of

1 Bioinformatics Group, Department of Biology, Darmstadt University of Technology, 64287 Darmstadt.
2 Institute of Applied Physics, Darmstadt University of Technology, 64289 Darmstadt.

a single element). Often these patterns emerge abruptly, when a critical value of a (slowly drifting) control parameter is passed (see, e. g., KELSO 1995, SOLÉ et al. 1992, BAR-YAM 1997). Many such processes of biological self-organization can be better understood with the help of mathematical models based upon coupled nonlinear oscillators. In such models cooperative behavior of many interacting elements, in particular synchronization and the loss of synchronization when internal parameters or external conditions are changed, can be studied and related to biological observation. The precise conditions leading to synchronization of two or more oscillators have been extensively investigated in the last decades (see, e. g., PIKOVSKY et al. 2001 for a recent account of the long history of this research). It is, however, not well understood, to what extent biological variability influences processes of pattern formation and self-organization, or, more specifically, to what extent dynamical function can be attributed to variability. Some theoretical investigations have shown that introducing variability is not only important for a better quantitative reproduction of experimental findings, but rather that in many cases variability might play an essential role in achieving a qualitative understanding of the processes at hand. The corresponding theoretical approaches range from variability as a driving force in evolutionary processes (LLOYD and GOULD 1993) to the generation of endogenous circadian oscillations from fast dynamics (SHINBROT and SCARBROUGH 1999). The vast field of research on synchronization in networks of nonlinear oscillators under the influence of stochastic contributions is described, e. g., from the point of view of synchronization (PIKOVSKY et al. 2001) and from the network point of view (STROGATZ 2001).

Our main question, how a parameter distribution influences synchronization properties of interacting nonlinear elements, has started to be addressed with the pioneering work of KURAMOTO (1984) on phase oscillators and has become a major topic in nonlinear dynamics (see, e. g., STROGATZ 2000 for a review on continuations of KURAMOTO's model). The influence of such *variability* has also been studied for the Ising model (MCCOY and WU 1973). MATTHEWS and STROGATZ (1990) have discussed variability (or "disorder" in their terminology) in a chain of limit-cycle oscillators. Its effect on spatiotemporal chaos has been studied by LINDNER et al. (1997), BRAIMAN et al. (1995) and GAVRIELIDES et al. (1998). Only few studies, however, focus on the biological or ecological implications of variability and its influence on spatiotemporal dynamics. One example is the work by SHINBROT and SCARBROUGH (1999). There it is discussed, how rhythms with a long time constant (e. g. circadian oscillations) can be generated by many elements oscillating with high frequency. Their main result is that variability leads to the appearance of oscillations with longer time constants. They give an explicit model, where an additive variability term regulates the time constant of the slow oscillation. Another example is the work by GUARDIOLA et al. (2000). These authors investigate how network topology influences the synchronization properties within a network of pulse-coupled FitzHugh-Nagumo oscillators. They vary the number of random links between oscillators and compare the resulting dynamics with a regular network of oscillators, where they introduce some variability. Their key result is that topological irregularity (number of random connections) and variability in a model parameter (or "population diversity" in their terminology) have a very similar effect on the dynamics of the network. Other work acknowledges the function of variability in dynamical systems from a more descriptive level (see, e. g., KEELING and

GRENFELL 1997). LLOYD and GOULD (1993) have emphasized that variability could be an important evolutionary trait, where selection could take place on the level of population, rather than only on the level of individuals. Apart from such theoretical investigation, a wide range of experimental work points out possible functional roles of biological variability in biological, ecological and sociological processes of pattern formation, e. g. in population dynamics (PFISTER 1998), in neurobiology (SINGER 1999) and in molecular biology (MITTAG 1996).

With the present paper, we address the dynamical consequences of variability in biological systems by studying a network of nonlinear elements with nearest-neighbor coupling. In the language of synchronization, we thus look at synchronization in oscillatory media. We show by numerical analysis that in a biologically motivated system, namely a chain of biochemical oscillators, an increase in variability may induce spatial waves and long-range spatiotemporal correlations.

2. The Model

We study a system of biochemical reactions given by the following set of differential equations:

$$\frac{dX}{dt} = \frac{a}{K+Z} - X, \quad \frac{dY}{dt} = X - Y, \quad \frac{dZ}{dt} = Y - \frac{k_1 Z}{K+Z}, \qquad [1]$$

where the three dynamical variables X, Y and Z can be thought of as (time-dependent) concentrations of some biochemically active substances. The first substance X goes over into a substance Y, which is transformed into a third substance Z. This last component, Z, inhibits the formation of X and is itself enzymatically depleted. These two properties of Z represent the two nonlinearities in the system, regulated by the two parameters a and k_1, respectively. The parameter k_0 regulating the onset of inhibition will be kept constant ($k_0 = 0.001$) throughout this investigation. This system has first been introduced and studied by THRON (1991) with the aim to formulate a minimal system of biochemical oscillation. Figure 1 *A* gives a schematic view by graphically representing the major regulatory elements. Such a system of biochemical reactions with backward inhibition is one of the simplest biologically motivated oscillatory systems. Later, BAIER and SAHLE (1998) used this system as a starting point for studying spatiotemporal patterns by coupling these Thron oscillators in one and two spatial dimensions. Recently we have investigated, how colored noise influences pattern formation in such a network of Thron oscillators (BUSCH et al. 2001). In the following, we first look at the dynamics of the individual oscillator and then later, in Section 3.2, we will turn to a chain of coupled oscillators. The dynamical variables $X(t)$, $Y(t)$ and $Z(t)$ display an oscillatory behavior in a certain region of the (a–k_1)-plane, which arises *via* a Hopf bifurcation, when a critical value in one of these two parameters is passed. Figure 1 *B* shows the time development of $X(t)$ for different values of the bifurcation parameter k_1. Above the critical value a stable oscillation occurs. Later, we will introduce biological variability as a distribution in one of these bifurcation parameters. Thus, it is important to understand the dynamics of the individual oscillator in more detail. From the differential equations, one can immediately compute the position of the fixed point as a function of k_1 and a, as well as the

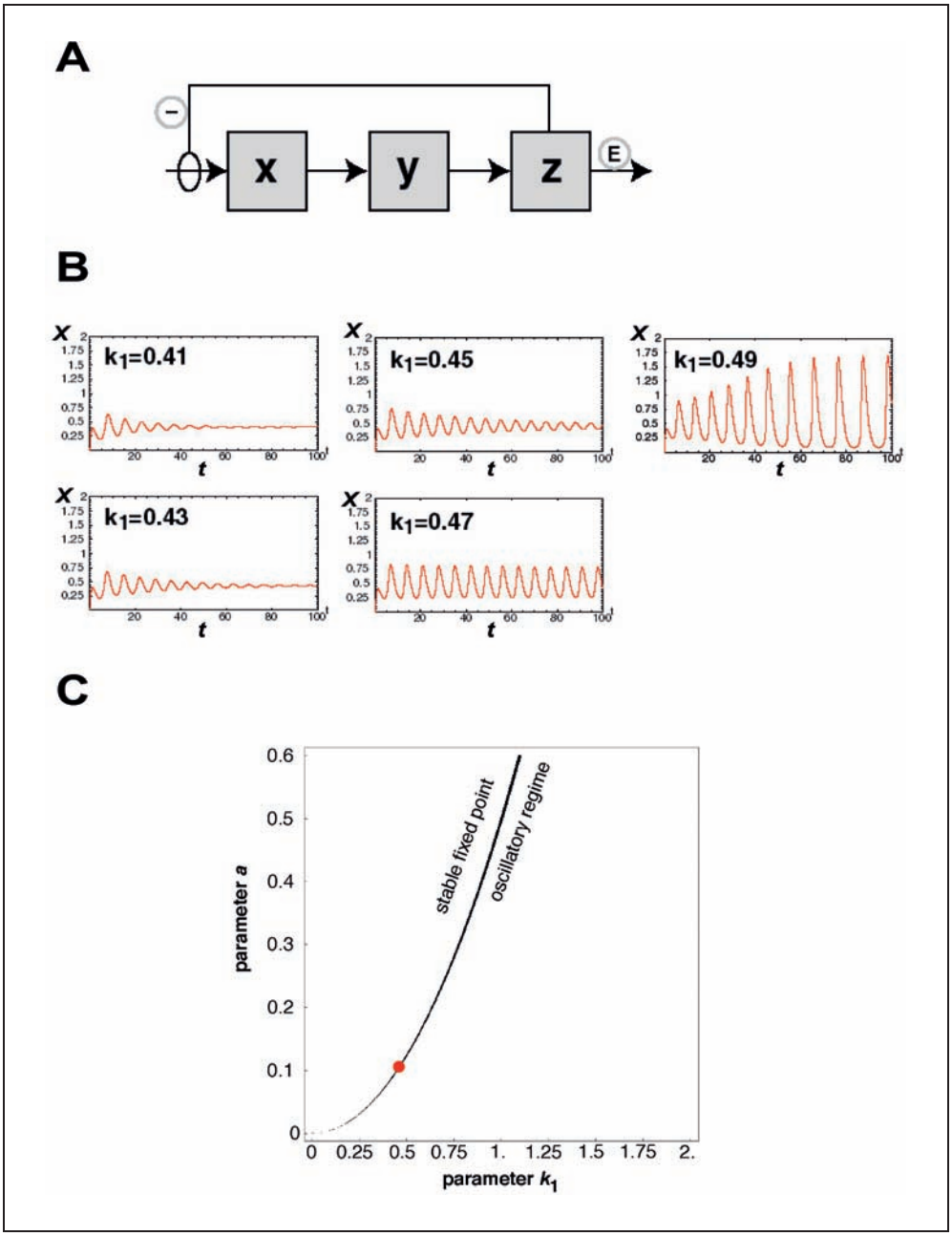

Fig. 1 Description of the Thron system. (*A*) Schematic view of the individual oscillator with the two nonlinear regulatory elements, namely inhibition [–] and enzymatic depletion [E]. (*B*) Typical time development of the *X*-variable in the vicinity of the Hopf bifurcation. Time is shown in dimensionless units. The parameter a has been set to $a = 0.11$. Here and in the following the parameter k_0 is set to $k_0 = 0.001$. (*C*) Phase diagram for a single Thron oscillator. The line shows the location of the Hopf bifurcation as a function of the two bifurcation parameters a and k_1.

eigenvalues governing the stability of the steady state. One can then calculate the zeroes of the real part of the complex eigenvalues as a function of the two parameters. From this result one obtains the bifurcation line separating the fixed-point regime from the oscillatory regime in the (a–k_1)-plane. This is shown in Figure 1 *C*. The point in parameter space, which corresponds to the bifurcation illustrated in Figure 1 *B* is indicated by the dot. The main dynamical feature of interest in the oscillatory regime is the period length, which also depends on a and k_1. Figure 2 shows some examples of this. There, the dynamical regions in the (a–k_1)-plane are depicted, as in Figure 1 *C*. In addition, for three cases the corresponding periods of oscillation are given, namely for $k_1 = 0.5$ and 1.4 as a function of a and for $a = 0.2$ as a function of k_1, respectively. It is seen that, e. g., for $a = 0.2$ and above a certain value of k_1 (around $k_1 = 0.8$) the period length T decreases almost linearly with k_1. In this way for example a distribution in the parameter k_1 corresponds to a distribution in period lengths.

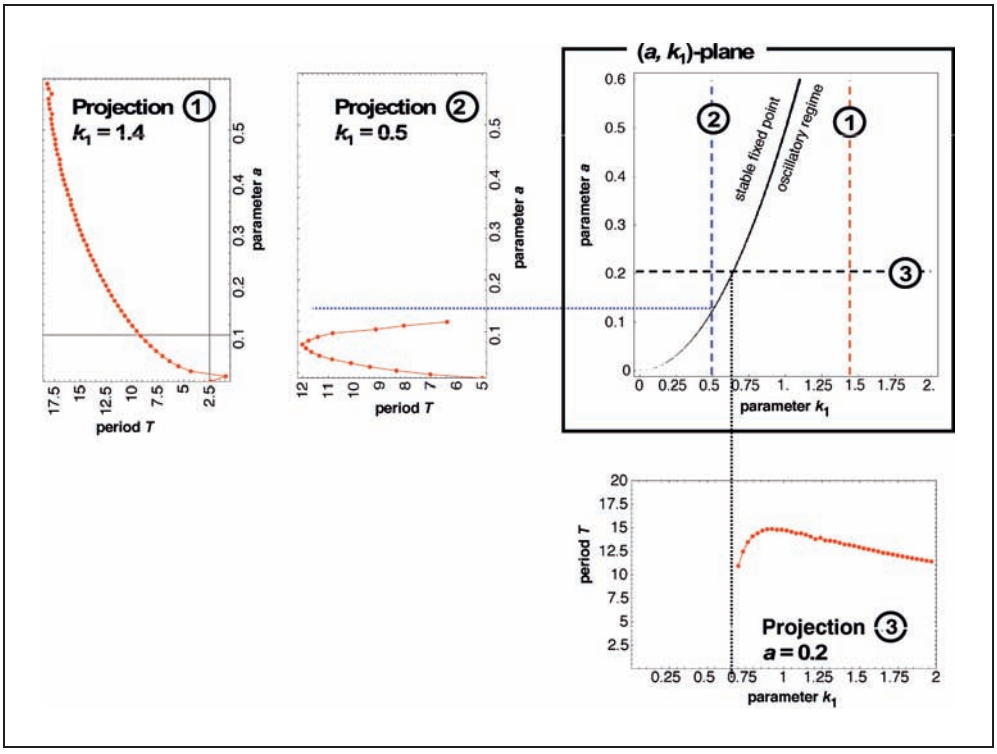

Fig. 2 Dependence of the period length T on the bifurcation parameters a and k_1. Starting from the (a–k_1)-plane three projections are considered, namely (1) $k_1 = 1.4$, (2) $k_1 = 0.5$ and (3) $a = 0.2$. For these projections the period length T is shown as a function of the remaining parameter (i. e. as a function of a for (1) and (2) and of k_1 for (3)). Dashed lines within the phase diagram indicate the intersection chosen to display period length. The dotted lines leading out of the phase diagram project the bifurcation points onto the period diagram. For projection (1) no bifurcation exists in the parameter range shown here. The period T has been obtained by computing the phase $\varphi_{xy} = \arctan(X/Y)$ for a long time series (10 000 time steps after a transient of 5 000) and then counting 2π changes in φ_{xy} in this time interval.

3. From the Single Oscillator to Coupled Oscillators

3.1 Example of Phase Oscillators

The previous section was devoted to studying some basic properties of the individual Thron oscillator. In order to understand, what typical dynamics arise when oscillatory units are coupled, it is convenient to first look at the simplest oscillatory unit, namely a phase oscillator. The idea is to design a limit-cycle oscillator in its simplest form as a fixed point of a radial component and an uniformly increasing phase. One then can ignore, with good accuracy, the amplitude dynamics (given by the radial component) and focus on the time evolution of the phase. In spite of the trivial single-oscillator dynamics (uniform increase of the phase with time) the coupled system is an interesting minimal model for investigating synchronization.

For this case the effect of variability on synchronization properties has been studied extensively. KURAMOTO (1984) has shown that in the case of globally coupled phase oscillators with a distribution of internal frequencies the number of synchronized oscillators changes with the coupling strength in a phase-transition-like manner. The critical coupling (i. e. the coupling strength at which the phase transition occurs) depends on the form and width of the frequency distribution as well as on the form of the coupling between oscillators. In more recent years, this fundamental result has been extended and further studied, both numerically and analytically (see STROGATZ 2000 for a review). In the case of a local (neighbor) coupling the essence of synchronization properties of phase oscillators can be grasped by discussing a simple numerical experiment introduced by PIKOVSKY et al. (2001). There, five phase oscillators with different internal frequencies are locally coupled in the order of their frequencies. The explicit form of these oscillators is given by a set of differential equations for the phases $\Phi_k(t)$:

$$\frac{d\Phi_k}{dt} = \omega_k + \varepsilon \sin(\Phi_{k-1} - \Phi_k) + \varepsilon \sin(\Phi_{k+1} - \Phi_k), \qquad [2]$$

i. e., a sinusoidal coupling to neighbors is used. Free boundary conditions are implied, i. e., when $k - 1 = 0$ or when $k + 1$ exceeds the number of oscillators the corresponding coupling term is omitted. The effective (relative) frequencies given by

$$\Omega_k = \langle d\Phi_k/dt \rangle \qquad [3]$$

are then monitored as a function of the coupling strength ε (braces denote time average). Figure 3 shows this relation for a certain choice of internal frequencies ω_k. In Figure 3 *A* one sees, how the oscillators, one after the other, are drawn into a synchronized cluster. Above a certain coupling strength all oscillators are synchronized. If more oscillators are added to this picture (Fig. 3 *B* and *C*) without changing the range of internal frequencies and without scaling the coupling strength, one observes that synchronization is shifted to higher values of ε (actually, it is known that using ε/N as a coupling strength, where N is the number of oscillators, accounts for this shift). In addition, in the intermediate regime, where few oscillators are synchronized, an oscillator may leave one cluster and join another. Otherwise, the situation remains the same. Note that the situation depicted in Figure 3 is somewhat artificial, as the oscillators are arranged with respect to the size of their natural (internal) frequencies. Nevertheless, the characteristic features of the time development, in particular the formation of ever fewer, ever larger clusters with

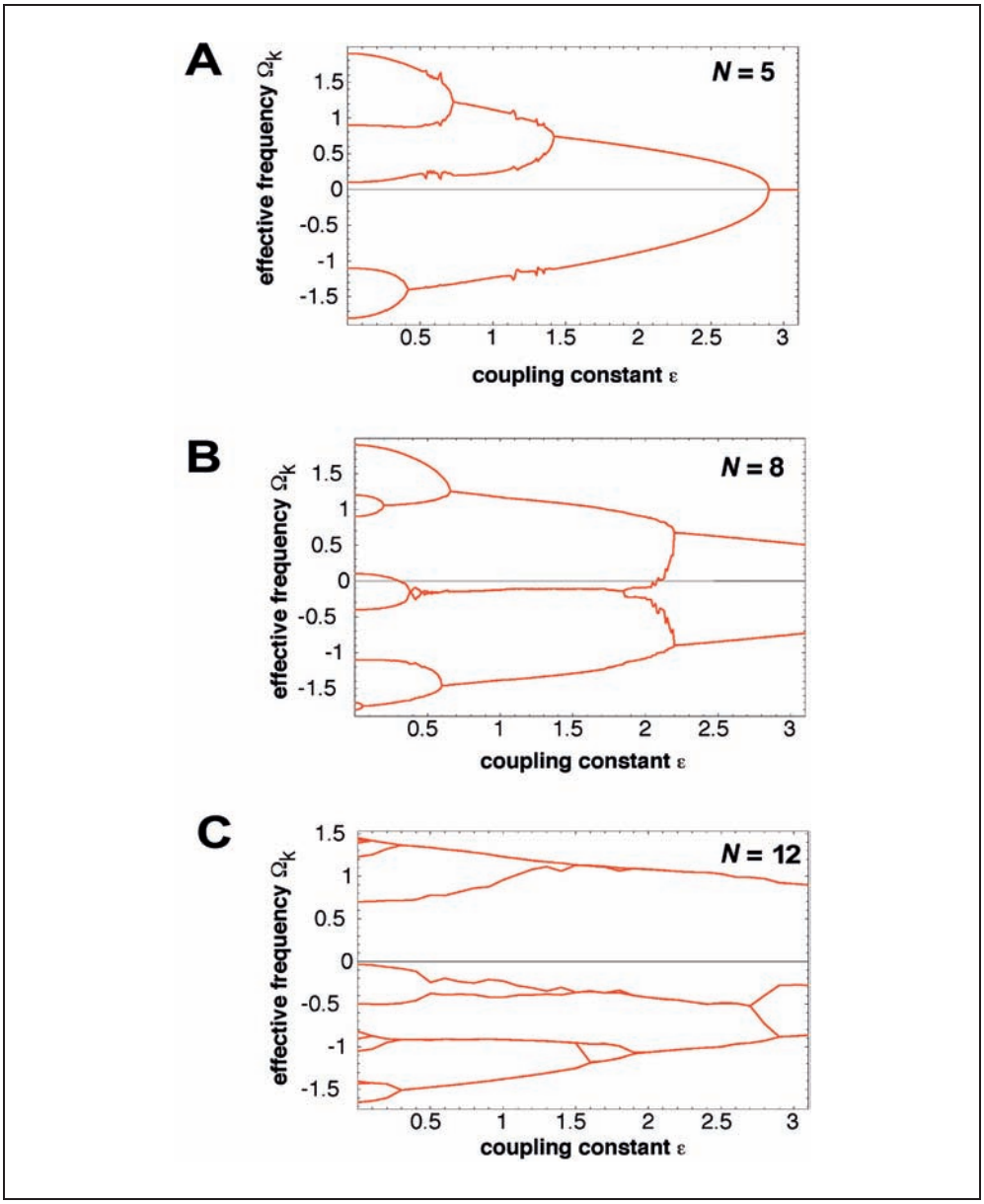

Fig. 3 Effective frequencies Ω_k as a function of the coupling strength ε for sinusoidally coupled phase oscillators. On an interval of $-1.7 < \Omega_k < 1.7$ different numbers N of phase oscillators have been distributed and locally coupled according to this order, namely (*A*) $N = 5$, (*B*) $N = 8$ and (*C*) $N = 12$ oscillators. The original frequencies can be seen in each diagram at $\varepsilon = 0$. Figure (*A*) has been adapted from Pikovsky et al. (2001).

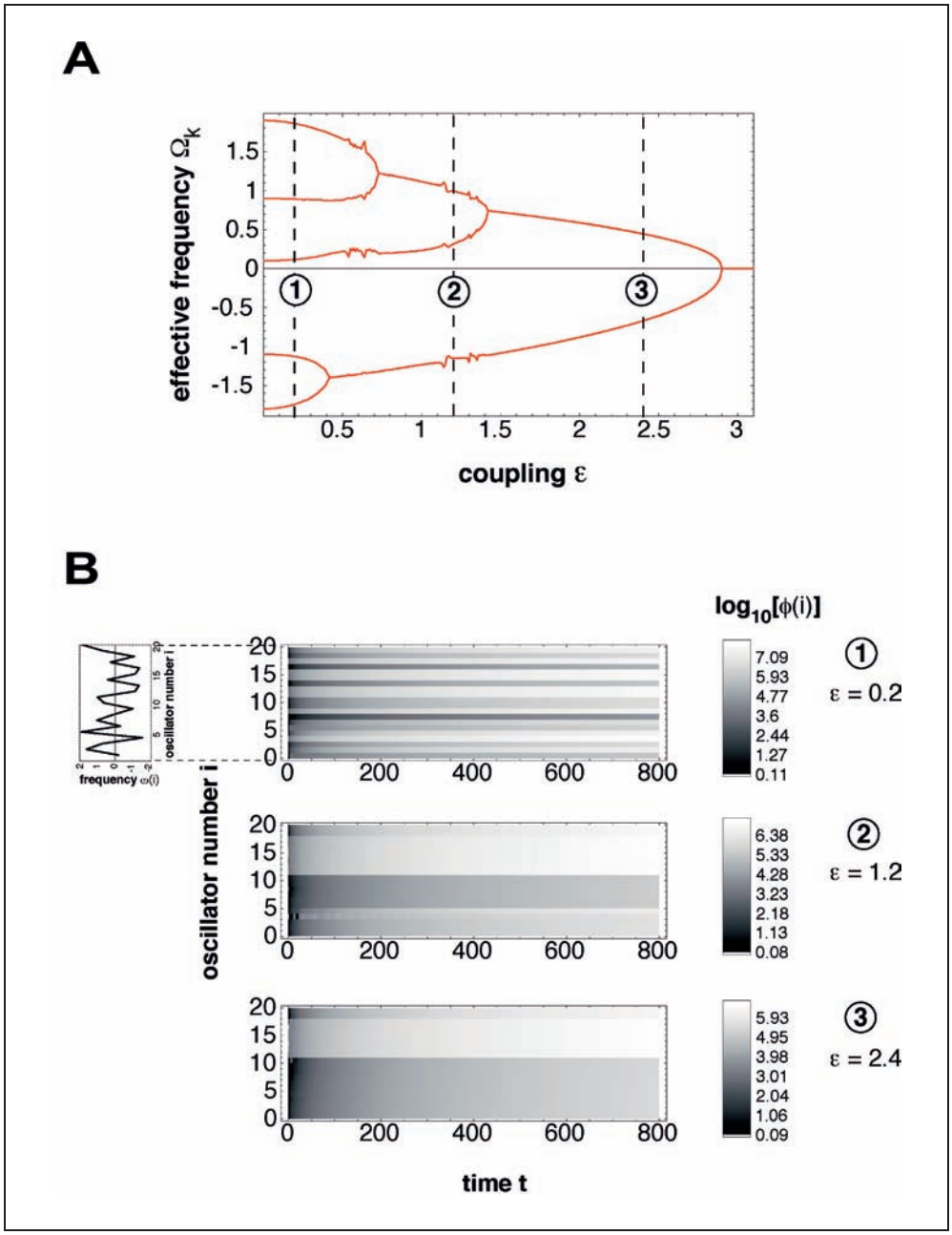

Fig. 4 Typical clusters of phase oscillators for different values of the coupling constant ε. In the diagram from Figure 3*A* displaying the effective frequencies of 5 phase oscillators as a function of the coupling constant ε three values of ε are singled out ($\varepsilon = 0.2$, $\varepsilon = 1.2$ and $\varepsilon = 2.4$, marked by (1), (2) and (3), respectively). For these values of e the time developments (coded in greyscale) are shown for 20 phase oscillators with randomized frequencies. For the first case ($\varepsilon = 0.2$) the distribution of internal frequencies is shown explicitly on the left.

increasing coupling, is also found, when one studies an ensemble of phase oscillators arranged randomly on a chain with respect to their natural frequencies. A schematic example for 20 phase oscillators is given in Figure 4. There the time developments of 20 phase oscillators is shown for three different values of the coupling constant ε. Now the internal frequencies are not ordered along the chain as for Figure 3, but they have been selected randomly between –2 and 2. It is seen that the general scheme (small coupling – few oscillators are synchronized, intermediate coupling – neighboring oscillators are synchronized and form clusters, large coupling – large clusters or full synchronization of all oscillators), which is summarized in Figure 4 *A*, is also found for the chain with randomized frequencies (Fig. 4 *B*).

3.2 A Chain of Coupled Thron Oscillators

When one attempts to reproduce this scenario for Thron oscillators, one finds that amplitude dynamics keep the system from such simple synchronization behavior. In order to illustrate this we couple the Thron oscillators diffusively in one of the dynamical variables as shown schematically in Figure 5. Coupling in the *Z*-pool leads to an additional term

$$+D_Z(Z_{i+1} + Z_{i-1} - 2Z_i) \qquad [4]$$

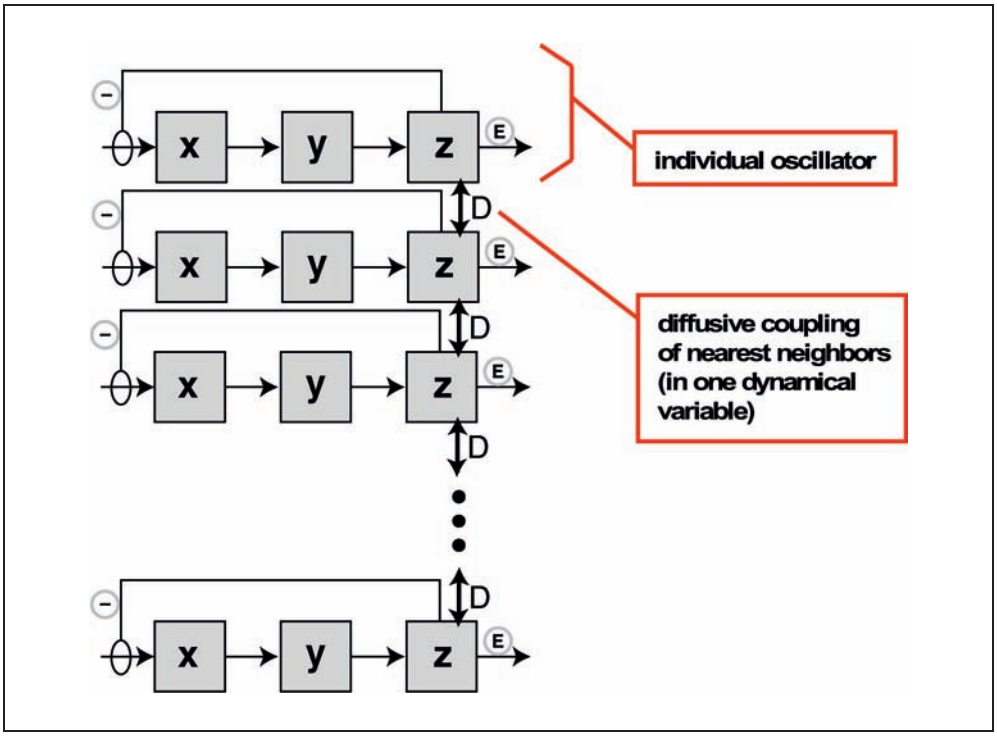

Fig. 5 Coupling scheme of the Thron oscillators. We consider a linear open chain of the oscillators depicted in Fig. 1 *A* with a diffusive coupling in the *Z*-variable.

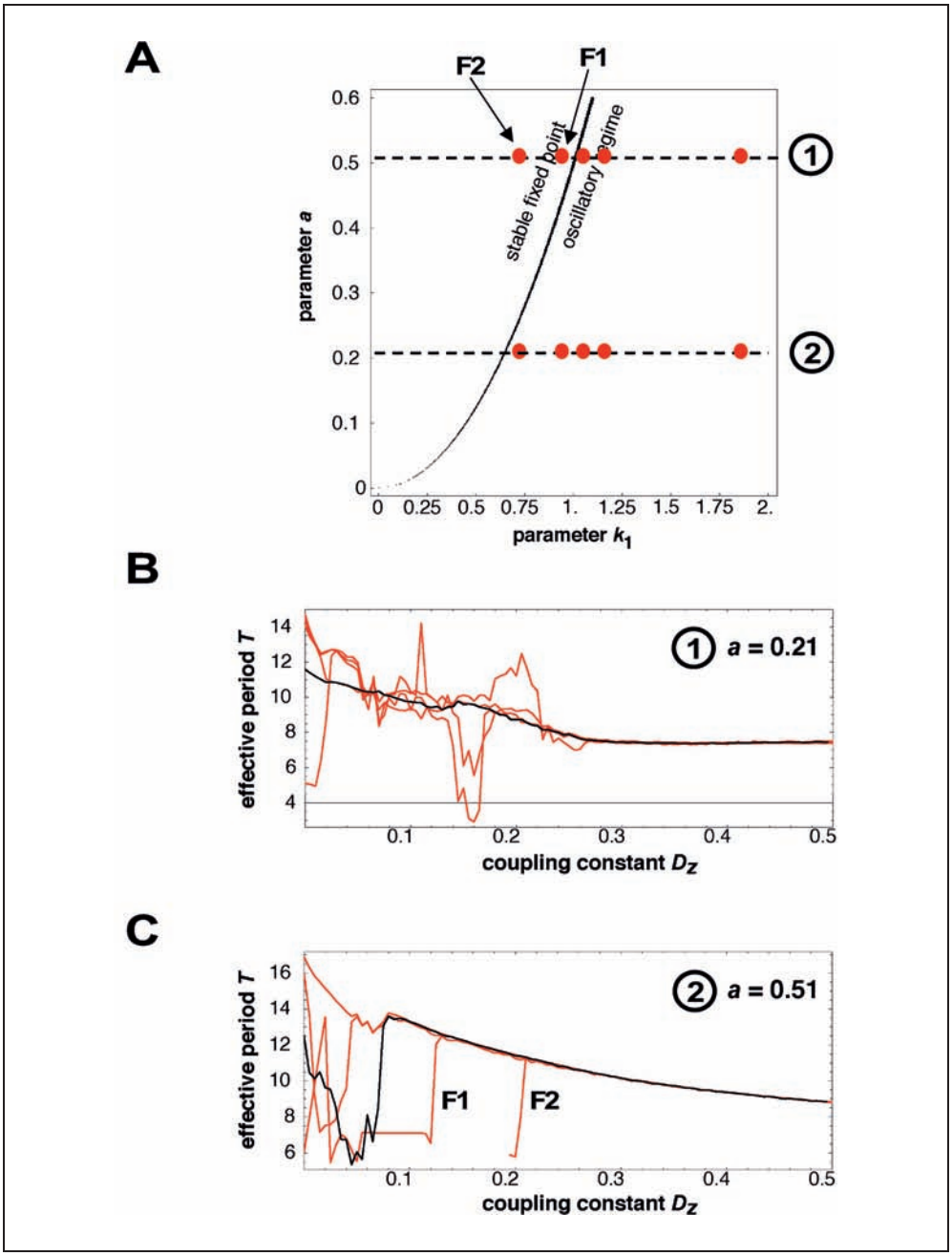

Fig. 6 Effective period T as a function of the diffusion constant D_Z for coupled Thron oscillators. The corresponding parameter values are indicated by the dots in (*A*). Five oscillators are considered with different values of k_1 at two different values of a, namely (*B*) $a = 0.21$ and (*C*) $a = 0.51$. For the latter case, two oscillators are in their fixed-point regime. These are marked F1 and F2, both in (*A*) and (*C*).

in the differential Equation [1] for the *Z*-variable of the *i*-th oscillator. In a similar numerical experiment as the one behind Figure 3*A*, we can now study the synchronization properties of five Thron oscillators at fixed a with different values of k_1. As for Figure 3, the oscillators are arranged corresponding to their k_1-values. Then time developments of this "chain" are simulated and the periods are extracted. This is done over a wide range of the diffusion constant D_Z. The results are shown in Figure 6 for two values of a. The k_1-values for the five oscillators are depicted in Figure 6*A* in the (a–k_1)-plane, as before, while Figures 6*B* and *C* show the effective period T as a function of coupling D_Z. In Figure 6*B* it is seen that although the Thron oscillators synchronize their behavior at high coupling, large deviations from the common period of the synchronized cluster are possible over a certain range in D_Z. The situation depicted in Figure 6*C* is somewhat clearer, as for this choice of a, while keeping the previous values of k_1, two of the oscillators are in their fixed-point regime (marked F1 and F2 in Fig. 6*A*). At a certain coupling, which depends on the distance from the bifurcation line, these oscillators are drawn into the synchronized cluster.

4. Effect of Variability

4.1 Variability-induced Patterns

If many oscillators are coupled to a chain, synchronization properties can be discussed in terms of properties of the spatiotemporal pattern produced by this chain. After the numerical experiment of the previous section, we can now turn to a more systematic study of variability on the basis of spatiotemporal patterns in a chain of Thron oscillators. For the case of identical Thron oscillators (i. e. a system without variability) an example of such a pattern is given in Figure 7 at zero variability (upper left space-time diagram), where the *Z*-value of 20 oscillators is plotted in grey-scale coding as a function of time. Starting from random initial conditions the oscillators synchronize their oscillation after a few time steps. This situation changes drastically, when variability is introduced. To this end we choose the value of the parameter k_1 for each oscillator individually from a distribution with width v. In the following, this quantity v is called the size of variability (or simply variability). The parameter $k_1^{(i)}$ of the i-th oscillator in the chain can then be written as

$$k_1^{(i)} = k_1(1 + v\eta_i) \qquad [5]$$

where η_i is a random number uniformly distributed in the interval [0, 1]. Note that these values $k_1^{(i)}$ do not change with time. They describe natural differences between the dynamical units as a static property of the system. Figure 7 shows typical spatiotemporal patterns for a chain of 30 Thron oscillators in the limit-cycle regime for different values of the variability v. Even for small v a significant change in the pattern is observed (compared to the case without variability, $v = 0$, shown in the first diagram in Fig. 7). Spatial waves are present in the system in addition to the oscillation of the elements with time. The complexity of the patterns increases with v and one observes patterns involving much longer scales in space and time than only a few elements and time steps. Results for a larger chain (128 oscillators) with longer time series are shown in Figure 8, where

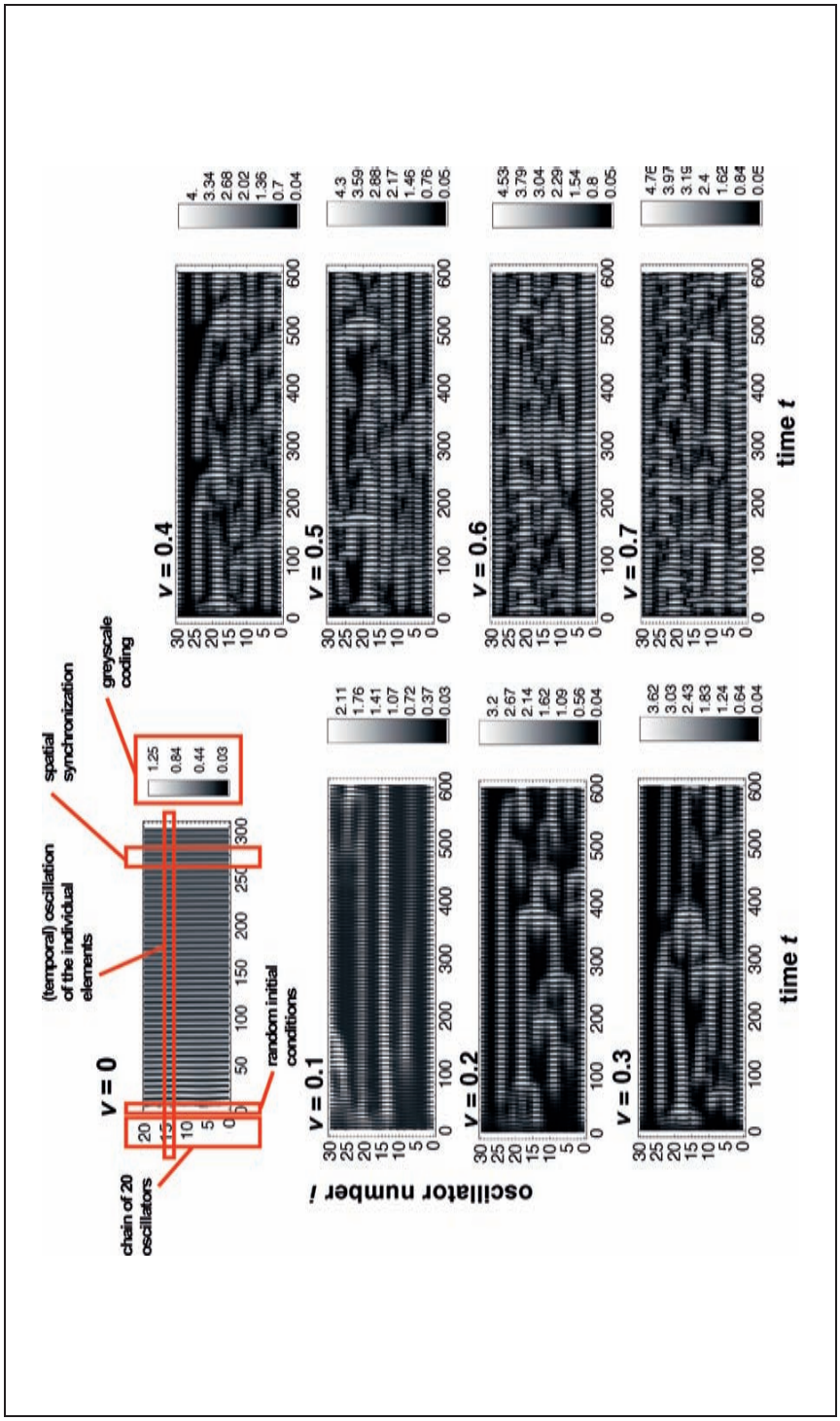

Fig. 7 Effect of variability ν on the spatiotemporal patterns produced by a chain of Thron oscillators. The parameters are $a = 0.11$, $k_1 = 0.49$ and $D_Z = 0.5$. For $\nu = 0$ (identical oscillators) the space-time diagram for 20 oscillators in the oscillatory regime is displayed for 300 time steps, together with details on the notation. For $\nu \neq 0$ chains of 30 oscillators are followed for 600 time steps. In all cases the grey-scale coded Z-values for each oscillator are shown as a function of (dimensionless) time t. Note that for visual clarity a shorter chain has been displayed for $\nu = 0$.

the long-range patterns induced by variability are seen more clearly. Again, the change from spatial waves to complex spatiotemporal patterns is obvious. At intermediate v one finds synchronized clusters slowly increasing or decreasing in size. Similar patterns arise, when variability is introduced in the parameter a. We also found that when one passes to the regime, where the period T decreases almost linearly with k_1 (i. e. $k_1 > 0.8$) the appearance of spatial waves at low nonzero variability disappears and complex patterns emerge abruptly, as soon as a certain value of v is passed (data not shown).

4.2 Quantification of Variability-induced Patterns

The structures shown in Figures 7 and 8 suggest a certain systematics behind the effect of variability on the synchronization properties of these oscillators. Variability seems to carry patterns from regular to complex and then, when increased further, to less complex. In order to quantify this visual impression that has been confirmed by a variety of model calculations varying both, the ranges of k_1 and the coupling constant D_Z, we use the

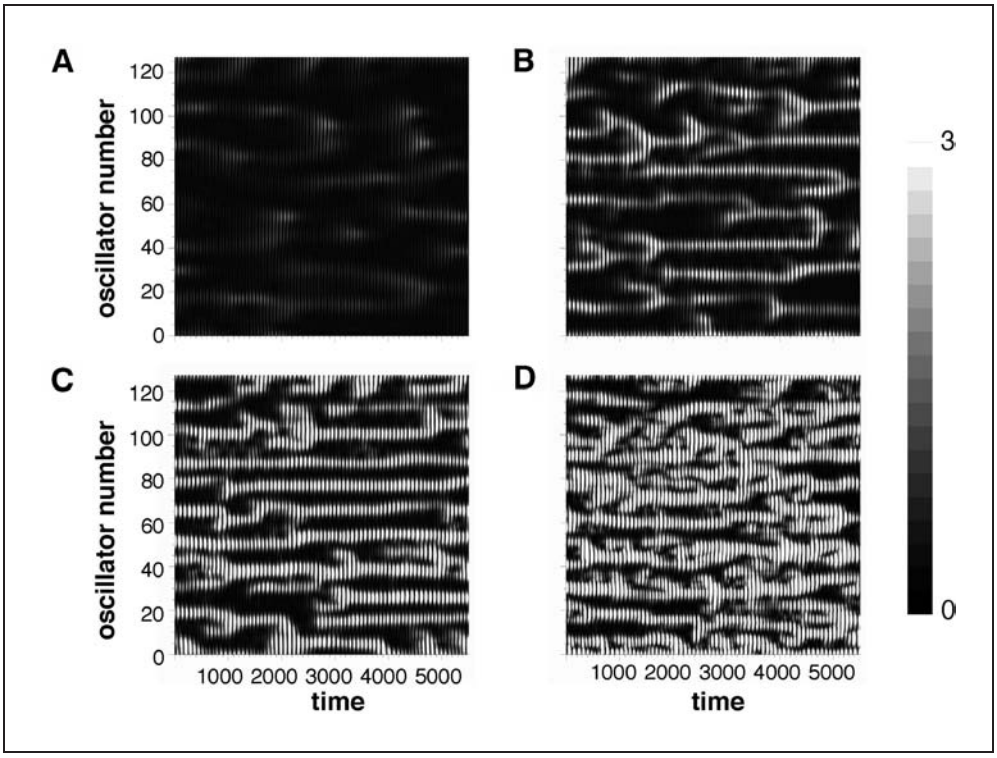

Fig. 8 Space-time diagrams for a chain of 128 Thron oscillators for different values of the variability in k_1, namely (*A*) $v = 0.05$, (*B*) $v = 0.2$, (*C*) $v = 0.4$ and (*D*) $v = 0.9$. For each value of the variability, 5 000 time steps are shown from a simulation, which has been started from random initial conditions and from which a transient of 1000 time steps has been dropped. The parameter values have been $a = 0.11$, $D_Z = 0.2$ and $k_1 = 0.49$ as a minimal value of the distribution in k_1. The parameter k_0 has been fixed at 0.001. As discussed in the text the width of the distribution is given by the variability v.

mutual information I, which is known to provide an efficient measure of pattern complexity.

The mutual information is defined as

$$I = \sum_{ij} p_{ij} \log \frac{p_{ij}}{p_i p_j} \qquad [6]$$

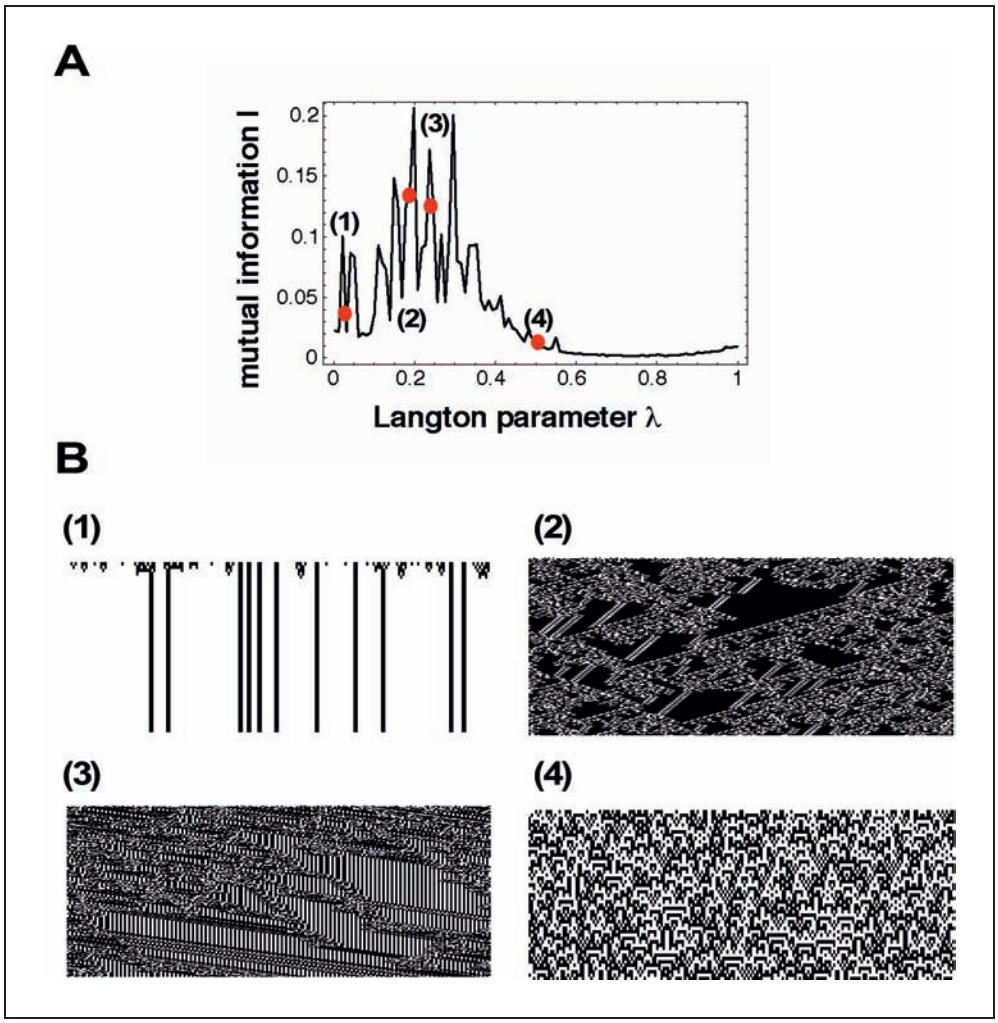

Fig. 9 (*A*) Mutual information I as a function of the Langton parameter λ for the case of one-dimensional cellular automata with a neighborhood size $K = 5$ and a state space of 4 elements. The curve is the average over ten paths through parameter space, where each path is parameterized by λ. For each λ a chain of 200 elements has been simulated over 300 time steps starting from initial conditions. The step size in λ has been 0.001. (*B*) For four values of λ (shown as dots in (*A*)) typical space-time diagrams of such cellular automata are given. Here the spatial dimension is shown horizontally and time runs from downwards. The state q selected for the definition of λ is shown in black, while all other states are represented in white (Figure adapted from Hütt 2001).

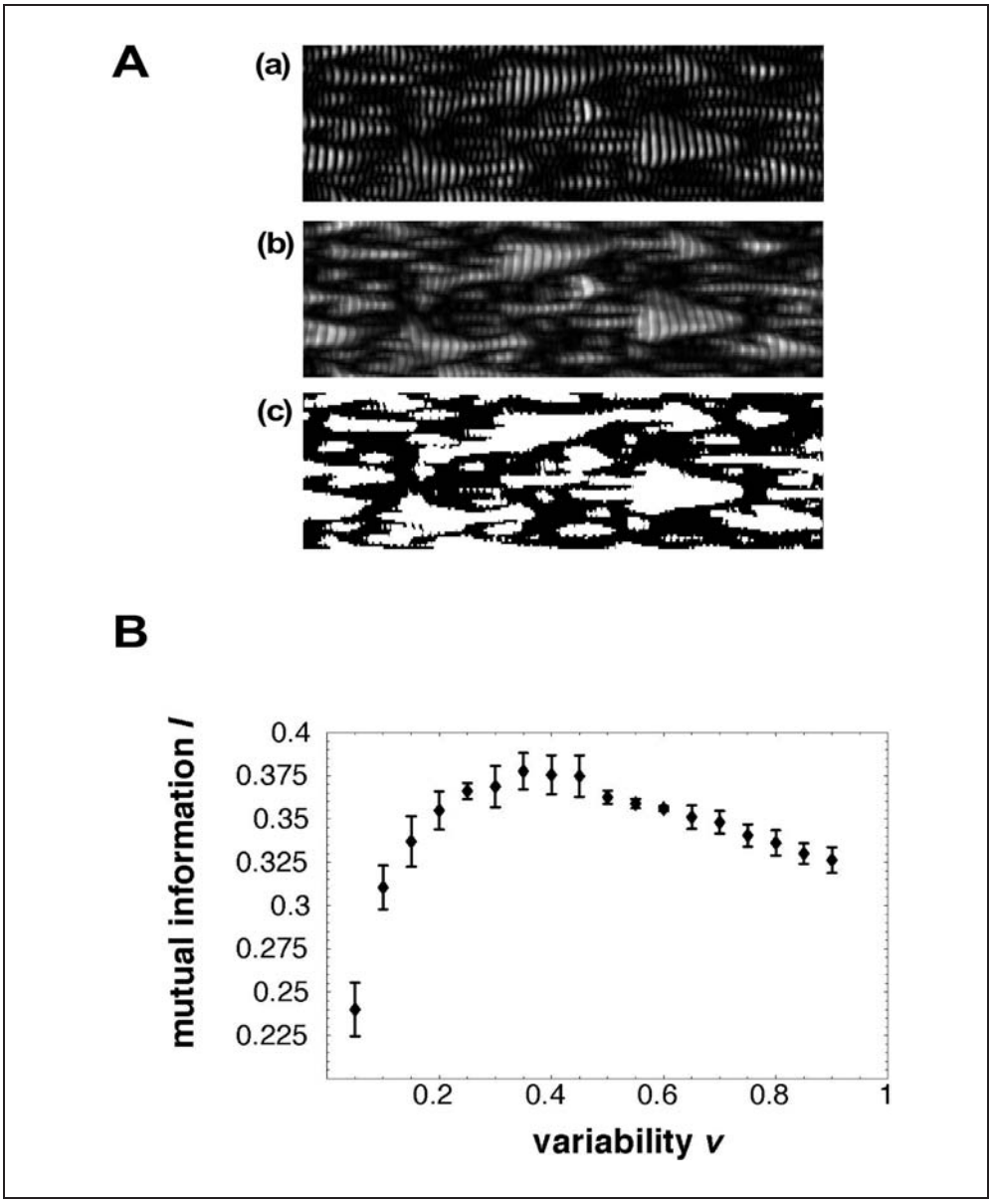

Fig. 10 Computation of the mutual information I as a function of variability v. (*A*) Treatment of the space-time data before applying the definition of I. First, in order to eliminate the fast oscillation underlying the large-scale variation of the spatiotemporal pattern (*a*) the first peak in the (temporal) Fourier spectrum of each oscillator is skipped (*b*). Next, the resulting grey-scale plot is converted into a black-and-white image (*c*) by applying an average-value threshold (i. e., every value below average is mapped onto 0, every value above is put to 1). (*B*) Mutual information I as a function of variability v for space-time data prepared in this manner. The choice of parameters is the same as in Figure 8. In all cases, the space-time data have been generated with a chain of 64 oscillators, where 2000 time steps after a transient of 1000 have entered the computation of I. Error bars have been generated by combining five independent runs.

where p_{ij} denotes the probability of finding the state j next to the state i in the spatiotemporal neighborhood, while p_i is the probability of finding the state i.

An example of the quantifying power of complex patterns is given by LANGTON's analysis of cellular automata (LANGTON 1990). Let us consider one-dimensional cellular automata with a state space consisting of N elements and a neighborhood of size K. So-called update rules determine the state of the i-th cell at time $t + 1$ from the state of the K-element neighborhood around the i-the cell at time t. The case $N = 2$ corresponds to binary automata, for $K = 3$ nearest neighbors are considered, while for $K = 5$ next-to-nearest neighbors are taken into account as well. It is known that such cellular automata can produce complex spatiotemporal patterns. LANGTON defined the parameter λ as the percentage of rules mapping neighborhoods to a chosen element q, e. g. to zero. His hypothesis was that sets of rules with a similar value of λ lead to a similar time development. Changing λ thus defined trajectories through the rule space of cellular automata, and even automata with more than two elements and neighborhoods larger than three became to a certain extent comparable from this global perspective. Figure 9 gives an example of such a behavior for cellular automata. In Figure 9*A* the mutual information I is shown as a function of the Langton parameter λ. For some values of λ typical space-time diagrams from such cellular automata are displayed in Figure 9*B*. The main result of LANGTON's investigation is that complex spatiotemporal patterns (i. e. patterns with long-range spatiotemporal correlations) appear at intermediate λ. The mutual information as a function of λ reflects this finding. The space-time diagrams given as examples in Figure 9*B* illustrate how pattern complexity is accounted for by the value of the mutual information.

We now adapt this analysis strategy to the variability-induced patterns in a chain of Thron oscillators. Analyzing the patterns shown in Figures 7 and 8 with the mutual information requires (*i*) omitting the fast oscillation present in the space-time plots for all values of the variability and (*ii*) reducing the state space of the system to, e. g., 0 and 1. The first step is achieved by omitting the first (high-frequency) peak in the Fourier spectrum. For the second step we use an average-value threshold projecting a value larger than average to 1 and a value smaller than average to 0. Figure 10*A* shows these two steps of preparing the space-time data. Starting from the original space-time diagram (*a*) fast oscillations are eliminated (*b*) and the threshold is applied (*c*). Computing the mutual information for such space-time data at different variability v leads to the curve displayed in Figures 10*B*, where a broad maximum of the mutual information at intermediate variability is seen with a slow decrease at higher v. This result confirms the visual impression that spatiotemporal patterns with strongest long-range correlations appear at intermediate variability.

5. Outlook: Dynamical Function of Variability in Experimental Data

Our investigations suggest a dynamical function of variability in nonlinear systems. It seems that variability strongly influences the complexity of space-time patterns produced by systems of diffusively coupled oscillators. It would be interesting to see, whether part of this behavior is also found in natural systems. This, however, requires the design of particular analysis tools capable of quantifying the size and distribution of

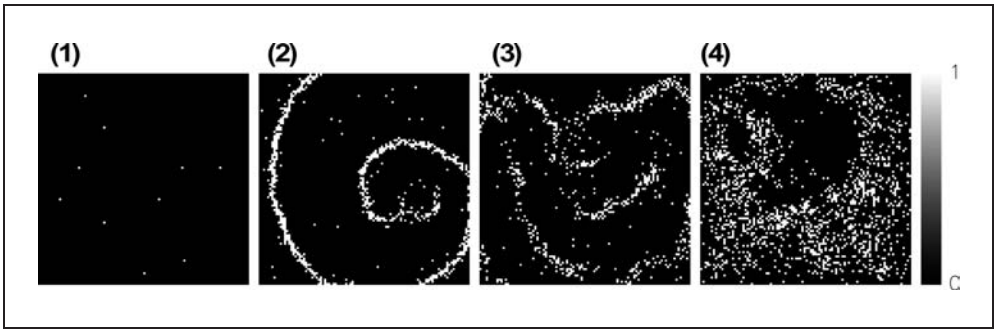

Fig. 11 Phenomenon of spatiotemporal stochastic resonance in the Jung system described by JUNG and MAYER-KRESS (1995). The images are typical snapshots of a 100 × 100 lattice for four different noise intensities σ, namely (1) $\sigma = 0.07$, (2) $\sigma = 0.10$, (3) $\sigma = 0.15$ and (4) $\sigma = 0.35$. For details on the model, see JUNG and MAYER-KRESS (1995), HÜTT et al. (2002).

variability in a given spatiotemporal data set. For the case of noise, i. e., the time-dependent counterpart of the static variability, we have already developed such tools and optimized them with the help of spatiotemporal data generated with mathematical models (HÜTT et al. 2002). Our main result concerns spatiotemporal stochastic resonance and will briefly be summarized here before discussing how similar analysis strategies for variability would look like.

The tools we use for quantifying the noise content in a spatiotemporal data set are dynamical filters based on cellular automata considerations (HÜTT and NEFF 2001). We tested them on data from mathematical model systems displaying spatiotemporal stochastic resonance. The term spatiotemporal stochastic resonance denotes a phenomenon when patterns in a spatially extended system are most pronounced at intermediate intensity of the noise present in the system. One of the main difficulties when attempting to find this phenomenon in natural systems has been that in most cases noise intensity is not immediately accessible by experiment (see, e. g., the contribution by MOSS and BALASZI, this volume). Our technique allows to reconstruct noise intensity from the spatiotemporal data set itself. Figure 11 shows typical snapshots from such model data (taken from HÜTT et al. 2002), namely from a system developed by JUNG and MAYER-KRESS (1995), the system, indeed, for which the phenomenon has first been described. It is clearly seen that at intermediate noise intensity (in particular snapshot #2) the spiral wave propagating through the system is most clearly visible. In Figure 12 *A* some measure of spatial order, the homogeneity, is plotted as a function of noise intensity. The homogeneity of a pattern is given by the average number of equal nearest neighbors (see HÜTT and NEFF 2001 for details). The characteristic feature of a spatiotemporal stochastic resonance is the pronounced peak at intermediate noise intensity. Figure 12 *B* shows our attempt to reconstruct the noise intensity from the data alone. There another spatiotemporal observable, the fluctuation number, is shown as a function of the real noise intensity used to generate the data. The monotonous relation between fluctuation number and noise intensity seen in Figure 12 *B* allows one to reconstruct the peak seen in Figure 12 *A* from the data alone, by plotting homogeneity and fluctuation number in a correlation diagram, as shown in Figure 12 *C*. These tools can form a basis for identifying and quantifying variability in spatiotemporal data sets from biological systems. The idea is to design similar

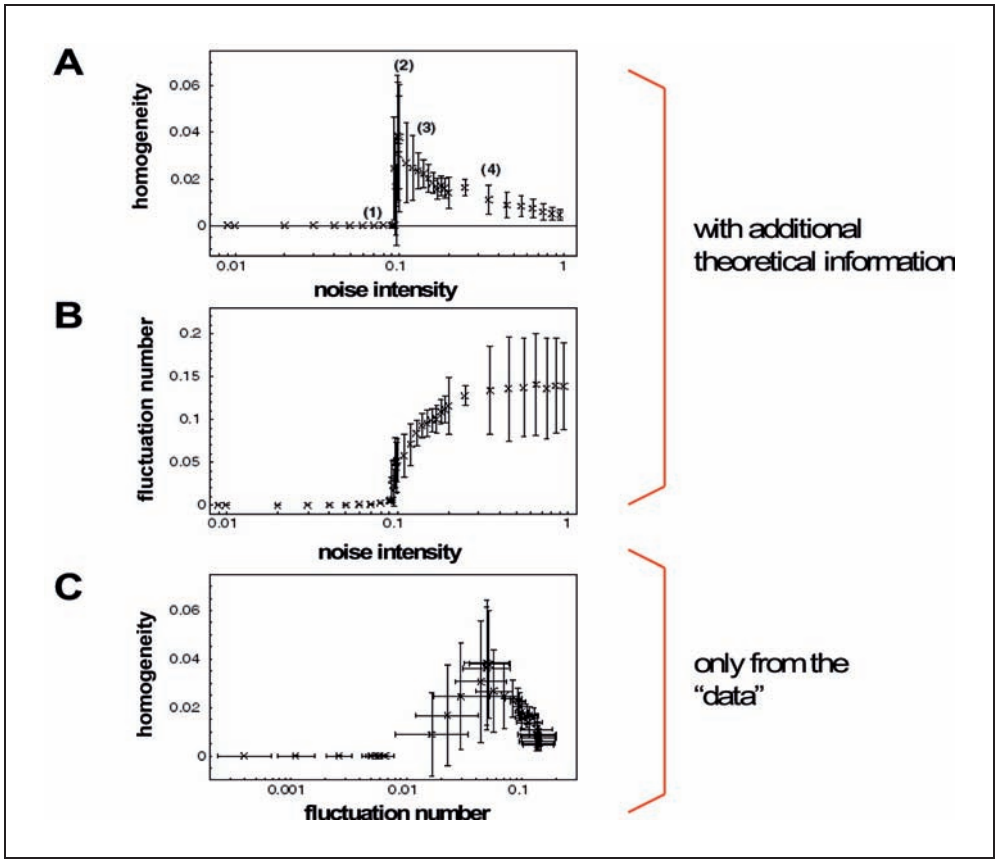

Fig. 12 Quantitative analysis of a spatiotemporal stochastic resonance using sample data from the Jung system. The first two diagrams show two spatiotemporal filters introduced by HÜTT and NEFF (2001) as a function of noise intensity σ, namely (*A*) the homogeneity and (*B*) the fluctuation number. The numbers (1)–(4) in (*A*) indicate the values of σ for the snapshots shown in Figure 11. The third diagram (*C*) shows a correlation diagram of these two filters. For further information on the spatiotemporal filters and this analysis, see HÜTT and NEFF (2001), HÜTT et al. (2002).

filters, measuring how similar neighboring states evolve in time. Systematic differences between the elements constituting the system can then be attributed to biological variability. A first approximation to such a filter would be a time-averaged (but spatially explicit) version of the above fluctuation number.

A fascinating model system, for which a regulation by biological variability seems possible, is the slime mould *Dictyostelium discoideum*. In this model system of biological pattern formation the individual cells aggregate under the effect of a chemotactic signal (cAMP) and form a multicellular organism capable of migration. Variability, in this case, could be responsible for certain stages of symmetry breaking in the usual course of development of *D. discoideum*. In this particular system the single-cell parameter, in which variability is functionally important, could be cell motility or the responsiveness to a chemotactical signal.

6. Conclusion

With the help of numerical simulation and subsequent analysis we have shown that biological variability (which enters the model as a static distribution in one of the parameters) can induce long-range spatiotemporal patterns. Within the model we studied, which represents a chain of biochemical oscillators, the complexity of the patterns is highest at intermediate variability. While the phenomenon of variability-induced patterns in a chain of biologically-motivated oscillators is clearly seen in the space-time plots shown here, as well as in the consecutive quantification attempts, it is clear that the theoretical frame needs more work to understand the systematics of this phenomenon. Quite obviously, it would be interesting to see how patterns are changed by variability in chains of other oscillators, both motivated from biology and otherwise. And even for our particular oscillator the systematics of the resonance shown in Figure 10 have to be analyzed in more detail. In particular, the relative roles of variability and coupling need to be studied to greater extent.

In the case of chains of other oscillators, two ways are, in principle, possible. One would be to explicitly take other (possibly also biologically motivated) systems of nonlinear differential equations, e. g. the Sel'kov system or a FitzHugh-Nagumo oscillator. The other method would be to start from the Thron system and modify the nonlinearities (e. g. the power in the Hill-type inhibition function). This would help to understand, in which biological systems this phenomenon can in principle be found.

Following this way, by studying both, mathematical model systems and real data using analysis tools optimized with the help of model data it could be possible to classify and understand the characteristic response scheme of biological systems to variability.

References

Baier, G., and Sahle, S.: Homogeneous and spatio-temporal chaos in biochemical reactions with feedback inhibition. J. Theor. Biol. *193*, 233–242 (1998)

Bar-Yam, Y.: Dynamics of Complex Systems. Reading, Mass.: Addison-Wesley 1997

Braiman, Y., Lindner, J. F., and Ditto, W. L.: Taming spatiotemporal chaos with disorder. Nature *378*, 465–467 (1995)

Busch, H., Hütt, M.-T., and Kaiser, F.: Effect of colored noise in networks of nonlinear oscillators. Phys. Rev. E *64*, 021105 (2001)

Gavrielides, A., Kottos, T., Kovanis, V., and Tsironis, G. P.: Spatio-temporal organization of coupled nonlinear pendula through impurities. Phys. Rev. E *58*, 5529–5534 (1998)

Guardiola, X., Diaz-Guilera, A., Lilas, M., and Perez, C. J.: Synchronization, diversity and topology of networks of integrate and fire oscillators. Phys. Rev. E *62*, 5565–5570 (2000)

Hütt, M.-T.: Datenanalyse in der Biologie. Heidelberg, Berlin: Springer 2001

Hütt, M.-T., and Neff, R.: Quantification of spatiotemporal phenomena by means of cellular automata techniques. Physica A *289*, 498 (2001)

Hütt, M.-T., Neff, R., Busch, H., and Kaiser, F.: A method for detecting the signature of spatiotemporal stochastic resonance. Phys. Rev. E *66*, 026117 (2002)

Jung, P., and Mayer-Kress, G.: Spatio-temporal stochastic resonance in excitable media. Phys. Rev. Lett. *74*, 2130–2133 (1995)

Keeling, M. J., und Grenfell, B. T.: Effect of variability in infection period on the persistence and spatial spread of infectuous diseases. Math. Biosci. *147*, 207–226 (1998)

Kelso, J. A. S.: Dynamic Patterns. The Self-Organization of Brain and Behavior. Bradford MIT Press 1995

Kuramoto, Y.: Chemical Oscillations, Waves, and Turbulence. Berlin: Springer 1984

Langton, C.: Computation at the edge of chaos. Physica D *42*, 12–26 (1990)
Lindner, F. J., Prusha, B. S., and Clay, K. E.: Optimal disorders for taming spatiotemporal chaos. Phys. Lett. A *231*, 164–172 (1997)
Lloyd, E. A., und Gould, S. J.: Species selection on variability. Proc. Natl. Acad. Sci. USA *90*, 595–599 (1993)
Matthews, P. C., and Strogatz, S. H.: Phase diagram for the collective behavior of limit-cycle oscillators. Phys. Rev. Lett. *65*, 1701–1704 (1990)
Mittag, M.: Conserved circadian elements in phylogenetically diverse algae. Proc. Natl. Acad. Sci. USA *93*, 14401–14404 (1996)
McCoy, B. M., and Wu, T. T.: The Two-dimensional Ising Model. Harvard: Havard University Press 1973
Pfister, C. A.: Patterns of variance in stage-structured populations: Evolutionary predictions and ecological implications. Proc. Natl. Acad. Sci. USA *95*, 213–218 (1998)
Pikovsky, A., Rosenblum, M., and Kurths, J.: Synchronization – A Universal Concept in Nonlinear Sciences. Cambridge: Cambridge University Press 2001
Shinbrot, T., und Scarbrough, K.: Using variability to regulate long term biological rhythms. J. Theor. Biol. *196*, 455–471 (1999)
Singer, W.: Time as coding space? Curr. Opin. Neurobiol. *9*, 189–194 (1999)
Solé, R. V., Manrubia, S. C., Luque, B., Delgado, J., and Bascompte, J.: Phase transitions and complex systems. Complexity *2*, 13 (1996)
Strogatz, S. H.: From Kuramoto to Crawford: exploring the onset of synchronization in coupled oscillators. Physica D *143*, 1–20 (2000)
Strogatz, S. H.: Exploring complex networks. Nature *410*, 268 (2001)
Thron, C. D.: Biochemical oscillations. Bull. Math. Biol. *53*, 383 (1991)

Prof. Dr. Marc-Thorsten Hütt
University of Technology Darmstadt
Bioinformatics Group
Department of Biology
Schnittspahnstraße 3–5
64287 Darmstadt
Germany
Phone: ++49 (0) 61 51 16 32 02
Fax: ++49 (0) 61 51 16 46 30
E-Mail: huett@bio.tu-darmstadt.de

Nova Acta Leopoldina NF *88*, Nr. 332, 401–405 (2003)

Synopsis

Friedrich Beck and Ulrich Lüttge, Academician (Darmstadt)

With 1 Figure

The main topics emerging from this symposium are nonlinear dynamics in general, stochastic resonance and synchronization in their recent foremost applications in biology. Now, the use of nonlinear models in biology as well as in chemistry is not a new invention. Verhulst introduced the logistic equation for the description of population dynamics in 1838, though he was not aware of (or did not dare to report on) its chaotic solutions. Lotka (1920) and Volterra (1926) opened with their feed-back model for predator and prey cycles the use of nonlinear rate equations in biological and chemical modeling. And, Robert May with his famous paper of 1976 on the logistic equation, as well as the later mathematical analysis by Grossmann and Thomas (1977), and Feigenbaum (1978), showed the richness in the solution manifold of this simple equation.

So, what is the new wisdom which makes the liaison between nonlinear dynamics and biology so fascinating? Structural biology was confronted with a vast amount of data, accumulated with new and refined experimental achievements. How can one deal with this situation? The choice of the hour was, naturally, *molecular biology.* In biology we now live in an era of "-omics". Technical breakthroughs take us in an ever accelerating pace of acquisition of information with genomics, proteomics, metabolomics ... and "channelomics", a new band waggon-term heard during this symposium. We need help for advancing from administration of these mountains of data to conceptual understanding, i. e. from description to explanation. Such rescue can come from theory. Construction of networks and systems of super-networks can assist in getting overview and outlook (e. g., Watts 1999, Hütt and Lüttge 2002). In the vein of our foreword, the concepts of nonlinear dynamics of physics to be merged with spatiotemporal biology as treated in this Symposium can lead the way. Only recently, and winning general acknowledgement rather slowly, it is realized that it is *not* enough to concentrate on the molecular structure of genes and their regulating power in cell performance alone, but that it is the whole spatiotemporal nonlinear dynamics of interacting cell agglomerations which is responsible for the behavior and conduct of living organisms. Here, the whole richness, variety and complexity of nonlinear systems come into play, as well as the fine-tuning of noise-enhanced signaling and the precise conditions for synchronization within a system. This Symposium offered a wealth of sometimes rather astonishing new findings along these lines.

Key elements of nonlinear dynamics emerging as a focus from the Symposium are oscillations, temporal and spatial synchronization/desynchronization and noise (Fig. 1). Oscillations scale from ultradian to circadian (LÜTTGE 2002, LÜTTGE and HÜTT 2003) and from individual enzymes to cells, organisms and populations (see contributions of W. SINGER, M. HAUSER, F. JÜLICHER, H. A. BRAUN, M. MALCHOW, M. MITTAG, U. RASCHER). Synchronization/desynchronization (see contributions of W. SINGER, A. PIKOVSKY, H. A. BRAUN) scales from hopping Brownian particles (see contributions of P. HÄNGGI and W. EBELING), ion channels (see contribution of G. THIEL), microalgae, Daphnias (see contribution of A. ORDEMANN), cells in an organ (see contribution of U. RASCHER), neurons in a brain (see contributions of W. WAGNER , S. GRÜN), development organizers (see contribution of T. W. HOLSTEIN), sardines in a vortex (see contribution of A. ORDEMANN) to plankton blooms in the ocean (see contribution of M. MALCHOW). Noise is differentiated into environmental and endogenous. Biological variability is, similar to the effect of noise, capable of inducing spatiotemporal patterns in nonlinear systems (see the contribution of M.-T. HÜTT).

Biology asks for positive effects driving evolution, or perhaps more explicitly, for benefits for fitness. Oscillations and clocks allow *timing*. Contributions to the Symposium unraveled *functions* of synchronization/desynchronization and noise in movements and transport with Brownian motors (contribution of P. HÄNGGI), in behavior and in the control of diseases (contribution of P. TASS) (Fig. 1).

One irrefutable conclusion of the Symposium was that nonlinear dynamics confer robustness to living systems. However, other questions regarding evolution and fitness remain. There are a lot of ideas and discussions regarding beneficial and even basically

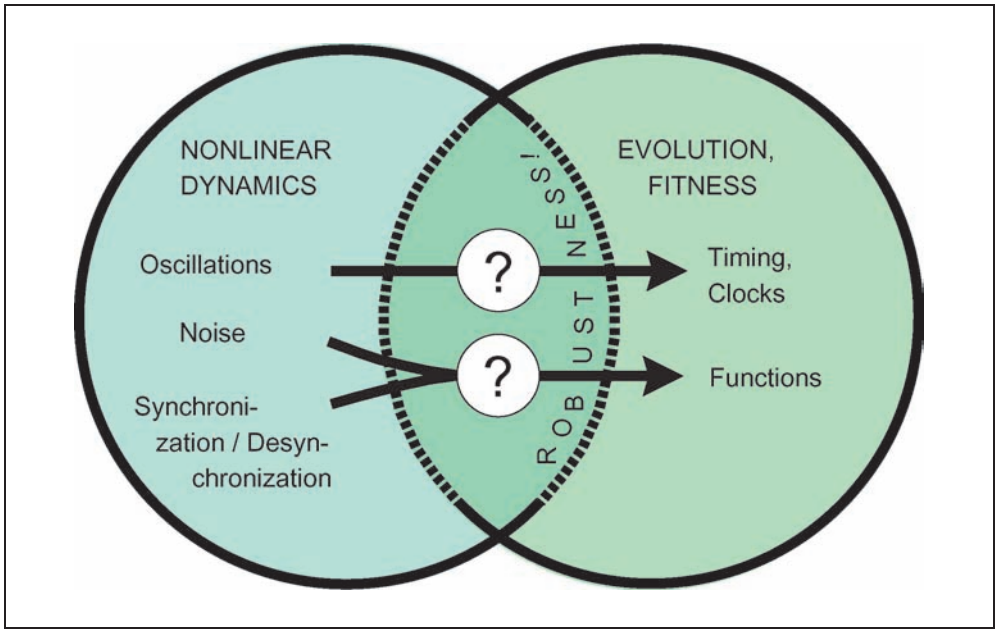

Fig. 1

essential functions of both ultradian (for review see LÜTTGE and HÜTT 2003) and circadian (for review see LÜTTGE 2002) rhythmicity in signaling, information transfer and timing in organisms. Nevertheless, the question still remains open, if they may not be just unavoidable by-products of nonlinear regulation dynamics. With respect to noise, with the newly developing insights in the impact of noise-induced structures and stochastic resonance on biological systems, the question becomes even more intriguing. Has evolution of organisms over billions of years under the non-escapable influence of thermal noise led to the selection of traits that are irreplaceably dependent on the noise?

Frank MOSS, in the final discussion of the Symposium, elaborated this question as follows, with reference to sensory evolution in animals: "Many animals have evolved surprisingly sensitive apparatus, some of which are as yet unrivalled by human engineering. Notable examples include the legendary electric field sensitivity of a few nanovolts per centimetre, of sharks and rays (KALMIJN 2000), one half-to-one microvolt per cm of freshwater cat- and paddle-fish (RUSSELL et al. 1999) and the remarkable sensitivity to seismic amplitudes of only a few Ångstroms by some frogs (NARINS and LEWIS 1984, NARINS 1990). Certainly the ability to detect ever weaker signals from predators, prey or potential mates is advantageous and therefore is selected for. Thus, weak signals at the threshold of perception drive the evolution of sensory nervous systems. Experiments with behaving animals (RUSSELL et al. 1999) have demonstrated that the detectability of such signals can be enhanced by Stochastic Resonance (SR), and we therefore expect it to have played a role in the evolution of sensory systems. SR requires three ingredients, a threshold, a subthreshold signal and noise, ingredients that are ubiquitous in the natural world, most especially in the world of animal perception. Indeed, the evolution of the long, electrically sensitive rostrum of the paddlefish is a textbook example. The rostrum grew longer and the electric sensitivity grew sharper as the animal's continued survival was enhanced by its ability to 'reach out' and perceive ever weaker signals from ever more distant planktonic prey." (See contributions by FREUND et al. and MOSS.) "Though this argument seems attractive, it is alas only speculative. There is, however, one experiment that offers compelling evidence of a role for SR in sensory evolution. Using experimental techniques similar to those described by JÜLICHER in this volume, JARAMILLO and WIESENFELD (1998) were able to mechanically manipulate hair bundles in the ear of a leopard frog at the sub-Brownian motion level while measuring the signal-to-noise ratio (SNR) of the corresponding discharge in the auditory neuron. They performed a classical SR experiment by adding a controlled amount of noise to subthreshold periodic motion of the hair bundle while measuring the SNR in the auditory nerve. They found, of course, the standard signature of SR: the SNR passed through a maximum at the optimum value of the noise intensity. What is remarkable is that the optimum noise found by JARAMILLO and WIESENFELD (1998), 2.5 – 0.5 nm r. m. s., was precisely in the midrange of the previously determined natural Brownian motion about 2 – 3 nm r. m. s. of the hair bundle moving in the cochlear fluid. Brownian motion is natural noise arising from thermal fluctuations present throughout the evolution of life on this planet. This experiment provides direct evidence that the mechanical properties of the hair bundles in the frog auditory system evolved in order to make use of SR at the threshold of perception."

There were some **specific points** from the various contributions, raised again in the synopsis discussion for further clarification:

Stochastic resonance is often explained qualitatively and pictorially as a subthreshold signal, pushed by internal noise above *threshold*, and, for a suitable window in the noise strength, *enhancing* the signal to noise ratio (SNR). Noise and signal amplitudes are added *linearly*, while stochastic resonance occurs in nonlinear systems only. Where enters the role of nonlinearity in this simple picture? It is the *nonlinear* production of the *threshold* in *non-dynamical stochastic resonance* of a system to which the external signal is applied.

In **coordinated motion** of swarms of animals, resulting from random walks of the individuals, e. g., the observed vortex motion of Daphnias around an external shaft of light (see contribution of A. ORDEMANN, see also the contribution of W. EBELING), the question arises where the breaking of rotational symmetry occurs. It is clear that such a vortex motion cannot occur in a *closed system*. There has to be a *substrate* (in the case of the quoted example the water) which takes up the angular momentum generated spontaneously by random motion. If the substrate is massive enough, the compensation needed for fulfilling the angular momentum conservation law can hardly be observed.

In stochastic resonance **noise tuning** is essential in order to obtain the amplitude window for which enhancement of SNR occurs. In biological systems, however, noise level and noise color are generally fixed by external control parameters (e. g. temperature) and internal dynamics. How can such a system profit in signal recognition from stochastic resonance? Is there an internal regulating mechanism (eventually produced in the process of evolution)? The question seems to be open at present. There is, however, an intriguing aspect, discussed in the contribution of H. KANTZ, that the fast dynamics, not explicitly described on the time scale of interest, can be replaced by a fluctuation term in the Liouville equation. This also relates to Frank MOSS' extensive contribution to the question of noise sensitivity, quoted above.

The role of **deterministic chaos** in biology is not yet clear. Unique identifications from time series analysis are often not possible since the amount of data, especially in diurnal rhythms, is not sufficiently large. Special care is needed since the interplay of noise, limit cycles and nearby fixed points can lead to irregular oscillations without chaos. Such situations can be effectively analyzed by adding noise in the Fokker-Planck equation (see contribution of H. KANTZ).

Modeling of biological processes is based completely on classical dynamics and classical mechanics. Could **quantum processes** show up significantly in biological systems? The general answer is *no*. The belief stems from the fact that noise, even if only thermal, destroys quantum coherence completely. One should, however, not rashly be consoled with this answer. In membrane processes *electron transfer* and *quantum tunneling* can play an important role for ion channel openings and signal transduction (as has been shown, e. g., for photobacteria in femtosecond spectroscopy; see also the contributions of P. HÄNGGI and T. DITTRICH). Molecular biology works generally with time scales down to nanoseconds. Quantum processes, which have to be in the time scale of pico- to femtoseconds in order to stay above thermal noise, escape therefore detection with present-day techniques.

This final synopsis highlighted once more important points put forward during the Symposium. It ended with a **wine reception** in the happy mood that one had witnessed three days of intriguing discussions on the most recent highlights of dynamic principles in biology.

References

FEIGENBAUM, M. J.: Quantitative universality for a class of nonlinear transformations. J. Stat. Phys. *19*, 25–52 (1978)

GROSSMANN, S., and THOMAS, S.: Invariant distributions and stationary correlation functions of one-dimensional critical processes. Z. Naturforsch.; *32 a*, 1353–1363 (1977)

HÜTT, M.-T., and LÜTTGE, U.: Nonlinear dynamics as a tool for data analysis and modeling in plant physiology. Plant Biology *4*, 281–297 (2002)

JARAMILLO, F., and WIESENFELD, K.: Mechanoelectrical transduction assisted by Brownian motion: a role for noise in the auditory system. Nature Neurosci.; 384–388 (1998)

KALMIJN, A. J.: Detection and processing of electromagnetic and near-field acoustic signals in elasmobranch fishes. Phil. Trans. R. Soc. London B *255*, 1135–1141 (2000)

LÜTTGE, U.: Circadian rhythmicity: Is the "biological clock" hardware or software? Progr. Bot. *64*, 277–319 (2002)

LÜTTGE, U., and HÜTT, M.-T.: High frequency or ultradian rhythms in plants. Progr. Bot. *65*, 235–263 (2003)

LOTKA, A. J.: Undamped oscillations derived from the law of mass action. J. Amer. Chem. Soc. *42*, 1595–1599 (1920)

MAY, R. M.: Simple mathematical models with very complicated dynamics. Nature *261*, 459–467 (1976)

NARINS, P. M.: Seismic communication in anuran amphibians. BioScience *40*, 268–274 (1990)

NARINS, P. M., und LEWIS, E. R.: The vertebrate ear as an exquisite seismic sensor. J. Accouist. Soc. Amer. *76*, 1384–1387 (1984)

RUSSEL, D., WILKENS, L., and MOSS, F.: Use of behavioral stochastic resonance by paddlefish for feeding. Nature *402*, 219–223 (1999)

VERHULST, P. F.: Notice sur la loi que la population suit dans son accroissement. Corr. Math. et Phys. *10*, 113–121 (1838)

VOLTERRA, V.: Variazionie fluctuationi del numero d'individui in specie animali conviventi. Mem. Acad. Lincei *2*, 31–113 (1926)

WATTS, D. J.: Small Worlds: The Dynamics of Networks between Order and Randomness. Princeton: Princeton University Press 1999

Prof. Dr. Friedrich BECK
Institut für Kernphysik
Technische Universität Darmstadt
Schloßgartenstraße 9
64289 Darmstadt
Germany
Phone: ++49 (0) 61 51 14 89 87
Fax: ++49 (0) 61 51 16 60 76
E-Mail: Freder.Beck@physik.tu-darmstadt.de

Prof. Dr. Ulrich LÜTTGE
Institut für Botanik
Technische Universität Darmstadt
Schnittspahnstraße 3–5
64287 Darmstadt
Germany
Phone: ++49 (0) 61 51 16 37 00
Fax: ++49 (0) 61 51 16 46 30
E-Mail: luettge@bio.tu-darmstadt.de